THE UNIVERSITY *of* EDINBURGH

Cell Fusion in *Neurospora crassa*

Alexander Lichius

Ph.D. Thesis

The University of Edinburgh

2010

To Daniela.

Honey,
you're the light
when darkness takes me,
you're the good
when evil breaks me,
you're the love
that won't forsake me.

('Honey', by Thomas Dybdahl)

Declaration

I hereby declare that I am the sole author of this thesis. The work, of which it is a record, has been carried out by myself. Results obtained through the collaboration with other individuals and institutions is appropriately indicated. All sources of information have been specifically acknowledged by means of referencing.

Alexander Lichius, Dipl.-Biol.

Edinburgh, May 2010

Abstract

The primary research aims of this thesis were the identification of novel cell fusion mutants of *Neurospora crassa* and the subsequent functional characterization of selected candidate proteins during conidial anastomosis tube (CAT)-mediated cell fusion by means of genetic, molecular, biochemical and live-cell imaging analysis. Chapter 1 provides a general introduction of the model organism and the cell fusion processes studied during different stages of the fungal lifecycle. Chapter 2 summarizes the materials and methods used. Chapter 3 introduces the comparative genomics screen conducted between appressorium-mediated plant infection by the rice blast fungus *Magnaporthe oryzae* and hyphal fusion in *Neurospora crassa*. Novel cell fusion mutants were identified in MAP kinase signalling, redox-signalling and Rho-type GTPase signalling pathways, whereas no functional overlap in the cAMP response pathway between both species could be found. Chapter 4 demonstrates how newly developed fluorescent reporters for F-actin and activated Rho GTPases in filamentous fungi lead to novel insights into the dynamic rearrangement of the F-actin cytoskeleton and cortical activation of Rho GTPases during cell symmetry breaking, polarized tip growth and cell fusion. Chapter 5 focuses on the role of the cell wall integrity (CWI) MAP kinase pathway during cell fusion, and in particular, on the function of the terminal MAP kinase MAK-1 during CAT homing and fusion pore formation. Inhibitor studies indicated that MAK-1 kinase activity is required for its own recruitment to the fusion site already during homing and for cell wall remodelling during fusion pore enlargement between interacting cells. Chapter 6 presents ultrastructural scanning electron microscope (SEM) studies which indicate that defects in hyphal attachment, extracellular matrix deposition and cell wall remodelling prematurely abort morphogenesis of the female fruitbody. These findings are put into context with defects observed in mutants of components acting in related signalling pathways which appear to regulate non-self fusion events at later stages of sexual development leading to fertilization in *N. crassa*. Chapter 7 provides the first evidence for a role of NADPH-oxidase (NOX)-generated reactive oxygen species (ROS) in the regulation of morphogenetic changes required for CAT-mediated cell fusion. Redox-modification of signalling proteins might be involved in cell-cell chemoattraction. Chapter 8 provides a summary of the key findings and discusses future directions.

Acknowledgements

I would like to thank all the people who have contributed through their advice, discussion, encouragement, friendship and inspiration to make my Ph.D. a unique, successful and invaluable experience. In a nutshell, the last 4 years have been exciting, frustrating, hard work, surprising and rewarding. Pretty much in that order, thus just a normal Ph.D..

First of all I would like to thank my supervisor Nick Read for giving me the opportunity and for skilfully guiding me through the Ph.D.. I have thoroughly enjoyed working with *Neurospora* in your lab and I am grateful for the support, unfailing reliability and encouragement I have received. Especially, for giving me numerous opportunities to present my work at international meetings.

I also would like to thank my second supervisor Karl Oparka for his enthusiastic support, sound advice and continued interest across kingdoms. Your objective thinking and 'second opinion' about my work will always be valued.

Chris Jeffree deserves a special mentioning and a very big thank you. Spending time with you at the cryo-SEM not only resulted in great science, but also provided a relaxing island of tranquillity in the rough waters of stressful molecular lab work. The great discussions we had alongside these fantastic journeys into the ultrastructural 3D world of fungi have been very influential for my scientific thinking.

Mathematical modelling is not my comfort zone, thus I am very grateful to Andrew Goryachev for enriching my work with his astonishing capabilities in that field. Extensive discussions with you on signalling network analysis have greatly contributed to the progression and output of this thesis. большое спасибо!

A special thank you also to Stephen Fry who helped me find my way through the intricate labyrinth of reactive oxygen species biochemistry of the cell wall. I still haven't found the exit but keep searching, and I will gladly come back for more enlightening discussions.

I would also like to thank all members of the Read lab, past and present, especially Gabriela Roca, Verena Seidl-Seiboth, Kathryn Lord, Patrick Hickey, Peter Marris, Graham Wright, Jun-ya Shoji, Alberto Muñoz and Adokiye Berepiki, who all have contributed to my work in some way, and all have been fantastic colleagues. Thanks guys!

Also a very pleased thank you to 'my' students Robert Dinwiddie, Radek Oborny and Patid Boonyarungsrit, who choose to do their honours or summer projects under my supervision. You all did a very good job and made significant contributions to this study.

There are far too many more colleagues from Edinburgh University to thank for helping out with strains, plasmids, chemicals, enzymes, protocols and borrowed equipment. Thus, a broad-spread thank you goes to members of the Rosalind Allen lab, the Jean Beggs lab, the Stephen Fry lab, the Karen Halliday lab, the Gary Loake lab, the Andrew Millar lab, and the Karl Oparka lab, and all the rest at the Institute of Molecular Plant Sciences (IMPS).

Nevertheless, two individuals deserve special mentioning: David Kelly who helped with various microscope set ups in The Centre Optical Instrumentation Laboratory (COIL) of the Welcome Trust Centre, and Lucas Black (Institute for Condensed

Matter and Complex Systems) for his help getting that chemiluminescent plate reader programmed.

Thanks also go to the British Mycological Society and the Royal Microscopical Society for their stimulating meetings and generous travel bursaries, as well as to The University of Edinburgh for awarding me with The College of Science and Engineering Studentship without which this scientific endeavour would not have been possible.

Thanks to collaborators that hosted me well in their labs for longer or shorter periods during my Ph.D.: Christian Kubicek and Verena Seidl-Seiboth at the TU Vienna for giving me a methodological kick-start and a few very enjoyable weeks in Vienna, Jan Knight and James Reeves, from Knight Scientific Ltd., for helping me to set up the first ever Pholasin® assays for *Neurospora*, and giving me a great time down South in Plymouth, as well as Nick Talbot and Martin Egan at the University of Exeter for advice and discussion on NOX in fungi.

Extra special thanks go to Arild Husby, Jens Tilsner, Gareth Hempson, Thomas Waibel, Euan James, Jürgen Prell and Dominique Hardy for being great colleagues and very good friends who contributed substantially to a fantastic time here in Scotland. Arild, I happily return many thanks for late Sunday guitar nights, introducing me to Thomas Dybdahl, fun badminton matches, regular running trips along the Canal, the odd night out, and improving my statistics skills. Jens, thanks for reliable belaying in the vertiginous heights of Alien Rock and holding me back from cycling home after climbing with all those fantastic Whiskies and great conversations, including cloning strategies. Gareth, thanks for your regular visits and bringing that relaxing mood into our flat. Also thanks for the continually renewed invites to South Africa, which kept me going when things were tough. I promise I'll come. Thomas, thanks for fun parties in your flat, chatting away lunch breaks on the golf course bench and wonderful hikes out and about. Euan, thanks for being an excellent route planner during many challenging walks in the Highlands. But most importantly, many thanks for getting me in touch with Nick in the first place. Otherwise all this would not have happened. For the same reason, and for good times in Aachen thanks to Jürgen Prell, now at the John Innes Centre in Norwich. Dominique, thanks for being a fast friend since Uni, and for wonderful times in Dundee.

Finally, I would like to sincerely thank my family. My parents for their faultless support in everything I choose to do, their encouragement and love. Thanks for the keen interest in my doings and raising me with a free spirit and curious mind. Special thanks also go to my brother Guido, who noticed my potential before I did and was reassuring when I was in doubt. You guys are amazing and laid the foundations for all my achievements many, many years ago. Thanks to my parents-in-law, Christiane and Ludwig. First of all for putting Daniela into this world, but also for the wonderful times at the coast of Spain, and for providing a haven of relaxation and reflection wherever we meet. Thanks to the rest of the pack for being there and for being who you are.

To my dearest Daniela, from the bottom of my heart I want to thank you for sharing your life with me over the past decade. During all ups and downs of our life in science. Whether in Aachen, Dresden or Edinburgh, you have been patient, supportive and loving, always. I am curiously looking forward to continuing this exciting journey together with you. I love you.

For those which I may have forgotten. This one is for you: THANK YOU!!

“In the year of 1657 I discovered very small living creatures in rain water.”

❖

“I've spent more time than many will believe [making microscopic observations], but I've done them with joy, and I've taken no notice those who have said why take so much trouble and what good is it?”

Antonie Philips van Leeuwenhoek, (born on October 24, 1632 and died on August 26, 1723) was a Dutch tradesman and scientist from Delft. He is commonly known as "the Father of Microbiology", and considered to be the first microbiologist. He is best known for his work on the improvement of the microscope and for his contributions towards the establishment of microbiology. Using his handcrafted microscopes he was the first to observe and describe single celled organisms, which he originally referred to as animalcules, and which we now refer to as microorganisms. (modified from http://en.wikipedia.org).

Table of Contents

Abbreviations

°C	degree Celcius
µg	microgram
µm	micrometer
1NM-PP1	1-(1,1-dimethylethyl)-3-(1-naphthalenylmethyl)-1H-pyrazolo[3,4-d]pyrimidin-4-amine
3D	three dimensional (x,y and z)
4D	four dimensional (x,y,z and time)
A	(deoxy)adenosine
A. fumigatus	*Aspergillus fumigatus*
A. gossypii	*Ashbya gossypii*
A. nidulans	*Aspergillus nidulans*
ABP	actin binding protein
ATP	adenosine triphosphate
bar	ignite resistance gene
BLASTp	basic local alignment search tool for proteins
bp	base pairs
BP	band pass
BR domain	basic rich domain
BROAD	Broad Institute at MIT
C	(deoxy)cytidine
C. albicans	*Candida albicans*
cAMP	cyclic adenosin monophosphate
CAT	conidial anastomosis tube
CCD	charge-coupled decive
CDK	cyclin-dependent kinase
cDNA	complementary DNA
CFEM domain	conserved fungi-specific extracellular-membrane spanning domain
CFW	calcofluor white
cGMP	cyclic guanosine monophosphate
CLSM	confocal laser scanning microscope/microscopy
cm	centimeter
COIL	Centre Optical Instrumentation Laboratory
CRIB	Cdc42- and Rac1-interactive binding
cryo-SEM	low-temperature SEM
CWI	cell wall integrity
D. discoideum	*Dictyostelium discoideum*
DAG	diacylglycerole
DAPI	4',6-diamidino-2-phenylindole
DC-STAMP	dendritic cell-specific transmembrane protein
dH_2O	distilled water
DIC	differential interference contrast

DMSO	dimethylsulfoxide
DNA	desoxyribonucleic acid
dNTP	desoxyribonucleotide triphosphate
DPI	diphenyleneiodonium
e.g.	*exempli gratia* (for example)
E. coli	*Escherichia coli*
E. festucae	*Epichloe festucae*
ECM	extracellular matrix
EDTA	ethylenediaminetetraacetic acid
EGF	epidermal growth factor
EIHM	extra-invasive hyphal membrane
ER	endoplasmic reticulum
EtOH	ethanol
F. graminearum	*Fusarium graminearum*
F-actin	filamentous actin
Fd	Faraday
FGSC	Fungal Genetics Stock Center
Fig.	figure
FIGS	fructose-glucose-sorbose
FKBP	FK506-binding protein
FM4-64	Fei Mao dye 4-64 (N-(3-triethylammoniumpropyl)-4-(6-(4-diethylamino)phenyl)hexatrienyl pyridinium dibromide)
fMLP	N-formylmethione-leucyl-phenylalanine
FP	fluorescent protein
G	(deoxy)guanosine
g	gram
G-actin	globular actin
GAP	GTPase activating-protein
GDI	guanine nucleotide dissociation inhibitor
gDNA	genomic DNA
GEF	guanine nucleotide exchange factor
GFP	green fluorescent protein
GPCR	G-protein-coupled receptor
GPI	glycosylphosphatidylinositol
GSHPx	glutathione peroxidase
GSSGR	glutathione reductase
GT	germ tube
GTPase	guanosine triphosphatase
h	hour
H1-GFP	histone H1-green fluorescent protein
het	heterokaryon incompatibility genes
HOG	high osmolarity glycerol
HP	homokaryon purification
hph	hygromycin B resistance gene

HRP	horse radish peroxidase
HygB	hygromycine B
hygR	hygromycine resistance
i.e.	*it est* (that is)
IL-4	interleukine 4
kb	kilo base pairs
kDA	kilo Dalton
KI	potassium iodine
KO	knock-out
kV	kilo volts
l	liter
LACS	low-affinity calcium influx system
Lat A	latrunculin A
LB	Luria Bertani
LED	light-emitting diode
LP	long pass
LSA	low-sucrose agar
LTSEM	low temperature scanning electron microscope/microscopy
M	molar
M. oryzae	*Magnaporthe oryzae*
MADS box	MCM1-agamous-deficiens-SRF sequence motif
MAPK	mitogen-activated protein kinase
MAPK	mitogen-activated protein kinase
MAPKK	mitogen-activated protein kinase kinase (MAP2K)
MAPKKK	mitogen-activated protein kinase kinase kinase (MAP3K)
MAPKKKK	mitogen-activated protein kinase kinase kinase kinase (MAP4K)
mat a	mating type locus a
mat A	mating type locus A
Mbp	mega base pairs
M-CSF	macrophage colony-stimulating factor
mg	milligram
min	minute
MIT	Massachusetts Institute of Technology
ml	milliliter
mm	millimeter
mM	millimolar
mRNA	messenger ribonucleic acid
mW	milli Watt
N. crassa	*Neurospora crassa*
N.A.	numerical aperture
NADP(H)	nicotinamid adenine dinucleotide phosphate
NBT	nitroblue tetrazolium
NCBI	National Centre for Biotechnology Information

N-free VM	nitrogen-free Vogel's medium
ng	nanogram
NIH	National Institutes of Health
nm	nanometer
NOX	NADPH-oxidase
NSF	N-ethylmaleimide sensitive fusion proteins
nt	nucleotide
OD_{600}	optical density at 600 nm
ORF	open reading frame
P. anserina	*Podospora anserina*
PAF	platelette activating factor
PAK	p21-activated kinase
PBD	p21-binding domain
PCD	programmed cell death
PCR	polymerase chain reaction
pDNA	plasmid DNA
pH	potentia hydrogenica
PH domain	Pleckstrin homology domain
PKA	protein kinase A
PKC	protein kinase C
PKS	polyketide synthase
PMA	phorbol-12-myristate-13-acetate
PR	pheromone response
RANKL	receptor activator for nuclear factor κ B ligand
redox	reduction-oxidation
RGS	regulator of G-protein signalling
RIP	repeat-induced point mutation
RLU	relative light units
RNA	ribonucleic acid
RNas	ribonuclease
RNS	reactive nitrogen species
ROS	reactive oxygen species
rpm	revolutions per minute
RT	room temperature (21 °C)
S. pombe	*Schizosaccharomyces pombe*
SBF	Swi4p/Swi6p/Mbp1p transcription factor complex
SCM	synthetic crossing medium
SDM	side-directed mutagenesis
sec	second
SEM	scanning electron microscope/microscopy
sGFP	synthetic GFP = GFP(S65T)
SMART	simple modular architecture research tool
SOC	super optimal broth with catabolite repression
SOD	superoxide dismutase

Spk	Spitzenkörper
STM	spore tip mucilage
T	(deoxy)thymidine
TagRFP	red fluorescent protein RFP from the sea anemone *Entacmaea quadricolor*
TagRFP-T	photostabilized TagRFP(S162T)
TB	transformation buffer
TEM	transmission electron microscope/microscopy
TF	transcription factor
TIFF	tagged image file format
T_m	melting temperature
TNF	tumor necrosis factor
TOR	target of rapamycin
t-SNARES	target soluble NSF attachment protein receptor
U	unit
U. maydis	*Ustilago maydis*
UV light	ultra-violet light
V	volt
v/v	volume per volume
VHF	vegetative hyphal fusion
VM	Vogel's medium
VMpc	pre-conditioned Vogel's medium
vol.	volume
v-SNARES	vesicle soluble NSF attachment protein receptor
w/v	weight per volume
WASP	Wiscott-Aldrich Syndrome protein
WAVE	WASP-family verprolin homology protein
WSC	wall integrity and stress-response component
wt	wild type
WW domain	protein domain with two signature tryptophane (W) residues
xg	times g-force
Ω	Ohm

Chapter 1 – General introduction

1.1. Abstract

The formation of interconnected hyphal networks is central to the organization and functioning of the filamentous fungal colony. It is brought about by the fusion of specialized hyphae during colony initiation and mature colony development. Within one colony the hyphae are genetically identical, and hence this process is termed hyphal self-fusion. Self-fusion occurs at two stages of vegetative colony development. The conidial anastomosis tube (CAT) is a specialized cell protrusion and functions in forming networks of conidial germlings during the earliest stages of colony establishment. Extraordinary new insights into the process of self-signalling that are a prerequisite for CAT-mediated cell fusion have recently been revealed by live-cell imaging of genetically engineered strains of *Neurospora crassa*. During colony extension morphologically distinct fusion hyphae establish the interconnected network of the mature colony. This chapter will introduce the filamentous model fungus *N. crassa,* review our current understanding of how cell fusion is regulated on the cellular level, and highlight the importance of cell fusion at various stages of the fungal lifecycle.

1.2. The model fungus *Neurosopora crassa*

Neurospora crassa is the best-characterised fungus among the filamentous ascomycetes, a group of organisms critically important to agriculture, medicine, and the environment. *Neurospora* is an extensively studied model filamentous fungus because of its numerous advantages for experimental research. A principal benefit of *N. crassa* is its ease of culture on defined media with rapid growth and large hyphae making it highly suited for cytological examination. Both, vegetative hyphae and asexual spores (conidia) are experimentally accessible and very convenient for microscopy compared with other filamentous fungi or yeast cells. A range of subcellular structures can be readily observed by simple light microscopy, and advanced live-cell imaging techniques are established that facilitate in depth analysis of complex cellular processes [31, 32]. In 2003 *N. crassa* became the first filamentous fungus to have its genome sequenced and annotated [6, 23]. With a total genome size of about 43 Mbp from which 9826 open reading frames (ORFs) are currently predicted *Neurospora* possesses nearly twice as many genes as the unicellular yeast *Saccharomyces cerevisiae*. Its complex organisation makes it an increasingly important eukaryotic model system for the investigation of multicellular differentiation and development, epigenetics and gene regulation in a multinuclear environment. Molecular details of the establishment and maintenance of cell polarity, cell recognition and cell fusion, are only a few of the many aspects of cell biology and biochemistry studied in *Neurospora*. As *N. crassa* is haploid throughout the majority of its life cycle recessive mutant alleles are not masked by dominant alleles on homologous chromosomes [85]. Furthermore, *Neurospora* possesses a wide variety of epigenetic phenomena, most importantly repeat-induced point mutation (RIP) [9, 10]. RIP efficiently detects repeated DNA sequences and subjects both copies of the sequence duplication to multiple G:C-to-A:T mutations. This contributes to an unusually low level of gene redundancy making the functional analysis of genes conveniently straight forward.

In addition to the experimental advantages of *N. crassa*, an established scientific community exists in which resources and strains are easily and readily shared. A foundation of this community is the Fungal Genetics Stock Centre (FGSC) based at the University of Kansas, Missouri (http://www.fgsc.net). The FGSC makes many resources, including protocols, strains and plasmids readily available for a range of different filamentous fungi. Especially in recent years a comprehensive collection of molecular tools for standard and advanced cloning and expression techniques [13, 21, 33] became available which filled important technical gaps that so far existed in comparison to the yeast field.

1.3. The life cycle of *Neurospora crassa*

Neurospora crassa has both asexual and sexual parts to its life cycle (Fig. 1.1). The asexual, vegetative colony grows on solid medium by means of radial extension of tip growing hyphae, which penetrate with force, and by digestion, through the substrate. Spatial confinement and nutrient limitation in the culture dish, as well as other factors including the circadian clock and light stimulation, induce the production of copious quantities of orange multinucleate asexual spores (macroconidia). Macroconidia are formed by budding and segmentation of aerial hyphae that emerge from the mycelium. The two other types of asexual spores of *Neurospora* are microconidia, formed by specialized microconidiophores, and arthroconidia, which form by fragmentation of macroconidiophores [49]. Environmental factors, but also defects in macroconidiation can promote the production of microconidia and arthroconidia, a pleiotropic phenomenon often seen in various gene deletion mutants [48].

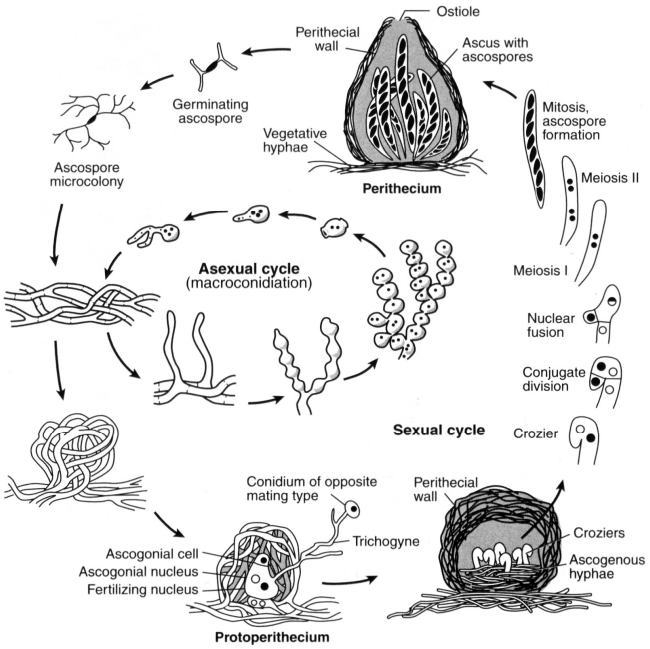

Figure 1.1 The life cycle of *Neurospora crassa*. The asexual cycle leading to the production of macroconidia is illustrated in the inner sequence. The outer sequence illustrates the main stages of the sexual cycle, in which the protoperithecium is fertilized by the fusion of the female trichogyne with a male conidium of the opposite mating type (*N. crassa* has two mating types *mat a* and *mat A*) and subsequent meiosis leads to the production of ascospores inside developing asci of the perithecium. Reproduced from [15].

Nitrogen starvation triggers the development of female reproductive structures (Fig. 1.1). Hyphal aggregates form which gradually become enveloped by primary and secondary enveloping hyphae to build the protoperithecium [61]. Upon maturation, this fruitbody sends out a specialized hypha (trichogyne) which is chemotropically attracted to the male mating partner [3, 4], which can be any cell of the opposite mating type, but in most cases is a macroconidium [53]. Upon fusion between female trichogyne and male conidium the male nucleus travels through the trichogyne into the mature fruitbody which triggers differentiation of the protoperithecium into the perithecium, and leads to fertilization of ascogenous hyphae inside. Dikaryon formation, karyogamy and meiosis eventually lead to the production of haploid sexual spores (ascospores) [59], which are shot out through the perithecial neck and are capable of founding a new vegetative colony [15].

1.4. Conidial germination and CAT-mediated cell fusion

1.4.1. Germ tube emergence and colony establishment

Primary functions of conidia are in asexual reproduction, dispersal and in acting as male fertilising agents during sexual reproduction (Fig. 1.1) (see section 1.6). Macroconidia, once in a favourable environment, hydrate then initiate a complex cascade of mRNA expression, and biochemical and metabolic changes (Tables 1.1, 1.2; Fig. 1.2) [14, 40, 70]. Following hydration prior conidia undergo isotropic expansion before cell symmetry is broken and a polarized germ tube (GT) emerges [2, 14]. Initially most of the organelles (e.g. nuclei and mitochondria) display a more-or-less uniform distribution within growing GTs. However, after about 10 h when GTs reach ~150 μm in length, the organelle organisation becomes polarized, and a small exclusion zone appears at the tip, followed by the development of a phase dark Spitzenkörper, which is characteristic of mature growing vegetative hyphae [2]. The colony explores its environment by extending highly polarised tip growing leading hyphae from the colony periphery. Maturation of the colony involves the formation of a complex interconnected hyphal network in the subperipheral region, starting a few hundred micrometers behind the leading edge, by means of hyphal self-fusion (Fig. 1.6) [31].

Table 1.1 Cytological events associated with the early stages of colony establishment in *N. crassa*. Modified from [2, 67].

< 2 h
Spore hydration
Isotropic expansion
2-3 h
Cell polarisation
GT emergence
CAT induction
> 3 h
CAT homing and fusion starts
> 5 h
GT elongation and branching
Uniform distribution of organelles
FM4-64 staining can be detected in vesicles in the tip
> 10 h
Exclusion zone establishes at tip
'Immature Spitzenkörper' develops
Increasingly polarized distribution of organelles (mitochondria and nuclei)
Phase dark mature Spitzenkörper observed

1.4.2. CAT-mediated cell fusion

In addition to GTs, cell polarisation can also lead to the protrusion of a morphologically and functionally distinct structure: the conidial anastomosis tube (CAT) [67]. CAT-mediated cell fusion in *Neurospora crassa* initially establishes cytoplasmic continuity between individual conidia, but with time leads to the formation of complex germling networks (Fig.1.3E). All three types of conidia produced by *N. crassa* (microconidia, macroconidia and arthroconidia) are able to undergo CAT fusion with each other [67]. GTs form directly from conidia, have an average diameter of about 4-5 μm, show indeterminate growth, have the ability to septate and branch, and eventually will differentiate into vegetative hyphae of the mature colony. GTs show avoidance, i.e. negative chemotropism towards each

other, thus tend to grow away from each other, and are generally unable to fuse (Fig.1.3A,B) [63, 67].

Table 1.2 The timing of the biochemical events leading to conidial germination in *N. crassa* after exposure to media. Modified from [15].

0-30 min
Hydration and loss of heat resistance
Rodlets solubilise and exocellular enzyme is released
γ-amino butyrate appears
Glutamate degraded
Aspartate forms
NADP(H) increases
Disulphides reduced
RNA synthesis begins
Polysomes assembled
1-2 h
Transport systems increase
Minimal amino acid pools appear
2-5 h
Transport further increases
DNA synthesis and nuclear divisions occur
Oxidative phosphorylation starts
Isoleucine-valine enzymes become localised in mitochondria
Arginine and ornithine pools enlarge
Chitin synthesis begins (~ 3 h)
> 7 h
Galactosamine polymers appear

In contrast, CATs are much thinner with an average diameter of only 2-2.5 μm, show determinate growth (rarely extend longer than 10–12 μm), do not branch and, most importantly, are chemotropically attracted to each other and fuse (Fig.1.3C,D). The CAT system in *N. crassa* provides a simple, experimentally amenable and genetically tractable system in which to study self-signalling and self-fusion in filamentous fungi [63, 64]. The whole process of CAT-mediated cell fusion

can be analysed within 6 h, which makes mutant screening, live-cell imaging and physiological experiments very easy to perform. CAT-mediated cell fusion can be divided into a continuum of events: CAT induction, CAT chemoattraction (homing), cell-cell adhesion, cell wall remodelling/degradation, and plasma membrane merger which ultimately achieves cytoplasmic continuity between cells (Fig. 1.4). The molecular regulation of these processes is currently being analysed in detail [17, 19, 20, 56, 68].

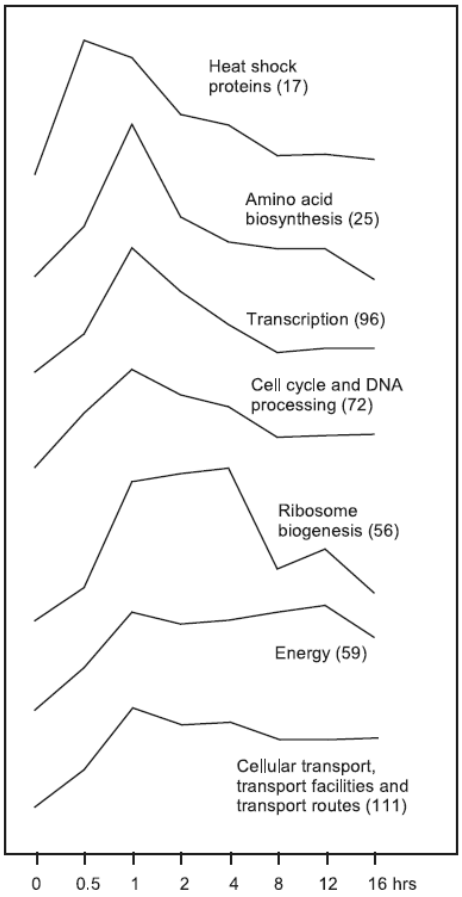

Figure 1.2 Expression profiles of genes in different functional categories during conidial germination. The number of genes in each category are indicated. Taken from [2].

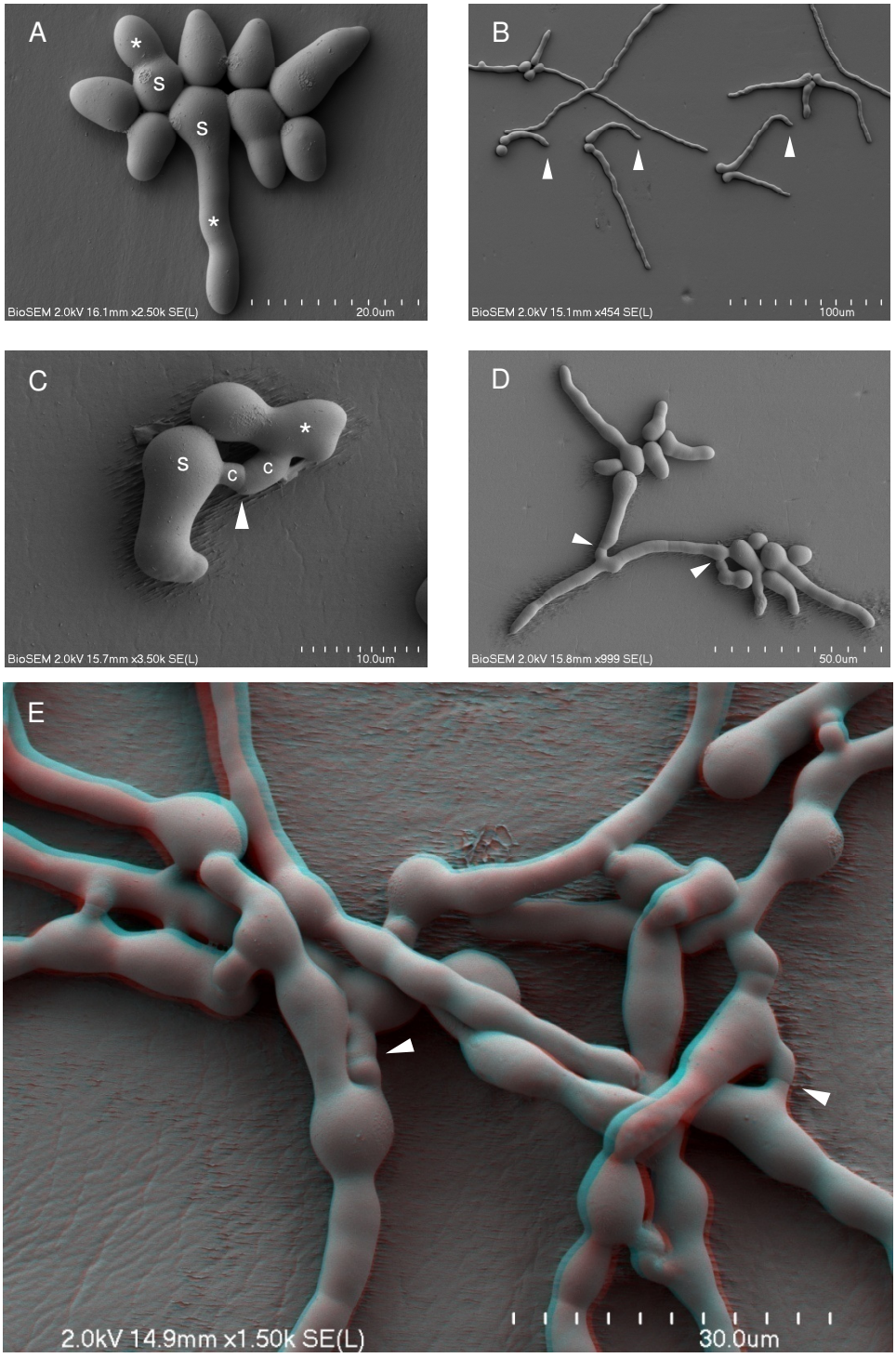

Figure 1.3 CATs are morphologically and functionally distinct from GTs. (A) Avoidance of GTs (asterisks) emerging from the spore body (s) ~2.5 h after inoculation. **(B)** GT tips redirecting growth away from each other (arrowheads) ~4 h after inoculation. **(C)** Fusion between two CATs (c; arrowhead indicates the fusion site) emerging from a GT (asterisk) and directly from the spore body (s); ~4 h after inoculation. **(D)** Fusion between several cells ultimately establishes an interconnected germling network (arrowheads mark fusion sites); ~4 h after inoculation. **(E)** Stereo image of an elaborate germling network established by

CAT-mediated cell fusion (arrowheads indicate fusion connections) ~5.5 h after inoculation. All images show macroconidia of *N. crassa* examined by low-temperature scanning electron microscopy. Images taken by C. M. Jeffree and A. Lichius.

1.4.3. CAT induction involves MAP kinase signalling, HAM-2 and SO

CAT induction probably involves an extracellular CAT inducer produced by ungerminated conidia [63, 67] or from the tips of other CATs in the vicinity (Fig. 1.4a,b). The nature of this signalling molecule, however, is still unknown. CAT induction involves the NRC-1/MEK-2/MAK-2 mitogen-activated protein kinase (MAPK) pathway and the transcription factor PP-1 [56, 63, 67]. Orthologs of these proteins are components of the pheromone response (PR) pathway in budding yeast [12]. Phosphorylation of the MAP kinase MAK-2 was found to increase during the period when CAT induction is most prolific [56]. CAT induction also involves a putative transmembrane protein called HAM-2 [81], which is an ortholog of the yeast Far11p [42], and involves a filamentous ascomycete-specific WW domain protein called SO [18, 20]. In contrast to *mak-2*, *nrc-1*, *pp-1* and *ham-2* mutants which all lack CATs [63], mutants defective in *so* still form CATs, but with lower efficiency than the wt. CATs of *so* are unable to chemotropically interact with each other or with wt conidia [20].

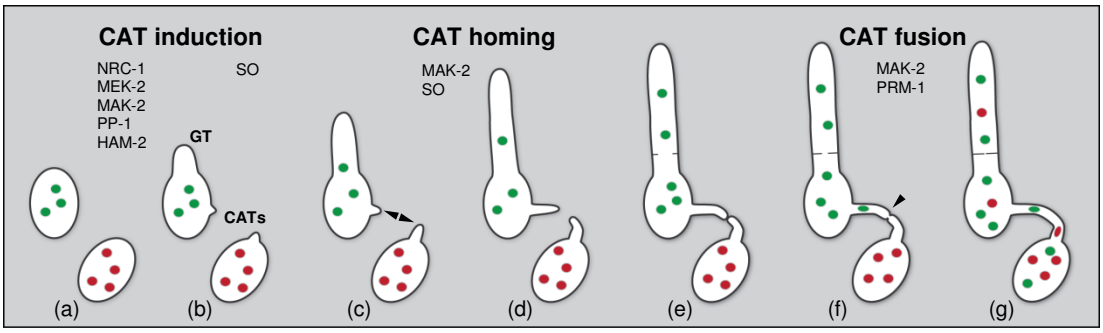

Figure 1.4 Diagram of CAT-mediated cell-cell fusion in *Neurospora crassa* and known proteins involved. The three main phases of CAT-mediated cell fusion are CAT induction, CAT homing and CAT fusion, and progress through a subset of consecutive stages: **(a)** Ungerminated conidia contain on average 3-6 nuclei (shown here in green and red to

indicate their origin from different but genetically identical cells), and initially grow exclusively by isotropic expansion. **(b)** Cell polarisation leads to the outgrowth of a germ tube (GT) and conidial anastomosis tubes (CATs). GTs avoid each other and are unable to fuse. **(c)** Genetically identical cells communicate by releasing an unknown chemoattractant from their tips which is perceived by opposing CAT tips (arrows). **(d)** Orientation along this chemoattractant gradient results in CATs growing towards each other (homing) to establish cell wall contact. **(e)** Contact induces tip growth arrest and CAT attachment, which most likely involves adhesive secretion and the buildup of new cell wall material around the contact site in order to prevent leakage during subsequent pore formation. **(f)** Fusion pore formation (arrowhead) includes localised cell wall remodelling/degradation and plasma membrane merger. **(g)** Upon establishment of cytoplasmic continuity, organelles, including nuclei, become mixed between fused germlings. Signalling and structural molecules involved at different stages of the process are indicated (see text for details).

1.4.4. CAT homing is regulated by a novel 'ping-pong' signalling mechanism involving MAK-2 and SO

CATs exhibit marked positive chemotropism towards each other (homing) (Fig. 1.4c,d). This has been most unambiguously demonstrated using optical (laser) tweezers to micromanipulate CATs which, after having their relative positions changed, readjusted their growth direction to make contact and fuse at their tips [20, 67, 78]. These results provide compelling evidence for a diffusible chemoattractant released from CAT tips and for a chemoattractant receptor located at CAT tips. If the assumption is correct that the CAT inducer and chemoattractant are the same molecule, then the findings that conidia of *mak-2*, *nrc-1*, *ham-2* and *so* mutants fail to attract wt CATs suggest that the proteins encoded by these genes are involved in either the chemoattractant release or chemoattractant response pathways [63]. Recent results have provided much stronger evidence for MAK-2 and SO being involved in signalling during CAT homing [19]. Previous evidence had shown that a Δ*mak-2* mutant lacks CATs [67] whilst a Δ*so* mutant produced CATs which were unable to chemotropically interact with other CATs [20]. It is now clear that CATs that are growing towards each other rapidly alternate between two different physiological states that may be associated with alternating signal delivery and response. This mechanism (which we have termed the '*ping-pong mechanism*', [64])

involves the rapidly alternating, anti-phase, pulsatile recruitment of MAK-2 and SO to CAT tips [19, 64]. It results in the simultaneous localization of MAK-2 and SO in opposing CAT tips that are homing towards each other. This highly coordinated, 'oscillatory' recruitment of signalling proteins is initiated when CATs are < 15 µm apart, the period of the 'oscillation' is 6-12 min, and each of these proteins can be repeatedly recruited to a single CAT tip 4-6 times during tip homing. The proteins become concentrated in particulate complexes of ~300 nm in diameter that mostly concentrate in cortical regions closest to their partner cells. Such spatio-temporal coordination of signalling allows genetically identical and developmentally equivalent cells to avoid self-stimulation and coordinate their behaviour to ultimately achieve cell fusion [19]. This ping-pong mechanism (Fig. 1.5) operates over a very short time scale and comparisons with non-self signalling during yeast cell mating indicate that this mechanism probably does not involve transcriptional regulation [64].

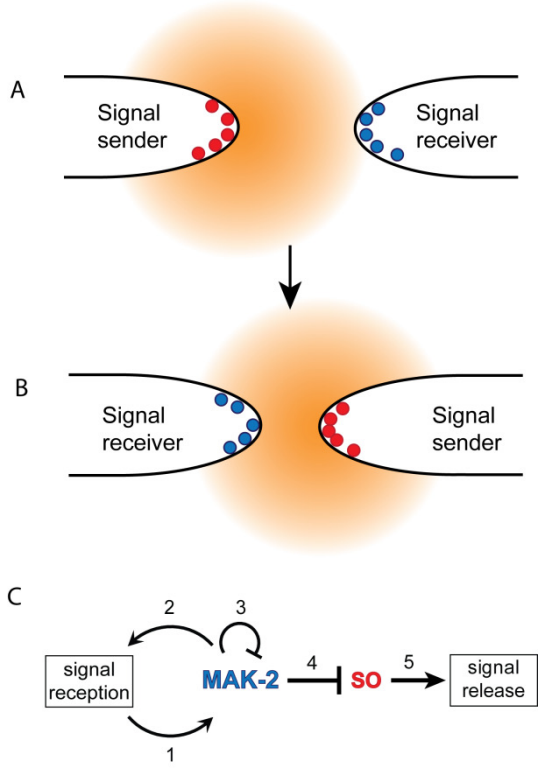

Figure 1.5. Ping-pong mechanism of self-signalling during CAT chemoattraction. **(A)** In the first half-period of the periodic signalling, the CAT tip on the left releases the chemoattractant signal while the one on the right responds to the signal by adjusting its growth direction along the gradient of the signalling molecule. **(B)** In the second half-period the roles reverse. **(C)** Proposed mechanism of intracellular signalling: **(1)** chemoattractant-receptor complex induces local recruitment and activation of MAK-2; **(2)** hypothetical positive feedback inherent in MAP kinase modules [43, 72] amplifies the received signal; **(3)** as its local concentration increases, MAK-2-p2 (MAK-2 activated by double phosphorylation) may induce disassembly of the MAP kinase protein complex by phosphorylating its upstream components [51, 72]; **(4)** resulting decrease in MAK-2-p2 derepresses the accumulation of SO and formation of SO-containing protein complexes at the CAT tip; **(5)**, SO-stimulated chemoattractant release occurs. As the other CAT tip responds to the released chemoattractant, the sequence **(1)-(5)** will be repeated until the two tips physically meet [19]. Taken from [64].

1.4.5. The final stages of CAT fusion involve MAK-2 and PRM-1

Upon contact, CATs cease tip growth and adhere to each other (Fig. 1.4e). Although mating-type specific adhesins, that enable fusion partners of *Saccharomyces cerevisiae* to tightly adhere at their shmoo tips, have been identified early on [86] (reviewed in [47]), orthologs of these proteins are not conserved in the *N. crassa* genome [30], and candidate proteins have not yet been recognized. Subsequent fusion pore formation involves localised remodelling and partial degradation of the intervening cell walls to allow plasma membrane merge between both CATs (Fig. 1.4f,g). MAK-2 also seems to play a role in fusion pore formation [19] and the plasma membrane protein PRM-1 is involved in membrane merger [17]. Cytoplasmic continuity is finally achieved and organelles, including nuclei, interchange between the two germlings.

1.5. Vegetative hyphal fusion in the mature colony

1.5.1. Specialized fusion hyphae establish a subperipheral network

The mature filamentous fungal colony develops as radialy extending and morphologically complex mycelium (Fig. 1.6A), and contains a variety of different hyphal types [5]. Leading hyphae and their branches at the periphery of a colony typically grow outward, exhibit a subapical branching pattern, and tend to avoid each other [8] (Fig. 1.6B). Hyphal anastomosis does not normally occur in this peripheral zone of a *N. crassa* colony [31]. A different but related process to germling self-fusion, however, does occur extensively behind the peripheral zone of leading hyphae to produce the characteristic interconnected state of the mature colony [27, 30, 31, 65]. In this subperipheral region, specialized fusion hyphae arise as branches

from established hyphae and grow towards each other and fuse (Fig. 1.6C and D). The interconnected state allows the fungal colony to operate as a coordinated individual and to regulate its overall homeostasis by the interchange of nutrients, water, signalling molecules, nuclei and other organelles [22, 62, 63]. Although fusion events are frequent within a colony they are not uniformly distributed, but highly regulated in order to adapt transport routes within the mycelium and overall colony architecture to changing environmental conditions, including heterogeneously distributed nutrient or water supply.

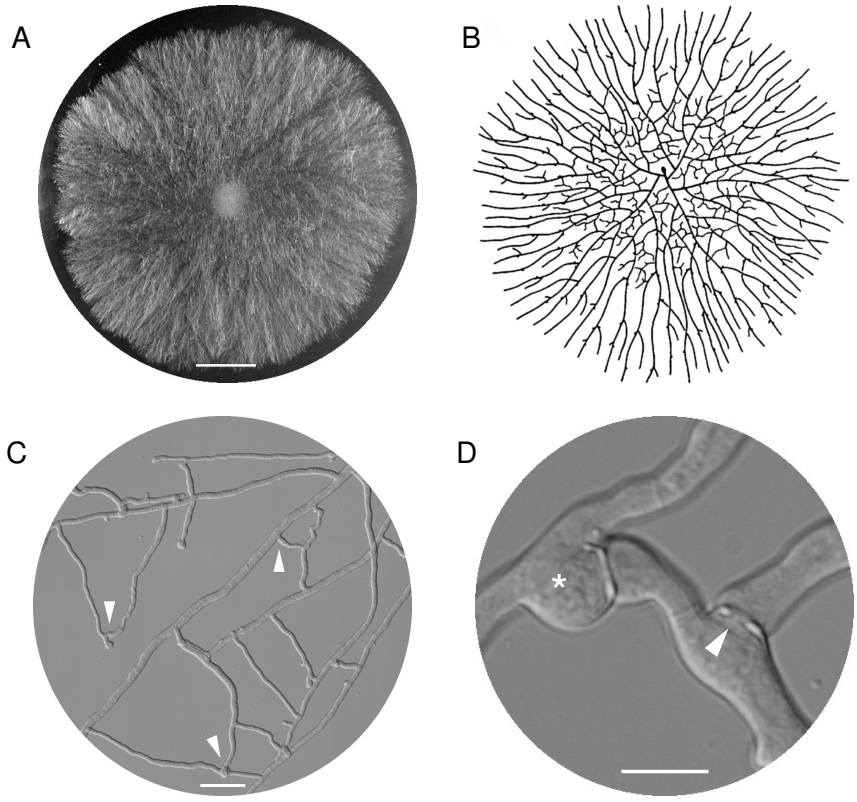

Figure 1.6 Colony architecture of filamentous fungi. (A) Radially extending colony of *Neurospora crassa* after overnight incubation in the dark. Scale bar, 1 cm. **(B)** Diagram showing the typical appearance of a filamentous fungal colony grown from a single spore in the centre. Leading hyphae at the colony periphery avoid one another, whilst hyphae in the interior of the colony actively fuse (adapted from [8]). **(C)** Hyphal network in the subperipheral fusion zone (some fusion connections are indicated with arrowheads). Scale bar, 50 µm. **(D)** Detail of hyphal fusion connections showing contact-induced tip growth arrest leading to isotropic swelling (asterisk), and a fusion pore (arrowhead). Scale bar, 10 µm.

Vegetative hyphal fusion (VHF) in *N. crassa* has been described in detail using time-lapse confocal microscopy [31] and currently known proteins regulating the various steps of the process have recently been reviewed [63]. Similar to CAT-mediated cell fusion of condidial germlings (Fig.1.4) the process can be divided into the three main phases of pre-contact, post-contact and post-fusion, which comprise various stages including: induction of fusion hyphae and fusion pegs, tip chemoattraction, tip growth arrest, tip depolarisation and adhesion, cell wall remodelling/degradation, plasma membrane merger, and achievement of cytoplasmic continuity between both compartments (Fig.1.7).

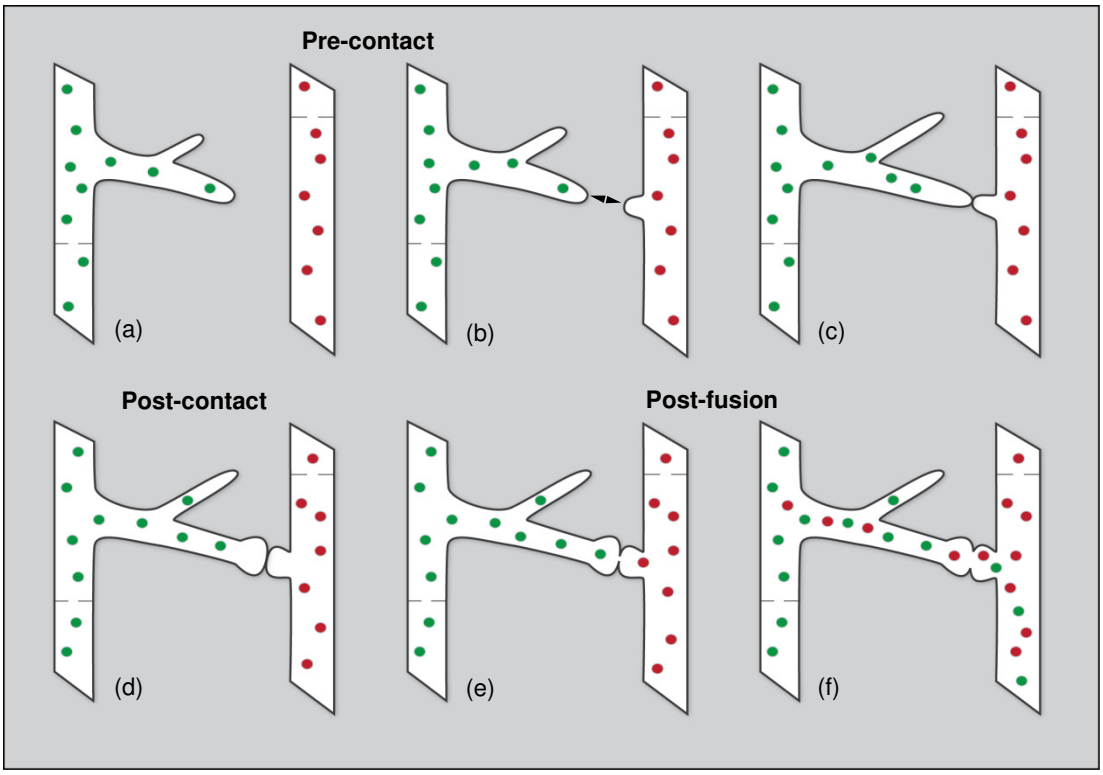

Figure 1.7 Vegetative hyphal fusion in the mature colony of *Neurospora crassa*. The three main phases of hyphal fusion are pre-contact, post-contact and post-fusion, and also progress through a subset of consecutive stages: **(a)** An approaching fusion hypha can induce the formation of a new fusion peg in a nearby hyphal branch. **(b)** Chemotropic interaction guides both structures towards each other. **(c)** Contact induces arrest of polarised tip growth and most likely coincides with secretion of adhesives which promote attachment. **(d)** Tip growth arrest is quickly followed by depolarisation of the cytoskeleton leading to pronounced swelling. **(e)** Localised cell wall remodelling and cell wall degradation creates a fusion pore. **(f)** Fusion pore expansion and plasma membrane merger establish cytoplasmic

continuity between both compartments and provides a new transport route within the colony network (see text for details).

During the pre-contact phase fusion hyphae are formed and home towards each other. Proximity of fusion hyphae usually induces *de novo* emergence of fusion pegs from the sides of other hyphal branches [8, 31] (Fig. 1.7b). Fusion hyphae in *Neurospora* are morphologically distinct from other hyphae and usually appear as secondary branches showing wiggly growth and dichotomous branching. This growth pattern might be associated with irregular displacement of the Spitzenkörper whose localisation correlates with tip re-orientation during hyphal homing [2, 24, 25, 31]. Upon contact, hyphal tips depolarise which results in immediate tip growth arrest and tip swelling (Fig. 1.7d), and is believed to be accompanied by secretion of adhesives to achieve firm attachment. Subsequent remodelling and digestion of the intervening cell walls creates a fusion pore through which the opposing membranes can fuse (Fig. 1.7e). The Spitzenkörper persists during this period, suggesting that it provides secretory vesicles for wall synthesis during tip swelling, and for the delivery of extracelluar adhesives and cell wall degrading enzymes during fusion pore formation [31]. Membrane merger marks the onset of the post-fusion phase which involves rapid cytoplasmic mixing and bulk flow of organelles from one compartment into the other. Fusion pore expansion and further strengthening of cell walls adjacent to the new connection most likely to prevent leakage finalizes the process (Fig. 1.7f).

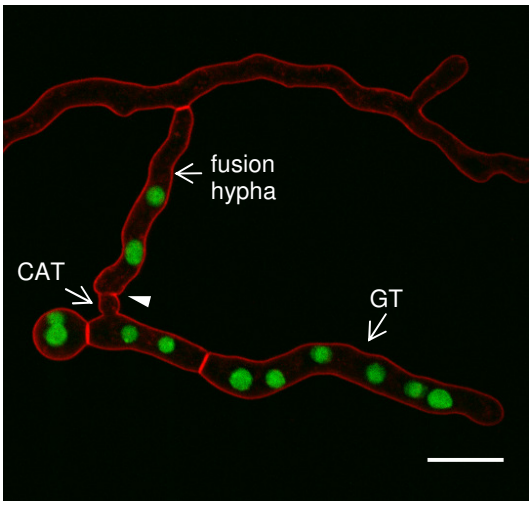

Figure 1.8 Fusion between conidial germling and fusion hypha of the mature colony. Confocal optical section showing transfer of green nuclei from the germling into the mature colony. Conidia of a wt strain expressing histone-H1-GFP (H1-GFP) as nuclear marker were added to an overnight culture of unlabelled wt and incubated together for 4 h to allow fusion to take place. Plasma membranes are labelled with FM4-64 dye. The fusion site is indicated by an arrowhead. Scale bar, 10 µm.

Although pronounced contact-induced tip swelling cannot be observed during CAT fusion, both processes share not only morphological similarities. To date, all identified fusion mutants of *N. crassa* were defective in both, CAT-mediated germling fusion and VHF in the mature colony [63]. This indicates considerable molecular and functional overlap of both fusion machineries, and is best demonstrated by the fact that CATs are able to establish cytoplasmic continuity with fusion hyphae of the mature colony (Fig. 1.8). Recent data from *N. crassa* demonstrates that glycosylphosphatidylinositol (GPI)- anchored proteins are required for hyphal fusion. Mutations in *gpig-1, gpip1-3* and *gpit-1* genes, which encode components of the *N. crassa* GPI-anchored protein biosynthetic pathway, result in mutants that were unable to undergo VHF in the mature colony [7]. Defects in CAT-mediated cell fusion still need to be verified, but it is possible that enzymes such as GPI-anchored chitinases participate in localised cell wall remodelling and degradation at fusing CAT tips [63, 84].

1.5.2. Non-self recognition and heterokaryon incompatibility

Non-self VHF between two colonies only leads to stable heterokaryon formation, i.e. nuclei of two individuals in a common cytoplasm, if both strains are genetically compatible. Non-self recognition in filamentous fungi is conferred by allelic specificity of *het* (heterokaryon incompatibility) loci, of which 11, including the mating type (*mat*) loci, have been documented in *N. crassa* [29, 57, 79]. If two individuals differ in allelic specificity at only one of their *het* loci they are genetically incompatible. Furthermore, non-allelic heterokaryon incompatibility mediated by protein-protein interactions of unlinked loci acts as an additional self/non-self recognition system in filamentous fungi [39, 79]. Fusion between heterokaryon incompatible individuals, however, does occur, and usually activates a programmed cell death (PCD) response resulting in rapid compartmentalisation

and autophagy of the heterokaryotic hyphal compartment which becomes physically isolated from the rest of the hyphal network [26].

Because heterokaryon incompatibility is usually expressed only during vegetative growth (and is also termed vegetative incompatibility) it does not affect non-self fusion during sexual reproduction of heterothallic (outbreeding) species, such as *N. crassa*. During sexual reproduction, vegetative incompatibility must be suppressed to allow opposite mating-type nuclei to proliferate in a common cytoplasm prior to karyogamy [28] (see next section). Two transcriptional regulators (TOL and VIB-1) have been identified that are involved in controlling mating-type-associated heterokaryon incompatibility during different developmental stages of the *N. crassa* lifecycle [36, 54, 73, 79, 80]. Most interestingly, non-self recognition is also suppressed for an extended period during conidial germling network formation [68], up until 14-16 h into colony development (M. G. Roca, personal communication). CAT-mediated cell fusion during this early period may provide a 'window of opportunity' for non-meiotic recombination between otherwise vegetatively incompatible genotypes [65]. How heterokaryon incompatibility is suppressed during this initial stage of colony establishment, and what genetic changes might occur after these 14-16 h is currently unknown.

1.6. The role of hyphal fusion during late stages of sexual development

As in many organisms, cell fusion also plays a critical role during sexual development and progression beyond certain points of the sexual cycle cannot be achieved unless a fusion event has occurred. Studies so far have concentrated on cell fusion events leading to fertilisation and crozier formation, which will be briefly discussed in this section.

In the Ascomycota hyphal fusion occurs during mating cell fusion and the formation and maintenance of the dikaryon during the sexual phase of the life cycle

(Fig. 1.1). Mating cell fusion in *Neurospora crassa* involves the fusion between a fertile receptive hyphae, the trichogyne, which is sent out from the ascogonium inside the unfertilised protoperithecium, and a compatible, i.e. opposite mating type, male partner. This can be a hypha from another mature colony, but in most cases will be a micro-, macro- or arthroconidium. The trichogyne is chemotropically attracted to the male conidium, establishes contact and then fuses with it [4, 45, 63]. As both partners are genetically different in their mating type loci, this process is a non-self fusion event. The only two prerequisites for successful non-self recognition and homing that have been described to date are the production and secretion of the sex pheromone by the male partner, and the expression of the cognate pheromone receptor by the female trichogyne. Genetic deletion of the pheromone in the female and of the pheromone receptor in the male did not affect sexual reproduction [41, 45, 46]. Gene deletion mutants of *N. crassa* that are defective in hyphal fusion are in the majority of cases female sterile. Conversely, mutations in the mating type loci (23), or genes encoding the sex pheromones (*mfa-1 and ccg-4*), the pheromone receptors (*pre-1 and pre-2*) and the associated heterotrimeric G-protein signalling subunits (*gna-1 to gna-3, gnb-1 and gng-1*) do not affect vegetative self-fusion in *N. crassa* [41, 45, 46].

Upon successful mating cell fusion the male nucleus travels through the trichogyne into the ascogonium inside the unfertilised protoperithecium. Arrival of the male nucleus fertilises the developing fruitbody, triggers differentiation of the protoperithecium into the perithecium, and initiates the dikaryotic phase of the life cycle [1]. Two nuclei of opposite mating type (one male and one female) are involved in the formation and proliferation of binucleate cells. In *N. crassa*, dikaryotic cells are generated and maintained by the formation of specialized hyphal compartments called crozier [59] (Fig. 1.9).

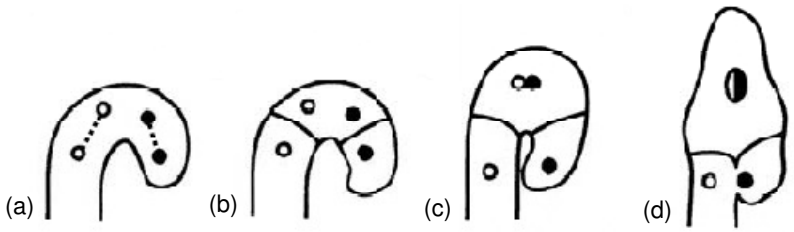

Figure 1.9 Diagram of crozier cell fusion in a typical ascomycete species. (a) A hooked-shaped crozier forms at the tip of an ascogenous hypha. The two nuclei within the crozier (one male one female, indicated as filled and empty circles) go through a simultaneous mitotic division. **(b)** They become separated by walls forming across the two mitotic spindles, which leads to the formation of a uninucleate terminal cell and a binucleate penultimate cell at the end of the ascogenous hypha. **(c)** The two "pre-fusion" nuclei in the penultimate cell undergo karyogamy, forming the diploid ascus mother cell which subsequently elongates and develops into the ascus ultimately containing eight haploid ascospores. **(d)** Meanwhile, the terminal cell grows back and fuses with the subtending ascogenous hyphae allowing the nuclei in these two compartments to pair up. In *N. crassa*, the two nuclei subtending the ascus also undergo karyogamy [59]. Modified from [63].

1.7. Cell-cell fusion in other eukaryotes

Cell-cell fusion is a highly regulated and complex cellular event that is essential for development and homeostasis in all eukaryotes. Chemoattraction between genetically identical cells, often followed by cell-cell fusion, is widely present in eukaryotes from amoebae to humans [11, 55]. Three contrasting examples in other organisms that provide interesting comparisons with fungal self-signalling and self-fusion are where there is: (1) chemoattraction without cell fusion (e.g. *Dictyostelium discoideum*); (2) chemoattraction with fusion between developmentally different cells (e.g. myoblasts); and (3) chemoattraction with fusion between developmentally similar cells (e.g. macrophages).

A well studied example of self-signalling at the cell population level, which does not lead to cell fusion, is displayed by the slime mould *D. discoideum*. In response to starvation, *Dictyostelium* unicellular amoebae initiate the pulsatile release of cAMP and follow its gradient to form large cell aggregates that eventually differentiate into multicellular fruiting bodies [60]. In contrast to chemoattraction

between two CATs in *Neurospora*, self-signalling in *Dictyostelium* amoebae is a long-range phenomenon that involves thousands of cells. Thus periodic signalling in *Dictyostelium* during chemoattraction is cell-autonomous unlike in *Neurospora* where the periodic response is induced by the presence of another CAT forming cell [19]. Moreover, cAMP signalling in *Dictyostelium* results in an in-phase synchronization of nearby cells while the oscillatory recruitment of MAK-2 (or SO) to homing CAT tips of *Neurospora* are always out-of-phase in the opposing CAT tips by half a period as necessitated by the ping-pong mechanism of self-signalling (see Fig. 1.5).

One of the most intriguing phenomena involving chemoattraction between developmentally different cells is the fusion of stem cells with differentiated tissue cells which may potentially result in the reversal of cellular senescence and tissue regeneration [75]. Fusion of muscle progenitor cells (myoblasts) during muscle development and regeneration is perhaps the best characterized example in this class. In *Drosophila,* fusion is initiated by founder cells that do not fuse with each other but instead attract and fuse with undifferentiated fusion-competent myoblasts [66]. This initial fusion event results in a nascent myotube that subsequently grows by 2 to 25 successive fusion events, the number of which is strictly developmentally regulated. Nascent mammalian myotubes, formed by the initial fusion of several differentiated myoblasts, subsequently grow by releasing cytokine interleukin-4 (IL-4) which chemoattracts more undifferentiated myoblasts precursor cells with which they fuse [34, 38]. Thus, in contrast to *Neurospora*, both signalling and fusion during muscle development are asymmetric and unilateral. However, all fusion events during myotube elongation are strictly pair-wise and require polarized "tip-to-tip" attachment of fusing cells, which is a feature in common with hyphal self-fusion.

Perhaps the best characterized example of self-fusion among developmentally similar cells is the fusion of mammalian macrophages. Uninucleate, macrophages fuse occasionally to form osteoclasts and giant cells. Interestingly, prostaglandins and IL-4, which mediate activation and chemoattraction of myoblasts, are also involved in macrophage fusion that results in

the differentiation of osteoclasts and giant cells. Other cytokines and growth factors, such as RANKL and M-CSF, have also been reported to regulate the complex process of macrophage fusion and differentiation [76]. RANKL induces the expression of the dendritic cell-specific transmembrane protein DC-STAMP that is crucial for macrophage fusion during multinucleate osteoclast formation [82, 83]. Interestingly, expression of DC-STAMP in one of the interacting macrophages is sufficient for fusion to occur [82], suggesting that two fusing macrophages are in different physiological states. One cell may take the role as fusion competent 'founder' cell and expresses DC-STAMP, whilst the other may act as a 'follower' cell that expresses a so far unknown DC-STAMP ligand [35, 77]. Thus it seems that macrophages "differentiate" into founder and follower cells (equivalent to signal sender and receiver cells in *Neurospora*) to avoid self-stimulation, whereas in CAT chemoattraction two interacting cells rapidly alternate between two physiological states to achieve this. These different strategies to achieve different physiological states in a population of genetically identical cells may be attributed to macrophages being motile and *Neurospora* conidia being non-motile. Thus macrophages are capable of exhibiting migratory movement to a fusion partner [35] whilst sessile conidia depend on being close enough to a potential fusion partner in order to bridge the distance by CAT growth and fusion. The ability to alternate between being a signal sender and receiver allows any fusion competent cell to fuse with any other fusion competent cell of similar genetic background in its vicinity. Therefore, the ping-pong mechanism of signalling might function to increase the efficiency of fusion between immobile cells.

Although the basic process of cell fusion, comprising self/non-self recognition, homing, attachment and fusion pore formation, is conserved amongst eukaryotes, the molecular fusion machineries are very diverse, suggesting they might have evolved independently [11]. An important research focus in higher eukaryotic model systems currently is the identification of proteins or protein complexes whose exclusive function is to directly mediate membrane-membrane

fusion. The first identified, so called 'fusogens', were v- and t-SNARES which mediate heterotypic fusion between viruses or vesicles and the plasma membrane [37, 44, 74], and more recently, the epithelial and anchor cell fusion failure proteins EFF-1 and AFF-1, which confer homotypic fusion between the plasma membranes of individual cells in *C. elegans* [16, 52, 58, 69, 71]. Identification of novel members of this class of proteins in other eukaryotic model systems, such as *N. crassa*, poses a major challenge as they elicit their membrane-joining function in various ways and do not seem to have highly conserved domain structures [50].

1.8. General introduction to the research aims of this thesis

The primary research aims of this thesis were the identification of novel cell fusion mutants of *N. crassa* and the subsequent functional characterization of selected candidate proteins during CAT-mediated cell fusion by means of genetic, molecular, biochemical and live-cell imaging analysis. Key questions that were addressed included:

1. Can the functional genomic comparison with appressorium-mediated host invasion by the rice blast fungus *Magnaporthe oryzae* facilitate the identification of novel fusion mutants of *Neurospora crassa*?
2. How much of the molecular machineries is conserved between cell fusion in *N. crassa* and appressorium-mediated infection of *M. oryzae*, and which pathways are differently used in a saprotrophic and pathogenic lifestyle?
3. Which signalling pathways are primarily involved in CAT homing, as opposed to those known to be essential for CAT formation?
4. Which of these pathways might translate positional information of the chemoattractant source into re-orientation of CAT tip growth during homing?

5. What is the role of the cytoskeleton in CAT formation, homing and fusion?
6. What is the role of the cell wall integrity MAP kinase pathway during CAT-mediated cell fusion, in particular during fusion pore formation?
7. How do defects in VHF affect the early stages of sexual fruitbody development?
8. Are H_2O_2 and other reactive oxygen species (ROS) potentially used as second messengers to initiate or guide CAT chemoattraction either directly or by redox-modification of signalling molecules?

Chapter 3 introduces the morphogenetic basis of the functional comparative genomics screen conducted between *Magnaporthe oryzae* and *Neurospora crassa*, and discusses the three major signalling pathways in which novel cell fusion mutants have been identified. These comprised MAP kinase signalling, redox-signalling and Rho-type GTPase signalling, and turned out to be functionally conserved between both species. Interestingly, cyclic AMP signalling was found to be dispensable for cell fusion, indicating significant functional divergence of the cAMP response pathway between saprotroph and pathogen.

New methods involving the selective disruption of cytoskeletal components improved the differentiation between CAT induction and CAT homing mutants, and put new emphasis on the role of the actin cytoskeleton for the process of CAT-mediated cell fusion. The development of new fluorescent reporters for F-actin and activated GTPases is subject of **Chapter 4**. Novel insights into the organisation of F-actin cables and patches, and their dynamic rearrangement during cell symmetry breaking, polarized tip growth and CAT fusion are presented. Furthermore, distinct functions of the actin cytoskeleton during septum formation have been revealed, showing that actin rings formed by localized condensation of F-actin. Novel insights into the molecular basis of opposite chemotropism of GTs and CATs will be

discussed in the context of differential tip recruitment of the two Rho GTPases CDC42 and RAC-1.

Chapter 5 focuses on the role of the cell wall integrity MAP kinase pathway during cell fusion, in particular on the function of the terminal MAP kinase MAK-1 during CAT homing and fusion pore opening. Inhibitor studies indicated that MAK-1 kinase activity is required for its own recruitment to the fusion site as well as for cell wall remodelling essential for the establishment of cytoplasmic continuity. Potential connections between MAK-1 activity and cytoskeletal rearrangements during that process will be discussed.

How defects in VHF affect the early stages of fruitbody development during the sexual cycle of *N. crassa* is evaluated in **Chapter 6**. The first evidence that defects in extracellular matrix (ECM) deposition, hyphal adhesion and probably cell wall remodelling abort protoperithecial morphogenesis and lead to autolysis and reabsorbtion of immature fruitbodies by the mycelium are presented. These findings are put into context with parallel signalling pathways that appear to regulate later stages of protoperithecium morphogenesis, which trigger the transition into perithecium maturation and prepare the fruitbody for subsequent non-self fusion processes.

The first evidence that NADPH-oxidase (NOX)-generated reactive-oxygen species (ROS) have a crucial role during cell fusion will be presented in **Chapter 7**. Biochemical evidence suggests that conidia of *N. crassa* modulate the amount of ROS in order to enable intracellular redox signalling whilst avoiding oxidative damage. Subsequent studies show that hydrogen peroxide has profound effects on CAT formation without affecting germ tube growth. This opens up the possibility that chemoatttraction between conidial germlings is mediated either directly by ROS or via redox modification of signalling molecules exchanged between cells.

Chapter 8 provides a summary of the key findings and will discuss future directions.

1.9. References

1. **Anderson, J. B., and L. M. Kohn.** 2007. Dikaryons, diploids, and evolution, p. 333-348. *In* J. Heitman (ed.), Sex in fungi: molecular determination and evolutionary implications. American Society of Microbiology, Washington D.C.

2. **Araujo-Palomares, C. L., E. Castro-Longoria, and M. Riquelme.** 2007. Ontogeny of the Spitzenkörper in germlings of *Neurospora crassa*. Fungal Genetics and Biology **44:**492.

3. **Backus, M. P.** 1939. The mechanics of conidial fertilization in *Neurospora sitophila*. Bulletin of the Torrey Botanical Club **1939:**63-67.

4. **Bistis, G. N.** 1981. Chemotropic interactions between trichogynes and conidia of opposite mating-type in *Neurospora crassa*. Mycologia **73:**959-975.

5. **Bistis, G. N., D. D. Perkins, and N. D. Read.** 2003. Different cell types in *Neurospora crassa*. Fungal Genetics Newsletter **50:**17-19.

6. **Borkovich, K. A., L. A. Alex, O. Yarden, M. Freitag, G. E. Turner, N. D. Read, S. Seiler, D. Bell-Pedersen, J. Paietta, N. Plesofsky, M. Plamann, M. Goodrich-Tanrikulu, U. Schulte, G. Mannhaupt, F. E. Nargang, A. Radford, C. Selitrennikoff, J. E. Galagan, J. C. Dunlap, J. J. Loros, D. Catcheside, H. Inoue, R. Aramayo, M. Polymenis, E. U. Selker, M. S. Sachs, G. A. Marzluf, I. Paulsen, R. Davis, D. J. Ebbole, A. Zelter, E. R. Kalkman, R. O'Rourke, F. Bowring, J. Yeadon, C. Ishii, K. Suzuki, W. Sakai, and R. Pratt.** 2004. Lessons from the genome sequence of *Neurospora crassa*: tracing the path from genomic blueprint to multicellular organism. Microbiological and Molecular Biological Reviews **68:**1-108.

7. **Bowman, S. M., A. Piwowar, M. e. Al Dabbous, J. Vierula, and S. J. Free.** 2006. Mutational analysis of the glycosylphosphatidylinositol (GPI) anchor pathway demonstrates that GPI-anchored proteins are required for cell wall biogenesis and normal hyphal growth in *Neurospora crassa*. Eukaryotic Cell **5:**587-600.

8. **Buller, A. H. R.** 1933. Researches on Fungi, vol. 5. Longman, London.

9. **Cambareri, E. B., B. C. Jensen, E. Schabtach, and E. U. Selker.** 1989. Repeat-induced G-C to A-T mutations in Neurospora. Science **244:**1571-1575.

10. **Cambareri, E. B., M. J. Singer, and E. U. Selker.** 1991. Recurrence of Repeat-Induced Point Mutation (RIP) in *Neurospora crassa*. Genetics **127:**699-710.

11. **Chen, E. H., E. Grote, W. Mohler, and A. Vignery.** 2007. Cell-cell fusion. FEBS Letters **581:**2181-2193.

12. **Chen, R. E., and J. Thorner.** 2007. Function and regulation in MAPK signaling pathways: lessons learned from the yeast *Saccharomyces cerevisiae*. Biochimica et Biophysica Acta - Molecular Cell Research **1773:**1311-1340.

13. **Colot, H. V., G. Park, G. E. Turner, C. Ringelberg, C. M. Crew, L. Litvinkova, R. L. Weiss, K. A. Borkovich, and J. C. Dunlap.** 2006. A high-throughput gene knockout procedure for *Neurospora* reveals functions for multiple transcription factors. Proceedings of the National Academy of Sciences of the USA **103:**10352-10357.

14. **d'Enfert, C.** 1997. Fungal spore germination: insights from the molecular genetics of *Aspergillus nidulans* and *Neurospora crassa*. Fungal Genetics and Biology **21:**163-173.

15. **Davis, R. H.** 2000. *Neurospora*: contributions of a model organism. Oxford University Press, Oxford.

16. **del Campo, J. J., E. Opoku-Serebuoh, A. B. Isaacson, V. L. Scranton, M. Tucker, M. Han, and W. A. Mohler.** 2005. Fusogenic activity of EFF-1 is regulated via dynamic localization in fusing somatic cells of *C. elegans*. Current Biology **15:**413-423.

17. **Fleißner, A., S. Diamond, and N. L. Glass.** 2009. The *Saccharomyces cerevisiae* PRM1 homolog in *Neurospora crassa* is involved in vegetative and sexual cell fusion events but also has postfertilization functions. Genetics **181:**497-510.

18. **Fleißner, A., and N. L. Glass.** 2007. SO, a protein involved in hyphal fusion in *Neurospora crassa*, localizes to septal plugs. Eukaryotic Cell **6:**84-94.

19. **Fleißner, A., A. C. Leeder, M. G. Roca, N. D. Read, and N. L. Glass.** 2009. Oscillatory recruitment of signaling proteins to cell tips promotes coordinated behaviour during cell fusion Proceedings of the National Academy of Sciences of the USA **106:**19387–19392.

20. **Fleißner, A., S. Sarkar, D. J. Jacobson, G. M. Roca, N. D. Read, and N. L. Glass.** 2005. The *so* locus is required for vegetative cell fusion and postfertilization events in *Neurospora crassa*. Eukaryotic Cell **4:**920-930.

21. **Freitag, M., P. C. Hickey, N. B. Raju, E. U. Selker, and N. D. Read.** 2004. GFP as a tool to analyze the organization, dynamics and function of nuclei and microtubules in *Neurospora crassa*. Fungal Genetics and Biology **41:**897-910.

22. **Fricker, M. D., L. Boddy, and D. Bebber.** 2007. Network organisation in filamentous fungi, p. 309-330. *In* R. J. Howard and N. A. R. Gow (ed.), Biology of the Fungal Cell. Springer-Verlag, Berlin.

23. **Galagan, J. E., S. E. Calvo, K. A. Borkovich, E. U. Selker, N. D. Read, D. Jaffe, W. FitzHugh, L.-J. Ma, S. Smirnov, S. Purcell, B. Rehman, T. Elkins, R. Engels, S. Wang, C. B. Nielsen, J. Butler, M. Endrizzi, D. Qui, P. Ianakiev, D. Bell-Pedersen, M. A. Nelson, M. Werner-Washburne, C. P. Selitrennikoff, J. A. Kinsey, E. L. Braun, A. Zelter, U. Schulte, G. O. Kothe, G. Jedd, W. Mewes, C. Staben, E. Marcotte, D. Greenberg, A. Roy, K. Foley, J. Naylor, N. Stange-Thomann, R. Barrett, S. Gnerre, M. Kamal, M. Kamvysselis, E. Mauceli, C. Bielke, S. Rudd, D. Frishman, S. Krystofova, C. Rasmussen, R. L. Metzenberg, D. D. Perkins, S. Kroken, C. Cogoni, G. Macino, D. Catcheside, W. Li, R. J. Pratt, S. A. Osmani, C. P. C. DeSouza, L. Glass, M. J. Orbach, J. A. Berglund, R. Voelker, O. Yarden, M. Plamann, S. Seiler, J. Dunlap, A. Radford, R. Aramayo, D. O. Natvig, L. A. Alex, G. Mannhaupt, D. J. Ebbole, M. Freitag, I. Paulsen, M. S. Sachs, E. S. Lander, C. Nusbaum, and B. Birren.** 2003. The genome sequence of the filamentous fungus *Neurospora crassa*. Nature **422:**859-868.

24. **Gierz, G., and S. Bartnicki-Garcia.** 2001. A three-dimensional model of fungal morphogenesis based on the vesicle supply centre concept. Journal of Theoretical Biology **208:**151-164.

25. **Girbardt, M.** 1957. Der Spitzenkörper von *Polysticus versicolor*. Planta **50:**47-59.

26. **Glass, N. L., and K. Dementhon.** 2006. Non-self recognition and programmed cell death in filamentous fungi. Current Opinion in Microbiology **9:**553-558.

27. **Glass, N. L., and A. Fleißner.** 2006. Re-wiring the network: understanding the mechnanism and function of anastomosis in filamentous ascomycete fungi, p. 123-135. *In* U. Kües and R. Fischer (ed.), The Mycota, vol. 1. Springer-Verlag, Berlin Heidelberg.

28. **Glass, N. L., D. J. Jacobson, and P. K. T. Shiu.** 2000. The genetics of hyphal fusion and vegetative incompatibility in filamentous ascomycete fungi. Annual Review of Genetics **34:**165-186.

29. **Glass, N. L., and I. Kaneko.** 2003. Fatal Attraction: Nonself recognition and heterokaryon incompatibility in filamentous fungi. Eukaryotic Cell **2:**1-8.

30. **Glass, N. L., C. Rasmussen, G. M. Roca, and N. D. Read.** 2004. Hyphal homing, fusion and mycelial interconnectedness. TRENDS in Microbiology **12:**135-141.

31. **Hickey, P. C., D. J. Jacobson, N. D. Read, and N. Louise Glass.** 2002. Live-cell imaging of vegetative hyphal fusion in *Neurospora crassa*. Fungal Genetics and Biology **37:**109-119.

32. **Hickey, P. C., S. R. Swift, G. M. Roca, and N. D. Read.** 2005. Live-cell imaging of filamentous fungi using vital fluorescent dyes and confocal microscopy. Methods in Microbiology **34:**63-87.

33. **Honda, S., and E. U. Selker.** 2009. Tools for Fungal Proteomics: Multifunctional Neurospora Vectors for Gene Replacement, Protein Expression and Protein Purification. Genetics **182:**11-23.

34. **Horsley, V., K. M. Jansen, S. T. Mills, and G. K. Pavlath.** 2003. IL-4 acts as a myoblast recruitment factor during mammalian muscle growth. Cell **113:**483-94.

35. **Ishii, M., and Y. Saeki.** 2008. Osteoclast cell fusion: mechanisms and molecules. Modern Rheumatology **18:**220-227.

36. **Jacobson, D. J.** 1992. Control of mating type heterokaryon incompatibility by the *tol* gene in *Neurospora crassa* and *Neurospora terasperma*. Genome **35:**347-353.

37. **Jahn, R., and R. H. Scheller.** 2006. SNAREs: engines for membrane fusion. Nature Reviews Molecular and Cellular Biology **7:**631-643.

38. **Jansen, K. M., and G. K. Pavlath.** 2008. Molecular control of mammalian myoblast fusion. Methods Mol Biol **475:**115-33.

39. **Kaneko, I., K. Dementhon, Q. Xiang, and N. L. Glass.** 2006. Nonallelic interactions between *het-c* and a polymorphic locus, *pin-c*, are essential for nonself recognition and programmed cell death in *Neurospora crassa*. Genetics **172:**1545-1555.

40. **Kasuga, T., J. P. Townsend, C. G. Tian, L. B. Gilbert, G. Mannhaupt, J. W. Taylor, and N. L. Glass.** 2005. Long-oligomer microarray profiling in *Neurospora crassa* reveals the transcriptional program underlying biochemical and physiological events of conidial germination. Nucleic Acid Research **33:**6469-6485.

41. **Kays, A. M., and K. A. Borkovich.** 2004. Severe impairment of growth and differentiation in a *Neurospora crassa* mutant lacking all heterotrimeric G-alpha proteins. Genetics **166:**1229-1240.

42. **Kemp, H. A., and G. F. Sprague, Jr.** 2003. Far3 and five interacting proteins prevent premature recovery from pheromone arrest in the budding yeast *Saccharomyces cerevisiae*. Molecular and Cellular Biology **23:**1750-1763.

43. **Kholodenko, B. N., and M. R. Birtwistle.** 2009. Four-dimensional dynamics of MAPK information-processing systems. Wiley Interdisciplinary Reviews: Systems Biology and Medicine **1:**28 - 44.

44. **Kielian, M., and F. A. Rey.** 2006. Virus membrane-fusion proteins: more than one way to make a hairpin. Nature Reviews Microbiology **4:**67-76.

45. **Kim, H., and K. A. Borkovich.** 2004. A pheromone receptor gene, *pre-1*, is essential for mating type-specific directional growth and fusion of trichogynes and female fertility in *Neurospora crassa*. Molecular Microbiology **52:**1781-1798.

46. **Kim, H., and K. A. Borkovich.** 2006. Pheromones are essential for male fertility and sufficient to direct chemotropic polarized growth of trichogynes during mating in *Neurospora crassa*. Eukaryotic Cell **5:**544-554.

47. **Lipke, P. N., and J. Kurjan.** 1992. Sexual agglutination in budding yeast - structure, function, and regulation of adhesion glycoproteins. Microbiological Reviews **56:**180-194.

48. **Maheshwari, R.** 1999. Microconidia of *Neurospora crassa*. Fungal Genetics and Biology **26:**1-18.

49. **Maheshwari, R.** 1991. Microcycle conidiation and its genetic basis in *Neurospora crassa*. Journal of General Microbiology **137:**2103-2115.

50. **Martens, S., and H. T. McMahon.** 2008. Mechanisms of membrane fusion: disparate players and common principles. Nature Reviews Molecular Cell Biology **9:**543-556.

51. **McKay, M. M., D. A. Ritt, and D. K. Morrison.** 2009. Signaling dynamics of the KSR1 scaffold complex. Proc Natl Acad Sci U S A **106:**11022-7.

52. **Mohler, W. A., G. Shemer, J. J. del Campo, C. Valansi, E. Opoku-Serebuoh, V. Scranton, N. Assaf, J. G. White, and B. Podbilewicz.** 2002. The Type I Membrane Protein EFF-1 Is Essential for Developmental Cell Fusion in *C. elegans*. Developmental Cell **2:**355-362.

53. **Nelson, M. A., and R. L. Metzenberg.** 1992. Sexual development genes of *Neurospora crassa.* Genetics **132:**149-162.

54. **Newmeyer, D.** 1970. A suppressor of the heterokaryon-incompatibility associated with mating type in *Neurospora crassa*. Canadian Journal of Genetics and Cytology **12:**914-926.

55. **Oren-Suissa, M., and B. Podbilewicz.** 2007. Cell fusion during development. Trends Cell Biol **17:**537-46.

56. **Pandey, A., G. M. Roca, N. D. Read, and N. L. Glass.** 2004. Role of a mitogen-activated protein kinase pathway during conidial germination and hyphal fusion in *Neurospora crassa*. Eukaryotic Cell **3:**348-358.

57. **Perkins, D. D.** 1988. Main features of vegetative incompatibility in *Neurospora crassa*. Fungal Genetics Newsletter **35:**44-46.

58. **Podbilewicz, B., E. Leikina, A. Sapir, C. Valansi, M. Suissa, G. Shemer, and L. V. Chernomordik.** 2006. The *C. elegans* developmental fusogen EFF-1 mediates homotypic fusion in heterologous cells and *in vivo*. Developmental Cell **11:**471-481.

59. **Raju, N. B.** 1980. Meiosis and ascospore genesis in *Neurospora*. European Journal of Cell Biology **23:**208-223.

60. **Rappel, W.-J., and W. F. Loomis.** 2009. Eukaryotic chemotaxis. Wiley Interdisciplinary Reviews: Systems Biology and Medicine **1:**141-149.

61. **Read, N. D.** 1994. Cellular nature and multicellular morphogenesis of higher fungi, p. 254-271. *In* D. Ingram and A. Hudson (ed.), Shape and Form in Plants and Fungi. Academic Press, London.

62. **Read, N. D.** 2007. Environmental sensing and the filamentous fungal lifestyle, p. 38-57. *In* G. M. Gadd, S. C. Watkinson, and P. S. Dyer (ed.), Fungi and the Environment. Cambridge University Press, Cambridge.

63. **Read, N. D., A. Fleißner, M. G. Roca, and N. L. Glass.** 2010. Hyphal fusion. *In* K. A. Borkovich and D. Ebbole (ed.), Cellular and Molecular Biology of Filamentous Fungi. American Society of Microbiology, Washington DC.

64. **Read, N. D., A. Lichius, J. Shoji, and A. B. Goryachev.** 2009. Self-signalling and self-fusion in filamentous fungi. Current Opinion in Microbiology **12:**608-615.

65. **Read, N. D., and G. M. Roca.** 2006. Vegetative hyphal fusion in filamentous fungi, p. 87-98. *In* F. Baluska, D. Volkmann, and P. W. Barlow (ed.), Cell-Cell Channels. Landes Bioscience.

66. **Richardson, B. E., S. J. Nowak, and M. K. Baylies.** 2008. Myoblast fusion in fly and vertebrates: new genes, new processes and new perspectives. Traffic **9:**1050-9.

67. **Roca, G. M., J. Arlt, C. E. Jeffree, and N. D. Read.** 2005. Cell biology of conidial anastomosis tubes in *Neurospora crassa*. Eukaryotic Cell **4:**911-919.

68. **Roca, G. M., N. D. Read, and A. E. Wheals.** 2005. Conidial anastomosis tubes in filamentous fungi. FEMS Microbiological Letters **249:**191-198.

69. **Sapir, A., J. Choi, E. Leikina, O. Avinoam, C. Valansi, L. V. Chernomordik, A. P. Newman, and B. Podbilewicz.** 2007. AFF-1, a FOS-1-regulated fusogen, mediates fusion of the anchor cell in *C. elegans*. Developmental Cell **12:**683-698.

70. **Schmit, J. C., and S. Brody.** 1976. Biochemical genetics of *Neurospora crassa* germination. Bacteriological Reviews **40:**1-41.

71. **Shemer, G., M. Suissa, I. Kolotuev, K. C. Q. Nguyen, D. H. Hall, and B. Podbilewicz.** 2004. EFF-1 is sufficient to initiate and execute tissue-specific cell fusion in *C. elegans*. Current Biology **14:**1587-1591.

72. **Shin, S. Y., O. Rath, S. M. Choo, F. Fee, B. McFerran, W. Kolch, and K. H. Cho.** 2009. Positive- and negative-feedback regulations coordinate the dynamic behavior of the Ras-Raf-MEK-ERK signal transduction pathway. J Cell Sci **122:**425-35.

73. **Shiu, P. K. T., and N. L. Glass.** 1999. Molecular characterization of *tol*, a mediator of mating-type-associated vegetative incompatibility in *Neurospora crassa*. Genetics **151:**545-555.

74. **Söllner, T. H.** 2004. Intracellular and viral membrane fusion: a uniting mechanism. Current Opinion in Cell Biology **16:**429-435.

75. **Stolzing, A., J. Hescheler, and S. Sethe.** 2007. Fusion and regenerative therapies: is immortality really recessive? Rejuvenation Res **10:**571-86.

76. **Vignery, A.** 2008. Macrophage fusion: molecular mechanisms. Methods Mol Biol **475:**149-61.

77. **Vignery, A.** 2005. Macrophage fusion: the making of osteoclasts and giant cells. J. Exp. Med. **202:**337-340.

78. **Wright, G. D., J. Arlt, W. C. K. Poon, and N. D. Read.** 2007. Optical tweezer micromanipulation of filamentous fungi. Fungal Genetics and Biology **44:**1-13.

79. **Xiang, Q., and N. L. Glass.** 2004. The control of mating type heterokaryon incompatibility by *vib*-1, a locus involved in *het*-c heterokaryon incompatibility in *Neurospora crassa*. Fungal Genetics and Biology **41:**1063-1076.

80. **Xiang, Q., and N. L. Glass.** 2002. Identification of *vib-1*, a locus involved in vegetative incompatibility mediated by *het-c* in *Neurospora crassa*. Genetics **162:**89-101.

81. **Xiang, Q., C. Rasmussen, and N. L. Glass.** 2002. The *ham-2* locus, encoding a putative transmembrane protein, is required for hyphal fusion in *Neurospora crassa*. Genetics **160:**169-180.

82. **Yagi, M., T. Miyamoto, Y. Sawatani, K. Iwamoto, N. Hosogane, N. Fujita, K. Morita, K. Ninomiya, T. Suzuki, K. Miyamoto, Y. Oike, M. Takeya, Y. Toyama, and T. Suda.** 2005. DC-STAMP is essential for cell-cell fusion in osteoclasts and foreign body giant cells. J. Exp. Med. **202:**345-351.

83. **Yagi, M., K. Ninomiya, N. Fujita, T. Suzuki, R. Iwasaki, K. Morita, N. Hosogane, K. Matsuo, Y. Toyama, T. Suda, and T. Miyamoto.** 2007. Induction of DC-STAMP by alternative activation and aownstream signaling mechanisms. Journal of Bone and Mineral Research **22:**992-1001.

84. **Yamazaki, H., A. Tanaka, J.-I. Kaneko, A. Ohta, and H. Horiuchi.** 2008. *Aspergillus nidulans* ChiA is a glycosylphosphatidylinositol (GPI)-anchored chitinase specifically localized at the polarized growth side. Fungal Genetics and Biology **45:**963-972.

85. **Zelter, A., M. Bencina, B. J. Bowann, O. Yarden, and N. D. Read.** 2004. A comparative genomic analysis of the calcium signaling machinery in *Neurospora crassa*, *Magnaporthe grisea*, and *Saccharomyces cerevisiae*. Fungal Genetics and Biology **41:**827-841.

86. **Zhao, H., Z.-M. Shen, P. C. Kahn, and P. N. Lipke.** 2001. Interaction of alpha-Agglutinin and a-agglutinin, *Saccharomyces cerevisiae* sexual cell adhesion molecules. Journal of Bacteriology **183:**2874-2880.

Chapter 2 – Materials and methods

2.1. Chemicals

Unless otherwise stated chemicals were purchased from Sigma or Fluka (both Sigma-Aldrich Company Ltd., Poole, Dorset, UK, www.sigmaaldrich.com).

2.2. Organisms and strains

Genetically modified *Neurospora crassa* (*N. crassa*) and *Escherichia coli* (*E. coli*) are containment level 1 organisms and the relevant procedures for their handling and disposal (Published by the Genetic Manipulation and Biological Safety Committee, University of Edinburgh) were followed at all times. Established sterile technique was used at all times.

2.2.1. *Neurospora crassa* strains

A total of 160 *N. crassa* strains, including 131 gene deletion mutants and 27 transformants, were used and produced in this study. Table 2.1 shows all strains created by the *Neurospora* Genome Project, Dartmouth Medical School, Dartmouth, USA, and other participating institutes, by the methods described elsewhere [9, 55], and supplied by the Fungal Genetics Stock Centre (FGSC, School of Biological Sciences, University of Missouri, Kansas City, USA). The list also includes strains that underwent homokaryon purification within this study, and strains received from other sources than the FGSC. Strains genetically modified within this study for ectopic expression of fluorescent fusion proteins are listed in Table 2.2.

Table 2.1 *Neurospora crassa* strains received from the FGSC or other sources. Gene deletion strains are ordered by ascending FGSC strain number. HP denotes strains that underwent homokaryon purification by single spore isolation of micro- or macroconidida (section 2.8) or sexual crosses (section 2.4.2.3). *hygR* encodes for the hygromycin resistance gene. *bar+* encodes for ignite (also known as phosphinothricin or basta) resistance gene. Asterisks indicate strains that were genotypically verified by PCR (section 2.7) for presence of nuclei with the correctly inserted knock-out (KO) cassette, absence (homokaryon) or presence (heterokaryon, het) of nuclei containing the *wt* gene locus, and tested whether or not Δ*mus-51* and Δ*mus-52* deletions, respectively, have been recovered after back-crossing to the wt.

Strain	***FGSC/strain number***	***Locus***	***Mating type***	***Genotype***	***Source***
wild type	FGSC2489	_	A	*74-OR23-1VA*	FGSC
wild type	FGSC4200	_	a	*ORS-SL6a*	FGSC
Δmus-52	FGSC15968	NCU00077.2	A*	*Δmus52::bar+*	FGSC
Δmus-51	FGSC20277	NCU08290.2	a*	*Δmus51::bar+*	FGSC
wt (H1-sGFP)	N2282	_	A	*his-3^{+}::Pccg1-hH1^{+}-sgfp*	[14]
wt (H1-sGFP)	N2283	_	a	*his-3^{+}::Pccg1-hH1^{+}-sgfp*	[14]
wt (BML-sGFP)	N2506	_	a	*rid^{RIP4} his3^{+} ::Pccg1-bml^{+} -sgfp^{+} + rid^{RIP4} his-3*	[14]
Δhex-1	_	NCU08332.2	A	*Δhex-1::pan^{-}*	[50]
Δpred.prot.	FGSC11010	NCU08652.2	A	*Δpred.prot.::hygR*	FGSC
Δsah-1	FGSC11132	NCU04179.2	a	*Δsah-1::hygR*	FGSC
Δnth-1	FGSC11133	NCU04211.2	a	*Δnth-1::hygR*	FGSC
Δspa-2	FGSC11141	NCU03115.2	a	*Δspa-2::hygR*	FGSC
Δrdi-1	FGSC11145	NCU06561.2	a*	*Δrdi-1::hygR*	FGSC
Δgnb-1	FGSC11199	NCU00440.2	A	*Δgnb-1::hygR*	FGSC
Δsod-1	FGSC11215	NCU02133.2	a*	*Δsod-1::hygR*	FGSC
Δabc-1	FGSC11238	NCU05591.2	a	*Δabc-1::hygR*	FGSC

Δspla-2	FGSC11246	NCU06650.2	a	*Δspla-2::hygR*	FGSC
Δacr-1	FGSC11254	NCU07617.2	A	*Δacr-1::hygR*	FGSC
Δso	FGSC11292	NCU02794.2	a*	*Δso::hygR*	FGSC
Δso	FGSC11293	NCU02794.2	A	*Δso::hygR*	FGSC
Δmek-1	FGSC11318	NCU06419.2	a*	*Δmek-1::hygR*	FGSC
Δmek-1	FGSC11319	NCU06419.2	A*	*Δmek-1::hygR*	FGSC
Δmak-1	FGSC11320	NCU09842.1	A*	*Δmak-1::hygR*	FGSC
Δmak-1	FGSC11321	NCU09842.1	a*	*Δmak-1::hygR*	FGSC
Δchm-1	FGSC11322	NCU00406.2	a*	*Δchm-1::hygR*	FGSC
Δste20	FGSC11324	NCU03894.2	A*	*Δste20::hygR*	FGSC
Δmik-1	FGSC11326	NCU02234.2	A*	*Δmik-1::hygR*	FGSC
Δmik-1	FGSC11327	NCU02234.2	a*	*Δmik-1::hygR*	FGSC
Δrho-3	FGSC11352	NCU00600.2	a	*Δrho-3::hygR*	FGSC
Δnit-2	FGSC11392	NCU09068.2	a	*Δnit-2::hygR*	FGSC
Δcons.hypot. protein	FGSC11420	NCU06648.2	A	*Δcons.prot.::hygR*	FGSC
Δaip-1	FGSC11424	NCU08468.2	a	*Δaip-1::hygR*	FGSC
Δpde-1	FGSC11429	NCU00237.2	a*	*Δpde-1::hygR*	FGSC
Δpde-2	FGSC11431	NCU00478.2	a*	*Δpde-2,::hygR*	FGSC
Δpkac-2	FGSC11433	NCU00682.2	a*	*Δpkac-2,::hygR*	FGSC
Δos-2	FGSC11436	NCU07024.2	A*	*Δos-2,::hygR*	FGSC
Δpp-1	FGSC11459	NCU00340.2	a (het)*	*Δpp-1::hygR, Δmus51::bar+*	FGSC
Δpp-1 (HP)	macroconidia	NCU00340.2	a*	*Δpp-1::hygR, Δmus51::bar+*	This study
Δnrc-1	FGSC11466	NCU06182.2	a*	*Δnrc-1::hygR, Δmus51::bar+*	FGSC

ΔsevK	FGSC11478	NCU00772.2	a (het)	*ΔsevK::hygR, Δmus51::bar+*	FGSC
ΔsevK (HP)	macroconidia/ sexual cross	NCU00772.2	a	*ΔsevK::hygR, Δmus51::bar+*	This study
Δmak-2	FGSC11482	NCU02393.2	a*	*Δmak-2::hygR*	FGSC
ΔsepA	FGSC11490	NCU01431.2	a (het)*	*ΔsepA::hygR, Δmus51::bar+*	FGSC
ΔsepA (HP)	macroconidia	NCU01431.2	a	*ΔsepA::hygR, Δmus51::bar+*	This study
Δrac-1	FGSC11495	NCU02160.2	a (het)*	*Δrac-1::hygR, Δmus51::bar+*	FGSC
Δrac-1 (HP)	microconidia	NCU02160.2	a*	*Δrac-1::hygR, Δmus51::bar+*	This study
Δpkac-1	FGSC11513	NCU06240.2	a (het)*	*Δpkac-1::hygR, Δmus51::bar+*	FGSC
Δpkac-1 (HP)	microconidia/ sexual cross	NCU06240.2	a*	*Δpkac-1::hygR, Δmus51::bar+*	This study
Δcrisp-1	FGSC11514	NCU08377.2	a (het)*	*Δcrisp-1::hygR, Δmus51::bar+*	FGSC
Δcrisp-1 (HP)	microconidia/ sexual cross	NCU08377.2	a*	*Δcrisp-1::hygR, Δmus51::bar+*	This study
Δnox-2	FGSC11516	NCU10775.2	a (het)*	*Δnox-2::hygR, Δmus51::bar+*	FGSC
Δnox-2 (HP)	macroconidia	NCU10775.2	a (het)*	*Δnox-2::hygR, Δmus51::bar+*	This study
Δcpc-1	FGSC11520	NCU04050.2	a	*Δcpc-1::hygR, Δmus51::bar+*	FGSC
Δmek-2	FGSC11524	NCU04612.2	a*	*Δmek-2::hygR, Δmus51::bar+*	FGSC
Δrac-1	FGSC11525	NCU02160.2	a*	*Δrac-1::hygR, Δmus51::bar+*	FGSC
Δmcb	FGSC11609	NCU01166.2	a (het)*	*Δmcb::hygR, Δmus51::bar+*	FGSC
Δmcb (HP)	microconidia/ sexual cross	NCU01166.2	a (het)*	*Δmcb::hygR, Δmus51::bar+*	This study
Δgna-3	FGSC11610	NCU05206.2	a (het)*	*Δgna-3::hygR, Δmus52::bar+*	FGSC
Δgna-3 (HP)	macroconidia	NCU05206.2	a*	*Δgna-3::hygR, Δmus52::bar+*	This study
Δmyo-5	FGSC11611	NCU02111.1	a (het)	*Δmyo-5::hygR, Δmus51::bar+*	FGSC
Δprm-1-like	FGSC11616	NCU03292.2	a (het)	*Δprm-1-like::hygR, Δmus51::bar+*	FGSC
ΔNapt-2	FGSC11620	NCU07443.2	a (het)	*ΔNapt-2::hygR, Δmus51::bar+*	FGSC

ΔNapt-2 (HP)	macroconidia	NCU07443.2	a (het)	*ΔNapt-2::hygR, Δmus51::bar+*	This study
Δpls-1	FGSC11630	NCU07432.2	a (het)	*Δpls-1::hygR, Δmus51::bar+*	FGSC
Δpred.prot.	FGSC11642	NCU02903.2	a	*Δpred.prot::hygR*	FGSC
Δpred.prot.	FGSC11647	NCU08038.2	A	*Δpred.prot::hygR*	FGSC
Δacw-2	FGSC11674	NCU00957.2	a	*Δacw-2::hygR*	FGSC
Δcdc-24	FGSC11721	NCU06067.2	a (het)*	*Δcdc-24::hygR, Δmus51::bar+*	FGSC
Δcdc-24 (HP)	macroconidia	NCU06067.2	a*	*Δcdc-24::hygR, Δmus51::bar+*	This study
Δrho-4	FGSC11726	NCU03407.2	a (het)	*Δrho-4::hygR, Δmus51::bar+*	FGSC
Δrho-4 (HP)	macroconidia	NCU03407.2	a	*Δrho-4::hygR, Δmus51::bar+*	This study
ΔnimA	FGSC11841	NCU03187.2	a (het)	*ΔnimA::hygR, Δmus51::bar+*	FGSC
ΔnimA (HP)	macroconidia	NCU03187.2	a (het)	*ΔnimA::hygR, Δmus51::bar+*	This study
Δeb-1	FGSC11851	NCU00243.2	a	*Δeb-1::hygR*	FGSC
Δsdc25	FGSC11866	NCU09758.2	a*	*Δsdc25::hygR, Δmus51::bar+*	FGSC
Δham-2	FGSC12091	NCU03727.2	A	*Δham-2::hygR*	FGSC
Δspr-7	FGSC12115	NCU07159.2	A	*Δspr-7::hygR*	FGSC
Δpks-4	FGSC12116	NCU08399.2	a	*Δpks-4::hygR*	FGSC
Δtrm-52	FGSC12280	NCU03498.2	a	*Δtrm-52::hygR*	FGSC
Δgpr-1	FGSC12363	NCU00786.2	A	*Δgpr-1::hygR*	FGSC
Δgna-1	FGSC12370	NCU06493.2	a (het)*	*Δgna-1::hygR*	FGSC
Δgna-1 (HP)	macroconidia	NCU06493.2	a (het)*	*Δgna-1::hygR*	This study
ΔflbA	FGSC12372	NCU08319.2	a	*Δ flbA::hygR*	FGSC
Δgna-2	FGSC12378	NCU06729.2	a*	*Δgna-2::hygR*	FGSC
Δpred.prot.	FGSC12401	NCU04170.2	a	*Δpred.prot::hygR*	FGSC

Δras2	FGSC12467	NCU03616.2	a*	*Δras2::hygR*	FGSC
ΔNatg-8	FGSC12506	NCU01545.2	a(het)	*ΔNatg-8::hygR, Δmus51::bar+*	FGSC
ΔNatg-8 (HP)	macroconidia	NCU01545.2	a(het)	*ΔNatg-8::hygR, Δmus51::bar+*	This study
Δhypoth.prot.	FGSC12522	NCU05521.2	a	*Δhypoth.prot.::hygR*	FGSC
Δtrm-30	FGSC12544	NCU07879.2	a	*Δtrm-30::hygR*	FGSC
Δnox-1	FGSC12867	NCU02110.2	a*	*Δnox-1::hygR*	FGSC
Δnox-1	FGSC12868	NCU02110.2	A*	*Δnox-1::hygR*	FGSC
Δpks-7	FGSC12932	NCU03584.2	a (het)	*Δpks-7::hygR, Δmus52::bar+*	FGSC
Δpred.prot.	FGSC13042	NCU07846.2	a (het)	*Δpred.prot.::hygR, Δmus51::bar+*	FGSC
Δccp-1	FGSC13189	NCU03297.2	a	*Δccp-1::hygR*	FGSC
Δpex-6	FGSC13219	NCU08373.2	a (het)	*Δpex-6::hygR, Δmus51::bar+*	FGSC
Δpex-6 (HP)	macroconidia/ secual cross	NCU08373.2	a (het)	*Δpex-6::hygR, Δmus51::bar+*	This study
Δeas	FGSC13318	NCU08457.2	a	*Δeas::hygR*	FGSC
Δtps-1	FGSC13320	NCU09715.2	a	*Δtps-1::hygR*	FGSC
Δrho-2	FGSC13322	NCU08683.2	a	*Δrho-2::hygR*	FGSC
Δlao	FGSC13350	NCU05113.2	a*	*Δlao::hygR*	FGSC
Δlao	FGSC13351	NCU05113.2	A*	*Δlao::hygR*	FGSC
Δrrg-1	FGSC13363	NCU01895.2	a*	*Δrrg-1::hygR*	FGSC
Δgdh-1	FGSC13417	NCU00461.2	a*	*Δgdh-1::hygR*	FGSC
Δgdh-1	FGSC13418	NCU00461.2	A*	*Δgdh-1::hygR*	FGSC
Δpth-1	FGSC13419	NCU01611.2	a	*Δpth-1::hygR*	FGSC
Δnor-1	FGSC13573	NCU07850.2	a (het)*	*Δnor-1::hygR, Δmus51::bar+*	FGSC
Δnor-1 (HP)	macroconidia	NCU07850.2	a*	*Δnor-1::hygR, Δmus51::bar+*	This study

Δprm-1	FGSC13594	NCU09337.2	a (het)	*Δprm-1::hygR, Δmus52::bar+*	FGSC
Δmhp-1	FGSC13752	NCU08192.2	a	*Δmhp-1::hygR*	FGSC
Δpks-3	FGSC14204	NCU04865.2	a	*Δpks-3::hygR*	FGSC
Δcyp	FGSC14340	NCU00726.2	a	*Δcyp::hygR*	FGSC
Δorp-1	FGSC14342	NCU04236.2	a	*Δorp-1::hygR*	FGSC
Δpten	FGSC14343	NCU06969.2	A	*Δpten::hygR*	FGSC
ΔtmpA	FGSC14453	NCU00848.2	a	*ΔtmpA::hygR*	FGSC
ΔtmpA-like	FGSC14467	NCU07231.2	a	*ΔtmpA::hygR*	FGSC
Δlpl	FGSC14506	NCU03141.2	A	*Δlpl::hygR*	FGSC
Δdnr-1	FGSC14662	NCU02806.2	a	*Δdnr-1::hygR*	FGSC
Δcons.hypot. protein	FGSC14847	NCU06834.2	A	*Δcons.prot.::hygR*	FGSC
Δhyr-1	FGSC15631	NCU09534.2	a*	*Δhyr-1::hygR*	FGSC
Δcys-9	FGSC15634	NCU08352.2	a (het)*	*Δcys-9::hygR*	FGSC
Δcys-9	FGSC15635	NCU08352.2	A*	*Δcys-9::hygR*	FGSC
Δpkc	FGSC15734	NCU06544.2	a (het)*	*Δpkc::hygR, Δmus52::bar+*	FGSC
Δcdc42	FGSC15833	NCU06454.2	a*	*Δcdc-42::hygR*	FGSC
Δcdc25	FGSC16014	NCU06500.2	a (het)*	*Δcdc25::hygR, Δmus51::bar+*	FGSC
Δcdc25 (HP)	macroconidia/ sexual cross	NCU06500.2	a (het)*	*Δcdc25::hygR, Δmus51::bar+*	This study
Δcdc2	FGSC16078	NCU09778.2	a (het)	*Δcdc2::hygR, Δmus51::bar+*	FGSC
Δrrg-2	FGSC16195	NCU02413.2	a	*Δrrg-2::hygR*	FGSC
Δste50	FGSC17041	NCU00455.2	A*	*Δste50::hygR*	FGSC
Δhypot.prot.	FGSC17212	NCU02609.2	a	*Δhypot.prot.::hygR*	FGSC
Δos-2	FGSC17933	NCU07024.2	A*	*Δos-2::hygR*	FGSC

Δnrc-1	FGSC18162	NCU06182.2	a	*Δnrc-1::hygR, Δmus51::bar+*	FGSC
Δos-4	FGSC18202	NCU03071.2	a*	*Δos-4::hygR*	FGSC
Δos-5	FGSC18203	NCU00587.2	a*	*Δos-5::hygR*	FGSC
Δcons.hypot. protein	FGSC19786	NCU10397.2	A	*Δcons.prot.::hygR*	FGSC
Δpp-1	FGSC21335	NCU00340.2	a	*Δpp-1::hygR, Δmus51::bar+*	FGSC

Table 2.2 *Neurospora crassa* transformants generated within this study.

Strain	***Strain number***	***Host strain***	***Mating type***	***Genotype***
wt sGFP	NCAL001	FGSC 4200	a	*Pccg-1::sfgp::bar^{+}*
wt sGFP	NCAL002	FGSC 2489	A	*Pccg-1::sfgp::bar^{+}*
wt Lifeact-tdTomato	NCAL003	FGSC 4200	a	*Pccg-1::lifeact-tdtomato::bar^{+}*
wt Lifeact-TagRFP	NCAL004	FGSC 4200	a	*Pccg-1::lifeact-tagrfp::bar^{+}*
wt Lifeact-TagRFP	NCAL005	FGSC 2489	A	*Pccg-1::lifeact-tagrfp::bar^{+}*
wt BML-sGFP + Lifeact-TagRFP	NCAL006	N2506	a	*rid^{RIP4} his3^{+}::Pccg-1-bml^{+}-sgfp^{+} + rid^{RIP4} his-3; Pccg-1::lifeact-tagrfp::bar^{+}*
wt MAK-1-sGFP	NCAL007	FGSC 4200	a	*Pccg-1::mak-1-sgfp::bar^{+}*
wt NOX-1-sGFP	NCAL008	FGSC 4200	a	*Pccg-1::nox-1-sgfp::bar^{+}*
wt NOR-1-sGFP	NCAL009	FGSC 4200	a	*Pccg-1::nor-1-sgfp::bar^{+}*
Δ*mak-1* MAK-1-sGFP	NCAL010	FGSC 11320	A	*Δmak-1::hygR ; Pccg-1::mak-1-sgfp::bar^{+}*
Δ*mak-1* MAK-1^{E104G}-sGFP	NCAL011	FGSC 11320	A	*Δmak-1::hygR ; Pccg-1::mak-1^{E104G}-sgfp::bar^{+}*
Δ*mak-1* Lifeact-tdTomato	NCAL012	FGSC 11320	A	*Δmak-1::hygR ; Pccg-1::lifeact-tdtomato::bar^{+}*
Δ*mak-1* Lifeact-TagRFP	NCAL013	FGSC 11320	A	*Δmak-1::hygR ; Pccg-1::lifeact-tagrfp::bar^{+}*

Δ*nox-1* NOX-1-sGFP	NCAL014	FGSC 12867	a	*Δnox-1::hygR ; Pccg-1::nox-1-sgfp::bar*$^{+}$
Δ*nor-1* NOR-1-sGFP	NCAL015	Δ*nor-1* (HS)	a	*Δnox-1::hygR ; Δmus51::bar+; Pccg-1::nor-1-sgfp::bar*$^{+}$
wt OS-2-sGFP	NCAL016	FGSC 2489	A	*Pccg-1::os-2-sgfp::bar*$^{+}$
wt OS-2-TagRFP	NCAL017	FGSC 2489	A	*Pccg-1::os-2-tagrfp::bar*$^{+}$
Δ*os-2* OS-2-sGFP	NCAL018	FGSC 11436	A	*Δos-2::hygR ; Pccg-1::os-2-sgfp::bar*$^{+}$
Δ*os-2* OS-2-TagRFP	NCAL019	FGSC 11436	A	*Δos-2::hygR; Pccg-1::os-2-tagrfp::bar*$^{+}$
Δ*os-2* OS-2-sGFP	NCAL020	FGSC 17933	A	*Δos-2::hygR; Pccg-1::os-2-sgfp::bar*$^{+}$
wt BML-sGFP + Lifeact-TagRFP-T	NCAL021	N2505	a	*rid*^{RIP4} *his3*$^{+}$*::Pccg-1-bml*$^{+}$*-sgfp*$^{+}$ *+ rid*^{RIP4} *his-3; Pccg-1::lifeact-tagrfp-t::bar*$^{+}$
wt Lifeact-TagRFP-T	NCAL022	FGSC 2489	A	*Pccg-1::lifeact-tagrfp-t::bar*$^{+}$
wt CRIB-sGFP	NCAL023	FGSC 4200	a	*Pccg-1::crib*$^{chm-1}$*-sgfp::bar*$^{+}$
wt CRIB-sGFP	NCAL024	FGSC 2489	A	*Pccg-1::crib*$^{chm-1}$*-sgfp::bar*$^{+}$
wt sCRIB-sGFP	NCAL025	FGSC 2489	A	*Pccg-1::scrib-sgfp::bar*$^{+}$
wt Lifeact-TagRFP	NCAL026	FGSC 4200	a	*Pccg-1::lifeact-tagrfp::nat1*$^{+}$
wt Lifeact-TagRFP	NCAL027	FGSC 2489	A	*Pccg-1::lifeact-tagrfp::nat1*$^{+}$
Δmak-1 MAK-1-sGFP + Lifeact-TagRFP	NCAL028	NCAL010	A	*Δmak-1::hygR ; Pccg-1::mak-1-sgfp::bar*$^{+}$*: Pccg-1::lifeact-tagrfp::nat1*$^{+}$
Δ*mak-1* MAK-1^{E104G}-sGFP + Lifeact-TagRFP	NCAL029	NCAL011	A	*Δmak-1::hygR ; Pccg-1::mak-1*^{E104G}*-sgfp::bar*$^{+}$
wt CRIB-sGFP + Lifeact-TagRFP	NCAL030	vegetative fusion of NCAL005 with NCAL024	A	*Pccg-1::crib-sgfp::bar+, Pccg-1::lifeact-tagrfp::bar*$^{+}$
wt CRIB-sGFP + Lifeact-TagRFP-T	NCAL031	vegetative fusion of NCAL022 with NCAL024	A	*Pccg-1::crib-sgfp::bar*$^{+}$*, Pccg-1::lifeact-tagrfp-t::bar*$^{+}$

2.2.2. Escherichia coli strains

E. coli strains used in this study for plasmid DNA (pDNA) selection and amplification are listed in Table 2.3.

Table 2.3 Bacterial strains used in this study.

Strain	*Description*	*Source*
DH5α	versatile chemically competent *E. coli* strain for everyday cloning applications	#18265-017, Invitrogen
Top10	chemically competent *E. coli* strain for high-efficiency cloning and plasmid propagation	#C4040-30, Invitrogen
Fusion-Blue	chemically ultra-competent *E. coli* K-12 strain used for In-Fusion™ cloning	#636700, Clontech

2.3. Plasmid DNA

Plasmids used and engineered in this study are listed in Table 2.4.

Table 2.4 Plasmids used and generated within this study. All fusion proteins were engineered as carboxy-terminal fusions of the fluorescent protein to the target protein.

Plasmid	*Description/Genotype*	*Source/Reference*
pBARGRG1	expression vector for *N. crassa* containing *Pccg1* promoter and *bar* resistance gene	[40]
pD-Nat	transformation vector for filamentous fungi containing the *nat1* resistance gene	[31]
pMF272	sGFP (GFP^{S65T}) containing expression plasmid for *N. crassa*	[14]
pJT580a	plasmid containing tdTomato fluorescent protein coding sequence	J. Tilsner, Edinburgh University, UK
pJT603f	plasmid containing Lifeact linked to a photostabilised TagRFP variant	J. Tilsner, Edinburgh University, UK
pAL1	transformation vector for cytoplasmic sGFP expression based on pBARGRG1 backbone;	This study

	Pccg-1::sgfp::bar^{+}	
pAL1-MAK-1	expression vector for MAK1-sGFP fusion protein; *Pccg-1::mak-1-sgfp::bar*$^{+}$	This study
pAL1-MAK-1^{E104G}	expression vector for inhibitable variant of MAK1-sGFP fusion protein; generated by side-directed mutagenesis of pAL1-MAK1	This study
pAL1-NOX-1	expression vector for NOX-1-sGFP fusion protein; *Pccg-1::nox-1-sgfp::bar*$^{+}$	This study
pAL1-NOR-1	expression vector for NOR-1-sGFP fusion protein; *Pccg-1::nor-1-sgfp::bar*$^{+}$	This study
pAL1-OS-2	expression vector for OS-2-sGFP fusion protein; *Pccg-1::os-2-sgfp::bar*$^{+}$	This study
pAL2	transformation vector for cytoplasmic tdTomato expression; *Pccg-1::tdTomato::bar*$^{+}$	This study
pAL2-Lifeact	expression vector for Lifeact-tdTomato fusion protein; *Pccg-1::lifeact-tdtomato::bar*$^{+}$	This study
pAL3-Lifeact	expression vector for Lifeact-TagRFP fusion protein; *Pccg-1::lifeact-tagrfp::bar*$^{+}$	This study
pAL3-OS-2	expression vector for OS-2-TagRFP fusion protein; *Pccg-1::os-2-tagrfp::bar*$^{+}$	This study
pAL4-Lifeact	expression vector for Lifeact-TagRFP fusion protein containing *nat1* resistance gene; *Pccg-1::lifeact-tagrfp::nat1*$^{+}$	This study
pAL5-Lifeact	expression vector for Lifeact-TagRFP-T (TagRFP^{S162T}) fusion protein; generated by side-directed mutagenesis from pAL3-Lifeact; *Pccg-1::lifeact-tagrfp-t::bar*$^{+}$	This study
pAL1-CRIB	expression vector for CRIB-sGFP fusion construct encoding amino acids 78-240 from *N. crassa* p21-activated kinase (PAK) CHM-1 linked to sGFP; *Pccg-1::crib*$^{chm-1}$*-sgfp::bar*$^{+}$	This study
pAL1-sCRIB	expression vector for synthetic CRIB-sGFP fusion construct encoding a synthetic gene of the CRIB motif linked to sGFP; *Pccg-1::scrib-sgfp::bar*$^{+}$	This study

2.4. Culture media and growth conditions

All media and salt solutions were made using distilled water (dH_2O) and sterilized before use by autoclaving at 121 °C, 2.1 bar for 21 min. Heat-sensitive components, such as antibiotics, other selection markers or sugars, were filter sterilized (using Millex® GP 0.22 μm filter units, Milipore, Cork, Ireland) and added to the main solution after the latter was autoclaved and allowed to cool to 50 °C.

Species were maintained and stored on the appropriate solid agar media in 8.5 cm Ø plastic Petri dishes (Greiner Bio-One, www.greinerbioone.com). If not otherwise stated, Oxoid agar No. 3 (www.oxoid.com) was used at an increased concentration of 2 % (w/v) to produce a firmer gel, encouraging growth to be limited to one plane on the agar surface, which is more suitable for light microscopy of filamentous fungi. Agar media were prepared in 300 ml batches contained in 500 ml flasks, and sterilized by autoclaving. They were then either allowed to set for storage, or when cooled to 50 °C poured into plastic Petri dishes, or made up as slants in plastic tubes (3 ml agar in 15 ml Greiner tubes, allowed to set at > 45°C, Greiner Bio-One www.greinerbioone.com) with plastic screw caps. If stored, the agar was melted by microwaving (650 W) set at medium power for 10-15 min, with swirl breakes in between, then allowed to cool to 50 °C in a water bath before pouring. Once poured plates and tubes were stored in the dark at 4 °C, and used within 12 weeks. Liquid media (for microscopy preparation and dilution of fluorescent dyes) were prepared in 100-500 ml batches to the same recipes, excluding agar, and stored at RT or 4 °C if required.

2.4.1. Culturing *Escherichia coli*

2.4.1.1. Culture media for *E. coli*

E. coli strains were grown on solid or in liquid lysogeny broth (LB) medium [4, 5] (Table 2.5). Working stock cultures were kept on LB plates at 4 °C. Glycerol stocks according to Sambrook and Russell [45] were used for long term storage of *E. coli* at - 80 °C. For selection of strains transformed with plasmids containing antibiotic resistance genes, antibiotics were added to the media after autoclaving and once media had cooled to 50 °C. Antibiotics used in this study are listed in Table 2.6. To increase survival rate and thus transformation efficiency after heat shock, *E.coli* were recovered in super optimal broth with catabolite repression (SOC) medium [17] (Table 2.7).

Table 2.5 Luria Bertani (LB) medium.

Component	*Quantity*
Tryptone	10 g
Yeast extract	5 g
NaCl	10 g
Agar	10 g
dH_2O	add 1 l

Table 2.6 Antibiotic selection markers for *E. coli* used in this study.

Selection marker	*Stock conc.*	*Solvent*	*Amount used*	*Final conc.*
Ampicillin	100 mg/ml	50% EtOH	100 µl/100 ml	100 µg/ml
Chloramphenicol	35 mg/ml	EtOH	100 µl/100 ml	35 µg/ml
Kanamycin	50 mg/ml	dH_2O	100 µl/100 ml	50 µg/ml
Gentamycin	20 mg/ml	dH_2O	100 µl/100 ml	20 µg/ml
Tetracyclin	50 mg/ml	50% EtOH	100 µl/100 ml	50 µg/ml

Table 2.7 Super-optimal broth with catabolite repression (SOC) medium.

Component	*Quantity*
Tryptone	10 g
Yeast extract	5 g
NaCl	10 g
Agar	10 g
KCl (1 M)	2.5 ml
$MgCl_2$ (2 M)	5 ml
dH_2O	972.5 m l
adjusted pH7 with NaOH, autoclaved and cooled down, then added:	
sterile glucose (1 M)	20 ml

Table 2.8 Composition of transformation buffer (TB).

Component	*Stock sol.*	*Final conc.*	*Quantity*
PIPES-HCl pH6.7	0.5 M	10 mM	20 ml
$CaCl_2$	0.5 M	15 mM	30 ml
KCl	2 M	0.25 M	125
$MnCl_2$	1 M	55 mM	55 ml
dH_2O (sterile)	1 M	55 mM	55 ml
filter sterilized and stored at 4 °C			

2.4.1.2. Types of culture and growth conditions

Solid LB medium (Table 2.5) plates were hand poured with approximately 20 ml LB per plate. Media were made, autoclaved and allowed to cool to 50 °C before addition of the appropriate antibiotic (Table 2.6) and pouring. Upon solidification and inoculation the plates were incubated upside down at 37 °C to prevent condensed water dripping onto the cells.

For plasmid minipreps 5 ml liquid LB cultures supplemented with the appropriate antibiotic were inoculated using a sterile pipette tip and incubated overnight in a shaking incubator at 37 °C and 200 rpm. For plasmid midipreps the LB culture volume was increased to 20-30 ml and the incubation time extended until sufficient bacterial growth has occurred (OD_{600} = 2-4).

2.4.2. Culturing *Neurospora crassa*

2.4.2.1. Culture media for *N. crassa*

All *N. crassa* strains were grown on solid or in liquid Vogel's medium (VM) prepared with Vogel's medium salts [53] (Table 2.10) using 2% sucrose as the sole carbon source. For solid media 2% agar were added before autoclaving and prepared according to Table 2.9. Liquid Vogel's medium followed the same recipe, excluding the agar.

Table 2.9 Vogel's sucrose minimal medium. pH of the single-strength medium is about 5.8; with no further adjustment required.

Component	*Quantity*
*Vogel's salts 50x stock solution	20 ml
Sucrose	20 g
Agar	20 g
dH_2O	add 1 l

* see Table 2.10

Table 2.10 Composition of Vogel's salts 50x stock solution (stored at 4 °C).

Component	*Quantity*
$Na_3Citrate\text{-}2H_2O$	126.7 g
KH_2PO_4	250 g
*NH_4NO_3	100 g
$MgSO_4\text{-}7H_2O$	10 g
$CaCl_2\text{-}2H_2O$	5 g
**Vogel's trace elements solution	5 ml
†Biotin solution	5 ml
dH_2O	add 1 l

* omitted for N-free VM, ** see Table 2.11, † see Table 2.12

Table 2.11 Composition of Vogel's trace elements stock solution (stored at 4 °C).

Component	*Quantity*
Citric acid-1H_2O	5 g
$ZnSO_4$-7H_2O	5 g
$Fe(NH_4)_2SO_4$-7H_20	1 g
$CuSO_4$-5H_2O	0.25 g
$MnSO_4$-1H_2O	0.05 g
H_2BO_4	0.05 g
Na_2MoO_4-2H_2O	0.05 g
dH_2O	add 1 l

Table 2.12 Composition of biotin stock solution (stored at 4 °C).

Component	*Quantity*
d-biotin	5 g
dH_2O	add 1 l

For VM to be used with Ignite selection (*bar* resistance gene), NH_4NO_3 was omitted from the VM 50x stock solution (Table 2.10) to yield nitrogen-free Vogel's medium (N-free VM). 0.5 % (w/v) proline was used as an alternative nitrogen source as this had been found to increase the potency of Ignite selection [19]. Ignite was extracted from the "Harvest" herbicide (Bayer Crop Science Ltd., Monheim, Germany). Extraction was performed using the methods described by Hays and Selker [19]. The effective concentration of Ignite was titrated against *Neurospora* wild type for each extraction (typical effective concentration was 400 µg/ml Ignite in N-free VM).

For VM plates using Hygromycin B selection (*hph* resistance gene) [49] or nourseothricin selection (*nat1* resistance gene) [31] standard VM plates were supplemented with the appropriate amounts of each drug after autoclaving to yield final concentrations given in Table 2.13.

Table 2.13 Selection markers for *N. crassa* used in this study.

Selection marker	*Stock conc.*	*Solvent*	*Amount used*	*Final conc.*
Hygromycin B	200 mg/ml	dH_2O	100 µl/100 ml	200 µg/ml
Ignite	400 mg/ml	dH_2O	100 µl/100 ml	400 µg/ml
Nourseothricin	5 mg/ml	dH_2O	100 µl/100 ml	50 µg/ml

To induce the sexual cycle in *Neurospora,* strains were grown under nitrogen- and carbon-limiting conditions on solid synthetic crossing medium (SCM) [56] (Table 2.14) or low-sucrose agar (LSA) (Table 2.16), respectively.

Table 2.14 Synthetic crossing medium (SCM). pH of the single-strength medium is about 6.5; with no further adjustment required.

Component	*Quantity*
‡Synthetic crossing medium 50x stock solution	20 ml
Sucrose	20 g
Agar	20 g
dH_2O	add 1 l

‡ see Table 2.15

Table 2.15 Composition of synthetic crossing medium (SCM) 50x stock solution.

Component	*Quantity*
KNO_3	50 g
K_2HPO_4	35 g
KH_2PO_4	25 g
$MgSO_4$-$7H_2O$	25 g
NaCl	5 g
$CaCl_2$-$2H_2O$	5 g
**Vogel's trace elements solution	5 ml
†Biotin solution	2.5 ml
dH_2O	add 1 l

** see Table 2.9, † see Table 2.12

Table 2.16 Composition of low-sucrose agar (LSA). If not otherwise stated the solidified agar was overlaid with a disc of sterile cellophane.

Component	*Quantity*
Sucrose	2 g
Agar	20 g
dH_2O	add 1 l

Table 2.17 Composition of bottom agar.

Component	*Quantity*
*Vogel's salts 50x stock solution	20 ml
L-Arginine hydrochloride	3 g
Agar	15 g
dH_2O	800 ml
autoclaved and cooled down	
¥FIGS 10x stock solution	100 ml
poured 20 ml dishes	

*see Table 2.10; ¥see Table 2.18

For plating and selection of *N. crassa* transformants after electroporation (section 2.10.2) specific recovery media are required. For Ignite selection N-free Vogel's salts (Table 2.10) were used.

Table 2.18 Composition of fructose-glucose-sorbose (FIGS) 10x stock solution.

Component	*Quantity*
Fructose	5 g
Glucose	5 g
Sorbose	200 g
Agar	20 g
dH_2O	add 1 l
filter sterilized and stored at RT	

Table 2.19 Composition of top agar.

Component	*Quantity*
*Vogel's salts 50x stock solution	20 ml
Sorbitol	182 g
Agar	15 g
dH_2O	800 ml
autoclave and cooled down	
¥FIGS 10x stock solution	100 ml
prepared 10 ml aliquots in 15 ml tubes	

*see Table 2.10; ¥see Table 2.18

Table 2.20 DNA extraction buffer.

Component	*Final conc.*	*Quantity for 100 ml*
Tris-HCl (pH8)	10 mM	10 ml
NaCl	1.4 M	8.2 g
EDTA (0.5 M)	5 mM*	1 ml
dH_2O	20 mg/ml	add 100 ml
autoclaved and stored at RT		

*Proteinase K is not required for EDTA concentrations < 8 mM.

Table 2.21 Lysis buffer.

Component	*Final conc.*	*Quantity for 5 ml*
Proteinase K* (20 µl/ µl)	100 mM	25 µl
SDS (5 %)	0.5 % w/v	500 µl
EDTA (0.5 M)	50 mM	50 µl
dH_2O	-	add 5 ml
stored at 4°C and used within 2-3 days		

* e.g. Proteinase K #19131, Qiagen

2.4.2.2. Types of culture and growth conditions

Mature colonies of *N. crassa*. For experiments requiring mature hyphal colonies Petri dishes were inoculated in the centre of the agar plate with either an agar plug from an established colony or a 5 µl drop of a dense conidial suspension. The plate was then sealed with Parafilm (www.parafilm.com) before being placed in the incubator. To enable better aeration and thus faster growth Parafilm could be replaced with Micropore tape (3M, www.3m.com), and for containment the plate was placed within a larger plastic Petri dish (14 cm Ø, Nunc, www.nuncbrand.com).

Conidial germling cultures. For experiments requiring asexual spores either agar slants or plates were inoculated with a drop (~10 µl) of a dense conidial

suspension, incubated for one day at 35 °C in the dark, then placed on the windowsill for another 1-2 days (or much longer for slow growing mutants) until sufficient amounts of conidia have been produced. Conidia were harvested in 1-5 ml of sterile water by either rinsing the colony surface on the plate, or by adding water to the slant, swirling and then aspirating. To break up chains of macroconidia, the spore suspension was vigorously vortexed. If necessary, the spore suspension was then filtered through a pipette tip containing a ball of sterile cotton wool to remove hyphal fragments and larger arthroconidia. The concentration of conidia was then determined using a Fuchs-Rosenthal cell counting chamber (Paul Marienfeld GmbH & Co. KG, www.marienfeld-superior.com) and adjusted by dilution in dH_2O to 1 x 10^7 spores/ml. From this stock suspension, working suspensions in VM containing 0.5-1 x 10^6 cells/ml were prepared prior to each experiment. Stock spore suspensions were kept at 4 °C and reused for up to one week. For quantification, all samples were prepared as duplicates and the experiment repeated at least once.

Long-term stock cultures. Stock cultures of *N. crassa* were grown in VM agar slants supplemented with selection marker where appropriate. The slant cultures were inoculated and allowed to grow at 25 °C for 7 days in continuous light (Sanyo MIR-153 incubator illuminated by a single 15 W 'warm white' fluorescent tube light, www.sanyo-biomedical.co.uk) by which time significant conidiation had occurred. These slants were then refrigerated at 4 °C and used for several weeks. Additionally similar slants were frozen at -20 °C as a backup for several years. To recover the cultures an inoculating loop was used to remove spores and transfer them into liquid media or onto agar plates.

2.4.2.3. Performing sexual crosses

Successful sexual reproduction in *Neurospora crassa* requires fusion between the female trichogyne and a male conidium of the opposite mating type. The trichogyne is sent out from the female reproductive structure, the protoperithecium, is chemoattracted towards the male conidium and fuses with it. The male nucleus

travels through the trichogyne into the protoperithecium where fertilization takes place. This event is thought to trigger differentiation of the protoperithecium into the mature perithecium [13], and eventually leads to the production of sexual progeny, the ascospores, which are shot out upon maturation. To investigate the relationship between vegetative hyphal fusion and sexual fusion, development of sexual reproductive structures was analysed in fusion defective KO mutants. For this heterozygous crosses between KO mutant and wild type strains were performed on synthetic crossing medium (SCM)(Table 2.15) and low-sucrose agar (LSA) (Table 2.16). Both media induce protoperithecium formation mainly by nitrogen starvation [56] and delay conidiation to different extends, facilitating microscopical analysis. Crossing assays were performed in three different ways:

Female Fertility Test: The KO mutant strain was inoculated onto SCM or LSA plates and incubated for 2-4 days at 25°C. In parallel, a wild type strain of opposite mating type was cultured on standard VM for 2-3 days at 30 °C. Conidiogenesis was enhanced by light exposure one day before usage. After 3-4 days the KO mycelium, unless severely defective, should have developed protoperithecia which then were fertilized with male conidia from the wild type. Fertilization was performed 'dry' or 'wet'. For dry fertilization male conidia were collected on the lid by inverting the Petri dish and gently tapping it. The lid was then placed over the female mycelium and male conidia sprinkled onto it. For wet fertilization male conidia were harvested in sterile tap water, adjusted to the desired conidial concentration in a 3 ml volume and either evenly distributed onto the female mycelium, or applied as droplets at various positions. In any case, the fertilized plate was put back into the 25 °C incubator and monitored over the following weeks.

Male Fertility Test: The same procedure, as described for female fertility tests, was employed except that the wild type was used as female partner and conidia of the opposite mating type KO mutant were used as male fertilizing agent.

Confrontation Crossing: The KO mutant was co-inoculated with a wild type strain of opposite mating type on the same SCM or LSA plate, and incubated at 25 °C over the next 2-3 weeks. Either of the strains is supposed to be able to act as male and female partner.

In all crosses, development of protoperithecia and differentiation into mature perithecia was monitored under the stereomicroscope (section 2.12.1) over the following three weeks after fertilization. Upon successful fertilization mature perithecia were formed that eventually shot out the meiotic progeny, the ascospores. Ascospores were easily collected from the Petri dish lid and microscopically analysed. The appearance of ascospores was the determining feature of successful sexual reproduction. In crosses where perithecia appeared within that time period, but no ascospores could be recovered, perithecia were cracked open and the development of asci and ascospores assessed.

2.5. Comparative genomics by BLASTp analysis

From the literature genes were identified that have been shown to create defects during various stages of the appressorium-mediated infection process when mutated or deleted in the rice blast fungus *Magnaporthe oryzae* (summarized most recently in [57]). Orthologous gene loci in the *N. crassa* genome were identified using the Basic Local Alignment Search Tool (BLAST) algorithm [1] applying BLOSUM62 substitution scores [22] and gapped alignment [2] on the basis of predicted protein sequences (BLASTp). Potential hypothetical protein orthologs from *N. crassa* and *M. oryzae* (reciprocally blasted and cross-compared with the *Saccharomyces cerevisiae* genome) were identified based on: E-value, % identities and number of positives, as well as conserved protein domains. The following genome and proteome online tools were used to compare and re-probe gene and protein sequences, and validate predicted functional domains:

Genome databases at the BROAD Institute of MIT and Cambridge

Neurospora crassa
http://www.broad.mit.edu/annotation/genome/neurospora/

Magnaporthe oryzae
http://www.broad.mit.edu/annotation/genome/magnaporthe_grisea/

Saccharomyces cerevisiae
http://www.broad.mit.edu/annotation/genome/saccharomyces_cerevisiae/

GenBank at NCBI	http://www.ncbi.nlm.nih.gov/Genbank/index.html
Functional Domains	http://www.ebi.ac.uk/InterProScan/
SMART	http://smart.embl-heidelberg.de/
ClustalW2	http://www.ebi.ac.uk/Tools/clustalw2/index.html

2.6. Molecular cloning techniques

2.6.1. Extraction of plasmid DNA from *E. coli*

Plasmid minipreps were performed using one of the following commercially available kits according to manufacturer's recommendations: Invisorb Spin Plasmid Mini kit II #IV-10101402, Invitek, Berlin, Germany; PureLink High Pure MiniPrep Kit #K2100-10, Invitrogen, Paisly, UK or Qiaprep Spin MiniPrep kit #27106, Qiagen, Crawley, UK. Accordingly Plasmid Midiprep kits form the following suppliers were used: PureLink Hi Pure Plasmid Midiprep kit #K2100-04, Invitrogen, Paisley, UK; Genopure Plasmid Midi kit #03143414001, Roche, Welwyn Garden City, UK or Qiagen Plasmid Midi kit #12243, Qiagen, Crawley, UK. To avoid problems with EDTA in downstream applications, such as transformation, sequencing or side-directed mutagenesis, DNA was always eluted in 10mM Tris-HCl or dH_2O.

2.6.2. Extraction of genomic DNA from *N. crassa*

2.6.2.1. Phenol/chloroform extraction from fungal mycelia

The desired strain was inoculated onto VM overlaid with sterile cellophane (525 gauge uncoated Rayophane, A.A. Packaging, www.aapackaging.co.uk) and then incubated for 2-3 days at 30 °C and constant light until the mycelium covered the whole plate surface. For biomass harvest, the mycelium was carefully scrapped off the cellophane using a sterile spatula and transferred onto a double-layered 10 x 10 cm square of sterile Miracloth (#475855, Calbiochem, Merk KGaA, Darmstadt, Germany). Folded together in the middle then sandwiched between paper towels the fungal biomass was dry-pressed to remove as much liquid as possible. The dried flakes of mycelium were then transferred into liquid nitrogen in a pre-chilled mortar. Under constant addition of liquid nitrogen the biomass was ground to a fine powder, then transferred into 2 ml Eppendorf tubes already containing 600 µl of DNA extraction buffer (Table 2.20) plus 1.5 µl RNase (#19101, Qiagen; 10 ng/µl final concentration). After vigorous vortexing the mixture was incubated for 20 min at 65 °C in a heat block, and subsequently cooled down on wet ice for 5 min. To extract gDNA, 300 µl phenol and 300 µl chloroform/isoamylalcohol 49:1 mixture were sequentially added with vigorous vortexing in between and afterwards. Phase separation was achieved by centrifugation for 10 min at 12000xg at 4 °C. The upper aqueous phase containing the gDNA was carefully taken off with a pipette and transferred into a fresh 1.5 ml Eppendorf tube containing 600 µl chloroform/isoamylalcohol 49:1 mix. After repeated vigorous vortexing, the phases were again separated by centrifugation, and the upper aqueous phase transferred in a fresh 1.5 ml Eppendorf tube containing 0.8 vol. (600-650 µl) pre-chilled (-20 °C) isopropanol. DNA precipitation occurred during a 30 min or overnight incubation period at -20 °C. The precipitated gDNA was pelleted by centrifugation for 15 min at 14000xg and 4 °C. After discarding the supernatant and washing the pellet once

in 0.8 vol. (~800 µl) 75% EtOH, as much of the supernatant as possible was removed and the gDNA dried at RT for 5-10 min, before being resuspended in a suitable volume (typically 50-100 µl) of 10mM TrisHCl or dH_2O. Incubation of the sample for 15-20 min at 65 °C in a heat block helped to dissolve very thick pellets. Optionally, remaining RNA was digested by adding 1/10 of the solution volume (5-10 µl) RNase (10 µg/µl stock) to the sample and incubate for 2 h at 37 °C. Purified gDNA was stored at - 20 °C.

2.6.2.2. Quick gDNA extraction protocol

A time saving alternative which obtained sufficient amounts of biomass for the extraction of gDNA was used prior to genetic verification by PCR (section 2.7). This method allowed to process several strains in parallel without the need of laborious biomass grinding in liquid nitrogen. 500 µl of liquid VM, supplemented with selection marker if desired, were inoculated with a small drop of spore suspension of the desired strain, and incubated overnight at 30-35 °C. The next morning, the formed biomass was pelleted by centrifugation for 10 min at 12000xg and room temperature, and the supernatant medium was discarded. 500 µl of lysis buffer (Table 2.21) were added and the sample incubated for 1 h at 60 °C in a heat block. Optionally, final gDNA yield could be increased by shock-freezing the biomass pellet in liquid nitrogen prior to lysis. Subsequently, 250 µl phenol and 250 µl of a chloroform/isoamylalcohol 24:1 mix were added and the sample vigorously vortexted. DNA purification was performed as describe in the previous section.

2.6.3. Extraction of total RNA and cDNA synthesis

Total RNA was extracted from mycelial biomass grown as described in section 2.6.2.1, using the RNeasy Plant Mini kit (#74904, Qiagen, Crawley, UK) according to manufacturer's recommendations. To enrich mRNA for subsequent

cDNA synthesis the Oligotex mRNA Mini kit (#70022, Qiagen) was used, as well according to manufacturer's recommendations. To facilitate first strand cDNA synthesis 1 µl of Oligo(dT)$_{15}$ primer (20 ng/µl stock concentration) (#C1101, Promega Biosciences, Inc., Southampton, UK) were mixed with 2 µg of enriched mRNA and 17 µl dH_2O, and the mixture incubated for 5 min at 70 °C in a thermal cycler (Piko® Thermal Cycler, Finnzymes Instruments Oy, Espoo, Finland; www.finnzymes.com) to resolve secondary mRNA structures. After the melting step the mixture was quickly transferred onto wet ice for 10 min to allow annealing of Oligo(dT)$_{15}$ primers to polyA-tails of the linearized mRNA molecules. For reverse transcription (RT), 5 µl RT-buffer 5x, 1.25 µl dNTP mix (#U1511, Promega) 1 µl RNasin® Plus RNase inhibitor (#N2611, Promega) and 1 µl M-MLV Reverse Transcriptase (#M170A, Promega) were added to the mix. After gently flicking the tube to mix all components cDNA synthesis occured during a 1 h incubation period at 42 °C in the thermal cycler. A final heat-inactivation step of 15 min at 70 °C terminated the reaction. 1-2 µl of the cDNA solution provided sufficient amounts of cDNA template for subsequent cloning of *wt* gene loci by PCR amplification.

2.6.4. Restriction and analysis of pDNA

Restriction digests were performed according to the manufacturer's instructions for the enzymes used. Restriction enzymes were purchased from New England Biolabs (New England Biolabs Ltd., Hitchin, UK; www.neb.com) or Promega (Promega Biosciences, Inc., Southampton, UK; www.promega.com). DNA agarose gel electrophoresis was performed as described in Sambrook and Russel [45], using 100 bp and 1 kb DNA ladders (#N3231 and #N3231, NEB) as size standards. Ethidium bromide containing gels were run in BioRad MiniSubTM (BioRad Laboratories Ltd., Herts, UK) DNA cells at 5 V/cm then visualized using UV light.

2.6.5. DNA extraction and purification from agarose gels

DNA bands were excised from agarose gels, transferred to 1.5 ml Eppendorf tubes and weighed. DNA was then purified with one of the following gel extraction kits according to the manufacturer's recommendations: Invisorb Spin DNA extraction kit #IV-10201102, Invitek, Berlin, Germany; Wizard SV Gel and PCR Clean-Up system #A9281, Promega, Southampton, UK or QiaQuick Gel Extraction Kit #28704, Qiagen, Crawley, UK,. DNA was eluded in 10 mM Tris-HCl or dH_2O.

2.6.6. Ethanol precipitation of DNA

0.1 vol. 3M sodium acetate (pH 5.2) was added to the DNA solution in an Eppendorf tube. Two volumes of chilled (- 20 °C) EtOH were added and the DNA precipitated for 30 min at - 20 °C. Subsequently the mix was centrifuged at 13000 rpm and 4 °C for 30 min, and the supernatant removed. The DNA pellet was washed in 1 vol. of 70 % ethanol and centrifuged for 5 min at 13000 rpm at 4 °C. After discarding the supernatant the pellet was dried for 5-10 min at RT and resuspended in the desired volume of 10 mM Tris-HCl or dH_2O.

2.6.7. Preparation and ligation of DNA

DNA fragments for ligation were prepared by restriction digest, separated by agarose gel electrophoresis and extracted, as described in sections 2.6.4 and 2.6.5. To prevent re-ligation of the vector, linearized pDNA was dephosphorylated using Antartic phosphatase (#M0289, New England Biolabs Ltd., Hitchin, UK) which was then removed by EtOH precipitation as described in section 2.6.6. DNA was ligated using T4 DNA (HC) ligase (#M1794, Promega Biosciences, Inc., South-ampton, UK), according to the manufacturer's instructions. Prior to salt-sensitive applications the ligation mix was desalted by micro-dialysis using a hydrophilic membrane filter

(MF-Millipore filter, #VSWP02500, Millipore, Livingston, UK) floating on 5-10 ml dH_2O for 10-15 min. After desalting 5 µl of the ligation mixture were transformed into *E. coli* as described in section 2.9.2, and *E. coli* transformants were analysed by miniprep pDNA extraction (section 2.6.1) and restriction digestion (section 2.6.4). Seemingly correct clones were verified by DNA sequencing (section 2.6.10).

2.6.8. In-Fusion™ cloning

Alternatively to traditional cloning approaches, a restriction/ligation-independent mechanism for plasmid cloning was used. The In-Fusion™ Advantage PCR Cloning Kit (#63961, Clontech Laboatories, Takara Bio Europe, Saint-Germain-en-Laye, France) facilitated an *in vitro* gap repair mechanism to seamlessly combine up to 5 different inserts into one linearized vector fragment, mediated by 15 bp homologous sequence overlaps, in one reaction. The manufacturer's protocol recommendations were followed (http://www.clontech.com).

2.6.9. Measuring DNA/RNA quantity and quality

Quantity and quality of all DNA and RNA samples, including recovered pDNA, extracted gDNA, PCR products, DNA fragments after gel purification, or RNA and cDNA, were measured using the NanDrop ND-1000 spectrophotometer (www.nanodrop.com).

2.6.10. Primer design and DNA sequencing

Primers were supplied by Invitrogen (Invitrogen Ltd., Paisley, UK). DNA sequencing PCRs were performed using the BigDye® Terminator v3.1 Cycle Sequencing kit (#4337455, Applied Biosystems, Warrington, UK), and analysed by The GenePool Sequencing Service, Ashworth Laboratories, University of Edinburgh, Edinburgh, UK. Sequence analysis was performed using FinchTV

vers.1.4.0 software from Geospiza Inc., Seattle, USA, and the ClustalW2 online alignment tool (http://www.ebi.ac.uk/Tools/clustalw2/index.html).

2.6.11. Polymerase Chain Reaction (PCR) and multiplex PCR

Polymerase chain-reaction [36] (PCR) was used to amplify specific DNA sequences from cDNA, pDNA and gDNA for molecular cloning purposes, as well as for site-directed mutagenesis (SDM) (see section 2.6.13). Multiplex PCR [21], a variant using more than one primer pair per reaction, was used to incorporate an internal standard for each individual PCR, when genotyping *N. crassa* gene deletion strains (see section 2.7). All PCRs were performed in the Piko® Thermal Cycler (Finnzymes Instruments Oy, Espoo, Finland; www.finnzymes.com) according to manufacturer's recommendations, and using one of the following DNA polymerases: Phire® High-Fidelity non-proof-reading DNA polymerase (#F-120, Finnzymes), Phusion® High-Fidelity proof–reading DNA polymerase (#F-530, Finnzymes), GoTaq® Flexi non-proof-reading DNA polymerase (#M8301, Promega Biosciences, Inc., Southampton, UK) or *Pfu* High-Fidelity proof-reading DNA polymerase (#M7741, Promega).

2.6.12. PCR purification

To facilitate downstream applications, enzymes and unwanted buffer ingredients were removed from PCR reactions using one of the following commercial PCR purification kits according to manufacturer's recommendations: PCRapace kit, #IV-10202003, Invitek, Berlin, Germany; PureLink PCR Purification kit, #K3100-01, Invitrogen, Paisly, UK or QIAquick PCR Purification kit #28104, Qiagen, Crawley, UK.

A cheaper custom purification method was used, when the purity of the DNA was not a major concern. For this, 2.5 vol. of 96.5% EtOH were added to the PCR reaction and left for 10-15 min at -20 °C to precipitate all DNA (including primers!). After centrifugation for 10 min at 13000xg, 4 °C, the supernatant was removed and the pellet dried at RT for 5-10 min. Finally the purified DNA was resuspended in 20-25 µl 10mM Tris-HCl or dH_2O.

An alternative method used 0.1 vol. of 7.5 M ammonium acetate (NH_4CH_3COO, final concentration 2 M) plus 3 vol. of 96.5 % ice-cold EtOH to precipitate PCR products at pH 4 for 15 min at – 80 °C (or > 1h at – 20 °C). The DNA was pelleted by centrifugation for 10 min at 14000xg and the supernatant discarded. After washing the DNA pellet once in 70 % EtOH and a second centrifugation step, the pellet was dried for 5-10 min at RT, and then resuspended in a suitable volume of 10 mM TrisHCl or dH_2O. Advantage was that deoxyribonucleotide triphosphates (dNTPs) remain in solution, and thus are removed. (The same protocol was used with 3 M sodium acetate instead of ammonium acetate to precipitate pDNA from any solution; section 2.6.6).

2.6.13. Side-directed mutagenesis (SDM)

Individual nucleotides or triplets within the open reading frame (ORF) of a gene were exchanged by site-directed mutagenesis using pairs of mutagenesis primers containing 1-3 nucleotide mismatches. Typical features of the used oligonucleotides were: 25-40 nt length, mismatch in the middle of the primer, 50-60 % GC content, ideally no GC at the 3' end and a melting temperature of T_m > 80 °C, which was calculated using the following equation:

$$T_m = 81.5°C + 0.41 \times \%GC - (675/nt_{total}) - \%mismatch$$

with $\%mismatch = 100\% \times (nt_{mismatch} / nt_{total})$

Primers, dNTPs, 50-100 ng of template pDNA, polymerase buffer and *Pfu* DNA polymerase (#M7741, Promega Biosciences, Inc., Southampton, UK) were combined with dH_2O in a 50 µl PCR mix. The mutagenised pDNA was amplified with 30 sec/kb in 20 repetitions in a thermal cycler, according to the recommendations of the polymerase manufacturer. Prior to transformation of 5-8 µl of the 50 µl PCR mix into 200 µl of ultra-competent *E. coli* (2.9.2), methylated template pDNA was digested with 20 u of *Dpn*I restriction enzyme (#R0176, New England Biolabs Ltd., Hitchin, UK) for 2-3 h at 37°C.

2.7. Genetic verification of gene deletion strains by PCR

Exchange of the open reading frame (ORF) of the target gene by a knock-out (KO) cassette carrying the Hygromycin B resistance gene (*hph*) was accomplished by homologous recombination as describe in [9] and shown in Figure 2.1. All gene deletion strains generated by the NIH *Neurospora* Genome Project have been verified by Southern analysis as described in [24], and accordingly classified as homokaryotic or heterokaryotic transformants. Heterokaryons contain both wild type and deletion mutant nuclei, whereas homokaryons only contain gene deletion nuclei. Detailed information about all currently available KO strains from the FGSC can be found at:
http://www.dartmouth.edu/~neurosporagenome/knockouts_completed.html

Due to the high-throughput approach of the KO project and the considerable size of the FGSC collection (currently 10.462 gene deletion strains available), errors are inevitable and lead to false positive and false negative gene deletion strains being deposited. To verify the genetic make up of individual KO strains received from the FGSC, the absence of the wild type gene from and presence of the *hph*

cassette at the target locus, were analysed by PCR within this study. A schematic drawing of the PCR set up is shown in Figure 2.1.

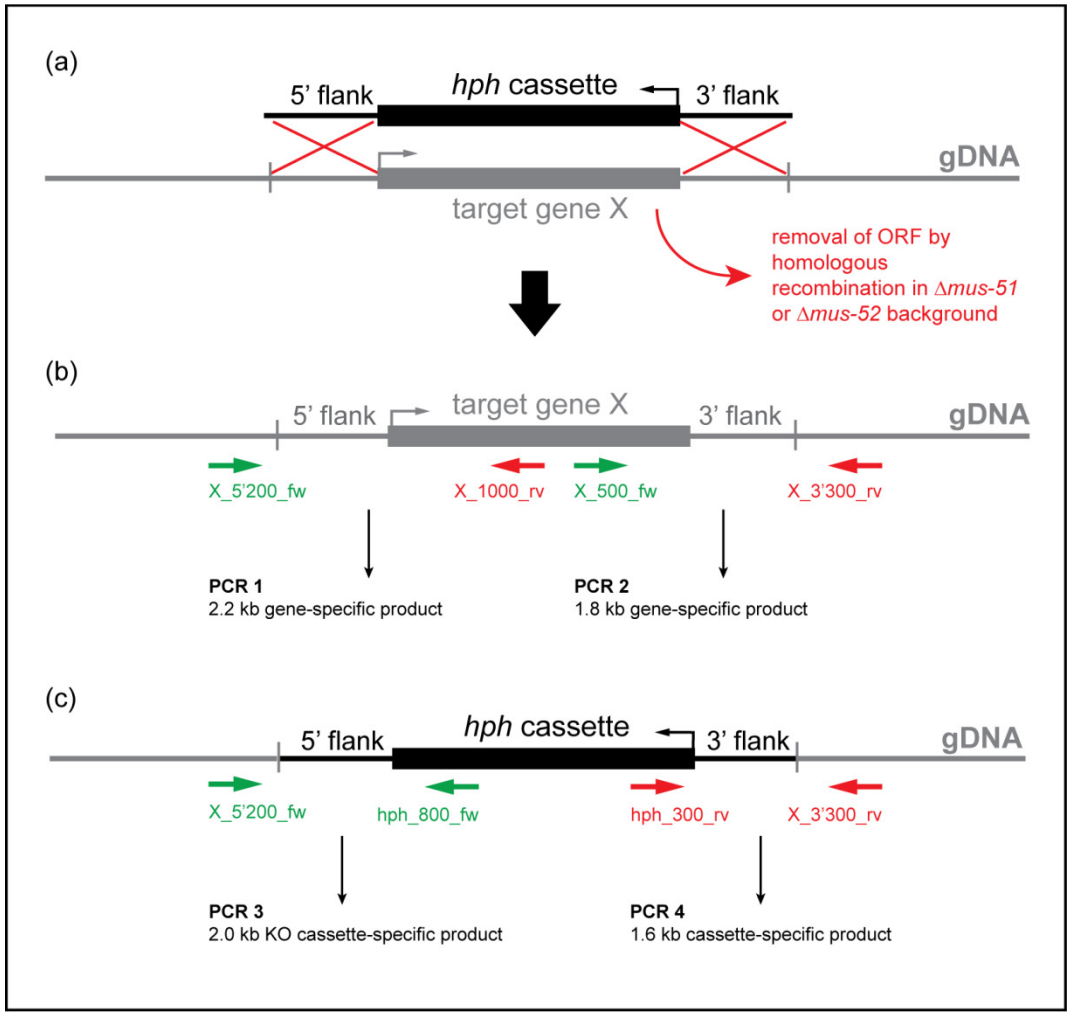

Figure 2.1 Generation and genetic verification of gene deletion strains in a nutshell. **(a)** Simplified representation of the gene deletion process by homologous recombination. The open reading frame (ORF) of the *hph* cassette and the target gene are in antisense. As macroconidia, which were used for KO cassette transformation, are multinucleate, gene deletion does not necessarily occur in all nuclei of a single spore. This may result in cells which contain both wild type and deletion mutant nuclei, therefore being Hygromycin B resistant but still expressing the *wt* target gene. **(b)** Presence of the target gene X in an individual strain is analysed using two gene-specific primers positioned inside the wild type ORF (X_1000_rv and X_500_fw) paired up with primers positioned outside of the 5' and 3' flank used for homologous recombination (X-5'200_fw and X-3'300_rv). In case, PCR 1 and PCR 2 result products of the predicted size, the target gene is still present in that strain. **(c)** Presence of the *hph* cassette in the target locus is analysed with primers specific for the cassette (hph_800_fw and hph_300_rv), paired up with the same primers outside of both flanks as described before. Analogous to (b), products from PCR 3 and PCR 4 confirm that

the *hph* cassette has been integrated into the correct location in the genome. Amplification products from PCRs 1-4 have relative size differences of at least 200 bp to one another, in order to facilitate differentiation after gelelectrophoresis. Green arrows represent forward primers, red arrows represent reverse primers. The *hph* cassette is oriented in antisense relative to the target gene locus. Therefore, in PCRs 3 and 4 seemingly non-matching primers are used, i.e. two forward and two reverse primers together.

In addition to the four PCRs shown, PCRs using primer pairs specific for the *mus-51* locus (NCU08290.3), the *mus-52* locus (NCU00077.3), and the *hph* resistance gene were carried out to verify if complementation of Δ*mus-51* and Δ*mus-52* deletions, respectively, has been accomplished by back-crossing to the wt, and to test whether the *hph* cassette might have been integrated somewhere else in the genome in case PCRs 3 and 4 would not produce expected signals. Furthermore, oligonucleotides binding within the actin locus (NCU04173.3) were added as second pair to each PCR tube to serve as internal positive control for each PCR, especially for those reactions where no signal was expected (e.g. PCR 1 and 2 in a homokaryotic KO). Finally, to probe for the presence of the targeted ORF somewhere else in the genome, a primer pair binding within the native gene sequence was included as well.

2.8. Homokaryon purification by single spore multiple passage isolation

To select conidia containing deletion mutant nuclei only from a heterokaryotic KO strain, single spore isolation was performed, either using macro- or microconidia. Micoconidia have the advantage to usually contain only one nucleus, whilst macroconidia are much more abundant and easier to harvest.

2.8.1. Homokaryon purification using macroconidia

The desired strain was grown on VM containing 200 μg/ml Hygromycin B until enough conidia have developed. Conidia were harvested in 1 ml sterile dH_2O

and adjusted by eye to yield a slightly cloudy, orange suspension. The spore suspension was diluted in two steps by first making a 1:100 dilution from the stock suspension and further diluting this 1:50. 150 µl of the final 1:5000 dilution were evenly distributed on fresh VM supplemented with Hygromycin B using glass beads, and subsequently incubated at 30 °C overnight. Developing monoconidial microcolonies were excised under the stereo microscope (section 2.12.1) using a sterile syringe needle and transferred into 5 ml capped tube slants containing 1 ml VM with Hygromycin B, loosely capped and sealed with micropore tape to allow aeration. Upon incubation at 30 °C and constant light for at least 48 h or until sufficient conidiation has occurred, the procedure was repeated 2-3 times or until prominent phenotype changes occurred. Strains that showed no phenotype changes were subjected to at least 5 isolation steps (some strains even up to 10) before gDNA was extracted (section 2.6.2) and potential changes in the genetic status were verified by PCR (section 2.7).

2.8.2. Homokaryon purification using microconidia

A weak macroconidial spore suspension was prepared as described in the previous section, but this time distributed on LSA (section 2.4.2) overlaid with sterile cellophane, as this has been found to promote development of microconidia. Plates were incubated at 25 °C for 5-7 days. Conidia were harvested from the colony in 2 ml dH_2O and passed through a syringe filter with a 5 µm size exclusion limit to enrich microconidia (2-3 µm average ∅) in the filtrate. This suspension was then plated out as described for multiple passage isolation of macroconidia (section 2.8.1) and microcolonies, which usually appeared after 2 days incubation at 25 °C, were isolated onto VM slants containing Hygromycin B and subsequently genetically validated by PCR (2.7).

2.9. Transformation of *E. coli*

2.9.1. Preparation of chemically ultra-competent *E. coli* cells

Chemically ultra-competent *E. coli* for heat shock transformation (section 2.9.2) were prepared as follows. An overnight 5 ml LB_{Tet} Top10 *E. coli* pre-culture supplemented with 100 µl 1 M $MgSO_4$ was used to inoculate 250 ml LB medium (Table 2.5) supplemented with 5 ml 1M $MgSO_4$ in a 2 l Erlenmeyer flask (20 mM $MgSO_4$ final), and grown at 23 °C and 250 rpm to an OD_{600} = 0.5. The cell suspension was transferred into sterile 500 ml centrifuge tubes and cooled down on wet ice for 10 min. In the meantime, enough 1.5 ml Eppendorf tubes were pre-chilled in the freezer. Chilled cells were pelleted by centrifugation at 6500xg and 4 °C for 10 min. The cell pellets were gently resuspended in 4 x 20 ml of ice-cold transformation buffer (TB) (Table 2.8) by swirling the bottles on ice, then left to rest for 10 min on wet ice, before centrifuging again for 10 min, 4 °C at 2000xg. After decanting the supernatant the cells were very gently resuspended in 4 x 5 ml ice-cold TB, pooled, and 1.5 ml of 7.5% DMSO were added. After incubating the mixture on ice for no longer than 10 min the cells were dispensed in 400 µl aliquots into pre-chilled (-20 °C) Eppendorf tubes using a multistep pipette and shock frozen in liquid nitrogen as quickly as possible; then stored at -80 °C until use.

2.9.2. Heat shock transformation and selection of *E. coli*

Amplification of plasmid DNA was performed by transformation of chemically competent *E. coli* strains (Table 2.4) using heat shock. In brief, a 50-200 µl aliquot of competent cells was slowly thawed on wet ice, and incubated with 8-12 ng of pDNA for 15-30 min. After a 45 sec heat shock at 42 °C in a water bath the cells were left on wet ice for 2 min, then recovered with 250-500 µl of pre-warmed

(42 °C) SOC medium (Table 2.7) and incubated for 45-60 min at 37 °C and 250 rpm. Cells were quickly pelleted (20 sec full speed in standard table top microfuge) and resuspended in 200 µl of fresh SOC. 50 and 150 µl were plated onto LB agar supplemented with the appropriate antibiotic (Table 2.6) and incubated at 37 °C overnight.

2.10. Transformation of *N. crassa*

2.10.1. Preparation of electrocompetent conidia

The desired strain was inoculated onto two VM agar plates (section 2.4.2.1) and incubated for 10-14 days at 25 °C and constant light or until sufficient conidiation has occured. Conidia were rinsed of the culture with 10-20 ml sterile water, collected in sterile 50 ml Falcon tubes and vigorously vortexed to break up conidial chains. The spore suspension was then passed through a sterile custom-made filter consisting of a Pasteur pipette filled with 0.5 cm thin strips of Miracloth (#475855, Calbiochem, Merk KGaA, Darmstadt, Germany) to separate out hyphal fragments and larger arthroconidia. After 10 min of centrifugation at 560xg and discarding the supernatant, macroconidia were washed twice in 20 ml ice-cold 1M sorbitol. Depending on the final pellet size the conidia were resuspended in 1-5 ml of ice-cold 1M sorbitol, and spore concentration determined using a Fuchs-Rosenthal cell counting chamber. Spore concentration was adjusted to $2.5x10^9$ cells/ml, and 50 µl aliquots of the spore suspension were dispensed into 1.5 ml Eppendorf tubes and, if not used immediately, frozen in liquid nitrogen and stored at -80 °C.

2.10.2. Electroporation and selection of *N. crassa* transformants

If not freshly prepared electrocompetent cells were used, a frozen 50 µl aliquote containing 2.5 x 10^9 cells/ml was slowly thawed on wet ice and washed twice with 500 µl of ice-cold 1M sorbitol, applying centrifugation steps of 20 sec at full speed in a standard table top centrifuge (~12.000-14.000xg) in between. The washed pellet was resuspended in ice-cold 1M sorbitol to a final volume of about 50 µl. 1-3 µg of ultra-pure DNA were added to the cells, briefly mixed, and left on ice for 15-30 min. Then 150 µl of ice-cold 1M sorbitol were added and the mixture was filled into a pre-chilled (-20 °C) 0.2 cm gapped electroporation cuvette (#Z706086-50EA, Sigma-Aldrich). Electroporation was performed in a BioRad Gene Pulser™ (BioRad Laboratories Ltd., Herts, UK) using the following settings: resistance 600 Ω, voltage 1.5 kV/cm and capacitance 25 µFd. Cells were immediately recovered by adding 800 µl of ice-cold 1M sorbitol, gently mixed by inverting the capped tube twice and placed back on ice.

For plating, 50–100 µl of electroporated conidia were added to 10 ml top agar – containing appropriate selection marker, if required - at 50 °C and poured onto a 20 ml bottom agar plate containing appropriate selection marker (Table 2.13). After the agar had set, plates were inverted and incubated at 25 °C until colonies appeared (usually after 2-3 days). Alternatively, 100 µl of a 1:10 dilution of electroporated conidia were directly spread onto bottom agar containing appropriate selection marker using glass beads, and incubated under identical conditions. Once individual colonies were visible they were analysed for expression of the fluorescent fusion protein under the fluorescence stereo microscope (section 2.12.1), and isolated onto small Petri dishes containing VM and incubated at 30 °C until conidiation. From these plates, conidia were harvested and germinated for 2-3 h in liquid VM (section 2.11.2), and expression level and localisation of the fluorescent fusion protein were analysed by widefield fluorescence microscopy (section 2.12.3). Depending on availability, at least 3-9 clones with identical

localisation pattern were replica 'plated' onto VM slants containing appropriate selection marker (Table 2.12) and put into long-term storage at 4 °C.

2.11. Sample preparation for live-cell imaging

2.11.1.1. Inverted agar block culture

For imaging mature hyphal colonies, strains were grown on solid agar medium as described in section 2.4.2.2. Using a sterile scalpel a quarter of the colony was excised, such that all developmental stages (colony centre to leading edge) of the extending mycelium were represented on the agar block. The agar was then inverted and transferred onto a droplet of liquid media on a large (48 x 64 mm #1.5, R.A. Lamb, www.ralamb.co.uk) glass coverslip (Fig. 2.2). During the preparation the hyphae suffer mechanical perturbation which can cause transient cessation of growth and apical swelling. Therefore, samples were placed on the microscope stage and allowed 10-30 min to recover and resume normal growth, indicated by rapid cytoplasmic bulk flow towards the colony edge. To prevent samples from drying out during longer time courses, the base from a plastic Petri dish, with a hole cut through the centre so as not to perturb the illumination, and containing a damp piece of filter paper was placed over the sample on the microscope stage. If required, liquid media was also refreshed from the side using a pipette.

For conidial germination assays, 200 µl of a 1 x 10^7 spores/ml stock solution (section 2.4.2.2) were evenly distributed onto VM agar plates using glass beads, and incubated at 30-35 °C. At desired time points 2 x 2cm agar blocks were cut out and mounted onto cover slips as described above. The technique was modified, when extra room beneath the agar was required (e.g. when observing bigger structures such as protoperithecia,), by supporting the agar on each side using strips of adhesive electricians insulation tape (Fig. 2.3).

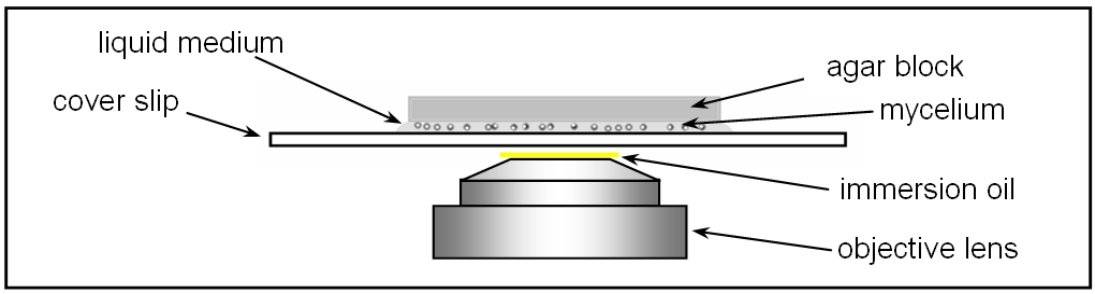

Figure 2.2 Inverted agar block culture method. Reproduced with permission from [58].

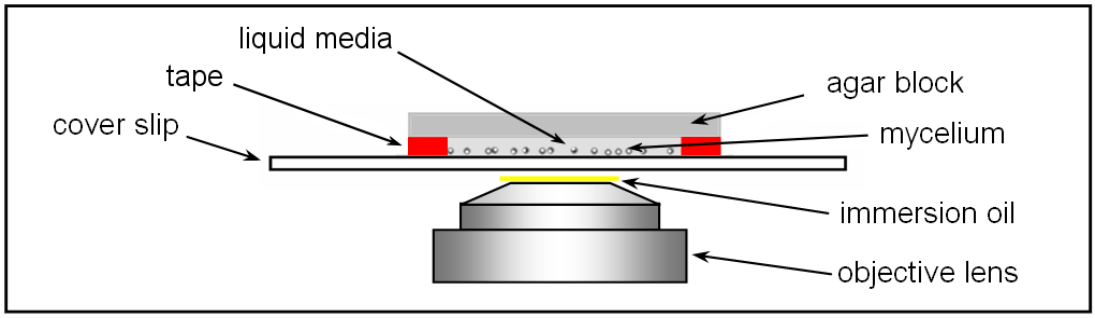

Figure 2.3 Modified inverted agar block method, using adhesive tape to raise the level of the agar providing extra room. Reproduced with permission from [58].

2.11.2. Liquid culture

Liquid culture techniques were commonly used in experiments monitoring the germination and fusion process of conidial germlings. A 1 x 10^7 spores/ml stock solution was prepared as described in section 2.4.2.2. 10-20 µl droplets of the spore solution were added to 180-190 µl of liquid VM into eight well slide culture chambers (Nalge Nunc International, www.nalgenunc.com), and incubated at 30-35 °C. In contrast to 'inverted agar' sample preparation, this type of culture made the application of biochemical inhibitors at any time point of the experiment much easier, as appropriate amounts of stock solution of the desired biochemical (Table 2.25) could simply be added into the medium. At selected time points the developmental stage of the cells was documented using DIC microscopy (section 2.12.2). Two reduce handling stress, usually two identical sample slides were prepared and used in an alternating manner.

2.11.3. Chemical gradient (halo) plate assays

An alternative method to assess effects of biochemical agents on spore germination and germling fusion was to prepare gradient agar plates. For this, 200 µl of a 1 x 10^7 spores/ml stock solution (section 2.4.2.2) of ungerminated conidia were evenly distributed onto VM agar plates using glass beads, and left open for about 10 min to dry. A 1.5 cm Ø filter disc was placed in the centre of the plate and soaked with 25 µl chemical solution (e.g. 4.9 M H_2O_2) and incubated at 30-35 °C for several hours. With time the drug or chemical diffused from the centre into the agar outwards establishing a radial gradient throughout the plate. At desired time points digital photographs of the whole plate were taken to document colony development. Biochemical agents that affected germination and cell fusion resulted in a gradient of developmental stages, with an area around the filter paper disc with no or severely impaired growth (halo), compared to areas further away from the drug source at which more growth occurred. Duplicates of these plates were also used to document the various stages of germling development in greater detail by DIC microcopy using the 'inverted agar method' (section 2.11.1).

2.12. Microscopy

A range of microscopy techniques were used throughout the study to enable enhanced visualisation of colony phenotypes and specific structures or organelles within conidial germlings and mature hyphae. For low-power magnification applications, such as assessment of general colony morphology or development of sexual fruitbodies, fluorescence stereomicroscopes were used (section 2.12.1). For higher-power visualisation of intracellular structures differential interference contrast (DIC) microscopy was used (section 2.12.2). Fluorescent dyes in combination with widefield fluorescence (section 2.12.3), including image restoration by deconvolution, (section 2.12.4) or confocal laser scanning microscopy

(CLSM; section 2.12.5) were used to further enhance the resolution of specific organelles or cellular processes, and to observe localisation and dynamics of fluorescent dyes and fusion proteins (sections 2.12.6 and 2.12.7). Often combinations of these techniques were applied, depending on the question addressed and system used. Apart from the Delta Vision RT system (section 2.12.4), Nikon TE2000-U Eclipse inverted microscopes (Nikon Inc., www.nikoninstruments.com) were used throughout the study, complemented by various extensions including different light sources, automated high-precision stages, confocal scanning heads, CCD cameras, etc., which are explained in detail where appropriate. For ultra-structural analysis of the 3D morphology and topography of conidial germlings and sexual fruitbodies low-temperature scanning electron microscopy (cryo-SEM; section 2.12.8) was used.

2.12.1. Stereomicroscopy

Two stereomicroscopes were used in this study. A Leica MZ 16F stereomicroscope (Leica Microsystems Ltd, Bucks, UK; www.leica-microsystems.com) with a magnifying range from 0.71x to 11.5x, and an attached Leica DFC300FX digital camera was used to assess the general colony morphology, monitor development of sexual structures, and for single colony isolation during homokaryon purification (section 2.8). Images were acquired with the implemented Leica QWin 3V software and stored in a lossless TIFF format.

Furthermore, a Nikon SMZ 1500 fluorescence stereomicroscope, with a magnifying range of 0.75x to 11.25x, and a mercury arc lamp excitation light source were used to assess expression of fluorescent fusion proteins within fungal colonies. GFP and TagRFP were visualized with a GFP (excitation 470/40 nm, 505 nm LP dichroic mirror, emission 530/40 nm) or a RFP (excitation 545/30 nm, 570 nm LP dichroic mirror, emission 620/60 nm) filter set, respectively, for the identification and isolation of fluorescent clones after transformation of *N. crassa* (section 2.10.2). It was also used to identify developing perithecia resulting from fertilization events

between two strains expressing different fluorescent markers. Images were acquired with Nikon ACT-1 software on a Nikon digital DXM 1200F colour camera and stored as TIFF files.

2.12.2. Brightfield and differential interference contrast microscopy

Standard light microscopy forms an image of an object based on its interaction with the transmission illumination passing through the sample (e.g. absorption, optical path differences and phase gradients). Prior to all experiments Köhler illumination [29, 30] was set up to ensure even illumination and maximal spatial resolution giving the best possible images for each sample and objective. Basic brightfield microscopy was usually set up with DIC to improve visibility of intracellular structures in the otherwise translucent cells and hypha of *N. crassa*.

DIC microscopy is a technique in which dual-beam interference optics are used to produce amplitude contrast in an image from local gradients in optical path length (a product of refractive index and thickness of an object through which light is travelling). The images produced are very distinctive for their shadow-cast, 3D-like appearance [38]. To implement DIC microscopy, in an inverted microscope, a polarizer and Wollaston prism are mounted in the condenser and complementary Wollaston prism slider and analyser are mounted beneath the objective lens. The sample is then focussed and DIC adjusted using the slider. A Nikon Plan Fluor 100× 1.4 N.A. DIC H oil immersion, a Nikon Plan Apo 60× 1.2 N.A. DIC H water immersion objective lens or a Nikon Plan Apo 20x 0.5 N.A. DIC M air objective were used, with their corresponding slider.

2.12.3. Widefield fluorescence microscopy

Fluorescence microscopy, in contrast to the techniques so far described, depends upon the presence of fluorescent molecules that when exposed to the appropriate excitation light will emit light of a longer wavelength [32, 38]. The plethora of recombinant fluorescent probes, chemical dyes and filter sets now available permit the visualisation of very specific molecules, organelles and cellular processes which can otherwise not be seen (a comprehensive overview on fluorescent labelling techniques can be found in [18]). Excitation light, from a mercury arc lamp, xenon arc lamp or more recently light-emitting diodes (LEDs), illuminates cells through the objective lens using epi-illumination. The same objective lens then functions to collect the emitted fluorescence light as it would in transmitted light microscopy. A filter set, constituting an excitation filter, a dichroic mirror and an emission filter serves to prevent any unwanted wavelengths of light reaching the detection device. High sensitivity CCD cameras, such as Hamamatsu ORCA® ER cooled CCD camera (www.hamamatsu.com) are then used to permit the limitation of the exposure to excitation light, which can be damaging to cells. The high contrast images produced have bright areas of fluorescence, corresponding to where the fluorescent probe is concentrated, on a black background. This allows for the selective imaging of cell components and cellular processes of interest. Either a standard Nikon mercury arc lamp (regulating the power with either an 8× or 4× neutral density filter), or a combination of the two, a Till Polychrome IV monochromator xenon arc lamp (www.till-photonics.com) or a CoolLED system (www.coolled.com) were used with a Nikon Plan Fluor 100× 1.4 N.A. DIC H oil immersion objective or a Nikon Plan Apo 60× 1.2 N.A. DIC H water immersion objective lens. For GFP, FM4-64 and Solophenyl Flavine imaging the Nikon B-2A filter cube was used, for dtTomato and TagRFP imaging the Nikon G-2A filter was used, and for imaging of Calcofluor White the Nikon UV-2A filter was used. All dyes used in this study are listed in Table 2.23.

To image GFP and TagRFP together, a Semrock BrightLine® GFP/DsRed-2X-A Dual-band filter (www.semrock.com) was used, with the two associated excitation filters for GFP and RFP separately fitted into the PE-2 collimator of the CoolLED unit. Together with fast-switching LED illumination alternating within 10 ms between 475nm (blue) and 550nm (green) excitation, this allowed quasi-simultaneous imaging of GFP and RFP on the whole chip of the attached EM-CCD Hamamatsu Orca camera.

Alternatively, the DualView2 (DV2) system (www.photometrics.com), a two-channel simultaneous-imaging system attached to the side port of the microscope, was used together with Semrock emission filters FF01-514/30-25 (GFP) and FF01-617/73-25 (RFP) and the same GFP/DsRed-2X-A Dual-band dichroic filter mentioned before, to allow simultaneous imaging of both channels under constant LED illumination at 475nm and 550nm. However, emission detection was limited onto half of the CCD chip for each channel. All used fluorescent filters are summarised in Table 2.22.

Table 2.22 Details of filter cubes used for widefield fluorescence microscopy.

Filter set	*Excitation filter*	*Dichroic mirror*	*Emission filter*
Nikon UV-2A	355/15 nm BP	400 nm LP	420 nm LP
Nikon B-2A	470/20 nm BP	500 nm LP	515 nm LP
Nikon G-2A	535/25 nm BP	565 nm LP	590 nm LP
Semrock GFP/DsRed-2X-A	470/22 nm BP 556/20 nm BP	500-529 nm 584-679 nm	512/25 nm BP 630/25 nm BP
Semrock for DV2	not required*	500-529 nm	514/25 nm BP
Semrock for DV2	not required*	584-679 nm	617/25 nm BP

* LEDs provide a very tight band of excitation light, therefore excitation filters are not required. Abbreviations: BP = band pass filter, LP = long pass filter

2.12.4. Deconvolution restoration microscopy

Deconvolution microscopy is a technique of processing image data, obtained on a highly automated widefield fluorescence microscope. A piezo-controlled stage drive allows the acquisition of optical z-sections with 0.2 μm precision. Detailed information on how the microscope system performs (e.g. exact shape and size of the point-spread function) is used to apply an iterative mathematical transformation that reassigns out-of-focus light to its point of origin, resulting in blur free confocal-like optical sections of the object. A DeltaVision RT system (Applied Precision, www.api.com) designed specifically for deconvolution microscopy and located in the Centre Optical Instrumentation Laboratory (COIL) of the University of Edinburgh, was used in this study. It consisted of an Olympus IX70 base (www.olympus.co.uk/microscopy/); Olympus Plan-Apo 100x 1.4 N.A. oil immersion objective; 75W HBO illuminator; Chroma Sedat Quad ET filter set (for GFP: excitation 490/20 nm, emission 528/38 nm; for RFP: excitation 545/30nm, emission 610/75 nm; Chroma Technology Corp., www.chroma.com); CoolSnap HQ EM-CCD camera (Photometrics, www.photomet.com); and SoftWorx software (Applied Precision) for image acquisition. Exposure times ranged from 200-400 ms. To acquire 3D (x,y,z) images, 30-40 optical sections were obtained at 0.2 μm steps. For 4D imaging (x,y,z and t), 10-15 optical sections were obtained at 0.4 or 0.5 μm steps and 30-120 s intervals. Images were processed through 10 iterative deconvolutions using implemented SoftWorx image processing and analysis software, and stored as TIFF files. Projections and further image processing were carried out with the MacBiophotonics package ImageJ 1.43b software (http://rsbweb.nih.gov/ij/).

2.13. Confocal microscopy

Confocal laser scanning microscopy (CLSM) allows the exclusion of fluorescent light emitted from parts of the sample above and below the focal plane

using an aperture (pinhole) in front of the detector, thereby increasing the resolution and contrast within an image [10, 41]. Confocal microscopy was performed using a Bio-Rad Radiance 2100 system (originally Bio-Rad Microscience, Hertfordshire, now Zeiss, www.zeiss.com) mounted on a Nikon TE2000-U Eclipse inverted microscope. GFP and FM4-64 were imaged after excitation with the 488 nm laser line of a 40 mW argon ion laser set to ≤ 15% and fluorescence detected at 510-560 nm and > 600 nm respectively. Staining of cell walls was performed by adding 0.12 μM Calcofluor White M2R (Sigma, Welwyn Garden, UK; prepared from a 1.2 M stock in ethanol) to macroconidial suspensions immediately after the conidia were harvested. Calcofluor White and GFP were imaged simultaneously by excitation with a 405 nm blue laser diode and 488 nm, respectively, and fluorescence detection at 420/7 nm (for Calcofluor White) and 500/30 nm (for GFP). A Nikon Plan Apo 60× 1.2 N.A. water immersion or a Plan Fluor 100× 1.4 N.A. DIC H oil immersion objective lens were used. Laser intensity and laser dwell time on individual germlings or hyphal compartments were kept to a minimum to reduce photobleaching and phototoxic effects. Simultaneous brightfield images were captured with a transmitted light detector. Time-lapse imaging was performed at 1-2 min intervals for periods of up to 30 min, or at longer time intervals for periods of several hours. Images were captured with a laser scan speed of 166 lines/sec and a resolution of 1024 x 1024 pixels using Lasersharp 2000 software (version 5.1; Bio-Rad Microscience), and stored as TIFF files.

2.13.1. Preparation of dyes for fluorescence microscopy

Fluorescent dyes (Table 2.23) were used as markers for specific cellular compartments and applied as liquid droplets of freshly made working solution either underneath the agar block when using the inverted agar method (section 2.11.1), or simply added to the cell suspension when working with liquid cultures

(section 2.11.2). Due to the limited solubility of most dyes in aqueous solution, stock solutions were prepared in the organic solvent dimethyl sulfoxide (DMSO), and further diluted when applied onto the cells to reach the final dye concentration. The DMSO concentration was always kept below 0.2% (w/v) in the final mix.

Table 2.23 Fluorescent dyes used in this study. FM4-64 (#T3166, Molecular Probes, Invitrogen), Solophenyl Flavine 7GFE 500 (#1485385V6, CIBA), Calcofluor White (#F3543, Sigma-Aldrich) and DAPI (#D1306, Molecular Probes, Invitrogen). Concentrations given are the final concentrations used on the cells; excitation and emission wavelengths given are those used for imaging, and not the excitation and emission maxima of the dyes.

Dye	*Selectivity*	*Conc. (µM)*	*Ex. (nm)*	*Em. (nm)*	*Mol. weight*
FM4-64	Membranes	2.5-10	488	> 600	608
Solophenyl Flavine	Cell wall	20	488	> 510	496
Calcofluor White	Cell wall	0.12	365	> 420	917
DAPI	Nuclei	0.3	359	> 420	277

FM4-64 = Frei Mao 4-64 [6], DAPI = 4',6-diamidino-2-phenylindole

2.13.2. Fluorescent proteins

Four different fluorescent proteins (FPs) were used in the course of this study to generate fusion constructs with target proteins. Table 2.24 briefly summarizes their characteristics.

Table 2.24 Fluorescent proteins used and produced in this study. More detailed information, e.g. on maturation time, brightness, photostability under laser illumination and fluorescence quantum yield of the individual fluorophores, can be found in the cited references.

Fluorescent protein	*Molecule type*	*Ex. max. (nm)*	*Em. max. (nm)*	*$t_{0.5}$ for bleach* (s)*	*Ref.*
sGFP (S65T)	monomer	488	507	174	[14, 20]
†TagRFP	monomer	555	584	>37	[3, 34], this study
†TagRFP-T (S162T)	monomer	555	584	>337	[48], this study
tdTomato	dimer	554	581	98	[47]

* Time to bleach to 50% emission intensity under arc-lamp illumination, at an illumination level that causes each molecule to emit 1,000 photons/s initially [48].
† Variant of TagRFP produced within this study by the addition of N- and C-terminal amino acids from GFP to increase its photostability and utility for 4D live-cell imaging.

2.13.3. Low-temperature scanning electron microscopy (cryo-SEM)

All samples for cryo-SEM were prepared and incubated identical to other applications described earlier (section 2.4.2), either on VM agar plates (mature hyphal colonies and conidial germlings) or SCM or LSA plates (development of protoperithecia) overlaid with sterile cellophane (525 gauge uncoated Rayophane, A.A. Packaging, www.aapackaging.co.uk). At desired time points ~ 12 mm² cellophane rectangles carrying the specimen were cut out and attached to the surface of a cryospecimen carrier (Gatan, Oxford, UK; www.gatan.com) with Tissue-Tek OCT compound (Sakura Finetek, Torrance, USA.) as an adhesive, and immediately cryofixed by plunging into subcooled liquid nitrogen. The specimen

carrier was transferred under low vacuum to the cold stage of a 4700II field emission scanning electron microscope (Hitachi, Wokingham, UK; www.hitachi-hitec-uk.com), where it was slowly warmed to –80 °C under continuous visual observation until surface ice had sublimated. After cooling back down to –120 °C, the specimen was returned onto the stage of the Gatan Alto 2500 cryopreparation system at –180 °C, and coated with ~10 nm of 60:40 gold-palladium alloy (Testbourne Ltd., Basingstoke, UK) in an argon gas atmosphere. The specimen was examined at about - 160 °C at a beam accelerating voltage of 2 kV, a beam current of 10 μA, and a working distances of 12 to 15 mm. Digital images were captured at a resolution of 2,560 x 1,920 pixels using in most cases the signal from the lower secondary electron detector, and saved as TIFF files.

2.14. Biochemical methods

2.14.1. Biochemical agents and inhibitors

A number of biochemical agents and inhibitors known to affect cell signalling (MAPK, TOR and ROS signalling pathways), cytoskeletal elements and the redox status of cells in general, have been tested for effects on germination and germling fusion in *N. crassa*. All chemicals have been applied by adding appropriate amounts of stock solutions to liquid germling cultures, prepared as described in section 2.4.2 and 2.11.2. Effects of H_2O_2 on spore germination and fusion have additionally been investigated using plate diffusion assays (halo assays; section 2.11.3). Developmental progress of the treated cells over time was qualitatively monitored by DIC microscopy (section 2.12.2) and quantitatively evaluated by cell counts, based on the acquired image data. All biochemical agents used within this study are listed in Table 2.25.

Table 2.25 Biochemical agents and enzymes used in this study.

Name	*Formula*	*Application*	*Concentr.*	*Ref.*
1NM-PP1	$C_{20}H_{21}N_5$	MAP kinase inhibitor	20 µM	[7, 8, 12]
benomyl	$C_{14}H_{18}N_4O_3$	microtubule inhibitor	8-10µM	[23, 44, 51]
latrunculin A	$C_{22}H_{31}NO_5S$	F-actin inhibitor	10 µM	[3]
rapamycin	$C_{51}H_{79}NO_{13}$	TOR inhibitor	0.2-1.2 µg/ml	[52]
NSC23766	$C_{24}H_{35}N_{73}HCl$	Rac1 inhbitor	50-200 µM	[16]
fMLP	$C_{21}H_{31}N_3O_5S$	NOX activation via Ca^{2+}	1 µM	[28]
PMA	$C_{36}H_{56}O_8$	NOX activation via PKC	0.8 µM	[28, 33]
DPI	$C_{12}H_{10}I.NO_3$	NOX inhibitor	20-200 µM	[11, 39]
NBT	$C_{40}H_{30}Cl_2N_{10}O_6$	$O_2^{\cdot-}$ indicator	0.05% (w/v)	[11, 37]
hydrogen peroxide	H_2O_2	ROS	0.1-50 µM	[15, 46]
potassium iodine	KI	H_2O_2 scavenger	1-20 mM	[46]
mannitol	$C_6H_{14}O_6$	$^{\cdot}OH$ scavenger	10-200 mM	[54]
Na-ascorbate	$C_6H_7NaO_6$	ROS scavenger	1-20 mM	[15, 25]
DMSO	$(CH3)_2SO$	$^{\cdot}OH$ scavenger	0.1-10%	[54]
catalase	Enzyme	H_2O_2 decomposition	1-200 u/ml	[27]
SOD	Enzyme	$O_2^{\cdot-}$ decomposition	1-200 u/ml	[43]

1NM-PP1= 1-(1,1-dimethylethyl)-3-(1-naphthalenylmethyl)-1H-pyrazolo[3,4-d]pyrimidin-4-amine, TOR = target of rapamycin, DPI = diphenyleneiodonium, NBT = nitroblue tetrazolium, NOX = nicotinamide adenine dinucleotide phosphate-oxidase, ROS = reactive oxygen species, fMLP = N-formylmethione-leucyl-phenylalanine, PMA = phorbol-12-myristate-13-acetate, PKC = protein kinase C, SOD = superoxide dismutase, DMSO = dimethyl sulfoxide.

2.14.2. Pholasin® chemiluminescence plate assays

To monitor levels of extracellular reactive oxygen species (ROS) during the time course of conidial germination and germling fusion, chemiluminescence assays were developed for *N. crassa*, using the chemiluminescent reporter protein Pholasin® (Knight Scientific Ltd, Plymouth, UK; www.knightscientific.com). Pholasin® is a thermostable 34 kDa photoprotein of the bioluminescent mollusc *Pholas dactylus*, and an ultra-sensitive detector of reactive oxygen species [26, 35], including extracellular superoxide generated by NADPH oxidases [27]. Pholasin® only releases photons from its light-emitting moiety Lucidalin® once when it

becomes irreversibly oxidised to oxypholasin by ROS. Thus, Pholasin® allows real-time measurements of increasing and decreasing ROS levels without the accumulation of background glow over time, as can be the case with fluorescent reporters. Pholasin® reacts with a broad range of ROS, including free radicals (superoxide anion, singlet oxygen, hydroxyl and ferryl radicals), as well as ROS generated by oxidants (hypochlorous and hypobromous acid, chloramines, bromamines and peroxynitrite) and peroxidases (horseradish peroxidise, myeloperoxidase, eosinophil peroxidase and others). Pholasin® exclusively measures extracellular ROS as it cannot cross the plasma membrane. It is most sensitive towards the superoxide anion ($O_2^{\cdot-}$), and does not react with hydrogen peroxide on its own. Hydrogen peroxide (H_2O_2) produced by cellular activity and released into the medium can be measured indirectly by adding peroxidases, such as horse radish peroxidase (HRP), into the assay buffer. The enzyme is converted by H_2O_2 into its active forms, compound I and II, which are subsequently able to oxidise Pholasin® generating signal in a concentration dependent manner [42].

Measurements were performed either on BMG FLUORstar Optima and LUMIstar Galaxy plate readers (BMG Labtech Ltd., Aylesbury Bucks, UK; www.bmglabtech.com), or on a BioOrbit 1251 tube luminometer (BioOrbit, Sweden) using various experimental set ups to adapt commercially available test kits (Knight Scientific, Plymouth, UK) to culture conditions of *N. crassa* (see below). Samples were prepared as triplicates, and data recording and analysis was performed with the implemented MARS software package and/or Microsoft Excel 2007.

2.14.2.1. Monitoring extracellular ROS levels in continuous cell cultures

White 96-well plates (flat bottomed 96 well opaque white 12.8 cm × 8.8 cm plates, Thermo Fisher Scientific, Loughborough, UK) were prepared with 50,000-150,000 cells/well in 190 µl liquid VM (section 2.4.2.1) and constantly maintained at

30°C in the plate reader. After 2 min/well background reading 10 µl of Pholasin® preconditioned in 0.1 M phosphate assay buffer (pH 6.5) were injected to yield a final concentration of 2.5 µg/ml in each well. Changes in extracellular ROS levels during germination and cell fusion were continuously measured by recording chemiluminescence signal (as relative light units; RLU) in comparison to cell-free controls over the following 5-6 h, and without any further perturbation of the system. At the end of the experiment 5 µl assay buffer containing 0.6 u superoxide dismutase (SOD) were injected into each well. The immediate drop of chemiluminescence signal demonstrated that superoxide anions and sufficient amounts of Pholasin® were still present to generate signal (adapted from ABEL® Superoxide Test kit, Knight Scientific Ltd.) Addition of the NOX inhibitor DPI (diphenyliodonium, 50-100 µM final) was used as negative control. All measurements were generally performed using triplicate samples, and were repeated at least once.

To test activation of NADPH-oxidases in conidial germlings the ABEL® Cell Activation kit (Knight Scientific, Plymouth, UK) was adapted for *N. crassa*. Briefly: liquid cell cultures were prepared and incubated in 96-well plates as described in the previous paragraph. Pholasin® (2.5-5 µg/ml final) and PMA (phorbol myristate acetate, 0.8 µM final) or fMLP (formylmethione-leucyl-phenylalanine, 1 µM final), both activators of NADPH oxidase, were reconstituted in either pre-conditioned Vogel's medium (VMpc) or 0.1 M phosphate buffer, and sequentially injected into the wells. Release of superoxide into the medium was measured over the following 20- 30 min. Additionally, the assay was adapted for the BioOrbit tube luminometer, which allowed a 4-times higher temporal resolution.

2.14.2.2. Measuring extracellular ROS/H_2O_2 in cell supernatant samples

Conidial spore cultures were prepared in 96-well plates as describe in the previous section, but kept in an extra incubator at 30 °C over the course of the experiment. To avoid potential problems with fluctuations in Pholasin® stability and availability over long time periods in continues culture, 100 µl of cell culture supernatant were removed from individual wells at desired time points and transferred onto fresh 96-well plates, then put into the plate reader. Alternatively, cell supernatant samples were collected into 1.5 µl Eppendorf tubes, shock frozen in liquid nitrogen and stored at – 80 °C until all measurements could be performed in one go. In any case, 5 µg/ml Pholasin® were reconstituted in 0.1 M phosphate buffer (pH6.5) and 180 µl injected into each well containing 20 µl sample. ROS levels in the cell supernatants were recorded in 2-10 min measurements and mean values of replicates plotted over time. This approach guaranteed that equal amounts of fresh Pholasin® and constant pH of the assay buffer were maintained throughout all measurements.

To measure the amounts of H_2O_2 in cell supernatants, cultures were prepared and samples collected as described in the previous paragraph, but this time the phosphate assay buffer contained 0.5 µg/ml Pholasin® and 0.1 u/ml HRP (#P-8250, Sigma). 20 µl sample/well were prepared in 96-well plates and 180 µl assay buffer were injected after baseline reading. Pre-incubation of Pholasin® and HRP together in assay buffer was required to establish a reaction equilibrium between both components, which otherwise would have distorted the first 30-60 sec of the actual measurement [27, 42]. As the reaction itself is extremely quick (peak after 1-2- sec) each measurement only lasted for 90 sec including a 30 sec baseline recording before injection of the reaction mix. The system was calibrated with 0-9 mM H_2O_2 solutions freshly prepared from phosphate-citrate-buffered (pH5) H_2O_2 tablets (#P-4560, Sigma). The biologically relevant concentrations of H_2O_2 for

germination and germling fusion have been determined in separate liquid culture and plate assays (section 2.11) to be between 25 μM-1 mM.

2.15. References

1. **Altschul, S. F., W. Gish, W. Miller, E. W. Myers, and D. J. Lipman.** 1990. Basic local alignment search tool. Journal of Molecular Biology **215:**403-410.
2. **Altschul, S. F., T. L. Madden, A. A. Schaffer, J. Zhang, Z. Zhang, W. Miller, and D. J. Lipman.** 1997. Gapped BLAST and PSI-BLAST: a new generation of protein database search programs. Nucleic Acids Research **25:**3389-3402.
3. **Berepiki, A., A. Lichius, J. Tilsner, and N. D. Read.** 2009. Live-cell imaging of the *Neurospora crassa* actin cytoskeleton. Eukaryotic Cell.
4. **Bertani, G.** 2004. Lysogeny at the mid-twentieth century: P1, P2, and other experimental systems. Journal of Bacteriology **186:**595-600.
5. **Bertani, G.** 1956. Studies on lysogenesis. I. The mode of phage liberation by lysogenic *Escherichia coli*. Journal of Bacteriology **62:**293-300.
6. **Betz, W. J., F. Mao, and S. C. B.** 1996. Imaging exocytosis and endocytosis. Current Opinion in Neurobiology **6:**365-371.
7. **Bishop, A. C., C.-y. Kung, K. Shah, L. Witucki, K. M. Shokat, and Y. Liu.** 1999. Generation of monospecific nanomolar tyrosine kinase inhibitors via a chemical genetic approach. Journal of the American Chemical Society **121:**627-631.
8. **Bishop, A. C., J. A. Ubersax, D. T. Petsch, D. P. Matheos, N. S. Gray, J. Blethrow, E. Shimizu, J. Z. Tsien, P. G. Schultz, M. D. Rose, J. L. Wood, D. O. Morgan, and K. M. Shokat.** 2000. A chemical switch for inhibitor-sensitive alleles of any protein kinase. Nature **407:**395-401.
9. **Colot, H. V., G. Park, G. E. Turner, C. Ringelberg, C. M. Crew, L. Litvinkova, R. L. Weiss, K. A. Borkovich, and J. C. Dunlap.** 2006. A high-throughput gene knockout procedure for *Neurospora* reveals functions for multiple transcription factors. Proceedings of the National Academy of Sciences of the USA **103:**10352-10357.
10. **Conchello, J.-A., and J. W. Lichtman.** 2005. Optical sectioning microscopy. Nat Meth **2:**920-931.
11. **Egan, M. J., Z. Y. Wang, M. A. Jones, N. Smirnoff, and N. J. Talbot.** 2007. Generation of reactive oxygen species by fungal NADPH oxidases is required for rice blast disease. Proceedings of the National Academy of Sciences of the USA **104:**11772-7.
12. **Fleißner, A., A. C. Leeder, M. G. Roca, N. D. Read, and N. L. Glass.** 2009. Oscillatory recruitment of signaling proteins to cell tips promotes coordinated behaviour during cell fusion Proceedings of the National Academy of Sciences of the USA **106:**19387–19392.

13. **Fleißner, A., S. Sarkar, D. J. Jacobson, G. M. Roca, N. D. Read, and N. L. Glass.** 2005. The *so* locus is required for vegetative cell fusion and postfertilization events in *Neurospora crassa*. Eukaryotic Cell **4:**920-930.

14. **Freitag, M., P. C. Hickey, N. B. Raju, E. U. Selker, and N. D. Read.** 2004. GFP as a tool to analyze the organization, dynamics and function of nuclei and microtubules in *Neurospora crassa*. Fungal Genetics and Biology **41:**897-910.

15. **Fry, S. C.** 1998. Oxidative scission of plant cell wall polysaccharides by ascorbate-induced hydroxyl radicals. Biochemical Journal **332:**507-515.

16. **Gao, Y., J. B. Dickerson, F. Guo, J. Zheng, and Y. Zheng.** 2004. Rational design and characterization of a Rac GTPase-specific small molecule inhibitor. Proceedings of the National Academy of Science of the USA **101:**7618-7623.

17. **Hanahan, D.** 1983. Studies on transformation of *Escherichia coli* with plasmids. Journal of Molecular Biology **166:**557-580.

18. **Haugland, R. P.** 2005. The Handbook: A guide to fluorescent probes and labeling technologies, 10th ed. Invitrogen, Molecular Probes Inc.

19. **Hays, S., and E. U. Selker.** 2000. Making the selectable marker *bar* tighter and more economical. Fungal Genetics Newsletter **47:**107.

20. **Heim, R., A. B. Cubitt, and R. Y. Tsien.** 1995. Improved green fluorescence. Nature **373:**663-664.

21. **Henegarin, O., N. A. Heerema, S. R. Dlouhy, G. H. Vance, and P. H. Vogt.** 1997. Multiplex PCR: Critical Parameters and Step-By-Step Protocol. BioTechniques **23:**504-511.

22. **Henikoff, S., and J. G. Henikoff.** 1992. Amino acid substitution matrices from protein blocks. Proceedings of the National Academy of Sciences of the USA **89:**10915-10919.

23. **Horio, T., and B. R. Oakley.** 2005. The role of microtubules in rapid hyphal tip growth of *Aspergillus nidulans*. Molecular Biology of the Cell **16:**918-926.

24. **Ivey, F. D., P. N. Hodge, G. E. Turner, and K. A. Borkovich.** 1996. The G alpha i homologue *gna-1* controls multiple differentiation pathways in *Neurospora crassa*. Molecular Biology of the Cell **7:**1283-1297.

25. **Kärkönen, A., and S. C. Fry.** 2006. Effect of ascorbate and its oxidation products on H_2O_2 production in cell-suspension cultures of *Picea abies* and in the absence of cells. Journal of Experimental Botany **57:**1633-1644.

26. **Knight, J.** 1997. The piddock and the immunologist. Immunology News **4:**26-31.

27. **Knight, J.** 1999. Reactions of Pholasin with superoxide and peroxidases: applications to cellular chemiluminescence, p. 251-254. *In* A. Roda, L. J. Kricka, and P. E. Stanley (ed.), Bioluminescence and chemiluminescence. Perspectives for the 21st century. John Wiley & Sons, Chichester, New York.

28. **Knight, J., and A. McCafferty.** 1997. Pholasin monitors neutrophil degranulation and activation, p. 334-337. *In* J. W. Hastings, L. J. Kricka, and P. E. Stanley (ed.), Bioluminescence and Chemiluminescence: molecular reporting with photons. John Wiley & Sons, Chishester, New York.

29. **Köhler, A. K. J. V.** 1893. Eine neues Beleuchtungsverfahren für mikrophotographische Zwecke. Zeitschrift für wissenschaftliche Mikroskopie und für mikroskopische Technik **10:**433-440.

30. **Köhler, A. K. J. V.** 1893. New method of illumination for photomicrographical purposes. American Monthly Microscopical Journal **14:**329.

31. **Kück, U., and B. Hoff.** 2006. Application of the nourseothricin acetyltrasnferase gene (*nat1*) as dominant marker for transformation of filamentous fungi. Fungal Genetics Newsletter **53:**9-11.

32. **Lichtman, J. W., and J.-A. Conchello.** 2005. Fluorescence microscopy. Nature Methods **2:**910-919.

33. **Meenan, B. J., J. McConnell, J. Knight, A. Boyd, and A. Bell.** 2002. Development of a sensitive whole blood chemiluminescence method for assessing the bioactivity of calcium phosphate powders. Biomaterials **23:**2431-2445.

34. **Merzlyak, E. M., J. Goedhart, D. Shcherbo, M. E. Bulina, A. S. Shcheglov, A. F. Fradkov, A. Gaintzeva, K. A. Lukyanov, S. Lukyanov, T. W. J. Gadella, and D. M. Chudakov.** 2007. Bright monomeric red fluorescent protein with an extended fluorescence lifetime. Nature Methods **4:**555-557.

35. **Michelson, A. M.** 1978. Purification and properties of Pholas dactylus luciferin and luciferase. Methods in Enzymology **57:**385-406.

36. **Mullis, K., F. Faloona, S. Scharf, R. Saiki, G. Horn, and H. Erlich.** 1986. Specific Enzymatic Amplification Of DNA *in-vitro* - The Polymerase Chain-Reaction. Cold Spring Harbor Symposia On Quantitative Biology **51:**263-273.

37. **Munkres, K.** 1990. Histochemical detection of superoxide radicals and hydrogen peroxide by *age-1* mutants of *Neurospora*. Fungal Genetics Newsletter **37**.

38. **Murphy, D. B.** 2001. Fundamentals of light microscopy and electronic imaging., 1st ed. Wiley-Liss, New York.

39. **O'Donnell, B. V., D. G. Tew, O. T. Jones, and P. J. England.** 1993. Studies on the inhibitory mechanism of iodonium compounds with special reference to neutrophil NADPH oxidase. Biochem Journal **290:**41-9.

40. **Pall, M. L., and J. P. Brunelli.** 1994. New plasmid and plasmid hybrid vectors and a Neurospora crassa genomic library containing the bar selectable marker and Cre/lox site-specific recombination system for use in filamentous fungi. Fungal Genetics Newsletter **41:**63-65.

41. **Pawley, J. B.** 1995. Fundamental limits in confocal microscopy, p. 19-37. *In* J. B. Pawley (ed.), Handbook of Biological Confocal Microscopy. Plenum Press, New York.

42. **Reichl, S., J. Arnhold, J. Knight, J. Schiller, and K. Arnold.** 2000. Reactions of pholasin with peroxidases and hypochlorous acid. Free Radical Biology and Medicine **28:**1555-1563.

43. **Reichl, S., S. Bernard, J. Arnhold, J. Schiller, and K. Arnold.** 1999. Factors inlfuencing the Pholasin chemiluminescence, p. 280-283. *In* A. Roda, L. J. Kricka, and P. E. Stanley (ed.), Bioluminescence and Chemiluminescence. Perspectives for the 21st century. John Wiley & Sons, Chichester, New York.

44. **Rossier, C., A. R. McDonald, and G. Turian.** 1993. Microtubular remnants in macroconidia of *Neurospora crassa* benomyl-induced to multipolar germination. Folia Microbiologica **39:**87-88.

45. **Sambrook, J., and D. W. Russell.** 2001. Molecular Cloning: A laboratory manual, 3 ed, vol. 1. Cold Spring Harbor Laboratory Press, Cold Spring Harbor, New York.

46. **Schopfer, P.** 2001. Hydroxyl radical-induced cell-wall loosening *in vitro* and *in vivo*: implications for the control of elongation growth. The Plant Journal **28:**679-688.

47. **Shaner, N. C., R. E. Campbell, P. A. Steinbach, B. N. G. Giepmans, A. E. Palmer, and R. Y. Tsien.** 2004. Improved monomeric red, orange and yellow fluorescent proteins derived from *Discosoma* sp. red fluorescent protein. Nature Biotechnology **22:**1567-1572.

48. **Shaner, N. C., M. Z. Lin, M. R. McKeown, P. A. Steinbach, K. L. Hazelwood, M. W. Davidson, and R. Y. Tsien.** 2008. Improving the photostability of bright monomeric orange and red fluorescent proteins. Nature Methods **5:**545-551.

49. **Staben, C., B. Jensen, M. Singer, J. Pollock, M. Schechtman, J. Kinsey, and E. U. Selker.** 1989. Use of a bacterial Hygromycin B reistance gene as a dominant selectable marker in *Neurospora crassa* transformation. Fungal Genetics Newsletter **36:**79-81.

50. **Tenney, K., I. Hunt, J. Sweigard, J. I. Pounder, C. McClain, E. J. Bowman, and B. J. Bowman.** 2000. *hex-1*, a Gene Unique to Filamentous Fungi, Encodes the Major Protein of the Woronin Body and Functions as a Plug for Septal Pores. Fungal Genetics and Biology **31:**205-217.

51. **Tognolli, M., A. Utz-Pugin, G. Turian, and C. Rossier.** 1998. Developmental abnormalities in benomyl-resistant strains of *Neurospora crassa*. Mycological Research **102:**869-875.

52. **Torres, J., C. J. Di Como, E. Herrero, and M. A. de la Torre-Ruiz.** 2002. Regulation of the cell integrity pathway by rapamycin-sensitive TOR function in budding yeast. Journal of Biological Chemistry **277:**43495-43504.

53. **Vogel, H. J.** 1956. A convenient growth medium for *Neurospora* (Medium N). Microbiology and Gentics Bulletin **13:**42-43.

54. **Vreeburg, R. A. M., and S. C. Fry.** 2005. Reactive oxygen species in cell walls, p. 215-249. *In* N. Smirnoff (ed.), Antioxidants and Reactive Oxygen Species in Plants. Blackwell, Oxford.

55. **Weld, R. J., K. M. Plummer, M. A. Carpenter, and H. J. Ridgway.** 2006. Approaches to functional genomics in filamentous fungi. Cell Research **16:**31-44.

56. **Westergaard, M., and H. K. Mitchell.** 1947. *Neurospora*. V. A synthetic medium favouring sexual reproduction. American Journal of Botany **34:**573-577.

57. **Wilson, R. A., and N. J. Talbot.** 2009. Under pressure: investigating the biology of plant infection by *Magnaporthe oryzae*. Nature Reviews Microbiology **7:**185-195.

58. **Wright, G. D.** 2007. Optical Tweezer Micromanipulation of Filamentous Fungi. University of Edinburgh, Edinburgh.

Chapter 3 – Functional comparative genomics for the identification of novel fusion mutants in *Neurospora crassa*

3.1. Abstract

This chapter will introduce the morphological and genetic basis of the functional comparative genomics screen performed between the rice blast fungus *Magnaporthe oryzae* and *Neurospora crassa* which led to the identification of novel cell fusion mutants in *Neurospora*. Signalling and enzymic pathways in which the candidate proteins are acting will be briefly summarized, and put into perspective of the pathogenic and non-pathogenic fungal lifestyle. Functional conservation between appressorium-mediated host penetration of *M. oryzae* and hyphal fusion in *N. crassa* was found to be focused on MAPK, Rho GTPase and redox signalling components. G-protein and cyclic AMP signalling were found to be non-essential for cell fusion in *Neurospora*, although known to be crucially important for appressorium maturation in the plant pathogen. The outcome of the comparative analysis also suggests that the analysis of upstream receptor components needs to be revisited in more detail.

3.2. Introduction

3.2.1. Infection structure development in *Magnaporthe oryzae*

The success of the rice blast fungus *Magnaporthe oryzae* [18] as a plant pathogen is strictly dependent on the formation of functional infection structures, called appressoria. They allow the fungus to gain access to the plant tissue and to spread invasively in the epidermal tissue of rice, millet and other commercially important grasses, thereby causing almost a million hectares annual crop loss worldwide [98]. Appressorium-mediated penetration and early stages of *in planta* growth of *M. oryzae* do not induce plant cell death. Therefore, the rice blast fungus is a classified hemibiotrophic pathogen [85], i.e. it switches from a biotrophic to necrotrophic life style during its development inside the host tissue. The prolonged biotrophic stage is characterised by a specialized extra-invasive hyphal membrane (EIHM) which provides a contact interface between invasive hyphae and the invaginated plasma membrane of cells of the plant epidermis [52]. This membrane interface appears to play a crucial role in evading or suppressing plant defence responses during penetration and *in planta* growth of the fungus [52]. During later stages of tissue colonisation, and coinciding with the appearance of lesions, the host's cells are finally killed by the action of fungal toxins and secreted lytic enzymes, which are most likely required to liberate large amounts of nutrients from the plant tissue and allow massive proliferation and production of mature spores [49]. To develop these highly specialized infection structures, conidia of the rice blast fungus undergo a series of complex morphogenetic differentiation processes [87, 90] which are schematically summarised in Figure. 3.1.

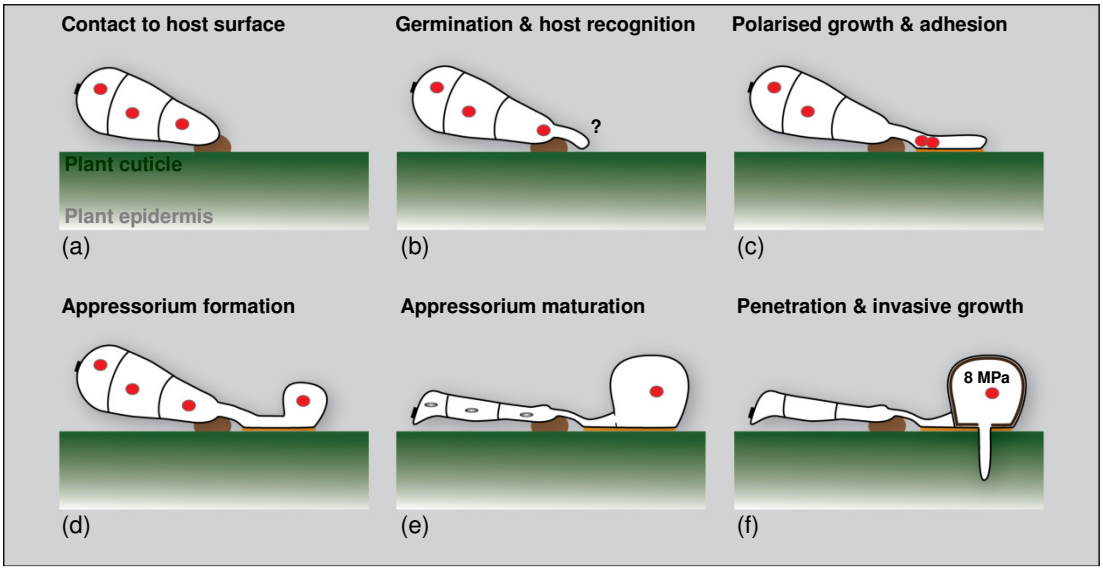

Figure 3.1 Appressorium-mediated host invasion of *Magnaporthe oryzae*. (a) The three-celled conidium anchors itself to the plant cuticle with pre-formed adhesives at the tip (brown). **(b)** In most cases the apical cell polarizes and protrudes a single GT which detects chemical and physical cues of the host surface. **(c)** On an inductive surface, such as the hydrophobic plant cuticle, the GT elongates by polarised tip growth, and secrets additional adhesives (orange) to establish firm contact. The nucleus (red) of the germinating cell migrates into the GT where it divides. **(d)** Eventually GT elongation arrests and tip growth switches to isotropic expansion leading to tip swelling and formation of the appressorium. One daughter nucleus travels into the incipient appressorium, the other nucleus migrates back into the conidium. **(e)** Upon autophagic cell death and recycling of the degradation products into the appressorium, it seals of and starts to accumulate glycerol to build up turgor pressure. **(f)** The appressorial wall becomes reinforced through the deposition of melanin and chitin, and a basal penetration pore is formed by localized cell wall degradation. The cell repolarises and translates the established 8 MPa of turgor pressure to pierce the emerging penetration hypha through the plant cuticle into the underlying epidermal cells, where it initiates invasive growth. See text for more details.

Soon after the three-celled conidium of *M. oryzae* has landed on a putative host it becomes firmly attached to the plant cuticle by its sticky extracellular matrix (ECM) [90], and by releasing pre-formed, adhesive spore tip mucilage (STM) [39, 43]. Free water on the leaf surface is sufficient to re-hydrate the conidium and trigger cell polarisation leading to the outgrowth of a single GT [90] which in most cases emerges from the apical cell [47]. Upon perception of a suitable hydrophobic surface [3], the GT elongates in a polarised fashion over the plant cuticle to which it attaches itself with secreted adhesives. The nucleus of the germinating cell migrates into the GT where it divides [92]. Arresting GT elongation and switching to

isotropic growth, the GT tip swells and differentiates into a domed-shaped rigid cell, the appressorium. One daughter nucleus moves into the incipient appressorium while the other returns into the conidium triggering autophagic cell death, which marks an essential check point for appressorium maturation [92]. Material from the degrading conidium is recycled into the developing appressorium before it completely seals of and becomes an independent cellular unit. The appressorium 'glues' itself to the leaf surface and accumulates glycerol to build up the extremely high internal osmotic pressure (> 8 MPa) required to provide the penetration force for host tissue invasion [19, 42, 88]. Cell wall remodelling including deposition of melanin and chitin within the inner layer of the appressorial wall is essential for the cell to generate and withstand high internal pressure, and to translate this into penetration force [9, 15, 19]. Localized cell wall remodelling, including degradation, forms a penetration pore at the appressorial base. The cell repolarises and protrudes an actin-filled penetration peg from that pore, which physically pierces through the cuticle and plant cell wall into the leaf epidermis [8]. Secreted cell wall degrading enzymes facilitate penetration, but are not essential [8, 9]. Inside the plant tissue, but still enveloped by the EIHM [52], the peg differentiates into primary and secondary infection hyphae to enter the *in planta* growth phase of its life cycle.

3.2.2. Major signalling pathways required for rice blast pathogenicity

Developmental progression from the ungerminated spore to a functional appressorium and the establishment of invasive growth is regulated by a complex network of signalling pathways, inlcuding G-protein signalling, the cyclic AMP (cAMP) response pathway, mitogen-activated protein (MAP) kinase signalling and

redox signalling mediated by NADPH-oxidase (NOX)-derived reactive oxygen species (ROS) [25, 98].

G-protein signalling. Host surface recognition is thought to be mediated via G-protein signalling involving the G-protein-coupled receptor (GPCR) Pth11 which contains a conserved fungi-specific extracellular-membrane spanning domain (CFEM domain) [22] and the G-protein α and β subunits MagA, MagB and Mgb1, respectively [62, 68], as potential downstream effectors. Deletion mutants in all these genes fail to initiate appressorium development from the undifferentiated GT, and are therefore non-pathogenic. This defect can be remediated in Δ*magB* through the addition of exogenous cAMP [62], indicating that external signal cues activate the cAMP response pathway to trigger appressorium morphogenesis and maturation (Fig. 3.2A).

cAMP response pathway. Deletion of the *Magnaporthe* adenylate cyclase Mac1 also results in mutants which cannot form appressoria and can be rescued by adding exogenous cAMP [14]. Deletion of the downstream acting cAMP-dependent protein kinase A (PKA) catalytic subunit CpkA, furthermore results in delayed formation of small, but non-functional appressoria [65, 102]. Interestingly, Δ*cpka* mutants are able to cause disease after wound inoculation, indicating that PKA activity is not required for invasive growth within the plant tissue. Together, this data indicates that activation of the cAMP response pathway is important for the maturation of infection-competent appressoria, but that it is not the only pathway regulating appressorium formation (Fig. 3.2A). G-protein signalling has been suggested as one possibility to provide a functional link between cAMP and MAPK signalling during appressorium initiation and maturation [102].

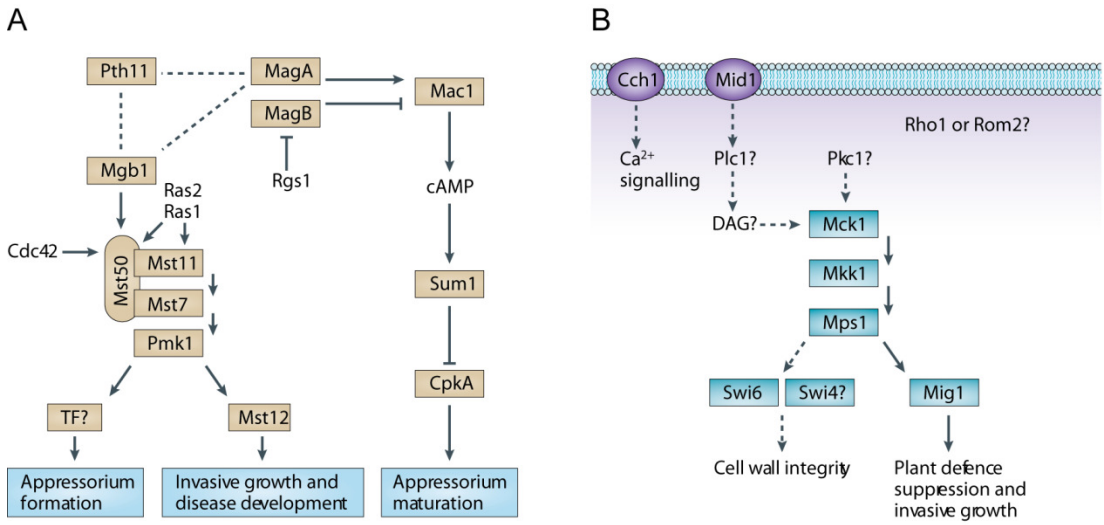

Figure 3.2 Signalling pathways involved in appressorium formation and invasive growth of *Magnaporthe oryzae*. (A) The fungus perceives the hard, hydrophobic rice leaf surface, which induces appressorium formation. The Pmk1 MAPK module is tethered by the Mst50 scaffold protein, and constitutes a phosphorelay that culminates in movement of the phosphorylated Pmk1 MAPK to the nucleus to activate transcription factors (TFs), such as Mst12. Activation of the Pmk1 pathway involves Ras proteins, Cdc42 and the Gβ-subunit protein Mgb1. Crosstalk with the cAMP pathway may occur through the Gα-subunit protein MagB. The cAMP response pathway seems to be regulated by the G-proteins MagA and MagB, which potentially interact with the Pth11 G-protein-coupled receptor. Adenylate cyclase Mac1 causes the accumulation of cAMP, which binds to the regulatory protein kinase A subunit Sum1, allowing detachment of the catalytic subunit CpkA. **(B)** Mps1 is necessary for penetration peg formation and plant tissue colonization. The transcription factor Mig1 is activated by Mps1 and is necessary for invasive growth and plant defence suppression. Activation of the Mps1 pathway occurs through calcium channel proteins (Cch1 or Mid1) or protein kinase C (PKC). Solid lines denote physical or genetic interactions that are supported by experimental evidence. Dotted lines denote tentative interactions that require further experimental testing. DAG, diacylglycerol. Taken from [98].

Pmk1 MAPK signalling pathway. Deletion mutants of the pathogenicity MAP kinase Pmk1 respond to inductive surfaces and the addition of exogenous cAMP with the production of swollen GT tips [102], indicating that host surface recognition via GPCRs and cAMP signalling is active and also transduced into the MAPK pathway of *Magnaporthe*, which is equivalent to the budding yeast pheromone response (PR) pathway. However, Δ*pmk1* mutants, as well as mutants of upstream components in this pathway, including Mst11 (MAPKKK), Mst7 (MAPKK) and their scaffold protein Mst50, are unable to differentiate appressoria

and non-pathogenic even after wound inoculation [101, 105, 106]. Interestingly, the associated downstream transcription factor Mste12 appears not to be required for appressorium formation and only has a role during invasive growth and disease development [72]. This places the Pmk1 MAPK signalling pathway at a central position for the initiation of appressorium morphogenesis, but also indicates a gene regulatory function during post-penetration processes (Fig. 3.2A).

Mps1 MAPK signalling pathway. Mck1 (MAPKKK) and Mps1 (MAPK) resemble components of the 'cell wall integrity' (CWI) pathway, and are dispensable for appressorium formation, but required for penetration peg formation and invasive growth of *Magnaporthe* [48, 101]. Conserved defects in cell wall biogenesis leading to increased autolysis in non-pathogenic deletion mutants of these genes emphasises that extensive cell wall remodelling is required for polarisation and protrusion of the penetration hypha. Interestingly, the recently identified MADS-box transcription factor Mig1, which might act as terminal phosphorylation target of Mps1, was shown to be dispensable for invasive growth and did not cause autolysis or overt cell wall defects when deleted [64]. Therefore, signalling through the Mps1 MAPK pathway is essential for the penetration and post-penetration phase of the infection process (Fig. 3.2B). Its function is to maintain cell wall integrity during host colonisation, including penetration and invasive growth, and to regulate gene expression during plant defence suppression via the transcription factor Mig1.

Redox signalling. Generation of ROS by the NADPH-oxidases Nox1 and Nox2 of *M. oryzae* has recently been found to be essential for appressorium function [26]. Similar to mutants of the CWI pathway, Δ*nox1* and Δ*nox2* mutants differentiate appressoria, but are unable to penetrate and colonize the host tissue, even when inoculated into wound sites. ROS serve a plethora of cellular functions [11, 84], but in this context might be important to promote oxidative cross-linking of cell wall polymers during appressorium maturation and protrusion of penetration hyphae [98]. Additionally, they might regulate the activity of infection-related proteins by reversible oxidation of thiol groups [25, 41]. How NOX activity is regulated in

Magnaporthe is currently unknown, but most likely involves the NOX regulator NoxR and the small GTPases Rho3 and Rac1 [26, 107].

Taken together, our current understanding places GPCR-mediated host surface recognition at the start of the differentiation process. Generated signals are transduced inside the cell via G-proteins which activate the Pmk1 MAPK cascade and the cAMP response pathway to initiate appressorium formation and maturation during the pre-penetration phase. The Mps1 MAPK cascade then triggers cell wall remodelling processes to reinforce the appressorial wall and allow the formation and protrusion of penetration hyphae. Cell wall remodelling during this crucial step of host cell entry is promoted by the action of NADPH-oxidase-derived ROS. Morphogenetic and functional changes required to enter the post-penetration phase, including differentiation of invasive hyphae and activation of infection-related proteins, such as plant defence suppressors, are transcriptionally regulated by Mig1 and Mste12 (activated through Pmk1 and Mps1 MAPK cascades), and potentially modulated in their activity by redox modification via ROS. Besides these five fundamental signalling pathways, a variety of other key players with vital roles during the appressorium-mediated infection process, have been identified. Those include up- and downstream effectors of the introduced pathways, such as calcium and PKC signalling, a great number of metabolic and structural proteins, and factors involved in cell cycle regulation. Very recent transcriptome analysis also revealed that protein degradation and amino acid metabolism are essential for appressorium formation and subsequent infection [69]. A more complete picture can be obtained from a number of excellent reviews [12, 20, 21, 69, 85, 90, 98, 100].

3.3. Results

3.3.1. Functional overlap between appressorium-mediated host infection by *M. oryzae* and hyphal fusion in *N. crassa*

Neurospora crassa and *Magnaporthe oryzae* resemble the ideal model pair to study molecular details of vegetative hyphal fusion and appressorium-mediated infection. Despite different lifestyles, these fungi are closely related [34], making the comparison between pathogen and non-pathogen a highly valuable investigative tool. Morphogenetic transitions leading from the ungerminated spore to the infection-competent appressorium in *M. oryzae* (section 3.1), and developmental stages taken during CAT-mediated cell fusion and hyphal fusion in the mature colony of *N. crassa* (sections 1.4 and 1.5), share a number of basic features in common (Table 3.1), and suggested that the underlying molecular machineries might be conserved between both species. Assuming significant morphogenetic and molecular overlap between both processes, one aim of this study was to assess the utility of *M. oryzae* as a functional model to facilitate the identification of novel cell fusion mutants in *N. crassa*.

Table 3.1 Morphogenetic features shared between appressorium-mediated infection of *M. oryzae* and hyphal fusion *N. crassa*. Although some processes are used for different purposes, especially the final stages of penetration and membrane fusion, respectively, the overlap of underlying cellular processes in both species is significantly large.

Process	***M. oryzae*** (host infection)	***N.* crassa** (cell fusion)
Cell polarisation	germination and outgrowth of a GT	induction/protrusion of a CAT or fusion hyphae
Recognition	perception of inducible host surface	recognition of fusion competent partner
Directed growth	GT elongation across plant cuticle	directed growth (homing) towards fusion partner
Tip depolarisation	tip growth arrest and switch to isotropic tip expansion leading to appressorium formation	contact-induced tip growth arrest of CATs and fusion hyphae, and tip swelling of fusion hyphae
Attachment	adhesion of GT and incipient appressorium to plant cuticle	secretion of adhesives to stabilise contact between fusing tips
Cell wall remodelling	remodelling and fortification of the appressorial wall and localized chitin degradation during penetration pore formation	localized chitin degradation during fusion pore formation and cell wall remodelling during fusion pore expansion
Membrane	membrane interface between fungal EIHM* and plant plasma membrane	plasma membrane merger to achieve cytoplasmic continuity

* EIHM = extra-invasive hyphal membrane [52]

The tractability of both genomes from this model pair [7, 21, 33, 103] enabled us to very specifically investigate cellular processes and concentrate on only hundreds of gene targets presumably involved in hyphal fusion rather than non-specifically screen thousands. To utilise the full potential of structural genomic information and perform a functional comparative genome analysis [40] of selected proteins from both species, pathogenicity associated genes of *M. oryzae* were identified in the *N. crassa* genome using BLASTp alignment (section 2.5). Additional comparison with the *S. cerevisiae* genome helped to map identified genes onto known signalling pathway models, as shown for the highly conserved MAPK

signalling cascades in Table 3.2. Interestingly, initial genomic comparison showed that *Neurospora*'s genome sequence contains numerous genes similar to those required by fungal pathogens for infection of humans or plants [7]. Strikingly, orthologs of a number of genes that have no other known function except in pathogenesis of the rice blast fungus *M. oryzae* [21], are present in the genome of *N. crassa* [33]. Thus, although *N. crassa* has a truly saprotrophic lifestyle, i.e. it exclusively feeds on dead and decaying matter, the genome sequence has revealed many genes with similarities to those required for pathogenicity, emphasising the close evolutionary relationship of both species.

Table 3.2 Alignment of proteins constituting MAPK signalling cascades in *M. oryzae*, *N. crassa* and *S. cerevisiae*.

	M. oryzae			***N. crassa***			***S. cerevisiae***	
Class of protein	**Name**	**MGG locus no.***	**e-value**	**Name**	**NCU locus no.***	**e-value**	**Name**	**SCRG locus no.***
Yeast pheromone-response (PR) pathway								
MAPKK Kinase	**Mst11**	12855.6	0.0	**NRC-1**	06182.3	1.0e-15	**Ste11p**	04305.1
MAPK Kinase	**Mst7**	00800.6	0.0	**MEK-2**	04612.3	0.0	**Ste7p**	00652.1
MAP Kinase	**Pmk1**	09565.6	0.0	**MAK-2**	02393.3	0.0	**Fus3p/Kss1p**	02978.1
transcription factor	**Mst12**	12958.6	0.0	**PP-1**	00340.3	0.0	**Ste12p**	04797.1
Yeast cell-wall-integrity (CWI) pathway								
MAPKK Kinase	**Mck1**	00883.6	0.0	**MIK-1**	02234.3	0.0	**Bck1p/Slk1p**	03576.1
MAP/ERK Kinase	**Mkk1**	06482.6	0.0	**MEK-1**	06419.3	0.0	**Mkk1p/Mkk2p**	01617.1
MAP Kinase	**Mps1**	04943.6	0.0	**MAK-1**	11376.3	0.0	**Slt2p/Mpk1p**	04738.1
Yeast high osmolarity glycerol (HOG) pathway								
MAPKK Kinase	**Wis4**	00183.6	0.0	**OS-4**	03071.3	0.0	**Ssk2p/Ssk22p**	03112.1
MAPK Kinase	**Pbs2**	10268.6	0.0	**OS-5**	00587.3	0.0	**Pbs2p**	03546.1
MAP Kinase	**Osm1**	01822.6	0.0	**OS-2**	07024.3	0.0	**Hog1p**	05095.1

* Locus numbers of the Broad MIT genome annotation (www.broad.mit.edu/annotation/genome).

3.3.2. Target loci identified by functional comparative genomics

As a result of the functional genomic comparison performed between *M. oryzae* and *N. crassa*, a list of 75 potential candidate proteins was compiled and extended to 110 by incorporating related genes, i.e. components of the same pathway or proteins believed to be involved in similar cellular processes. For 85 of these, gene deletion strains of *N. crassa* were or became available from the FGSC during the course of this project (section 2.2.1). Together with a number of control strains, including already published fusion mutants (e.g. components of the MAPK PR pathway) and known fusion competent KOs (e.g. components of the GPCR pheromone receptor complex), as well as strains of genetic backgrounds in which the KOs have been produced (Δ*mus-51* and Δ*mus-52*), and strains of both mating types of the same gene deletion, the list of *Neurospora* KO strains subjected to phenotypic analysis finally contained 125 strains comprising 98 different gene loci (Table 2.1, section 2.2.1).

3.3.3. Identification of fusion mutants

Live-cell imaging (section 2.12) was used to screen obtained gene deletion mutants of *N. crassa* for cell fusion defects at two developmental stages: CAT-mediated cell fusion between conidial germlings (section 1.4) and vegetative hyphal fusion (VHF) between specialized fusion hyphae in the subperiphery of the mature colony (section 1.5). Samples were prepared as described in sections 2.4.2.2. and 2.11.

Vegetative hyphal fusion defects cause 'chaotic' tip growth in the mature colony. Fusion competent strains established an organised and ordered hyphal network in the subperipheral zone, whereas fusion defective mutants were unable

to form an interconnected hyphal network and commonly produced mycelia that were disorganized and chaotic (Fig. 3.3).

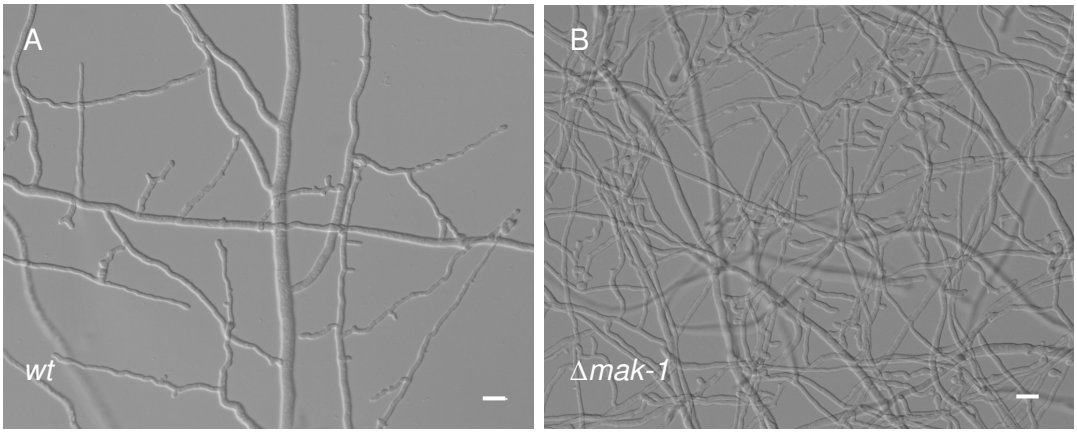

Figure 3.3 Architecture of the *N. crassa* mycelium in the subperiphery after 12 h incubation at 30 °C on solid Vogel's medium. (A) Hyphal tips of the wt strain arrested tip growth prior to fusion, resulting in the establishment of an ordered, interconnected hyphal network. **(B)** The fusion defective Δ*mak-1* mutant displayed a chaotic mycelial organization as hyphae were not restricted in polarised elongation. Scale bars, 50 µm.

Interacting hyphal tips in the wt colony showed the typical features of successful fusion: contact-induced tip growth arrest, tip depolarisation leading to tip swelling, formation of fusion pores by localized cell wall breakdown and establishment of cytoplasmic continuity (Fig. 3.4). Whereas, in fusion defective KO mutants, as for example Δ*mek-2*, hyphal tips continued polarised tip growth upon contact, did not depolarise (no tip swelling) and did not attempt to establish fusion connections (Fig. 3.4).

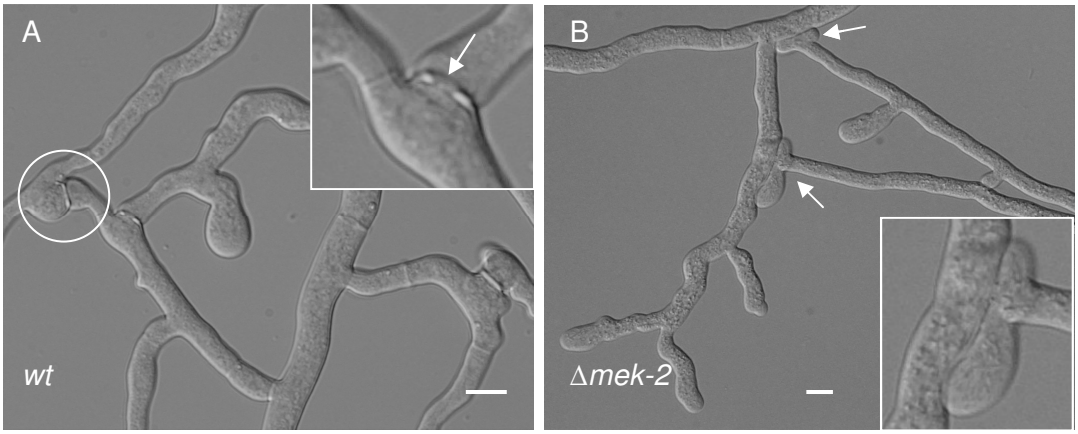

Figure 3.4 Touch sensing potentially induces hyphal fusion. (A) VHF connections in the wt colony. Upon contact, interacting hyphal tips arrested tip growth switching from polarised to isotropic expansion (circle). Cell wall remodelling and localized breakdown form the fusion pore which often can be identified as a gap between the tightly attached cell walls (arrow in inset). **(B)** Contacting fusion hyphae of Δ*mek-2* mutant did not respond with morphogenetic changes upon hyphal contact and did not attempt to establish fusion connections. Hyphal tips continued polarised tip growth (inset). Scale bars, 10 µm.

Vegetative hyphal fusion defects cannot be rescued by the wt. To test whether putative fusion defects in KO strains could be rescued by the wt, VHF was assessed in compatible confrontations between fusion mutants and wt strains expressing the nuclear fluorescent marker H1-GFP. Upon successful fusion, fluorescent nuclei were readily transferred from the labelled into the unlabelled strain (Fig. 3.5A). However, nuclear transfer was never observed in interactions involving fusion defective KO mutants (Fig. 3.5B and C). Most interestingly, fusion hyphae of the wt that grew towards hyphae of fusion defective strains displayed the same response upon contact as fusion mutants did, i.e. absence of tip growth arrest and fusion, but continuation of polarised growth. This clearly showed that physical contact alone is insufficient to trigger the fusion process, and most likely the activation of a signalling cascade is required that might involve mechanosensors.

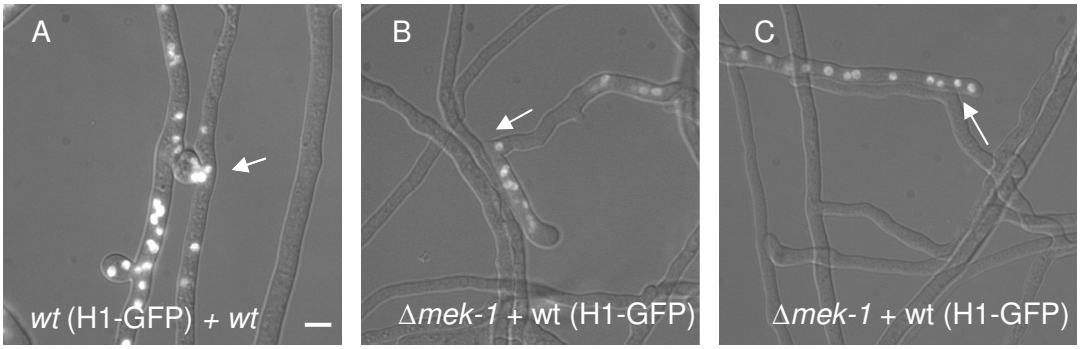

Figure 3.5 Nuclear transfer was never observed between a H1-GFP expressing wt and a fusion defective KO mutant strain. (A) Successful fusion between wt strains became evident by nuclear migration from the labelled into the unlabelled strain (arrow). **(B)** Fusion hypha of wt (H1-GFP) approached and got into contact with Δ*mek-1* hypha. However, fusion and thus transfer of nuclei did not occur between both strains. **(C)** This time, a hypha of Δ*mek-1* approached and got into contact with the wt. Tip growth arrest and hyphal fusion, however, were not established. Scale bar, 10 µm.

Cytoplasmic streaming through fusion connections demonstrated their functionality. The determining feature of successful VHF is the achievement of cytoplasmic continuity which can be observed as cytoplasmic streaming through established fusion connections (Fig. 3.6).

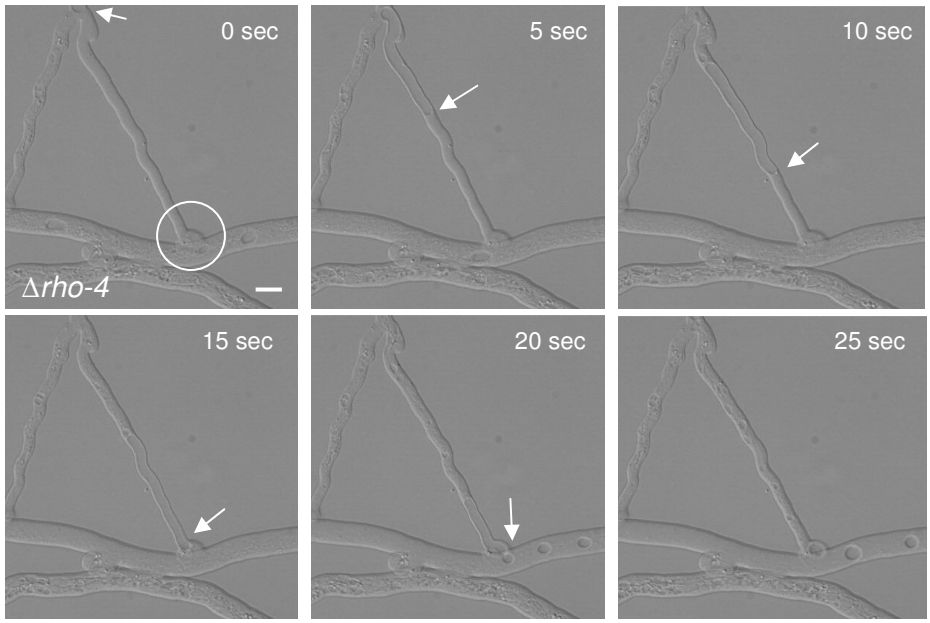

Figure 3.6 Cytoplasmic continuity established by VHF in the mature colony. Time course of vacuolar passage through a fusion connection in the fusion impaired (developmentally delayed and reduced number of fusion connections) Δ*rho-4* mutant. A large vacuole (arrow) that passed through the fusion connection (circle) and eventually split up into smaller vacuoles. Scale bar, 10 µm.

All KO strains that clearly showed networked hyphae and cytoplasmic streaming through the established fusion pores were classified as fusion competent. Distinguishing features between hyphal fusion competency and incompetency used in this analysis are summarised in Table 3.3.

Table 3.3 Characteristic features of VHF competency and incompetency in the mature colony.

VHF competent strain	*VHF defective strain*
• ordered mycelial network with interconnected hyphae • contact-induced tip growth arrest and depolarisation (swelling) • fusion pores visible • fast cytoplasmic streaming throughout the hyphal network • cytoplasmic streaming through fusion connections	• disorganised, chaotic mycelium lacking hyphal interconnectedness • upon physical contact hyphal tips continue polarised growth • no fusion pores visible • extremely slow cytoplasmic flow, mainly in thicker leading hyphae • no cytoplasmic continuity between contacting hyphae

Fusion defects equally affected early and late developmental stages. All fusion mutants identified so far were defective in VHF and CAT-mediated cell fusion. Conidial germling fusion assays (aka: CAT fusion assays) (section 2.11.2), with conidia harvested from the same cultures used for initial VHF assays, were used to confirm fusion defects found in mature colonies of screened KO mutant strains. In the wt, CAT-mediated cell fusion usually was completed within 5-6 h, and therefore CAT fusion assays could be easily completed within one day. After more than 6 h, normally a very dense germling network would have formed and developed so much biomass, that microscopical analysis was extremely difficult (Fig. 3.7). CAT fusion assays, in contrast to investigating the fusion phenotype in the mature colony alone, allowed to determine at which stage of the fusion process (CAT induction, CAT homing or CAT fusion; see Fig. 1.4) a particular mutant was blocked. In half of the tested fusion mutants CAT induction was blocked and only GTs were formed (which *per se* are unable to fuse).

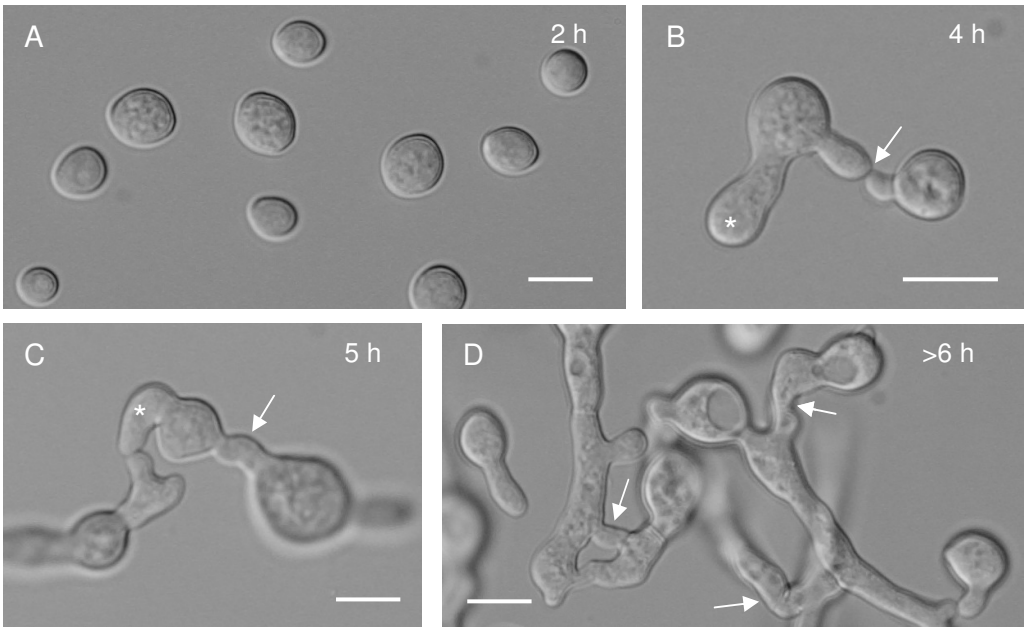

Figure 3.7 Conidial anastomosis in the *N. crassa* wt. (A) Macroconidia after 2 h incubation in liquid VM at 30°C. **(B)** After 3-4 h conidia germinated (GT marked with asterisk) and also formed CATs which homed towards each other and established contact (arrow). **(C)** After 4-5 h more homing CATs could be observed (asterisk) and fusion connections have been established (arrow). **(D)** After more than 5-6 h germling network have been formed, in which cytoplasm was freely distributed throughout all compartments. Scale bars, 10 µm.

However, a number of novel fusion mutants were identified that in addition to GTs also formed much smaller protrusions that resembled CATs as seen in the wt, but which were unable to home towards each other and establish fusion. These strains were of particular interest for this study as only these were likely to be CAT homing mutants and essential for investigating the process of cell-cell communication and the regulation of directed chemotropic growth. Figure 3.8 shows the phenotype of both conditions.

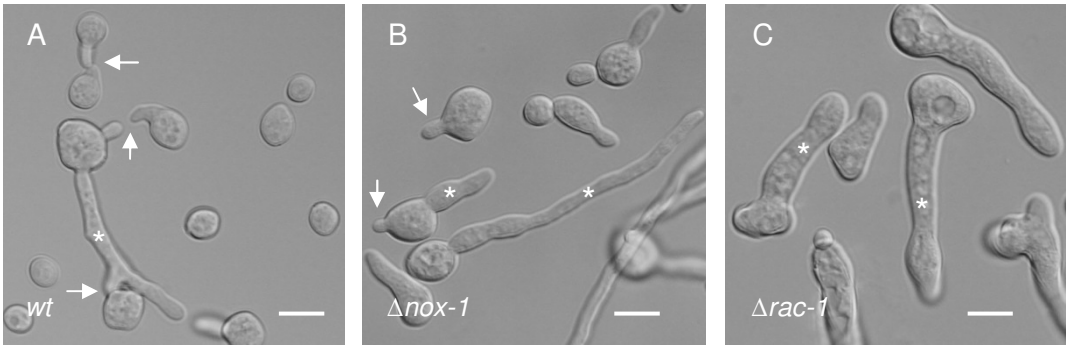

Fig. 3.8 CAT fusion assays distinguished CAT homing from CAT induction defects. (A) Wt cells in the process of CAT homing and fusion. **(B)** Cells of Δ*nox-1* differentiated CAT-like protrusions in addition to elongated GTs, but were unable to chemotropically interact, and therefore classified as homing deficient. **(C)** Conidia of Δ*rac-1* were unable to form CATs (CAT induction defect) and only protrude GTs. In all images, GTs are marked with asterisks, and CATs are indicated by arrows. Scale bars, 10 µm.

Equivalent to confrontation assays between mature colonies (Fig. 3.5), conidia of gene deletion mutants were mixed with fluorescently labelled H1-GFP wt cells to test whether existing fusion defects could be compensated by the wt at this early developmental stage. Consistent with findings in the mature colony, cells of fusion competent mutants homed and fused with the wt, whilst fusion defective gene deletion mutants never interacted with wt cells (Fig. 3.9).

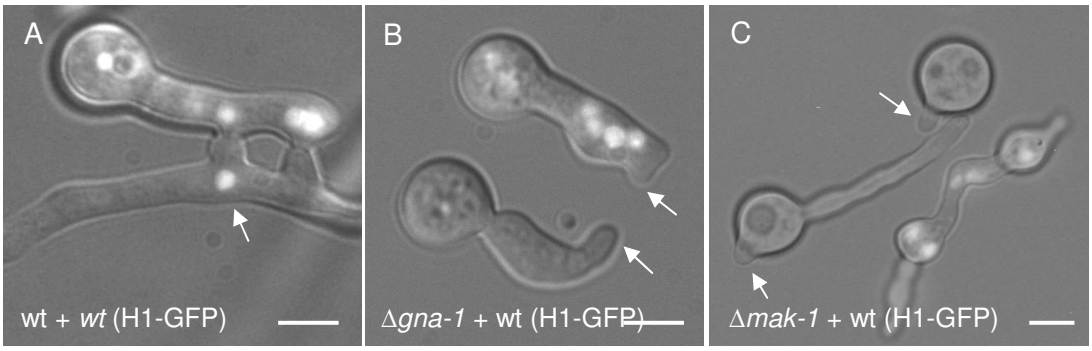

Figure 3.9 Confrontation assays in mixed cultures of gene deletion mutants and wt conidia expressing nuclear H1-GFP. (A) Nuclear migration upon CAT fusion from the labelled into an unlabelled *wt* cell (arrow). **(B)** A homing CAT (lower arrow) of the fusion competent Δ*gna-1* mutant induced the formation of a CAT (upper arrow) in the H1-GFP labelled wt conidium. **(C)** CAT-like protrusions (arrows) of fusion defective mutants did not chemotropically interact although nearby *wt* cells (fluorescent nuclei) were fusing. Fusion between the two cell populations was never observed. Scale bars, 10 µm.

Table 3.4 summarises characteristic features that were employed to differentiate between CAT fusion competent and CAT fusion defective strains.

Table 3.4 Characteristic features of CAT fusion competency and incompetency of conidial germlings of *N. crassa*.

CAT fusion competent strain	*CAT fusion defective strain*
• formation of CATs in addition to GTs	• CAT induction defect: only GTs emerge from the spore
• induction of CATs by CATs approaching neighbouring conidia or GTs	• even presence of CATs from wt conidia does not induce CAT formation in the KO mutants
• recognition and homing response between interacting CATs	• CAT homing defect: CATs are formed, but they do not chemotropically interact and fuse with each other or wt conidia
• nuclear migration between fused cells	• nuclear transfer even with wt cells does not occur
• establishment of an interconnected germling network	• conidia are always separate from each other and do not network

3.3.4. PCR-based genotyping

In order to provide the causal link between observed phenotypic defects and the absence of the target gene after integration of the knock-out cassette at the intended locus, screened mutants were genetically verified by PCR. Genomic DNA was extracted as described in section 2.6.2.2 and analysed by PCR as explained in section 2.7. Strains whose heterokaryotic status, according to the FGSC classification based on Southern blotting, could be confirmed by PCR were subjected to homokaryon purification (HP) as explained in section 2.8. After 3-5 generations of single spore isolation, or when noticeable phenotypic changes occurred (see below; section 3.2.5), the presumably purified strains were reassessed by PCR. Figure 3.10 summarises representative examples of this approach.

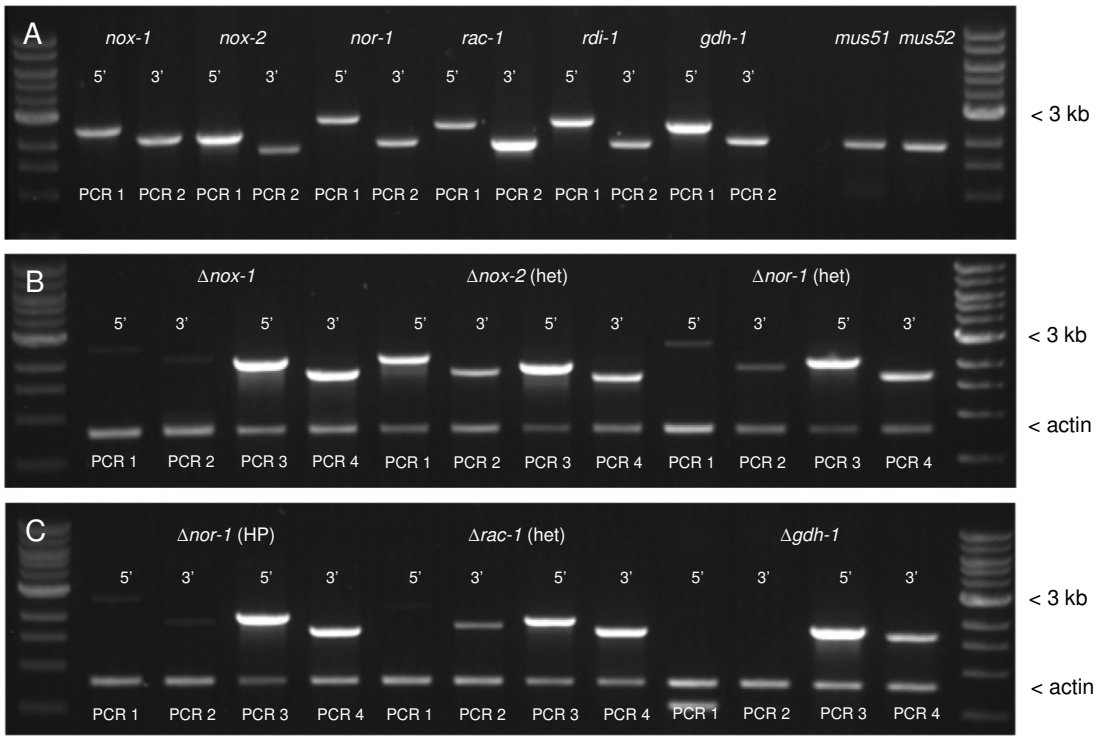

Figure 3.10 PCR genotyping I. PCRs were designed as outlined in Fig. 2.1. **(A)** All primers were initially tested on wt gDNA. Primers binding within the KO cassette were tested and optimized accordingly. **(B)** Multiplex PCRs on gDNA of gene deletion strains. For Δ*nox-1*, in stark contrast to Δ*nox-2* (het), only very minute wt background signal could be detected and thus was confirmed as practically homokaryotic. The clear wt signal obtained from Δ*nox-2* (het) confirmed the presence of wt nuclei and thus its classification as heterokaryon. This was also the case for the Δ*nor-1* (het) strain as received from the FGSC, but with a much weaker wt background. **(C)** The detectable wt background in Δ*nor-1* was further reduced after homokaryon purification (HP) and coincided with a phenotypic change including a cell fusion defect. Genotyping of Δ*rac-1* (het) resulted in a wt background signal, but only at the 3' flank of the locus, potentially indicating presence of nuclei where only part of the ORF has been removed or a double integration event has occured. No wt nuclei could be detected in the Δ*gdh-1* strain, confirming its homokaryotic classification. Abundance of nuclei with the correctly inserted knock-out cassette could be confirmed for all strains equally well, and all strains grew on hygromycin containing selection medium. Also, the internal PCR controls using the actin multiplex primer pair worked for all PCRs in (B) and (C). About 100 ng of gDNA template were used in each PCR. Genotypic details of all strains can be found in Table 2.1.

All gene deletion strains were generated in a Δ*mus-51* or Δ*mus-52* *mat a* mutant background [17, 67]. Therefore all deposited heterokaryons are *mat a* and carry a *mus-51* or *mus-52* deletion, and in fact are double KOs. To recover the *mus-51* or *mus-52* deletions, respectively, and to obtain the *mat A* version of any particular KO strain, the original transformants were crossed with a *mat A* wt, and *mat a* and

mat A progeny was selected on hygromycin containing medium, and distinguished using the mating type tester strain fluffy [73]. Obtained KO strains of either mating type were verified for the presence of the *hph* knock-out cassette by Southern analysis and, if positive, deposited in the KO strain collection as homokaryons (all details under 'Available KO strains' at the following URL:

http://www.dartmouth.edu/~neurosporagenome/knockouts_completed.html).

To confirm that during back-crossing Δ*mus-51* or Δ*mus-52* successfully have been recovered, and that the newly selected *mat A* and *mat a* strains are free of wt nuclei, thus exclusively contain nuclei with the intended gene deletion, genotypic analysis within this project was extended by incorporating *mus-51* and *mus-52* specific primer pairs. Two examples are given in Figure 3.11.

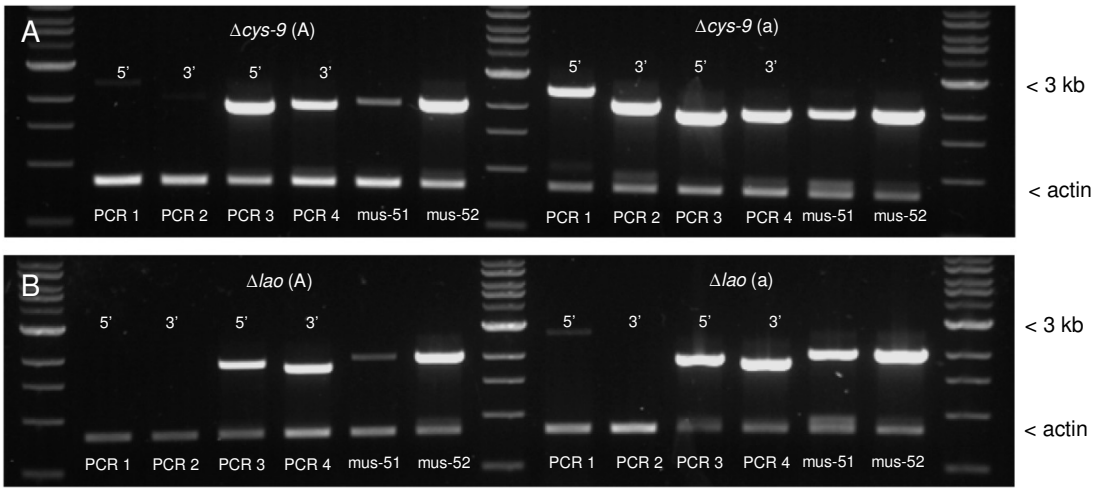

Figure 3.11 PCR genotyping II. PCRs were designed as outlined in Fig. 2.1, including *mus-51* and *mus-52* specific primer pairs. **(A)** The m*us* deletion has been recovered in Δ*cys-9* (A) and no significant wt background can be detected. Δ*cys-9* (a) however, does produce a significant amount of wt signal, suggesting that this strain is a heterokaryon, although back-crossing worked and recovered Δ*mus*. **(B)** Apart from a faint signal at the 5' flank in Δ*lao* (a), the homokaryotic status of both Δ*lao* mating types inlcuding recovery of the *mus* deletion could be confirmed. Genotypic details of all strains are listed in Table 2.1.

3.3.5. Homokaryon purification (HP)

In order to remove or at least significantly reduce wt nuclei from a heterokaryotic strain, homokaryon purification was performed as explained in section 2.8, mainly using macro- or microconidia of *N. crassa*, but also by performing sexual crosses as described in section 2.4.2.3. For a few strains dramatic phenotypic changes in colony morphology and cell biology were observed after the procedure, indicating that the true mutant phenotype of the strain has been exposed (Fig. 3.12). Further live-cell imaging analysis revealed that in some cases the phenotypic change coincided with a vegetative hyphal fusion defect, which was further confirmed in CAT fusion assays. Figures 3.13 and 3.14 give one example.

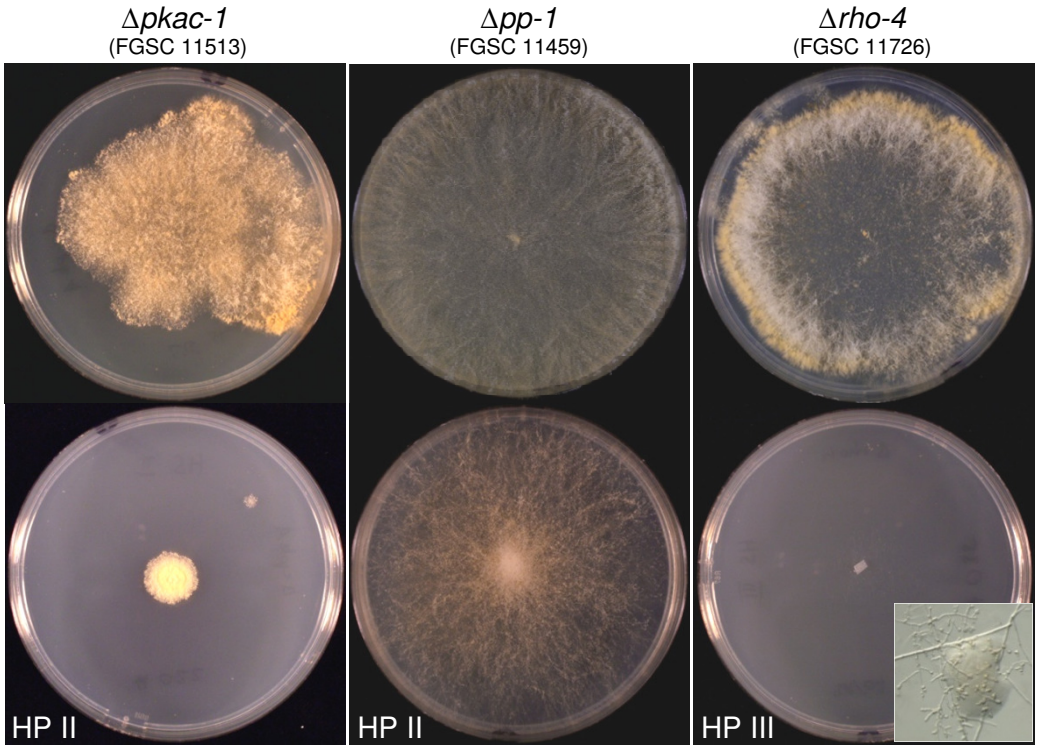

Figure 3.12 Phenotypic changes upon homokaryon purification. Top row: colony morphologies of heterokaryotic KO strains as originally received from the FGSC. **Bottom row:** changed morphologies of the same strains after 2-3 rounds of homokaryon purification (HP II-III). The extremely slow developing mycelium of Δ*rho-4* (HP) is magnified in the inset. All cultures were imaged after 36 h incubation on solid Vogel's medium at 30°C. Equivalent results were obtained on VM plates containing selection marker (data not shown).

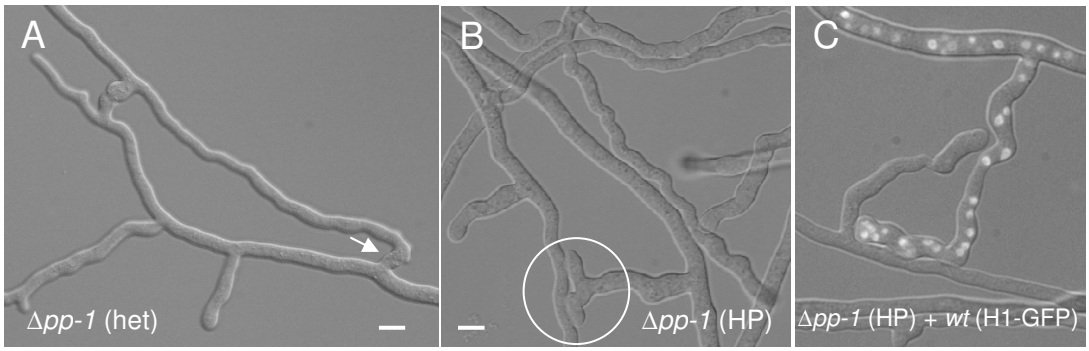

Fig. 3.13 Fusion defect after homokaryon purification. (A) Due to the presence of wt nuclei, the heterokaryotic Δ*pp-1*(het) strain could undergo VHF. Cytoplasmic streaming occurred through the fusion connections (arrows). **(B)** After two rounds of homokaryon purification hyphae of Δ*pp-1* (HP) lost fusion competency (circle). **(C)** The fusion defect could not be compensated by the wt (expressing nuclear H1-GFP) in a compatible confrontation assay. Scale bars, 10 µm.

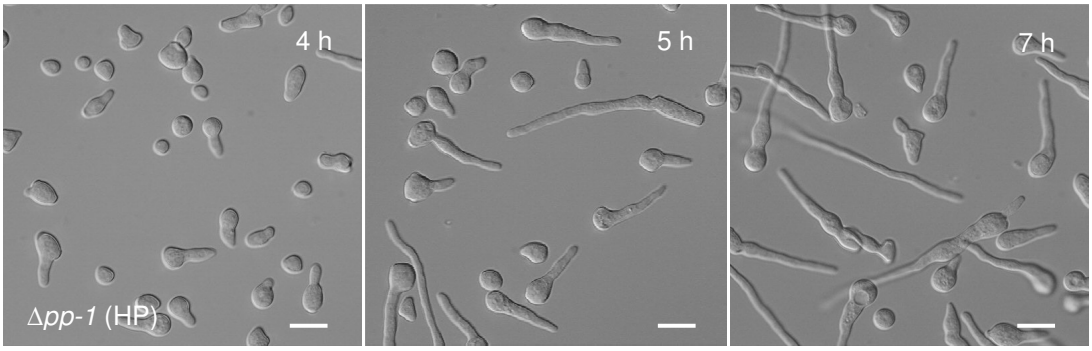

Figure 3.14 CAT induction defect in the Δ*pp-1* mutant after homokaryon purification. Over the course of 7 h in a standard CAT fusion assay only GTs were formed, and fusion between conidial germlings did not occur. Scale bars, 10 µm.

In total, 20 strains were processed through homokaryon purification by means of single spore isolation of macro- and microconidia, and through sexual crosses within this study. As a result, 9 strains showed recognisable changes in colony morphology (e.g. Δ*pkac-1*, Fig. 3.12) and 5 of those defects in hyphal fusion, which were not present in the wt-like heterokaryotic strains (e.g. Δ*nor-1*, see chapter 7). Three strains, although classified as heterokaryons by the FGSC, were fusion defective and verified as homokaryons by PCR, did not change phenotype after 3 rounds of single spore isolation. One strain classified as a homokaryon (Δ*gna-1*)

proved to be heterokaryotic as analysed by PCR and, together with 7 other strains, has so far not been successfully be purified. Table 3.5 summarises these results.

Table 3.5 Results of homokaryon purification and subsequent genotypic and phenotypic analysis.

Gene deletion	*Original strain #*	*Phenotypic change*	*PCR verification*	*Fusion defect*
Δ*pp-1*	FGSC11459	yes	homokaryon	yes
Δ*sevK*	FGSC11478	yes	n.d.	no
Δ*sepA*	FGSC11490	yes	n.d.	no
Δ*pkac-1*	FGSC11513	yes	homokaryon	no
Δ*crisp-1*	FGSC11514	yes	homokaryon	no
Δ*gna-3*	FGSC11610	yes	homokaryon	reduced
Δ*cdc24*	FGSC11721	yes	homokaryon	yes
Δ*rho-4*	FGSC11726	yes	n.d.	reduced
Δ*nor-1*	FGSC13573	yes	homokaryon	yes
Δ*nrc-1*	FGSC11466	no	homokaryon	yes
Δ*mak-2*	FGSC11482	no	homokaryon	yes
Δ*rac-1*	FGSC11495	no	homokaryon	yes
Δ*nox-2*	FGSC11516	no	heterokaryon	no
Δ*mcb*	FGSC11609	no	heterokaryon	no
Δ*Napt-2*	FGSC11620	no	n.d.	no
Δ*nimA*	FGSC11841	no	n.d	no
Δ*gna-1*	FGSC12370	no	heterokaryon	no
Δ*Natg-8*	FGSC12506	no	n.d.	no
Δ*pex-6*	FGSC13219	no	n.d	no
Δ*cdc25*	FGSC16014	no	heterokaryon	no

3.3.6. Outcome of comparative genomics screen

The outcome of the comparative screen of 98 different gene loci was the identification of 10 novel fusion mutants with complete blocks in hyphal fusion, and 9 severely impaired mutants which displayed reduced or delayed cell fusion, often associated to defects during the establishment and maintenance of cell polarity. Table 3.6 summarises all investigated loci and attempts to correlate the individual gene products with the various stages of appressorium-mediated infection at which the orthologous proteins of *M. oryzae* are known or believed to act.

Table 3.6 Alignment of orthologous genes from *N. crassa* and *M. oryzae* with the various morphogenetic stages of appressorium-mediated infection of the rice blast fungus. Gene deletions that result in a total loss or impairment of fusion competency in *N. crassa* are highlighted.

N. crassa strain	Locus	Molecule Pathway / Process	*M. oryzae* gene	Locus	Ref.
Surface recognition and induction of appressorium formation					
Δgnb-1	NCU00440.2	G-beta subunit G-protein singalling	*MGB1*	MGG_05201.6	[62, 68]
Δpred.prot.	NCU02903.2	CFEM-GPCR G-protein singalling	*PTH11*	MGG_05871.6	[22, 56]
Δeas	NCU08457.2	hydrophobin precursor host recognition	*MPG1*	MGG_10315.6	[79, 86]
Δpred.prot.	NCU04170.2	cellulose-binding elicitor host recognition /attachment	*CBEL*	MGG_05865.6	[35, 50]
Δmhp-1	NCU08192.2	hydrophobin host recognition / attachment	*MHP1*	MGG_01173.6	[80]
*Δgna-1**	NCU06493.2	G-alpha subunit 1 cAMP	*MAGB*	MGG_00365.6	[62]
Δacw-2	NCU00957.2	secreted adhesive cuticle attachment	*EMP1*	MGG_00527.6	[2]
Δpkac-1	NCU06240.2	PKA catalytic subunit 1 cAMP response	*CPKA*	MGG_06368.6	[65, 88, 102]
Δcrisp-1	NCU08377.2	adenylate cyclase cAMP response	*MAC1*	MGG_09898.6	[14]
Δste50	NCU00455.2	MAPK scaffold pheromone response	*STE50*	MGG_05199.6	[71]
Δacr-1	NCU07617.2	putative transcription factor	*ACR1*	MGG_09847.6	[57]
Appressorium formation and invasive growth					
Δnrc-1	NCU06182.2	MAPKKK pheromone response	*MST11*	MGG_12855.6	[105, 106]
Δmek-2	NCU04612.2	MAPKK pheromone response	*MST7*	MGG_00800.6	[106]
Δmak-2	NCU02393.2	MAPK pheromone response	*PMK1*	MGG_09565.6	[88, 99]
Δpp-1	NCU00340.2	transcription factor pheromone response	*MSTE12*	MGG_12958.6	[72]
Appressorium maturation					
Δgdh-1	NCU00461.2	NAD-specific glutamate dehydrogenase 1 amino acid metabolism	*MGD1*	MGG_05247.6	[69, 89]

Δhex-1	NCU08332.2	hexagonal protein 1 Woronin body	*MHEX1*	MGG_02696.6	[81]
*Δpex-6**	NCU08373.2	peroxisomal biogenesis factor Woronin body	*PEX6*	MGG_00529.6	[37, 96]
Δrho-3 (reduced)	NCU00600.2	Rho GTPase 3 cell polarity/redox signalling	*RHO3*	MGG_10323.6	[107]
Δsah-1	NCU04179.2	transcription factor	*CON1*	MGG_03977.6	[78]
*ΔNatg-8**	NCU01545.2	autophagy-related ubiquitin-like modifier autophagic cell death	*ATG8*	MGG_01062.6	[36, 92]
*Δmcb**	NCU01166.2	cpkA regulatory subunit cAMP response	*SUM1*	MGG_07335.6	[1, 88]
*ΔnimA**	NCU03187.2	G2-specific protein kinase cell cycle control	*NIMA*	MGG_03026.6	Nick Talbot, Nancy '06
Δchm-1 (delayed)	NCU00406.2	p21-activated kinase (PAK) pheromone response	*CHM1*	MGG_06320.6	[60]

Cell wall remodelling, repolarisation and penetration

Δmik-1	NCU02234.2	MAPKKK cell wall integrity	*MCK1*	MGG_00883.6	[48, 105]
Δmek-1	NCU06419.2	MAPKK cell wall integrity	*MKK1*	MGG_06482.6	[105]
Δmak-1	NCU09842.1	MAPK cell wall integrity	*MPS1*	MGG_04943.6	[58, 101]
Δnox-1	NCU02110.2	NADPH-oxidase 1 NOX redox signalling	*NOXA*	MGG_00750.6	[25, 26]
Δnor-1	NCU07850.2	NOX regulator NOX redox signalling	*NOXR*	MGG_05280.6	[25, 26]
Δrac-1	NCU02160.2	Rho GTPase NOX redox signalling	*MRAC1*	MGG_02731.6	[13]
*Δnox-2**	NCU10775.2	NADPH oxidase 2 NOX redox signalling	*NOXB*	MGG_06559.6	[26]
Δras2 (delayed)	NCU03616.2	GTPase Kras pheromone response	*RAS2*	MGG_09499.6	[71]
Δtps-1	NCU09715.2	trehalose-6-phosphat synthase subunit 1 turgor generation	*TPS1*	MGG_03860.6	[30, 97]
Δcyp	NCU00726.2	cyclophilin turgor generation	*CYP1*	MGG_10447.6	[93]
Δpth-1	NCU01611.2	carnitine acetyl transferase	*PTH2*	MGG_01721.6	[37, 83]
Δorp-1	NCU04236.2	S-phase regulator	*ORP1*	MGG_06873.6	[44, 94]
Δhypoth.prot	NCU05521.2	putative cell-wall degrading transmembrane protein	*PATH531*	MGG_00438.6	[32]
Δabc-1	NCU05591.2	ABC type ATPase	*ABC1*	MGG_13624.6	[91]
Δmmt-2	NCU07879.2	Mitochondrial metal transporter 2	*MMT2*	MGG_06247.6	Nick Talbot, Nancy '06

Δpde-1	NCU06281.4	P-type ATPase aminophospholipid translocase	*PDE1*	MGG_00111.6	[5]
*ΔNapt-2**	NCU07443.2	Golgi-associated P-type ATPase secretion	*APT2*	MGG_02767.6	[36]
*Δpks-7**	NCU03584.2	polyketide synthase melanin synthesis / turgor generation	*ALB1*	MGG00428.6	[20, 43]
*Δpls-1**	NCU07432.2	tetraspanin turgor generation	*PLS1*	MGG_12594.6	[16, 92]
*Δpred.prot.**	NCU07846.2	transcriptional regulator	*SMO1/ CON7*	MGG_05287.6	[38, 39, 78]
Δnth-1	NCU04211.2	neutral trehalase	*NTH1/ PTH9*	MGG_09471.6	[30, 83]
Δpks-3	NCU04865.2	polyketide synthase (PKS)	*SYN6*	MGG_15100.6	[6]
Δpks-4	NCU08399.2	PKS-NRPS	*SYN2/ ACE1*	MGG_12447.6	[6]
Δspr-7	NCU07159.2	proteinase T precursor secretion	*SPM1*	MGG_03670.6	[69]
Δpred.prot.	NCU08652.2	fungal specific transcriptional activator	*?*	MGG_10529.6	[24, 44]
Δpred.prot.	NCU08038.2		*MAS3/ GAS1*	MGG_12337.6	[7, 104]

Genes shown to be dispensable for infection

Δgna-2	NCU06729.2	G-alpha subunit 2 G-protein singalling	*MAGC*	MGG_04204.6	[62]
Δgna-3 (delayed)	NCU05206.2	G-alpha subunit 3 G-protein signalling	*MAGA*	MGG_01818.6	[53]
Δos-4	NCU03071.2	MAPKKK osmosensitivity	*WIS4*	MGG_00183.6	[105]
Δos-5	NCU00587.2	MAPKK osmosensitivity	*PBS2*	MGG_10268.6	[105]
Δos-2	NCU07024.2	MAPK osmosensitivity	*OSM1*	MGG_01822.6	[23, 90]
Δste20	NCU03894.2	p21-activated kinase (PAK) pheromone response	*STE20*	MGG_12821.6	[60]
ΔflbA (delayed)	NCU08319.2	Regulator of G-protein signalling (RGS)	*RGS1*	MGG_14517.6	[61]

No published information on *M. oryzae* orthologs available

Δcdc24	NCU06067.2	Rho GEF Rho signalling / polarity	*SCD1*	MGG_09697.6	
Δcdc42	NCU06454.2	Rho GTPase Rho signalling / polarity	*CDC42*	MGG_00466.6	
Δsoft	NCU02794.2	WW-TM protein ?	*MHAM-1*	MGG_00731.6	[29]
Δham-2	NCU03727.2	hyphal anastomosis protein ?	*?*	MGG_00731.6	[70]

Δlao	NCU05113.2	L-ascrobate oxidase -like ?	?	MGG_13464.6	
*Δpkc**	NCU06544.2	Ca^{2+}-dependent protein kinase C	*?*	MGG_08689.6	

Genes associated with the above pathways, but not yet annotated in *M. oryzae*

Δgpr-1	NCU00786.2	G-protein coupled receptor G-protein singalling			
Δpkac-2	NCU00682.2	PKA catalytic subunit 2 cAMP response			
*Δcdc25**	NCU06500.2	cell division control cAMP response			
*Δcdc2**	NCU09778.2	cyclin dependent kinase (CDK); cAMP response			
Δpde-2	NCU00478.2	P-type ATPase cAMP response			
Δrrg-1	NCU01895.2	response regulator MAPK singalling			
Δrrg-2	NCU02413.2	response regulator MAPK signalling			
Δsdc25	NCU09758.2	Ras-like GTPase			
Δrho-4 (reduced)	NCU03407.2	Rho protein Rho signalling			[74]
Δrho-2 (reduced)	NCU08683.2	Rho GTPase Rho signalling			
ΔsepA	NCU01431.2	cytokinesis protein polarity			
Δspa-2 (reduced)	NCU03115.2	polarisome protein polarity			[4]
Δrdi-1 (delayed)	NCU06561.2	Rho GDI alpha homol. redox signalling			
Δtrm-52	NCU03498.2	ferroxidase redox signalling			
Δcys-9	NCU08352.2	thioredoxin reductase redox signalling			
Δhyr-1	NCU09534.2	glutathione peroxidase redox signalling			
Δccp-1	NCU03297.2	cytochrome C peroxidase redox signalling			
Δsod-1	NCU02133.2	superoxide dismutase redox signalling			
Δprm-1 (reduced)	NCU03292.2	P-type ATPase membrane fusion			[28]
*Δprm-1-like**	NCU09337.2	Pheromone-regulated membrane protein 1-like			
Δeb-1	NCU00243.2	microtubule associated protein			
Δaip-1	NCU08468.2	actin-intertactinG-protein 1 actin disassembly			

*Δmyo-5**	NCU02111.1	myosin 5 polarity / vesicle transport
Δpten	NCU06969.2	phosphate tenside cAMP signalling
ΔsevK	NCU00772.2	similar to severin kinase A cAMP signalling
Δcons.hypot. protein	NCU10397.2	PI-3,4-kinase cAMP signalling
ΔtmpA	NCU00848.2	
ΔtmpA-like	NCU07231.2	
Δdnr-1	NCU02806.2	14-3-3 protein homolog (Raf-1 binding)
Δlpl	NCU03141.2	cytosolic PLA-2
Δcpc-1	NCU04050.2	cross-pathway control protein 1
Δcons.hypot. protein	NCU06648.2	cytoskeleton component
ΔsPLA-2	NCU06650.2	secretory phospholipase A
Δcons.hypot. protein	NCU06834.2	disintegrin
Δnit-2	NCU09068.2	nitrogen regulator protein

* Genetic status of KO strain unclear (not determined), but most likely heterokaryon.

Table 3.7 Novel cell fusion mutants of *N. crassa* identified in this study.

N. crassa strain	*Locus*	*Gene product*	*Process/ Pathway*	*Cell fusion stage blocked*
Gene deletion strains unable to establish cell fusion				
Δcdc24	NCU06067.2	Rho GEF	cell polarity	CAT induction
Δcdc42	NCU06454.2	Rho GTPase	cell polarity	CAT induction
Δrac-1	NCU02160.2	Rho GTPase	cell polarity/ NOX activation	CAT induction
Δmik-1	NCU02234.2	MAPKKK	cell wall remodelling	CAT homing
Δmek-1	NCU06419.2	MAPKK	cell wall remodelling	CAT homing
Δmak-1	NCU09842.1	MAPK	cell wall remodelling	CAT homing/ pore opening
Δnox-1	NCU02110.2	NADPH-oxidase 1	cell wall remodelling/ redox signalling	CAT homing
Δnor-1	NCU07850.2	NOX regulator	cell wall remodelling/ redox signalling	CAT homing
Δgdh-1	NCU00461.2	NAD-specific glutamate dehydrogenase 1	hyphal adhesion/ protein oxidation	CAT induction (?)
Δlao	NCU05113.2	Laccase (L-ascorbate oxidase –like)	cell wall remodelling via 'Fenton reaction' in the apoplast (?)	CAT homing
Gene deletion strains with significantly reduced or delayed onset of cell fusion				
Δchm-1 (delayed)	NCU00406.2	p21-activated kinase (PAK)	pheromone response/ cell polarity	
Δspa-2 (reduced)	NCU03115.2	? GTPase activation	cell polarity	
Δras2 (reduced)	NCU03616.2	GTPase Kras Rab GTPase protein	pheromone response/ cell polarity	
Δgna-3 (delayed)	NCU05206.2	G-alpha subunit 3 G-protein signalling		
Δrho-2 (reduced)	NCU08683.2	Rho2-GTPase Rho GTPase signalling	cell polarity	
Δrho-3 (reduced)	NCU00600.2	Rho3-GTPase Rho GTPase signalling	cell polarity	
Δrho-4 (reduced)	NCU03407.2	Rho protein Rho GTPase signalling	cell polarity	
Δrdi-1 (delayed)	NCU06561.2	Rho GDI alpha Rho GTPase signalling		
ΔflbA (delayed)	NCU08319.2	Rho GAP Rho GTPase signalling		

In total, 53 annotated orthologous loci have been compared between *N. crassa* and *M. oryzae*, containing 48 genes that are essential for pathogenicity in the rice blast fungus. Of those, only 9 have been found to be essential for hyphal fusion, whereas 4 displayed severe developmental delays leading to a reduction or very late onset of cell fusion. According to our analysis, a functional overlap between hyphal fusion and appressorium-mediated infection was seen at three stages: appressorium formation, appressorium maturation and cell wall remodelling. Molecular pathways involved and conserved in both species comprise the PR and CWI MAPK signalling pathways, NOX-mediated redox signalling and metabolic processes involving NAD-specific glutamate dehydrogenase.

The extended analysis of *N. crassa* gene deletion mutants also revealed that the establishment and maintenance of cell polarity is a crucial process for hyphal fusion. Several Rho GTPases and associated regulatory proteins are indispensable for cell fusion or lead to severe impairments if removed from the genome. It is conceivable that, due to their central and comprehensive function, these proteins also play vital roles during rice blast infection, but at the time of analysis almost no information was available about corresponding mutants of *M. oryzae*.

3.4. Discussion

To initiate the search for novel fusion mutants in *N. crassa,* a functional genomic comparison with the infection process of the rice blast fungus *M. oryzae* was a helpful and successful approach. Besides the identification of novel fusion mutants, it also revealed new insights into functional overlaps and differences of the molecular machineries regulating both processes. About 25% of the screened orthologs annotated in both species were equally essential, and showed that MAPK signalling pathways and NOX-derived ROS have similar cellular functions in both processes. GPCR-mediated cAMP signalling, which is extremely important for the induction of appressorium formation in the rice blast fungus, had no obvious role in

hyphal fusion. KOs of 18 components associated with G-protein and cAMP signalling have been screened in *Neurospora* (8 of those with known non-pathogenic orthologs in *Magnaporthe*) and did not display defects in hyphal fusion.

Cyclic AMP is not essential for hyphal fusion. The underlying model of the cAMP signalling pathway in *N. crassa* (Fig. 3.15) has been proposed by Andrew B. Goryachev (Edinburgh University, pers. comm.) and is based on orthologous pathways in yeast and higher eukaryotes.

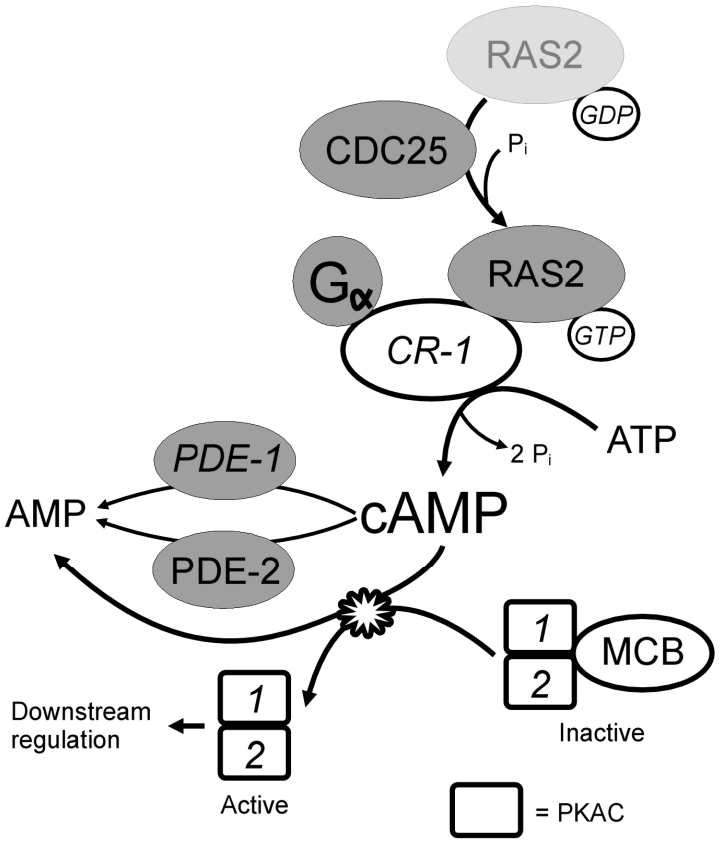

Figure 3.15 Suggested model of cAMP response pathway in *N. crassa*. Adapted from a model by A.B. Goryachev, University of Edinburgh. Design by Robert Dinwiddie, honours student, Read lab. See text for details.

The *cr-1* gene codes for adenylate cyclase in *N. crassa* (CR-1) which generates cAMP by converting ATP into cAMP. The *cr-1* mutant undergoes intense condidation in the absence of intracellular cAMP [54, 55]. It is regulated by guanine nucleotide binding-protein (RAS-2) and three Gα-protein subunits associated with upstream GPCRs (not depicted in Fig. 3.13). In higher eukaryotes the cAMP dependent protein kinase A (PKA) complex forms a tetramer with two regulatory subunits and two catalytic subunits [31]. In *N. crassa* two cAMP-dependent catalytic PKA subunits (PKAC-1 and 2) are responsible for activating downstream targets. In contrast to other eukaryotes only one regulatory subunit of cAMP-dependent protein kinase (MCB) has been found in the *Neurospora* genome to date, indicating that important functional differences exist in the architecture of the pathway between different species. When MCB is bound to the catalytic subunits it forms an inactive PKA complex. cAMP separates the complex by binding to MCB, inducing conformational changes allowing it to act on downstream effectors. In yeast the sole function of cAMP is to activate PKA [82]. All three Gα subunits (GNA-1, GNA-2 and GNA-3) have been implicated in the cAMP pathway in earlier studies [45, 53]. Δ*gna-1* was found to only have 10-15% of adenylate cyclase activity, while Δ*gna-2* was found to have normal levels with no phenotypic differences [45]. Δ*gna-3* displays a colony morphology described as similar to Δ*cr-1* [53], and so does Δ*pkac-1* according to our analysis (Fig. 3.16).

Figure 3.16 Colony phenotype of Δ*pkac-1*. Initially received as heterokaryotic strain with wt-like appearance, removal of wt nuclei by homokaryon purification resulted in a colony morphology identical to Δ*cr-1*. Colony diameter approximately 4 cm.

Δ*ras-2* has previously been reported to have defects in cell wall synthesis and a slower rate of growth [51], which we could confirm. The regulatory subunit of the PKA complex (MCB) has been shown to be involved in hyphal growth polarity and septal morphology [10]. Nevertheless, apart from Δ*cr-1* [75], the role of these proteins in hyphal fusion was not explored in these papers.

The extended KO mutant analysis of cAMP response pathway components in this study comprehensively confirms previous findings that cAMP is not essential for cell fusion in *N. crassa* [75]. This does not fully exclude the involvement of cAMP in hyphal fusion, although the delayed fusion observed in Δ*gna-3* and Δ*ras-2* may be secondary effects of cAMP's involvement elsewhere. The >20 h delay observed in Δ*gna-3* might implicate that another pathway is initiated to allow hyphal fusion or CAT formation and that, in the case of CATs, it may take about 20 h to activate this alternative signalling route. Slower growth in these mutants may also induce slower CAT induction, although the slower growth and pronounced conidiation observed in Δ*pkac-1* and Δ*cr-1* did not impair or delay CAT homing and fusion, supporting Δ*gna-3* involvement in other pathways. This might also indicate a potentially different regulation at early and late developmental stages of colony development. In previous studies the slow growth of Δ*gna-3* could be reversed through the addition of exogenous cAMP, but the observed short aerial hyphae and pronounced conidiogenesis phenotype remained [53].

Neurospora possesses two phosphodiesterases, PDE-1 and PDE-2. The lack of phenotype in both of them may arise from their ability to compensate for each other. A double knock out of PDE-1 and PDE-2 could give a better understanding of what effects the low turnover of cAMP may have on cell fusion. This could potentially lead to a general cytotoxic effects. Although having a previously reported phenotype [10], no homokaryon was successfully generated for Δ*mcb* in this project. A KO of MCB would generate a constitutive over expression of PKAC-1 and PKAC-2 targets. As the complete loss of signal in the cAMP pathway (cAMP deficient Δ*cr-1*

mutant) did not prevent cell fusion, the analysis of over expression might bring a more conclusive result about the requirement of the cAMP pathway for cell fusion.

Cyclic guanosine monophosphate (cGMP) may act as a replacement for cAMP in the pathway to recover a hyphal fusion defect. As the structure between the nucleotides differs slightly, it would implicate a possible lower affinity for respective binding site of the opposite nucleotide and potentially explain why fusion occurs delayed and reduced in some of these mutants. An *in vitro* experiment with the PKA complex would show whether the addition of cGMP could compensate the lack of cAMP.

The concluding notion is that the cAMP pathway in *N. crassa* does not play an essential role in cell fusion and has other functions yet to be discovered. One of those functions obviously includes the regulation of conidiogenesis which in comparison to the vital role of cAMP-induced appressorium formation in *Magnaporthe* is another crucial morphogenetic transition in the fungal life cycle.

MAPK signalling is highly conserved in both species. Components of the pheromone response MAPK pathway, including NRC-1, MAK-2 and PP-1, were amongst the first to be found as essential determinants of hyphal fusion in *Neurospora* [59, 70, 75]. Results obtained previously were confirmed within this study using independently generated gene deletion mutants. Extending this work onto other MAPK cascades of *Neurospora* it was not surprising to find that components of the parallel cell wall integrity pathway, including the MIK-1/MEK-1/MAK-1 cascade, were also essential for hyphal fusion, which in the meantime has been independently confirmed [63]. However, the reason for a cell fusion defect caused by removal of the terminal MAP kinase MAK-1 has not been elucidated and novel insights into the molecular function of this essential protein will be discussed in detail in chapter 5. The most interesting aspect so far is the fact that disruption of the PR pathway leads to a CAT induction defect, whereas increasing evidence points towards CAT homing defects when disrupting the CWI pathway. On this

background, it was surprising to find that the third osmoregulatory (HOG) MAPK cascade conserved in *Neurospora*, comprising OS-4/OS-5/OS-2 (see Table 3.2), seems to be dispensable for hyphal fusion. Although this is consistent with findings in *M. oryzae*, where deletion of all three orthologous MAP kinases WIS4/PBS2/OSM-1 did not affect pathogenicity [23, 102, 105], it contradicts recent findings in *Neurospora* made by observing VHF in the mature colony of gene deletion mutants [63]. This conflict might potentially be explained by the use of incorrect mutant strains in previous studies, which in addition to the intended gene deletion carried other genetic defects creating a false phenotype. To clarify the involvement of this MAPK cascade in cell fusion in *Neurospora*, comparison and genetic validation of various available mutants of this pathway is ongoing research emanating from this project. However, when assuming osmosensing is nonessential for hyphal fusion, it would indicate that the molecular and functional overlap of MAPK signalling is 100% conserved between *Neurospora* and *Magnaporthe*. Similar to the rice blast fungus a future challenge will be to broaden our understanding of the up- and downstream components feeding signals in and out of this central molecular switchboard of MAPK cascades.

Gene deletion mutant screening. Being able to obtain KO mutants from the NIH *Neurospora* Gene Disruption Project provided an unprecedented opportunity for various reasons: first of all it would not have been possible to produce and screen > 100 KO mutants, and analyse the cell biological roles of interesting targets within one Ph.D. project. Secondly, the possibility to obtain the KOs from one source guarantees a consistent quality of the strains, and finally, specific KOs can be produced upon request and become available within a relatively short time, usually after 2-3 months. Within the *Neurospora* Genome Project almost all selected gene deletion strains are genetically verified for the presence of the KO-cassette by Southern analysis before deposition. Initially a Southern probe directed against the whole KO-cassette for each individual ORF was used which included 5′ flank, *hph*-

cassette and 3′ flank, and therefore could verify the integration of the KO cassette at its target locus. Motivated by the high success rate of correctly generated gene deletion mutants, this approach was simplified at later stages of the project, by using one and the same Southern probe directed against the *hph*-cassette only for the verification of every new strain. This also reliably detects the presence of the KO-cassette in the genome and further speeds up the throughput of generated strains, but does not detect KO-cassettes that might have been integrated somewhere else in the genome. Although the frequency for homologous recombination in Δ*mus-51* and Δ*mus-52* backgrounds has been experimentally determined to be 100% [67], a minute error rate of incorrect strains must be expected. Errors can occur at various stages of the process. Mistakes in the sequence of synthesised primers used for amplification of the flanking regions or errors within these flanks introduced by the DNA polymerase can lead to the amplification of mismatching flanks that under suboptimal PCR conditions generate mismatching KO-cassettes which integrate at similar but not identical regions to the targeted ORF. Unwanted recombination events might also occur during backcrossing of the initial transformants, or during the selection procedure of rescued clones. Potential mistakes during the Southern analysis might lead to misinterpretation of the data and deposition of wrong strains. Undetected contaminations during handling can further change the genotype of an individual strain. As mentioned before, the overall error rate was very low, but according to our experience within this project it was not zero. Therefore, it proved to be essential to verify the genetic content of all KO mutants by alternative methods before progressing the work. The introduced PCR-based approach provided a very versatile, quick and extremely sensitive method to genotype gene deletion strains. Of course, it is also not error free, but together with the published verification data for each strain, and phenotypic analysis, it was a highly useful additional control and avoided working with wrong strains on at least five occasions. Furthermore, it was an essential tool to monitor the progress of homokaryon purification of selected strains. In the end, confirming that

the observed phenotype was exclusively caused by disruption of the intended target gene was absolutely essential for the interpretation of the experimental data.

First evidence for novel enzymic activity during cell fusion. Without the resources of both genomes and the availability of the gene deletion strain collection, the unexpected and interesting roles of the NADPH-oxidase system, comprising NOX-1, NOR-1 and RAC-1, or the L-ascorbate-oxidase–like laccase LAO and the NAD^+-dependent glutamate dehydrogenase 1 (GDH-1), in hyphal fusion would not have been discovered. Identification of these proteins provided the first evidence for enzymic processes essential for hyphal fusion, and added a new level of complexity to the process. Preliminary results on the potential role of NOX-derived ROS during hyphal fusion, and how enzymic activity of other oxidases and dehydrogenases might fit into the picture are the subject of chapter 7.

Establishment and maintenance of cell polarity is required for cell fusion. Another central topic impacting cell fusion in *N. crassa* was cell polarity. Gene deletion of members of the Rho family of small GTPases (RAC-1, CDC42, RHO-2, RHO-3 and RHO-4) and their regulatory proteins, including guanine nucleotide dissociation inhibitors (GDIs), guanine nucleotide exchange factors (GEFs) and GTPase activating-proteins (GAPs) [46], have been identified that either were completely blocked or severely impaired in cell fusion (Table 3.7). These proteins coordinate cell symmetry breaking, polarised cell wall protrusion of GTs and CATs, and orientation of the cytoskeleton to guide targeted vesicle delivery in order to establish and maintain polarised growth and allow chemotropic tip re-orientation (reviewed in [66]). Due to their numerous cellular functions, and consequently the extremely pleiotropic phenotypes of the corresponding mutants, it was and still is a major challenge to elucidate specific functions of these components during the cell fusion process. Identification of Δ*rac-1*, Δ*cdc42* and Δ*cdc24* mutant strains of *Neurospora*, with their extreme phenotypes caused by defects in cell polarity (Fig.

3.17), motivated a closer investigation of the role of the cytoskeleton, in particular F-actin-based structures, during cell fusion. A great body of evidence has already been accumulated on how polarised tip growth is achieved in the mature fungal colony [27, 76, 77, 95], but how these processes are regulated to establish fusion between conidial germlings has not been investigated so far. Novel insights into the dynamic rearrangements of the F-actin cytoskeleton during CAT-mediated cell fusion are subject of the following chapter.

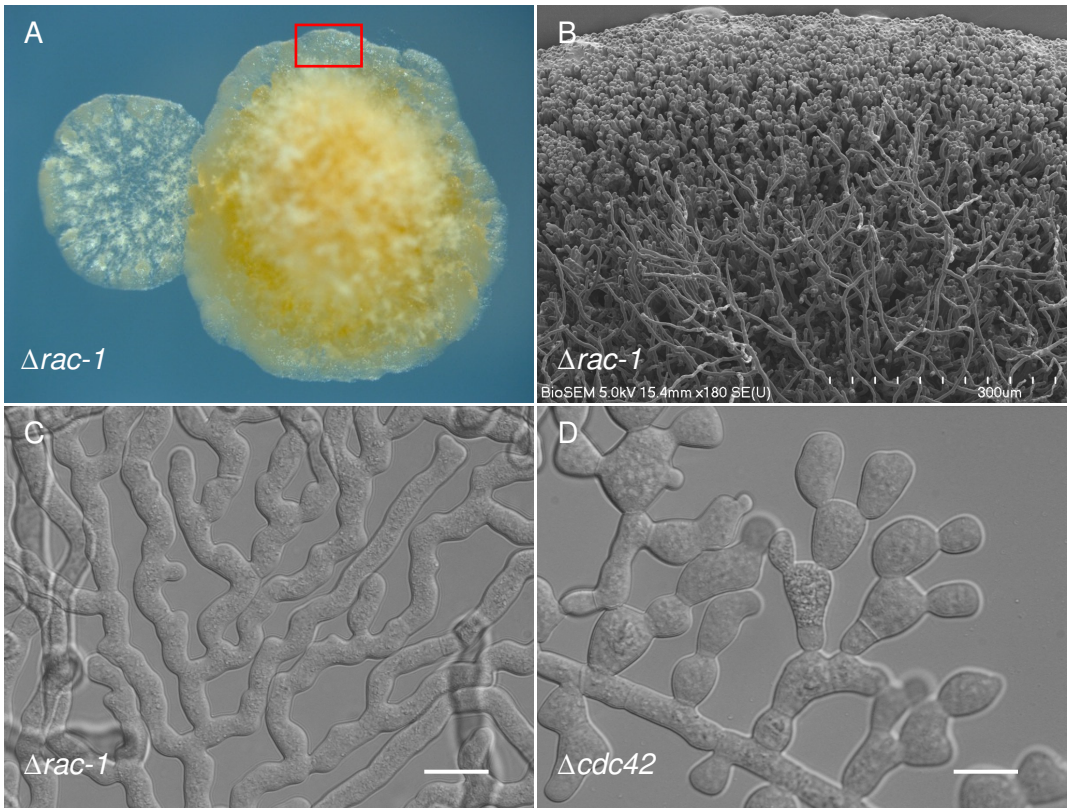

Figure 3.17 Polarity defects of Rho GTPase mutants severely affect colony architecture. (A) Five day old colony of Δ*rac-1*, with an approximate diameter of 8 mm. The rectangle indicates a similar area as magnified in (B). **(B)** SEM of the colony edge of Δ*rac-1* formed by extremely dense growing, undifferentiated hyphae. Towards the colony centre aerial hyphae are emerging. **(C)** Strictly dichotomous branching pattern of Δ*rac-1* hyphae. **(D)** Hyphae of Δ*cdc42* also show dichotomous branching, but additionally are defective in polarised hyphal elongation and thus display extremely bulbous growth. The colony morphology of Δ*cdc42* is equally dense than that seen in Δ*rac-1*, but shows even slower extension rates. Scale bars, 10 µm.

3.5. Summary

This chapter demonstrated that the functional genomic comparison to the infection process of *M. oryzae* provided a feasible way to identify novel hyphal fusion mutants in *N. crassa*:

- Genomic comparison identified 98 target loci - including 53 annotated orthologs of both species - for mutant screening
- The NIH *Neurospora* Genome Project together with the FGSC provided invaluable resources for obtaining gene deletion mutants
- PCR-based genetic verification of gene deletion mutants proved to be an essential control prior to further phenotypic analyses
- Ten novel fusion mutants with complete blocks in cell fusion, and nine mutants with severely impaired cell fusion phenotypes, were identified within this study
- MAPK signalling was found to be functionally highly conserved in both fungal species, with the pheromone response and cell wall integrity pathways being equally essential
- Although crucial for the establishment of rice blast infection, G-protein and cAMP signalling were confirmed to be non-essential for hyphal fusion in *N. crassa*
- Novel enzymic pathways, involving NADPH-oxidase, L-ascorbate-oxidase-like laccase and NAD^+-dependent glutamate dehydrogenase activity, were identified for the first time to be important for cell fusion
- The Rho GTPases CDC42 and RAC-1 were found to be essential for the establishment and maintenance of cell polarity during CAT-mediated cell fusion, triggering more detailed investigations of this topic

3.6. References

1. **Adachi, K., and J. E. Hamer.** 1998. Divergent cAMP signaling pathways regulate growth and pathogenesis in the rice blast fungus *Magnaporthe grisea*. Plant Cell **10:**1361-1374.

2. **Ahn, N., S. Kim, W. Choi, K.-H. Im, and Y.-H. Lee.** 2004. Extracellular matrix protein gene, EMP1, is required for appressorium formation and pathogenicity of the rice blast fungus, Magnaporthe grisea. Molecules and Cells **17:**166-173.

3. **Allen, A. E., B. E. Hazen, H. C. Hoch, Y. Kwon, and G. M. E. Leinhos.** 1991. Appressorium formation in response to topographical signals by 27 rust species. Phytopathology **81:**323-331.

4. **Araujo-Palomares, C. L., M. Riquelme, and E. Castro-Longoria.** 2009. The polarisome component SPA-2 localizes at the apex of *Neurospora crassa* and partially colocalizes with the Spitzenkörper. Fungal Genetics and Biology **46:**551-563.

5. **Balhadere, P. V., and N. J. Talbot.** 2001. PDE1 encodes a P-type ATPase involved in appressorium-mediated plant infection by the rice blast fungus *Magnaporthe grisea*. Plant Cell **13:**1987-2004.

6. **Bohnert, H. U., I. Fudal, W. Dioh, D. Tharreau, J.-L. Notteghem, and M.-H. Lebrun.** 2004. A putative polyketide synthase/peptide synthetase from *Magnaporthe grisea* signals pathogen attack to resistant rice. Plant Cell **16:**2499-2513.

7. **Borkovich, K. A., L. A. Alex, O. Yarden, M. Freitag, G. E. Turner, N. D. Read, S. Seiler, D. Bell-Pedersen, J. Paietta, N. Plesofsky, M. Plamann, M. Goodrich-Tanrikulu, U. Schulte, G. Mannhaupt, F. E. Nargang, A. Radford, C. Selitrennikoff, J. E. Galagan, J. C. Dunlap, J. J. Loros, D. Catcheside, H. Inoue, R. Aramayo, M. Polymenis, E. U. Selker, M. S. Sachs, G. A. Marzluf, I. Paulsen, R. Davis, D. J. Ebbole, A. Zelter, E. R. Kalkman, R. O'Rourke, F. Bowring, J. Yeadon, C. Ishii, K. Suzuki, W. Sakai, and R. Pratt.** 2004. Lessons from the genome sequence of *Neurospora crassa*: tracing the path from genomic blueprint to multicellular organism. Microbiological and Molecular Biological Reviews **68:**1-108.

8. **Bourett, T. M., and R. J. Howard.** 1992. Actin in penetration pegs of the fungal rice blast pathogen, *Magnaporthe grisea*. Protoplasma **168:**20-26.

9. **Bourett, T. M., and R. J. Howard.** 1990. *In vitro* development of penetration structures in the rice blast fungus *Magnaporthe grisea*. Canadian Journal of Botany **68:**329-342.

10. **Bruno, K. S., R. Aramayo, P. F. Minke, R. L. Metzenberg, and M. Plamann.** 1996. Loss of growth polarity and mislocalization of septa in a *Neurospora* mutant altered in the regulatory subunit of cAMP-dependent protein kinase. EMBO Journal **15:**5772-5782.

11. **Buchanan, B. B., and Y. Balmer.** 2005. Redox regulation: a broadening horizon. Annual Reviews of Plant Biology **56:**187-220.

12. **Caracuel-Rios, Z., and N. J. Talbot.** 2007. Cellular differrentiation and host invasion by the rice blast fungus *Magnaporthe grisea*. Current Opinion in Microbiology **10:**339-345.

13. **Chen, J., W. Zheng, S. Zheng, D. Zhang, W. Sang, X. Chen, G. Li, G. Lu, and Z. Wang.** 2008. Rac1 is required for pathogenicity and Chm1-dependent conidiogenesis in rice fungal pathogen *Magnaporthe grisea*. PLoS Pathog **4:**e1000202.

14. **Choi, W., and R. A. Dean.** 1997. The adenylate cyclase gene *MAC1* of *Magnaporthe grisea* controls appressorium formation and other aspects of growth and development. Plant Cell **9:**1973-1983.

15. **Chumley, F. G., and B. Valent.** 1990. Genetic analysis of melanin-deficient, nonpathogenic mutants of *Magnaporthe grisea*. Molecular Plant and Microbe Interactions **3:**135-145.

16. **Clergeot, P.-H., M. Gourgues, J. Cots, F. Laurans, M.-P. Latorse, R. Papin, D. Tharreau, J.-L. Notteghem, and M.-H. Lebrun.** 2001. *PLS1*, a gene encoding a tetraspanin-like protein, is required for penetration of rice leaf by the fungal pathogen *Magnaporthe grisea*. Proceedings of the National Academy of Sciences of the United States of America **98:**6963-6968.

17. **Colot, H. V., G. Park, G. E. Turner, C. Ringelberg, C. M. Crew, L. Litvinkova, R. L. Weiss, K. A. Borkovich, and J. C. Dunlap.** 2006. A high-throughput gene knockout procedure for *Neurospora* reveals functions for multiple transcription factors. Proceedings of the National Academy of Sciences of the USA **103:**10352-10357.

18. **Couch, B. C., and L. M. Kohn.** 2002. A multilocus gene genealogy concordant with host preference indicates segregation of a new species *Magnaporthe oryzae* from *M. grisea*. Mycologia **94:**683-693.

19. **de Jong, J. C., B. J. McCormack, N. Smirnoff, and N. J. Talbot.** 1997. Glycerol generates turgor in rice blast. Nature **389:**471-483.

20. **Dean, R. A.** 1997. Signal pathways and appressorium morphogenesis. Annual Review of Phytopathology **35:**211-234.

21. **Dean, R. A., N. J. Talbot, D. J. Ebbole, M. L. Farman, T. K. Mitchell, M. J. Orbach, M. Thon, R. Kulkarni, J.-R. Xu, H. Pan, N. D. Read, Y.-H. Lee, I. Carbone, D. Brown, Y. Y. Oh, N. Donofrio, J. S. Jeong, D. M. Soanes, S. Djonovic, E. Kolomiets, C. Rehmeyer, W. Li, M. Harding, S. Kim, M.-H. Lebrun, H. Bohnert, S. Coughlan, J. Butler, S. Calvo, L.-J. Ma, R. Nicol, S. Purcell, C. Nusbaum, J. E. Galagan, and B. W. Birren.** 2005. The genome sequence of the rice blast fungus *Magnaporthe grisea*. Nature **434:**980-986.

22. **DeZwaan, T. M., A. M. Carroll, B. Valent, and J. A. Sweigard.** 1999. *Magnaporthe grisea* Pth11p is a novel plasma membrane protein that mediates appressorium differentiation in response to inductive substrate cues. Plant Cell **11:**2013-2030.

23. **Dixon, K. P., J.-R. Xu, N. Smirnoff, and N. J. Talbot.** 1999. Independent signaling pathways regulate turgor during hyperosmotic stress and appressorium-mediated plant infection by *Magnaporthe grisea*. Plant Cell **11:**2045-2058.

24. **Dufresne, M., S. Perfect, A.-L. Pellier, J. A. Bailey, and T. Langin.** 2000. A GAL4-like protein is involved in the switch between biotrophic and necrotrophic phases of the infection process of *Colletotrichum lindemuthianum* on common bean. Plant Cell **12:**1579-1590.

25. **Egan, M. J., and N. J. Talbot.** 2008. Genomes, free radicals and plant cell invasion: recent developments in plant pathogenic fungi. Current Opinion in Plant Biology **11:**367-372.

26. **Egan, M. J., Z. Y. Wang, M. A. Jones, N. Smirnoff, and N. J. Talbot.** 2007. Generation of reactive oxygen species by fungal NADPH oxidases is required for rice blast disease. Proceedings of the National Academy of Sciences of the USA **104:**11772-7.

27. **Fischer, R., N. Zekert, and N. Takeshita.** 2008. Polarized growth in fungi - interplay between the cytoskeleton, positional markers and membrane domains. Molecular Microbiology **68:**813-826.

28. **Fleißner, A., S. Diamond, and N. L. Glass.** 2009. The *Saccharomyces cerevisiae* PRM1 homolog in *Neurospora crassa* is involved in vegetative and sexual cell fusion events but also has postfertilization functions. Genetics **181:**497-510.

29. **Fleißner, A., and N. L. Glass.** 2007. SO, a protein involved in hyphal fusion in *Neurospora crassa*, localizes to septal plugs. Eukaryotic Cell **6:**84-94.

30. **Foster, A. J., J. M. Jenkinson, and N. J. Talbot.** 2003. Trehalose synthesis and metabolism are required at different stages of plant infection by *Magnaporthe grisea*. EMBO J **22:**225-235.

31. **Francis, S. H., and J. D. Corbin.** 1994. Structure and function of cyclic nucleotide-dependent protein kinase. Annual Review of Physiology **56:**237-272.

32. **Fujimoto, D., Y. Shi, D. Christian, J. B. Mantanguihan, and H. Leung.** 2002. Tagging quantitative loci controlling pathogenicity in *Magnaporthe grisea* by insertional mutagenesis. Physiological and Molecular Plant Pathology **61:**77-88.

33. **Galagan, J. E., S. E. Calvo, K. A. Borkovich, E. U. Selker, N. D. Read, D. Jaffe, W. FitzHugh, L.-J. Ma, S. Smirnov, S. Purcell, B. Rehman, T. Elkins, R. Engels, S. Wang, C. B. Nielsen, J. Butler, M. Endrizzi, D. Qui, P. Ianakiev, D. Bell-Pedersen, M. A. Nelson, M. Werner-Washburne, C. P. Selitrennikoff, J. A. Kinsey, E. L. Braun, A. Zelter, U. Schulte, G. O. Kothe, G. Jedd, W. Mewes, C. Staben, E. Marcotte, D. Greenberg, A. Roy, K. Foley, J. Naylor, N. Stange-Thomann, R. Barrett, S. Gnerre, M. Kamal, M. Kamvysselis, E. Mauceli, C. Bielke, S. Rudd, D. Frishman, S. Krystofova, C. Rasmussen, R. L. Metzenberg, D. D. Perkins, S. Kroken, C. Cogoni, G. Macino, D. Catcheside, W. Li, R. J. Pratt, S. A. Osmani, C. P. C. DeSouza, L. Glass, M. J. Orbach, J. A. Berglund, R. Voelker, O. Yarden, M. Plamann, S. Seiler, J. Dunlap, A. Radford, R. Aramayo, D. O. Natvig, L. A. Alex, G. Mannhaupt, D. J. Ebbole, M. Freitag, I. Paulsen, M. S. Sachs, E. S. Lander, C. Nusbaum, and B. Birren.** 2003. The genome sequence of the filamentous fungus *Neurospora crassa*. Nature **422:**859-868.

34. **Galagan, J. E., M. R. Henn, L.-J. Ma, C. A. Cuomo, and B. Birren.** 2006. Genomics of the fungal kingdom: insights into eukaryotic biology. Cold Spring Harbor Monograph Series **46:**41-69.

35. **Gaulin, E., A. Jauneau, F. Villalba, M. Rickauer, M.-T. Esquerre-Tugaye, and A. Bottin.** 2002. The CBEL glycoprotein of Phytophthora parasitica var-nicotianae is involved in cell wall deposition and adhesion to cellulosic substrates. Journal of Cell Science **115:**4565-4575.

36. **Gilbert, M. J., C. R. Thornton, G. E. Wakley, and N. J. Talbot.** 2006. A P-type ATPase required for rice blast disease and induction of host resistance. Nature **440:**535-539.

37. **Gurpreet, K. B., W. Zheng-Yi, M. S. Darren, E. W. Gavin, and J. T. Nicholas.** 2006. Peroxisomal carnitine acetyl transferase is required for elaboration of penetration hyphae during plant infection by *Magnaporthe oryzae*. Molecular Microbiology **61:**46-60.

38. **Hamer, J. E., B. Valent, and F. G. Chumley.** 1989. Mutations at the SMO genetic locus affect the shape of diverse cell types in the rice blast fungus. Genetics **122:**351-361.

39. **Hamer, S. K., R. J. Howard, F. G. Chumley, and B. Valent.** 1988. A mechanism for surface attachment in spores of a plant pathogenic fungus. Science **239:**288-290.

40. **Hieter, P., and M. Boguski.** 1997. Functional Genomics: It's all how you read it. Science **278:**601-602.

41. **Hogg, P. J.** 2003. Disulfide bonds as switches for protein function. Trends in Biochemical Sciences **28:**210-214.

42. **Howard, R. J., M. A. Ferrari, D. H. Roach, and N. P. Money.** 1991. Penetration of hard substrates by a fungus employing enormous turgor pressures. Proceedings of the National Academy of Sciences of the USA **88:**11281-11284.

43. **Howard, R. J., and B. Valent.** 1996. Breakingand entering: host penetration by the fungal rice blast pathogen *Magnaporthe grisea*. Annual Review of Microbiology **50:**491-512.

44. **Idnurm, A., and B. J. Howlett.** 2001. Pathogenicity genes in phytopathogenic fungi. Molecular Plant Pathology **2:**241-255.

45. **Ivey, F. D., P. N. Hodge, G. E. Turner, and K. A. Borkovich.** 1996. The G alpha i homologue *gna-1* controls multiple differentiation pathways in *Neurospora crassa*. Molecular Biology of the Cell **7:**1283-1297.

46. **Jaffe, A. B., and A. Hall.** 2005. Rho GTPases: biochemistry and biology. Annual Review of Cell and Developmental Biology **21:**247-269.

47. **Jelitto, T. C., H. A. Page, and N. D. Read.** 1994. Role of external signals regulating the pre-penetration phase of infection by the rice blast fungus, *Magnaporthe grisea*. Planta **194:**471-477.

48. **Jeon, J., J. Goh, S. Yoo, M.-H. Chi, J. Choi, H.-S. Rho, J. Park, S.-S. Han, B. R. Kim, S.-Y. Park, S. Kim, and Y.-H. Lee.** 2008. A putative MAP kinase kinase kinase, MCK1, is required for cell wall integrity and pathogenicity of the rice blast fungus, *Magnaporthe oryzae*. Molecular Plant-Microbe Interactions **21:**525-534.

49. **Kahmann, R., and C. Basse.** 2001. Fungal gene expression during pathogenesis-related development and host colonization. Current Opinion in Microbiology **4:**374-380.

50. **Kamakura, T., S. Yamaguchi, K.-i. Saitho, T. Teraoka, and I. Yamaguchi.** 2002. A novel gene, CBP1, encoding a putative extracellular chitin-binding protein, may play an important role in the hydrophobic surface sensing of *Magnaporthe grisea* during appressorium differentiation. Molecular Plant-Microbe Interactions **15:**437-444.

51. **Kana-uchi, A., C. T. Yamashiro, S. Tanabe, and T. Murayama.** 1997. A *ras* homologue of *Neurospora crassa* regulates morphology. Molecular Genetics and Genomics **254:**427-432.

52. **Kankanala, P., K. Czymmek, and B. Valent.** 2007. Roles for rice membrane dynamics and plasmodesmata during biotrophic invasion by the blast fungus. Plant Cell **19:**706-724.

53. **Kays, A. M., and K. A. Borkovich.** 2004. Severe impairment of growth and differentiation in a *Neurospora crassa* mutant lacking all heterotrimeric G-alpha proteins. Genetics **166:**1229-1240.

54. **Kore-Eda, S., T. Murayama, and I. Uno.** 1991. Isolation and charcterization of the adenylate cyclase structural gene of *Neurospora crassa*. Japanese Journal of Genetics **66:**317-334.

55. **Kothe, G. O., and S. J. Free.** 1998. The isolation and characterization of *nrc-1* and *nrc-2*, two genes encoding protein kinases that control growth and development in *Neurospora crassa*. Genetics **149:**117-130.

56. **Kulkarni, R. D., M. R. Thon, H. Pan, and R. A. Dean.** 2005. Novel G-protein-coupled receptor-like proteins in the plant pathogenic fungus *Magnaporthe grisea*. Genome Biology **6:**R24.1-14.

57. **Lau, G. W., and J. E. Hamer.** 1998. Acropetal: a genetic locus required for conidiophore architecture and pathogenicity in the rice blast fungus. Fungal Genetics and Biology **24:**228-239.

58. **Lengeler, K. B., R. C. Davidson, C. D'Souza, T. Harashima, W.-C. Shen, P. Wang, X. Pan, M. Waugh, and J. Heitman.** 2000. Signal transduction cascade regulating fungal development and virulence. Microbiology and Molecular Biology Reviews **64:**746-785.

59. **Li, D., P. Bobrowicz, H. H. Wilkinson, and D. J. Ebbole.** 2005. A mitogen-activated protein kinase pathway essential for mating and contributing to vegetative growth in *Neurospora crassa*. Genetics **170:**1091-1104.

60. **Li, L., C. Y. Xue, K. Bruno, M. Nishimura, and J. R. Xu.** 2004. Two PAK kinase genes, CHM1 and MST20, have distinct functions in *Magnaporthe grisea*. Molecular Plant-Microbe Interactions **17:**547-556.

61. **Liu, H., A. Suresh, F. S. Willard, D. P. Siderovski, S. Lu, and N. I. Naqvi.** 2007. Rgs1 regulates multiple G alpha subunits in *Magnaporthe* pathogenesis, asexual growth and thigmotropism. EMBO J **26:**690-700.

62. **Liu, S., and R. A. Dean.** 1997. G protein alpha subunit genes control growth, development, and pathogenicity of *Magnaporthe grisea*. Molecular Plant and Microbe Interactions **10:**1075-1086.

63. **Maerz, S., C. Ziv, N. Vogt, K. Helmstaedt, N. Cohen, R. Gorovits, O. Yarden, and S. Seiler.** 2008. The nuclear Dbf2-related kinase COT1 and the mitogen-activated protein kinases MAK1 and MAK2 genetically interact to regulate filamentous growth, hyphal fusion and sexual development in *Neurospora crassa*. Genetics **179:**1313-1325.

64. **Mehrabi, R., S. Ding, and J.-R. Xu.** 2008. MADS-box transcription factor Mig1 is required for infectious growth in *Magnaporthe grisea*. Eukaryotic Cell **7:**791-799.

65. **Mitchell, T. K., and R. A. Dean.** 1995. The cAMP-dependent protein kinase catalytic subunit is required for appressorium formation and pathogenesis be the rice blast pathogen *Magnaporthe grisea*. The Plant Cell **7:**1869-1878.

66. **Nelson, W. J.** 2003. Adaptation of core mechanisms to generate cell polarity. Nature **422:**766-774.

67. **Ninomiya, Y., K. Suzuki, C. Ishii, and H. Inoue.** 2004. Highly efficient gene replacements in Neurospora strains deficient for nonhomologous end-joining. Proceedings of the National Academy of Sciences of the USA **101:**12248-53.

68. **Nishimura, M., G. Park, and J.-R. Xu.** 2003. The G-beta subunit MGB1 is involved in regulating multiple steps of infection-related morphogenesis in *Magnaporthe grisea*. Molecular Microbiology **50:**231-243.

69. **Oh, Y., N. Donofrio, H. Pan, S. Coughlan, D. Brown, S. Meng, T. Mitchell, and R. Dean.** 2008. Transcriptome analysis reveals new insight into appressorium formation and function in the rice blast fungus *Magnaporthe oryzae*. Genome Biology **9:**R85.

70. **Pandey, A., G. M. Roca, N. D. Read, and N. L. Glass.** 2004. Role of a mitogen-activated protein kinase pathway during conidial germination and hyphal fusion in *Neurospora crassa*. Eukaryotic Cell **3:**348-358.

71. **Park, G., C. Xue, X. Zhao, Y. Kim, M. Orbach, and J. R. Xu.** 2006. Multiple upstream signals converge on the adaptor protein Mst50 in *Magnaporthe grisea*. Plant Cell **18:**2822-2835.

72. **Park, G., G. Y. Xue, L. Zheng, S. Lam, and J. R. Xu.** 2002. *MST12* regulates infectious growth but not appressorium formation in the rice blast fungus *Magnaporthe grisea*. Molecular Plant-Microbe Interactions **15:**183-192.

73. **Perkins, D. D., B. C. Turner, V. C. Pollard, and A. Fairfield.** 1989. Neurospora strains incorporating fluffy, and their use as testers. Fungal Genetics Newsletter**:**64-67.

74. **Rasmussen, C. G., and N. L. Glass.** 2007. Localization of RHO-4 indicates differential regulation of conidial versus vegetative septation in the filamentous fungus *Neurospora crassa*. Eukaryotic Cell **6:**1097-1107.

75. **Roca, G. M., J. Arlt, C. E. Jeffree, and N. D. Read.** 2005. Cell biology of conidial anastomosis tubes in *Neurospora crassa*. Eukaryotic Cell **4:**911-919.

76. **Rolke, Y., and P. Tudzynski.** 2008. The small GTPase Rac and the p21-activated kinase Cla4 in *Claviceps purpurea*: interaction and impact on polarity, development and pathogenicity. Molecular Microbiology **68:**405-423.

77. **Seiler, S., and M. Plamann.** 2003. The genetic basis of cellular morphogenesis in the filamentous fungus *Neurospora crassa*. Molecular Biology of the Cell **14:**4352-4364.

78. **Shi, Z., and H. Leung.** 1995. Genetic analysis of sporulation in *Magnaporthe grisea* by chemical and insertional mutagenesis. Molecular Plant-Microbe Interactions **8:**949-959.

79. **Soanes, D. M., M. J. Kershaw, R. N. Cooley, and N. J. Talbot.** 2002. Regulation of the *MPG1* hydrophobin gene in the rice blast fungus *Magnaporthe grisea*. Molecular Plant-Microbe Interactions **15:**1253-1267.

80. **Soonok, K., A. Il-Pyung, R. Hee-Sool, and L. Yong-Hwan.** 2005. *MHP1*, a *Magnaporthe grisea* hydrophobin gene, is required for fungal development and plant colonization. Molecular Microbiology **57:**1224-1237.

81. **Soundararajan, S., G. Jedd, X. Li, M. Ramos-Pamplona, N. H. Chua, and N. I. Naqvi.** 2004. Woronin body function in *Magnaporthe grisea* is essential for efficient pathogenesis and for survival during nitrogen starvation stress. Plant Cell **16:**1564-1574.

82. **Stark, M. J. R.** 2004. Protein phosphorylation and dephosphorylation, p. 284-344. *In* J. R. Dickinson and M. Schweizer (ed.), The metabolism and molecular physiology of *Saccharomyces cerevisiae*, 2nd ed. CRC Press LLC, Boca Raton.

83. **Sweigard, J. A., A. M. Carroll, L. Farrall, F. G. Chumley, and B. Valent.** 1998. *Magnaporthe grisea* pathogenicity genes obtained through insertional mutagenesis. Molecular Plant-Microbe Interactions **11:**404-412.

84. **Takemoto, D., A. Tanaka, and B. Scott.** 2007. NADPH oxidases in fungi: diverse roles of reactive oxygen species in fungal cellular differentiation. Fungal Genetics and Biology **44:**1065-1076.

85. **Talbot, N. J.** 2003. On the trail of a cereal killer: exploring the biology of *Magnaporthe grisea*. Annual Review of Microbiology **57:**177-202.

86. **Talbot, N. J., D. J. Ebbole, and J. E. Hamer.** 1993. Identification and characterization of *MPG1*, a gene involved in pathogenicity from the rice blast fungus *Magnaporthe grisea*. Plant Cell **5:**1575-1590.

87. **Talbot, N. J., A. J. Foster, P. V. Balhadere, S. L. Tucker, L. J. Holcombe, J. L. Jenkinson, E. Thines, and R. W. S. Weber.** 2002. Molecular genetics of appressorium-mediated plant infection by *Magnaporthe grisea*. Biology of Plant-Microbe Interactions **3:**197-202.

88. **Thines, E., R. W. S. Weber, and N. J. Talbot.** 2000. MAP kinase and protein kinase A-dependent mobilization of triacylglycerol and glycogen during appressorium turgor generation by *Magnaporthe grisea*. Plant Cell **12:**1703-1718.

89. **Toledo, I., J. Aguirre, and W. Hansberg.** 1994. Enzyme inactivation related to a hyperoxidant state during conidiation of *Neurospora crassa*. Microbiology **140:**2391-2397.

90. **Tucker, S. L., and N. J. Talbot.** 2001. Surface attachment and pre-penetration stage development by plant pathogenic fungi. Annual Review of Phytopathology **39:**385-417.

91. **Urban, M., E. Mott, T. Farley, and K. Hammond-Kosack.** 2003. The *Fusarium graminearum MAP1* gene is essential for pathogenicity and development of perithecia. Molecular Plant Pathology **4:**347-359.

92. **Veneault-Fourrey, C., M. Barooah, M. Egan, G. Wakley, and N. J. Talbot.** 2006. Autophagic fungal cell death is necessary for infection by the rice blast fungus. Science **312:**580-583.

93. **Viaud, M. C., P. V. Balhadere, and N. J. Talbot.** 2002. A *Magnaporthe grisea* cyclophilin acts as a virulence determinant during plant infection. Plant Cell **14:**917-930.

94. **Villalba, F., M.-H. Lebrun, A. Hua-Van, M.-J. Daboussi, and M.-C. Grosjean-Cournoyer.** 2001. Transposon impala, a novel tool for gene tagging in the rice blast fungus *Magnaporthe grisea*. Molecular Plant-Microbe Interactions **14:**308-315.

95. **Virag, A., M. P. Lee, H. Si, and S. D. Harris.** 2007. Regulation of hyphal morphogenesis by *cdc42* and *rac1* homologues in *Aspergillus nidulans*. Molecular Microbiology **66:**1579-1596.

96. **Wang, Z.-Y., J. M. Jenkinson, L. J. Holcombe, D. M. Soanes, C. Veneault-Fourrey, G. K. Bhambra, and N. J. Talbot.** 2005. The molecular biology of appressorium turgor generation by the rice blast fungus *Magnaporthe grisea*. Biochemical Society Transactions **33:**384-388.

97. **Wilson, R. A., J. M. Jenkinson, R. P. Gibson, J. A. Littlechild, Z.-Y. Wang, and N. J. Talbot.** 2007. Tps1 regulates the pentose phosphate pathway, nitrogen metabolism and fungal virulence. EMBO J **26:**3673-3685.

98. **Wilson, R. A., and N. J. Talbot.** 2009. Under pressure: investigating the biology of plant infection by *Magnaporthe oryzae*. Nature Reviews Microbiology **7:**185-195.

99. **Xu, J.-R.** 2000. MAP kinases in fungal pathogens. Fungal Genetics and Biology **31:**137-152.

100. **Xu, J.-R., Y.-L. Peng, M. B. Dickmann, and A. Sharon.** 2006. The dawn of fungal pathogen genomics. Annual Review of Phytopathology **44:**337-366.

101. **Xu, J.-R., C. J. Staiger, and J. E. Hamer.** 1998. Inactivation of the mitogen-activated protein kinase Mps1 from the rice blast fungus prevents penetration of host cells but allows activation of plant defense responses. Proceedings of the National Academy of Sciences of the USA **95:**12713-12718.

102. **Xu, J. R., and J. E. Hamer.** 1996. MAP kinase and cAMP signaling regulate infection structure formation and pathogenic growth in the rice blast fungus *Magnaporthe grisea*. Genes and Development **10:**2696-2706.

103. **Xu, J. R., X. Zhao, and R. A. Dean.** 2007. From genes to genomes: a new paradigm for studying fungal pathogenesis in *Magnaporthe oryzae*. Advances in Genetics **57:**175-218.

104. **Xue, C. Y., G. Park, W. B. Choi, L. Zheng, R. A. Dean, and J. R. Xu.** 2002. Two novel fungal virulence genes specifically expressed in appressoria of the rice blast fungus. Plant Cell **14:**2107-2119.

105. **Zhao, X. H., Y. Kim, G. Park, and J. R. Xu.** 2005. A mitogen-activated protein kinase cascade regulating infection-related morphogenesis in *Magnaporthe grisea*. Plant Cell **17:**1317-1329.

106. **Zhao, X. H., and J. R. Xu.** 2007. A highly conserved MAPK-docking site in Mst7 is essential for Pmk1 activation in *Magnaporthe grisea*. Molecular Microbiology **63:**881-894.

107. **Zheng, W., J. Chen, W. Liu, S. Zheng, J. Zhou, G. Lu, and Z. Wang.** 2007. A Rho3 homolog is essential for appressorium development and pathogenicity of *Magnaporthe grisea*. Eukaryotic Cell **6:**2240-2250.

Chapter 4 – Cell polarity and the actin cytoskeleton during cell fusion

4.1. Abstract

The establishment and maintenance of cell polarity is an obvious prerequisite for spore germination and cell fusion in *Neurospora crassa*. Without the ability to break cell symmetry, a cell is limited to isotropic growth and unable to differentiate polarised cell protrusions, including GTs and CATs. During CAT homing, polarised tip growth is spatially directed along a chemoattractant gradient to facilitate cell-cell contact and fusion. The molecular mechanisms involving cortical markers and the cytoskeleton to achieve directionality during CAT homing is virtually unknown. This chapter will briefly review how cell polarity and directed tip growth is achieved in filamentous fungi, and how two newly developed fluorescent reporters for the visualization of the actin cytoskeleton and activated Rho GTPases provided new insights into this vital process in living cells of *N. crassa*. The novel live-cell imaging markers Lifeact-TagRFP/-T and CRIB-sGFP were developed and used for the first time in filamentous fungi, and revealed that highly dynamic rearrangements of F-actin cables and patches, as well as localized activation of CDC42/RAC-1 GTPases at the cell cortex are essential for CAT formation, homing and fusion. Co-expression of Lifeact-TagRFP with the microtubule marker BML-sGFP, furthermore, allowed simultaneous imaging of both cytoskeletal elements and revealed distinct yet coordinated dynamics during cell symmetry breaking and GT and CAT polarised protrusion.

4.2. Introduction

4.2.1. Generating cell polarity

In single cell ascomycete yeasts, such as *Saccharomyces cerevisiae* and *Schizosaccharomyces pombe*, polarised growth is restricted to certain times of the cell cycle occuring only during budding, mating and fission [20]. Studies in these systems, however, allowed invaluable insights into how cell polarity is established [93, 94], and identified the central role of the cytoskeleton in this process [33, 34, 70, 94]. Although the yeast models provide an extremely useful framework, some unique features of polarised growth in filamentous fungi, cannot be explained by simple extrapolation from the yeast paradigm [45]. These include the ability to establish and permanently maintain multiple axis of polarity [147], the formation of morphologically and physiologically distinct protrusions from one cell during vegetative growth (germ tubes and conidial anastomosis tubes) [100, 105, 106], and the extremely rapid extension rates of mature hyphae [132, 133]. Tip growth of mature hyphae has recently been found to be determined by three main conditions: permanent presence of the polarity machinery in a confined cortical area, organized accumulation of vesicles and a subset of polarity components close to this area, and spatial separation of the zones of exocytosis (tip front) and endocytosis (tip rim) [65]. The formation and maintenance of sustained polarised growth during hyphal morphogenesis is a defining feature of filamentous fungi [44] making them attractive models for studying the role of the fungal cytoskeleton in cell polarity, tip growth and organelle transport. These topics have been intensively studied and substantially progressed in recent years, especially since genomes of numerous filamentous fungal species became available [16, 37, 44, 114, 131]. Polarity establishment occurs at three distinct points in the vegetative growth phase of filamentous fungi: (1) the elaboration of a germ tube (GT) which elongates, septates and eventually develops into the vegetative hyphae of the mature mycelium [16, 82], (2) the formation of conidial anastomosis tubes (CATs) directly from conidia or

GTs that are attracted to and fuse with other CATs to form a germling network [99, 105, 106], as well as the initiation of apical and lateral branches from mature hyphae [44, 82, 132].

Disruption of the cytoskeleton, either genetically or chemically, generally causes severe defects during spore germination, hyphal tip growth, septation and branching [28, 55, 108, 130, 138]. Furthermore, filamentous fungi use different sets of proteins that are not present or not associated with budding or mating in yeasts [45, 64] or *vice versa*, including the Rho-type GTPase RAC-1, which is not encoded in the *S. cerevisiae* or *S. pombe* genomes [59], or polarity markers, such as TeaC and TeaR from *A. nidulans*, which share only very little homology with the functional yeast counterparts [37].

The basic toolbox of core molecular mechanisms to organise polar growth, however, appears to be conserved amongst eukaryotes, and includes landmark proteins providing positional cues for the assembly of modular protein scaffolds at the cell cortex, which then direct localized formation and orientation of the cytoskeleton, and specify targeted vesicle delivery to the incipient growth site [37, 86]. Several protein pathways interactively regulate the polarity machinery and are schematically summarized in Fig. 4.1.

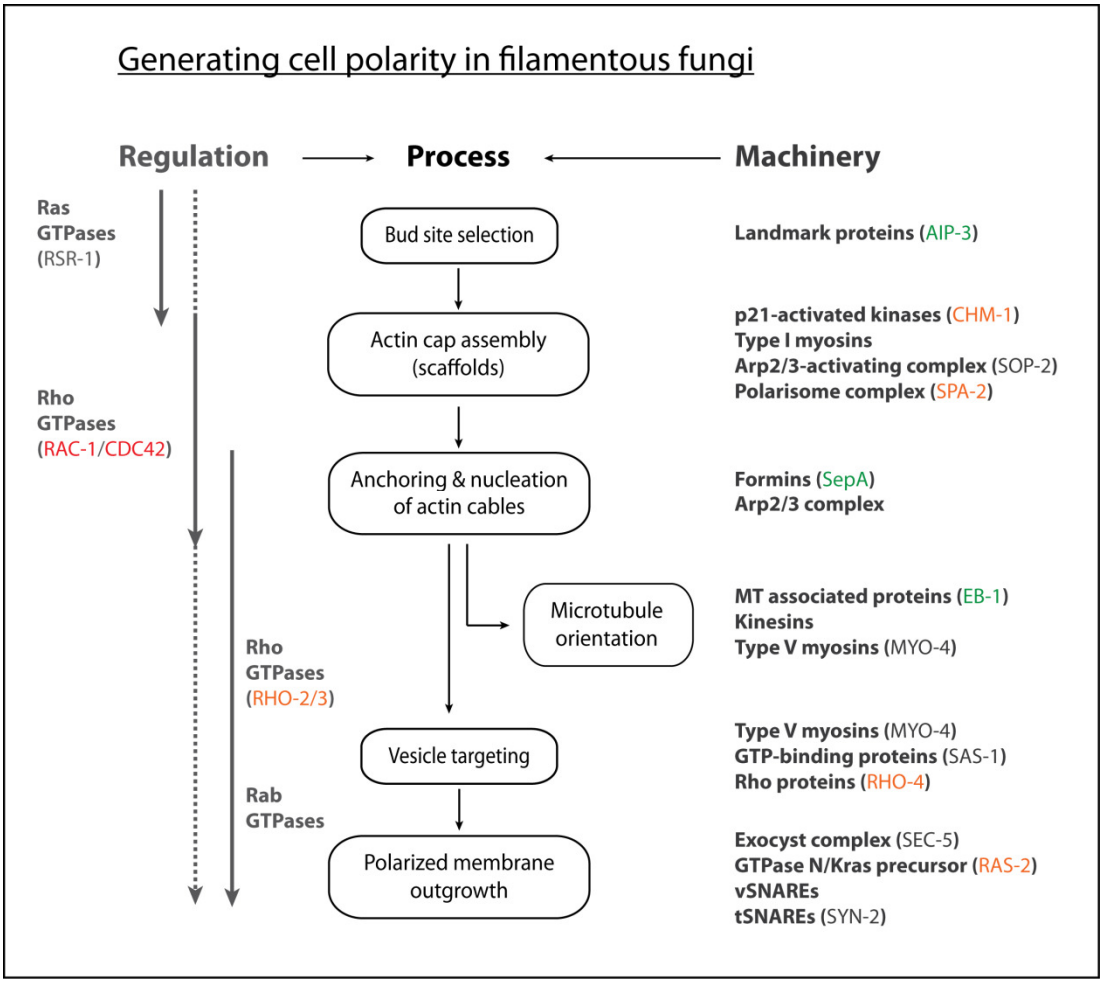

Figure 4.1 Protein pathways generating cell polarity in filamentous fungi. Hierarchical organization of morphogenetic regulators, cellular processes and molecular machineries linking bud-site selection to assembly of an actin cap, anchoring and nucleation of actin cables, recruitment of microtubules, and targeted vesicle secretion ultimately resulting in polarised outgrowth of GTs, CATs or hyphal branches. Selected proteins acting in these various processes are indicated in brackets; some of which have been investigated within this study. Proteins highlighted in red are essential for hyphal fusion, whereas proteins highlighted in orange have been found to severely reduce or delay cell fusion in gene deletion mutants (Table 3.6). Proteins marked in green have been found to be dispensable for hyphal fusion, although often leading to other severe defects. Gene deletion mutants of proteins marked in grey were not included in this study. Diagram adapted from [86] for filamentous fungi; additional information in [18, 33, 37, 44, 64, 114, 122, 140].

4.2.2. The role of the Spitzenkörper in organizing polarity

The Spitzenkörper (Spk) is a complex, multicomponent structure dominated by vesicles and tethered to the apical plasma membrane of mature hyphae [17, 47, 51]. It has a unique role in spatially and temporally organizing the polarity machinery. It moves within the apical dome and controls the directionality of tip growth [30, 41, 72, 103]. New Spk arise at sites of branch initiation supporting the idea that it acts as vesicle supply centre for targeted secretion of new cell wall material involved in cell surface expansion [8, 51, 101]. However, the mechanism of Spk motility is unknown, but might involve concerted action of the actin and microtubule cytoskeleton, in order to maintain the integrity of the Spk at the growing tip [120], and also might act as a 'relay station' from long-distance transport along microtubules to short-distance F-actin-mediated targeted vesicle delivery [47, 98]. Integrity of the Spk is crucial for the initiation and directed growth of fusion hyphae and persists until fusion pore widening occurs (Fig. 1.7e) [42, 50]. Very recent data indicates that the Spk itself is functionally stratified [136]. Macrovesicles containing components of the glucan synthase machinery and chitin synthase laden microvesicles arrive separately at the apex, but congregate in distinct strata of the Spk. The functional reason for this discrimination is not yet understood but could be related to different and morphogenetically relevant patterns of migration and exocytotic discharge for each vesicle type [136]. Interestingly, an equivalent vesicular accumulation within germlings of *N. crassa* has not yet been reported, leaving the fundamental questions of how directionality of tip growth is controlled during GT avoidance and CAT homing currently unanswered. A phase-dark immature Spk does not appear before 10 h after germination and may be considered to mark the transition from GTs to mature hyphae (Table 1.1). It might be expected, although has yet to be shown, that the same molecular components that already have been identified in mature hypha will be required to regulated tip

orientation in GTs and CATs, but how they are organized and interact with the cytoskeleton requires further investigation.

4.2.3. Microtubules are not essential for the generation of cell polarity

In *S. cerevisiae* actin-mediated vesicle transport is sufficient for the establishment and maintenance of polar cell extension, whereas in *S. pombe* microtubules are additionally required to specify the polarisation site [25, 37]. In filamentous fungi cytoplasmic microtubules typically exist in longitudinal arrays that are oriented parallel to the axis of hyphal extension [44]. They serve as tracks for directed long-distance transport of endo- and exocytotic vesicles: dynein moves towards the minus end of microtubules, and kinesins take their cargo to the plus end towards the tip apex [120, 135]. But unlike actin filaments, microtubules are not required for the establishment of polarised hyphal growth [49]. When assembly of microtubules is disrupted, e.g. by treatment with benomyl or the mutational inactivation of tubulin genes, fungal cells still polarize [23, 55]. However, in the absence of microtubules correct positioning of the Spk is affected, leading to the formation of unstable polarity axes and the inability of hyphae to extend in a linear manner [103], and to achieve maximal extension rates [55].

4.2.4. The major components of the fungal actin cytoskeleton

Actin is a highly conserved protein found in all eukaryotes and exists in a monomeric form (globular actin or G-actin) and polymeric form (filamentous actin or F-actin). Actin monomers bind and hydrolyse ATP in order to self-assemble into the polymer. G-actin nucleation is the rate-limiting step in actin filament formation

and therefore aided by a variety of actin-binding proteins (ABPs), such as profilins and formins (comprehensively reviewed in [84]). Numerous pharmacological and genetic studies in fungi have demonstrated crucial roles for F-actin in cell polarity, exocytosis, endocytosis and organelle movement [6, 7, 88, 118, 119, 138]. Phalloidin staining, immunofluorescent labelling, and fluorescent protein-based live-cell imaging have revealed three distinct sub-populations of F-actin-containing structures in fungi: patches, cables and rings [1, 31, 63, 142, 152]. Actin patches are associated with the plasma membrane and represent an accumulation of F-actin around endocytic vesicles [4, 58, 134]. Actin cables are bundles of F-actin stabilized by cross-linking proteins such as tropomyosins [94] and fimbrin [60]. They are assembled by formins [33, 34, 109] at sites of active growth where they form tracks for myosin-V-dependent polarised secretion and organelle transport [20, 35, 112]. Cables, unlike patches, are absolutely required for polarised growth in *S. cerevisiae* [84, 93]. Contractile actomyosin rings are essential for cytokinesis in yeasts, whereas in filamentous fungi actin rings are less well studied but are known to be involved in septum formation [46, 63, 96, 97]. In *N. crassa* and other filamentous fungi, disruption of the actin cytoskeleton leads to rapid tip swelling, indicating perturbation of polarised tip growth, and clearly demonstrates a critical role for F-actin in targeted secretion to particular sites on the plasma membrane [7, 23, 49].

4.2.5. Rho GTPase shuttling and the CRIB motif

Cellular polarisation can occur as a response to distinct intracellular or extracellular cues, such as cortical landmarks, nutrient gradients or pheromones. However, in the absence of such signals cells can still select a polarisation axis at random [90]. In any case, symmetry breaking depends on the localized recruitment of activated small GTPases which in turn activate their effectors to initiate formation of a crescent-shaped polar cap. Within this region rearrangements of the actin cytoskeleton and targeted secretion are orchestrated to initiate polarised protrusion

of the plasma membrane (Fig. 4.1). The Ras superfamily of small guanosine triphosphatases (GTPases), such as the Rho-type GTPases Cdc42 and Rac-1, have a central role in this event [59, 140, 149]. They switch between a GDP-bound inactive and GTP-bound active state whilst being shuttled between cytoplasm and plasma membrane [43]. The GTP-bound form interacts with effector molecules to regulate a plethora of cellular processes, and its intrinsic GTPase activity switches the signal off by hydrolysing GTP. A number of accessory proteins including guanine nucleotide dissociation inhibitors (GDIs) [113], guanine nucleotide exchange factors (GEFs) [111] and GTPase activating proteins (GAPs) [12], regulate and catalyse this process. This shuttling mechanism is energy dependent and results in focussing activated GTPase clusters – both in amplitude and spatial confinement – in a specific region at the apical plasma membrane (Fig. 4.2) .

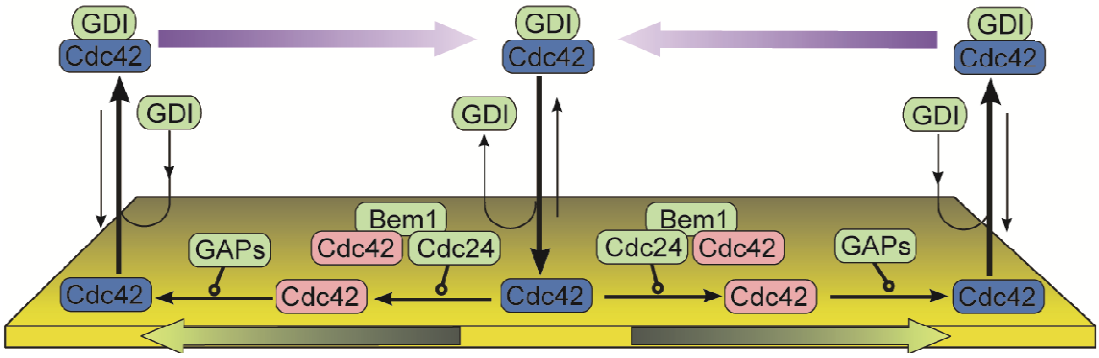

Figure 4.2 Membrane-cytoplasmic shuttling mechanism of yeast Rho GTPases. GDI reversibly deposits inactive Cdc42p (blue) on the membrane and recycles it back to the cytoplasm. Cdc24p (GEF) and Bem1p (scaffold) independently shuttle between cytoplasm (not shown in diagram). Cdc24p-Bem1p complex formation increases retention of Cdc24p in the membrane and resembles the catalytically potent form to activate membrane-bound Cdc42p. In the heterotrimeric complex Cdc42p is active (pink) and in turn activates its effectors. Activated Cdc42p remains at the membrane until it is deactivated by a GAP and extracted by GDI. Thick black arrows represent the predominant direction of the membrane-cytoplasmic exchange; open circle arrowheads indicate catalysis; colored arrows represent the diffusion flux direction on the membrane and in the cytoplasm. Modified from [43].

The Cdc42- and Rac-interactive binding (CRIB) motif is embedded within the p21-binding domain (PDB) and a hallmark of important effector proteins of Rho

GTPases. Six highly conserved residues within the CRIB consensus sequence (x I x x P- - x F x H x x H x x x D) are essential for the interaction of these effectors with GTP-bound Cdc42 and Rac-1 [21, 75]. A broad range of downstream effectors has been identified, including MAP kinases, p21-activated kinases (PAK), and the Wiscott-Aldrich Syndrome protein (WASP) family [14]. MAP kinases activity inside the nucleus can elicit changes in gene expression and important targets of PAKs include myosin light-chain kinases and other cytoskeletal components participating in Cdc42- and/or Rac-1-mediated actin rearrangements [53, 124]. *S. cerevisiae* possesses three PAKs (Ste20p, Cla4p and Skm1p) which are implicated in cytoskeletal rearrangements during modulation of cell morphology and polarity [69, 77, 150], and Cla4p has recently been shown to have a major role in cell symmetry breaking [57, 66]. The WASP family of proteins interact with the Arp2/3 complex to initiate F-actin polymerisation [13]. Specificity of either Cdc42- or Rac-1 mediated responses is regulated via different WASP-type effectors (N-WASP/Toca1 for Cdc42 and WAVE for Rac-1) that subsequently act on the Arp2/3 complex [59]. Fluorescent CRIB reporter constructs have been successfully used as biosensors to visualize the changing activation of endogenous Cdc42 in mammalian cells [85], and recently to monitor bipolarisation in fission yeast [128].

Besides the mere initiation of actin nucleation and elongation, structural changes to the actin cytoskeleton, including filament bundling, cross-linking, membrane-binding and severing, require an additional level of regulation. This has been best characterized for RHO-induced assembly of contractile actomyosin rings during cytokinesis in yeast, and recently been shown for RHO-4 during septa formation in *N. crassa* [97]. Detailed information about the activity and potential functional differences of the other Rho GTPases in filamentous fungi is to date very limited.

In *Neurospora* the major body of evidence on polarised tip growth has been accumulated through studies on mature hyphae and to a lesser extent by investigations on individual cells. Especially with respect to CAT-mediated cell

fusion a number of open questions remained: (1) is the establishment and maintenance of cell polarity differently regulated and achieved in GTs and CATs?, (2) how is directional growth of GTs and CATs controlled and by which cytoskeletal components is it facilitated?, (3) why do CATs show determinate growth?, (4) is depolarisation of CATs required prior to fusion, as indicated by tip swelling of fusion hyphae in the mature colony (Fig. 1.5)?, and (5) what roles do actin cables and patches play during cell fusion? Localized nucleation and remodelling of F-actin by spatially focused activity of Rho GTPases must play a key role in both, GT and CAT formation and during CAT-mediated cell fusion. However, live-cell imaging of F-actin architecture and dynamics during the establishment, maintenance and disruption of cell polarity has not been previously accomplished in *N. crassa*. Neither has the temporal and spatial correlation of these processes with the predicted recruitment of activated CDC42/RAC-1 GTPases been demonstrated. Research presented in this chapter aimed to fill these gaps.

4.3. Results

4.3.1. Lifeact-FP cloning and expression

The plasmid pAL2-Lifeact for the expression of Lifeact-tdTomato in *N. crassa* was prepared by subcloning the coding region for Lifeact-tdTomato from pJT580a into pBARGRG1 via *Eco*RI restriction digestion/ligation as described in sections 2.6.4-7. The plasmid pAL3-Lifeact encoding Lifeact-TagRFP was generated by amplifying the Lifeact-TagRFP coding region from pJT603f with oligonucleotides LA_if_BamHI_fw 5′-TTTCCTCGACGGATCCATGGGTGTCGCAGATTTGATCAAGA-3′ and TagRFP_if_EcoRV_rv 5′-ATCGATAAGCTTGATATCTTACTTGTACAGCTCGTCCATGCCA-3′ (underlined are the 15 bp overlaps to the host vector), and subsequently joining the purified PCR

product (section 2.6.12) into *BamH*I/*Eco*RV-linearized and gel purified (sections 2.6.4.-2.6.5) pBARGRG1 using In-Fusion® cloning (section 2.6.8). TagRFP used in this study was modified from its original version [80] by the addition of N- and C-terminal amino acids from GFP (VSKGE and LNGMDELYK, respectively), increasing its photostability and utility for 4D live-cell imaging [11]. To further increase the photostability of the reporter, pAL5-Lifeact, encoding Lifeact-TagRFP-T was generated by side-directed mutagenesis using oligonucleotides TagRFP_S162T_fw 5'-CCTGGAAGGCAGAA**A**<u>**C**</u>**C**GACATGGCCCTGAAGC-3' and its reverse complement TagRFP_S162T_rv 5'-GCTTCAGGGCCATGTC**G**<u>**G**</u>**T**TCTGCCTTCCAGG-3' (underlined is the mismatching nucleotide conferring S162T exchange). As verified by sequencing (section 2.6.10), all three strategies resulted in correct pDNA clones encoding Lifeact in-frame to each particular fluorescent protein (FP). Selected pDNA clones were amplified/extracted from *E.coli* using midiprep (section 2.6.1), and transformed into *N. crassa* by electroporation (section 2.10). As the integration of the expression plasmid was not targeted to a specific locus, but occurred randomly within the genome, at least five (on average nine) fluorescent transformants per construct were analysed by live-cell imaging (section 2.12), and those which showed consistently high expression under control of the inducible P*ccg-1* promotor [79], without artefactual localization of the reporter, were selected for further studies. Lifeact-TagRFP and Lifeact-TagRFP-T were of comparable brightness and showed markedly increased photostability compared to Lifeact-tdTomato. Lifeact-TagRFP-T was on average at least 10x more photostable than Lifeact-TagRFP *in vivo* (Fig. 4.3), which is consistent with the reported photophysical properties of the original TagRFP and TagRFP-T versions [117].

A

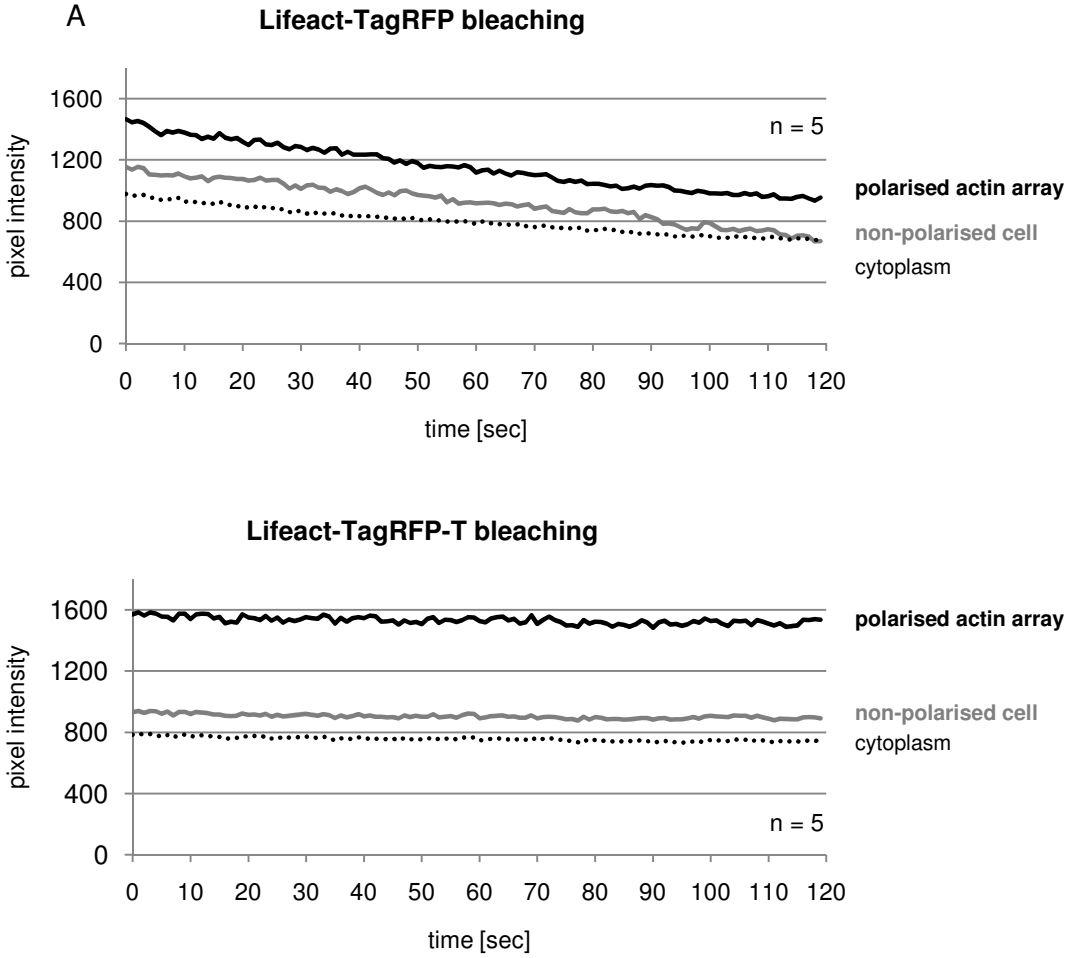

B

Bleaching rates [decrease grey levels/sec]	***Lifeact-TagRFP***	***Lifeact-TagRFP-T***
apical F-actin polarised cell	4.28	0.30
F-actin non-polarised cell	4.03	0.33
cytoplasmic F-actin	2.47	0.36
average (n=15)	**3.59**	**0.33**

Figure 4.3 Lifeact-TagRFP-T is on average 10x more photostable than Lifeact-TagRFP. **(A)** Cells expressing Lifeact-TagRFP or Lifeact-TagRFP-T were imaged with 1 frame/sec and 0.5 sec exposure to 60% of a 550 nm LED excitation light source over 2 minutes. Bleaching rates were measured in 20 µm² areas in three intracellular regions with different F-actin content. Graphs represent the mean of measurements from five individual cells. **(B)** On average, Lifeact-TagRFP lost 3.6 grey levels/sec, whereas Lifeact-TagRFP-T only bleached with 0.33 grey levels/sec, corresponding to average decay constants (k) of 0.003 ± 0.0007 and 0.0004 ± 0.0002, respectively.

Two clones for each fusion construct were selected for further investigations. All wt transformants chosen for live-cell imaging studies possessed normal colony morphologies and conidiation patterns, and isotropic or polarised tip growth were not affected (Fig. 4.4). In general, transformants which displayed phenotypic changes after random integration of the fusion construct were excluded from further analysis (Fig. 4.16 shows one example).

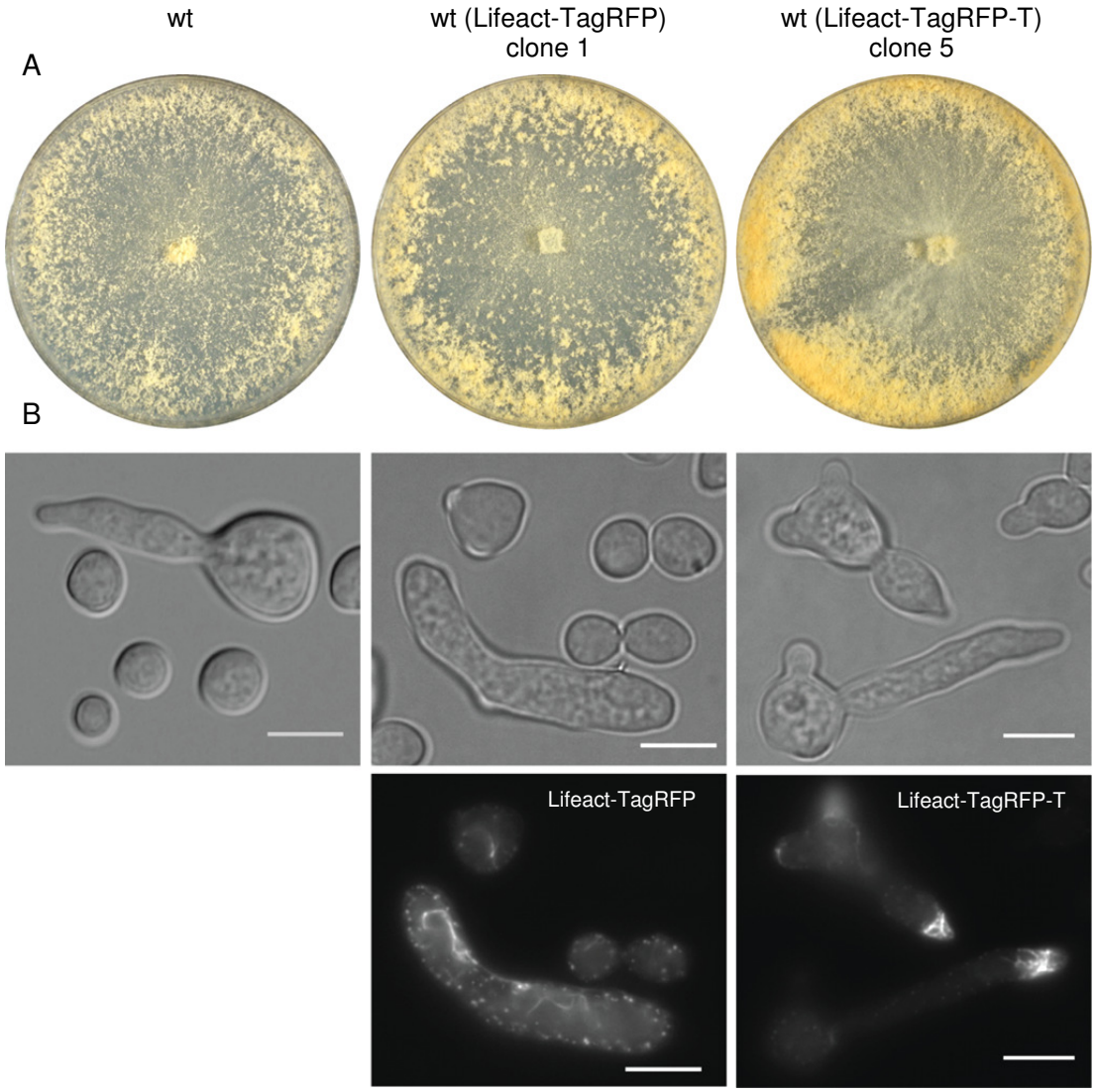

Figure 4.4 Ectopic expression of Lifeact-TagRFPs did not induce phenotypic defects. **(A)** Colony development and conidiation pattern of Lifeact-TagRFPs expressing transformants were unaffected and equivalent to the wt, after 72 h incubation on VM at 25°C and constant light. **(B)** Brightfield and epifluorescence images of conidial germlings. In comparison to the wt (left), spore morphologies of the transformants did not show unusual

phenotypic variation or obvious alterations during isotropic (middle) or polarised growth (right). In ungerminated conidia F-actin was evenly distributed throughout the cell, whereas during polarised tip growth dense arrays of actin cables accumulated at the tip apex. As these condensed F-actin arrays were usually extremely bright, F-actin elsewhere in the cell appeared much dimmer compared to non-polarised cells. Scale bars, 5 µm. See supplementary movies 4.1- 4.3.

4.3.2. Lifeact-TagRFPs robustly labelled F-actin patches, cables and rings

To image Lifeact-FPs widefield epifluorescence microscopy, often in combination with image deconvolution, was used as described in sections 2.12.3 and 2.12.4. Lifeact-TagRFP and Lifeact-TagRFP-T robustly labelled F-actin patches, cables and rings (Fig. 4.5). Although basic labelling of F-actin cables and patches was identical to that seen with Lifeact-TagRFPs, strains expressing Lifeact-tdTomato additionally showed mutlimerization artefacts in the form of brightly fluorescent rings in the cytoplasm which were not associated to any known cellular structure, as well as vacuolar accumulation of the reporter construct (Fig. 4.5B to D). Therefore, Lifeact-tdTomato was excluded from the project and all further studies were performed with Lifeact-TagRFP/-T, henceforth referred to as Lifeact-TagRFPs. The labelling pattern of both reporters was also identical to F-actin structures visualized with Lifeact-sGFP prepared in a parallel project [11].

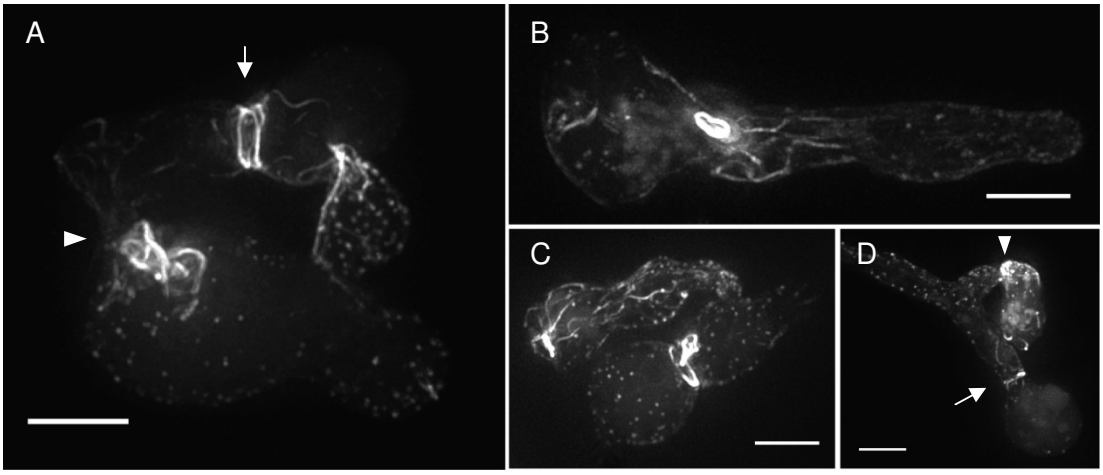

Figure 4.5 Lifeact-TagRFPs labelled F-actin cables, patches and rings. (A) Two fused wt cells expressing Lifeact-TagRFP. F-actin cables stretched throughout the spore body of the upper cell, whilst actin patches were distributed over the surface of the bottom cell. Dense arrays of actin cables were localized at the CAT fusion site (arrowhead), and condensed into an actin ring at the spore neck prior to septum formation (arrow). **(B to D)** Examples of wt conidia expressing Lifeact-tdTomato. **(B)** Conidial germling with actin cables aligned with the long axis of the GT. An extremely bright fluorescent ring is obvious but not associated to any known cellular structure. Also vacuolar accumulation of the fusion construct created artefactual background. **(C)** Two fusing germlings with bright fluorescent rings at different localizations within the cells. **(D)** Conidia in the process of CAT homing, apparent by the intense accumulation of actin patches and cables in the tip of the smaller cell (arrowhead). Formation of a cortical actin ring at the spore neck is again indicated with an arrow. All images show maximum intensity projection of deconvolved z-stacks. Scale bars, 5 µm.

4.3.3. Latrunculin A caused rapid loss of Lifeact-TagRFP labelled structures

Although Lifeact-TagRFP localization observed here was remarkably consistent with previous reports of F-actin distribution in yeast and filamentous fungi, we confirmed specificity of the probe for F-actin using Latrunculin A (Lat A). Latrunculins are potent inhibitors of F-actin polymerization and have been shown to cause rapid disruption of the actin cytoskeleton in fungi [6, 49, 92, 152]. Treatment with 10 µM Lat A led to a rapid loss of Lifeact-TagRFP fluorescence associated with patches and cables and a concomitant increase in cytoplasmic signal (Fig. 4.6A). After >5 min of incubation with Lat A Lifeact-TagRFP fluorescence became distributed uniformly within the cytoplasm indicating a complete loss of patches

and cables (Fig. 4.6 B), and confirmed that Lifeact-TagRFPs bind to F-actin in *N. crassa*. Assuming that Lat A only inhibited actin polymerization [6], these findings also indicated that complete turnover of F-actin in patches and most of the cables occurs within 4-5 min. Interestingly, we observed that dense cable arrays persisted much longer upon Lat A addition, especially those located in CAT connections. These cables eventually disassembled but their initial insensitivity to Lat A showed that the rate of F-actin polymerization varies within the population of cables. Occasionally a sub-population of cables was observed that did not appear to be tethered to a particular site and displayed random motion within the cytoplasm, and often formed ring-like aggregates (Fig. 4.6B).

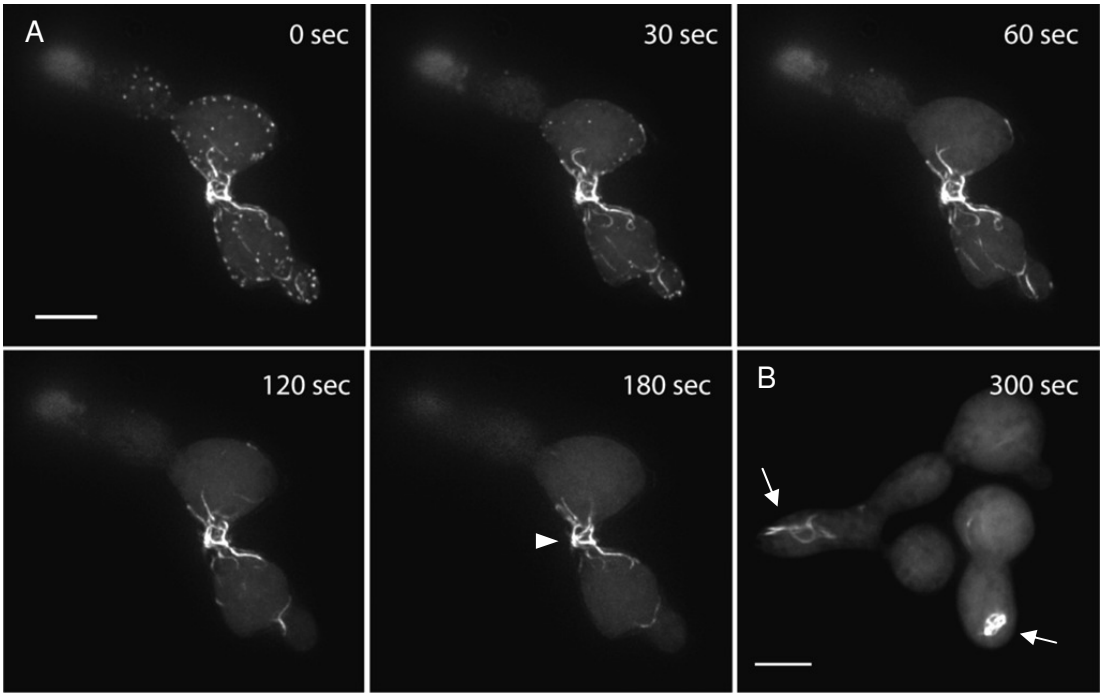

Figure 4.6 Disruption of F-actin upon Latrunculin A treatment. (A) Two fused wt conidia expressing Lifeact-TagRFP were treated with 10 µM Lat A (final concentration) at time point 10 sec. Cortical actin patches disappeared within 20 sec upon addition of Lat A, reflecting their high turnover rate. Thinner actin cables began to shrink shortly after and were lost within the first 1.5 min. Denser actin arrays within the cell connecting tube (arrowhead) remained largely unaffected for up to 3 min, indicating a slower turnover rate. **(B)** Fused germlings after 5 min of Lat A treatment. Cortical actin patches and cables have completely disappeared. Occasionally, residual actin aggregates remained (arrows). Scale bars, 5 µm.

4.3.4. F-actin caps marked sites of cell polarisation

In ungerminated conidia of *N. crassa* actin cables and patches were randomly and evenly distributed throughout the cell and along the cell cortex, respectively (Figs. 4.4, 4.8 and 4.10). Cell polarisation and germination always coincided with the localized assembly of an 'actin cap' at the cell cortex. Initiated polar caps were not immediately fixed at a specific site of the membrane, but were dynamically displaced and changed their position within minutes. Often more than one polar actin cap per cell could be observed, but usually only one persisted and was maintained prior to and during GT emergence (Fig. 4.7).

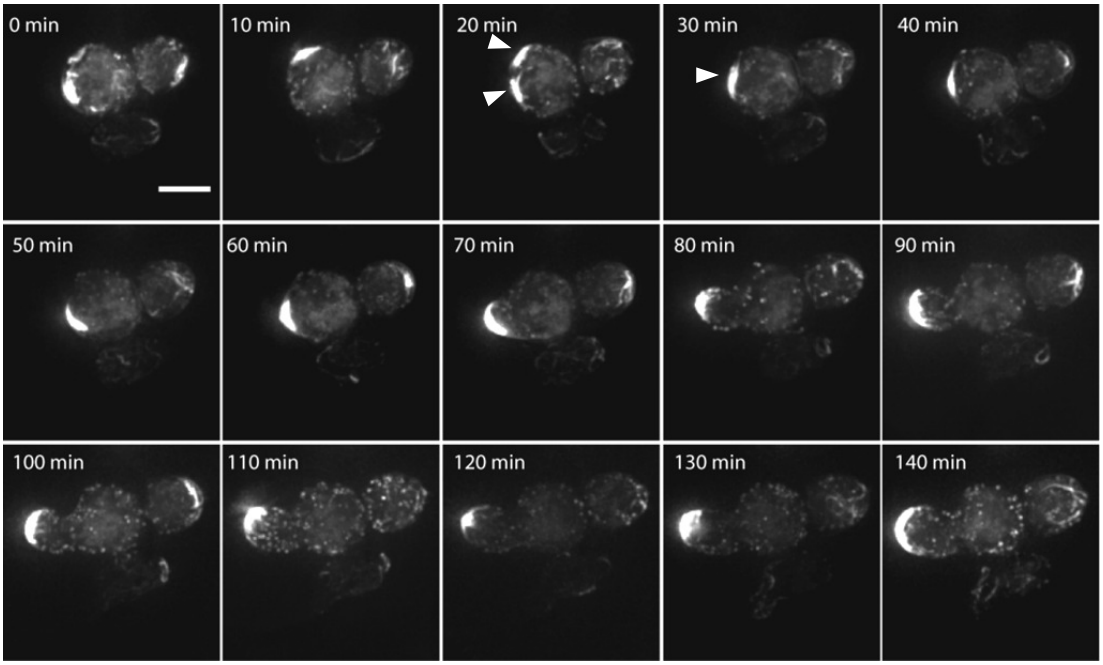

Figure 4.7 Actin cap formation during cell polarisation and germination. Within the first 20 min the cortical actin cap changed position and the cell established two polarisation sites at the same time (arrowheads), but eventually maintained only one. This cap appeared quite static over the following 30 min, and GT outgrowth was potentially arrested during nuclear division (see supplementary figure 4.1). After 60 min a GT bud emerged from that site and extended over the following hour. Over the entire time course a cortical F-actin cap was maintained at the GT apex. Scale bar, 5 µm.

Further analysis revealed another striking aspect of cable dynamics during GT emergence and elongation (after 2-4 h of incubation). Actin arrays were associated with sites of polarised growth in germlings; intriguingly, these arrays were not static but underwent recurrent retrograde flow from the elongating tip into the cell body (Fig. 4.8; Supplementary movie 4.4a). This behavior was commonly observed during GT elongation, and in almost all cases where an actin array was present at the growing tip we could follow its eventual retrograde flow. If the same tip was observed at a later time point it was possible to monitor the formation of a new cable array and its subsequent retrograde flow. The whole process of actin array formation, retrograde flow and dissolution generally occurred over a 2-10 min period.

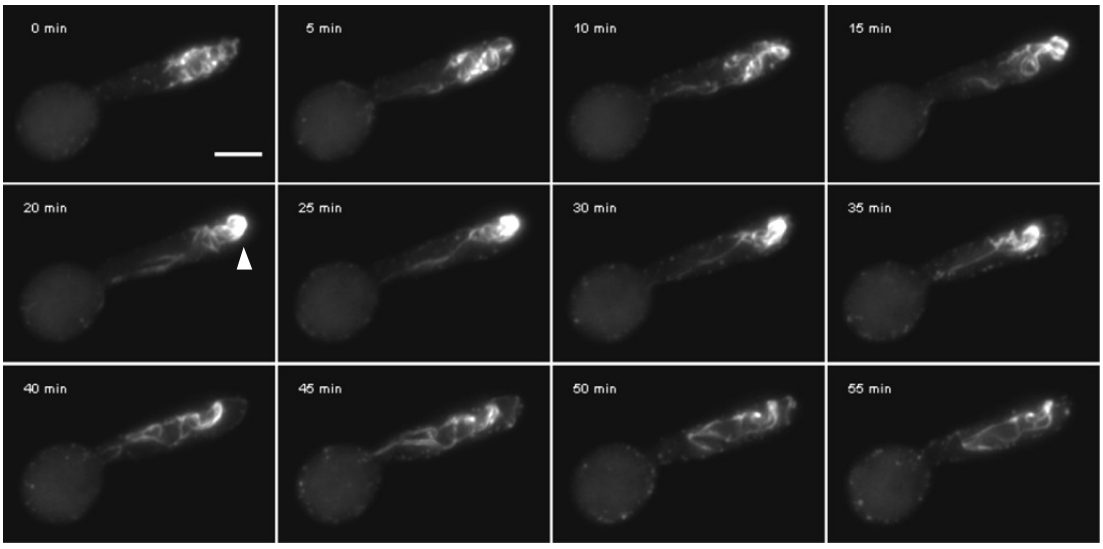

Figure 4.8 Dynamic rearrangement of apical F-actin arrays during GT tip growth. A loosely organized array of F-actin cables in the sub-apical region of the GT dispersed shortly before a new actin cap assembled at the tip apex (arrowhead). This actin cap underwent retrograde movement and finally converted into loose cables as well. See full sequence in supplementary movies 4.4a-c. Scale bar, 5 µm.

4.3.5. F-actin had an essential role during CAT-mediated cell fusion

The dynamic organization of F-actin during CAT formation was in general very similar to that observed during GT initiation and outgrowth (Fig. 4.9). Cell polarity was established by localized accumulation of an actin array at the cortex, which then lead to polarised protrusion of a CAT. Further accumulation of actin cables and patches to the tip region were typically seen during CAT protrusion.

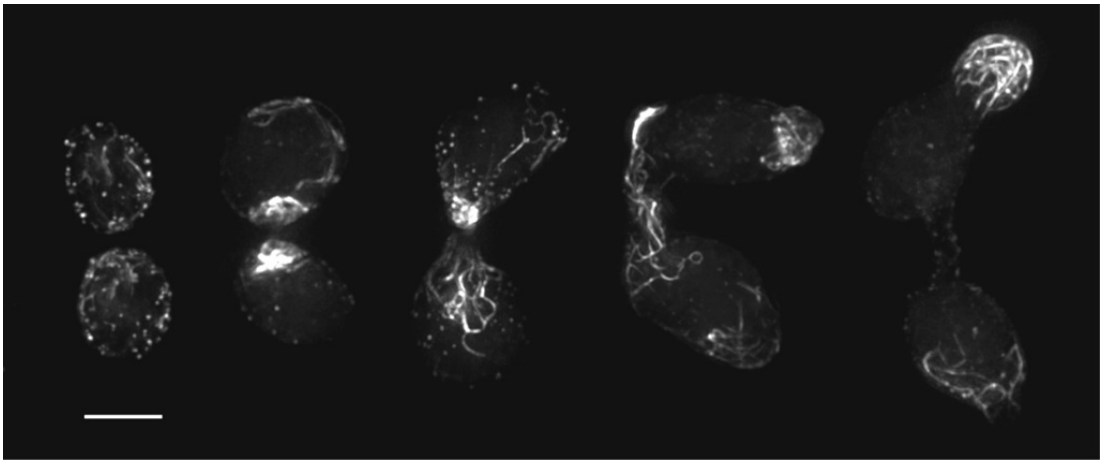

Figure 4.9 F-actin dynamics during CAT-mediated cell fusion. Arranged sequence representing key stages of the CAT formation, homing and fusion process (compare with Fig. 1.4). Z-projections of interacting cell pairs expressing Lifeact-TagRFP. In ungerminated, non-polarised conidia F-actin cables and patches were randomly distributed throughout the cell and along the cell cortex. Isotropic expansion within the first 1-2 h of the germination process led to an increase in cell size. Cell symmetry breaking was indicated by localized accumulation of actin at the cell cortex, and was followed by protrusion of a CAT (compare with GT initiation in Fig. 4.7). CATs in close vicinity (< 15 µm) homed towards each other and established contact. The homing process was accompanied by dynamic rearrangements of actin arrays, including cables and patches, at the CAT tip. Shortly after contact has been established F-actin started to disappear from the connection, and was almost completely lost after cytoplasmic continuity has been achieved; with only cortical patches remaining. Due to the bright signal from condensed F-actin arrays at specific regions, cables and patches elsewhere in the cells appear very dim. Scale bar, 5 µm.

An equal accumulation of fluorescence in either CAT apex could be observed during homing. Upon contact, apical fluorescence of Lifeact-TagRFPs gradually disappeared from the fusion site, indicating cessation of polarised tip growth. However, residual actin cables persisted at the fusion site suggesting that they may be involved in fusion pore formation. A new polar axis was often established, initiating GT extension from a different localization at the cell cortex. Once cytoplasmic continuity was fully established, actin cables had completely disappeared from the fusion connection, whereas a few cortical actin patches remained, probably involved in endocytic recycling of membrane-bound components.

4.3.6. Microtubules were not required for CAT-mediated cell fusion

Very recently we have found that although cells with disrupted microtubules showed isotropic enlargement and were unable to elongate initiated GT buds, almost 90% of the treated cells still formed CATs and successfully established cell fusion [107]. These findings suggested that without the ability to form elongated GTs, any polarised protrusion emerging from conidial germlings must be a CAT. Therefore, in this study, the microtubule depolymerizing drug benomyl was used at sub-lethal concentrations of < 5 μg/ml to distinguish fusion mutants that are blocked in CAT formation from those that are able to form CATs and therefore are indicated to be defective in homing and fusion (Fig. 4.10).

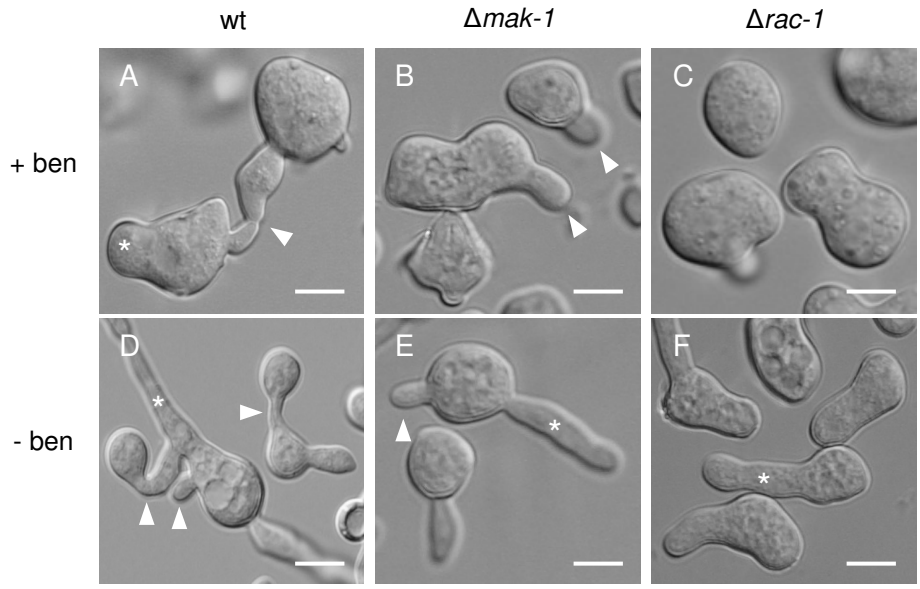

Figure 4.10 CAT formation assay. (A-C) Treatment of cells with the anti-tubulin drug benomyl (ben) caused pronounced isotropic swelling and prevented GT elongation, but did not prevent CAT formation and cell fusion. **(A)** Wt cells fused in the presence of ~3 µg/ml benomyl. An initiated GT bud is mark by an asterisk. **(B)** Cells of the fusion mutant Δ*mak-1* also formed CAT-like protrusions – but no GTs - in the presence of benomyl, but were unable to chemotropically interact and fuse. **(C)** The Rho GTPase mutant Δ*rac-1* did neither form CATs nor GTs, most likely due to a defect in F-actin nucleation required for CAT polarisation (see below). **(D-F)** Controls of the same strains in growth medium supplemented with 0.1% DMSO. CATs and fusion connections are indicated by arrowheads. Elongated GTs are marked with asterisks. Scale bars, 5 µm.

Benomyl treatment of cells expressing Lifeact-TagRFP revealed interesting effects that the lack of microtubules has on the actin cytoskeleton (Fig. 4.11). Although the overall distribution and integrity of F-actin cables and patches was not markedly different to untreated cells, formation of multiple actin caps at various locations at the cell cortex could be frequently observed, and sometimes led to the protrusion of the plasma membrane in the presence of more than one polar cap. With functional microtubules, generally fewer polarisation sites per cell were observed and usually only one was maintained during plasma membrane protrusion (Fig. 4.7). These observations suggest that actin is sufficient for the establishment of cell polarity and for initial plasma membrane protrusion, but that the elongation of GTs requires microtubules. Furthermore, it indicates that the formation of multiple GTs might be caused by a deregulated organisation of the

actin cytoskeleton in the absence of microtubules, and suggests that both cytoskeletal elements function cooperatively in this process.

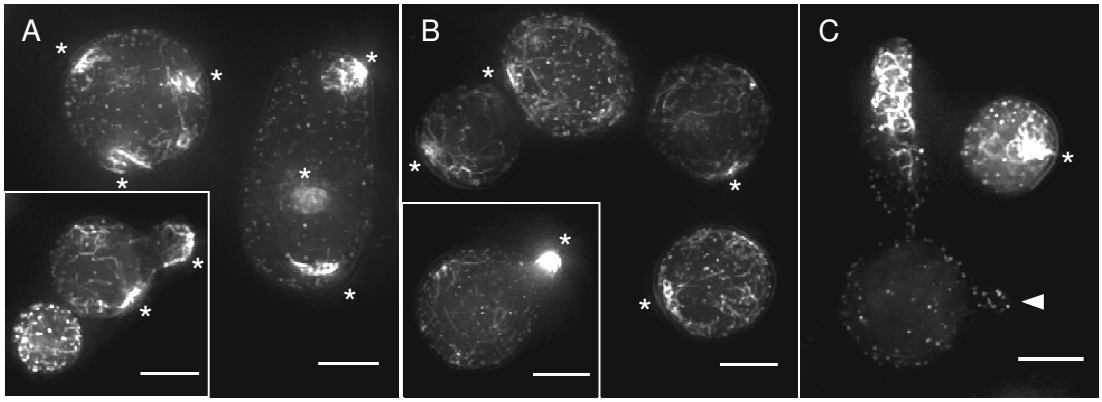

Figure 4.11 Disruption of microtubules caused defects in F-actin organization. (A) Cells after 2 h incubation in the presence of ~3 µg/ml benomyl. Without functional microtubules cells had problems in initiating polarised growth and therefore showed pronounced isotropic expansion. This was most likely caused by disorganised arrangement of polar actin caps leading to the uncontrolled protrusion of plasma membrane (inset A). **(B)** Untreated cells usually maintained only one polar cap during plasma membrane protrusion (inset B). **(C)** Elongated GT with complex actin array at its apex in comparison to a much smaller CAT which has formed at the side (arrowhead). Polar actin arrays and caps are indicated with asterisks. Scale bars, 5 µm.

4.3.7. Co-expression of Lifeact-TagRFP and β-tubulin-GFP revealed distinct spatial organization of F-actin and microtubules

In order to investigate the spatial and functional relationship between F-actin and microtubules during cell polarisation, maintenance of tip growth and cell fusion, strains NCAL006 and NCAL021 (Table 2.2) stably co-expressing Lifeact-TagRFPs with BML-sGFP (β-tubulin-sGFP) were generated by transforming pAL3-Lifeact and pAL5-Lifeact (Table 2.3) into *N. crassa* strain N2506 [38] as described in section 2.10. Both marker proteins accurately labelled their intended target polymers and showed no unspecific background staining (see supplementary movie 4.5). Microtubules and F-actin showed distinctive spatial distribution in conidial

germlings of *N. crassa*. We commonly observed regions within germlings occupied by F-actin that contained no or only very few microtubules (Fig. 4.12C.a), as well as the opposite situation, where microtubules extended into the GT tip in the absence of F-actin arrays (Fig. 4.12C.b). Recruitment of F-actin to the cell cortex during polarity establishment was not accompanied by accumulation of microtubules to that site (Fig. 4.12C.c). This suggests that spatial organization of both cytoskeletal elements can occur independently from each other, and confirms the notion that actin has a pronounced role during the establishment of cell polarity in filamentous fungi (see below Figs. 4.13 and 4.14, and supplementary movie 4.4c).

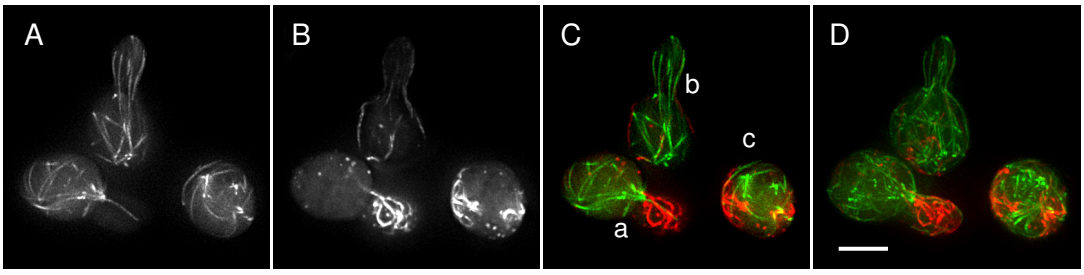

Figure 4.12 F-actin and microtubules show distinct spatial organization in conidia and germlings. (A) BML-sGFP signal from the middle section of a group of cells showing distribution of microtubules (green). **(B)** Lifeact-TagRFP signal from the same section showing F-actin distribution (red). **(C)** Merged image of (A) and (B) showing F-actin in red and microtubules in green. **(a)** Germling with an F-actin array at the tip, but only very few microtubules extending into this region. **(b)** Cell with microtubules extending into the GT tip, but with no dense accumulation of F-actin currently present. **(c)** Distribution of F-actin and microtubules in an ungerminated cell. **(D)** Z-projection of all optical sections taken through the cells. Scale bar, 5 µm. Full set of z-sections is shown in supplementary Fig. 4.2.

4.3.8. Actin organization during CAT formation is similar to that during GT emergence

The organization of F-actin during CAT formation was in general very similar to that observed during GT initiation and outgrowth (supplementary movie 4.2). CAT formation also coincided with localized accumulation of F-actin at the cell cortex and protrusion of a small bud (Fig. 4.13, arrowheads). An apical actin cap

formed at the tip of the protrusion and remained present during CAT extension, but eventually disappeared (Fig. 4.13g to i), suggesting that the CAT had stopped growing as it reached its determinate length [105]. In the observed cell, CAT formation coincided with transient dissolution of the F- actin array present at the GT tip (Fig. 4.13d-h, arrow), and appeared to coincide with a decrease in tip extension speed. In neighboring cells which did not form CATs actin arrays remained present at the GT tips throughout the time course (Fig. 4.13).

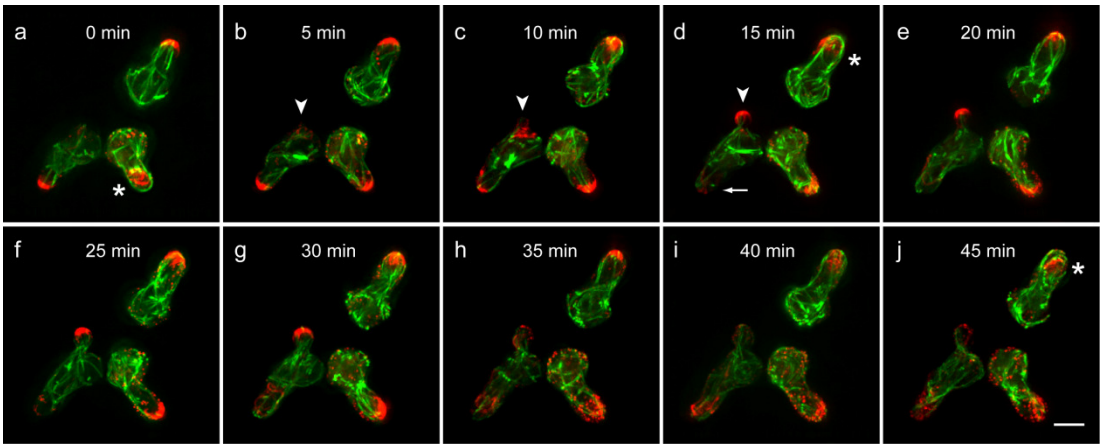

Figure 4.13 CAT polarisation and protrusion. Microtubules were labelled with BML-sGFP (green) and F-actin was labelled with Lifeact-TagRFP (red). **(a)** Apical F-actin was present at GT tips in all three conidial germlings. Over time these actin caps underwent retrograde movement and dissipation (asterisks). **(b)** The bottom left cell established a new site of cell polarity as indicated by the recruitment of F-actin to the cell cortex (arrowhead). **(c)** Actin array formation coincided with bud emergence. **(d)** As the CAT elongated an actin cap formed at its apex. Formation of this CAT coincided with the disappearance of the actin cap in the GT tip of the same cell (arrow). **(e-g)** The CAT extended over the following 10 min, but did not elongate beyond 4-5 µm in length, and **(h-j)** between 30-35 min the actin cap finally disappeared. During the period of CAT formation **(c-h)** GT extension was slower (0.04 µm/min) in the cell forming the CAT, compared to the two cells not forming CATs (0.06 and 0.10 µm/min, respectively). CAT elongation on the other hand was more rapid (0.14 µm/min). Scale bar, 5 µm

4.3.9. Actin arrays localized to CAT tips during homing and disappeared after fusion, but were re-deployed during GT re-polarisation

During CAT-mediated cell fusion, we found that actin cables and patches localized to CAT tips (Figs. 4.9, 4.13 and 4.14). When two CATs were homing towards each other, we generally observed an equal accumulation of fluorescence in either cell protrusion. If only one of the interacting CATs was growing, pronounced actin arrays were only observed in this one (Fig. 4.14). Upon contact, actin flurorescence gradually disappeared from the fusion site, indicating cessation of polarised tip growth. Once cytoplasmic continuity was fully established, actin cables disappeared from the connecting tube, whereas cortical actin patches remained (Fig. 4.9). At this stage a new site of polarised growth was often established, suggesting re-initiation of GT extension (Fig. 4.14, arrowhead at 20 min), which coincided with the formation of an actin array at the cell cortex localizing to the previously established site of polar outgrowth (Fig. 4.14, 20-25 min). Subsequent to F-actin re-deployment, further elongation of the GT involved dynamic rearrangement of the actin array including reassembly close to the GT tip (Fig. 4.14, 45 min). The re-initiation of GT growth was also accompanied by extension of microtubules into the tip. These observations suggest that recruitment of both cytoskeletal elements occurs in a distinct but coordinated manner and might influence which protrusion is being formed and maintained at any point in time.

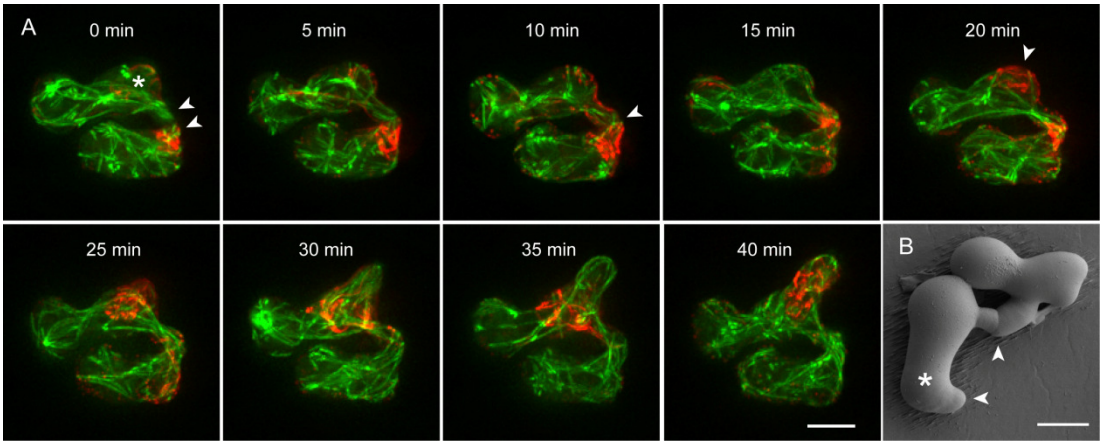

Figure 4.14 F-actin dynamics during CAT-mediated cell fusion and GT re-initiation. Microtubules were labelled with BML-sGFP (green) and F-actin was labelled with Lifeact-TagRFP (red). **(A)** Two CATs establishing cell-cell contact. CATs are indicated by arrowheads; the GT is indicated by an asterisk. **(5-20 min)** Gradual re-polarisation of F-actin from the fusion site (arrowhead at 10 min) to the GT tip (arrowhead at 20 min). **(25-45 min)** F-actin undergoes dynamic rearrangement whilst microtubules extend into the growing GT. In this instance, GT extension increased by a factor of nine after cell fusion was completed (0.02 µm/min before fusion, 0.18 µm/min after fusion). **(B)** Scanning electron micrograph showing a similar scenario of germling fusion. Asterisks mark GTs from which CATs (arrowheads) have emerged and fused (image centre). Scale bars, 5 µm.

4.3.10. Localized condensation of F-actin rings preceded septation

Accumulation of F-actin in brightly fluorescent rings was also visualized with Lifeact-TagRFPs (Fig. 4.15). Formation of these rings occurred by an initially loose accumulation of actin cables in a defined area of the hypha, which gradually condensed and shaped into a ring closely associated to the inner perimeter of the GT or mature hypha. The fluorescence intensity of these rings was extremely bright compared to fluorescent signals from actin cables and patches, indicating a very high concentration of F-actin (see supplementary figure 4.3). As has been previously reported, these cortical actin rings serve as landmarks and building platforms for the formation of septa in filamentous fungi [96, 97]. *Neurospora* is a multinucleate organism and nuclear division occurs asynchronously [38, 73, 95, 107, 115]. Actin ring formation was observed at various developmental stages and at various

locations within conidial germlings and germling networks, and therefore not obviously associated with the cell cycle. This is interesting, as a spatial or temporal coordination of actin ring formation with microtubules involved in nuclear division was not apparent, pointing towards fundamental functional differences to contractile actin-myosin rings required for mitotic cell division in yeasts.

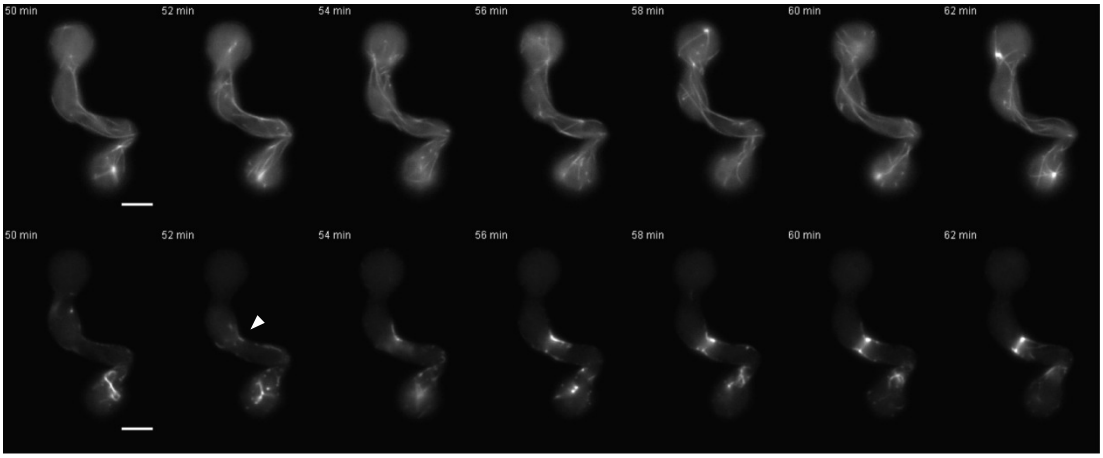

Figure 4.15 Condensation of F-actin into a cortical ring. Post-fusion and preceding septum formation a cortical actin ring was formed within 10 min by localized condensation of F-actin cables along the inner perimeter of a GT (arrowhead). Epifluorescence images of one optical plane. Microtubules were labelled with BML-sGFP (top row), F-actin was labelled with Lifeact-TagRFP-T (bottom row). See supplementary movies 4.6a-b for full sequence. Scale bars, 5 µm.

Taken together, Lifeact-TagRFPs enabled a more comprehensive understanding of the cell polarisation process in *Neurospora crassa* and revealed for the first time the dynamic rearrangements of the actin cytoskeleton required to maintain polarised extension of GTs and CATs. The exclusive and essential role of the actin cytoskeleton during CAT-mediated cell fusion could be demonstrated and, in combination with the microtubule marker BML-sGFP, initial evidence for important functional differences between, but also coordinated recruitment of both cytoskeletal elements in these processes could be collected. Further studies with higher spatial and temporal resolution will be necessary to resolve more details of

the cooperative interaction between microtubules and the actin cytoskeleton in filamentous fungi.

4.3.11. CRIB-reporter cloning and expression

Neurospora crassa possesses two p21-activated kinases (PAKs) with p21-binding domains (PBDs), which contain the Cdc42- and Rac-interactive binding (CRIB) motif. Figure 4.16 shows the protein sequence aligment used to identify the CRIB consensus motif of *N. crassa*, as well as a schematic representation of the final CRIB-sGFP reporter construct used in this study.

A

```
STE20(327-363)       GSPKKPLISAP--ENPVHVTHVGYDSNTGQFTGLPKEW 36
CHM-1(193-229)       RCPGMGGVSNP--TNFSHAVHVGFDPQTGEFVGLPPEW 36
CRIB consensus       -------ISXPXXSXFXHXXHXGXD------------- 18
                            :* *       *  * * *

CRIB consensus N. crassa   XSXP--XNXXHXXHVGXD
```

B

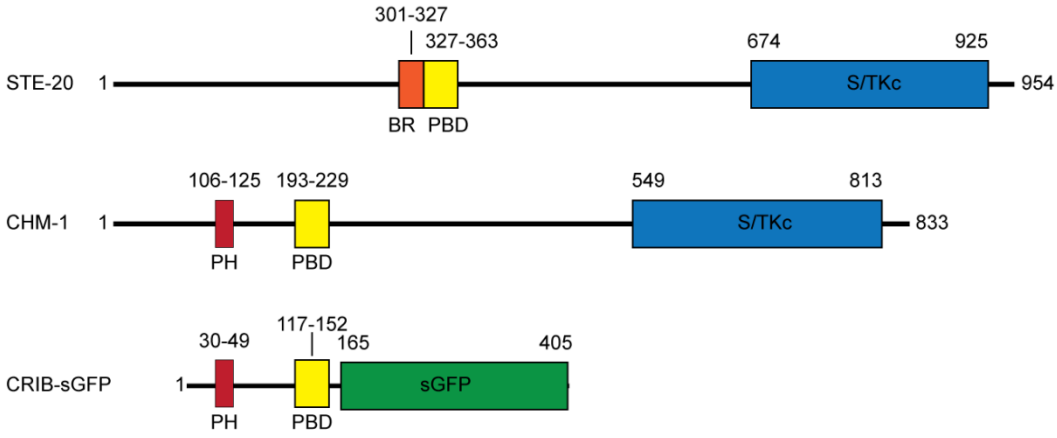

Figure 4.16 Construction of a CRIB-sGFP biosensor for *N. crassa* (A) The *N. crassa* genome encodes two PAKs: STE20 (NCU03894.2) and CHM-1 (NCU00406.2). The CRIB motif within the PBDs of both PAKs has been identified by alignment with the eukaryotic CRIB consensus sequence [14, 53]. Red denotes small/hydrophobic, blue acidic, magenta basic and green hydroxyl/ amine amino acids. **(B)** Each PAK of *Neurospora* contains a PBD

and a catalytic Serine/Threonine Kinase (S/TKc) domain, as well as additional domains required for membrane-localized activation of the kinase. STE-20 contains a basic-rich (BR) membrane-interaction domain, whereas CHM-1 utilizes a pleckstrin homology (PH) domain. Numbers denote amino acid positions at the beginning and end of conserved domains, respectively. Both, BR and PH domains are essential for functional localization of PKAs, and the BR domain of Ste20p can functionally substitute loss of the PH domain of Cla4p [126].

Plasmid pAL1-CRIB (Table 2.3) for the expression of CRIB-sGFP under control of the inducible P*ccg-1* promotor was generated by amplifying the coding region for amino acids 78-240 of CHM-1 from *N. crassa* wt cDNA (section 2.6.3) using oligonucleotides PHPBD_if_BamHI_fw 5′-TTTCCTCGACGGATCCCAAATGTCAAACAACGACGGC-3′ and PHPBD_GS_if_rv 5′-AGACACCATCGAGCCTTCTTGGGTAATGGCTGAAGAG-3′, then amplifying the sGFP coding region from pAL1-MAK-1 (Table 2.3) using oligonucleotides GS_sGFP_if_fw 5′-CCGCCGCAAGGCTCGATGGTGAGCAAGGGCGAGG-3′ and sGFP_if_EcoRV_rv 5′- ATCGATAAGCTTGATATCTTACTTGTACAGCTCGTCCATGCC-3′ (underlined are the 15 bp overlaps between both fragments and host vector), and subsequently joining both purified PCR products (section 2.6.12) with *BamH*I/*EcoR*V-linearized and gel purified (sections 2.6.4.-2.6.5) pBARGRG1 using In-Fusion® PCR cloning (section 2.6.8). Selected pDNA clones were propagated through *E.coli* and transformed into *N. crassa* wt as described earlier (section 4.3.1). Six transformant strains were selected for further investigations. Apart from one, all transformants showed no phenotypic changes after random integration of the fusion construct into the genome (Fig. 4.17).

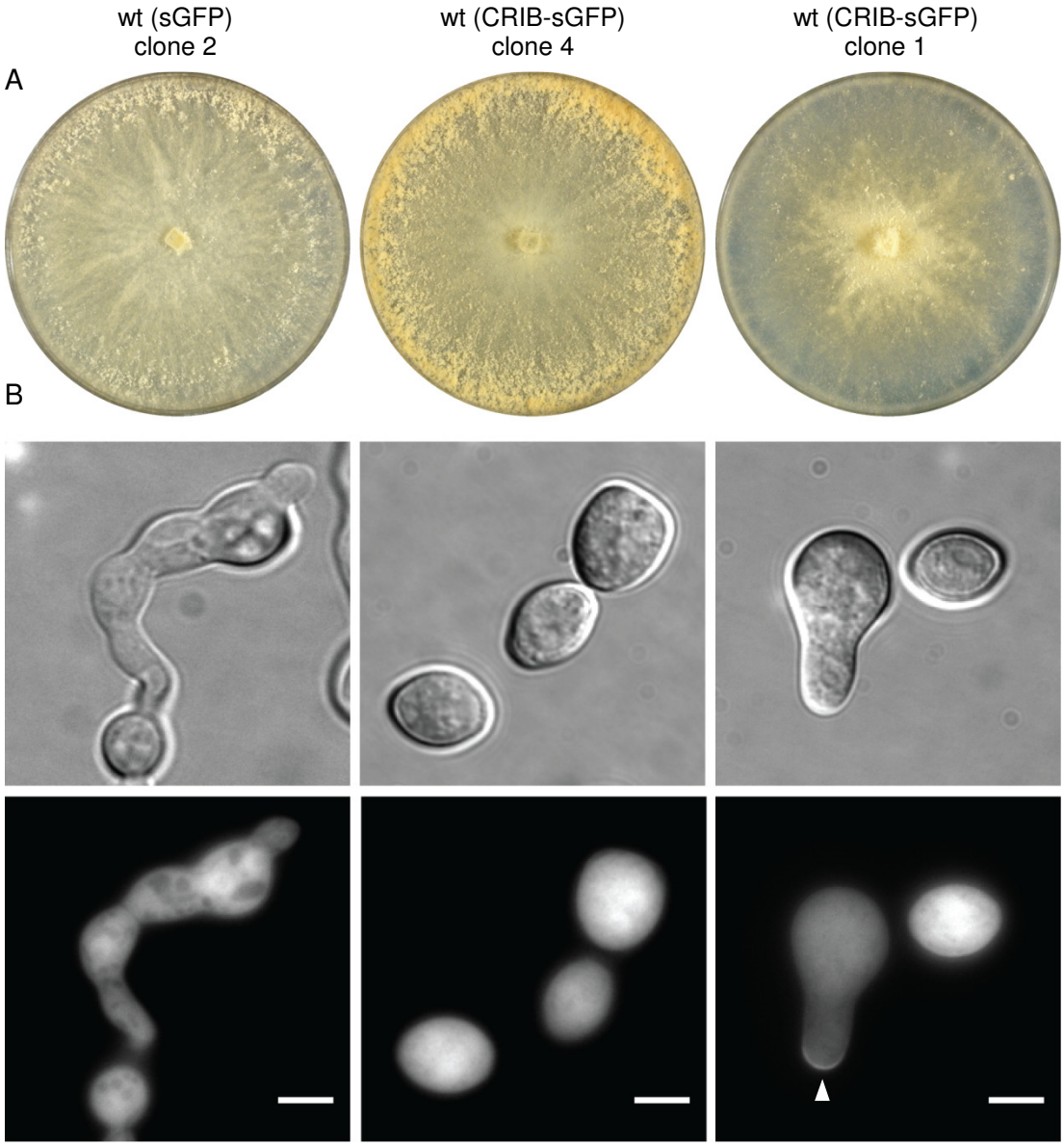

Figure 4.17 Ectopic expression of CRIB-sGFP *per se* did not induce phenotypic defects. (A) Colony development and conidiation pattern of CRIB-sGFP expressing transformants were in most cases (five out of six) unaffected and equivalent to the wt expressing free sGFP. Here shown after 72 h incubation on VM at 25°C. One transformant however (clone 1), was recovered with altered colony morphology and conidiation pattern, and was therefore excluded from further analyses. **(B)** Brightfield and epifluorescence images of conidia. In comparison with the sGFP expressing wt (left), spore morphologies of the transformants did not show any obvious abnormalities. Free sGFP showed cytoplasmic localization and nuclear accumulation, but was excluded from other organelles. In ungerminated conidia CRIB-sGFP showed a more homogeneous cytoplasmic localization and nuclear accumulation (middle). During polarised growth CRIB-sGFP formed a polar crescent at GT tips (arrowhead). Scale bars, 5 µm.

4.3.12. CRIB-sGFP marked sites of polarised plasma membrane protrusion

In ungerminated, non-polarised cells CRIB-sGFP was homogeneously distributed in the cytoplasm. Cell polarisation coincided with the recruitment of the reporter into a cortical cap, marking the prospective protrusion site. During polarised plasma membrane protrusion, i.e. GT and CAT formation, an apical crescent was constantly present at polarized tips (Fig. 4.18; supplementary movie 4.7). A synthetic CRIB-sGFP construct, only containing the CRIB motif and lacking the associated PH domain, did not localize (data not shown).

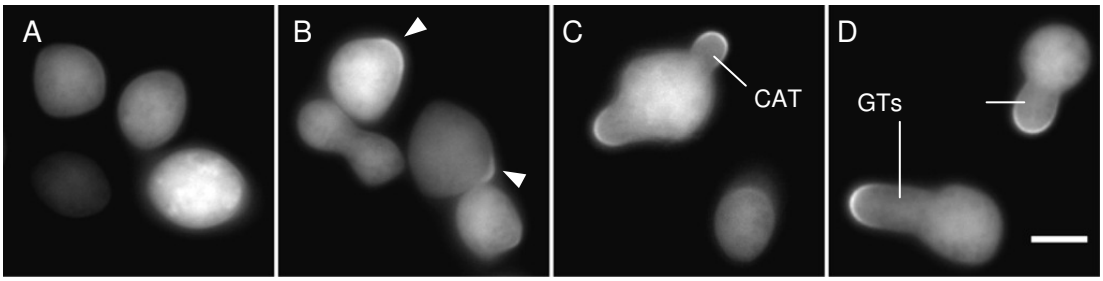

Figure 4.18 CRIB-sGFP marked sites of polarised growth. (A) Ungerminated, non-polarised conidia showed an even distribution of the fluorescent biosensor. **(B)** Cell polarisation led to localized recruitment of CRIB-sGFP indicating accumulation of activated Rho GTPases at the cell cortex (arrowheads). **(C-D)** Crescent-shaped polar caps were constantly present during GT and CAT protrusion. Scale bar, 5 µm.

4.3.13. Rho GTPases have a central role in hyphal fusion

As indicated in section 3.4, gene deletion mutants of both *N. crassa* Rho GTPases CDC42 and RAC-1, as well as one of their effector PAKs, CHM-1, showed severe cell polarity defects. Interestingly, Δ*chm-1* cells were generally able to undergo hyphal fusion in the mature colony and between conidial germlings, whilst Δ*cdc42* and Δ*rac-1* were complete blocked in CAT formation (Fig. 4.19).

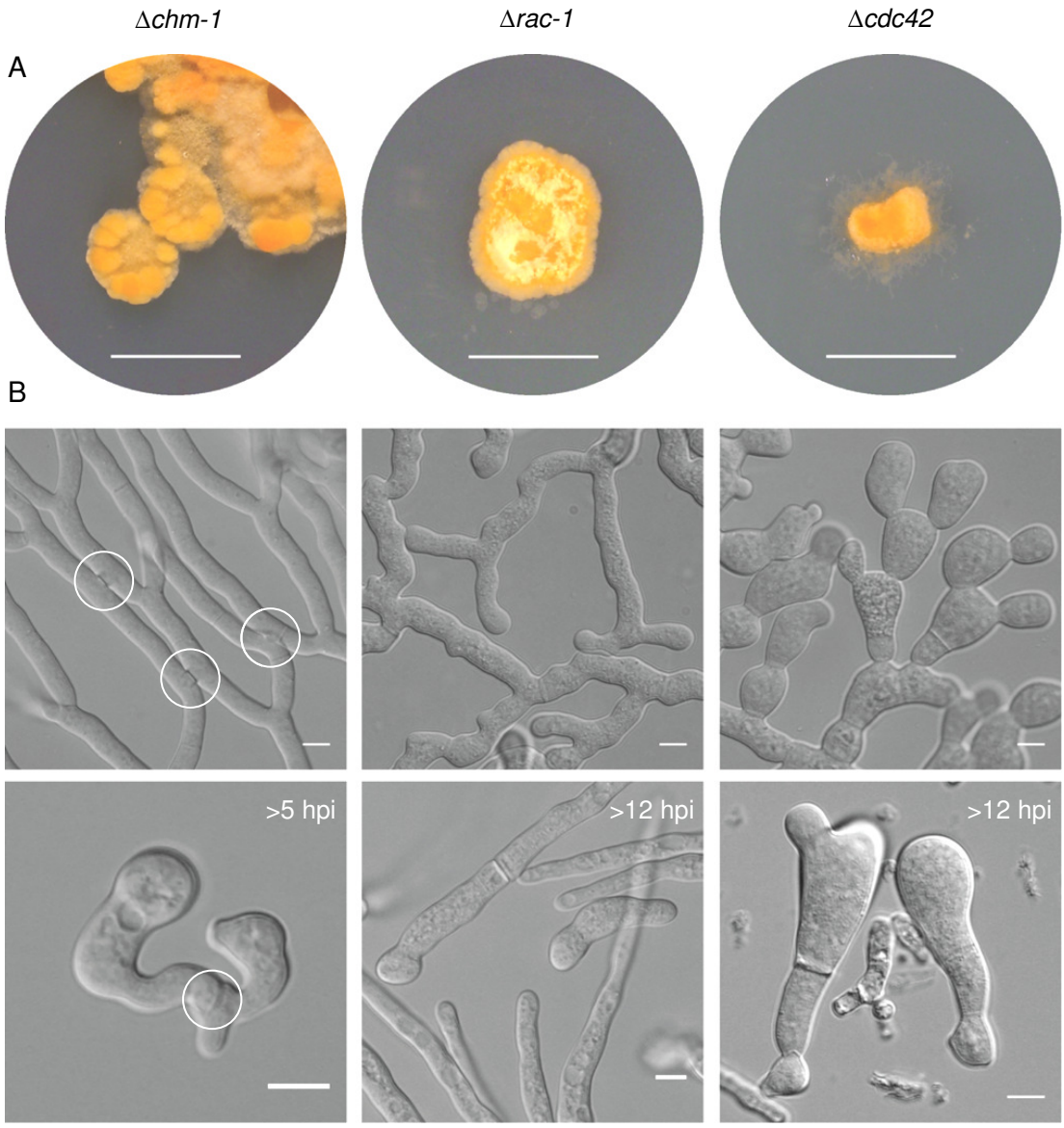

Figure 4.19 Phenotypes of cell polarity mutants. (A) Deletion of the PAK CHM-1 and the Rho GTPases CDC42 or RAC-1 caused severe developmental delays (radial extension reduced to < 2 mm/day compared to wt with > 45 mm/day) and led to extremely dense growing colonies. Images taken after 3 days of incubation at 30°C. Scale bars, 10 mm. **(B) Top row:** Mature hyphae after 4 days incubation at 30°C. All three mutants displayed a strictly dichotomous branching pattern and lacked hyphal differentiation, i.e. all hyphae looked essentially the same. However, Δ*chm-1* was still able to establish fusion connections (circled), whereas fusion was never observed in Δ*rac-1* and Δ*cdc42* strains. **Bottom row:** Despite a significant developmental delay (onset of CAT fusion in Δ*chm-1* about 2-3 h later compared to wt), conidial germlings of Δ*chm-1* were generally able to fuse. Under identical conditions, germlings of Δ*rac-1* or Δ*cdc42* did never form CATs, even after extended incubation times for up to 12.5 h. Scale bars, 10 µm.

The observed phenotypic defects of both GTPase mutants confirmed the crucial functions of these proteins during the establishment and maintenance of polarised tip growth in *N. crassa*. Both GTPase mutants displayed very distinct phenotypes indicating different roles in the regulation of polarised growth (Fig. 4.19B). Whilst Δ*rac-1* cells managed to initiate and maintain elongated GTs, conidia of Δ*cdc42* appeared almost unable to set and maintain a polar axis, which led to extremely swollen germlings and greatly reduced hyphal elongation rates. Interestingly, both mutants formed normal septa, which suggests that neither CDC42 nor RAC-1 are essential for this process, and points towards an exclusive role of the RHO GTPases (RHO isoforms 1 to 4) in septum formation [96, 97]. Absence of the GTPase-effector CHM-1 did not prevent hyphal fusion, indicating that loss of function in this mutant can be compensated, most likely by the second PAK of *Neurospora*, STE20. Further investigations using CRIB-sGFP confirmed that activated GTPases were constantly present at homing and fusion CAT tips, but disappeared shortly after cytoplasmic continuity has been established (Fig. 4.20; supplementary movie 4.8).

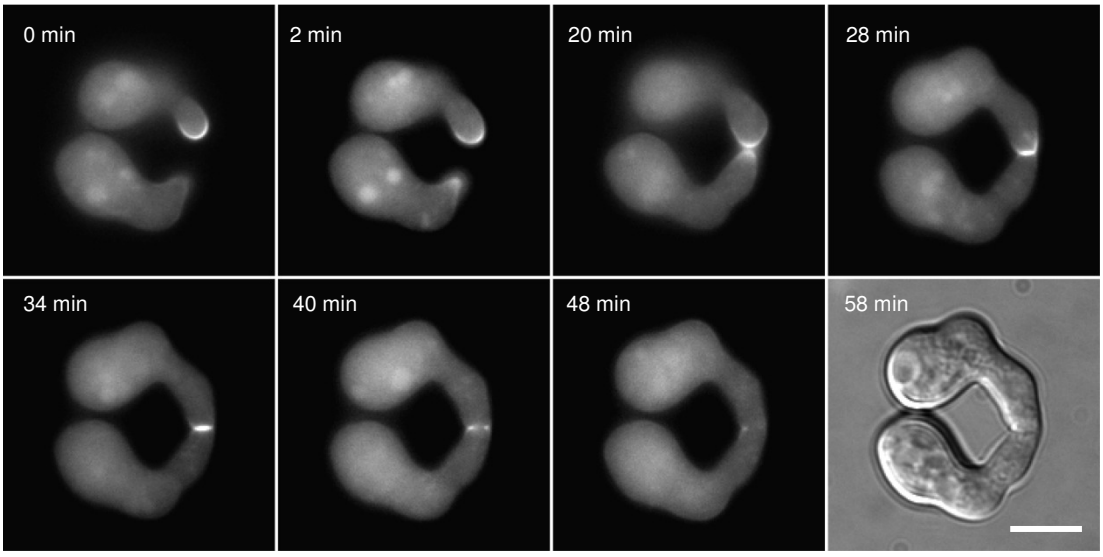

Figure 4.20 Rho GTPase activity is maintained at homing and fusing CAT tips. CRIB-sGFP was constantly present at tips of homing and fusion CATs until cytoplasmic continuity was established. Selected key stages of the process included: directed growth of CATs

towards each other which coincided with recruitment of CRIB-sGFP to both tips at 2 min. Contact and attachment was being made between 20 and 28 min. From 28 min onwards fluorescence focused to the attachment area. At 40 min fusion pore opening established cytoplasmic continuity between both cells. Subsequently, CRIB-sGFP fluorescence disappeared from the fusion site and was completely gone after 50 min, indicating that Rho GTPase activity was no longer required at this site. Scale bar, 5 µm.

Fluctuating fluorescence intensity of the CRIB-sGFP reporter within the apical crescents were observed during GT extension (supplementary movie 4.7) and CAT homing (supplementary movie 4.8). To verify these observations fluorescence intensity changes within locally defined regions of the tip apex (left side, centre and right side) were measured and plotted against time (Fig. 4.21). During CAT homing, signal intensity peaks could be identified that locally correlated with the displacement of activated GTPase towards the fusion partner, and subsequent re-orientation of tip extension. Tip contact coincided with a third very strong peak and the transition into cell wall fusion (Fig. 4.21A). During linear GT extension constant 'flickering' of the CRIB-GFP signal could be observed, but significant changes indicating focused recruitment of activated GTPase to a specific side could not be measured (Fig. 4.10B). Tip growth arrest at the 18-20 min time point coincided with a general decrease of fluorescent signal. Fluorescence intensity of the CRIB-sGFP reporter inside the cytoplasm (indicated as dashed line in both graphs) remained constant throughout both time courses, showing that observed changes of apical fluorescence indeed represent locally defined changes in GTPase activity.

These initial measurements support the notion that localization of activated GTPase clusters at the apical membrane changes in response to chemoattractant perception and induces tip re-orientation towards the source. In the absence of chemotropic stimuli, as for example during linear GT extension, a locally defined accumulation within the tip apex did not occur. The flickering of the CRIB biosensor in this case might represent constant fluctuation of the shuttling GTPases.

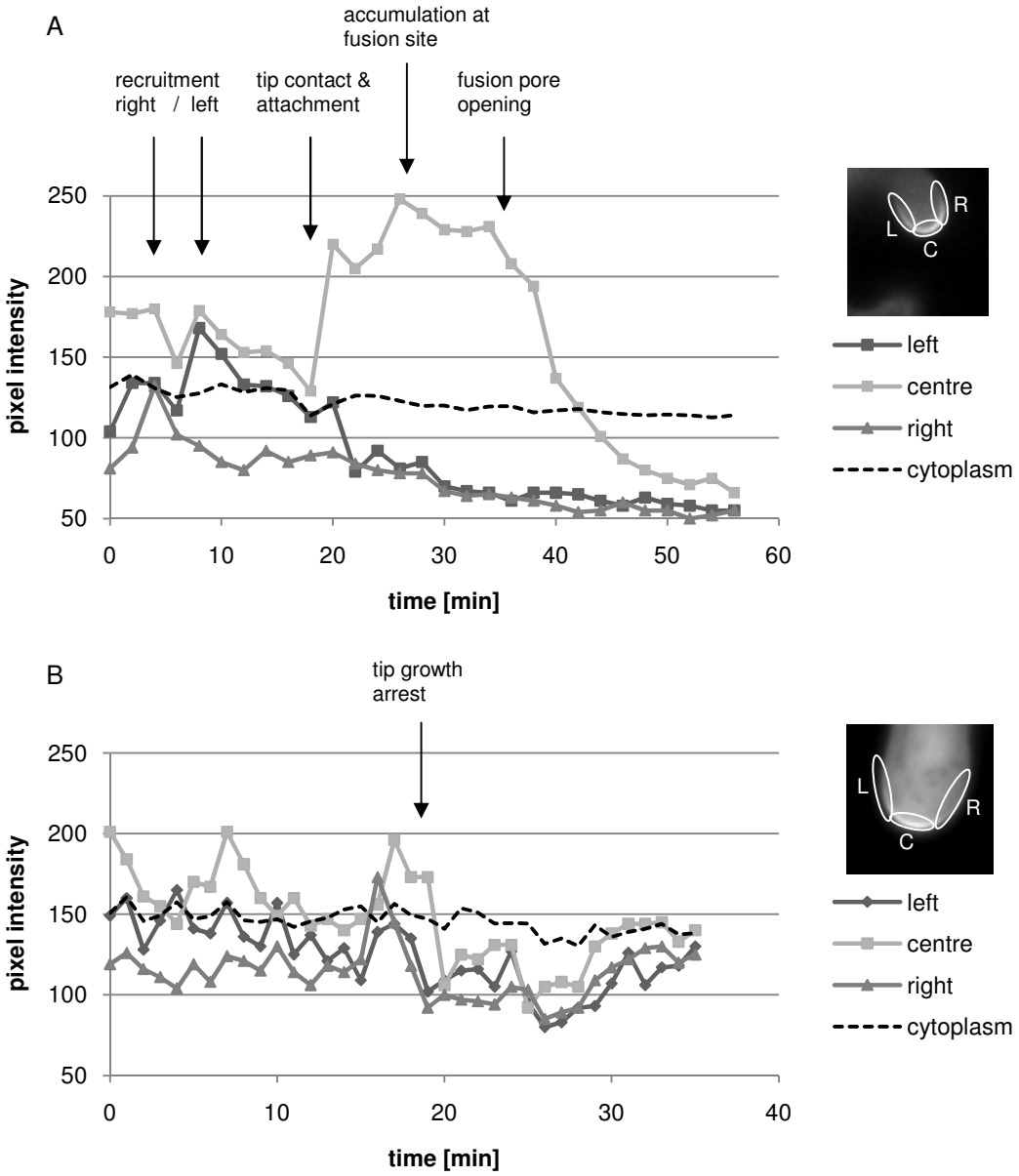

Figure 4.21 Recruitment and relocation of activated CDC42/RAC-1 GTPase clusters along the tip apex during CAT fusion and GT extension. Fluorescence intensities of CRIB-sGFP were measured in three defined regions at the tip apex (left side, centre and right side of the tip) as indicated in the insets. **(A)** During CAT homing (supplementary movie 4.8) GTPase activity initially peaked at the right side, then got relocated to the left side, which induced promoted tip growth at this location, towards the interacting CAT. Subsequently, GTPase activity became focused in the centre and engaged into cell wall attachment and fusion pore formation. Finally, the marker dispersed form the fusion site. **(B)** During linear tip extension of the GT (supplementary movie 4.7) slight variations in signal intensity occurred along the complete tip apex without being focused to a particular location. Tip growth arrest coincided with a general signal decrease.

Taken together, this data demonstrates that the presence and localized activation of the Rho GTPases RAC-1 and CDC42 is essential for polarised growth in general, and CAT-mediated cell fusion in particular.

4.3.14. Activated Rho GTPases and the F-actin cytoskeleton were functionally linked

To further investigate functional differences between both GTPases and verify the spatio-temporal relationship between GTPase activity and F-actin recruitment during cell symmetry breaking, GT elongation and CAT fusion, strains co-expressing CRIB-sGFP and Lifeact-TagRFP or Lifeact-TagRFP-T were generated by vegetative fusion of the heterokaryon compatible strains NCAL005 and NCAL022 with NCAL024, respectively (Table 2.2). Figure 4.22 shows one example of the close spatio-temporal relationship between locally defined Rho GTPase activation and the formation of apical F-actin caps .

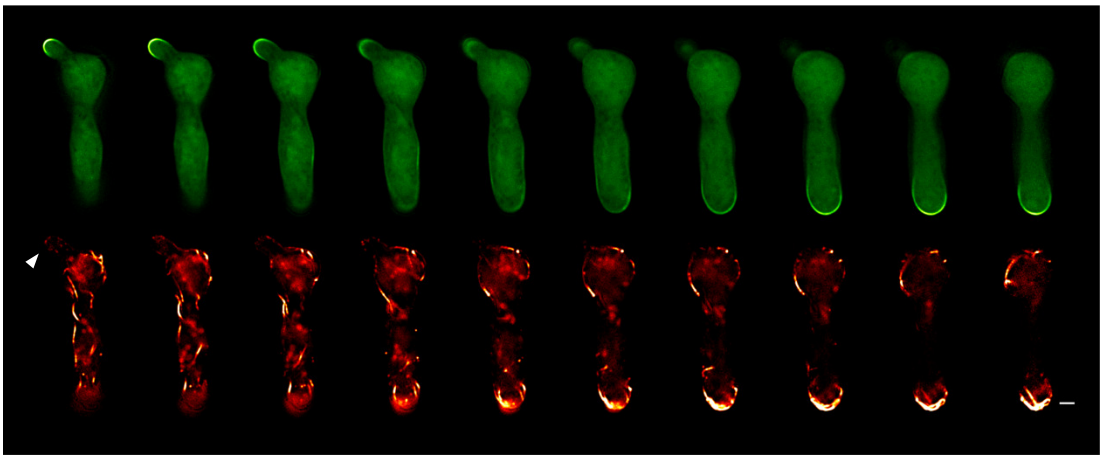

Figure 4.22 Co-localization of activated Rho GTPases and F-actin. Optical z-sections through a *N. crassa* germling co-expressing CRIB-sGFP (green) and Lifeact-TagRFP-T (red). Co-localization of the CRIB marker with an apical F-actin cap in the GT tip was evident. The apical CRIB crescent in the CAT is accompanied by less pronounced F-actin patches and cables (arrowhead). Fluorescence is intensity-coloured, with white indicating the strongest signal. Scale bar, 5 µm.

As shown above (Fig. 4.11), disruption of microtubules caused defects in F-actin organization which can lead to multipolar germination in *N. crassa* [108, 130]. Treatment of cells co-expressing CRIB-sGFP confirmed that the efficiency and accuracy of localized recruitment of activated Rho GTPases, and consequently polarisation fidelity, is compromised in the absence of microtubules (Fig. 4.23). This confirms the already suggested functional cooperation between microtubules, activated Rho GTPases and the F-actin cytoskeleton in symmetry breaking and polarised plasma membrane and cell wall protrusion.

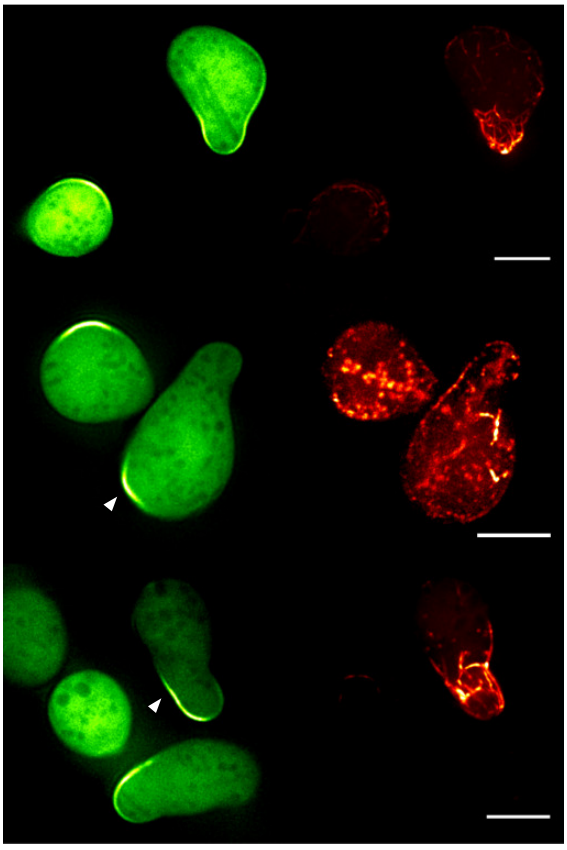

Figure 4.23 Disruption of microtubules compromised 'polarisation fidelity'. Examples of **c**ells co-expressing CRIB-sGFP (green) and Lifeact-TagRFP (red) treated with ~3 µg/ml Benomyl for 4 h. Delocalization of activated Rho GTPases (arrowheads) and extended isotropic swelling demonstrated that functional interaction between microtubules and F-actin was required for efficient establishment and maintenance of cell polarity. Fluorescence is intensity-coloured, with white being the strongest signal. Scale bars, 5 µm.

4.3.15. CDC42 and RAC-1 are differentially recruited to GT and CAT tips

Dimethyl sulfoxide (DMSO) is the standardly used organic solvent for drugs such as benomyl or latrunculins. In control experiments, involving the treatment of conidia of *N. crassa* with DMSO alone, the interesting observation was made that GTs were more sensitive to DMSO than CATs. Whereas GT formation and elongation were blocked in the presence of 1% DMSO, CAT-mediated cell fusion progressed normally (Figure 4.24). Furthermore, DMSO addition resulted in rapid dispersal of the CRIB biosensor from GT tips, but left CRIB-sGFP unaffected in homing and fusion CATs (Fig. 4.25).

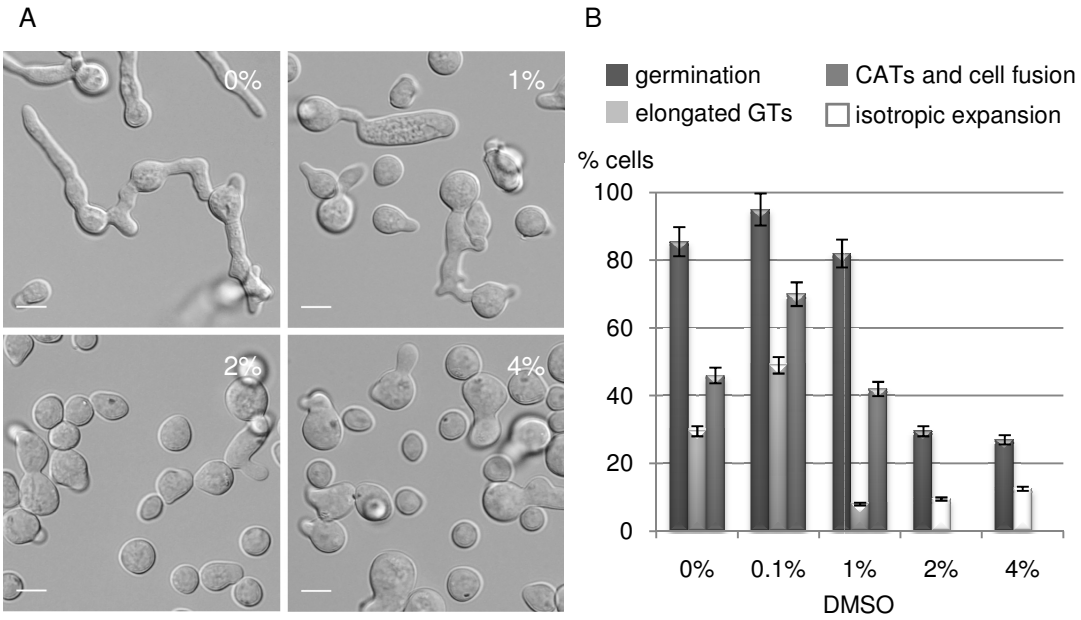

Figure 4.24 Selective inhibition of GT growth with 1% DMSO. (A) Cells of *N. crassa* incubated in the presence of 0-4% DMSO for 3 h at 35°C. 1% DMSO blocked GT formation but not CAT formation and cell fusion. More than 1% significantly reduced germination, CAT fusion and induced extensive isotropic swelling. Scale bars, 5 µm. **(B)** Quantification of (A).

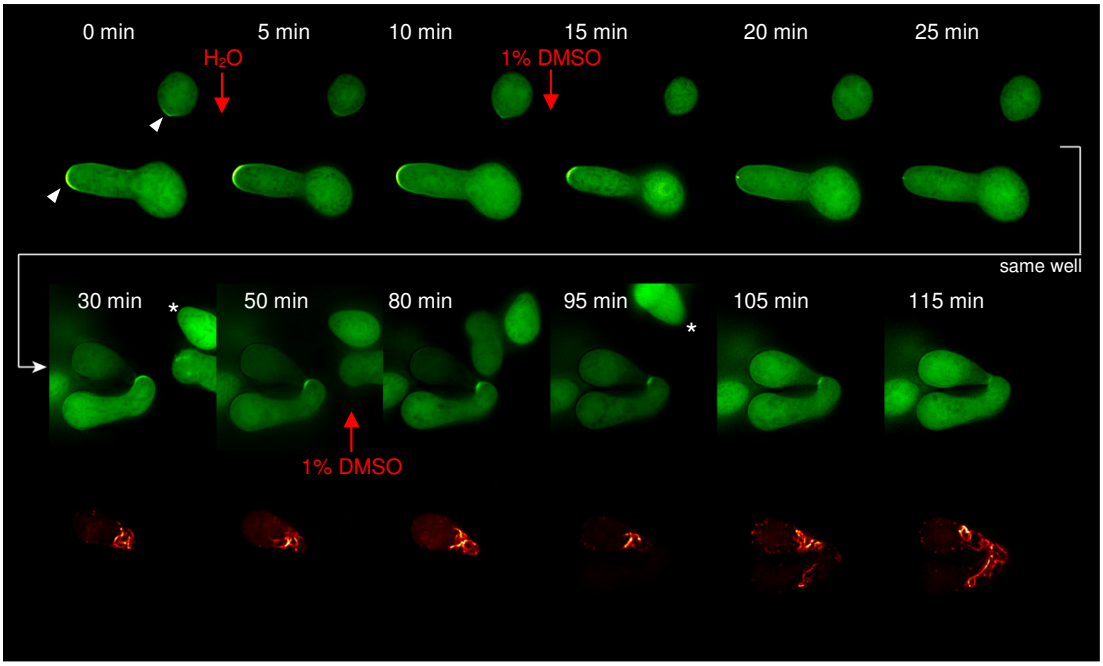

Figure 4.25 Differential sensitivity of activated Rho GTPases in GT and CAT tips towards DMSO treatment. Time points of DMSO addition to cells co-expressing CRIB-sGFP (green) and Lifeact-TagRFP-T (red) are indicated in the figure. CRIB-sGFP dispersed from GT tips and polarisation sites (arrowheads) within 5 min upon addition of 1% DMSO, and remained absent (asterisks). Addition of equal volumes of water to simulate mechanical perturbation had no effect. A final concentration of 2% DMSO did not lead to dispersal of CRIB-sGFP from CAT tips, and furthermore, did not interfere with cell fusion; evident by transfer of the Lifeact marker from the upper into the lower, previously non-expressing cell. Fluorescence is intensity-coloured, with white being the strongest signal. Time course was continuously recorded in the same well. Scale bars, 5 µm.

To verify these observations, the Rac GTPase-specifc small molecule inhibitor NSC23766 was used. NSC23766 was identified through structure-based virtual screening of compounds that fit into a surface groove of Rac1 known to be critical for GEF specification, and has been shown to specifically block Rac1/GEF interaction *in vitro* and *in vivo* in mammalian cells [40]. Incubation of cells in the presence of $\geq$ 50 µM NSC23677 completely blocked CAT formation and fusion in *Neurospora*, and instead lead to promoted GT elongation (Supplementary figures 4.4 and 4.5). Addition of 100 µM NSC23766 to growing germlings lead to rapid dispersal of CRIB-sGFP from CAT tips and abrogated cell fusion (Fig. 4.26A), whereas no effects on polarised tip growth of GTs were observed (Fig. 4.26B).

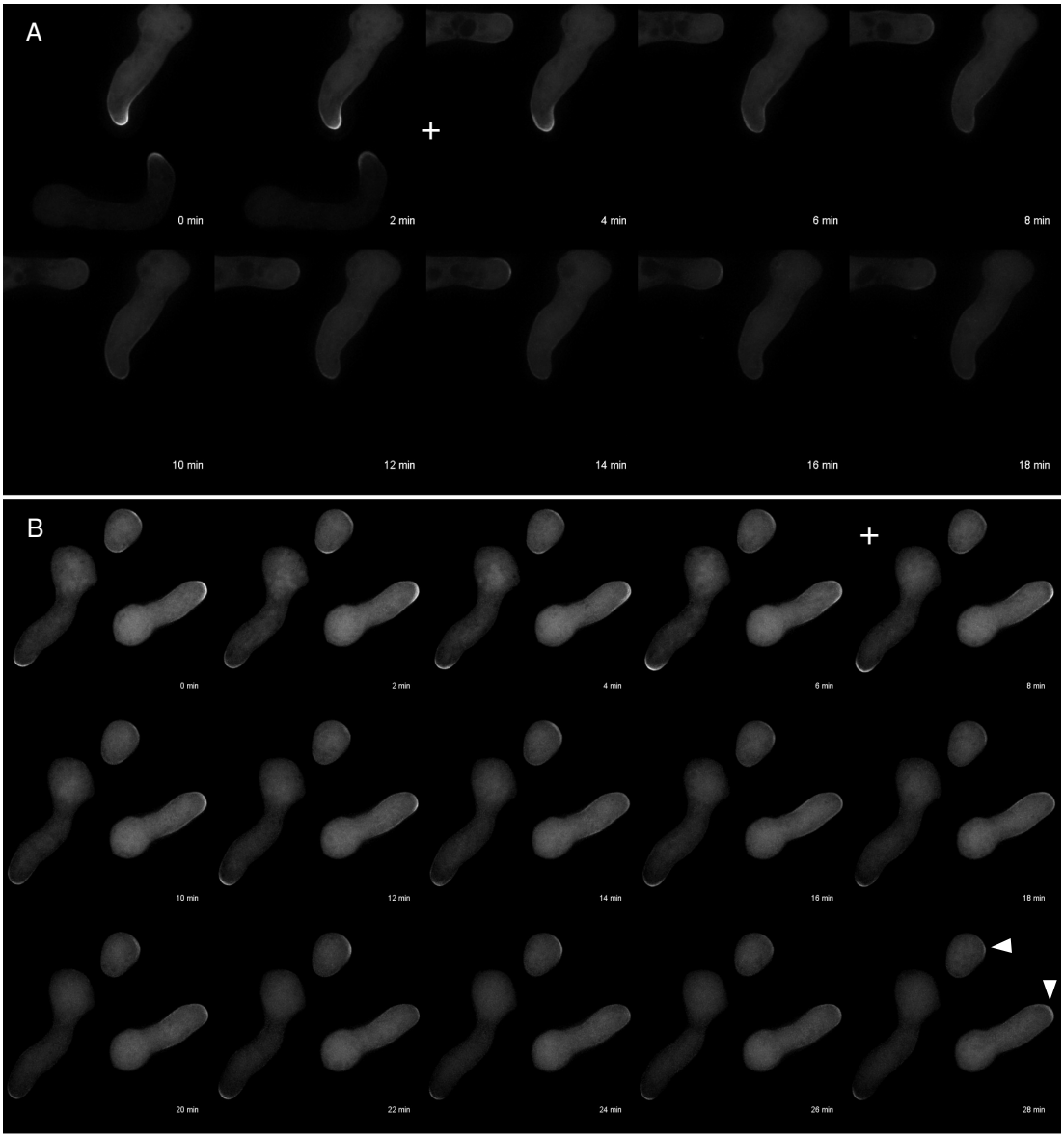

Figure 4.26 Exclusive recruitment of RAC-1 to CAT tips. Z-projections of cells expressing CRIB-sGFP. Cells were treated with 100 µM of the Rac inhibitor NSC23766 [40] at indicated time points (+). **(A)** Within 5 min upon addition, CRIB-sGFP complete dispersed from CAT tips. **(B)** Even after > 25 min upon addition of the Rac inhibitor, activated Rho GTPases still resided in apical crescents at GT tips and symmetry breaking conidia (arrowheads).

Taken together, this data strongly suggests that both Rho GTPases CDC42 and RAC-1 are differentially recruited to polarised growing GT and CAT tips, which provides one possible explanation for the morphological and functional distinction of both cell protrusion.

4.4. Discussion

Cell polarisation marks the decision point for colony establishment from the ungerminated spore. Maintenance of sustained tip growth at multiple growth sites, and the continued elaboration of new polar axes are essential for colony extension and a hallmark of filamentous fungi. Research presented in this chapter investigated the different roles of the F-actin cytoskeleton and of microtubules during cell symmetry breaking, polarised protrusion of GTs and CATs, and during conidial germling fusion.

Filamentous fungi use distinct mechanisms to generate and maintain polarised growth. Polarised outgrowth during budding or mating projection formation in budding yeast involves deposition and detection of cortical landmarks which define the new polarity site. Recruitment and activation of the small GTPase Cdc42p promotes the formation of the polarisome complex at this site, leading to localized nucleation of F-actin cables. Along these cables post-Golgi vesicles are transported and dock with the exocyst complex which regulates vesicle fusion and allows polarised plasma membrane protrusion. *S. cerevisiae* has been the prime model system to study cell polarity, and molecular details of the process have been comprehensively summarized in [91]. Genome comparison and research over the past years involving various fungal model organisms with yeast and yeast-like growth, pseudohyphal or filamentous hyphal growth, and including *Schizosaccharomyces pombe*, *Candida albicans*, *Ashbya gossypii*, *Aspergillus nidulans*, *Ustilago maydis* and *Neurospora crassa*, showed that the core molecular mechanisms for generating cell polarity and maintaining hyphal tip growth are highly conserved within the fungal kingdom [29, 44, 48, 78, 104, 120, 146]. The significant morphogenetic differences between filamentous fungi and yeasts, however, make it seem unlikely that hyphal tip growth utilizes orthologous components in the same way as during budding or pseudohyphal growth. Furthermore, additional factors exclusive to the polarity machinery of filamentous fungi have been identified and

provide an opportunity to search for mechanisms that have not been exemplified in other model systems. Our understanding about how sustained tip growth of mature hyphae is maintained in filamentous fungi has greatly improved and revealed fascinating insights, e.g. into the crucial role of the Spitzenkörper as vesicle supply centre and its interaction with the cytoskeleton to allow hyphal orientation. The increase in knowledge over recent years is reflected in the considerable number of excellent reviews on these topics [16, 37, 44, 45, 120, 122, 139]. But how does it all work at the earliest stages of colony initiation?

'Historical' cell cortex markers, i.e. landmarks remaining from previous morphogenetic events, such as bud scars, that could provide positional cues for cell polarisation and GT or CAT emergence have not been identified in filamentous fungi. Also, a number of classical landmark proteins known from yeasts are absent from filamentous fungal genomes [15, 44]. Therefore, it remains unclear how polarity in fungal spores lacking obvious morphological landmarks is specified. One possibility is the determination of polarity sites at random, based on localized build-up of activated CDC42 GTPase (Fig. 4.2) which then leads to nucleation of actin cables and assembly of the polarisome. Random symmetry breaking by positive feedback loops which amplify Cdc42 concentration at certain spots of the plasma membrane have been demonstrated in budding yeast [90]. For filamentous fungi this might be in doubt, as in most species CDC42 has been reported to be largely dispensable for polarity establishment [16, 44]. Our analysis showed that gene deletion mutants of CDC42 and RAC-1 in *N. crassa* have severe polarity defects which on a cellular level impair normal GT formation and extension, and can lead to a CAT induction defect (Fig. 4.19B). In the mature colony these defects translate into a dichotomous branching pattern and extremely dense growth (Fig. 4.19A). Although both GTPases are structurally very similar (59% amino acid sequence homology), the phenotypes of Δ*cdc42* and Δ*rac-1* are distinct, suggesting different regulatory functions for both GTPases. Functional specificity of GTPases is normally generated through selective interaction with GDIs, GEFs and GAPs, specific for each

particular GTPase. A *CDC42* deletion results in a lethal phenotype in both *S. cerevisiae* and *S. pombe* [2, 81], but is tolerated in filamentous fungi due to the presence of the second CDC42-like GTPase RAC-1 [74]. CDC42/RAC-1 double KOs are expected to be lethal in filamentous fungi, too. Therefore, it needs to be considered that in the *N. crassa* single KOs loss-of-function from one of the two GTPases might be at least partially compensated by the other. However, the availability of viable single KOs, due to the presence of RAC-1 orthologs, is a great advantage for studying their separate functions in filamentous fungi. A second possibility for how polarity in fungal spores is determined is that not intrinsic but external signals break cell symmetry, which in *N. crassa* is indicated by the fact that GT and CAT formation are cell density dependent, and show opposite chemotropisms [99, 105, 106]. At low cell concentrations GT formation is favoured, at a medium range of 0.5–1 x 10^6 cells/ml CAT formation and fusion occurs at maximal rates, whereas with further increasing cell density germination is inhibited. These early findings suggest that conidia of *N. crassa* display a kind of quorum sensing and respond with the initiation of cell polarisation according to their environment: low cell numbers, i.e. no close-by fusion partners, increases GT formation, whereas presence of potential fusion partners 'within range' triggers CAT formation. Quorum sensing, initially described in bacteria [68, 145], has also been recognized in various fungal species as means of population-level regulation [54]. In *C. albicans*, farnesol was identified as the 'quorum sensing' molecule, which at concentrations between 1-50 μM repressed hyphal development [56, 83]. Tyrosol, on the other hand stimulates the formation of filamentous protrusions under conditions otherwise permissive for GT development [27]. A number of recent reviews provide updated information on these intriguing autoregulatory molecules in fungi [54, 67, 87]. Interestingly, results from systematic mutant screens imply that distinct mechanisms may underlie polarity establishment and maintenance events occurring in different types of hyphae, as shown for primary hyphae and secondary side branches in *N. crassa* [114]. Therefore, polarity establishment and maintenance

might be differently regulated in spores compared with that in mature hyphae of the same organism. More work is required to uncover regulatory differences between polarised growth in germlings and mature hyphae. Two of the most pressing questions for us were: (1) what are the functional differences between CDC42 and RAC-1 in this context, and (2) how, once polarity is established and plasma membrane protrusion underway, is displacement of the polarisome and exocyst complexes accomplished to facilitate changes in growth direction?

Investigating cell polarity in conidial germlings of *N. crassa*. Conidial germlings of *N. crassa* provide a very interesting model system as they allow to study the cell polarity machinery of a filamentous fungus in a cellular system which is more readily comparable to unicellular yeasts than mature hyphae are. Although Spitzenkörper-like structures have not been identified in either GTs or CATs, both are capable of re-orientating tip growth, and interestingly show opposite chemotropisms. GTs avoid other GTs and cells (Fig. 1.3A and B), thus show negative chemotropism, whereas CATs show positive chemotropism towards each other (Fig. 1.3 C to E). One fascinating aspect clearly is that both responses can be regulated from one cell at apparently the same time. Our molecular understanding of this phenomenon is virtually non-existent. Therefore, the central questions of the work presented in this chapter were: (1) how is cell polarity in conidial germlings of *N. crassa* established, (2) what differences exist between the formation and polar maintenance of GTs compared to CATs, and (3) how is directionality during CAT homing achieved?

Our studies involving pharmacological disruption of cytoskeletal components in combination with the development of new molecular markers made two important findings: (1) the actin cytoskeleton is the sole requirement for cell polarisation and CAT fusion (Fig. 4.10) [107], and (2) microtubules, although essential for GT elongation and colony development, are dispensable for CAT-mediated cell fusion. The pronounced effects microtubule-disrupting drugs, such as

benomyl, have on GT formation have been recognized early on [108], but the importance of the F-actin cytoskeleton for cell symmetry breaking and in particular CAT-mediated cell fusion has not been fully appreciated.

Lifeact-TagRFPs reliably labelled F-actin cables, patches and rings in *N. crassa*. Although considerable effort has been expended in attempts to visualize F-actin distribution and dynamics in living fungal cells, satisfactory solutions have not yet been achieved. Previous strategies mostly relied on fusions between fluorescent proteins (FPs) and actin or actin binding proteins (ABPs) [31, 142, 152]. The use of FP-actin fusions as reporters for F-actin is problematic as only a fraction of actin is present in microfilaments resulting in a low signal-to-noise ratio, and, more importantly, the relatively large FP moiety has been shown to perturb actin dynamics in a variety of cell types [3, 102, 151]. Therefore, FP-actin fusion constructs are likely to alter actin dynamics in filamentous fungi, too. Fluorescent protein tagging of ABPs is preferable as there is generally less perturbation of actin dynamics *in vivo* but this approach may only reveal a small population of F-actin and the fusion protein may compete with unlabelled endogenous ABPs [22, 144].

To overcome these limitations, we took advantage of a recently developed live-cell imaging probe for F-actin, called Lifeact. Lifeact is a 17-amino-acid peptide derived from the N-terminus of the budding yeast actin-binding protein Abp140 [5, 152], and has recently been demonstrated to be a universal live-cell imaging marker for F-actin in eukaryotes, providing clear labelling of F-actin cables and patches in a variety of cell types without interfering with actin dynamics [32, 102, 137]. We constructed synthetic genes consisting of Lifeact fused to either the homodimer tdTomato [116], GFP and photostabilized versions of the monomeric red fluorescent proteins TagRFP [80] and TagRFP-T, respectively, and expressed these constructs in various *N. crassa* strains. In all strain backgrounds, fluorescent Lifeact constructs clearly labelled actin patches, cables and rings, and revealed a direct association of F-actin structures with sites of cell polarisation and active tip growth (Figs. 4.4 and

4.5). Labelling artefacts in the form of cytoplasmic rings and pronounced vacuolar accumulation were only seen with the Lifeact-tdTomato construct (Fig. 4.4B and C), and were most likely associated with multimerisation of the dimer. Both Lifeact-TagRFPs performed equally well and produced reliable labelling of F-actin patches, cables and rings (Fig. 4.3 to 4.5) identical to those labelled with a GFP tagged version of Lifeact [11], and displayed a localization pattern of F-actin consistent with previous studies in *N. crassa* and other filamentous fungi using immunofluorescent labelling, phalloidin staining, and FP-based live-cell imaging [4, 49, 63, 123, 125, 134, 138]. Due to its >10-fold increased photostability, Lifeact-TagRFP-T (Fig. 4.3) was particular well suited for long time course imaging, especially in combination with GFP-labelled markers (Fig 4.12 to 4.14), where unwanted cross-excitation of TagRFPs with 488 nm noticeably increased their bleaching rate. Latrunculin A treatment, which prevents F-actin polymerization [6], confirmed specificity of Lifeact-FPs for F-actin [11]. Treatment with 10 μM Lat A led to a rapid loss of Lifeact-TagRFP-labelled patches and cables demonstrating a generally high rate of F-actin turnover in *N. crassa* (Fig. 4.6). Interestingly, although usually all cables disassembled within 5-10 min of Lat A treatment, some cables appeared to be initially insensitive to Lat A implying that different subpopulations of actin cables with different turnover rates exist in *N. crassa*.

Roles of cables and patches during polarised secretion. In budding yeast, actin cables form tracks for myosin-V-dependent transport of secretory vesicles, whereas actin patches are considered to be platforms for endocytosis and membrane invagination [84]. Both patches and cables localize to new buds in *S. cerevisae* but only actin cables are required for polarised secretion [58, 94, 152]. The localization of actin patches and cables to the tips of GTs and CATs in *N. crassa* suggests active exo- and endocytosis in these regions and indicates a tight coupling of both processes (Fig. 4.4 and Supplementary movie C4.3). Accumulation of highly dynamic actin cables and patches at sites of active growth in *N. crassa* confirmed that polarisation

of the actin cytoskeleton underlies apical extension, indicating consistency with the yeast model. Prior to GT emergence cortical F-actin caps formed at the incipient bud site (Fig. 4.7). Interestingly, these caps were mobile and reformed along the cortex before being fixed at a specific position which then determined the site of GT emergence. Tip extension was accompanied by dynamic rearrangement of F-actin, which usually formed as an apical cap that slowly dissolved into a highly dynamic cable array undergoing retrograde movement (Fig. 4.8; Supplementary movie 4.4a). This phenomenon was recurrent and was commonly observed during the initial stages of GT emergence and elongation. Assuming that secretory vesicles are transported along actin cables in *N. crassa*, as has been indicated in budding yeast [58], a perplexing question is raised by these observations: how are vesicles transported to the growing tip while actin cables are constantly being rearranged and move in the opposite direction? Retrograde flow of actin cables has been reported during polarised growth in budding yeast [152], which is somewhat at odds with the notion of myosin-V-dependent transport of secretory vesicles along actin cables. It appears that the velocity of myosin-V anterograde transport is great enough to overcome retrograde cable flow; in *S. cerevisiae*, myosin-V movement along actin cables is approximately ten times more rapid than the rate of cable extension [84, 112, 152]. A similar mechanism is conceivable for filamentous fungi and would provide a logical explanation of how tip extension can occur while the F-actin array falls back. If and how these dynamic actin rearrangements are coordinated with long-distance transport along microtubules is subject of ongoing research.

The process of cell polarisation and bud protrusion is similar between GTs and CATs. The importance of F-actin for polarised growth is further highlighted by cable and patch accumulation during and after CAT-mediated cell fusion. Similar to the formation of polar caps and subsequent plasma membrane protrusion leading to GT formation (Fig. 4.7), F-actin arrays have also been found to

assemble at the cell cortex prior to CAT formation and condense into apical caps during CAT extension and homing (Figs. 4.9 and 4.13). Shortly after cytoplasmic continuity has been established by pore opening, actin cables gradually disappeared from the fusion site while patches usually persisted (Figs. 4.8 and 4.13). It has been proposed that the polarised secretion of biosynthetic material for plasma membrane and cell wall extension is compensated by endocytosis, maintaining the polarised state of cortical markers and receptors [76, 121, 134]. Given the role of actin patches in endocytosis, it is possible that the accumulation of actin patches at the tips of homing CATs and their persistence shortly after fusion facilitates the recycling of membrane receptors and polarity factors no longer required at this site. Disassembly of F-actin post-fusion indicates rapid depolarisation, and would be consistent with tip swelling regularly observed during hyphal fusion in the mature colony (Figs. 1.5 and 1.6).

Besides likely roles in targeted secretion during polarised extension and directed growth of GTs and CATs, additional roles of actin cables during the cell-cell fusion process are mostly unknown. The direct involvement of actin cables in the pore opening mechanism is a possibility. Recent work on cell fusion in mammalian systems suggests an important role for F-actin networks, in concert with myosins, in resisting and thereby slowing down membrane pore opening, allowing better control over the fusion process in order to prevent leakage [10, 26]. Due to the small size and dynamic nature of the fusion pore, elucidating further details of how cytoplasmic continuity is established on a structural level will be an important focus of future investigations.

Actin ring formation prior to septation. Lifeact-FPs also showed that actin cables are not always associated with tip growth, but have an additional role in septum formation [11]. F-actin rings were formed by accumulation and gradual condensation of cables at the cortex (Figs. 4.5 and 4.15). Previous work has shown that this process is dependent on the activity of RHO-4 GTPase [96, 97]. Besides

CDC42 and RAC-1, *N. crassa* possesses four other Rho GTPases (RHO-1 to RHO-4 isoforms), all with implicated functions in cytoskeletal organization and cell wall integrity. In contrast to Δ*cdc42* and Δ*rac-1* KOs (Fig. 4.19B), Δ*rho-4* mutants of *N. crassa* are aseptate and show leakage defects at hyphal tips due to insufficient cell wall strength [97]. This severe impairment however did not generally prevent hyphal fusion (Fig. 3.6), but lead to a noticeable reduction of hyphal fusion according to our findings; a feature shared in common with gene deletion mutants of RHO-2 and RHO-3 (Table 3.6). RHO-1 of *N. crassa* also has implicated functions in establishing cell polarity [141], but viable deletion strains that would permit a more detailed analysis have not yet been recovered. Taken together, these findings suggest that the recruitment and organization of the actin cytoskeleton for cell polarity establishment and polarised tip growth in the one hand, and actin ring formation on the other, is independently regulated by the two groups of Rho-type GTPases.

Morphogenetic differences between GTs and CATs might be regulated by selective recruitment of both cytoskeletal elements. One outstanding structural difference between GTs and CATs has been revealed by selectively disrupting microtubules. Cell polarisation and initiation of both protrusions occurred in the absence of microtubules (Fig. 4.10). GT elongation, however, required the presence of microtubules, whereas CAT formation, homing and fusion proceeded independently of microtubules. A phenomenon robust enough to be used as additional control for the differentiation between CAT induction defective and CAT homing defective fusion mutants (Fig. 3.8 and 4.8; Table 3.7). Previous studies on *Neurospora* reported several defects in the absence of microtubules, including pronounced isotropic growth and the induction of multiple GTs [23, 108]. Our observations confirm that GT initiation (but not elongation) can be achieved without microtubules, and furthermore indicate that the efficiency and accuracy of actin-mediated bud site selection (polarisation fidelity) is disturbed in the absence of

microtubules (Fig. 4.11). This led to surplus polarisation sites at the cell cortex which delayed germination and probably caused prolonged isotropic growth, but also can lead to multipolarisation. This demonstrates that certain cellular processes, such as GT elongation, require both cytoskeletal elements, whereas others sufficiently function with only one, such as CAT-mediated cell fusion. Therefore, the selective recruitment of either actin or microtubules, and their concerted action provide means of morphogenetic control.

Co-expression of Lifeact-TagRFPs and BML-sGFP revealed distinct but coordinated recruitment of both cytoskeletal elements during different stages of cell polarisation and tip extension. Sequential time lapse imaging indicated that further protrusion (and potentially stabilization) of the initial GT bud involved microtubules extending into the growing GT, and coincided with dynamic rearrangement of actin arrays which initially accumulated in the bud apex (Fig. 4.14). This is consistent with previous studies using microtubule-depolymerizing drugs which showed that GT emergence (but not elongation) in *N. crassa* can be achieved without microtubules [7]. Our data showing that polarisation of F-actin always preceded polarisation of microtubules further reinforces the notion that GT emergence and elongation occurs in two stages [18, 44], which first involves F-actin to break cell symmetry and establish a polarised bud, and secondly recruits microtubules which build on this asymmetry, maintain the stability of the polarised organization and drive further tip protrusion [71]. Crosstalk between regulatory pathways coordinates the functions of the two cytoskeletal systems. A similar phenomenon was never observed during CAT formation and fusion. Although, microtubules were recruited into protruding CATs, they did not extend beyond the present actin caps before tip growth was arrested and actin dispersed (Fig. 4.13), or cytoplasmic continuity has been achieved (Fig. 4.14). In contrast, CATs are thinner than GTs, show determinate growth [105], and do not require microtubules to facilitate cell fusion [107]. Consistently, we observed dynamic rearrangement of actin organization during CAT formation and fusion, suggesting a predominant role

of actin in these processes. This notion is supported by findings in *U. maydis* where it has been demonstrated that cell-cell recognition and cell-cell fusion exclusively depend on F-actin during all stages of polar growth whereas microtubules are only required for long-distance growth of hyphae [39]. The function of CATs is to connect cells which are less than 15 μm apart, i.e. CATs do not need to extend further than ~7 μm. The F-actin cytoskeleton is apparently sufficient to support this short-distance growth and facilitate fusion. Therefore, it is tempting to speculate that the morphological and functional differences between GTs and CATs are achieved by selective regulation of either cytoskeletal element. The two-step nature of establishing then stabilizing a polarity axis has been described for filamentous fungi and pseudohyphal GT growth of *C. albicans* (20, 9), but so far not been connected to selective but cooperative interaction of both cytoskeletal components. Although the existence of functional links between actin and microtubules is generally accepted, and especially well researched in the context of mitotic cell division in yeasts [153], signalling pathways regulating these interactions in fungi require further analysis. Orthologs of the mammalian IQGAP multidomain proteins, cytoskeletal scaffolding effectors that directly bind and cross-link F-actin [9, 143], but also have the ability to capture microtubules at their plus ends [19], have the potential to functionally link microtubules and cortical F-actin during polarity establishment in *N. crassa*. IQGAP-related proteins in fungi were first identified in yeast [89], but shortly after have been shown to have essential roles during septation in filamentous fungi [148]. The gene products of the *N. crassa* loci NCU03116.3 and NCU06122.4 are promising candidates for future analysis of how actin organization is coordinated with that of microtubules.

Unravelling molecular details of how conidial germlings of *N. crassa* establish and maintain two functionally distinct cell protrusions by regulated interaction of F-actin and microtubules will contribute novel aspects to this area of cell biology, especially as these processes appear to occur independently of cell cycle regulation in *N. crassa*.

Regulating directional growth of CATs. As mentioned earlier, a Spitzenkörper, which is crucially involved in regulating directionality of hyphal growth in mature hyphae, has not been identified in GTs or CATs within the initial hours of colony initiation. Still, GTs and CATs orientate their growth according to chemotropic signals. In CATs this is possible in the absence of microtubules (Fig. 4.10A), suggesting that it greatly relies on directed vesicle delivery along the actin cytoskeleton. But how is re-orientation of CAT tips accomplished? As recently reviewed for *C. albicans* [18], directionality of growth of fungal hyphae is determined by activation of at least three signalling pathways: (1) cell cortex landmark proteins, (2) G-protein-coupled mating pheromone receptors, or (3) plasma membrane calcium channels. All three ultimately provide positional feedback onto the actin cytoskeleton via CDC42 activation, which leads to reorientation of growth. Regulation via stretch- or voltage-activated Ca^{2+} channels is an option in *N. crassa* as well, although mechanical stimuli must be excluded, as CAT homing occurs prior to physical contact and works equally well on solid medium and in liquid culture, thus is not a response to specific surface cues. Touch sensing, however, might have an important role in triggering depolarisation and tip growth arrest once CATs made contact. Although responsible molecules are unknown, chemotropism is the accepted stimulus for CAT homing [100]. Mating pheromone is required for directed chemotropic growth during the sexual stage of *N. crassa's* lifecycle [61, 62], but can be ruled out as stimulus for CAT orientation as deletion of both sex pheromones, their respective GPCRs and all G-protein α and β subunits did not interfere with mature hyphal fusion or germling fusion in *N. crassa* (Tables 3.5 to 3.7). The currently most promising candidates are orthologs of cell end markers from *S. pombe*, such as Tea1 and Tea4, that have been recently identified in the filamentous fungus *A. nidulans* [52]. Deletion of TeaC affected polarised growth and hyphal directionality, whereas overexpression repressed septation and caused abnormal swelling of germinating conidia. In both fungi these cell end markers are recruited to the growing hyphal tip where they assemble into multiprotein

complexes and initiate actin nucleation via formin activation [36, 37]. Intact sterol-rich microdomains within the plasma membrane are required for cell-end marker localization which is mediated via prenylation motifs [110, 127]. This is interesting because it provides a functional link to CDC42 activation. The Cdc42-effector PAK Ste20p has been connected to sterol synthesis and is involved in regulating cell polarity in yeast [126, 129]. If sterol-rich domains were to act as accumulation spots of activated CDC42 in filamentous fungi as hypothesized [37], displacement of these domains would effectively relocate actin nucleation and re-orientate tip growth. Therefore, investigating the functional relationship between activated CDC42 and RAC-1 GTPases, putative cell end marker orthologs and the actin cytoskeleton during CAT homing is an important next step in this area of research. Identification of TeaC orthologs in filamentous fungi, as recently accomplished for *A. nidulans* [52], unfortunately is not straight forward, as the protein sequence is only poorly conserved amongst fungi (~12-14% sequence homology). The advances in fluorescent F-actin and Rho GTPase markers presented in this chapter, however, allowed some intial new insights.

Differential recruitment of the Rho GTPases CDC42 and RAC-1, respectively, determine functional distinction of GTs and CATs. Polarised activation of evolutionary conserved Cdc42-type GTPases is a key determinant of cellular F-actin organization and cell polarity in eukaryotes [59]. Using a CRIB motif containing biosensor it has very recently been demonstrated that active growth sites in *S. pombe* are accompanied by the GTP-bound, active form of Cdc42 [128]. To investigate GTPase activity during spore germination and CAT fusion we developed a similar marker for *N. crassa*. CRIB-sGFP labelled polarity sites in conidial germlings before plasma membrane protrusion and bud emergence, and accompanied polarised tip growth in GTs and CATs (Figs. 4.17 and 4.18). The crescent-shaped labelling pattern was identical to that documented for fission yeast cells [128], and also resembled localization of fluorescently labelled PAK in budding

yeast [126]. Furthermore, CRIB-sGFP fluorescence was constantly present at homing and fusing CAT tips, and allowed the visualization of fusion pore opening (Fig. 4.20). As soon as cytoplasmic continuity between cells has been established, fluorescence disappeared, indicating that activated GTPases were no longer required. Co-expression of CRIB-sGFP with Lifeact-TagRFP-T confirmed the expected, close spatio-temporal association of activated Rho GTPases with the F-actin cytoskeleton during cell symmetry breaking and polarised tip growth (Fig. 4.22). Furthermore, using both markers showed that disruption of microtubules has a direct influence on the efficiency and accuracy of cell polarisation and polarised GT growth (Fig. 4.23). Defects in polarisation fidelity due to the absence of microtubules provide an explanation for previous observations in *Neurospora crassa*, describing multipolar germination in the presence of benomyl [108], and clearly demonstrate that functional interaction between both cytoskeletal components is essential for these processes to occur normally.

The most important insight from this work is the functional distinction of CDC42 and RAC-1 in CAT-mediated cell fusion. Differential recruitment of both Rho GTPases to either protrusion became evident upon treatment with $\geq$ 1% DMSO (Figs. 4.24 and 4.25). The developed CRIB-sGFP biosensor is expected to equally bind to activated forms of both Rho GTPases at the plasma membrane. Therefore, the finding that dispersal of this biosensor upon DMSO treatment was only seen in GTs but not in CATs can be interpreted in various ways. In case both Rho GTPases would be present at the tips of both, GTs and CATs, the lipid composition in both tips could be markedly different, and insensitive to disruption through DMSO in CATs, consequently resulting in Rho GTPase dispersal only in GTs. In case each Rho GTPase is specifically recruited to either GT or CAT tips, the membrane-binding mechanisms of CDC42 and RAC-1 have different sensitivities towards DMSO treatment. Alternatively, DMSO could specifically interfere with activation of one of the two Rho GTPases at the membrane (e.g. by blocking GTPase-GEF interaction) leading to the loss of apical CRIB-sGFP fluorescence in GTs. This again

would argue for the differential recruitment of CDC42 and RAC-1 to either cell protrusion, as it does not occur in CATs.

Experiments conducted with the Rac GTPase-specific inhibitor NSC23766 (Fig. 4.26) strongly support the notion that CDC42 and RAC-1 are specifically activated in GTs and CATs, respectively. Germination of conidia in the presence of $\geq$ 50 μM NSC23766 completely blocked CAT formation and thus cell fusion, without blocking GT formation and elongation. Interestingly, in the presence of the Rac1 inhibitor, GT elongation was markedly promoted, leading to an increase of the average GT length by a factor of two (Supplementary figure 4.5). This alone demonstrated that RAC-1 is not required for GT growth, and is consistent with the phenotype of Δ*rac-1* cells, which can grown GTs, but are unable to differentiate CATs and establish cell fusion (Figs. 4.10 and 4.18). Furthermore, addition of NSC23766 to growing germlings expressing the CRIB biosensor resulted in CRIB-sGFP dispersal in CATs (Fig. 4.26A) but not in GT tips (Fig. 4.26B). Provided that NSC23766 is as specific for Rac GTPases in *Neurospora* as it is in mammalian cells [40], this clearly demonstrates that RAC-1 specifically functions in CATs, and that blockage of CAT formation defaults the cells into a 'GT-elongation pathway'.

Further analysis will be required to verify the binding specificity of the CRIB reporter for CDC42 and RAC-1 of *Neurospora crassa*. Based on the validated interaction of RAC-1 with NOR-1 [24], ongoing work attempts to develop a novel reporter which is specific for RAC-1. Furthermore, co-expression of CRIB-sGFP and Lifeact-TagRFP in Δ*rac-1* and Δ*cdc42* mutant backgrounds will help to elucidate additional details of the different roles both GTPases might have during cell polarisation and cell fusion. Based on the current findings and the fact that Δ*rac-1* cells of *N. crassa* display less severe polar extension defects compared to Δ*cdc42* (Fig. 4.19) we speculate that CDC42 has an exclusive role in establishing and maintaining polarised growth of GTs, whereas RAC-1 has an exclusive function in the establishment and polarised growth of CATs. This is in contrast to what is currently believed for mature hypha of *Neurospora*, where no significant functional differences

between both GTPases have been reported. This, however, might reflect different modes of regulation at early and late developmental stages of the organism.

Special attention in future investigations will also be focused on the interplay between perception of the chemotropic signal, dislocation of GTPase activity at the cell cortex and subsequent rearrangement of the actin cytoskeleton. Concerted action of all three processes is crucial for tip re-orientation during CAT homing in order to establish CAT contact and facilitate cell fusion, but also during GT avoidance responses. Based on the above results, CDC42 and RAC-1 are expected to have distinct roles in the regulation of negative chemotropism in GTs and positive chemotropism in CATs, respectively.

4.5. Summary

This chapter demonstrated the crucial and exclusive role of the actin cytoskeleton for cell symmetry breaking of *N. crassa* conidia during germination in general and CAT-mediated cell fusion in particular, and provided a causal link between localized activation of Rho GTPase at the cell cortex and dynamic rearrangement of F-actin during directed tip growth. Key achievements were:

- Development of a novel live-cell imaging marker for F-actin in filamentous fungi, which allowed the detailed analysis of F-actin cable and patch dynamics during the establishment and maintenance of polarised hyphal growth and CAT-mediated cell fusion:
    - cortical F-actin caps formed prior to plasma membrane protrusion and accompanied polarised tip growth of GTs and CATs
    - GT elongation involved the dynamic rearrangement of F-actin cable arrays that underwent retrograde movement

  - F-actin cable arrays disappeared after successful CAT fusion, whilst actin patches remained and were probably involved in endocytic recycling of membrane receptors and polarity factors

- Generation of filamentous fungal strains stably expressing dual colour labelling of microtubules and F-actin allowed visualization of the entire fungal cytoskeleton for the first time, and provided initial evidence for functionally distinct but coordinated rearrangement of both cytoskeletal elements:
  - disruption of microtubules affected polarisation fidelity, i.e. the accuracy and efficiency of actin-mediated bud site selection, and furthermore blocked GT elongation, but did not inhibit CAT formation and fusion
  - CATs are determinate in length because microtubules are not recruited to promote further elongation
  - actin rings formed by localized condensation of F-actin cables prior to septum formation and without obvious connection to microtubules or the cell cycle

- Identification and phenotypic description of the two closely related Rho-type GTPases CDC42 and RAC-1 of *N. crassa*, which indicated functionally diverse roles of both GTPases in the cell polarity machinery of conidial germlings:
  - more severe polar extension defect in Δ*cdc42* compared with Δ*rac-1* indicated a primary role for CDC42 in maintaining polar tip growth in GTs
  - CDC42 and RAC-1 were essential for polarised growth but dispensable for septum formation, indicating that F-actin nucleation for polarity establishment is differently regulated than F-actin recruitment for actin ring formation (which is controlled by the RHO isoform GTPases)

- Development of a novel live-cell imaging biosensor (CRIB-sGFP) to monitor activated CDC42 and RAC-1 GTPases during polarised growth:

- GTPase activity focused to polar crescents during cell symmetry breaking, GT elongation and CAT protrusion, providing a functional link to F-actin organization at these sites, and explaining the CAT induction defect in Δ*cdc42* and Δ*rac-1* strains
- concentration of GTPase activity to mobile, presumably sterol-rich plasma membrane microdomains suggests that relocation of F-actin nucleation towards the chemoattractant source is responsible for tip re-orientation during CAT homing

- Initial evidence that RAC-1 exclusively functions during the establishment and polarised growth of CATs
  - Δ*rac-1* cells were unable to differentiate CATs, but grew normal GTs
  - DMSO specifically blocked Rho GTPase recruitment/activation in GT tips
  - the small molecule Rac GTPase inhibitor NSC23766 specifically blocked Rho GTPase activation/recruitment in CAT tips

4.6. References

1. **Adams, A., and J. Pringle.** 1984. Relationship of actin and tubulin distribution to bud growth in wild-type and morphogenetic-mutant *Saccharomyces cerevisiae*. Journal of Cell Biology **98:**934-945.

2. **Adams, A. E., D. I. Johnson, R. M. Longnecker, B. F. Sloat, and J. R. Pringle.** 1990. CDC42 and CDC43, two additional genes involved in budding and the establishment of cell polarity in the yeast *Saccharomyces cerevisiae*. Journal of Cell Biology **111:**131-142.

3. **Aizawa, A., M. Sameshima, and I. Yahara.** 1997. A green fluorescent protein-actin fusion protein dominantly inhibits cytokinesis,cell spreading, and locomotion in *Dictyostelium*. Cell Structure and Function **22:**335-345.

4. **Araujo-Bazán, L., M. A. Penalva, and E. A. Espeso.** 2008. Preferential localization of the endocytic internalization machinery to hyphal tips underlies polarization of the actin cytoskeleton in *Aspergillus nidulans*. Molecular Microbiology **67:**891-905.

5. **Asakura, T., T. Sasaki, F. Nagano, A. Satoh, H. Obaishi, H. Nishioka, H. Imamura, K. Hotta, K. Tanaka, H. Nakanishi, and Y. Takai.** 1998. Isolation and characterization of a novel actin filament-binding protein from *Saccharomyces cerevisiae*. Oncogene **16:**121-130.

6. **Ayscough, K. R., J. Stryker, N. Pokala, M. Sanders, P. Crews, and D. G. Drubin.** 1997. High rates of actin filament turnover in budding yeast and roles for actin in establishment and maintenance of cell polarity revealed using the actin inhibitor Latrunculin-A. Cell Biology **137:**399-416.

7. **Barja, F., M.-L. Chappuis, and G. Turian.** 1993. Differential effects of anticytoskeletal compounds on the localization and chemical patterns of actin in germinating conidia of *Neurospora crassa*. FEMS Microbiological Letters **107:**261-266.

8. **Bartnicki-Garcia, S.** 2002. Hyphal tip growth: outstanding questions., p. 29-58. *In* H. D. Osiewaqcz (ed.), Molecualr Biology of Fungal Development. Marcel Dekker, New York.

9. **Bashour, A. M., A. T. Fullerton, M. J. Hart, and G. S. Bloom.** 1997. IQGAP1, a Rac- and Cdc42-binding protein, directly binds and cross-links microfilaments. Journal of Cell Biology **137:**1555-1566.

10. **Bath, P., and P. Thorn.** 2009. Myosin 2 maintains an open exocytic fusion pore in secretory epithelial cells. Mol. Biol. Cell **20:**1795-1803.

11. **Berepiki, A., A. Lichius, J.-y. Shoji, J. Tilsner, and N. D. Read.** 2010. F-actin dynamics in *Neurospora crassa*. Eukaryotic Cell **9:**547-57.

12. **Bernards, A., and J. Settleman.** 2004. GAP control: regulating the regulators of small GTPases. Trends in Cell Biology **14:**377-385.

13. **Bi, E., and S. H. Zigmond.** 1999. Actin polymerization: Where the WASP stings. Current Biology **9:**R160-R163.

14. **Bishop, A. L., and A. Hall.** 2000. Rho GTPases and their effector proteins. Biochemical Journal **348:**241-255.

15. **Borkovich, K. A., L. A. Alex, O. Yarden, M. Freitag, G. E. Turner, N. D. Read, S. Seiler, D. Bell-Pedersen, J. Paietta, N. Plesofsky, M. Plamann, M. Goodrich-Tanrikulu, U. Schulte, G. Mannhaupt, F. E. Nargang, A. Radford, C. Selitrennikoff, J. E. Galagan, J. C. Dunlap, J. J. Loros, D. Catcheside, H. Inoue, R. Aramayo, M. Polymenis, E. U. Selker, M. S. Sachs, G. A. Marzluf, I. Paulsen, R. Davis, D. J. Ebbole, A. Zelter, E. R. Kalkman, R. O'Rourke, F. Bowring, J. Yeadon, C. Ishii, K. Suzuki, W. Sakai, and R. Pratt.** 2004. Lessons from the genome sequence of *Neurospora crassa*: tracing the path from genomic blueprint to multicellular organism. Microbiological and Molecular Biological Reviews **68:**1-108.

16. **Boyce, K. J., and A. Andrianopoulos.** 2006. Morphogenesis: Control of Cell Types and Shape, p. 3-20. *In* R. Fischer and U. Kües (ed.), The Mycota I, vol. I. Springer Verlag, Berlin/Heidelberg.

17. **Bracker, C. E., D. J. Murphy, and R. Lopez-Franco.** 1997. Laser beam micromanipulation of cell morphogenesis in growing fungal hyphae, p. 67-80. *In* D. L. Farkas and B. J. Tromberg (ed.), Functional Imaging of Optical Manipulation of Living Cells. Proceedings of SPIE., vol. 2983. International Society of Optical Engineering, Bellingham, Washington, USA.

18. **Brand, A., and N. A. R. Gow.** 2009. Mechanisms of hypha orientation of fungi. Current Opinion in Microbiology **12:**350-357.

19. **Brandt, D. T., and R. Grosse.** 2007. Get to grips: steering local actin dynamics with IQGAPs. EMBO reports **8:**1019-1023.

20. **Bretscher, A.** 2003. Polarized growth and organelle segregation in yeast: the tracks, motors, and receptors. Journal of Cell Biology **160:**811-816.

21. **Burbelo, P. D., D. Drechsel, and A. Hall.** 1995. A conserved binding motif defines numerous candidate target proteins for both Cdc42 and Rac GTPases. Journal of Biological Chemistry **270:**29071-29074.

22. **Burkel, B. M., G. von Dassow, and W. M. Bement.** 2007. Versatile fluorescent probes for actin filaments based on the actin-binding domain of utrophin. Cell Motility and the Cytoskeleton **64:**822-832.

23. **Caesar-Ton That, T. C., C. Rossier, F. Barja, G. Turian, and U.-P. Ross.** 1988. Induction of multiple germ tubes in *Neurospora crassa* by antitubulin agents. European Journal of Cell Biology **46:**68-79.

24. **Cano-Dominguez, N., K. Alvarez-Delfin, W. Hansberg, and J. Aguirre.** 2008. NADPH oxidases NOX-1 and NOX-2 require the regulatory subunit NOR-1 to control cell differentiation and growth in *Neurospora crassa*. Eukaryotic Cell **7:**1352-1361.

25. **Chang, F., and M. Peter.** 2003. Yeasts make their mark. Nature Cell Biology **5:**294-299.

26. **Chen, A., E. Leikina, K. Melikov, B. Podbilewicz, M. M. Kozlov, and L. V. Chernomordik.** 2008. Fusion-pore expansion during syncytium formation is restricted by an actin network. Journal of Cell Science **121:**3619-3628.

27. **Chen, H., M. Fujita, Q. Feng, J. Clardy, and G. R. Fink.** 2004. Tyrosol is a quorum-sensing molecule in *Candida albicans*. Proceedings of the National Academy of Sciences of the United States of America **101:**5048-5052.

28. **Czymmek, K. J., T. M. Bourett, Y. Shao, T. M. DeZwaan, J. A. Sweigard, and R. J. Howard.** 2005. Live-cell imaging of tubulin in the filamentous fungus *Magnaporthe grisea* treated with anti-microtubule and anti-microfilament agents. Protoplasma **225:**23-32.

29. **d'Enfert, C.** 1997. Fungal spore germination: insights from the molecular genetics of *Aspergillus nidulans* and *Neurospora crassa*. Fungal Genetics and Biology **21:**163-173.

30. **Dijksterhius, J.** 2003. Confocal microscopy of Spitzenkörper dynamics during growth and differentiation of rust fungi. Protoplasma **222:**53-59.

31. **Doyle, T., and D. Botstein.** 1996. Movement of yeast cortical actin cytoskeleton visualized *in vivo*. Proceedings of the National Academy of Sciences **93:**3886-3891.

32. **Era, A., M. Tominaga, K. Ebine, C. Awai, C. Saito, K. Ishizaki, K. T. Yamato, T. Kohchi, A. Nakano, and T. Ueda.** 2009. Application of Lifeact reveals F-actin dynamics in *Arabidopsis thaliana* and the liverwort, *Marchantia polymorpha*. Plant and Cell Physiology **50:**1041-1048.

33. **Evangelista, M., D. Pruyne, D. C. Amberg, C. Boone, and A. Bretscher.** 2002. Formins direct Arp2/3-independent actin filament assembly to polarize cell growth in yeast. Nature Cell Biology **4:**32-34.

34. **Evangelista, M., S. Zigmond, and C. Boone.** 2003. Formins: signaling effectors for assembly and polarization of actin filaments. Journal of Cell Science **116:**2603-2611.

35. **Fehrenbacher, K. L., H.-C. Yang, A. C. Gay, T. M. Huckaba, and L. A. Pou.** 2004. Live-cell imaging of mitochondrial movement along actin cables in budding yeast. Current Biology **14:**1996-2004.

36. **Feierbach, G., F. Verde, and F. Chang.** 2004. Regulation of the formin complex by microtubule plus ends and contribute to growth directionality. Eukaryotic Cell **6:**555-562.

37. **Fischer, R., N. Zekert, and N. Takeshita.** 2008. Polarized growth in fungi - interplay between the cytoskeleton, positional markers and membrane domains. Molecular Microbiology **68:**813-826.

38. **Freitag, M., P. C. Hickey, N. B. Raju, E. U. Selker, and N. D. Read.** 2004. GFP as a tool to analyze the organization, dynamics and function of nuclei and microtubules in *Neurospora crassa*. Fungal Genetics and Biology **41:**897-910.

39. **Fuchs, U., I. Manns, and G. Steinberg.** 2005. Microtubules are dispensable for the initial pathogenic development but required for long-distance hyphal growth in the corn smut fungus Ustilago maydis. Molecular Biology of the Cell **16:**2746-2758.

40. **Gao, Y., J. B. Dickerson, F. Guo, J. Zheng, and Y. Zheng.** 2004. Rational design and characterization of a Rac GTPase-specific small molecule inhibitor. Proceedings of the National Academy of Science of the USA **101:**7618-7623.

41. **Girbardt, M.** 1957. Der Spitzenkörper von *Polysticus versicolor*. Planta **50:**47-59.

42. **Glass, N. L., C. Rasmussen, G. M. Roca, and N. D. Read.** 2004. Hyphal homing, fusion and mycelial interconnectedness. TRENDS in Microbiology **12:**135-141.

43. **Goryachev, A. B., and A. V. Pokhilko.** 2008. Dynamics of Cdc42 network embodies a turing-type mechanism of yeast cell polarity. FEBS letters **582:**1437-1443.

44. **Harris, S. D.** 2006. Cell polarity in filamentous fungi: shaping the mold. International Review of Cytology **251:**41-77.

45. **Harris, S. D., and M. Momany.** 2004. Polarity in filamentous fungi: moving beyond the yeast paradigm. Fungal Genetics and Biology **41:**391-400.

46. **Harris, S. D., J. L. Morrell, and J. E. Hamer.** 1994. Identification and characterization of *Aspergillus nidulans* mutants defective in cytokinesis. Genetics **136:**517-532.

47. **Harris, S. D., N. D. Read, R. W. Roberson, B. Shaw, S. Seiler, M. Plamann, and M. Momany.** 2005. Polarisome meets Spitzenkörper: microscopy, genetics, and genomic converge. Eukaryotic Cell **4:**225-229.

48. **Hazan, I., and H. P. Liu.** 2002. Hyphal tip-associated localization of Cdc42 is F-actin dependent in *Candida albicans*. Eukaryotic Cell **1:**856-864.

49. **Heath, I. B., G. Gupta, and S. Bai.** 2000. Plasma membrane-adjacent actin filaments, but not microtubules, are essential for both polarization and hyphal tip morphogenesis in *Saprolegnia ferax* and *Neurospora crassa*. Fungal Genetics and Biology **30:**45-62.

50. **Hickey, P. C., D. J. Jacobson, N. D. Read, and N. Louise Glass.** 2002. Live-cell imaging of vegetative hyphal fusion in *Neurospora crassa*. Fungal Genetics and Biology **37:**109-119.

51. **Hickey, P. C., S. R. Swift, M. G. Roca, and N. D. Read.** 2005. Live-cell Imaging of filamentous fungi using vital fluorescent dyes and confocal microscopy, p. 63-87, Methods in Microbiology, vol. Volume 34. Elsevier B. V.

52. **Higashitsuji, Y., S. Herrero, N. Takeshita, and R. Fischer.** 2009. The cell end marker protein TeaC is involved in both growth directionality and septation in *Aspergillus nidulans*. Eukaryotic Cell **8:**957-967.

53. **Hoffman, G. R., and R. A. Cerione.** 2000. Flipping the switch: the structural basis for signaling through the CRIB motif. Cell **102:**403-406.

54. **Hogan, D. A.** 2006. Talking to themselves: autoregulation and quorum sensing in fungi. Eukaryotic Cell **5:**613-619.

55. **Horio, T., and B. R. Oakley.** 2005. The role of microtubules in rapid hyphal tip growth of *Aspergillus nidulans*. Molecular Biology of the Cell **16:**918-926.

56. **Hornby, J. M., E. C. Jensen, A. D. Lisec, J. J. Tasto, B. Jahnke, R. Shoemaker, P. Dussault, and K. W. Nickerson.** 2001. Quorum sensing in the dimorphic fungus *Candida albicans* is mediated by farnesol. Applied and Environmental Microbiology **67:**2982-2992.

57. **Howell, A. S., N. S. Savage, S. A. Johnson, I. Bose, A. W. Wagner, T. R. Zyla, H. F. Nijhout, M. C. Reed, A. B. Goryachev, and D. J. Lew.** 2009. Singularity in polarization: rewiring yeast cells to make two buds. Cell **139:**731-743.

58. **Huckaba, T. M., A. C. Gay, L. F. Pantalena, H.-C. Yang, and L. A. Pon.** 2004. Live-cell imaging of the assembly, disassembly, and actin cable-dependent movement of endosomes and actin patches in the budding yeast, *Saccharomyces cerevisiae*. Journal of Cell Biology **167:**519-530.

59. **Jaffe, A. B., and A. Hall.** 2005. Rho GTPases: biochemistry and biology. Annual Review of Cell and Developmental Biology **21:**247-269.

60. **Karpova, T. S., K. Tatchell, and J. A. Cooper.** 1995. Actin filaments in yeast are unstable in the absence of capping protein or fimbrin. Journal of Cell Biology **131:**1483-1493.

61. **Kim, H., and K. A. Borkovich.** 2004. A pheromone receptor gene, *pre-1*, is essential for mating type-specific directional growth and fusion of trichogynes and female fertility in *Neurospora crassa*. Molecular Microbiology **52:**1781-1798.

62. **Kim, H., and K. A. Borkovich.** 2006. Pheromones are essential for male fertility and sufficient to direct chemotropic polarized growth of trichogynes during mating in *Neurospora crassa*. Eukaryotic Cell **5:**544-554.

63. **Knechtle, P. J., F. Dietrich, and P. Philippsen.** 2003. Maximal polar growth potential depends on the polarisome component AgSpa2 in the filamentous fungus *Ashbya gossypii*. Mol. Biol. Cell **14:**4140-4154.

64. **Knechtle, P. J., J. Wendland, and P. Philippsen.** 2006. The SH3/PH domain protein AgBoi1/2 collaborates with the Rho-type GTPase AgRho3 to prevent nonpolar growth at hyphal tips of *Ashbya gossypii*. Eukaryotic Cell **5:**1635-1647.

65. **Köhli, M., V. Galati, K. Boudier, R. W. Roberson, and P. Philippsen.** 2008. Growth-speed-correlated localization of exocyst and polarisome components in growth zones of *Ashbya gossypii* hyphal tips. Journal of Cell Science **121:**3878-3889.

66. **Kozubowski, L., K. Saito, J. M. Johnson, A. S. Howell, T. R. Zyla, and D. J. Lew.** 2008. Symmetry-breaking polarization driven by a Cdc42p GEF-PAK complex. Current Biology **18:**1719-1726.

67. **Langford, M. L., A. L. Atkin, and K. W. Nickerson.** 2009. Cellular interactions of farnesol, a quorum-sensing molecule produced by *Candida albicans*. Future Microbiology **4:**1353-1362.

68. **Lazazzera, B. A.** 2000. Quorum sensing and starvation: signals for entry into stationary phase. Current Opinion in Microbiology **3:**177.

69. **Leberer, E., D. Dignard, D. Harcus, D. Y. Thomas, and M. Whiteway.** 1992. The protein kinase homologue Ste20p is required to link the yeast pheromone response G-protein beta gamma subunits to downstream signalling components. EMBO Journal **11:**4815-4824.

70. **Lew, D. J.** 2002. Formin' actin filament bundles. Nature Cell Biology **4:**E29-E30.

71. **Li, R., and G. G. Gundersen.** 2008. Beyond polymer polarity: how the cytoskeleton builds a polarized cell. Nature Reviews Molecular Cell Biology **9:**860-873.

72. **Lopez-Franco, R., and C. E. Bracker.** 1996. Diversity and dynamics of the Spitzenkörper in growing hyphal tips of higher fungi. Protoplasma **195:**90-111.

73. **Lu, B. C.** 2006. Karyotyping of *Neurospora crassa* using synaptonemal complex spreads of translocation quadrivalents. Genome **49:**612-618.

74. **Mahlert, M., L. Leveleki, A. Hlubek, B. Sandrock, and M. Bölker.** 2006. Rac1 and Cdc42 regulate hyphal growth and cytokinesis in the dimorphic fungus *Ustilago maydis*. Molecular Microbiology **59:**567-578.

75. **Manser, E., T. Leung, H. Salihuddin, Z.-s. Zhao, and L. Lim.** 1994. A brain serine/threonine protein kinase activated by Cdc42 and Rac1. Nature **367:**40-46.

76. **Marco, E., R. Wedlich-Söldner, R. Li, S. J. Altschuler, and L. F. Wu.** 2007. Endocytosis optimizes the dynamic localization of membrane proteins that regulate cortical polarity. Cell **129:**411-422.

77. **Martin, H., A. Mendoza, J. M. Rodriguez-Pachon, M. Molina, and C. Nombela.** 1997. Characterization of SKM1, a *Saccharomyces cerevisiae* gene encoding a novel Ste20/PAK-like protein kinase. Molecular Microbiology **23:**431-444.

78. **Martin, S. G., and C. F.** 2005. New end take off: regulating cell polarity during the fission yeast cell cycle. Cell Cycle **4:**1046-1049.

79. **McNally, M. T., and S. J. Free.** 1988. Isolation and characterization of a *Neurospora* glucose-repressible gene. Current Genetics **14:**545-551.

80. **Merzlyak, E. M., J. Goedhart, D. Shcherbo, M. E. Bulina, A. S. Shcheglov, A. F. Fradkov, A. Gaintzeva, K. A. Lukyanov, S. Lukyanov, T. W. J. Gadella, and D. M. Chudakov.** 2007. Bright monomeric red fluorescent protein with an extended fluorescence lifetime. Nature Methods **4:**555-557.

81. **Miller, P. J., and D. I. Johnson.** 1994. Cdc42p GTPase is involved in controlling polarized cell growth in *Schizosaccharomyces pombe*. Molecular and Cellular Biology **14:**1075-1083.

82. **Momany, M.** 2002. Polarity in filamentous fungi: establishment, maintenance and new axes. Current Opinion in Microbiology **5:**580-585.

83. **Mosel, D. D., R. Dumitru, J. M. Hornby, A. L. Atkin, and K. W. Nickerson.** 2005. Farnesol concentrations required to block germ tube formation in *Candida albicans* in the presence and absence of serum. Applied and Environmental Microbiology **71:**4938-4940.

84. **Moseley, J. B., and B. L. Goode.** 2006. The yeast actin cytoskeleton: from cellular function to biochemical mechanism. Microbiology and Molecular Biology Reviews **70:**605-645.

85. **Nalbant, P., L. Hodgson, V. Kraynov, A. Toutchkine, and K. M. Hahn.** 2000. Activation of endogenous Cdc42 visualized in living cells. Science **305:**1615-1619.

86. **Nelson, W. J.** 2003. Adaptation of core mechanisms to generate cell polarity. Nature **422:**766-774.

87. **Nickerson, K. W., A. L. Atkin, and J. M. Hornby.** 2006. Quorum sensing in dimorphic fungi: farnesol and beyond. Applied and Environmental Microbiology **72:**3805-3813.

88. **Novick, P., and D. Botstein.** 1985. Phenotypic analysis of temperature-sensitive yeast actin mutants. Cell **40:**405-416.

89. **Osman, M. A., and R. A. Cerione.** 1998. Iqg1p, a yeast homologue of the mammalian IQGAPs, mediates Cdc42p effects on the actin cytoskeleton. The Journal of Cell Biology **142:**443-455.

90. **Ozbudak, E. M., A. Becskei, and A. von Oudenaarden.** 2005. A system counteracting feedback loops regulates Cdc42p activity during spontaneous cell polarization. Developmental Cell **9:**565-571.

91. **Park, H.-O., and E. Bi.** 2007. Central roles of small GTPases in the development of cell polarity in yeast and beyond. Microbiology and Molecular Biology Reviews **71:**48-96.

92. **Pelham, R. J., and F. Chang.** 2001. Role of actin polymerization and actin cables in actin-patch movement in *Schizosaccharomyces pombe*. Nature Cell Biology **3:**235-244.

93. **Pruyne, D., and A. Bretscher.** 2000. Polarization of cell growth in yeast. I. Establishment and maintenance of polarity states. Journal of Cell Science **113:**365-375.

94. **Pruyne, D., D. H. Schott, and A. Bretscher.** 1998. Tropomyosin-containing actin cables direct the Myo2p-dependent polarized delivery of secretory vesicles in budding yeast. Journal of Cell Biology **143:**1931-1945.

95. **Raju, N. B.** 1984. Use of enlarged cells and nuclei for studying mitosis in *Neurospora*. Protoplasma **121:**139-149.

96. **Rasmussen, C. G., and N. L. Glass.** 2007. Localization of RHO-4 indicates differential regulation of conidial versus vegetative septation in the filamentous fungus *Neurospora crassa*. Eukaryotic Cell **6:**1097-1107.

97. **Rasmussen, C. G., and N. L. Glass.** 2005. A rho-type GTPase, *rho-4*, is required for septation in *Neurospora crassa*. Eukaryotic Cell **4:**1913-1925.

98. **Read, N. D.** 2006. Environmental sensing and the filamentous fungal lifestyle, p. 38-57. *In* G. M. Gadd, S. C. Watkinson, and P. S. Dyer (ed.), Fungi and the Environment. Cambridge University Press, Cambridge.

99. **Read, N. D., A. Fleißner, M. G. Roca, and N. L. Glass.** 2010. Hyphal fusion. *In* K. A. Borkovich and D. Ebbole (ed.), Cellular and Molecular Biology of Filamentous Fungi. American Society of Microbiology, Washington DC.

100. **Read, N. D., A. Lichius, J. Shoji, and A. B. Goryachev.** 2009. Self-signalling and self-fusion in filamentous fungi. Current Opinion in Microbiology **12:**608-615.

101. **Reynaga-Pena, C. G., and S. Bartnicki-Garcia.** 1997. Apical branching in a temperature sensitive mutant of *Aspergillus niger*. Fungal Genetics and Biology **22:**153-167.

102. **Riedl, J., A. H. Crevenna, K. Kessenbrock, J. H. Yu, D. Neukirchen, M. Bista, F. Bradke, D. Jenne, T. A. Holak, Z. Werb, M. Sixt, and R. Wedlich-Söldner.** 2008. Lifeact: a versatile marker to visualize F-actin. Nature Methods **5:**605-607.

103. **Riquelme, M., C. G. Reynaga-Pena, G. Gierz, and S. Bartnicki-Garcia.** 1998. What determines growth direction in fungal hyphae? Fungal Genetics and Biology **24:**101-109.

104. **Rittentour, W. R., H. Si, and S. D. Harris.** 2009. Hyphal morphogenesis in *Aspergillus nidulans*. Fungal Biology Reviews **23:**20-29.

105. **Roca, G. M., J. Arlt, C. E. Jeffree, and N. D. Read.** 2005. Cell biology of conidial anastomosis tubes in *Neurospora crassa*. Eukaryotic Cell **4:**911-919.

106. **Roca, G. M., N. D. Read, and A. E. Wheals.** 2005. Conidial anastomosis tubes in filamentous fungi. FEMS Microbiological Letters **249:**191-198.

107. **Roca, M. G., H.-C. Kuo, A. Lichius, M. Freitag, and N. D. Read.** 2010. Nuclear dynamics, mitosis and the cytoskeleton during the early stages of colony initiation in *Neurospora crassa*. Eukaryotic Cell.

108. **Rossier, C., A. R. McDonald, and G. Turian.** 1993. Microtubular remnants in macroconidia of *Neurospora crassa* benomyl-induced to multipolar germination. Folia Microbiologica **39:**87-88.

109. **Sagot, I., S. K. Klee, and D. Pellman.** 2002. Yeast formins regulate cell polarity by controlling the assembly of actin cables. Nature Cell Biology **4:**42-50.

110. **Sawin, K. E., and P. T. Tran.** 2006. Cytoplasmic microtubule organization in fission yeast. Yeast **23:**1001-1014.

111. **Schmidt, A., and A. Hall.** 2002. Guanine nucleotide exchange factors for Rho GTPases: turning on the switch. Genes and Development **16:**1587-1609.

112. **Schott, D. H., R. N. Collins, and A. Bretscher.** 2002. Secretory vesicle transport velocity in living cells depends on the myosin-V lever arm length. Journal of Cell Biology **156:**35-39.

113. **Seabra, M. C., and C. Wasmeier.** 2004. Controlling the location and activation of Rab GTPases. Current Opinion in Cell Biology **16:**451-457.

114. **Seiler, S., and M. Plamann.** 2003. The genetic basis of cellular morphogenesis in the filamentous fungus *Neurospora crassa*. Molecular Biology of the Cell **14:**4352-4364.

115. **Serna, L., and D. Stadler.** 1978. Nuclear division cycle in germinating conidia of *Neurospora crassa*. Journal of Bacteriology **136:**341-351.

116. **Shaner, N. C., R. E. Campbell, P. A. Steinbach, B. N. G. Giepmans, A. E. Palmer, and R. Y. Tsien.** 2004. Improved monomeric red, orange and yellow fluorescent proteins derived from *Discosoma* sp. red fluorescent protein. Nature Biotechnology **22:**1567-1572.

117. **Shaner, N. C., M. Z. Lin, M. R. McKeown, P. A. Steinbach, K. L. Hazelwood, M. W. Davidson, and R. Y. Tsien.** 2008. Improving the photostability of bright monomeric orange and red fluorescent proteins. Nature Methods **5:**545-551.

118. **Shortle, D., J. E. Haber, and D. Botstein.** 1982. Lethal disruption of the yeast actin gene by integrative DNA transformation. Science **217:**371-373.

119. **Shortle, D., P. Novick, and D. Botstein.** 1984. Construction and genetic characterization of temperature-sensitive alleles of the yeast actin gene. Proceedings of the National Academy of Sciences **81:**4889-4893.

120. **Steinberg, G.** 2007. Hyphal Growth: a tale of motors, lipids and the Spitzenkörper. Eukaryotic Cell **6:**351-360.

121. **Steinberg, G.** 2007. On the move: endosomes in fungal growth and pathogenicity. Nature Reviews Microbiology **5:**309-316.

122. **Sudbery, P. E.** 2008. Regulation of polarised growth in fungi. Fungal Biology Reviews **22:**44-55.

123. **Suei, S., and A. Garrill.** 2008. An F-actin-depleted zone is present at the hyphal tip of invasive hyphae of *Neurospora crassa*. Protoplasma **232:**165-172.

124. **Szczepanowska, J.** 2009. Involvement of Rac/Cdc42/PAK pathway in cytoskeletal rearrangements. Acta Biochimica Polonica **56:**225-234.

125. **Taheri-Talesh, N., T. Horio, L. Araujo-Bazán, X. Dou, E. A. Espeso, M. A. Penalva, S. A. Osmani, and B. R. Oakley.** 2008. The tip growth apparatus of *Aspergillus nidulans*. Molecular Biology of the Cell **19:**1439-1449.

126. **Takahashi, S., and P. M. Pryciak.** 2007. Identification of novel membrane-binding domains in multiple yeast Cdc42 effectors. Molecular Biology of the Cell **18:**4945-4956.

127. **Takeshita, N., Y. Higashitsuji, S. Konzack, and R. Fischer.** 2008. Apical sterol-rich membranes are essential for localizing cell end markers that determine growth directionality in the filamentous fungus *Aspergillus nidulans*. Molecular Biology of the Cell **19:**339-351.

128. **Tatebe, H., K. Nakano, R. Maximo, and K. Shiozaki.** 2008. Pom1 DYRK regulates localization of the Rga4 GAP to ensure bipolar activation of Cdc42 in fission yeast. Current Biology **18:**322-330.

129. **Tiedje, C., D. G. Holland, U. Just, and T. Hofken.** 2007. Proteins involved in sterol synthesis interact with Ste20 and regulate cell polarity. Journal of Cell Science **120:**3613-3624.

130. **Tognolli, M., A. Utz-Pugin, G. Turian, and C. Rossier.** 1998. Developmental abnormalities in benomyl-resistant strains of *Neurospora crassa*. Mycological Research **102:**869-875.

131. **Torralba, S., and I. B. Heath.** 2001. Cytoskeletal and Ca^{2+} Regulation of Hyphal Tip Growth and Initiation, p. 135-187. *In* G. P. Schatten (ed.), Current Topics in Developmental Biology, vol. 51. Academic Press, San Diego/London.

132. **Trinci, A. P. J.** 1978. The duplication cycle and vegetative development in moulds, p. 132-163. *In* J. E. Smith and D. E. Berry (ed.), The Filamentous Fungi, vol. III. John Wiley, New York.

133. **Trinci, A. P. J.** 1973. Growth of wild-type and spreading colonial mutants of *Neurospora crassa* in batch culture and on agar medium. Archives of Microbiology **91:**113-126.

134. **Upadhyay, S., and B. D. Shaw.** 2008. The role of actin, fimbrin and endocytosis in growth of hyphae in *Aspergillus nidulans*. Molecular Microbiology **68:**690-705.

135. **Vale, R. D.** 2003. The molecular motor toolbox for intracellular transport. Cell **112:**467-480.

136. **Verdín, J., S. Bartnicki-Garcia, and M. Riquelme.** 2009. Functional stratification of the Spitzenkörper of *Neurospora crassa*. Molecular Microbiology **74:**1044-1053.

137. **Vidali, L., C. M. Rounds, P. K. Hepler, and M. Bezanilla.** 2009. Lifeact-mEGFP reveals a dynamic apical F-actin network in tip growing plant cells. PLoS ONE **4:**e5744.

138. **Virag, A., and A. Griffiths.** 2004. A mutation in the *Neurospora crassa* actin gene results in multiple defects in tip growth and branching. Fungal Genetics and Biology **41:**213-225.

139. **Virag, A., and S. D. Harris.** 2006. The Spitzenkörper: a molecular perspective. Mycological Research **110:**4-13.

140. **Virag, A., M. P. Lee, H. Si, and S. D. Harris.** 2007. Regulation of hyphal morphogenesis by *cdc42* and *rac1* homologues in *Aspergillus nidulans*. Molecular Microbiology **66:**1579-1596.

141. **Vogt, N., and S. Seiler.** 2008. The RHO1-specific GTPase-activating protein LRG1 regulates polar tip growth in parallel to Ndr kinase signalling in *Neurospora*. Molecular Biology of the Cell **19:**4554-4569.

142. **Waddle, J. A., T. S. Karpova, R. H. Waterstone, and J. A. Cooper.** 1996. Movement of cortical actin patches in yeast. Journal of Cell Biology **132:**861-870.

143. **Wang, S., T. Watanabe, J. Noritake, M. Fukata, T. Yoshimura, N. Itoh, T. Harada, M. Nakagawa, Y. Matsuura, N. Arimura, and K. Kaibuchi.** 2007. IQGAP3, a novel effector of Rac1 and Cdc42, regulates neurite outgrowth. Journal of Cell Science **120:**567-577.

144. **Washington, R. W., and D. A. Knecht.** 2008. Actin binding domains direct actin-binding proteins to different cytoskeletal locations. BMC Cell Biology **9:**10.

145. **Waters, C. M., and B. L. Bassler.** 2005. Quorum sensing: cell-to-cell communication in bacteria. Annual Review of Cell and Developmental Biology **21:**319-346.

146. **Wedlich-Söldner, R., S. C. Wai, T. Schmidt, and R. Li.** 2004. Robust cell polarity is a dynamic state established by coupling transport and GTPase signaling. Journal of Cell Biology **166:**889-900.

147. **Wendland, J., and P. Philippsen.** 2001. Cell polarity and hyphal morphogenesis are controlled by multiple rho-protein modules in the filamentous ascomycete *Ashbya gossypii*. Genetics **157:**601-610.

148. **Wendland, J., and P. Philippsen.** 2002. An IQGAP-related protein, encoded by *Ag*CYK1, is required for septation in the filamentous fungus *Ashbya gossypii*. Fungal Genetics and Biology **37:**81-88.

149. **Wennerberg, K., K. L. Rossman, and C. J. Der.** 2005. The Ras superfamily at a glance. Journal of Cell Science **118:**843-846.

150. **Wu, C., V. Lytvyn, D. Y. Thomas, and E. Leberer.** 1997. The phosphorylation site for Ste20p-like protein kinases is essential for the function of myosin-I in yeast. Journal of Biological Chemistry **272:**30623-30626.

151. **Wu, J. Q., and T. D. Pollard.** 2005. Counting cytokinesis proteins globally and locally in fission yeast. Science **310:**310-314.

152. **Yang, H.-C., and L. A. Pon.** 2002. Actin cable dynamics in budding yeast. Proceedings of the National Academy of Sciences of the USA **99:**751-756.

153. **Yarm, F., I. Sagot, and D. Pellman.** 2001. The social life of actin and microtubules: interaction versus cooperation. Current Opinion in Microbiology **4:**696-702.

Chapter 5 – Sustaining cell wall integrity during cell fusion

5.1. Abstract

This chapter will introduce mitogen-activated protein (MAP) kinase signalling pathways and review our current understanding of how MAPKs regulate hyphal fusion in *Neurospora crassa*. The specific role of the cell wall integrity (CWI) MAPK pathway network in that process will be highlighted and novel insights about the function of MAK-1, the terminal MAP kinase in that cascade, during CAT homing and fusion pore opening will be presented. Results will be discussed in comparison with related processes during mating cell fusion of the budding yeast *Saccharomyces cerevisiae* and appressorium-mediated host penetration by the rice blast fungus *Magnaporthe oryzae*.

5.2. Introduction

5.2.1. MAPK signal transduction pathways in fungi

Mitogen-activated protein (MAP) kinase pathways regulate a variety of cellular processes. Functionally distinct MAPK modules and their tightly regulated cross-communication with each other as well as up- and downstream pathways are best characterized for the budding yeast *Saccharomyces cerevisiae*. In budding yeast, a total of 16 MAPKs constitute five partially overlapping pathways that are involved in regulating pheromone-induced mating, filamentous growth, cell wall integrity, responses to high osmolarity and ascospore wall assembly [7, 19, 85, 117, 125]. MAPK signalling pathways comprise three basic modules: (1) upstream receptor/sensor components that often reside within the plasma membrane and perceive external stimuli which are then passed onto cytoplasmic signalling molecules, (2) a central MAPK phosphorylation cascade which becomes activated by the upstream input pathway, integrates the signal and phosphorylates downstream effectors, (3) MAPK phosphorylation targets that regulate gene transcription or elicit immediate cellular changes via direct protein-protein interaction. The central MAPK cascade consists of a three-tiered kinase relay which progresses through subsequent phosphorylation steps at highly conserved serine/threonine and tyrosine residues [21], in which an activated MAPK kinase kinase (MAPKKK) activates a MAPK kinase (MAPKK), which in turn activates a terminal MAPK [164]. Negative regulation of MAPK signalling can be achieved either via dephosphorylation of MAPK by serine/threonine, tyrosine, or dual specificity phosphatases [53], or by attenuation of pathway activity by ubiquitin-mediated degradation of pathway components [19]. Upstream events that can lead to activation of the MAPKKK, include ligand binding to cognate G-protein-coupled receptors (GPCRs) [82] or other classes of receptors that stimulate production of activated monomeric G-proteins. MAPK cascade activation is often triggered through Rho GTPase-mediated activation of protein kinase C (PKC) [71, 120], and

can involve lateral stimulation through a Cdc42/p21-activated kinase (PAK) module [83, 84, 121]. These upstream activators are usually associated with the plasma membrane – e.g. linked by membrane-bound small GTPases or lipids – and are usually referred to as MAPKKK kinases (MAPKKKK) [29, 127]. Although the central MAPK cascade appears very simple and might comprise only a small number of components (e.g. only nine MAPKs in *N. crassa*), a selection of MAPKKKKs that feed into them and numerous downstream targets that are acted upon, greatly diversify the signal [81]. The ability of MAPKs to transmit different, even opposing signals in the same cells raises the question as to how specificity of adequate responses is regulated. Several mechanisms that participate in this specificity determination have been proposed, including (1) duration and strength of signal, (2) interaction with various scaffold proteins, (3) subcellular localization, (4) presence of several isoforms, at each tier of the cascade, (5) extensive cross-talk between MAPK cascades and other pathways, and (6) post-translational modifications other than phosphorylation. Examples of each of these mechanisms are discussed in detail elsewhere [81]. A very recent review using the CWI pathway of *S. cerevisiae* as an example, comprehensively discussed how the coordinated effort from multiple pathways around the central MAPK cascade allows the cell to respond to numerous, diverse stress events appropriately [42]. To what extent the principal MAPK pathway architecture known from the yeast models applies to filamentous fungal species, and in particular to the cell fusion process in *N. crassa*, is a primary research focus of this chapter.

5.2.2. MAPK signalling modules regulating cell fusion in *N. crassa*

Three MAPK cascade modules have been identified in *Neurospora crassa* [13, 45], resembling the pheromone response (PR) pathway, the CWI/filamentous growth pathway, and the high osmolarity glycerol (HOG)/stress response pathway

originally described in yeast (see Table 3.2) [19, 85]. Mutations in the genes encoding components of the PR pathway, including the MAPKKK NRC-1, MAPK MAK-2 and the associated transcription factor PP-1, produced some of the first hyphal fusion mutants identified in *N. crassa*. Δ*nrc-1* and Δ*mak-2* strains of *N. crassa*, containing gene deletions of the yeast orthologs Ste11p and Fus3p, respectively, were unable to undergo hyphal fusion in the mature colony or between conidial germlings [114, 135]. Conidia of either mutant did not form CATs or attracted wt CATs, indicating defects in CAT inducer/chemoattractant production and perception. As discussed in detail in previous sections (1.4.3 to 1.4.5), recent findings revealed that MAK-2 has essential functions in the novel "ping-pong mechanism" during CAT homing, and showed that MAK-2 activity is also required at later stages of the fusion process [40, 132] (details in the following section). Recent data confirmed earlier predictions [50, 136], that the deletion strain of the pheromone response pathway MAPKK MEK-2 is also vegetative hyphal fusion (VHF) defective [98]. An analysis of MEK-2 localization and function during germling fusion, however, has so far not been reported. Disruption of the downstream transcription factor Ste12p ortholog, PP-1, in *N. crassa* resulted in a hyphal fusion mutant with a phenotype very similar to Δ*nrc-1, Δmek-2* and Δ*mak-2* strains [94]. Notably, upstream components, including sex pheromones (MFA-1 and CCG-4), pheromone membrane receptors (PRE-1 and PRE-2) and associated heterotrimeric G-protein subunits (GNA-1 to GNA-3, GNB-1 and GNG-1) were found to be dispensable for hyphal fusion as assessed by heterokaryon tests and germling fusion assays [76, 95]. This is in stark contrast to mating cell fusion in *S. cerevisiae*, where endocytosis of the sex pheromone/receptor complex is essential to trigger polarization of the cytoskeleton resulting in mating projection protrusion and chemotropism [153]. Binding of **a** or α-pheromone to the cognate GPCRs Ste3p or Ste2p, respectively, results in the disassociation of a heterotrimeric G-protein (Gα; Gpa1p, Gβ; Ste4p and Gγ; Ste18p), and subsequent interaction between G$\beta\gamma$ and the PAK Ste20p (acting as MAPKKKK) activates the Ste11p/Ste7p/Fus3p MAP kinase cascade [25, 38].

Taken together, these studies suggest that only parts of the PR pathway, including the central MAPK cascade and downstream components, are required for hyphal fusion in *Neurospora*, and that the chemotropic interaction must involve an upstream input pathway distinct from sex pheromone/GPCR signalling. The requirement of the MAK-2 MAP kinase pathway for vegetative hyphal fusion is also conserved in other filamentous ascomycete fungi, such as *A. nidulans* in which a mutant disrupted in the MAPKKK NRC-1 homolog, SteC, failed to form heterokaryons [163].

In contrast to the MAK-2 MAPK pathway, our knowledge about the functions of components of the other two MAPK modules during hyphal fusion in *Neurospora* is much more limited. Thanks to advanced cloning techniques [22] and the increased availability of *N. crassa* gene deletion mutants through the NIH *Neurospora* Genome Project, a more rapid identification and analysis of predicted orthologs to the yeast model has been faciliated, and recent data is starting to fill existing gaps. The second MAP kinase module of *Neurospora* resembles the cell wall integrity/filamentous growth pathway from *S. cerevisiae* which becomes activated under a number of different conditions that stress the structure and function of the cell wall, including hypotonic medium, depolarization of the actin cytoskeleton and pheromone-induced morphogenesis [57, 88]. It is believed that the common element sensed in all of these cases is stretching of the plasma membrane and/or alterations of its connection to the cell wall [19]. Experimental data indicates that cell wall stresses can modulate at least three distinct MAPKKK kinases acting between the GTPase and the MAPK cascade, and suggest that different stresses provide various lateral inputs into this regulatory pathway, rather than just operating in a linear "top-down" manner [57]. Due to its universal importance the CWI pathway can be expected to have a key role during directed tip growth of fusion hyphae and CATs, as well as during tip growth arrest and subsequent fusion pore formation once cell-cell contact has been established. In budding yeast this pathway comprises a MAPKKK (Bck1p), two redundant MAPKKs (Mkk1p/2p) and MAPKs

(Slt2p/Mpk1p). During pheromone-induced morphogenesis, the polarized outgrowth of mating projections involves new cell wall synthesis, which requires activation and localization of the CWI MAP kinase Mpk1p to the shmoo tip [16, 17]. In *N. crassa*, mutations in the *MPK1* ortholog, *mak-1*, and predicted upstream MAP kinase genes, *mek-1* and *mik-1* have been found to result in severe defects during vegetative and sexual development, including short aerial hyphae, mature hyphal lysis, reduced macroconidiogenesis and the absence of protoperithecia [116]. Furthermore, these mutants have recently been reported to result in strains that fail to undergo VHF [98]. This is consistent with results from the mutant screen presented in this study (Table 3.6), but again detailed analysis of the function of these components during the actual fusion process is still missing. In pathogenic filamentous fungi, such as *Magnaporthe oryzae* and *Colletotrichum lagenarium*, mutations in the MAP kinase gene orthologous to *MPK1* affect conidial germination, sporulation, and the ability to form functional appressoria and establish plant infection [78, 165, 166]. Defects in vegetative fusion were not assessed in these mutants.

The third MAP kinase pathway identified and extensively studied in a number of filamentous fungal species [44, 157, 169] is orthologous to the HOG/stress response MAPk pathway from *S. cerevisiae*, comprising the Ssk2p/Pbs2p/Hog1p cascade. Common phenotypic defects in deletion mutants of the central MAPK components include the inability to grow on high-osmolarity medium (e.g. > 3% NaCl or 1 M sorbitol), cell lysis and increased pigmentation of macroconidia, female sterility due to the lack of protoperithecia and increased resistance to phenylpyrrole fungizides, such as fenpliconil [169]. In *N. crassa*, strains containing deletion mutations in the MAPKKK (*os-4*), the MAPKK *(os-5*) or the MAPK (*os-2*) genes show all the above mentioned typical defects of *os* mutants, and also have recently been reported to be hyphal fusion defective [98]. The latter finding is not supported by data from this study (Table 3.6) and thus requires further detailed analysis.

Therefore, ongoing work characterizes involvement of HOG MAPK cascade components during cell fusion in *N. crassa* in greater detail.

It can be concluded that considerable overlap between MAPK signalling pathways in yeast and *Neurospora* exists, especially in respect to the core MAPK phosphorylation cascades. The integration with up- and downstream pathways appears to be slightly different, and species- as well as process-specific. The most recent data furthermore indicates that especially during vegetative cell fusion the short-term regulation of MAPK activity is rather accomplished by localized accumulation and protein-protein interaction at the cell cortex rather than by transcriptional regulation or phosphorylation [40, 132]. A phenomenon that very recently has also been found to regulate activity of the pathogenicity-related MAPK Chk1 in the corn leaf pathogen *Cochliobolus heterostrophus* [87]. Chk1 was required for appressorium formation and its function manifested by its local accumulation rather than through significant changes in phosphorylation or increase in total protein quantity. In summary, two of the three MAPK pathways in filamentous fungi, namely orthologs of the PR and CWI cascades, do have crucial roles during hyphal fusion, whereas the participation of the HOG pathway is not yet fully resolved.

5.2.3. What can studies on yeast mating tell us about MAPK-mediated self-signalling during cell fusion in filamentous fungi?

Budding yeast mating is the most studied and best understood MAPK signal transduction pathway in eukaryotes. The overwhelming complexity of the MAPK pathway network in *S. cerevisiae* has recently been reviewed in great detail [19, 42]. Pheromone-induced yeast mating triggers morphogenetic events leading to non-self-fusion between cells of opposite mating type. During this process, pheromone binding to cognate GPCRs leads to phosphorylation of Fus3p MAP kinase (ortholog

of MAK-2 in *N. crassa*) [18, 35, 127]. Phosphorylated Fus3p arrests cells in G1 phase, promotes actin nucleation and polymerization leading to polarized outgrowth of mating projections, and also induces expression of mating-related proteins that are involved in the formation of mating projections and cell-cell fusion. Once mating projections from two cells of opposite mating type made contact, their cell walls become attached via GPI-anchored agglutinin proteins. Build up of new cell wall material around the contact site stabilizes attachment and prevents leakage during subsequent fusion steps. Cell wall remodelling and local degradation of their intervening cell walls forms a pore that allows the merging of plasma membranes. This indicates that in spite of their different physiological roles, molecular mechanisms underlying mating cell fusion in yeast and CAT-mediated cell fusion in *Neurospora* are highly conserved (Fig. 5.1). However, the unknown upstream signal transduction components involved in *Neurospora* self-signalling seem to be significantly different from those in budding yeast, as to date all evidence indicates that pheromone GPCR signalling is not involved (see below).

Somewhat analogous to the oscillatory recruitment of MAK-2 (section 1.4.4) during CAT fusion [40], its yeast ortholog Fus3p exhibits 'oscillatory' phosphorylation, and thus activation, during mating [63]. Active Fus3p also preferentially localizes to mating projection tips [97, 143] but oscillatory recruitment of Fus3p to these tips has not been reported. In *Neurospora*, increased phosphorylation of MAK-2 was associated with conidial germination and cell fusion [114], but whether the phosphorylation status of MAK-2 coincides with its pulsatile recruitment has not yet been determined. However, a key difference in the oscillatory MAP kinase behaviour of yeast compared with that in *Neurospora* is the period of MAP kinase oscillation/activity. Whereas the pulsatile recruitment of MAK-2 in *Neurospora* has a period of 6-12 min [40], the oscillatory phosphorylation of Fus3p in yeast has a period of ~ 150 min. This much longer period of oscillation in yeast is achieved by transcriptional negative feedback of Fus3p mediated by the RGS protein Sst2p and the Fus3p phosphatase Msg5p whose expression is

upregulated by a positive feedback loop involving active Fus3p [63, 131]. In addition, non-transcriptional negative feedback regulates the active Fus3p level to fine-tune pheromone signalling during yeast mating. This feedback regulation is mediated through the inhibition of MAP kinase scaffold recruitment by active Fus3p, and achieves an initial increase and a subsequent decrease to a plateau in the active Fus3p level within 5-7 min [167], a timescale similar to that of the MAK-2 oscillation period (Fig. 5.1).

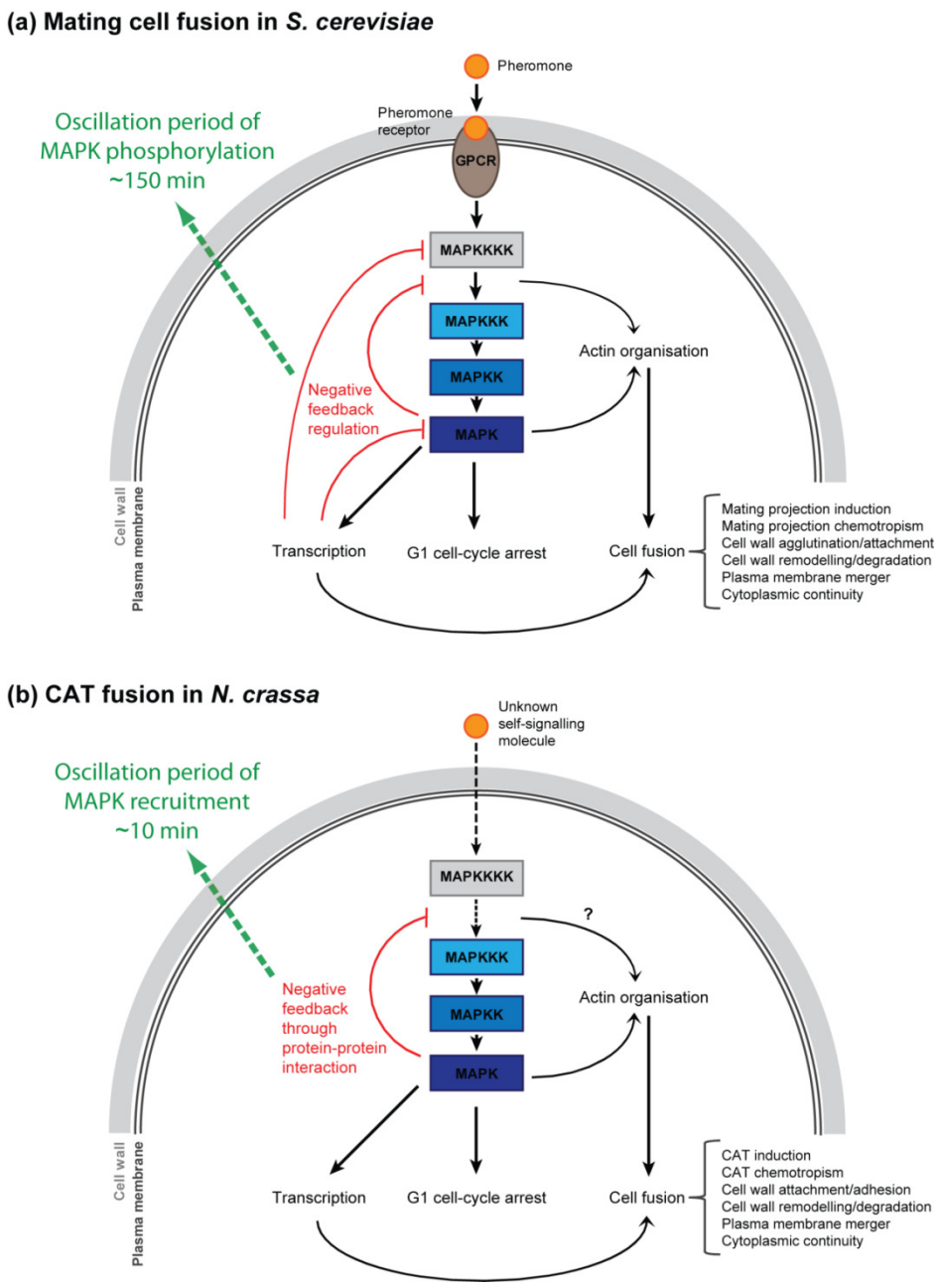

Figure 5.1 MAPK signal transduction pathway. Comparison of non-self signalling during mating in *Saccharomyces cerevisiae* and self-signalling during CAT fusion in *Neurospora crassa*. **(a)** Pheromone signalling in budding yeast. Pheromone binding to cognate G protein-coupled receptors (GPCRs; Ste2p and Ste3p) leads to activation of a MAPKKKK (Ste20p), which in turn activates the MAP kinase cascade (MAPKKK; Ste11p, MAPKK; Ste7p, MAPK; Fus3p). Activated Fus3p causes G1 cell-cycle arrest, and promotes actin nucleation and polymerization to form mating projections. Fus3p also induces expression of mating-related proteins which are required for mating projection formation, attachment between two cells of opposite mating type, and cell-cell fusion, through activation of the Ste12p transcription factor. The signalling pathway also involves negative feedback loops (red lines) consisting of transcriptional and non-transcriptional feedback regulation, which are crucial for cells to

optimally respond to the pheromone stimulus. **(b)** Signalling during CAT-mediated cell fusion in *Neurospora*. An unidentified chemoattractant is recognized by an unknown receptor, and believed to activate a MAPKKKK, which then activates the MAP kinase cascade (MAPKKK; NRC-1, MAPKK; MEK-2, MAPK; MAK-2). Downstream events in CAT fusion, which are probably regulated by MAK-2, seem to be similar to those of yeast mating, and involve G1 cell-cycle arrest, actin organization, cell wall attachment and cell fusion. A key difference to signalling during yeast mating is that CAT chemoattraction does not seem to involve transcriptional negative feedback regulation of the MAP kinase signalling cascade, but instead occurs by direct protein-protein interaction (see text for details). Figure modified from [132].

Other examples of biochemical oscillations mediated by transcriptional negative feedback have been reported to have periods greater than 90 min [64, 86], whereas oscillations involving non-transcriptional negative feedback tend to have much shorter periods of ~10 min [67, 167]. Thus, the pulsatile recruitment of MAK-2 is most likely achieved by negative feedback regulation that involves protein-protein interaction but not transcription. During yeast mating, negative feedback regulation of the Fus3p MAP kinase pathway is essential for the formation of multiple mating projections if the first projection fails to fuse with a mating projection from another cell [63, 105]. This suggests that downregulation of Fus3p activity is crucial for cells to respond to new pheromone stimulation. In a similar manner, downregulation of the signalling cascade involved in CAT chemoattraction may be important for MAK-2 to be dispersed from CAT tips allowing CATs to respond to the chemoattractant secreted by the opposing cell again, and thus undergo repeated ping-pong self-signalling and tip re-orientation (Fig. 1.5).

5.2.4. Cell wall maintenance in fungi

In all fungi, the need for a sturdy cell wall which resists environmental stresses and maintains cell shape during unfavourable conditions has to be balanced against the needs of growth, branching, cell fusion and other morphogenetic events, which all require drastic remodelling of its plastic and rigid structure, and therefore temporarily increase the risk of cell lysis [33]. The CWI pathway provides a means to monitor the structural integrity of the cell wall and repair damage caused by diverse stress conditions, including osmotic changes, pH stress, heat shock, nutrient limitation, oxidative stress, and responses to antifungal agents and chemical compounds [42].

In most cases stress conditions stimulate the CWI pathway through sensors located in the plasma membrane, but in some instances, such as oxidative challenge through hydrogen peroxide, activation is elicited by intracellular receptors [156]. Upon stimulation, the CWI pathway utilizes guanine nucleotide exchange factors (GEFs) and GTPase activating proteins (GAPs) to control the activity of Rho1 GTPase which exerts two main functions: (1) it serves as an integral regulatory subunit of the 1,3-β-glucan synthase complex (including the 1,3-β-D-glucan synthase components Fks1/2p) which stimulates cell wall biosynthesis in a GTP-dependent manner [36, 126], and (2) Rho1p also binds and activates PKC [71, 110], which then activates the CWI MAPK cascade leading to transcriptional regulation of cell wall integrity genes and rearrangement of the cytoskeleton [60, 74].

Interestingly, although cell wall stress-induced hyperactivation of Rho1p triggers actin depolarization and depends on PKC, it does not seem to require the complete downstream MAPK cascade [34]. Actin repolarization, however, depends on the complete PKC-MAPK cascade. Thus, activated Rho1p can mediate both polarized and depolarized cell growth via the same effector, PKC, suggesting that Rho1p may function as a signal modulator rather than being a simple on-off switch [34]. Loss of PKC function, or of any of the MAP kinase cascade components under

its control [88, 91], as well as defects in the biosynthesis of particular cell wall components (e.g. 1,3-β-glucans, 1,6-β-glucans and chitin) results in a cell lysis defect that is attributable to a deficiency in cell wall construction [89, 90, 115] and can generally be rescued by osmotic stabilization [52, 104]. Furthermore, strains defective in any of the above components show characteristic alterations in the biochemical composition and architecture of their walls that seem to compensate for the loss in strength caused by the mutations [33]. Activation of this salvage mechanism [99, 144] involves the cell wall stress sensor Mid2p [32, 75] and leads to increased deposition of chitin [124], upregulation of the expression of several cell wall proteins [72], and activation of alternative glucan synthase subunits [101, 129].

In budding yeast 25 genes encoding known or suspected cell wall proteins and enzymes involved in cell wall biogenesis, whose regulation is altered by activity of the terminal CWI MAPK Mpk1p, have been identified [69]. At least 18 were upregulated involving the transcription factor Rlm1p, which is a direct phosphorylation target of Mpk1p [162]. Besides these relatively slow responses - transcriptional upregulation and supply of new cell-wall-maintenance proteins through the secretory pathway - it has been previously suggested that the CWI pathway also must include a set of rapid responses, such as localized activation of cell wall synthases [33]. The final stages of hyphal fusion in *N. crassa* require rapid morphogenetic transitions from polarized tip growth (required to establish contact) to tip growth arrest and tight cell-cell attachment (in order to prevent leakage) over to localized degradation of intervening cell walls during fusion pore formation. The post-contact steps of the fusion event usually occur within less than 5 min (see Fig. 5.11) indicating that activities of the CWI pathway induce very quick molecular processes which occur most likely independently of transcriptional regulation. Cell wall remodelling is furthermore closely associated to dynamic rearrangement of the actin cytoskeleton. On the one hand F-actin cables provide tracks for targeted secretion during polarized tip extension, but also become remodelled in a PKC-MAPK dependent manner in response to a variety of environmental stresses [34].

Most interestingly, *slt2* and *bck1* mutants of yeast have been reported to display a depolarized actin cytoskeleton, with delocalization of actin cortical spots, abnormal accumulation of secretory vesicles, and defects in polarized cell growth [23, 102].

Taken together, these studies demonstrate that the PKC-MAPK pathway is required for cell polarity and maintenance of cell wall integrity during phases of rapid polarized growth, such as bud formation and mating projection formation, but also in response to transient actin perturbation during morphogenetic transitions, and to restore growth once cells adapted to environmental stresses. Experimental pertubation of the actin cytoskeleton by the addition of latrunculins induces an Slt2p/Mpk1p-mediated G2 cell cycle arrest which appears to be differently regulated than those mediated by the other two MAPK pathways [56]. It is a fascinating question what set of input signals triggers these quick morphogenetic transitions required for CAT-mediated cell fusion between *N. crassa* germlings, and how these signals are processed through the CWI MAPK cascade onto the actin cytoskeleton and the cell wall.

5.2.5. The CWI pathway network

The high level of regulation required to elicit appropriate morphogenetic changes under various conditions is achieved by cross-talk between the CWI MAPK pathway with other signalling pathways as part of a sequential or composite signal response. Essential lateral influences that enhance and modulate the signalling capabilities of the CWI pathway include components of the PR and HOG MAPK pathways, cAMP-dependent PKA signalling, target of rapamycin (TOR) signalling, Ca^{2+}/calcineurin signalling, and other Rho-type GTPase family members, such as Cdc42p, Rho3p and Rho4p and their regulators [42, 57]. The best studied example within this signalling network is the CWI MAPK Slt2/Mpk1 from budding yeast which can be activated by Hog1p MAPK upon hyperosomotic shock, as well as by

Fus3p MAPK upon pheromone stimulation [16, 53]. This secondary enlistment of the Slt2/Mpk1 pathway is thought to facilitate cell wall remodelling processes that must occur during the mating process, but also to cope with any damage incurred during the loss in turgor pressure under hyperosmotic conditions [19]. It has very recently been shown that the filamentous growth pathway in budding yeast, comprising the Rho GTPase Cdc42p, the PAK Ste20p, and components of the PR MAPK cascade (Ste11p/Ste7p/Kss1p), contributes to cell wall integrity in parallel with the CWI MAPK pathway [9]. Interestingly, this occurred in opposition to the HOG MAPK pathway and provided new insights into the combinatorial effects of signalling networks. In *N. crassa*, combinatorial effects of orthologs of the PR pathway MAP kinase MAK-2 and CWI pathway MAP kinase MAK-1 have also been recently described to interactively oppose the HOG pathway MAP kinase OS-2 [98]. In some situations however, e.g. during the formation of sexual fruitbodies and hyphal fusion, concerted activity of all three MAPK cascades has been suggested, too [98]. These studies again highlight the fact that MAPK pathways usually act in a coordinated manner, but that the type of coordination between individual components is process specific. Our understanding of how pathway-specific identity is maintained when certain components are shared is very limited in *N. crassa*. Figures 5.2 to 5.6 summarize core signalling molecules within the fungal CWI pathway network and, based on genomic comparisons with other fungi, attempt to sketch particular signal transduction pathways (highlighted in red in all figures) that are likely to lead to the activation of the MAP kinase MAK-1 of *N. crassa* under various stress conditions which impact cell wall integrity and require morphogenetic adaptation.

Osmotic changes. In accordance with the yeast model, phosphorylation of MAK-1 is expected to occur without specificity towards osmotic solutes, which can include molecules such as sorbitol, NaCl or glucose [42]. Variable solute concentrations however should trigger different signals to elicit adequate changes in cell wall architecture. Using separate branches of the pathway network facilitates

specific responses to opposing osmotic conditions (Figs. 5.2A and 5.2B). Hypoosmotic changes are perceived and processed in a PKC dependent manner, whereas hyperosmotic changes are likely to be signalled in a PKC independent but OS-2 dependent way, involving cross-talk between the CWI and the HOG pathway. Transmembrane osmosensors that respond to hypotonic conditions and transduce signals via RHO-1 GTPase onto the CWI MAPK cascade of *N. crassa* are likely to be WSC-2 or WSC-3, orthologs of the wall integrity and stress-response component (WSC) protein family from *S. cerevisiae* [134] (Fig. 5.2A). Additional lateral input into the MAPK cascade downstream of PKC is very likely; putative signalling components however have not yet been identified in *N. crassa*.

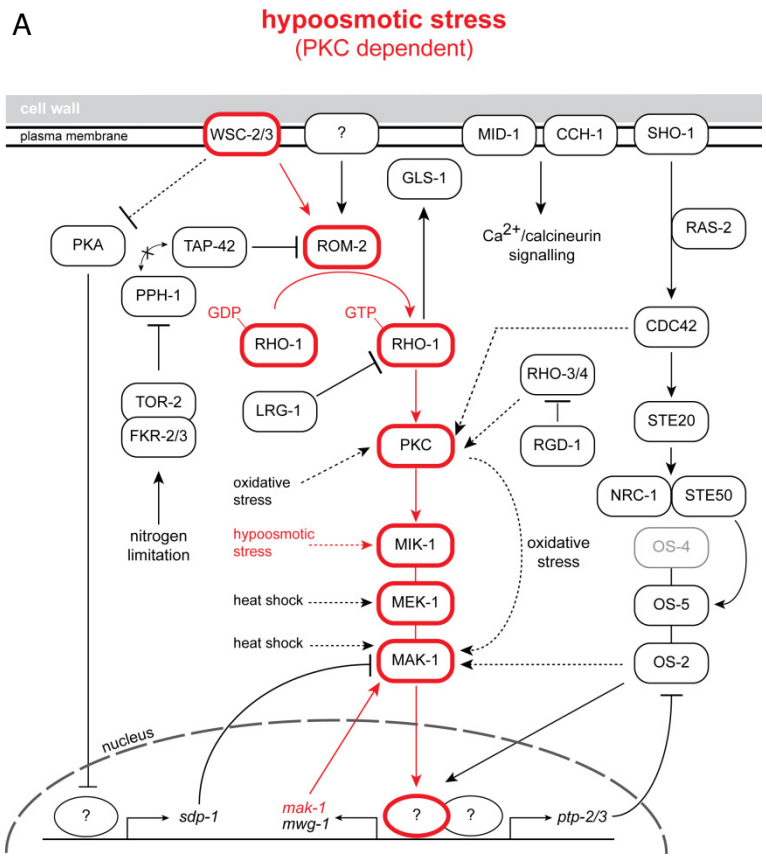

Figure 5.2A Activation of MAK-1 through the CWI pathway network under hypoosmotic stress conditions. Sensors of the WSC protein family are likely to activate RHO-1 GTPase and its effector PKC. PKC acts as MAPKKKK and triggers the CWI MAPK cascade, ultimately leading to MAK-1 activation. Additional lateral input directly into the

MAPK cascade might specify the response, but have not yet been identified in *N. crassa*. See text for details.

Mild osmostress leading to the activation of osmoregulatory genes (as opposed to cell wall genes) in *N. crassa* is sensed by a phosphorelay system including the histidine kinase OS-1 (not shown in diagram) and transduced through the OS-4/OS-5/OS-2 MAPK cascade [109]. The complete HOG MAPK cascade (i.e. excluding the MAPKK OS-4), however, does not seem to be required to elicit cell wall changes under osmotic stress in ascomycetes [8, 46].

Higher osmotic stress is likely to be perceived in an OS-1 independent manner and might rather happen through the second osmosensing branch, which in yeast involves the plasma membrane sensor kinase Sho1p, which recruits downstream signalling components to the cell surface and leads to the activation of Hog1p [8, 128]. In this case, Cdc42p, Ste50p, and Sho1p act as adaptor proteins that control the flow of the osmostress signal from Ste20p/Cla4p to Ste11p, and onto Pbs2p, the OS-5 ortholog [148]. An alternative membrane sensor in this context (not shown in diagram) could be the *N. crassa* mucin (encoded by locus NCU04373.3), orthologous to Msb2p and Hkr1p, which very recently have been shown to differentially regulate the filamentation and osmosensing pathways in yeast [123]. In any case, activation of MAK-1 would occur through a 'mixed' pathway comprising the Rho GTPase CDC42 (activated with the help of the small GTP-binding protein RAS-2) which activates the PAK STE20 (acting as MAPKKK), the pheromone response pathway MAPKKK NRC-1 which interacts with MAPKK OS-5 via the MAPK scaffolding protein STE50, and the final phosphorylation target OS-2 (Fig. 5.2B). MAPK OS-2 either directly activates the transcription factor RLM-1 to induce *mak-1* expression, or modulates MAK-1 activity via protein-protein interaction, most likely in complex with the HSP90 co-chaperone CDC37 [58] (not shown in diagram).

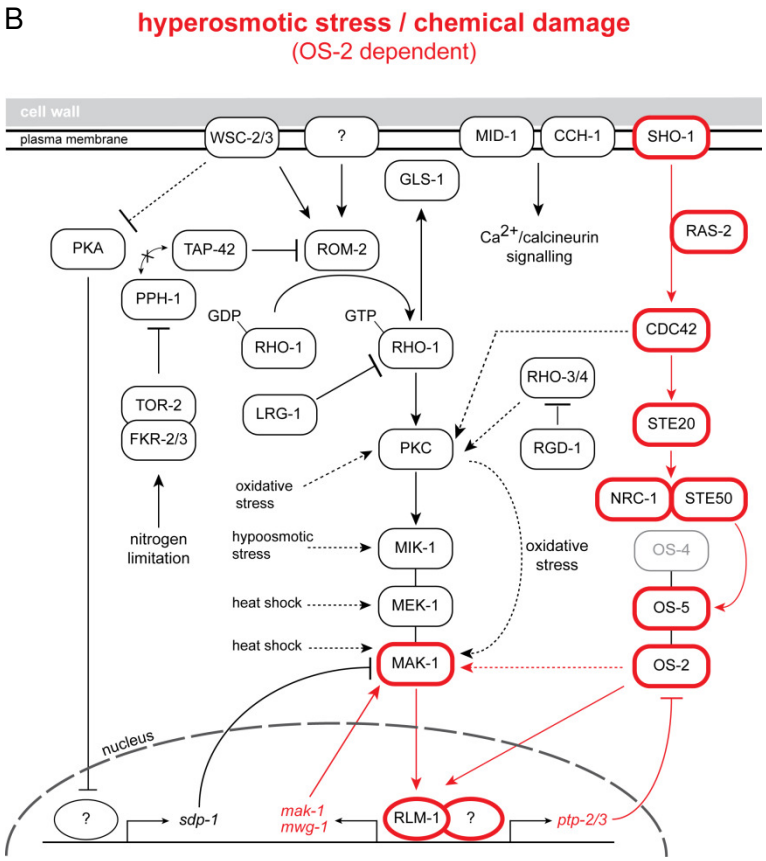

Figure 5.2B Activation of MAK-1 through the CWI pathway network under hyperosmotic stress conditions. In this model, MAK-1 activation does not occur through the 'classical' CWI pathway, but by interaction with components from the two other MAPK pathways. Membrane sensors activate CDC42 GTPase and thus its effector PAK STE20. STE20 acts as MAPKKKK for NRC-1 which interacts with OS-5 via the MAPK scaffolding protein STE50. The phosphorylation signal is passed onto OS-2 which either activates MAK-1 by direct protein-protein interaction or induces RLM-1 dependent expression of *mak-1*. See text for details.

Expression of cell wall genes from the glycosyl hydrolase family, such as *mwg-1*, are one likely outcome of this activity. Negative feedback regulation of OS-2 can occur through RLM-1-mediated expression of the putative tyrosine phosphatase PTP-2, or, involving a yet unidentified transcription factor, expression of phosphatase PTP-3 [53, 100]. Data from *A. nidulans* contradicts this pathway model for filamentous fungi by indicating that OS-2 activation solely depends on two-component histidine kinase and MAPK signalling and thus would not involve the

non-histidine kinase SHO-1 as potential sensor [44]. These findings, however, do not necessarily exclude that this (or a similar) pathway is used to activate MAK-1 in order to promote cell wall remodelling under non-osmotic stress conditions. In *S. cerevisiae*, this cross-talking pathway network is indeed used in response to chemical damage to the cell wall, for example by the 1,3-β-glucan hydrolyzing enzyme zymolyase [46]. The OS-4 homologs Ssk2p/Ssk22p are not required in that response [8, 46], and so far there are no reports that OS-4 in filamentous fungi is involved.

Changes in pH. In *S. cerevisiae*, changes in external pH are sensed by two dedicated plasma membrane sensors, Wsc1p and Mid2p [141]. Wsc1p exclusively senses alkaline stress, whilst Mid2p primarily responds to acidic stress, but might also have a minor role under high pH conditions (potential participation of the second sensor under alkaline stress is indicated as dashed box in Fig. 5.3A) [20, 141]. The *N. crassa* genome contains no ortholog of Mid2p or Wsc1p, but orthologs of the related Wsc2/3p. Whether WSC-2 and WSC-3 are redundant or facilitate different responses in *N. crassa* (similar to Wsc1p and Mid2p) has not yet been determined. Nevertheless, transmission of signals related to changes in external pH are likely to occur via the 'classical' CWI pathway, including activation of the small GTPase RHO-1 by its GEF ROM-2 and downstream transduction through the PKC-MAPK cascade onto MAK-1 [122]. Direct effects of RHO-1 activity include activation of 1,3-β-D-glucan synthase component GLS-1 (ortholog of the yeast Fks1p), which participates in cell wall biogenesis. Negative regulation of Rho1p occurs through activation of the Rho GAP Lrg1p [161]. Most interestingly, Lrg1p has been suggested to locally inhibit cell wall synthesis and to aid in the close apposition of the plasma membranes during mating cell fusion [39], making it an interesting candidate during vegetative cell fusion in *N. crassa*. Deletion of the PKC-encoding gene *pkcA* led to an altered cell wall structure and defects in polarized growth in *A. nidulans* [138]. Recent work has identified LRG-1 as a RHO-1-specific GAP that regulates PKC/MAK-1 pathway activities during polar tip growth in *Neurospora*

[160], strongly supporting this pathway model for filamentous fungi. A recent overview about the pH sensing and response mechanism in *A. nidulans* has been provided by Peñalva *et al.*, 2008 [118]. The transcription factor PacC/RIM101 takes a central role in pH adaptation, as it acts as an activator for genes expressed in alkaline conditions and a repressor of those expressed in acidic conditions. This is accomplished by two processing proteolyses of the protein, the first being pH signal dependent and the second proteasomal [119]. A PacC/RIM101 ortholog is encoded by the *N. crassa* locus NCU00090, but whether this transcription factor has any role in the regulation of cell wall genes has so far not been investigated. As the yeast Hog1p MAPK is not phosphorylated under alkaline conditions [141], cellular responses to high pH conditions, however, are likely to be independent of its ortholog OS-2 in *N. crassa*.

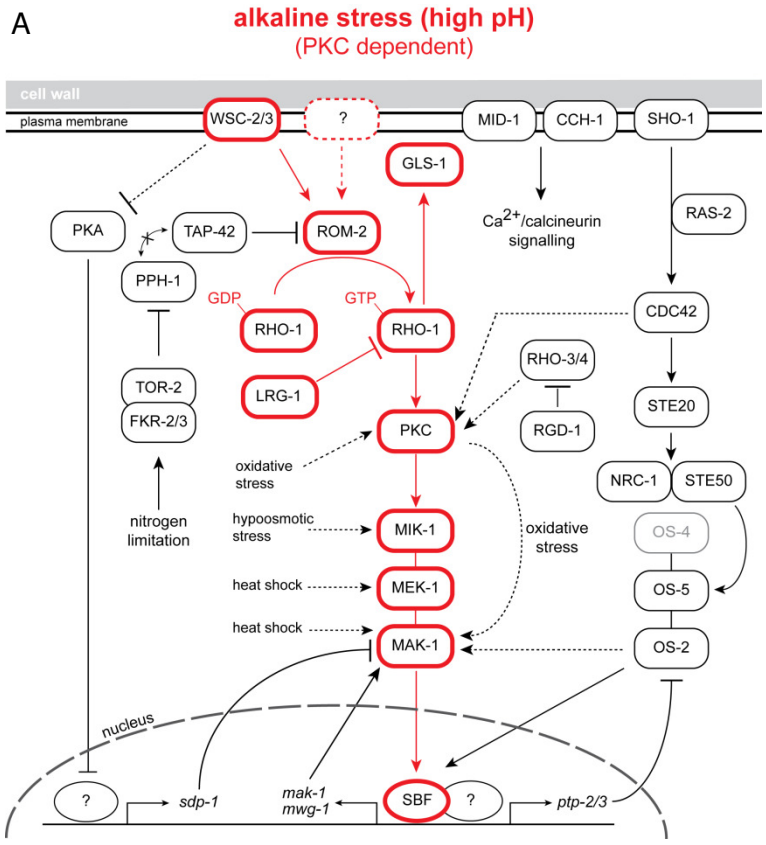

Figure 5.3A Activation of MAK-1 through the CWI pathway network under alkaline stress conditions. Differential cellular responses to opposing pH conditions are likely to be generated through receptor specificity and activation of different transcription factors. In

addition to osmotic changes, WSC-type membrane receptors also sense high pH conditions. Parallel activation of additional receptors (dashed box) is possible, but candidates have not been identified in *N. crassa*. Activation of MAK-1 occurs through the 'classical' CWI cascade and leads to the activation of SBF (Swi4p/Swi6p/Mbp1p) transcription factor complex-dependent genes. See text for details.

Signals elicited from yet unknown membrane receptors under low pH conditions are likely to be transduced along the same pathway, but modification of the signal through lateral input might occur in an OS-2 dependent manner, thus involving cross-talk between the CWI and HOG pathway (Fig. 5.3B). OS-2 can influence the expression of RGD-1 [48], a GAP for RHO-3 and RHO-4 GTPases, which both are suggested to modulate PKC activity thereby ultimately influencing MAK-1 [31]. In this context, Slt2p/Mpk1p in yeast has the capacity to activate two different transcription factors. Alkaline-induced Wsc1p-mediated signalling leads to activation of SBF (Swi4p/Swi6p/Mbp1p) complex-dependent genes (Fig. 5.3A), whereas acidic-induced Mid2p-mediated signalling leads to Rlm1p-dependent gene expression [141] (Fig. 5.3B). *N. crassa* possesses orthologs for all four transcription factors (SBF complex and RLM-1) making it feasible that a similar level of regulation exists in filamentous fungi. Notably, another pH-dependent transcription factor of *Neurospora* is PacC, whose activity also might result in expression of two heat shock genes, *hsp70-1* and *hsp70-2*, preferentially in an acidic milieu [145] (not shown in diagram).

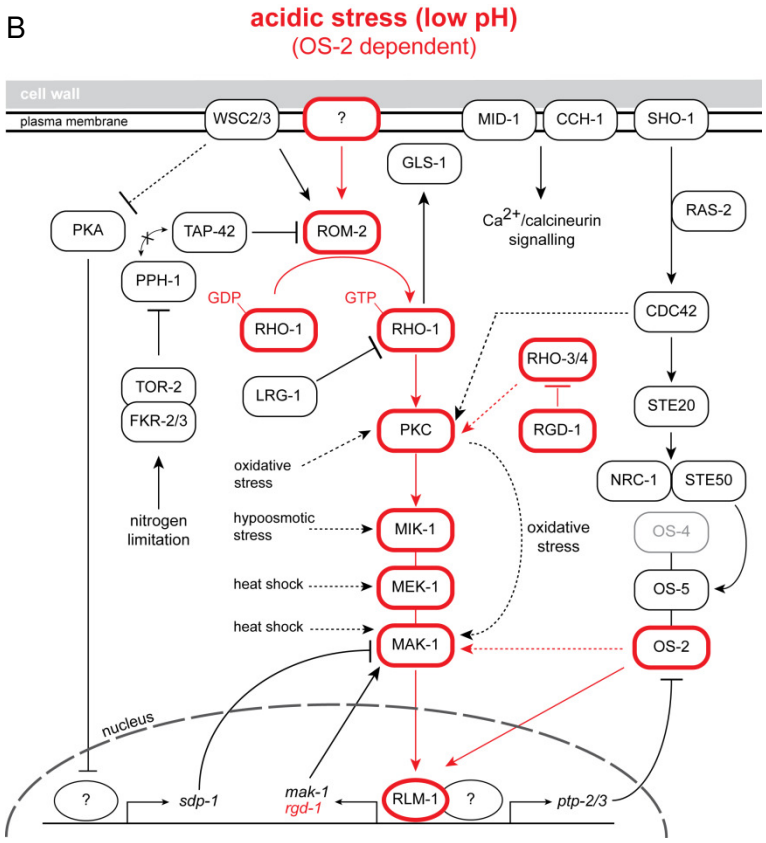

Figure 5.3B Activation of MAK-1 through the CWI pathway network under acidic stress conditions. Differential cellular responses to opposing pH conditions are likely to be generated through receptor specificity and activation of different transcription factors. Signal transduction under low pH conditions uses the same pathway components than under high pH conditions, but lateral input signals from RHO-3/4 proteins and OS-2 MAPK specify the response. Furthermore, MAK-1 activation under these conditions is likely to lead to activation of RLM-1 instead of SBF transcription factors and thus other genes will be transcriptionally regulated compared to high pH conditions. See text for details.

Heat shock. In budding yeast, heat shock, i.e. the rapid elevation of culture temperature by 7-23°C dependent on pre-culture condition and strain used, causes phosphorylation of Slt2p/Mpk1p in a Wsc1p-dependent manner [155] and, due to its general importance in stress responses, is suggested to require signal transduction through the entire PKC-MAPK cascade [42]. Interestingly, activation of Slt2p/Mpk1p by heat shock can also occur independently of Pkc1p and Bck1p [57], suggesting stress-specific lateral activation of the MAPK cascade. Slt2p/Mpk1p is

negatively regulated through direct dephosphorylation by the dual-specificity MAPK phosphatase Sdp1p. Sdp1p expression is regulated by the zinc-finger transcription factors Msn2p/4p which become activated under heat shock upon release of cAMP-PKA-mediated inhibition [53]. Negative feedback regulation of Slt2p also occurs through Rlm1p dependent expression of the tyrosine phosphatase Ptp2p [53]. Projected onto *N. crassa*, responses to heat shock could occur via the 'classical' CWI pathway, involving WSC-2 or WSC-3 as heat sensors in the plasma membrane, or, in case PKC and MIK-1 are not required (dashed boxes in Fig. 5.4), by lateral signal input onto the MAPKK MEK-1 or directly onto MAK-1. Negative regulation of MAK-1 activity could be accomplished by cAMP-PKA-mediated expression of the dual-specificity phosphatase Sdp1p homolog or induced expression of tyrosine phosphatase Ptp2/3p homologs by yet unknown transcription factors. The first two, recently identified genes expressed upon heat shock in *N. crassa* are *heat shock factor 1* and *2* (*hsf-1/2*) [149] (not shown in diagram). *Hsf-1* proved to be an essential gene, whereas Δ*hsf-2* gene deletion mutants were viable but virtually aconidiate due to severe defects in cell wall constriction during macroconidiogenesis.

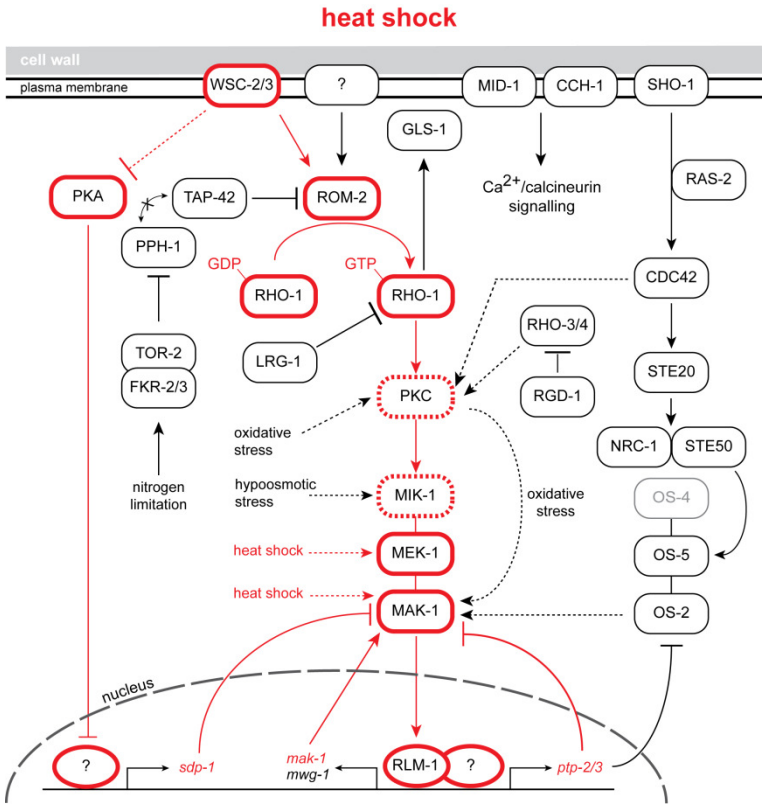

Figure 5.4 Activation of MAK-1 during heat shock. Phosphorylation of MAK-1 can occur via the CWI pathway, potentially modified through the substitution of PKC and MIK-1 (dashed boxes) either by yet unidentified components, or by providing direct lateral signal input into the MAPK cascade [57]. Suppression of MAK-1 activity can be accomplished either by RLM-1-mediated expression of tyrosine phosphatases (PTP-2/3) or via cross-talk between the cAMP-PKA and the CWI pathway which releases inhibition of the dual-specificity phosphatase Sdp1p ortholog [53]. See text for details.

Furthermore, mutants took longer to recover from heat stress compared to wt and showed an altered expression profile of *heat shock protein 90* (*hsp90*). Hsp90p in yeast facilitates activation of Slt2p/Mpk1p required for cell wall integrity [151] and is involved in the regulation of Ca^{2+}-calcineurin responses [146], demonstrating that heat shock factors are important for the regulation of expression and activity of several non-heat shock proteins in higher organisms. Based on these findings it is possible that components of the heat shock response pathway are used to facilitate cell wall remodelling under non-stress conditions in *N. crassa*. Dispensability of certain components of the 'classical' PKC-MAPK cascade (PKC and MIK-1) would

provide the opportunity to allow regulation by lateral input pathways in order to generate a specific response which is different from those required under changing pH conditions, which otherwise uses the same pathway components (Fig. 5.3A and B).

Nutrient deprivation. The availability of nutrients dictates basic cellular functions and determines whether or not cells can grow and develop. The target of rapamycin (TOR) signalling pathway balances protein synthesis and protein degradation in response to nutrient quality and quantity [130]. TOR signalling is active in the presence of sufficient nutrients thereby promoting translation, ribosome biosynthesis, and cell cycle progression. At the same time it inhibits starvation-induced gene transcription and prevents autophagy. TOR proteins are conserved amongst eukaryotes and the best studied fungal examples are Tor1p and Tor2p from *S. cerevisiae* and *S. pombe*, respectively [24, 112]. *TOR1* and *TOR2* encode serine/threonine kinases with overlapping function [59]. Both mediate protein synthesis and cell cycle progression, whereas Tor2p in addition and exclusively regulates cell cycle-dependent organization of the actin cytoskeleton [60, 140]. This function is shared with the CWI pathway and is most likely regulated by cross-talk between both pathways (Fig. 5.5). Similar to *C. albicans* [26], *N. crassa* possesses only a single copy of TOR, with higher homology to Tor2p (45% aa sequence homology) than to Tor1p (19% aa sequence homology). All other components of the basic TOR cascade, including FK506-binding proteins (FKBPs)(FKR-2 to FKR-5), as well as orthologs of the Sit4p serine/threonine-protein phosphatase (PPH-1) and the Tap42-protein catalytic subunit (TAP42) are present in *N. crassa.* Under 'natural' conditions, nitrogen limitation inhibits TOR signalling resulting in the release of ROM-2 inhibition, which then activates MAK-1 through the 'classical' CWI pathway, inducing adaptive cell wall changes.

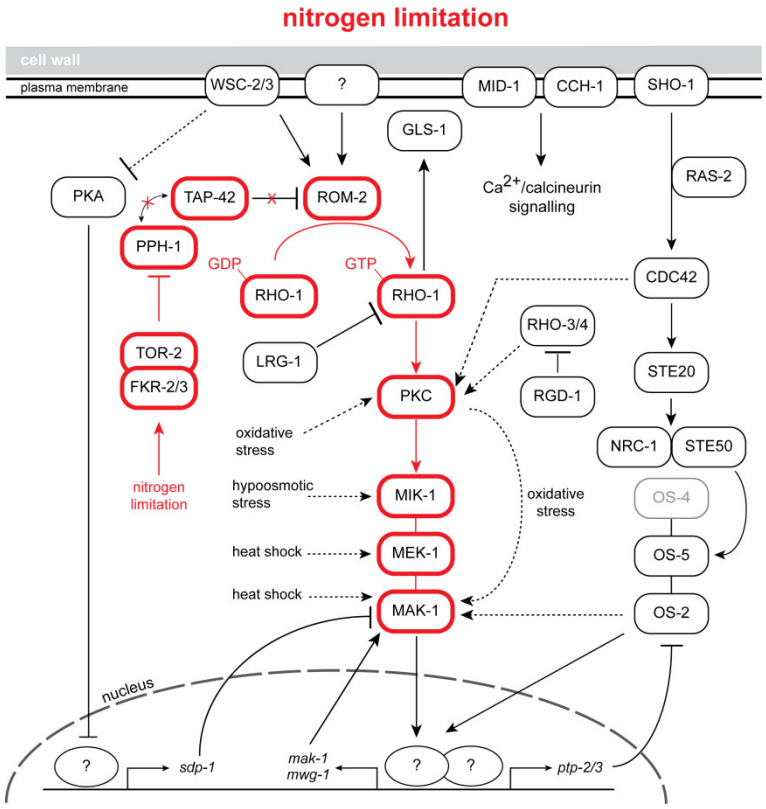

Figure 5.5 Activation of MAK-1 under nitrogen limiting conditions. Cross-talk between TOR and CWI pathway signalling leads to MAK-1 activation and is likely to have a primary role in actin cytoskeleton rearrangements and cell wall remodelling under nitrogen limiting conditions. See text for details.

The agent rapamycin synthetically inhibits TOR signalling by forming a complex with the FKBP ortholog FKR-2/3, which then binds to TOR-2 kinase and prevents association between PPH-1 and TAP42 resulting in ROM-2 activation. In budding yeast, rapamycin-dependent activation of Slt2p/Mpk1p depends on Rom2p, Pkc1p and Bck1p [150], supporting this pathway model for *N. crassa*.

Connection between Ca^{2+}/calcineurin signalling and the CWI pathway. A number of studies in yeast and yeast-like fungi support an interplay between Ca^{2+}/calcineurin signalling and the CWI pathway. Signalling through the calcium-calcineurin pathway is required for a multitude of cellular processes involving cell wall rearrangements, and include survival under stress conditions, such as high

cations and antifungal treatment [12, 27], as well as during morphogenetic processes, such as budding, mating and cytoskeletal reorganization [6, 139] (recently reviewed in [146]). Calcium has been found to induce phosphorylation of the MAK-1 ortholog MKC-1 in *C. albicans* in a Hog1p (OS-2 ortholog) dependent manner [107, 108]. A similar effect has been reported upon inhibition of calcineurin function in *C. neoformans* [80], suggesting that calcineurin and Mpk1p play complementing roles in regulating cell wall integrity. That Ca^{2+}-calcineurin signalling can compensate for some defects in the CWI pathway is further supported by the finding that constitutively active calcineurin partially rescues the lysis phenotype of *pkc1* and *slt2/mpk1* mutants of *S. cerevisiae* [47]. Calcium signalling commonly utilizes the Ca^{2+}-binding protein calmodulin and the Ca^{2+}-calmodulin-dependent serine/threonine protein phosphatase calcineurin to activate the zinc-finger-type transcription factor Crz1p, which might be solely responsible for calcineurin-dependent transcriptional responses [28, 73, 111]. Calcium influx in fungi is regulated by basically two integral plasma membrane channels: the voltage-gated high-affinity calcium channel Cch1p, which is functionally associated with the stretch-activated channel component Mid1p [96], and the low-affinity calcium channel Fig1p [106]. Orthologs of all three components have been identified in various filamentous fungal species including *N. crassa* [134, 168] (Fig. 5.6). Their precise roles, however, are still largely unknown. *Δmid-1* mutants of N. *crassa* only display a very mild phenotype, limited to slower hyphal growth and the inability to maintain homeostatic Ca^{2+} levels [93]. Hyphal fusion defects were not observed, which is also the case for *Δcch-1* single mutants and Δ*cch-1*Δ*mid-1* double mutants (Chu, M. & Read, N., unpublished results). Interestingly, Fig1p was found to be required for cell-cell fusion during yeast mating [106], suggesting a potentially similar role for a low-affinity calcium influx system (LACS) in filamentous fungi. Activation of the CWI MAPK Mpk1p, however, was not required for LACS activity, suggesting that Mpk1p and Fig1p define two independent signalling branches in that process. To our knowledge, a functional analysis of the putative Fig1p ortholog

of *N. crassa*, encoded by locus NCU02219.3, has so far not been conducted. Of course, it is an interesting and conceivable possibility that opening of stretch-activated calcium channels upon CAT tip contact triggers further steps of the fusion process. The involvement of MAK-1 in this signalling cascade, however, remains to be determined. For this reason, putative pathway connections between calcium channels and MAK-1 have been omitted from Fig. 5.6.

Further analysis of putative plasma membrane Ca^{2+}-channel components and their potential downstream targets in *N. crassa* is urgently required to achieve a better understanding of the potential connection between Ca^{2+}-calcineurin signalling and the CWI pathway machinery. Important roles of cation transporting channels in internal membranes, such as the Ca^{2+}-pumping ATPases NCA-1 to NCA-3 and PMR-1, and vacuolar Ca^{2+} channels, such as the Yvc1p ortholog encoded by locus NCU11361.3, need to be considered as well. A comprehensive summary of calcium signalling components in *N. crassa* has been provided by Zelter *et al.*, 2004 [168]; the latest overview of the fungal calcium system has been assembled by Rispail *et al.*, 2009 [134], who compared genomes of 10 different fungal species. According to a recent model, cofactors that influence calcineurin activity in fungi include HSP90, FKBP and the calcineurin regulator Rcn1p [77, 146]. Interestingly, Rcn1p-mediated modulation of calcineurin activity depends on the concomitant action of priming MAPKs (e.g. MAK-1) and effector kinases (e.g. GSK-3), thereby providing a 'reverse' link between the CWI MAPK cascade and calcineurin signalling [61, 62, 133]. For now, it can be concluded that calcineurin-dependent gene expression directs synthesis of components of stimulus-induced stress-response pathways that function in cell wall integrity and repair. The molecular connection between Ca^{2+}-calcineurin signalling and the CWI pathway in filamentous fungi, however, requires detailed experimental analysis, especially in respect to cell wall remodelling processes during cell fusion.

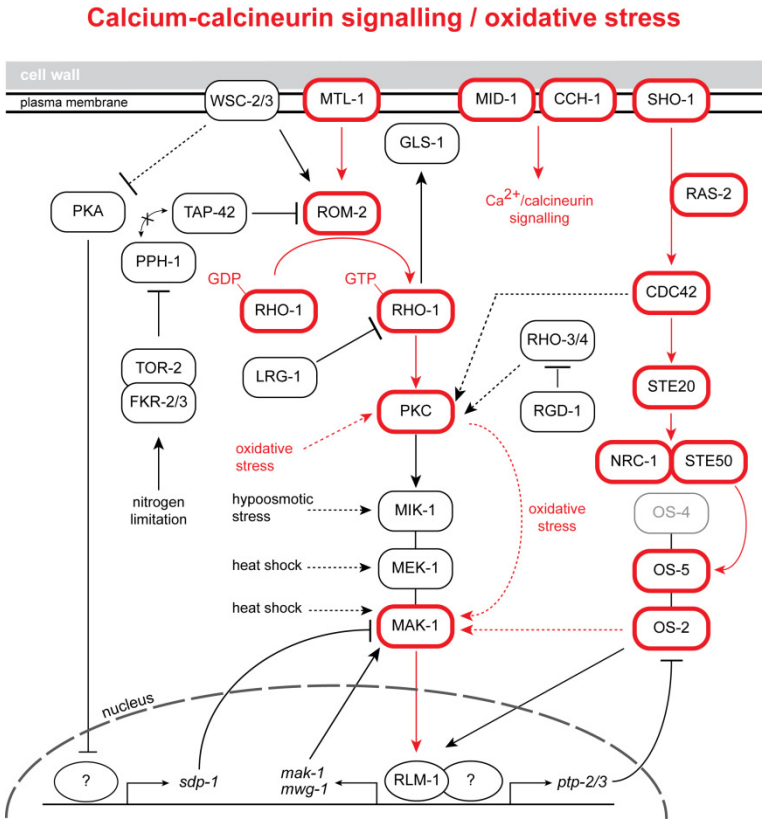

Figure 5.6 Activation of MAK-1 via Ca^{2+}-calcineurin signalling and under oxidative stress. Various lines of evidence strongly suggest that calcium influx through the MID-1/CCH-1 Ca^{2+}-channel complex ultimately leads to MAK-1 activation. The molecular link between Ca^{2+}/calcineurin signalling and the CWI MAPK cascade however is not clear, and thus not depicted in the diagram. Cells have the ability to differentiate between oxidative stressors that impact cell wall structure and those that act intracellularly, such as H_2O_2. In the first case, activation of MAK-1 occurs via plasma membrane sensors either in a PKC-dependent fashion through MTL-1, or in an OS-2-dependent way via SHO-1. In the later case, direct activation of PKC most likely involves H_2O_2-sensing peroxiredoxins (not shown in diagram). MIK-1, MEK-1 and OS-4 appear to be dispensable in this context. See text for details.

Oxidative stress. Fungi encounter oxidative stress in any aerobic environment in the presence of UV light. Under these conditions, the concentration of reactive oxygen species (ROS), including superoxide anion, hydroxyl radicals and hydrogen peroxide, can damage directly or indirectly cellular components, such as DNA, proteins or lipids. Fungal pathogens are additionally challenged by ROS, as well as nitrogen and chlorine species, released during plant and animal host defence

reactions. Although the molecular detection machinery can differ between evolutionary divergent fungal pathogen species, the cellular responses evoked appear to be universal, but specific towards different oxides [15, 42]. The cell wall provides the first protective layer to prevent oxidative damage to the cell. It is backed up by a number of detoxifying enzymes, including superoxide dismutase (SOD), catalase, glutathione peroxidase (GSHPx) and glutathione reductase (GSSGR) which are produced in response to oxide attacks [42], as well as by constantly present, non-enzymic antioxidants, such as L-ascorbic acid (vitamin C), tocopherols (vitamin E) and glutathione [5, 14, 147]. In yeasts, oxidative stress regulation involves cross-talk between the HOG and the CWI PKC-MAPK pathways. Activation of the highly conserved MAPKKs and MAPKs (Pbs2p, Hog1p and Slt2p/Mpk1p) upon addition of oxidant agents, however, occurs in a species-dependent manner [3]. Although *hog1* mutants are sensitive to H_2O_2, Hog1p is not phosphorylated in *S. cerevisiae*, whereas phosphorylation of the orthologous MAPKs occurs in *C. albicans* and *S. pombe* [3, 4, 142]. Furthermore, *hog1* and *pbs2* mutants respond differently to oxidative stress, suggesting that although Pbs2p and Hog1p function within the same pathway, both proteins have additional and separate roles in mediating oxidative stress responses [4]. Interestingly, activation of Slt2p/Mpk1p by H_2O_2 does not require any of the known 'classical' CWI plasma membrane sensors, nor the MAPKKK Bck1p or MAPKK Mkk1p/Mkk2p, but relies on Rom2p and Pkc1p as upstream components [156]. Although this appears to be species-specific [49, 156], equivalent pathway models have been reported in other yeasts, including *C. neoformans* [49] and *C. albicans* [108], suggesting that a similar signalling route may extend from PKC directly onto MAK-1 in *N. crassa* (Fig. 5.6). Alternatively, direct activation of PKC might occur through a yet unidentified lateral input pathway, involving an intracellular receptor, or via orthologs of the plasma membrane sensors Sho1p and Mtl1p [137, 156]. Most interestingly, Vilella *et al.* [156] found that Mtl1p activated PKC upon external oxidative stress that impacted cell wall structure directly (e.g. by the addition of diamide), whereas

addition of H_2O_2 which did not lead to structural damage of the cell wall activated the pathway at the intracellular level. Both stresses led to transient depolarization of the actin cytoskeleton in a concentration dependent manner, and all upstream components of the PKC-MAPK pathway, including Mtl1p, Rom2p and Pkc1p, were found to be required to restore actin organization. This suggests signal transduction from the putative MTL-1 membrane sensor via RHO-1 onto PKC, but so far has not been experimentally confirmed under oxidizing conditions in *N. crassa*. The ability of the CWI pathway to differentiate between various types of oxidative stresses has also recently been reported for *A. fumigatus* [152]. Similar to *C. albicans* [108], but in contrast to *S. cerevisiae* [79], deletion of the MAK-1 ortholog MpkA in *A. fumigatus* enhanced tolerance to H_2O_2, but increased sensitivity to menadione and diamide [152]. Besides its role in osmosensing (Fig. 5.2), Sho1p has also been implicated in the response to oxidative stress [137]. Interestingly, under these conditions the membrane sensor seems to have only a minor role in transmitting signals that lead to the phosphorylation of Hog1p, but appears to be important for linking oxidative stress to Mkc1p-mediated cell wall repair [137]. With respect to intracellular sensors for changing oxidative conditions, peroxiredoxins are likely candidates [2, 159]. Studies in *S. pombe* suggested that dependent on H_2O_2 concentration, the thioredoxin peroxidase Tpx1p activates alternative pathways that first induce adaptation by stimulation of Pap1p-mediated transcription, before triggering a more complex Sty1p MAPK-mediated (OS-2 ortholog) cell survival program (reviewed in [158]).

Orthologs of almost all aforementioned CWI pathway network components are present in the *N. crassa* genome and summarized in Table 5.1. To elucidate their molecular interactions required for cytoskeletal and structural cell wall rearrangements during cell-cell fusion in *N. crassa* will be a major future challenge.

Table 5.1 Components of the CWI MAPK pathway network featured in Figs. 5.2 to 5.6. Orthologous genes of *N. crassa* were identified by reciprocal BLASTp analysis against the *S. cerevisiae* genome. Where several close orthologs could be identified the one with the highest sequence homology and domain structure similarity was chosen.

Neurospora crassa		***Saccharomyces cerevisiae***		
Gene	**Locus**	**Gene**	**Locus**	**Protein**
wsc-2	NCU00309.3	*WSC2*	SCRG03410.1	plasma membrane sensor
wsc-3	NCU04170.3	*WSC3*	SCRG01299.1	plasma membrane sensor
pkac-1	NCU06240.3	*TPK1*	SCRG03512.1	cAMP-dependent PKA type 1
pkac-2	NCU00682.2	*TPK2*	SCRG02295.1	cAMP-dependent PKA type 2
msn-2	NCU02671.3	*MNS2*	SCRG01934.1	zinc finger transcription factor
msn-4	NCU02671.3	*MNS4*	SCRG03958.1	zinc finger transcription factor
sdp-1	NCU06252.3	*SDP1*	SCRG05285.1	dual-specificity phosphatase
no hit	no hit	*MID2*	SCRG04278.1	plasma membrane Ca^{2+}-channel
rom-2	NCU00668.3	*ROM2*	SCRG04313.1	Rho GEF
rho-1	NCU01484.3	*RHO1*	SCRG02640.1	Rho1 GTPase
pkc	NCU06544.2	*PKC1*	SCRG03062.1	protein kinase C
mik-1	NCU02234.2	*BCK1*	SCRG03576.1	MAPKKK
mek-1	NCU06419.2	*MKK1/MKK2*	SCRG01617.1	MAPKK
mak-1	NCU09842.1	*SLT2/MPK1*	SCRG04738.1	MAPK
rlm-1	NCU02558.3	*RLM1*	SCRG02406.1	transcription factor
swi6	NCU07587.3	*SWI4*	SCRG04587.1	transcription factor
swi6	NCU07587.3	*SWI6*	SCRG04142.1	transcription factor
mbp-1	NCU07246.3	*MBP1*	SCRG00555.1	transcription factor
mwg-1	NCU05974.3	*CRH1*	SCRG00832.1	cell wall protein
ccg15	NCU08936.3	*PST1*	SCRG00460.1	secreted cell wall protein
lrg-1	NCU02689.3	*LRG1*	SCRG00727.1	Rho GAP
gls-1	NCU06871.3	*FKS1*	SCRG04285.1	1,3-β-D-glucan synthase
gls-1	NCU06871.3	*FKS2/GSC2*	SCRG00980.1	1,3- β-D-glucan synthase
gls-1	NCU06871.3	*FKS3*	SCRG02203.1	1,3- β-D-glucan synthase
gs-1	NCU04189.3	*SIM1*	SCRG00795.1	1,3- β-D-glucan synthase
rho-3	NCU00600.2	*RHO3*	SCRG05290.1	Rho3 GTPase
rho-4	NCU03407.2	*RHO4*	SCRG04070.1	Rho4 protein
rgd-1	NCU00553.3	*RGD1*	SCRG02709.1	Rho3/4 GAP
pacC	NCU00090.3	*RIM101*	SCRG04676.1	transcription factor
mid-1	NCU06703.3	*MID1*	SCRG03417.1	stretch-activated Ca^{2+}-channel

cch-1	NCU02762.3	*no hit*	no hit	voltage-gated Ca^{2+}-channel
fig-1	NCU02219.3	*FIG1*	SCRG02926.1	plasma membrane Ca^{2+}-channel
mtl-1	NCU02187.3	*MTL1*	SCRG00988.1	plasma membrane sensor
sho-1	NCU08067.3	*SHO1*	SCRG04594.1	plasma membrane sensor
ras-2	NCU08823.3	*RAS2*	SCRG03234.1	small GTP-binding protein
cdc42	NCU06454.2	*CDC42*	SCRG04185.1	Rho GTPase
ste20	NCU03894.2	*STE20*	SCRG04697.1	PAK
nrc-1	NCU06182.3	*STE11*	SCRG04305.1	MAPKKK
ste50	NCU00455.2	*STE50*	SCRG05376.1	MAPK scaffold
os-4	NCU03071.2	*SSK2/SSK22*	SCRG03112.1	MAPKKK
os-5	NCU00587.2	*PBS2*	SCRG03546.1	MAPKK
os-2	NCU07024.2	*HOG1*	SCRG05095.1	MAPK
hsf-1	NCU08512.3	*HSF1*	SCRG01073.1	heat shock factor
hsf-2	NCU08480.3	no hit	no hit	heat shock factor
ptp-2	NCU02257.3	*PTP2*	SCRG01596.1	tyrosine phosphatase
ptp-3	NCU05364.3	*PTP3*	SCRG04551.1	tyrosine phosphatase
fkr-2	NCU04140.3	*FPR2*	SCRG00024.1	FK506-binding protein
fkr-3	NCU04372.3	*FPR2*	SCRG00024.1	FK506-binding protein
tor-2	NCU05608.3	*TOR2*	SCRG03828.1	phosphatidylinositol 3-kinase
no hit	no hit	*TOR1*	SCRG03718.1	phosphatidylinositol 3-kinase
ppe-1	NCU03436.3	*SIT4*	SCRG00547.1	protein phosphatase
pph-3	NCU00043.3	*SIT4*	SCRG00547.1	protein phosphatase
pph-1	NCU06630.3	*SIT4*	SCRG00547.1	protein phosphatase
tap-42	NCU08268.3	*TAP42*	SCRG01924.1	Tap42 catalytic subunit
hsp90	NCU04142.3	*HSP90*	SCRG02260.1	heat shock protein 90
cdc-37	NCU00472.3	*CDC37*	SCRG00355.1	Hsp90 co-chaperone
rcn-1	NCU01504.3	*RCN1*	SCRG03869.1	regulator of calcineurin
gsk-3	NCU04185.3	*MCK1*	SCRG03431.1	protein kinase
crz-1	NCU07952.3	*CRZ1*	SCRG03162.1	transcription factor
yap-1	NCU03905.3	*YAP1*	SCRG01889.1	transcription factor
prx-1	NCU06031.3	*TSA1*	SCRG01867.1	thioredoxin peroxidase
prx-1	NCU06031.3	*TSA2*	SCRG00086.1	thioredoxin peroxidase

One important advantage of using *Neurospora* as a model system is that CAT-mediated cell fusion occurs 'naturally' under experimental conditions, i.e. addition of excess amounts of pheromones or other chemicals to induce the process

is not required. Therefore, cell communication and cell fusion can be investigated in an experimentally stress-free environment. Of course, it is arguable whether or not the process of germling network formation by CAT fusion is a stress situation in itself. Most studies which contributed to the development of current CWI pathway models usually applied external stress stimuli to evoke cellular responses. It will be interesting to see whether this simple yet fundamental difference in experimental design will gain novel insights into pathway architecture in the future. Initial insights into the role of the central CWI MAPK MAK-1 of *Neurospora* will be presented in the following section.

5.3. Results

5.3.1. Cell fusion involved rapid cell wall remodelling and mechanical stress adaptation

Cell fusion in *N. crassa* requires extensive and rapid remodelling of the cell wall at at least four key stages of the process: (1) localized softening of the cell wall to allow protrusion of CATs and fusion hyphae, (2) cell wall biogenesis during directed tip growth towards the fusion partner, (3) strengthening of the attachment site to prevent cell leakage, and (4) localized degradation of the cell wall during fusion pore formation. Cell wall biogenesis can be visualized using the fluorescent dye calcofluor white (CFW) [30]. In contrast to other cell wall dyes, e.g. solophenyl flavine, CFW bleaches relatively quickly [65] and therefore, when using low concentrations (< 0.2 μM) of the dye any increase in fluorescence signal reliably indicates areas where new chitin polymers have been incorporated into the cell wall. CAT attachment preceded fusion pore formation and usually coincided with a 'germling torque' response, i.e. rotation of one conidial germling around the attachment point (Fig. 5.7). This movement might occur due to differential mechanical stress and tightening of the cell wall-cell wall connection. Assembly of

new chitin material during that process appeared to be targeted to those areas of CATs that experienced the greatest mechanical stress.

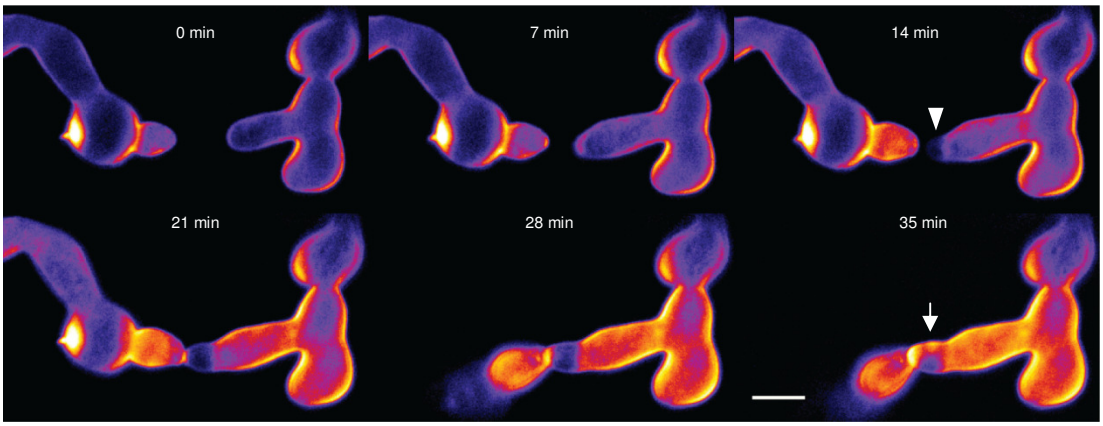

Figure 5.7 Cell wall remodelling during CAT homing and attachment. Time course of CAT homing, tip contact and germling torque. Tight attachment became apparent by the germling torque response (21 to 28 min). Calcofluor white (0.12 µM final concentration) was used to stain fungal cell walls, and is displayed in false-colours to indicate regions with little (dark blue) and intense (yellow) fluorescence which is assumed to relate to chitin deposition. During rapid cell wall extension the CAT tip of the right cell was initially weakly stained, indicating low chitin content (arrowhead), but became reinforced upon attachment (> 21 min). Addition of new cell wall material was not symmetrical, but appeared to be focused in that area experiencing the greatest stress during germling torque (arrow). Scale bar, 5 µm. See supplementary movies 5.1a and b for full animated sequence.

5.3.2. Defects in the CWI MAPK cascade prevented contact-induced tip growth arrest and hyphal fusion

Both mating types of the gene deletion mutants Δ*mik-1*, Δ*mek-1* and Δ*mak-1* were obtained from the FGSC (see Table 2.1). Integration of the knock-out cassette at the correct locus was verified in all strains by Southern analysis prior to strain deposition. Genotypes of all received strains were additionally verified by PCR within this project (section 3.3.4), and proved to be correct, i.e. absence of the native

gene from the genome and recovery of the Δ*mus-51* or Δ*mus-52* deletion, respectively, after back-crossing to the wt (data not shown).

All three CWI MAPK mutants showed a rosetta-like colony morphology, short aerial hyphae and reduced conidiation (Fig. 5.8A); features indicative of cell wall defects. Furthermore, all strains were blocked in hyphal fusion in the mature colony and between conidial germlings (Fig. 5.8B to D). In the mature colony, hyphae were unable to induce tip growth arrest and fusion upon cell wall contact, but rather continued polarized tip growth (Fig. 5.8C). This behaviour overall led to 'chaotic' hyphal growth (Fig. 5.8B), typical for fusion mutants of *N. crassa* (section 3.3.3). Conidial germlings of CWI mutants were blocked in CAT fusion and thus unable to establish germling networks (Fig. 5.8D). Most interestingly, all three mutants formed small protrusions that were different to GTs (arrowheads in Fig. 5.8D). These CAT-like protrusions were much less abundant (< 20% of cells, data not shown) compared to the wt, but frequently seen in all three MAPK mutants, Δ*mak-1*, Δ*mik-1* and Δ*mek-1* (also see Figs. 3.6 and 3.7 for comparison). No differences were observed between strains of opposite mating type (data not shown).

The morphological defects conserved amongst all three MAPK mutants strongly suggested an essential role of the CWI MAPK pathway in cell fusion in *N. crassa*. To confirm this notion and elucidate the role of this signalling pathway in more detail we decided to initially focus on the terminal phosphorylation target of this MAPK cascade, MAK-1. A great body of evidence has been accumulated on the functional role of MAK-2 during cell fusion in *N. crassa* [40, 114], providing the opportunity for interesting comparisons between the CWI and PR pathways.

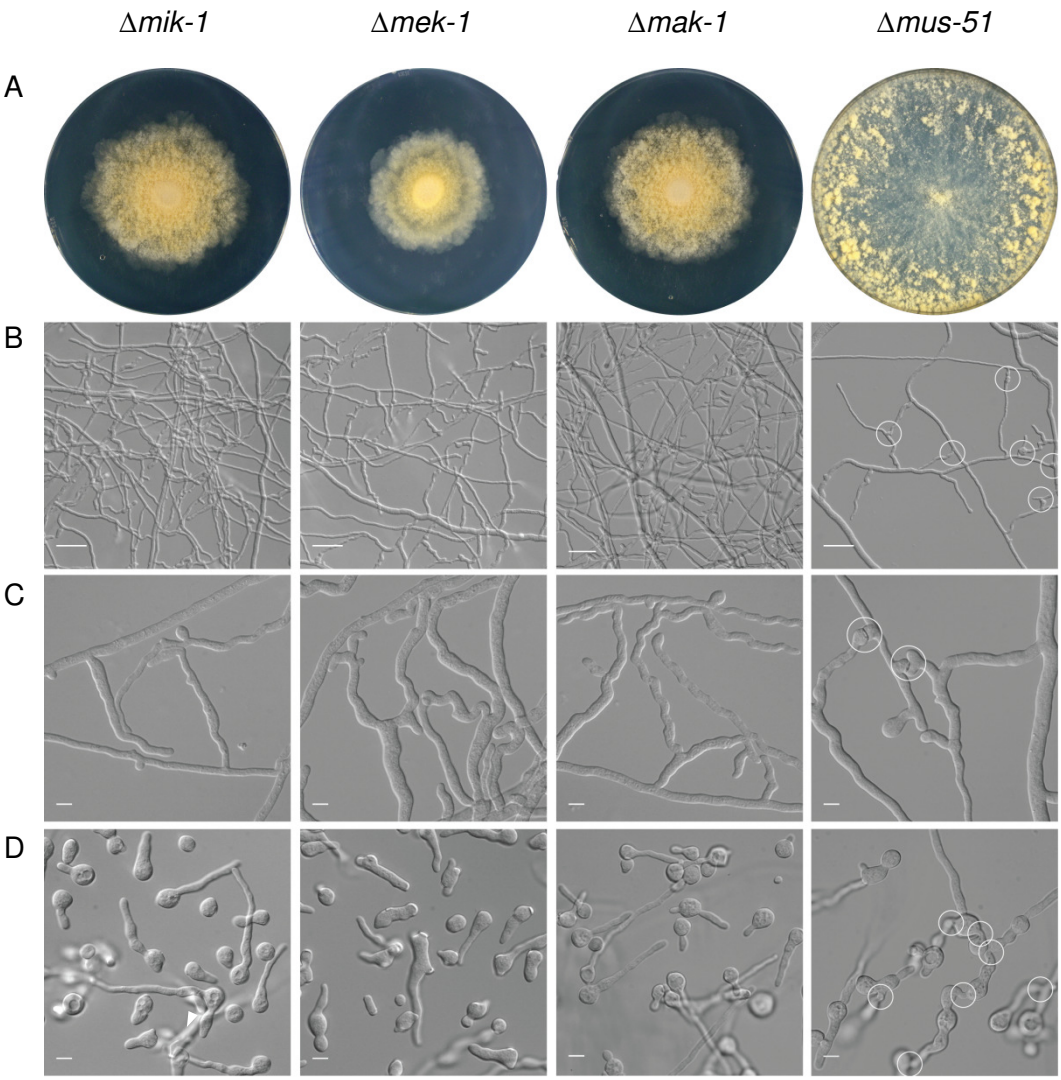

Figure 5.8 Phenotypes of CWI mutants Δ*mik-1* (MAP3K), Δ*mek-1* (MAP2K) and Δ*mak-1* (MAPK). (A) Mature colonies of all three CWI MAPK mutants displayed a rosetta-like morphology which was caused by greatly reduced colony extension and hyphal autolysis. Colonies furthermore showed reduced aerial hyphae and a conidiation pattern concentrated in the colony centre. Colonies have been grown for 3 days on standard VM. In comparison, the Δ*mus-51* strain which has been used as genetic background for gene deletion mutant production was indistinguishable from the wt (see Fig. 3.1). The mycelium has covered the whole plate and produced abundant aerial hyphae and condia concentrated along the edge already after 2 days of incubation. **(B)** All three MAPK mutants were unable to undergo VHF in the mature colony. This prevented the formation of a hyphal network and led to a chaotic mycelial architecture. The Δ*mus-51* deletion did not affect hyphal fusion and thus the strain was able to build up an organized hyphal network. Fusion connections are indicated with circles. Scale bars, 50 µm. **(C)** The hyphal fusion defect in CWI MAPK mutants was presumably caused by the inability of hyphal tips to respond to each other and trigger the fusion program, including contact-induced tip growth arrest, tip depolarization, attachment and fusion pore formation. Fusion connections between hypha of Δ*mus-51* are circled. Scale bars, 10 µm. **(D)** Conidial germlings of Δ*mik-1*, Δ*mek-1* and Δ*mak-1* were completely blocked in CAT-mediated cell fusion. To a low percentage conidia formed CAT-like structures, which

appeared to be most pronounced in Δ*mak-1* (indicated with arrowheads). Germling network established by CAT fusion between Δ*mus-51* cells; fusion connections are circled. Scale bars, 10 µm.

5.3.3. MAK-1-sGFP cloning and expression

To express a MAK-1-sGFP fusion protein in *N. crassa*, the plasmid pAL1-MAK-1 was constructed by first generating the GFP expression vector pAL1 through subcloning the sGFP coding region from pMF272 [41] into pBARGRG1 [113] using *Bam*HI/*Eco*RI restriction/ligation (section 2.6), and subsequently inserting the *mak-1* gene amplified from *N. crassa* wt cDNA using oligonucleotides mak1_*BamH*I_fw 5′-GATCGGATCCATTCGCCATGGCTGATCTCGTG-3′ and mak1_*Xma*I_rv 5′-GATCCCCGGGATTCGCCATGGCTGATCTCGTG-3′ (*BamH*I and *Xma*I restriction sites underlined) into *Bam*HI/*Xma*I linearized pAL1 in-frame to sGFP whilst omitting the *mak-1* stop codon. Recovered pAL1-MAK-1 plasmids were verified by sequencing and transformed into wt and Δ*mak-1* strains by electroporation (section 2.10). Transformants were selected on Ignite medium and expression of the fusion protein assessed in at least 8 clones per strain under the stereomicroscope, and in greater detail by epi-fluorescence and laser scanning confocal microscopy (section 2.12).

In ungerminated conidia MAK-1-sGFP was diffusely localized inside the cytoplasm and nuclei, but excluded from smaller organelles, comprising small vacuoles, vesicles and mitochondria (Fig. 5.9). Upon germination localization usually became more defined and a circular exclusion zone within nuclei became more obvious, most likely marking the nucleolus, and indicating release of MAK-1-sGFP into the nucleoplasm. During normal GT growth this basal cytoplasmic and nucleoplasmic localization of MAK-1-sGFP did not change (Fig. 5.9F).

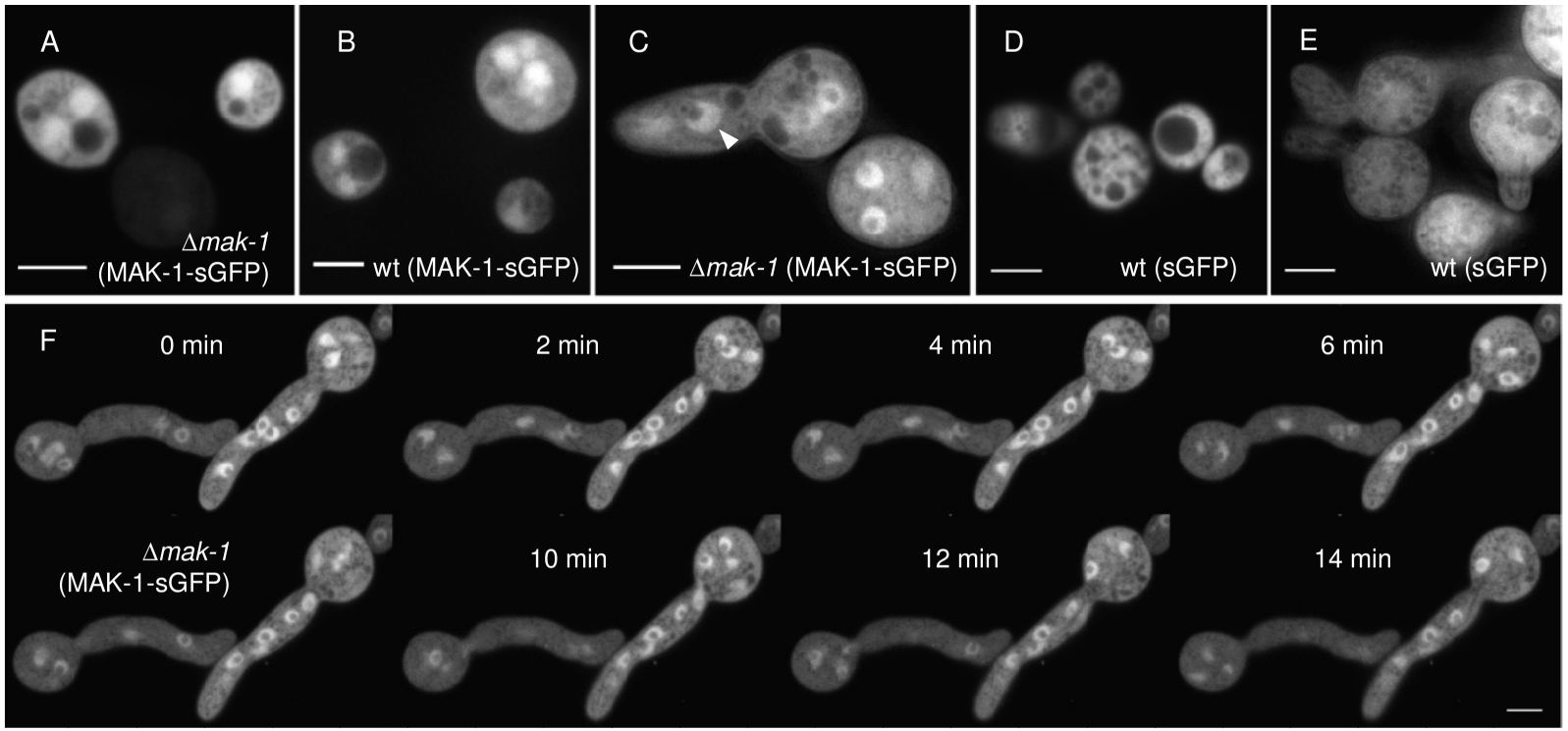

Figure 5.9 Intracellular localization of MAK-1-sGFP. In ungerminated conidia of **(A)** Δ*mak-1* and **(B)** wt, MAK-1-sGFP was diffusely localized inside nuclei and the cytoplasm, but excluded from vacuoles and other small organelles. **(C)** With the onset of isotropic expansion and germination MAK-1-sGFP localization became more discrete, including exclusion from the nucleolus (arrowhead). No differences in localization were observed between Δ*mak-1* and wt cells expressing the same construct. **(D)** Localization of free sGFP inside wt cells was different, in that pronounced nuclear accumulation and localization changes upon germination **(E)** were not observed. **(F)** During GT elongation obvious changes in the basal MAK-1-sGFP localization were not observed, nor pronounced cortical accumulation of MAK-1 before or upon tip contact (also see Fig. 5.12). Scale bars, 5 µm.

5.3.4. Ectopic expression of MAK-1 rescued Δ*mak-1* mutant phenotype

Re-introduction of fluorescently labelled MAK-1 fully restored wt-like phenotype in Δ*mak-1* strains, including rescue of fusion defects in the mature colony and between conidial germlings of Δ*mak-1* transformants, as well as between Δ*mak-1* transformants and wt cells expressing the nuclear marker H1-GFP (Fig. 5.10).

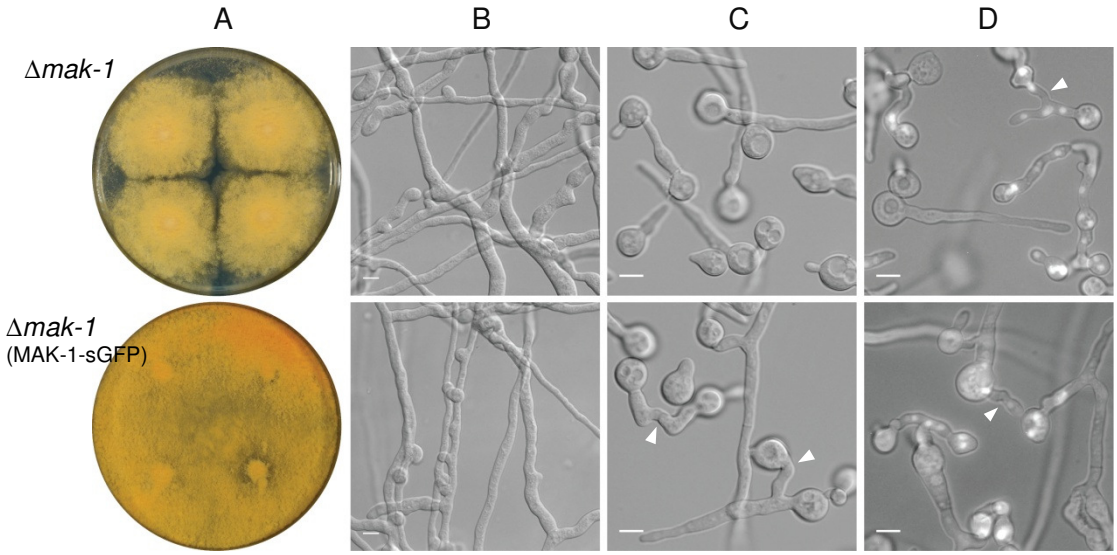

Figure 5.10 Recovery of wt-like phenotype after re-introduction of MAK-1 into Δ*mak-1* conidia. The top row shows the Δ*mak-1* gene deletion mutant; the bottom row Δ*mak-1* transformed with pAL1-MAK-1. **(A)** Agar plates that were inoculated at four positions and incubated for 3 days. Δ*mak-1* colonies show avoidance responses along the colony edges, whereas this defect, and all other morphological alterations of the mutant (section 5.3.1), were restored to wt-like appearance after re-introduction of *mak-1* into the genome. (Δ*mik-1* and Δ*mek-1* strains showed identical avoidance responses along colony edges, not shown.) **(B)** Vegetative hyphal fusion in the mature colony and **(C)** CAT-mediated cell fusion (arrowheads) between germlings of Δ*mak-1* were rescued, as well. **(D)** The cell fusion defect of Δ*mak-1* cells could not be compensated by wt cells (expressing the nuclear marker H1-GFP for identification purposes). Fusion between wt cells (arrowhead) occurred normally in the presence of mutant cells. Heterokaryon formation between gentically compatible cells of Δ*mak-1* (MAK-1-sGFP) transformant and *wt* (H1-GFP) conidia (arrowhead) however occurred. Due to the extreme brightness of the fluorescent H1-GFP nuclei, MAK-1-sGFP appears only as relatively weak cytoplasmic glow in these merged images. Scale bars, 10 µm.

5.3.5. MAK-1 accumulation peaked during fusion pore formation

MAK-1 became recruited into small apical clusters at CAT tips already during homing, but strongly accumulated upon tip contact and peaked shortly before fusion pore opening (Fig. 5.11). MAK-1-sGFP remained present at the fusion site throughout the fusion pore expansion process and disappeared shortly after cytoplasmic continuity was established. This type of localized accumulation at fusing CAT tips was never observed in cells expressing free sGFP only (data not shown).

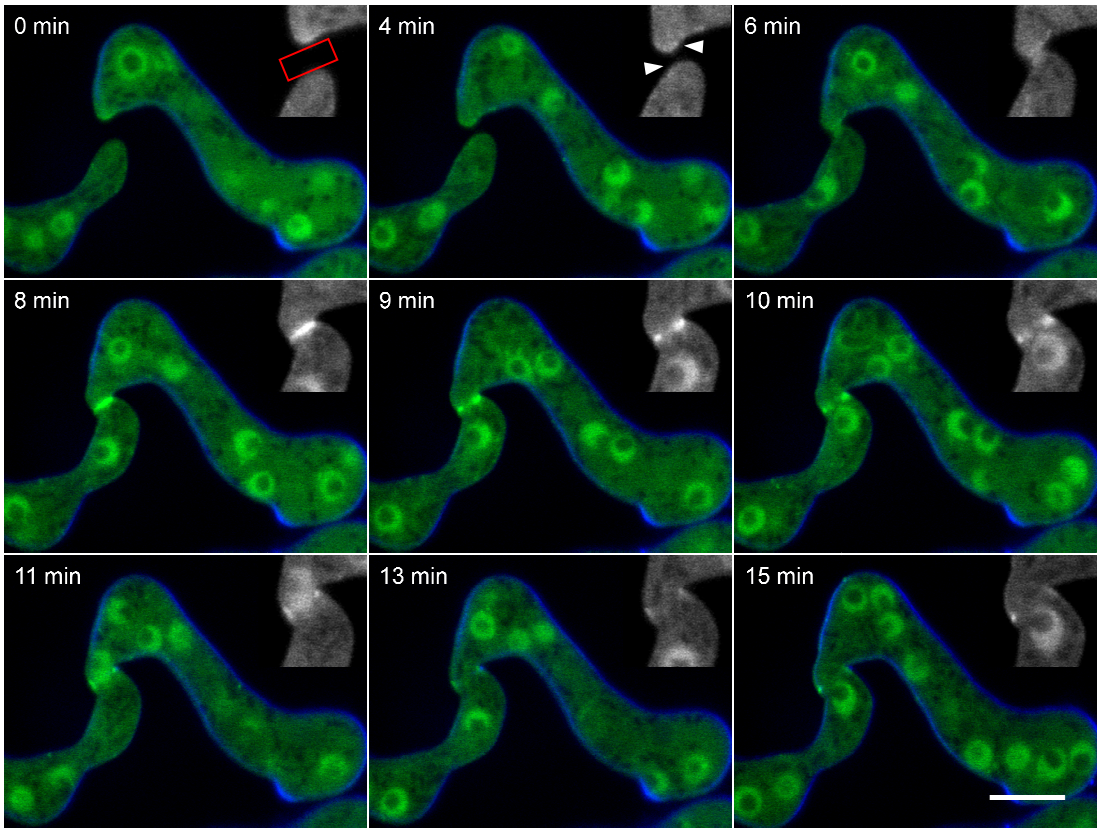

Figure 5.11 MAK-1 accumulation during CAT homing and fusion. Cells of Δ*mak-1* expressing MAK-1-sGFP (green); cell walls were stained with CFW (blue). MAK-1 became recruited into discrete spots at CAT tips during homing (arrowheads in insets), however, strong accumulation occurred in response to tip contact (6-8 min). MAK-1 remained localized during pore opening (9-11 min), but disappeared shortly after cytoplasmic continuity was fully

established (>11 min). Nuclear transit through the newly established connection occurred between 10-13 min. In this example, germling torque (Fig. 5.7) did not occur as cells were prepared by the inverted agar method (section 2.11.1), and thus spatially confined between cover glass and agar. Scale bar, 5 µm. Insets show magnification of the fusion site. The red rectangle marks the area in which MAK-1 fluorescence intensity was measured over time (see Fig. 5.18B). See supplementary movie 5.2 for full animated sequence.

When two GTs came into contact - of which one had potentially differentiated a CAT at its tip - the cell fusion process was not triggered, and thus MAK-1 recruitment to the contact site was not observed (Fig. 5.12). Instead, GT elongation was re-oriented and commenced away from the contact site. A slight increase in MAK-1-sGFP fluorescence at the re-polarization site opposite of the contact area (2-4 min), might suggest cell wall remodelling processes prior to bud emergence. Notably, accumulation of MAK-1 in discrete and highly mobile clusters along the GT cortex could be observed as well (see supplementary movie 5.3).

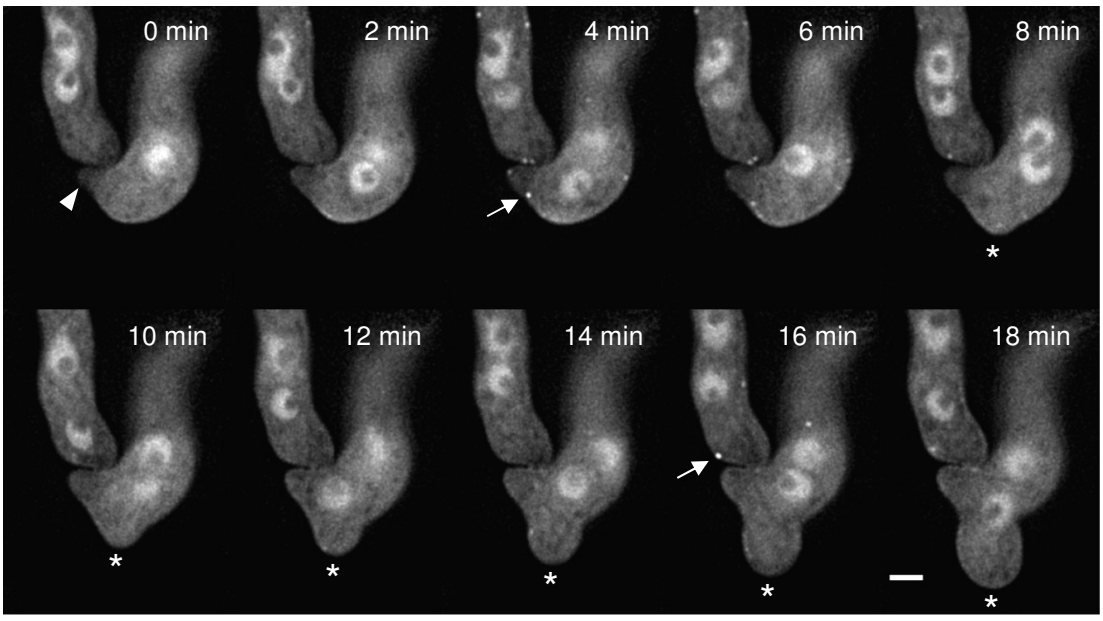

Figure 5.12 MAK-1 recruitment was not induced upon GT contact. Two GT tips of Δ*mak-1* (MAK-1-sGFP) conidia in close contact. One cell might have formed a CAT at its GT tip (arrowhead). However, cell fusion was not initiated, therefore MAK-1 was not recruited to the contact site, and GT elongation commenced away (asterisk) from the other GT. Bright cortical clusters of MAK-1-sGFP are marked with arrows. Scale bar, 2 µm.

5.3.6. Conidia of Δ*mak-1* formed CATs, but were unable to chemotropically interact and fuse

To verify initial observations of CAT-like protrusions (Fig. 5.8) and determine whether or not Δ*mak-1* conidia were only defective in homing and fusion (but not CAT formation), CAT formation assays (Fig. 4.10) were conducted. For this, the number of conidial germlings forming GTs and CATs in the presence and absence of the GT inhibiting drug benomyl (see Fig. 4.10) were quantified after 4 and 6 hours of incubation (Fig. 5.13). Although about 4-fold less efficient compared with the wt under identical conditions, Δ*mak-1* cells did form CATs. This reduction in CAT formation was fully restored in Δ*mak-1* (MAK-1-sGFP) transformants. Expression of the same construct in a wt background led to a significant decrease in CAT formation, which potentially was attributed to overexpression of MAK-1.

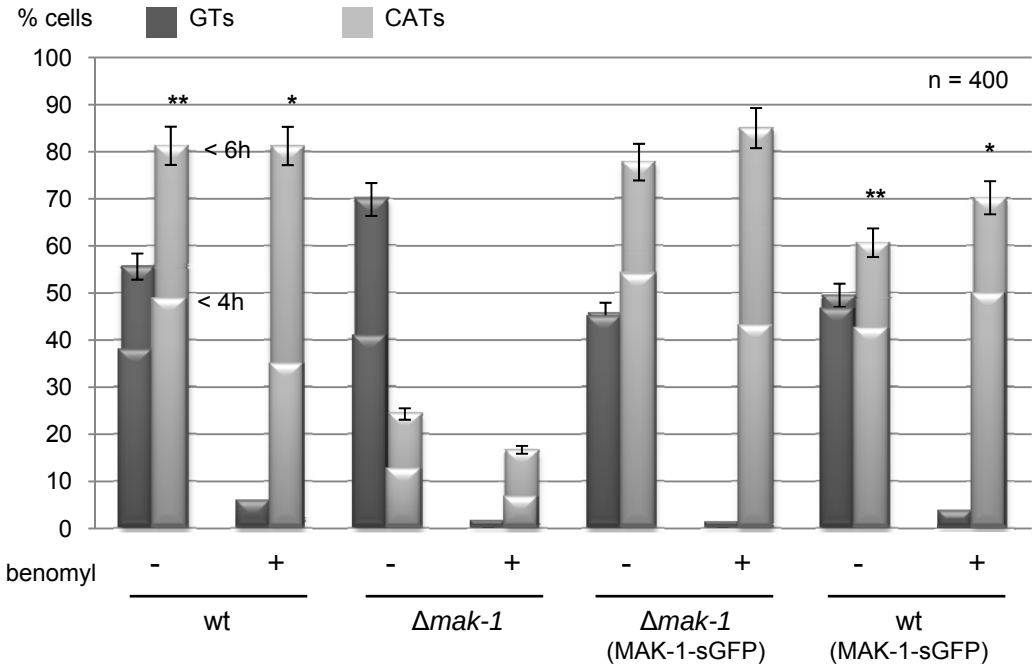

Figure 5.13 CAT formation in Δ*mak-1*. The microtubule disrupting drug benomyl prevents the formation of GTs but not CATs (Fig. 4.10), and was used to distinguish CAT formation in the wt, Δ*mak-1*, and both strains ectopically expressing MAK-1-sGFP. The number of cells forming GTs and CATs was quantified after 4 and 6 h incubation in the absence or presence of ~3 µg/ml benomyl. The disruption of microtubules did not influence the rate of CAT

formation in any of the four strains; variations seen are statistically not significant. CAT formation was reduced 4-fold in Δ*mak-1* cells compared to wt (Δ*mak-1*, 20% compared to wt, 80%; similar results obtained for Δ*mik-1* and Δ*mek-1*, supplementary figure 5.1), but fully restored by MAK-1-sGFP re-introduction. Ectopic expression of MAK-1-sGFP led to a statistically significant reduction of CAT formation in the wt which was independent of benomyl treatment (**$F_{3,3}$=0.18,p>0.05; $t_{3.6}$=6.24, p<0.01; *$F_{3,3}$=0.27, p>0.05; $t_{4.5}$=3.8, p=0.01; n=400 for each condition).

5.3.7. Generation of a chemically inhibitable *mak-1* allele

To facilitate a more detailed functional analysis of MAK-1 a Δ*mak-1* strain expressing a chemically inhibitable variant of MAK-1, MAK-1^{E104G}-sGFP, was generated. The exchange of glutamic acid (E) to glycine (G) within the ATP-binding motif (LY**E**ELME → LY**G**ELME) of MAK-1 confers sensitivity to the ATP-analogue inhibitor 1NM-PP1 [10, 11]. Side-directed mutagenesis (section 2.3.16) was performed on pAL1-MAK-1 pDNA using oligonucleotide MAK1_E104G_GGC_fw 5′-CGAGACCTATCTCTACGGCGAGTTGATGGAGTGCGATCTTGC-3′ and its reverse complement MAK1_E104G_GGC_rv 5′-GCAAGATCGCACTCCATCAACTCGCCGTAGAGATAGGTCTCG-3′ (triple base pair mismatch is underlined). Resulting plasmids were verified by sequencing, and transformation into Δ*mak-1* conidia as well as subsequent clone selection were performed as described earlier (section 5.3.3).

5.3.8. MAK-1 kinase activity was required for CAT-mediated cell fusion

Identical to the non-inhibitable variant, ectopic expression of MAK-1^{E104G}-sGFP in Δ*mak-1* cells fully restored the wt-like phenotype including the ability to undergo CAT-mediated cell fusion (Fig. 5.14). Most importantly, in the presence of the ATP-analogue 1NM-PP1 cell fusion was completely inhibited, although, similar

to the Δ*mak-1* KO, CAT formation occurred in about 20% of the cells. Formed CATs, however, did not home or fuse. Addition of the solvent (0.1% DMSO) only, or addition of 1NM-PP1 to wt cells not carrying the inhibitable *mak-1* allele had no inhibitory effects on germination and CAT fusion.

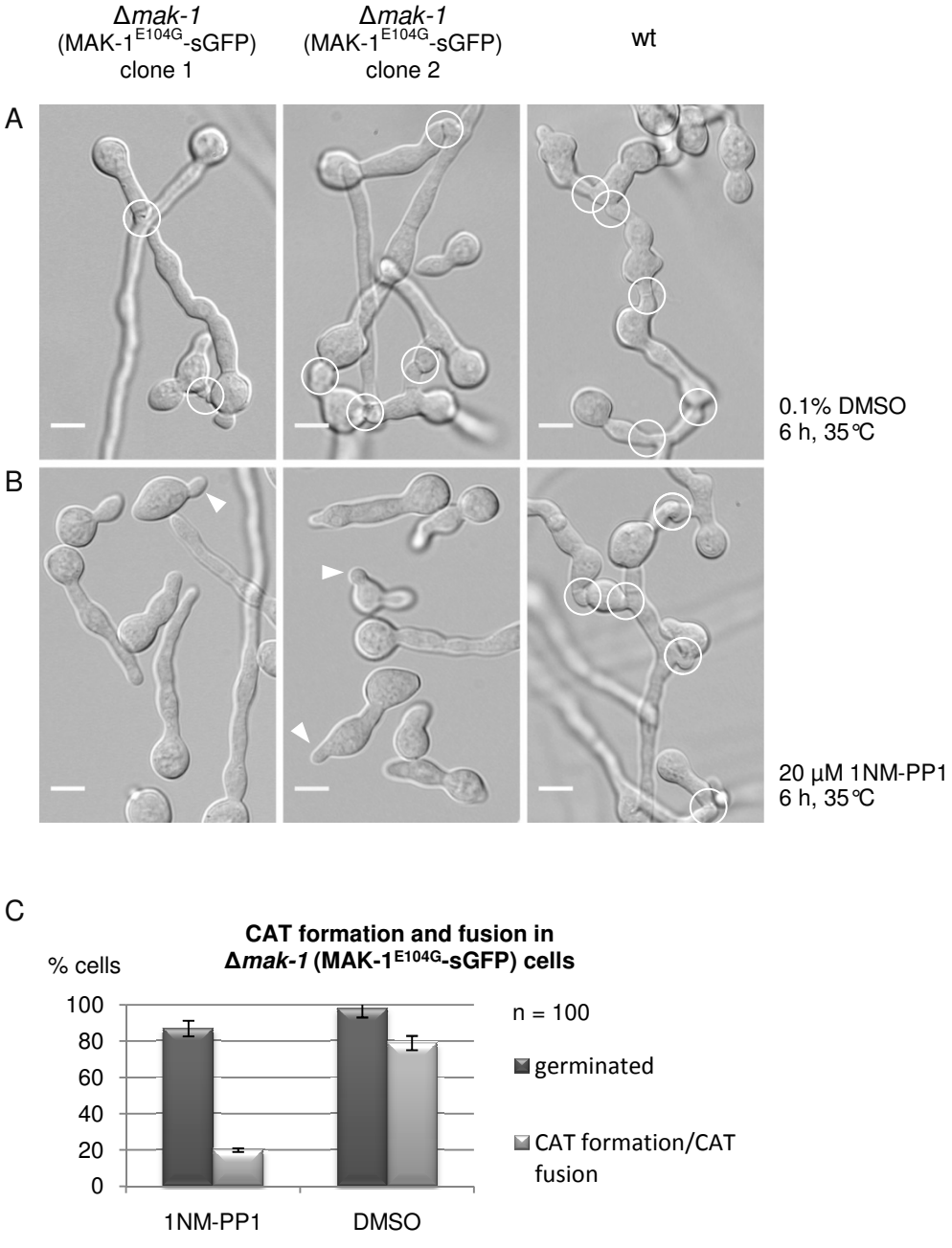

Figure 5.14 Inhibition of MAK-1 kinase activity blocked cell fusion but permitted CAT formation. (A) In the absence of 1NM-PP1 inhibitor, but presence of its solvent DMSO, germling network formation was restored in Δ*mak-1* strains expressing the inhibitable MAK-1

variant. **(B)** Addition of 20 µM 1NM-PP1 at the start of incubation efficiently blocked cell fusion for >6 h in the transformants, but did not affect wt cells not carrying the inhibitable *mak-1* allele. Fusion connections are circled. Interestingly, similar to Δ*mak-1* conidia CAT-like protrusions could be observed in 1NM-PP1 sensitive cells (arrowheads). Scale bars, 10 µm. **(C)** Quantification of CAT formation after 6 h incubation of Δ*mak-1* (MAK-1^{E104G}-sGFP) cells in the presence of 1NM-PP1 and CAT fusion in the presence of 0.1% DMSO, respectively. MAK-1 inhibition blocked CAT fusion, but permitted CAT formation at a reduced level. Incubation in the presence of DMSO alone had no inhibitory effects on germination and CAT fusion.

Furthermore, under standard conditions the intracellular localization of the inhibitable MAK-1 variant was identical to that of the native kinase. MAK-1^{E104G}-sGFP localized to the cytoplasm and nucleoplasm of conidial germlings, strongly accumulated at CAT fusion sites (Fig. 5.15) and remained present throughout the fusion pore formation process (Fig. 5.16A). Interestingly, although cell fusion was blocked in the presence of 1NM-PP1 inhibitor the basal cytoplasmic and nucleoplasmic localization of the kinase did not change. As CAT homing and fusion were inhibited under these conditions, localized recruitment of MAK-1 to CAT tips did of course not occur, but interestingly, accumulation of the kinase in cortical clusters was also absent from conidial germlings (Fig. 5.15C). The important difference to Fig. 5.9C and F is that without kinase inhibition cortical clusters of MAK-1-sGFP were present in conidial germlings, even when no CATs were being formed. But when MAK-1 activity was blocked, cortical clusters were not seen at all (Fig. 5.15C), indicating that formation of these clusters requires MAK-1 kinase activity.

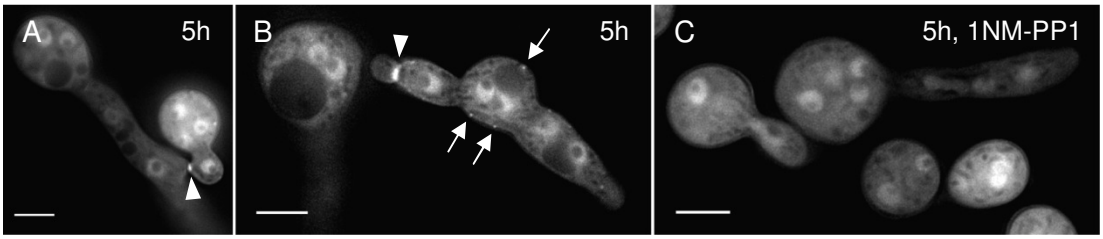

Figure 5.15 Cytoplasmic and nucleoplasmic localization of MAK-1^{E104G}-sGFP was not altered by 1NM-PP1 treatment. (A) Cytoplasmic and nucleoplasmic localization of MAK-1-sGFP in rescued Δ*mak-1* cells. During fusion MAK-1 became recruited to the contact site

(arrowhead). **(B)** Identical localization and recruitment pattern of the inhibitable MAK-1^{E104G}-sGFP variant during cell fusion between rescued Δ*mak-1* conidia. Accumulation of MAK-1^{E104G}-sGFP at the fusion site is indicated with an arrowhead, accumulation of the kinase in cortical clusters by arrows. **(C)** After 5 h of germination in the presence of 20 µM 1NM-PP1 the cytoplasmic and nucleoplasmic localization of MAK-1^{E104G}-sGFP was not different to both untreated controls, but most interestingly, accumulation of the kinase in cortical spots was also not observed. Scale bars, 5 µm.

The fact, that 1NM-PP1 sensitive cells germinated normally in the presence of the inhibitor, strongly suggested that MAK-1 kinase activity had a more important role in processes leading to CAT-mediated cell fusion than for GT extension.

5.3.9. MAK-1 kinase activity was required for its recruitment to CAT tips during homing and fusion pore formation

To investigate immediate effects of 1NM-PP1 on MAK-1 localization, and identify the stages of CAT fusion which depend on MAK-1 kinase activity, live-cell imaging experiments were conducted which involved the inhibition of MAK-1 at different time points during the fusion process. Addition of 1NM-PP1 before MAK-1 became visible at the CAT tip generally prevented apical recruitment of the kinase and thus CAT homing and fusion (data not shown). Therefore, interacting cell pairs were monitored until recruitment of MAK-1 to homing CAT tips became obvious, before the inhibitor was added, in order to establish the causal link between kinase inhibition and cellular effect. Similarly, germling torque was used as an indicator of successful CAT attachment, i.e. the starting point of the post-contact stage of fusion. Addition of 1NM-PP1 during the pre-contact stage resulted in a rapid decrease of MAK-1-sGFP fluorescence signal from homing CAT tips, indicating dispersal of the kinase from the putative fusion site (Figs. 5.16B and 5.17A). Once 1NM-PP1 was added cell attachment and fusion no longer occurred in that sample.

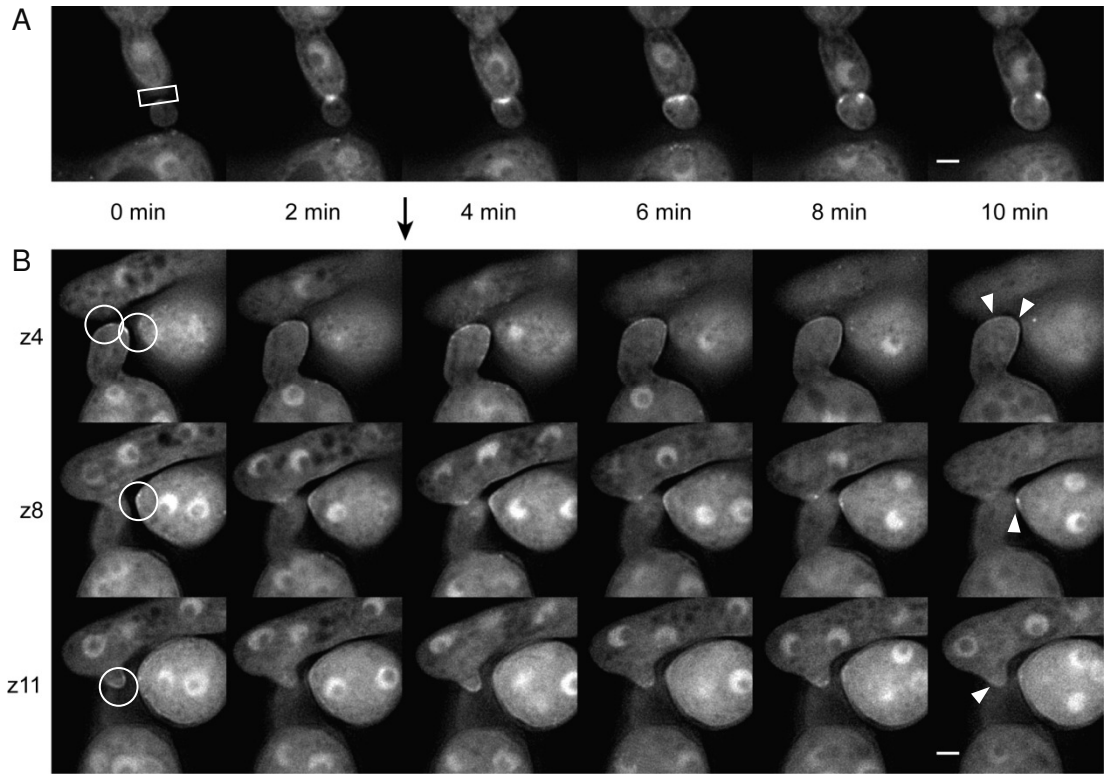

Figure 5.16 Dispersal of MAK-1^{E104G}-sGFP from interacting CAT tips upon addition of 1NM-PP1 kinase inhibitor. (A) In the absence of inhibitor, MAK-1^{E104G}-sGFP was normally recruited to homing CAT tips of rescued Δ*mak-1* transformants, and present during fusion pore formation; thus behaved identical to the non-inhibitable, native MAK-1 kinase (compare with Fig. 5.11). The rectangle marks the area in which MAK-1-sGFP fluorescence intensity was measured over time (see Fig. 5.18B). **(B)** Time series of three *N. crassa* cells interacting at two CAT fusion sites (circled). Displayed are three optical sections (z4, z8 and z11), showing areas of maximum MAK-1-sGFP accumulation at CAT tips in focus. Addition of 1NM-PP1 before CATs attached (time point of drug administration is indicated with an arrow) caused rapid dispersal of the kinase from CAT tips and prevented attachment and fusion pore formation (arrowheads). Scale bars, 2 µm. See supplementary movies 5.4 for full sequences and supplementary figure 5.2 for individual z-stacks, respectively.

Addition of 1NM-PP1 during the post-contact stage also caused rapid dispersal of apical MAK-1 (Fig. 517B), although less pronounced compared to inhibition at an earlier time point (see Fig. 5.18 for measurements). Further increase in MAK-1-sGFP fluorescence and fusion pore formation, however, were not observed, suggesting that the completion of cell fusion was prevented.

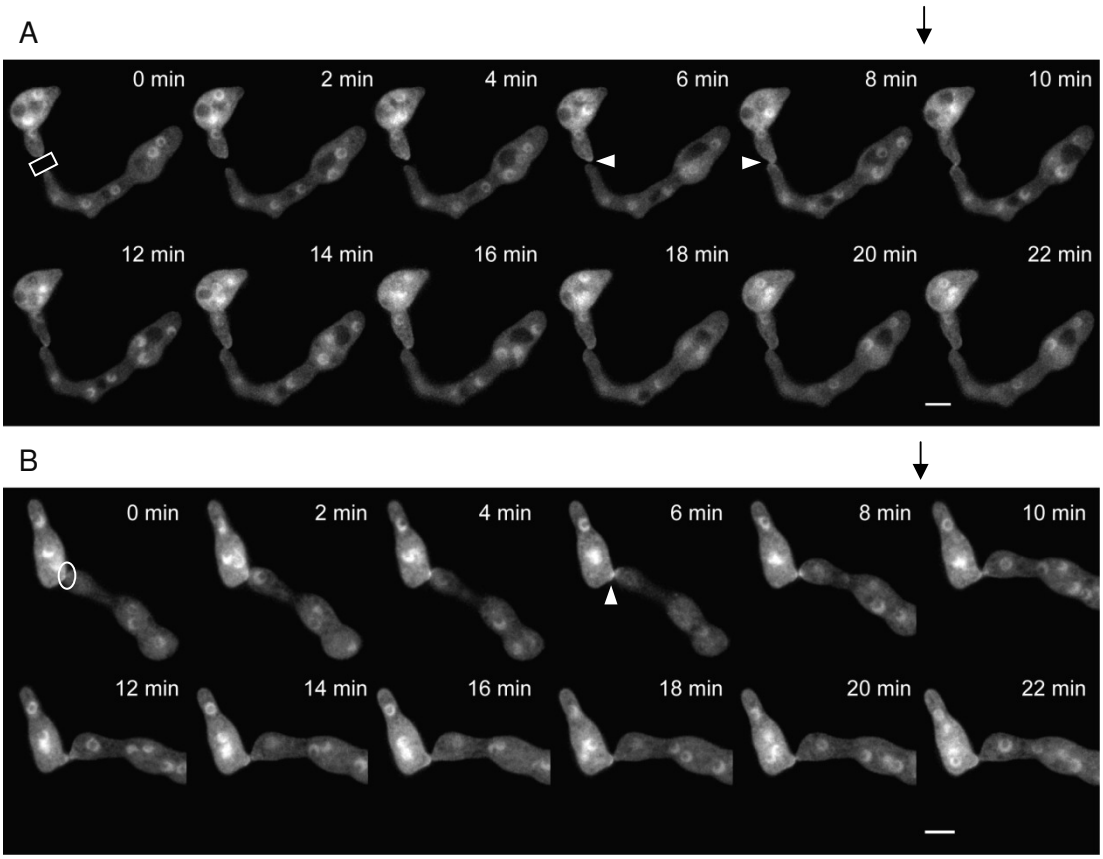

Figure 5.17 Inhibition of MAK-1 kinase activity before and after CAT attachment blocked the completion of cell fusion. (A) During the first eight minutes of the time course, MAK-1^{E104G}-sGFP became recruited to homing CAT tips (arrowheads). Just before tip attachment 1NM-PP1 inhibitor was added (time point indicated with arrow). Further increase of MAK-1^{E104G}-sGFP fluorescence at the contact site, germling torque and fusion pore formation were not observed over the following 14 minutes. **(B)** Within the first eight minutes, MAK-1^{E104G}-sGFP accumulated at the contact site (arrowhead) and germling torque occurred between 6-8 min, indicating successful cell attachment. Then 1NM-PP1 was added (time point indicated with arrow). Rapid dispersal of MAK-1 did not occur, but further increase in MAK-1-sGFP fluorescence and opening of a fusion pore were not observed either. Every image represents the maximum intensity projection of four optical sections, two below and two above the middle plane of the CAT contact site. Scale bars, 2 µm. Rectangle and oval mark areas in which MAK-1-sGFP fluorescence intensities were measured in both time courses (see Figs. 5.18C and D). See supplementary movies 5.5 and 5.6 for full z-stack sequences.

In order to verify the observed spatial and temporal dynamics of MAK-1 during cell fusion (Figs. 5.11 and 5.16A), particularly in dependence of kinase activity (Fig. 5.17), fluorescence intensity profiles of apical MAK-1-sGFP and MAK-1^{E104G}-sGFP, respectively, in the CAT contact regions were plotted (Fig. 5.18). Due to differences in experimental design and varying expression levels of the constructs

between individual cells, only the relative changes in pixel intensity during the process can be compared between samples.

Under standard conditions, i.e. native MAK-1 (Fig. 5.18A) or inhibitable MAK-1 variant in the absence of 1NM-PP1 (Fig. 5.18B), MAK-1-sGFP fluorescence increased at CAT tips during homing. A more rapid signal increase occurred upon tip contact and reached its maximum just before fusion pore formation. Signal intensity remained stable during the pore opening process, until the full width of the fusion pore was established. Subsequently, fluorescence intensity gradually decreased, indicating MAK-1 dispersal.

When 1NM-PP1 was added before cells could firmly attach (Fig. 5.18C), the initial signal increase during CAT homing rapidly decreased and did not significantly recover over the following 20 min, indicating immediate dispersal of the kinase and blockage of further recruitment. Addition of 1NM-PP1 during the post-contact stage, i.e. after CATs attached, MAK-1 strongly accumulated at the fusion site and germling torque had started (Fig. 5.18D), did result in a much slower decrease of MAK-1 fluorescence over the following 20 minutes. In both cases, further accumulation of MAK-1-sGFP and fusion pore formation were not observed.

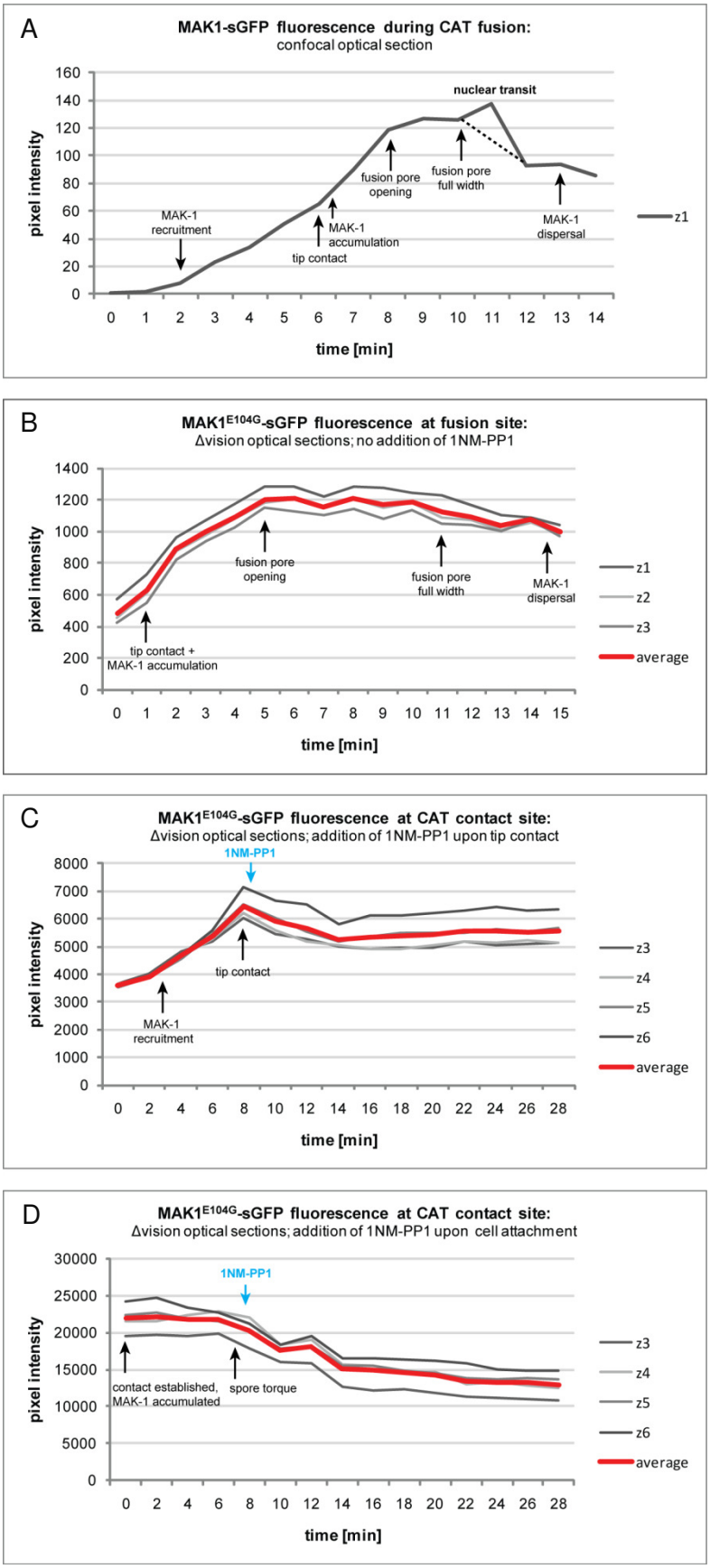

Fig. 5.18 Fluorescence intensity profiles of MAK-1-sGFP during CAT fusion and 1NM-PP1 inhibition. (A) MAK-1-sGFP signal during CAT fusion was measured in the tip contact area (rectangle in Fig. 5.11). The different stages observed in the time course are indicated in the diagram. The sudden peak in the fluorescence signal at the 11 min time point resulted from nuclear transit through the newly established fusion pore. Dotted line indicates putative curve progression in absence of nuclear transit. **(B)** MAK-1^{E104G}-sGFP signal in the absence of inhibitor (Fig. 5.16A). Three optical sections (z1-z3) were measured individually, then averaged (red curve). The profile reflects behaviour of native MAK-1 during the equivalent stages of cell fusion (7-11 min in (A)). **(C)** Addition of 1NM-PP1 immediately upon CAT contact (Fig. 5.17A) caused rapid decrease of tip localized MAK-1 fluorescence and blocked further increase of the signal over the following 20 min. Fusion pore formation was not observed. **(D)** Addition of 1NM-PP1 upon cell attachment (Fig. 5.17B) also led to a decrease in tip localized MAK-1-sGFP fluorescence. Again, further increase of the signal and fusion pore formation were not observed over the following 20 min. See text for details.

5.3.10. Influence of Δ*mak-1* deletion on F-actin organization

To investigate functional connections between MAK-1 and cytoskeletal elements, MAK-1-sGFP localization during CAT fusion in cells with disrupted microtubules was observed, as well as the distribution of F-actin in germinating cells of Δ*mak-1* expressing Lifeact-TagRFP (strain NCAL013, Table 2.2) (Fig. 5.19). As demonstrated earlier (section 4.3.6), chemical disruption of microtubules did not affect CAT formation and cell fusion, showing that microtubules are not essential for the process. MAK-1 recruitment during CAT homing and fusion also occurred normally in the absence of microtubules (Fig. 5.19A), confirming that a functional connection essential for cell fusion does not exist between the microtubule cytoskeleton and MAK-1 kinase. Polarization of the F-actin cytoskeleton, however, appeared disturbed, i.e. less polarized, in Δ*mak-1* cells (Fig. 5.19B). This would confirm suggested links between CWI signalling, and MAK-1 kinase in particular, and organization of the actin cytoskeleton. As discussed in sections 4.3.4 and 4.3.5, recruitment of F-actin into apical caps and cable arrays is essential for cell polarization and CAT fusion. Whereas in ungerminated Δ*mak-1* cells, i.e. even before isotropic expansion started, F-actin cables and patches were as randomly distributed as in the wt, the highly polarized organization of F-actin seen prior to symmetry breaking in wt cells was not observed in Δ*mak-1* condida incubated under identical conditions (Fig. 5.19B and C). MAK-1-dependent defects in F-actin polarization could explain the severe reduction in CAT formation under conditions where MAK-1 activity is disrupted, either genetically (Δ*mak-1*) or biochemically (1NM-PP1).

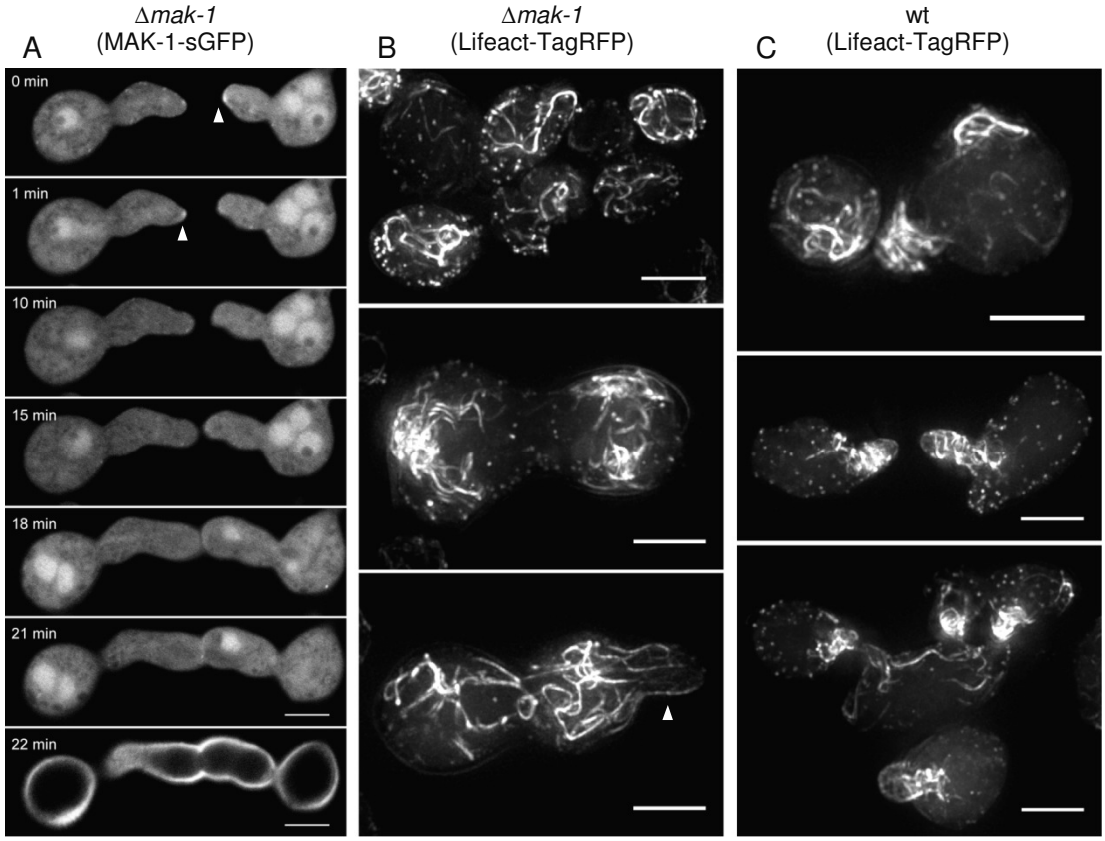

Figure 5.19 Functional relationship between MAK-1 kinase and the cytoskeleton. (A) Time course of CAT homing and fusion between Δ*mak-1* (MAK-1-sGFP) cells in the presence of ~3 µg/ml benomyl. Disruption of microtubules did not influence the subcellular localization or functionality of MAK-1 during cell fusion. MAK-1 became recruited to homing CAT tips (arrowheads), which successfully fused. Accumulation of MAK-1 at the fusion site and pore opening occurred just below the focal plane and is not clearly shown. Establishment of cytoplasmic continuity between both cells (breakdown of intervening cell walls), however, became evident by calcofluor white staining (22 min; recorded after readjusting the focal plane). (Also see supplementary movie 5.7 for second example.) **(B)** Δ*mak-1* cells expressing Lifeact-TagRFP. **Top:** randomly distributed F-actin cables and patches in ungerminated conidia of the mutant, as seen in wt cells (compare with Fig. 4.9). **Middle:** upon isotropic expansion, apical accumulation of F-actin arrays is less discrete and occurs at multiple sites more frequently as seen in the *wt* (compare with Fig. 4.11). **Bottom:** during GT emergence (arrowhead) F-actin was less focused into an apical array, but still distributed randomly throughout the spore body. **(C)** *N. crassa* wt cells expressing Lifeact-TagRFP. **Top:** cell polarization and GT or CAT emergence always coincided with concentrated F-actin arrays focused at defined sites in the cell apices, whilst the spore body was almost free of F-actin cables. **Middle and bottom:** highly polarized F-actin arrays in homing and fusing CATs. Scale bars, 5 µm.

5.4. Discussion

Precise regulation of cell wall remodelling processes, including rapid and directed cell wall extension during homing, cell wall reinforcement upon attachment (Fig. 5.7) in order to prevent leakage during locally defined cell wall breakdown for pore formation (Fig. 5.11), is a crucial requirement for CAT-mediated cell fusion in *N. crassa*. Gene deletion mutant analysis strongly suggested that the CWI MAPK pathway takes a central position in the signalling network which induces and controls the underlying cellular machinery (Fig. 5.8). How this network is regulating cell fusion in *N. crassa* has so far not been understood. Fortunately, components of this signalling network are highly conserved amongst fungal species (Table 5.1) and a massive body of evidence on the functional connection of its molecular components has been collected over past decades in a range of yeast and filamentous fungal species. This greatly facilitated the development of a pathway model for *N. crassa*, which is likely to lead to the activation of the central MAPK MAK-1 in response to a range of stimuli that demand structural cell wall changes (Figs. 5.2 to 5.6).

Which stimuli induce cell wall remodelling processes accompanying CAT fusion and how are they regulated? Recent work showed that, although considerable molecular overlap to pheromone-induced mating cell fusion in budding yeast exists, CAT homing in *N. crassa* is regulated in a very different way. The novel 'ping-pong' mechanism of CAT homing (sections 1.4.4 and 5.2.3) does not seem to be mediated via sex pheromone/GPCR-receptor signal transduction, although final proof from double and triple G-protein subunit knock-outs is still missing. Interacting cells create physiological differences between them by alternating recruitment of MAK-2 and SO protein to homing CAT tips [40, 132]. This system almost certainly does not use transcriptional negative feedback regulation, but rather direct protein-protein interactions instead, to rapidly downregulate the

induced signal. Due to these fundamental differences, it seems likely that morphogenetic cell wall changes during cell fusion in *N. crassa* are also differently regulated than comparable processes during yeast mating. Here we report the first detailed molecular analysis of MAK-1 and its essential function during cell fusion between genetically identical cells. Strikingly, and in contrast to MAK-2, strong apical accumulation of MAK-1 coincided with CAT tip contact (Fig. 5.11). This suggests a functional connection between cell wall/plasma membrane deformation, MAK-1 recruitment and induction of cell wall/plasma membrane fusion, and might also be reflected in the phenotype of fusion defective mature hyphae. A feature that all three CWI MAPK gene deletion mutants (Δ*mik-1*/Δ*mek-1*/Δ*mak-1*) of *N. crassa* share in common is a 'chaotic' hyphal architecture in the mature colony (Fig. 5.8B and C). Fusion hyphae which usually would arrest tip growth, depolarize and initiate the final stages of the fusion process upon contact (Fig. 1.7), lack this response in fusion defective mutants that are lacking MAP kinases (Fig. 3.1). Mechanosensors in the plasma membrane are predicted to play a role in the initiation of tip growth arrest, cell wall attachment and fusion pore formation. Stretch-activated Ca^{2+}-channels are one obvious possibility. Unfortunately, to date, there is only negative evidence for an involvement of the known calcium channel proteins, MID-1 and CCH-1, of *N. crassa* in cell fusion. Although indicated in other fungal species, there are so far no reports of a signal transduction pathway, leading from plasma membrane Ca^{2+} channels into the CWI MAPK cascade of *N. crassa* (Fig. 5.6). Recent identification of a third calcium channel, FIG-1, in the genome of *N. crassa* (Table 5.1) [134], opens up new possibilities for investigating this important issue further. However, preliminary data indicates that this receptor also is dispensable for cell fusion (Chu, M. & Read, N., unpublished results). Nevertheless, it is still possible that stretch-activated channels in *N. crassa* remain to be discovered and that an alternative pathway exists that transduces signals into the CWI MAPK cascade. Interestingly, Fig1p has been found to facilitate Ca^{2+} influx and mating cell fusion in *S. cerevisiae* [1, 106]. A second possibility is the involvement of another

sensor of mechanical stress. Promising candidates are the membrane sensors of the WSC family, which recently have been shown in yeast to act like nano-springs capable of sensing mechanical forces which act either on the cell wall or on the plasma membrane [37]. If similar to the yeast system, WSC-2/3 of *N. crassa* could activate MAK-1 in response to cell wall/plasma membrane deformation upon tip contact. Gene deletion mutants of *wsc-2* or *wsc-3* have so far not been tested for defects in cell fusion in *Neurospora*.

Other external stimuli, addressed in the depicted pathway model (Figs. 5.2 to 5.5), including osmotic, pH and temperature changes, as well as changes in nutrient availability, do not seem to be relevant candidates for signals being exchanged between CATs in order to initiate fusion. All these factors induce cellular responses when applied as stressors, i.e. at concentrations or within ranges beyond what would occur under standard conditions in a cell population. CAT fusion, however, does occur under 'stress-free' conditions in minimal medium without the addition of any inductive chemical or heat treatment being necessary. This, of course, does not at all exclude that the same molecular components which regulate stress responses are used to signal the more subtle interaction of fusing *Neurospora* cells.

Changes in the extracellular or intracellular oxidative state, on the other hand, provide another interesting possibility to activate the CWI network and mediate cell fusion. Results which indicate that germinating cells of *N. crassa* actively lower the oxidative state of their environment, before CAT formation and fusion can occur will be presented and discussed in chapter 7. Cells possess membrane located, but also intracellular sensors for ROS, such as H_2O_2, which would enable them to respond to very small oxidant changes, far below cell damaging concentrations (Fig. 5.6). In addition to direct intracellular H_2O_2 perception, e.g via the *N. crassa* peroxiredoxin PRX-1, which is likely to activate OS-2 [2, 156], which in turn acts on MAK-1, modulation of the intracellular redox status by peroxidases, such as HYR-1 of *N. crassa*, can influence oxidation states of cysteine

residues and thus regulate the activity of many proteins [54, 55], including those required for fusion. H_2O_2 is ideally suited as cellular second messenger as it readily crosses biological membranes, and a variety of enzymic and non-enzymic ways for its production and degradation are in place (see section 7.2.2).

Taken together, the putative sensor that amplifies apical accumulation of MAK-1 and triggers the cell fusion program upon tip contact has not been identified yet. A combination of plasma membrane mechanosensors and redox signals that could be generated within the cell wall, quickly enter the cytoplasm and activate cell internal receptor molecules, are the most likely candidates for future investigations. As MAK-1-sGFP is already recruited to homing CAT tips a second sensor/receptor might be involved during the pre-contact stage.

It is arguable whether the state of being non-fused or the process itself constitutes a stress situation. As we know, the percentage of CAT formation and fusion depends on cell density [131]. The optimum concentration for maximal CAT formation and CAT-mediated cell fusion, repectively, within a cell population is 0.5–1 x 10^6 cells per ml. Below this optimum less CATs are being formed and GT elongation is promoted. Above this optimum germination is inhibited (Roca, M. & Read, N. D., in preparation). As apart from cell number all outside environmental factors (pH, temperature, nutrient availability, etc.) were identical in these experiments, a type of quorum-sensing mechanism [135] can be suggested which must be the result of cellular activity. In this context a helpful observation is that a number of fusion mutants grow much longer and thinner GTs under standard conditions than the wt would do. This type of hyphal morphology, however, can be mimicked in the wt under nutrient limiting conditions, i.e. under stress. Longer and thinner GTs can be the result of more rapid tip growth in order to grow away from stress quicker, e.g. to reach nutrient rich areas sooner. A more rapid tip extension could therefore be the outcome of increased MAK-1 activity under nutrient limiting conditions, as depicted in Fig. 5.5. This however, remains to be shown.

Main function of MAK-1 appears to be focused on cell attachment and fusion pore formation. Re-introduction of MAK-1-sGFP into Δ*mak-1* by transformation restored the wt phenotype in all respects (Fig. 5.10) confirming the functionality of the construct, and the causal connection between MAK-1 and the observed morphological defects. CAT formation and fusion rates were restored to wt levels in the transformants (Fig. 5.13), which suggest that the basal CAT formation rate of about 20% occurred independent of MAK-1 activity. This phenotype was conserved between all three CWI MAPK mutants (Supplementary figure 5.1). In order to increase this rate and to produce functional CATs, MAK-1 is essential. The fact that overexpression of MAK-1 in a wt background reduced CAT formation and fusion might be indicative of a negative feedback regulation mechanism for MAK-1 acting on upstream components; potentially similar to or in interaction with that reported for MAK-2 (Fig. 5.1) [132]. It would be interesting to test whether partial inhibition of 1NM-PP1 sensitive MAK-2 in a Δ*mak-1* background would further decrease this basal rate of CAT formation. This probably would indicate interaction of both MAPKs during the initial stages of CAT-mediated cell fusion.

The main function of MAK-1, however, seemed to be focused on the post-contact stage of cell fusion. Although small clusters of MAK-1-sGFP already appeared at homing CAT tips, its accumulation at the fusion site peaked upon contact and during fusion pore formation (Figs. 5.11 and 5.16A). This type of recruitment was specific for fusing CATs, and never observed between contacting GTs (Fig. 5.12), confirming physiological and functional distinctiveness between GTs and CATs [131]. Apart from germling network formation, lack of MAK-1 did not prevent GT formation and colony establishment. Although both developmental stages were impaired – especially colony morphology was heavily defective - Δ*mak-1* was still able to progress through its complete vegetative cycle, as were Δ*mik-1* and Δ*mek-1* strains (Fig. 5.8). MAK-1 also accumulated in bright cortical clusters along the whole surface of conididal germlings. Although the function of these clusters is

currently unclear, their accumulation was dependent on MAK-1 activity (Fig. 5.15), but not obviously associated to specific developmental stages. Superficially, similar cortical clusters have been observed in cells expressing MAK-2-GFP [40]. These however, were directly associated with oscillatory recruitment during CAT homing and dispersed upon 1NM-PP1 treatment in case of the inhibitable MAK-2 variant.

Recruitment and accumulation of the inhibitable MAK-1 variant (MAK-1^{E104G}-sGFP) could be blocked at the pre- and post-contact stages of CAT fusion by the addition of 1NM-PP1 inhibitor (Fig. 5.16 to 5.18), which in all cases induced dispersal of the kinase from CAT tips and the contact site. The facility to block MAK-1 kinase activity at any point in the experiment proved to be an extremely useful tool in correlating intracellular localization, protein activity, cellular process and possible function. Taken together, 1NM-PP1 inhibitor studies provided evidence that kinase activity of MAK-1 is important during three essential stages of the cell fusion process. Firstly, for its targeted recruitment to homing CAT tips during the pre-contact phase, and localized accumulation at the fusion site during the post-contact stage. In both cases, addition of 1NM-PP1 led to rapid dispersal of already recruited MAK-1 and blocked further accumulation. Secondly, kinase activity was required for the fusion pore enlargement process. 1NM-PP1-induced inhibition of MAK-1 kinase activity prevented localized breakdown of intervening cell walls between firmly attached cells. Finally, kinase activity is also involved, but not exclusively required, for CAT formation (sections 5.3.6. and 5.3.8). Identical to the Δ*mak-1* gene deletion strain, only 20% of cells with inhibited MAK-1 activity formed CATs, these however were non-functional.

PKC is another central kinase in the CWI pathway network and will be a highly interesting next candidate to engineer a 1NM-PP1 sensitive variant of. This will be particularly useful because genetic deletion of PKC resulted in lethality in other fungal model species, including *S. cerevisiae* and *A. nidulans* [66, 92]. This is very likely the case for *Neurospora* as well, as our attempts to purify the

heterokaryotic Δ*pkc* strain obtained from the FGSC have so far not yielded viable, homokaryotic colonies.

CWI MAPK functions in other fungal systems. During yeast budding, the CWI MAP kinases Mpk1p and Mkk1/2, and their scaffolding protein Spa2p become recruited to the bud tip and mother-bud neck region [154]. In the same study, addition of α factor induced mating projection formation which coincided with strong apical accumulation of all four CWI pathway components, which was dependent on Spa2p. Interestingly, although LatA treatment blocked mating projection protrusion, recruitment of Mpk1p, Mkk1p and Spa2p to the incipient bud site was not inhibited. This type of MAPK localization is different to that observed in *N. crassa*, as during CAT formation and homing strong apical MAK-1 recruitment was never observed. Although the MAK-1 homolog MPS-1 appears to be dispensable for appressorium formation in the rice blast fungus *M. oryzae*, it has a crucial role in cell wall biosynthesis during penetration peg formation and infectious growth [166]. This function appears to be conserved within the CWI MAPK cascade of the rice blast fungus as the same defect has recently been reported for the MIK-1 ortholog Mck1 [68]. In yeast-two-hybrid screens it has been shown that Mps1 interacts with the MADS-box transcription factor Mig1, a Rlm1p homolog [103]. In *A. nidulans* it was found that transcription of *mpkA* (*mak-1* homolog) was auto-regulated by MpkA itself and independent of RlmA and AnSwi4-AnSwi6 transcription factor activity [43]. Transcriptional regulation of the α-1,3-glucan synthase genes *agsA* and *agsB*, however, occurred via these transcription factors in response to MpkA signalling. These data supports the pathway model of MAK-1 dependent RLM-1 activation during cell wall remodelling processes in filamentous fungi, but it also shows that transcriptional regulation of cell wall genes upon CWI pathway stimulation differs significantly from that in *S. cerevisiae*, and very likely also amongst other filamentous fungal species. Although Mig1-GFP could be localized inside nuclei of conidia, appressoria and infection hyphae, detailed analysis of Mps1-GFP localization and dynamics during appressorium formation

and the penetration process are so far missing. Although nucleo-cytoplasmic shuttling of Slt2p-GFP upon heat shock has been observed in budding yeast [53, 70], changes in subcellular localization of the protein during shmoo formation and mating cell fusion have so far not been described. A more detailed live-cell imaging analysis of these orthologous components in other fungi would provide extremely valuable data for a comparison with *N. crassa*.

The CWI pathway probably acts in conjunction with the PR pathway during CAT fusion. Our analysis of genetically and biochemically induced MAK-1 loss-of-function mutants in *N. crassa* (sections 5.3.2, 5.3.6 and 5.3.8) showed that MAK-1, although not crucially required, has a role in CAT formation. About 20% of cells without functional MAK-1 were still able to form CATs, but these were non-functional (Figs. 5.13 and 5.14). This was an important finding as it contrasts key functions of the CWI and PR MAPK pathways during CAT formation. All three MAPK gene deletion mutants of the PR pathway in *N. crassa* (Δ*nrc-1*/Δ*mek-1*/Δ*mak-2*) are unable to form CATs [94, 114, 135]. This might point to a sequential activity of both pathways during the initiation of CAT formation, in which first an inductive signal needs to be perceived and processed through the NRC-1/MEK-2/MAK-2 cascade before it feeds into the MIK-1/MEK-1/MAK-1 cascade to elicit cell wall changes required for CAT protrusion. A defect in the PR MAPK cascade cannot be compensated, whereas a lack in the CWI MAPK cascade – verified at least for MAK-1 within this study – partially can. At later stages, combined activity seems more likely. Directed tip growth during homing is coordinated via the MAK-2 dependent 'ping-pong' mechanism and necessary cell wall changes are probably mediated via MAK-1/MAK-2 induced cytoskeletal rearrangements coordinating vesicle delivery. As MAK-2 activity is oscillating, MAK-1 which is constantly present at the CAT tip, might be important to drive constant tip extension. MAK-1 recruitment to CAT tips accompanied homing, and inhibition of kinase activity at this stage stopped the process (Figs. 5.16 and Fig. 5.17A). Upon tip contact, MAK-1 strongly accumulated

at the fusion site and remained present during pore opening. Inhibition of MAK-1 kinase activity blocked fusion pore formation even at the post-contact stage (Fig. 5.17). In combination with data on MAK-2 recruitment and dynamics [40], these experiments demonstrate that both MAPKs, and thus supposedly both MAPK pathways, interact during the whole process from CAT formation to CAT fusion. When cytoplasmic continuity was successfully established MAK-1 dispersed from the site (Figs. 5.18A and B). Accumulation in a ring around the opening pore has also been reported for MAK-2 [40], but if and how its localization changed post-fusion was not described in detail.

MAK-1 is involved in the regulation of cell wall biogenesis and polarization of the actin cytoskeleton. The cell wall provides structural support and thus its remodelling during morphogenesis must occur in a controlled way as not to compromise the integrity of the cell and cause leakage. Mechanical stress on the cell wall certainly occurs during cell attachment, germling torque and subsequent fusion pore enlargement. The incorporation of chitin during CAT fusion was visualized with CFW (Fig. 5.7), and indicated that cell wall biogenesis might be targeted to regions that experience the greatest stress during germling torque. A molecular connection between the CWI pathway and cell wall biogenesis exists through RHO-1 dependent activation of the glucan synthase machinery (e.g. via GLS-1), but this however, is supposed to occur upstream of MAK-1 (Fig. 5.2). Cell wall defects, including a weaker structural composition are commonly attributed to CWI mutants [33], and become apparent by increased sensitivity to cell wall degrading agents, such as Novozyme [98]. A novel regulatory feedback connection between Mpk1p and Rho1p activity has recently been established in yeast [51]. Mpk1p directly influences Rom2p (GEF for Rho1p) activity, induces its redistribution and thus terminates Rho1p activity at a specific location. Circumventing transcriptional regulation, this direct protein-protein interaction very quickly can control the localization of cell wall synthesis and polarization of

the actin cytoskeleton. A similar feedback mechanism involving MAK-1 and ROM-2/RHO-1 in *N. crassa* is an exciting possibility, and would explain why in the absence of the kinase (Δ*mak-1*), the actin cytoskeleton and thus CAT formation are disturbed, and GT elongation proceeds much quicker (see below). The observed accumulation of MAK-1 in cortical clusters (Fig. 5.15) might be associated with MAK-1 dependent nucleation of F-actin cables. Co-localization studies of MAK-1-sGFP and Lifeact-TagRFP should resolve this issue.

Cell wall remodelling is closely associated to dynamic rearrangement of the cytoskeleton, and signalling through the CWI pathway is believed to have a direct affect on actin organization during cell fusion. Interestingly, CWI MAPK mutants in budding yeast (orthologs of Δ*mik-1* and Δ*mak-1*) have been reported to display a depolarized actin cytoskeleton [34, 102]. Using a Δ*mak-1* strain expressing the Lifeact-TagRFP marker, confirmed this notion in *N. crassa* germlings. Cells beyond the isotropic growth phase showed a less polarized actin distribution compared with wt cells, and even when GT emergence was finally achieved unusually many F-actin cables were still found randomly distributed within the spore body (Fig. 5.19B). This defect in F-actin polarization and organization in Δ*mak-1* cells may partially explain the defect in CAT formation and fusion. Although, in contrast to F-actin, microtubules are not required for CAT formation and fusion, they are crucial for GT protrusion (section 4.3.6). Therefore, it was not surprising to find that chemical disruption of microtubules did not affect MAK-1 recruitment and accumulation during CAT fusion (Fig. 5.19A). That cells of CWI MAPK gene deletion mutants were able to polarize and develop long GTs, whilst assuming that actin organization was defective in all of them, suggests that other parts of the CWI pathway network are able to compensate for the individual loss of those proteins.

Assessment of germination and CAT formation/fusion rates in wt and Δ*mak-1* cells of *N. crassa* in the presence of 0.25–1.25 μg/ml rapamycin to synthetically increase activation of the CWI pathway so far did not yield meaningful results (data not shown). This might have been a matter of too low concentrations, as for

applications in other filamentous fungi 10-20 μg/ml have standardly been used (Sarah Gurr, personal communication). Future work therefore, should aim at providing a functional link between F-actin organization and MAK-1 activity during CAT fusion by treating wt and Δ*mak-1* cells expressing Lifeact-TagRFP with higher doses of rapamycin.

5.5. Summary

This chapter presented the first detailed molecular analysis of the CWI signalling pathway during cell fusion in *N. crassa*, including a description of the role of the terminal MAP kinase MAK-1 in this process. Major achievements were:

- Development of a comparative model of the fungal CWI pathway network which highlights key molecules of *N. crassa* likely to be involved in the initiation and regulation of cell wall remodelling processes. Two aspects covered were:
    - the identification of 11 different input pathways which can lead to the activation of MAK-1 by external signals
    - the identification of five putative plasma membrane sensors that could act in contact-induced initiation of tip growth arrest, cell attachment and cell fusion
- Visualization of cell wall remodelling during CAT-mediated cell fusion and recognition of the associated germling torque response as an experimental marker for CAT attachment. Two important aspects were:
    - CFW was used as a tool to visualize asymmetric cell wall biosynthesis and mechanical stress during cell attachment
    - the germling torque response was shown to accompany firm cell-cell attachment and provided a valuable experimental indicator for the

transition from the pre-contact stage to the post-contact stage of cell fusion

- Detailed characterization of phenotypic defects in CWI MAPKs gene deletion mutants associated with hyphal fusion. Key findings were:
    - a lack of contact-induced tip growth arrest and tip attachment prevented hyphal fusion in the mature colony and lead to 'chaotic' mycelial architecture in Δ*mik-1*, Δ*mek-1* and Δ*mak-1*
    - the inability of the wt to rescue the fusion defect of gene deletion mutants indicated that the process relies on signal exchange between interacting individuals, and cannot be based on contact alone
    - the identification of a basal CAT formation rate in Δ*mak-1* germlings, which increases to wt levels upon re-introduction of MAK-1, lead to the classification of Δ*mak-1* as CAT homing mutant
- Generation of Δ*mak*-1 rescue strains which expressed either the native or inhibitable allele of *mak-1*. Important aspects of this work were:
    - full recovery of all phenotypic defects upon re-introduction of MAK-1-sGFP and MAK-1^{E104G}-sGFP
    - application of 1NM-PP1 to inhibitor-sensitive strains allowed chemical induction of the phenotype at will
- Detailed localization studies of MAK-1-sGFP during germination and CAT-mediated cell fusion. These studies showed that:
    - MAK-1 resided in the nucleus and cytoplasm but became clearly excluded from the nucleolus upon germination
    - this basal localization pattern did not change during GT growth or GT tip contact
    - recruitment of MAK-1 to CAT tips during homing, but massive accumulation to the putative fusion site upon tip contact
    - MAK-1 resided around the opening fusion pore, then dispersed upon successful fusion

  - inhibition of MAK-1 kinase activity prevented its apical recruitment and blocked CAT attachment when applied during the pre-contact stage, and blocked fusion pore formation when applied at the post-contact stage
  - thus, MAK-1 is involved in CAT homing and crucially important for cell attachment and fusion pore formation
  - accumulation of MAK-1 into cortical clusters was dependent on its own kinase activity, suggesting that it requires interaction with a phosphorylation target for its own recruitment
- Confirmation of the functional relationship between CWI signalling and the F-actin cytoskeleton. These studies showed that:
  - Δ*mak-1* cells are impaired in F-actin polarization, which is one likely explanation for the significant reduction in CAT formation
  - microtubules are not required for MAK-1 recruitment and cell fusion

5.6. References

1. **Aguilar, P. S., A. Engel, and P. Walter.** 2007. The plasma membrane proteins Prm1 and Fig1 ascertain fidelity of membrane fusion during yeast mating. Molecular Biology of the Cell **18:**547-556.

2. **Aguirre, J., M. Rios-Momberg, D. Hewitt, and W. Hansberg.** 2005. Reactive oxygen species and development in microbial eukaryotes. Trends in Microbiology **13:**111-118.

3. **Alonso-Monge, R., F. Navarro-Garcia, E. Roman, A. I. Negredo, B. Eisman, C. Nombela, and J. Pla.** 2003. The Hog1 mitogen-activated protein kinase is essential in the oxidative stress response and chlamydospore formation in *Candida albicans*. Eukaryotic Cell **2:**351-361.

4. **Arana, D. M., C. Nombela, R. Alonso-Monge, and J. Pla.** 2005. The Pbs2 MAP kinase kinase is essential for the oxidative-stress response in the fungal pathogen *Candida albicans*. Microbiology **151:**1033-1049.

5. **Atkinson, J., R. F. Epand, and R. M. Epand.** 2008. Tocopherols and tocotrienols in membranes: a critical review. Free Radical Biology and Medicine **44:**739-764.

6. **Bader, T., K. Schroppel, S. Bentink, N. Agabian, G. Kohler, and J. Morschhauser.** 2006. Role of calcineurin in stress resistance, morphogenesis, and virulence of a *Candida albicans* wild-type strain. Infection and Immunity **74:**4366-4369.

7. **Bahn, Y.-S., C. Xue, A. Idnurm, J. C. Rutherford, J. Heitman, and M. E. Cardenas.** 2007. Sensing the environment: lessons from fungi. Nature Reviews Microbiology **5:**57-69.

8. **Bermejo, C., E. Rodriguez, R. Garcia, J. M. Rodriguez-Pena, M. L. Rodriguez de la Concepcion, C. Rivas, P. Arias, C. Nombela, F. Posas, and J. Arroyo.** 2008. The sequential activation of the yeast HOG and SLT2 pathways is required for cell survival to cell wall stress. Molecular Biology of the Cell **19:**1113-1124.

9. **Birkaya, B., A. Maddi, J. Joshi, S. J. Free, and P. J. Cullen.** 2009. Role of the cell wall integrity and filamentous growth mitogen-activated protein kinase pathways in cell wall remodeling during filamentous growth. Eukaryotic Cell **8:**1118-1133.

10. **Bishop, A. C., C.-y. Kung, K. Shah, L. Witucki, K. M. Shokat, and Y. Liu.** 1999. Generation of monospecific nanomolar tyrosine kinase inhibitors via a chemical genetic approach. Journal of the American Chemical Society **121:**627-631.

11. **Bishop, A. C., J. A. Ubersax, D. T. Petsch, D. P. Matheos, N. S. Gray, J. Blethrow, E. Shimizu, J. Z. Tsien, P. G. Schultz, M. D. Rose, J. L. Wood, D. O. Morgan, and K. M. Shokat.** 2000. A chemical switch for inhibitor-sensitive alleles of any protein kinase. Nature **407:**395-401.

12. **Blankenship, J. R., and J. Heitman.** 2005. Calcineurin is required for *Candida albicans* to survive calcium ctress in serum. Infection and Immunity **73:**5767-5774.

13. **Borkovich, K. A., L. A. Alex, O. Yarden, M. Freitag, G. E. Turner, N. D. Read, S. Seiler, D. Bell-Pedersen, J. Paietta, N. Plesofsky, M. Plamann, M. Goodrich-Tanrikulu, U. Schulte, G. Mannhaupt, F. E. Nargang, A. Radford, C. Selitrennikoff, J. E. Galagan, J. C. Dunlap, J. J. Loros, D. Catcheside, H. Inoue, R. Aramayo, M. Polymenis, E. U. Selker, M. S. Sachs, G. A. Marzluf, I. Paulsen, R. Davis, D. J. Ebbole, A. Zelter, E. R. Kalkman, R. O'Rourke, F. Bowring, J. Yeadon, C. Ishii, K. Suzuki, W. Sakai, and R. Pratt.** 2004. Lessons from the genome sequence of *Neurospora crassa*: tracing the path from genomic blueprint to multicellular organism. Microbiological and Molecular Biological Reviews **68:**1-108.

14. **Branduardi, P., T. Fossati, M. Sauer, R. Pagani, D. Mattanovich, and D. Porro.** 2007. Biosynthesis of Vitamin C by yeast leads to increased stress resistance. PLoS ONE **2:**e1092.

15. **Brown, A. J. P., K. Haynes, and J. Quinn.** 2009. Nitrosative and oxidative stress responses in fungal pathogenicity. Current Opinion in Microbiology **12:**384-391.

16. **Buehrer, B. M., and B. Errede.** 1997. Coordination of the mating and cell integrity mitogen-activated protein kinase pathways in *Saccharomyces cerevisiae*. Molecular and Cellular Biology **17:**6517-6525.

17. **Changwei, Z., X. Mingyong, and W. Ranran.** 2007. Afr1p has a role in regulating the localization of Mpk1p at the shmoo tip in *Saccharomyces cerevisiae*. FEBS Letters **581:**2670-2674.

18. **Chen, E. H., E. Grote, W. Mohler, and A. Vignery.** 2007. Cell-cell fusion. FEBS Letters **581:**2181-2193.

19. **Chen, R. E., and J. Thorner.** 2007. Function and regulation in MAPK signaling pathways: lessons learned from the yeast *Saccharomyces cerevisiae*. Biochimica et Biophysica Acta - Molecular Cell Research **1773:**1311-1340.

20. **Claret, S., X. Gatti, F. Doignon, D. Thoraval, and M. Crouzet.** 2005. The Rgd1p Rho GTPase-activating protein and the Mid2p cell wall sensor are required at low pH for protein kinase C pathway activation and cell survival in *Saccharomyces cerevisiae*. Eukaryotic Cell **4:**1375-1386.

21. **Cobb, M. H., and E. J. Goldsmith.** 1995. How MAP kinases are regulated. Journal of Biological Chemistry **270:**14843-14846.

22. **Colot, H. V., G. Park, G. E. Turner, C. Ringelberg, C. M. Crew, L. Litvinkova, R. L. Weiss, K. A. Borkovich, and J. C. Dunlap.** 2006. A high-throughput gene knockout procedure for *Neurospora* reveals functions for multiple transcription factors. Proceedings of the National Academy of Sciences of the USA **103:**10352-10357.

23. **Costigan, C., S. Gehrung, and M. Snyder.** 1992. A synthetic lethal screen identifies SLK1, a novel protein kinase homolog implicated in yeast cell morphogenesis and cell growth. Molecular and Cellular Biology **12:**1162-1178.

24. **Crespo, J. L., and M. N. Hall.** 2002. Elucidating TOR signaling and rapamycin action: lessons from *Saccharomyces cerevisiae*. Microbiology and Molecular Biology Reviews **66:**579-591.

25. **Cross, F.** 1988. Conjugation in *Saccharomyces cerevisiae*. Annual Review in Cell Biology **4:**429-457.

26. **Cruz, M. C., A. L. Goldstein, J. Blankenship, M. Del Poeta, J. R. Perfect, J. H. McCusker, Y. L. Bennani, M. E. Cardenas, and J. Heitman.** 2001. Rapamycin and less immunosuppressive analogs are toxic to *Candida albicans* and *Cryptococcus neoformans* via FKBP12-dependent inhibition of TOR. Antimicrobial Agents and Chemotherapy **45:**3162-3170.

27. **Cruz, M. C., A. L. Goldstein, J. R. Blankenship, M. Del Poeta, D. Davis, M. E. Cardenas, J. R. Perfect, J. H. McCusker, and J. Heitman.** 2002. Calcineurin is essential for survival during membrane stress in *Candida albicans*. EMBO J **21:**546-559.

28. **Cyert, M. S.** 2003. Calcineurin signaling in *Saccharomyces cerevisiae*: how yeast go crazy in response to stress. Biochemical and Biophysical Research Communications **311:**1143-1150.

29. **Dan, I., N. M. Watanabe, and A. Kusumi.** 2001. The Ste20 group kinases as regulators of MAP kinase cascades. Trends in Cell Biology **11:**220-230.

30. **Darken, M. A.** 1961. Applications of fluorescent brighteners in biological techniques. Science **133:**1704-1705.

31. **De Bettignies, G., D. Thoraval, C. Morel, M. F. Peypouquet, and M. Crouzet.** 2001. Overactivation of the protein kinase C-signaling pathway suppresses the defects of cells lacking the Rho3/Rho4-GAP Rgd1p in *Saccharomyces cerevisiae*. Genetics **159:**1435-1448.

32. **de Nobel, H., C. Ruiz, H. Martin, W. Morris, S. Brul, M. Molina, and F. M. Klis.** 2000. Cell wall perturbation in yeast results in dual phosphorylation of the Slt2/Mpk1 MAP kinase and in an Slt2-mediated increase in FKS2-lacZ expression, glucanase resistance and thermotolerance. Microbiology **146:**2121-2132.

33. **de Nobel, H., H. van den Ende, and F. M. Klis.** 2000. Cell wall maintenance in fungi. Trends in Microbiology **8:**344-345.

34. **Delley, P.-A., and M. N. Hall.** 1999. Cell wall stress depolarizes cell growth via hyperactivation of Rho1. Journal of Cell Biology **147:**163-174.

35. **Dohlman, H. G., and J. W. Thorner.** 2001. Regulation of G-protein-initiated signal transduction in yeast: paradigms and principles. Annual Review of Biochemistry **70:**703-754.

36. **Drgonova, J., T. Drgon, K. Tanaka, R. Kollar, G.-C. Chen, R. A. Ford, C. S. M. Chan, Y. Takai, and E. Cabib.** 1996. *Rho1*p, a yeast protein at the interface between cell polarization and morphogenesis. Science **272:**277-279.

37. **Dupres, V., D. Alsteens, S. Wilk, B. Hansen, J. J. Heinisch, and Y. F. Dufrene.** 2009. The yeast Wsc1 cell surface sensor behaves like a nanospring *in vivo*. Nature Chemical Biology **5:**857-862.

38. **Elion, E. A.** 2000. Pheromone response, mating and cell biology. Current Opinion in Microbiology **3:**573-581.

39. **Fitch, P. G., A. E. Gammie, D. J. Lee, V. Brizzio de Candal, and M. D. Rose.** 2004. Lrg1p is a Rho1 GTPase-activating protein required for efficient cell fusion in yeast. Genetics **168:**733-746.

40. **Fleißner, A., A. C. Leeder, M. G. Roca, N. D. Read, and N. L. Glass.** 2009. Oscillatory recruitment of signaling proteins to cell tips promotes coordinated behaviour during cell fusion Proceedings of the National Academy of Sciences of the USA **106:**19387–19392.

41. **Freitag, M., P. C. Hickey, N. B. Raju, E. U. Selker, and N. D. Read.** 2004. GFP as a tool to analyze the organization, dynamics and function of nuclei and microtubules in *Neurospora crassa*. Fungal Genetics and Biology **41:**897-910.

42. **Fuchs, B. B., and E. Mylonakis.** 2009. Our paths might cross: the role of the fungal cell wall integrity pathway in stress response and cross talk with other stress response pathways. Eukaryotic Cell **8:**1616-1625.

43. **Fujioka, T., O. Mizutani, K. Furukawa, N. Sato, A. Yoshimi, Y. Yamagata, T. Nakajima, and K. Abe.** 2007. MpkA-dependent and -independent cell wall integrity signaling in *Aspergillus nidulans*. Eukaryotic Cell **6:**1497-1510.

44. **Furukawa, K., Y. Hoshi, T. Maeda, T. Nakajima, and K. Abe.** 2005. *Aspergillus nidulans* HOG pathway is activated only by two-component signalling pathway in response to osmotic stress. Molecular Microbiology **56:**1246-1261.

45. **Galagan, J. E., S. E. Calvo, K. A. Borkovich, E. U. Selker, N. D. Read, D. Jaffe, W. FitzHugh, L.-J. Ma, S. Smirnov, S. Purcell, B. Rehman, T. Elkins, R. Engels, S. Wang, C. B. Nielsen, J. Butler, M. Endrizzi, D. Qui, P. Ianakiev, D. Bell-Pedersen, M. A. Nelson, M. Werner-Washburne, C. P. Selitrennikoff, J. A. Kinsey, E. L. Braun, A. Zelter, U. Schulte, G. O. Kothe, G. Jedd, W. Mewes, C. Staben, E. Marcotte, D. Greenberg, A. Roy, K. Foley, J. Naylor, N. Stange-Thomann, R. Barrett, S. Gnerre, M. Kamal, M. Kamvysselis, E. Mauceli, C. Bielke, S. Rudd, D. Frishman, S. Krystofova, C. Rasmussen, R. L. Metzenberg, D. D. Perkins, S. Kroken, C. Cogoni, G. Macino, D. Catcheside, W. Li, R. J. Pratt, S. A. Osmani, C. P. C. DeSouza, L. Glass, M. J. Orbach, J. A. Berglund, R. Voelker, O. Yarden, M. Plamann, S. Seiler, J. Dunlap, A. Radford, R. Aramayo, D. O. Natvig, L. A. Alex, G. Mannhaupt, D. J. Ebbole, M. Freitag, I. Paulsen, M. S. Sachs, E. S. Lander, C. Nusbaum, and B. Birren.** 2003. The genome sequence of the filamentous fungus *Neurospora crassa*. Nature **422:**859-868.

46. **Garcia, R., J. M. Rodriguez-Pena, C. Bermejo, C. Nombela, and J. Arroyo.** 2009. The high osmotic response and cell wall integrity pathways cooperate to regulate transcriptional responses to Zymolyase-induced cell wall stress in *Saccharomyces cerevisiae*. Journal of Biological Chemistry **284:**10901-10911.

47. **Garrett-Engele, P., B. Moilanen, and M. S. Cyert.** 1995. Calcineurin, the Ca2+/calmodulin-dependent protein phosphatase, is essential in yeast mutants with cell integrity defects and in mutants that lack a functional vacuolar H(+)-ATPase. Molecular and Cellular Biology **15:**4103-4114.

48. **Gatti, X., G. de Bettignies, S. Claret, F. Doignon, M. Crouzet, and D. Thoraval.** 2005. RGD1, encoding a RhoGAP involved in low-pH survival, is an Msn2p/Msn4p regulated gene in *Saccharomyces cerevisiae*. Gene **351:**159-169.

49. **Gerik, K. J., M. J. Donlin, C. E. Soto, A. M. Banks, I. R. Banks, M. A. Maligie, C. P. Selitrennikoff, and J. K. Lodge.** 2005. Cell wall integrity is dependent on the *PKC1* signal transduction pathway in *Cryptococcus neoformans*. Molecular Microbiology **58:**393-408.

50. **Glass, N. L., and A. Fleißner.** 2006. Re-wiring the network: understanding the mechnanism and function of anastomosis in filamentous ascomycete fungi, p. 123-135. *In* U. Kües and R. Fischer (ed.), The Mycota, vol. 1. Springer-Verlag, Berlin Heidelberg.

51. **Guo, S., X. Shen, G. Yan, D. Ma, X. Bai, S. Li, and Y. Jiang.** 2009. A MAP kinase dependent feedback mechanism controls Rho1 GTPase and actin distribution in yeast. PLoS ONE **4:**e6089.

52. **Gustin, M. C., J. Albertyn, M. Alexander, and K. Davenport.** 1998. MAP kinase pathways in the yeast *Saccharomyces cerevisiae*. Microbiology and Molecular Biology Reviews **62:**1264-1300.

53. **Hahn, J.-S., and D. J. Thiele.** 2002. Regulation of the *Saccharomyces cerevisiae* Slt2 kinase pathway by the stress-inducible Sdp1 dual specificity phosphatase. Journal of Biological Chemistry **277:**21278-21284.

54. **Hancock, J., R. Desikan, J. Harrison, J. Bright, R. Hooley, and S. Neill.** 2006. Doing the unexpected: proteins involved in hydrogen peroxide perception. Journal of Experimantal Botany **57:**1711-1718.

55. **Hancock, J. T.** 2008. The role of redox in signal transduction, p. 1-9. *In* J. Hancock (ed.), Redox-Mediated Signal Transduction, Methods and Protocols. Humana Press, New York.

56. **Harrison, J. C., E. S. G. Bardes, Y. Ohya, and D. J. Lew.** 2001. A role for the Pkc1p/Mpk1p kinase cascade in the morphogenesis checkpoint. Nature Cell Biology **3:**417-420.

57. **Harrison, J. C., T. R. Zyla, E. S. G. Bardes, and D. J. Lew.** 2004. Stress-specific activation mechanisms for the "cell integrity" MAPK pathway. Journal of Biological Chemistry **279:**2616-2622.

58. **Hawle, P., D. Horst, J. P. Bebelman, X. X. Yang, M. Siderius, and S. M. van der Vies.** 2007. Cdc37p is required for stress-induced high-osmolarity glycerol and protein kinase C mitogen-activated protein kinase pathway functionality by interaction with Hog1p and Slt2p (Mpk1p). Eukaryotic Cell **6:**521-532.

59. **Helliwell, S. B., I. Howald, N. Barbet, and M. N. Hall.** 1998. TOR2 is part of two related signaling pathways coordinating cell growth in *Saccharomyces cerevisiae*. Genetics **148:**99-112.

60. **Helliwell, S. B., A. Schmidt, Y. Ohya, and M. N. Hall.** 1998. The Rho1 effector Pkc1, but not Bni1, mediates signalling from Tor2 to the actin cytoskeleton. **8:**1211-S2.

61. **Hilioti, Z., and K. W. Cunningham.** 2003. The RCN family of calcineurin regulators. Biochemical and Biophysical Research Communications **311:**1089-1093.

62. **Hilioti, Z., D. A. Gallagher, S. T. Low-Nam, P. Ramaswamy, P. Gajer, T. J. Kingsbury, C. J. Birchwood, A. Levchenko, and K. W. Cunningham.** 2004. GSK-3 kinases enhance calcineurin signaling by phosphorylation of RCNs. Genes & Development **18:**35-47.

63. **Hilioti, Z., W. Sabbagh, S. Paliwal, A. Bergmann, M. D. Goncalves, L. Bardwell, and A. Levchenko.** 2008. Oscillatory phosphorylation of yeast Fus3 MAP kinase activity through a reaction-diffusion mechanism in yeast pheromone signalling. Current Biology **18:**1700-1706.

64. **Hirata, H., S. Yoshiura, T. Ohtsuka, Y. Bessho, T. Harada, K. Yoshikawa, and R. Kageyama.** 2002. Oscillatory expression of the bHLH factor Hes1 regulated by a negative feedback loop. Science **298:**840-843.

65. **Hoch, H. C., C. D. Galvani, D. H. Szarowski, and J. N. Turner.** 2005. Two new fluorescent dyes applicable for visualization of fungal cell walls. Mycologia **97:**580-588.

66. **Ichinomiya, M., H. Uchida, Y. Koshi, A. Ohta, and H. Horiuchi.** 2007. A protein kinase C-encoding gene, *pkcA*, is essential to the viability of the filamentous fungus *Aspergillus nidulans*. Bioscience, Biotechnology, and Biochemistry **71:**2787-2799.

67. **Jacquet, M., G. Renault, S. Lallet, J. De Mey, and A. Goldbeter.** 2003. Oscillatory nucleocytoplasmic shuttling of the general stress response transcriptional activators Msn2 and Msn4 in *Saccharomyces cerevisiae*. Journal of Cell Biology **161:**497-505.

68. **Jeon, J., J. Goh, S. Yoo, M.-H. Chi, J. Choi, H.-S. Rho, J. Park, S.-S. Han, B. R. Kim, S.-Y. Park, S. Kim, and Y.-H. Lee.** 2008. A putative MAP kinase kinase kinase, MCK1, is required for cell wall integrity and pathogenicity of the rice blast fungus, *Magnaporthe oryzae*. Molecular Plant-Microbe Interactions **21:**525-534.

69. **Jung, U. S., and D. Levin, E. .** 1999. Genome-wide analysis of gene expression regulated by the yeast cell wall integrity signalling pathway. Molecular Microbiology **34:**1049-1057.

70. **Kamada, Y., U. S. Jung, J. Piotrowski, and D. E. Levin.** 1995. The protein kinase C-activated MAP kinase pathway of *Saccharomyces cerevisiae* mediates a novel aspect of the heat shock response. Genes & Development **9:**1559-1571.

71. **Kamada, Y., H. Qadota, C. P. Python, Y. Anraku, Y. Ohya, and D. E. Levin.** 1996. Activation of yeast protein kinase C by Rho1 GTPase. Journal of Biological Chemistry **271:**9193-9196.

72. **Kapteyn, J. C., H. Van Den Ende, and F. M. Klis.** 1999. The contribution of cell wall proteins to the organization of the yeast cell wall. Biochimica et Biophysica Acta **1426:**373-383.

73. **Karababa, M., E. Valentino, G. Pardini, A. T. Coste, J. Bille, and D. Sanglard.** 2006. *CRZ1*, a target of the calcineurin pathway in *Candida albicans*. Molecular Microbiology **59:**1429-1451.

74. **Katayama, S., D. Hirata, M. Arellano, P. Perez, and T. Toda.** 1999. Fission yeast alpha-glucan synthase Mok1 requires the actin cytoskeleton to localize the sites of growth and plays an essential role in cell morphogenesis downstream of protein kinase C function. Journal of Cell Biology **144:**1173-1186.

75. **Ketela, T., R. Green, and H. Bussey.** 1999. *Saccharomyces cerevisiae* Mid2p is a potential cell wall stress sensor and upstream activator of the PKC1-MPK1 cell integrity pathway. Journal of Bacteriology **181:**3330-3340.

76. **Kim, H., and K. A. Borkovich.** 2004. A pheromone receptor gene, *pre-1*, is essential for mating type-specific directional growth and fusion of trichogynes and female fertility in *Neurospora crassa*. Molecular Microbiology **52:**1781-1798.

77. **Kingsbury, T. J., and K. W. Cunningham.** 2000. A conserved family of calcineurin regulators. Genes and Development **14:**1595-1604.

78. **Kojima, K., T. Kikuchi, Y. Takano, E. Oshiro, and T. Okuno.** 2002. The mitogen-activated protein kinase gene MAF1 is essential for the early differentiation phase of appressorium formation in *Colletotrichum lagenarium*. Molecular Plant-Microbe Interactions **15:**1268-1276.

79. **Krasley, E., K. F. Cooper, M. J. Mallory, R. Dunbrack, and R. Strich.** 2006. Regulation of the oxidative stress response through Slt2p-dependent destruction of cyclin C in *Saccharomyces cerevisiae*. Genetics **172:**1477-1486.

80. **Kraus, P. R., D. S. Fox, G. M. Cox, and J. Heitman.** 2003. The *Cryptococcus neoformans* MAP kinase Mpk1 regulates cell integrity in response to antifungal drugs and loss of calcineurin function. Molecular Microbiology **48:**1377-1387.

81. **Krishna, M., and H. Narang.** 2008. The complexity of mitogen-activated protein kinases (MAPKs) made simple. Cellular and Molecular Life Sciences **65:**3525-3544.

82. **Ladds, G., A. Goddard, and J. Davey.** 2005. Functional analysis of heterologous GPCR signalling pathways in yeast. Trends in Biotechnology **23:**367-373.

83. **Lamson, R. E., M. J. Winters, and P. M. Pryciak.** 2002. Cdc42 regulation of kinase activity and signaling by the yeast p21-activated kinase Ste20. Molecular and Cellular Biology **22:**2939-2951.

84. **Leeuw, T., C. Wu, J. D. Schrag, M. Whiteway, D. Y. Thomas, and E. Leberer.** 1998. Interaction of a G-protein beta-subunit with a conserved sequence in Ste20/PAK family protein kinases. Nature **391:**191-195.

85. **Lengeler, K. B., R. C. Davidson, C. D'Souza, T. Harashima, W.-C. Shen, P. Wang, X. Pan, M. Waugh, and J. Heitman.** 2000. Signal transduction cascade regulating fungal development and virulence. Microbiology and Molecular Biology Reviews **64:**746-785.

86. **Lev Bar-Or, R., R. Maya, L. A. Segel, U. Alon, A. J. Levin, and M. Oren.** 2000. Generation of oscillations by teh p53-Mdm2 feedback loop: a theoretical and experimental study. Proceedings of the National Academy of Sciences of the USA **97**.

87. **Lev, S., H. Tal, M. S. Rose, and B. A. Horwitz.** 2009. Signaling by the pathogenicity-related MAP kinase of *Cochliobolus heterostrophus* correlates with its local accumulation rather than phosphorylation. Molecular Plant-Microbe Interactions **22:**1093-1103.

88. **Levin, D. E.** 2005. Cell wall integrity signaling in *Saccharomyces cerevisiae*. Microbioloy and Molecular Biology Reviews **69:**262-291.

89. **Levin, D. E., and E. Bartlett-Heubusch.** 1992. Mutants in the *S. cerevisiae* PKC1 gene display a cell cycle-specific osmotic stability defect. Journal of Cell Biology **116:**1221-1229.

90. **Levin, D. E., B. Bowers, C. Chen, Y. Kamada, and M. Watanabe.** 1994. Dissecting the protein kinase C/MAP kinase signalling pathway of *Saccharomyces cerevisiae*. Cellular and Molecular Biology Research **40:**229-239.

91. **Levin, D. E., and B. Errede.** 1995. The proliferation of MAP kinase signaling pathways in yeast. Current Opinion in Cell Biology **7:**197-202.

92. **Levin, D. E., F. O. Fields, R. Kunisawa, J. M. Bishop, and J. Thorner.** 1990. A candidate protein kinase C gene, *PKC1*, is required for the *S. cerevisiae* cell cycle. Cell **62:**213-224.

93. **Lew, R. R., Z. Abbas, M. I. Anderca, and S. J. Free.** 2008. Phenotype of a mechanosensitive channel mutant, *mid-1*, in a filamentous fungus, *Neurospora crassa*. Eukaryotic Cell **7:**647-655.

94. **Li, D., P. Bobrowicz, H. H. Wilkinson, and D. J. Ebbole.** 2005. A mitogen-activated protein kinase pathway essential for mating and contributing to vegetative growth in *Neurospora crassa*. Genetics **170:**1091-1104.

95. **Li, L., S. J. Wright, S. Krystofova, G. Park, and K. Borkovich.** 2006. Heterotrimeric G protein signaling in filamentous fungi. Annual Review of Microbiology.

96. **Locke, E. G., M. Bonilla, L. Liang, Y. Takita, and K. W. Cunningham.** 2000. A homolog of voltage-gated Ca^{2+} channels stimulated by depletion of secretory Ca^{2+} in yeast. Molecular and Cellular Biology **20:**6686-6694.

97. **Maeder, C. I., M. A. Hink, A. Kinkhabwala, R. Mayr, P. I. H. Bastiaens, and M. Knop.** 2007. Spatial regulation of Fus3 MAP kinase activity through a reaction-diffusion mechanism in yeast pheromone signalling. Nature Cell Biology **9:**1319-1326.

98. **Maerz, S., C. Ziv, N. Vogt, K. Helmstaedt, N. Cohen, R. Gorovits, O. Yarden, and S. Seiler.** 2008. The nuclear Dbf2-related kinase COT1 and the mitogen-activated protein kinases MAK1 and MAK2 genetically interact to regulate filamentous growth, hyphal fusion and sexual development in *Neurospora crassa*. Genetics **179:**1313-1325.

99. **Martín, H., J. M. Rodríguez-Pachón, C. Ruiz, C. Nombela, and M. Molina.** 2000. Regulatory mechanisms for modulation of signaling through the cell integrity Slt2-mediated pathway in *Saccharomyces cerevisiae*. Journal of Biological Chemistry **275:**1511-1519.

100. **Mattison, C. P., S. S. Spencer, K. A. Kresge, J. Lee, and I. M. Ota.** 1999. Differential regulation of the cell wall integrity mitogen-activated protein kinase pathway in budding yeast by the protein tyrosine phosphatases Ptp2 and Ptp3. Molecular and Cellular Biology **19:**7651-7660.

101. **Mazur, P., N. Morin, W. Baginsky, M. el-Sherbeini, J. A. Clemas, J. B. Nielsen, and F. Foor.** 1995. Differential expression and function of two homologous subunits of yeast 1,3-beta-D-glucan synthase. Molecular and Cellular Biology **15:**5671-5681.

102. **Mazzoni, C., P. Zarov, A. Rambourg, and C. Mann.** 1993. The SLT2 (MPK1) MAP kinase homolog is involved in polarized cell growth in *Saccharomyces cerevisiae*. Journal of Cell Biology **123:**1821-1833.

103. **Mehrabi, R., S. Ding, and J.-R. Xu.** 2008. MADS-box transcription factor Mig1 is required for infectious growth in *Magnaporthe grisea*. Eukaryotic Cell **7:**791-799.

104. **Mellor, H., and P. J. Parker.** 1998. The extended protein kinase C superfamily. Biochemical Journal **332:**281-292.

105. **Moore, T. I., C.-S. Chou, Q. Nie, N. L. Jeon, and T.-M. Yi.** 2008. Robust spatial sensing of mating pheromone gradients by yeast cells. PLoS ONE **3:**e3865.

106. **Muller, E. M., N. A. Mackin, S. E. Erdman, and K. W. Cunningham.** 2003. Fig1p facilitates Ca^{2+} influx and cell fusion during mating of *Saccharomyces cerevisiae*. Journal of Biological Chemistry **278:**38461-38469.

107. **Navarro-Garcia, F., R. Alonso-Monge, H. Rico, J. Pla, R. Sentandreu, and C. Nombela.** 1998. A role for the MAP kinase gene MKC1 in cell wall construction and morphological transitions in *Candida albicans*. Microbiology **144:**411-424.

108. **Navarro-Garcia, F., B. Eisman, S. M. Fiuza, C. Nombela, and J. Pla.** 2005. The MAP kinase Mkc1p is activated under different stress conditions in *Candida albicans*. Microbiology **151:**2737-2749.

109. **Noguchi, R., S. Banno, R. Ichikawa, F. Fukumori, A. Ichiishi, M. Kimura, I. Yamaguchi, and M. Fujimura.** 2007. Identification of OS-2 MAP kinase-dependent genes induced in response to osmotic stress, antifungal agent fludioxonil, and heat shock in *Neurospora crassa*. Fungal Genetics and Biology **44:**208.

110. **Nonaka, H., K. Tanaka, H. Hirano, T. Fujiwara, H. Kohono, M. Umikawa, A. Mino, and Y. Takai.** 1995. A downstream target of RHO1 small GTP-binding protein is PKC1, a homolog of protein kinase C, which leads to activation of the MAP kinase cascade in *Saccharomyces cerevisiae*. EMBO Journal **14:**5931-5938.

111. **Onyewu, C., F. L. Wormley, Jr., J. R. Perfect, and J. Heitman.** 2004. The calcineurin target, Crz1, functions in azole tolerance but Is not required for virulence of *Candida albicans*. Infection and Immunity **72:**7330-7333.

112. **Otsubo, Y., and M. Yamamato.** 2008. TOR signaling in fission yeast. Critical Reviews in Biochemistry and Molecular Biology **43:**277-283.

113. **Pall, M. L., and J. P. Brunelli.** 1994. New plasmid and plasmid hybrid vectors and a Neurospora crassa genomic library containing the bar selectable marker and Cre/lox site-specific recombination system for use in filamentous fungi. Fungal Genetics Newsletter **41:**63-65.

114. **Pandey, A., G. M. Roca, N. D. Read, and N. L. Glass.** 2004. Role of a mitogen-activated protein kinase pathway during conidial germination and hyphal fusion in *Neurospora crassa*. Eukaryotic Cell **3:**348-358.

115. **Paravicini, G., M. Cooper, L. Friedli, D. J. Smith, J. L. Carpentier, L. S. Klig, and M. A. Payton.** 1992. The osmotic integrity of the yeast cell requires a functional PKC1 gene product. Molecular and Cellular Biology **12:**4896-4905.

116. **Park, G., S. Pan, and K. A. Borkovich.** 2008. Mitogen-activated protein kinase cascade required for regulation of development and secondary metabolism in *Neurospora crassa*. Eukaryotic Cell **7:**2113-2122.

117. **Paul, A., S. Wilson, C. M. Belham, C. J. M. Robinson, S. P. H., G. W. Gould, and R. Pelvin.** 1997. Stress-activated protein kinases: activation, regulation and function. Cellular Signaling **9:**403-410.

118. **Peñalva, M. A., J. Tilburn, E. Bignell, and H. N. Arst Jr.** 2008. Ambient pH gene regulation in fungi: making connections. Trends in Microbiology **16:**291-300.

119. **Penas, M. M., A. Hervas-Aguilar, T. Munera-Huertas, E. Reoyo, M. A. Penalva, H. N. Arst, Jr., and J. Tilburn.** 2007. Further characterization of the signaling proteolysis step in the *Aspergillus nidulans* pH signal transduction pathway. Eukaryotic Cell **6:**960-970.

120. **Perez, P., and T. M. Calonge.** 2002. Yeast protein kinase C. Journal of Biochemistry **132:**513-517.

121. **Peter, M., A. M. Neiman, H. O. Park, M. van Lohuizen, and I. Herskowitz.** 1996. Functional analysis of the interaction between the small GTP binding protein Cdc42 and the Ste20 protein kinase in yeast. The EMBO Journal **15:**7046-7059.

122. **Philip, B., and D. E. Levin.** 2001. Wsc1 and Mid2 are cell surface sensors for cell wall integrity signaling that act through Rom2, a guanine nucleotide exchange factor for Rho1. Molecular and Cellular Biology **21:**271-280.

123. **Pitoniak, A., B. Birkaya, H. M. Dionne, N. Vadaie, and P. J. Cullen.** 2009. The signaling mucins Msb2 and Hkr1 differentially regulate the filamentation mitogen-activated protein kinase pathway and contribute to a multimodal response. Molecular Biology of the Cell **20:**3101-3114.

124. **Popolo, L., D. Gilardelli, P. Bonfante, and M. Vai.** 1997. Increase in chitin as an essential response to defects in assembly of cell wall polymers in the *ggp1*delta mutant of *Saccharomyces cerevisiae*. Journal of Bacteriology **179:**463-469.

125. **Posas, F., M. Takekawa, and H. Saito.** 1998. Signal transduction by MAP kinase cascades in budding yeast. Current Opinion in Microbiology **1:**175-182.

126. **Qadota, H., C. P. Python, S. B. Inoue, M. Arisawa, Y. Anraku, Y. Zheng, T. Watanabe, D. E. Levin, and Y. Ohya.** 1996. Identification of yeast *Rho1*p GTPase as a regulatory subunit of 1,3-beta-glucan synthase. Science **272:**279-281.

127. **Qi, M., and E. A. Elion.** 2005. MAP kinase pathways. Journal of Cell Science **118:**3569-3572.

128. **Raitt, D. C., F. Posas, and H. Saito.** 2000. Yeast Cdc42 GTPase and Ste20 PAK-like kinase regulate Sho1-dependent activation of the Hog1 MAPK pathway. EMBO J **19:**4623-4631.

129. **Ram, A. F. J., J. C. Kapteyn, R. C. Montijn, L. H. P. Caro, J. E. Douwes, W. Baginsky, P. Mazur, H. van den Ende, and F. M. Klis.** 1998. Loss of the plasma membrane-bound protein Gas1p in *Saccharomyces cerevisiae* results in the release of beta 1,3-glucan into the medium and induces a compensation mechanism to ensure cell wall integrity. Journal of Bacteriology **180:**1418-1424.

130. **Raught, B., A.-C. Gingras, and N. Sonenberg.** 2001. The target of rapamycin (TOR) proteins. Proceedings of the National Academy of Sciences of the USA **98:**7037-7044.

131. **Read, N. D., A. Fleißner, M. G. Roca, and N. L. Glass.** 2010. Hyphal fusion. *In* K. A. Borkovich and D. Ebbole (ed.), Cellular and Molecular Biology of Filamentous Fungi. American Society of Microbiology, Washington DC.

132. **Read, N. D., A. Lichius, J. Shoji, and A. B. Goryachev.** 2009. Self-signalling and self-fusion in filamentous fungi. Current Opinion in Microbiology **12:**608-615.

133. **Reedy, J. L., S. G. Filler, and J. Heitman.** 2009. Elucidating the *Candida albicans* calcineurin signaling cascade controlling stress response and virulence. Fungal Genetics and Biology **In Press, Corrected Proof**.

134. **Rispail, N., D. M. Soanes, C. Ant, R. Czajkowski, A. Grünler, R. Huguet, E. Perez-Nadales, A. Poli, E. Sartorel, V. Valiante, M. Yang, R. Beffa, A. A. Brakhage, N. A. R. Gow, R. Kahmann, M.-H. Lebrun, H. Lenasi, J. Perez-Martin, N. J. Talbot, J. Wendland, and A. Di Pietro.** 2009. Comparative genomics of MAP kinase and calcium-calcineurin signalling components in plant and human pathogenic fungi. Fungal Genetics and Biology **46:**287-298.

135. **Roca, G. M., J. Arlt, C. E. Jeffree, and N. D. Read.** 2005. Cell biology of conidial anastomosis tubes in *Neurospora crassa*. Eukaryotic Cell **4:**911-919.

136. **Roca, G. M., N. D. Read, and A. E. Wheals.** 2005. Conidial anastomosis tubes in filamentous fungi. FEMS Microbiological Letters **249:**191-198.

137. **Roman, E., C. Nombela, and J. Pla.** 2005. The Sho1 adaptor protein links oxidative stress to morphogenesis and cell wall biosynthesis in the fungal pathogen *Candida albicans*. Molecular and Cellular Biology **25:**10611-10627.

138. **Ronen, R., H. Sharon, E. Levdansky, J. Romano, Y. Shadkchan, and N. Osherov.** 2007. The *Aspergillus nidulans* pkcA gene is involved in polarized growth, morphogenesis and maintenance of cell wall integrity. Current Genetics **51:**321-329.

139. **Sanglard, D., F. Ischer, O. Marchetti, J. Entenza, and J. Bille.** 2003. Calcineurin A of *Candida albicans*: involvement in antifungal tolerance, cell morphogenesis and virulence. Molecular Microbiology **48:**959-976.

140. **Schmidt, A., J. Kunz, and M. N. Hall.** 1996. TOR2 is required for organization of the actin cytoskeleton in yeast. Proceedings of the National Academy of Sciences of the USA **93:**13780-13785.

141. **Serrano, R., H. Martin, A. Casamayor, and J. Arino.** 2006. Signaling alkaline pH stress in the yeast *Saccharomyces cerevisiae* through the Wsc1 cell surface sensor and the Slt2 MAPK pathway. Journal of Biological Chemistry **281:**39785-39795.

142. **Singh, K. K.** 2000. The *Saccharomyces cerevisiae* Sln1p-Ssk1p two-component system mediates response to oxidative stress and in an oxidant-specific fashion. Free Radical Biology and Medicine **29:**1043-1050.

143. **Slaughter, B. D., J. W. Schwartz, and R. Li.** 2007. Mapping dynamic protein interactions in MAP kinase signaling using live-cell fluorescence fluctuation spectroscopy and imaging. Proceedings of the National Academy of Sciences of the USA **104:**20320-20325.

144. **Smits, G. J., J. C. Kapteyn, H. van den Ende, and F. M. Klis.** 1999. Cell wall dynamics in yeast. Current Opinion in Microbiology **2:**348-352.

145. **Squina, F., J. Leal, V. Cipriano, N. Martinez-Rossi, and A. Rossi.** 2010. Transcription of the *Neurospora crassa* 70-kDa class heat shock protein genes is modulated in response to extracellular pH changes. Cell Stress and Chaperones **15:**225-231.

146. **Stie, J., and D. Fox.** 2008. Calcineurin regulation in fungi and beyond. Eukaryotic Cell **7:**177-186.

147. **Tan, S.-X., D. Greetham, S. Raeth, C. M. Grant, I. W. Dawes, and G. G. Perrone.** 2009. The thioredoxin-thioredoxin reductase system can function in vivo as an alternative system to reduce oxidized glutathione in *Saccharomyces cerevisiae*. Journal of Biological Chemistry**:**-.

148. **Tatebayashi, K., K. Yamamoto, K. Tanaka, T. Tomida, T. Maruoka, E. Kasukawa, and H. Saito.** 2006. Adaptor functions of Cdc42, Ste50, and Sho1 in the yeast osmoregulatory HOG MAPK pathway. EMBO Journal **25:**3033-3044.

149. **Thompson, S., N. J. Croft, A. Sotiriou, H. D. Piggins, and S. K. Crosthwaite.** 2008. *Neurospora crassa* heat shock factor-1 is an essential gene; a second heat shock factor-like gene, *hsf-2*, is required for asexual spore formation. Eukaryotic Cell **7:**1573-1581.

150. **Torres, J., C. J. Di Como, E. Herrero, and M. A. de la Torre-Ruiz.** 2002. Regulation of the cell integrity pathway by rapamycin-sensitive TOR function in budding yeast. Journal of Biological Chemistry **277:**43495-43504.

151. **Truman, A. W., S. H. Millson, J. M. Nuttall, M. Mollapour, C. Prodromou, and P. W. Piper.** 2007. In the yeast heat shock response, Hsf1-directed induction of Hsp90 facilitates the activation of the Slt2 (Mpk1) mitogen-activated protein kinase required for cell integrity. Eukaryotic Cell **6:**744-752.

152. **Valiante, V., T. Heinekamp, R. Jain, A. Härtl, and A. A. Brakhage.** 2008. The mitogen-activated protein kinase MpkA of *Aspergillus fumigatus* regulates cell wall signaling and oxidative stress response. Fungal Genetics and Biology **45:**618-627.

153. **Vallier, L. G., J. E. Segall, and M. Snyder.** 2002. The alpha-factor receptor C-terminus is important for mating projection formation and orientation in *Saccharomyces cerevisiae*. Cell Motility and the Cytoskeleton **53:**251-266.

154. **van Drogen, F., and M. Peter.** 2002. Spa2p functions as a scaffold-like protein to recruit the Mpk1p MAP kinase module to sites of polarized growth. Current Biology **12:**1698-1703.

155. **Verna, J., A. Lodder, K. Lee, A. Vagts, and R. Ballester.** 1997. A family of genes required for maintenance of cell wall integrity and for the stress response in *Saccharomyces cerevisiae*. Proceedings of the National Academy of Sciences of the USA **94:**13804-13809.

156. **Vilella, F., E. Herrero, J. Torres, and M. A. de la Torre-Ruiz.** 2005. Pkc1 and the upstream elements of the cell integrity pathway in *Saccharomyces cerevisiae*, Rom2 and Mtl1, are required for cellular responses to oxidative stress. Journal of Biological Chemistry **280:**9149-9159.

157. **Vitalini, M. W., R. M. de Paula, C. S. Goldsmith, C. A. Jones, K. A. Borkovich, and D. Bell-Pedersen.** 2007. Circadian rhythmicity mediated by temporal regulation of the activity of p38 MAPK. Proceedings of the National Academy of Sciences of the USA **104:**18223-18228.

158. **Vivancos, A., M. Jara, A. Zuin, M. Sansó, and E. Hidalgo.** 2006. Oxidative stress in *Schizosaccharomyces pombe*: different H_2O_2 levels, different response pathways. Molecular Genetics and Genomics **276:**495-502.

159. **Vivancos, A. P., E. A. Castillo, B. Biteau, C. Nicot, J. Ayté, M. B. Toledano, and E. Hidalgo.** 2005. A cysteine-sulfinic acid in peroxiredoxin regulates H_2O_2-sensing by the

antioxidant Pap1 pathway. Proceedings of the National Academy of Sciences of the USA **102:**8875-8880.

160. **Vogt, N., and S. Seiler.** 2008. The RHO1-specific GTPase-activating protein LRG1 regulates polar tip growth in parallel to Ndr kinase signalling in *Neurospora*. Molecular Biology of the Cell **19:**4554-4569.

161. **Watanabe, D., M. Abe, and Y. Ohya.** 2001. Yeast Lrg1p acts as a specialized RhoGAP regulating 1,3-beta-glucan synthesis. Yeast **18:**943-951.

162. **Watanabe, Y., G. Takaesu, M. Hagiwara, K. Irie, and K. Matsumoto.** 1997. Characterization of a serum response factor-like protein in *Saccharomyces cerevisiae*, Rlm1, which has transcriptional activity regulated by the Mpk1 (Slt2) mitogen-activated protein kinase pathway. Molecular and Cellular Biology **17:**2615-2623.

163. **Wei, H., N. Requerra, and R. Fischer.** 2003. The MAPKK kinase SteC regulates conidiophore morphology and is essential for heterokaryon formation and sexual development in the homothallic fungus *Aspergillus nidulans*. Molecular Microbiology **47:**1577-1588.

164. **Widmann, C., S. Gibson, M. B. Jarpe, and G. L. Johnson.** 1999. Mitogen-activated protein kinase: conservation of a three-kinase module from yeast to human. Physiological Reviews **79:**143-180.

165. **Xu, J.-R.** 2000. MAP kinases in fungal pathogens. Fungal Genetics and Biology **31:**137-152.

166. **Xu, J.-R., C. J. Staiger, and J. E. Hamer.** 1998. Inactivation of the mitogen-activated protein kinase Mps1 from the rice blast fungus prevents penetration of host cells but allows activation of plant defense responses. Proceedings of the National Academy of Sciences of the USA **95:**12713-12718.

167. **Yu, R. C., C. G. Pesce, A. Colman-Lerner, L. Lok, D. Pincus, E. Serra, M. Holl, K. Benjamin, A. Gordon, and R. Brent.** 2008. Negative feedback that improves information transmission in yeast signalling. Nature **456:**755-761.

168. **Zelter, A., M. Bencina, B. J. Bowann, O. Yarden, and N. D. Read.** 2004. A comparative genomic analysis of the calcium signaling machinery in *Neurospora crassa*, *Magnaporthe grisea*, and *Saccharomyces cerevisiae*. Fungal Genetics and Biology **41:**827-841.

169. **Zhang, Y., R. Lamm, C. Pillonel, S. Lam, and J.-R. Xu.** 2002. Osmoregulation and fungicide resistance: the *Neurospora crassa os-2* gene encodes a HOG1 mitogen-activated protein kinase homologue. Applied and Environmental Microbiology **68:**532-538.

Chapter 6 – The role of hyphal fusion during sexual development

6.1. Abstract

This chapter will briefly introduce the main stages of fruitbody morphogenesis in *Neurospora crassa* and review our current understanding of how defects in vegetative hyphal fusion affect sexual development. Recent insights into how disruption of the early stages of protoperithecium formation and maturation can lead to female sterility will be presented for a range of fusion mutants, and shall be discussed in the context of ongoing investigations. This work has been done in collaboration with Kathryn M. Lord and Dr. Chris E. Jeffree from the University of Edinburgh. Special credit needs to be given for Kathryn's detailed characterisation of the initial stages of protoperithecial development in *Neurospora*, and for Chris's invaluable expertise and extensive help with the cryo-SEM.

6.2. Introduction

6.2.1. Perithecium morphogenesis in *N. crassa*

The perithecium is the female sexual reproductive organ, or fruitbody, of *Neurospora crassa* within which ascospores, the products of meiosis, are generated [50]. The perithecium is comprised of at least 14 different cell types [6], and is formed by hyphal aggregation and adhesion, hyphal branching and septation, physical dissolution of adjacent compartments leading to cell specialization, and probably hyphal fusion. Through these processes, fungi achieve multicellularity in a fundamentally different way in which plant and animal cells achieve multicellularity [40]. Therefore, perithecial morphogenesis in *N. crassa* provides an excellent model system for the study of multicellular development in filamentous fungi [7, 42]. Recent work by Kathryn M. Lord has provided a detailed description of the protoperithecial and perithecial stages of fruitbody morphogenesis in the *N. crassa* wt (Lord, K.M. & Read, N.D., in prep.). Key findings are briefly summarized in the following section.

Neurospora is an ascomycete of the family *Sordariaceae* and is heterothallic, i.e. for sexual reproduction to occur interaction of two parents of opposite mating type, *mat A* and *mat a*, is required. The *mat A* locus encodes three genes, *mat A-1*, *mat A-2* and *mat A-3*, whereas the *mat a* locus contains two genes, *mat a-1* and *mat a-2* [9, 12, 36]. The function of the putative *mat a-2* transcript, however, is unknown, as so far a gene product has not been identified [36]. A role of this potentially non-coding gene in transcriptional regulation of *mat a-1* is one interesting possibility. Mutations in *mat A-1* or *mat a-1* result in strains that have lost mating identity and vegetative incompatibility (section 1.5.2) when confronted with strains of opposite mating type, whereas *mat A-2*, *mat A-3* and *mat a-2* single mutants are indistinguishable from the wt [13, 35]. Furthermore, all *mat a* and *mat A* mating-type gene deletion mutants are able to undergo vegetative hyphal fusion (VHF), even though such

mutants are sterile [17]. In sexual crosses each mating type can behave as male or female (section 2.4.2.3).

The sexual phase of the *N. crassa* lifecycle (Fig. 1.1) commences with the formation of the ascogonium, a specialized coiled hyphal branch which emerges from the vegetative mycelium, and forms septa and branches (Fig. 6.1A and B) [40, 41]. It becomes surrounded by primary and secondary enveloping hyphae to form a more-or-less spherical, immature protoperithecium (Fig. 6.1C). Primary enveloping hyphae form directly as branches from the developing ascogonial coil, whereas secondary enveloping hyphae emerge from the surrounding mycelium. Fruitbody expansion and further differentiation leads to the mature protoperithecium, which sends out specialized hyphae, trichogynes, involved in non-self fusion with cells of the opposite mating type (Fig. 6.1D). The fertilizing agent may be an asexual conidium, a germinated ascospore or indeed any vegetative cell or hypha of the mating partner [10, 29]. Trichogynes grow towards male elements, make contact and establish cell fusion prior to fertilization [5]. Protoperithecia can form one or more trichogynes which can grow great distances and also form branches [2]. The pheromone emitted by conidia of the opposite mating type triggers the homing response of trichogynes [2, 5]. Closely related, homothallic (self-fertile) species, such as *Sordaria macrospora*, lack trichogynes [30].

Immediately after trichogyne-conidium fusion, male nuclei travel through the trichogyne to pair up with female nuclei and form a dikaryon within the ascogenous tissue, inside the protoperithecium [10]. Fertilization is usually achieved by a single nucleus. However, mixed male and female parentage does occur [18]. Successful fertilization induces continued growth, differentiation and further expansion of the protoperithecium, and thus leads into the perithecial stage. Increasing melanisation is a visual marker of continued perithecial development. The heavily melanised, flask-shaped perithecium is the mature fruitbody within which asci and ascospores are formed (Fig. 6.2C and D). Asci develop from successively produced croziers at the apices of ascogenous hyphae (Fig. 1.8). The

nuclei of both mating types come together and share the same cytoplasm within the dikaryotic cells of the ascogenous hyphae, and fuse in the ascus mother cell. Nuclear fusion yields the only diploid stage of the life cycle which is very short-lived [37, 43].

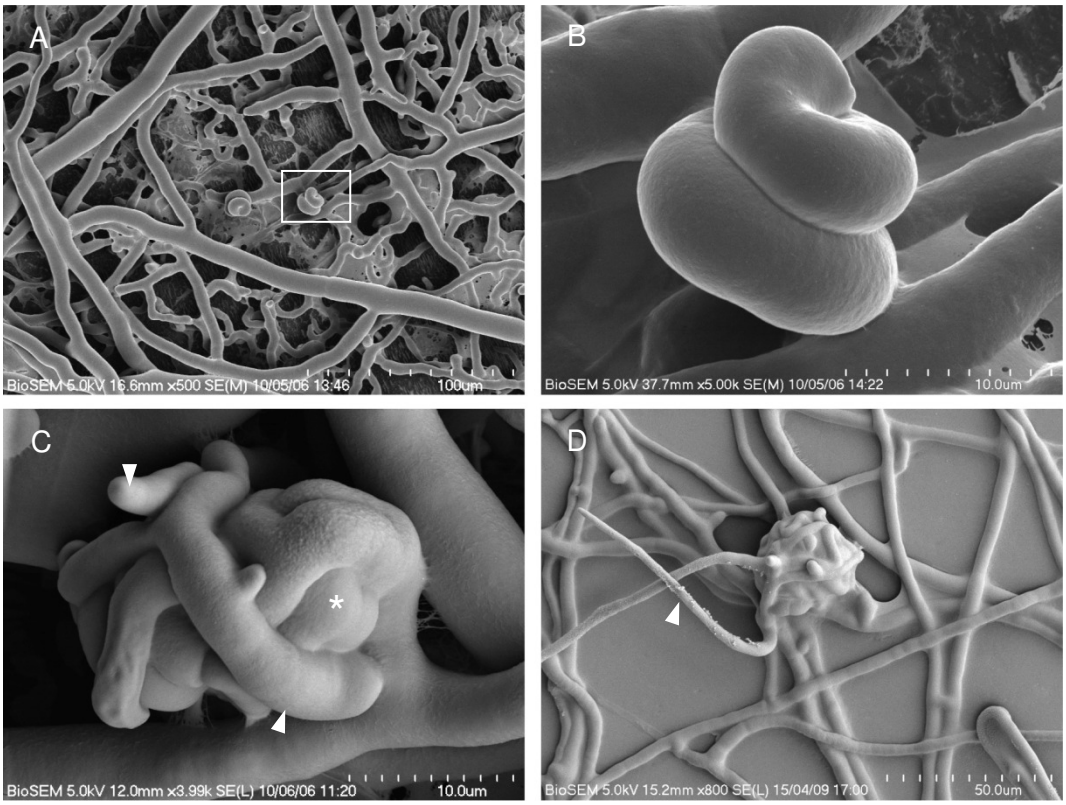

Figure 6.1 Protoperithecium morphogenesis of *Neurospora crassa*. Low-temperature SEM micrographs of the main stages of protoperithecial development. **(A)** Two ascogonial coils (one framed) differentiated from the vegetative mycelium. **(B)** High-power magnification of the ascogonial coil framed in (A). **(C)** Enveloping hyphae (arrowheads) wrapped around the ascogonial coil (asterisk). **(D)** More enveloping hyphae, which adhered to each other by means of extracellular matrix (ECM) secretion, contribute to fruitbody expansion. A trichogyne (arrowhead) emerged from the mature protoperithecium. Images A to C kindly provided by K.M. Lord. Image D taken by K.M. Lord, A. Lichius and C.E. Jeffree.

The ascus develops into a large cell, of about 175 μm x 20 μm, within which meiosis and mitosis takes place (Fig. 6.2D and E) [33]. The diploid nucleus undergoes two meiotic divisions followed by one mitotic division, resulting in each

ascus containing eight ordered haploid nuclei [10, 37]. After completion of the three nuclear divisions, the ascospore walls are laid down around the eight resulting nuclei. Ascospores are discharged through an apical pore at the top of the ascus (Fig. 6.2E) and subsequently ejected through the ostiole, an opening at the top of the perithecium. Further details on perithecium and ascospore morphogenesis can be found in chapter 2 of Davis, 2000 [10], and chapter 8 of Webster & Weber, 2007 [46].

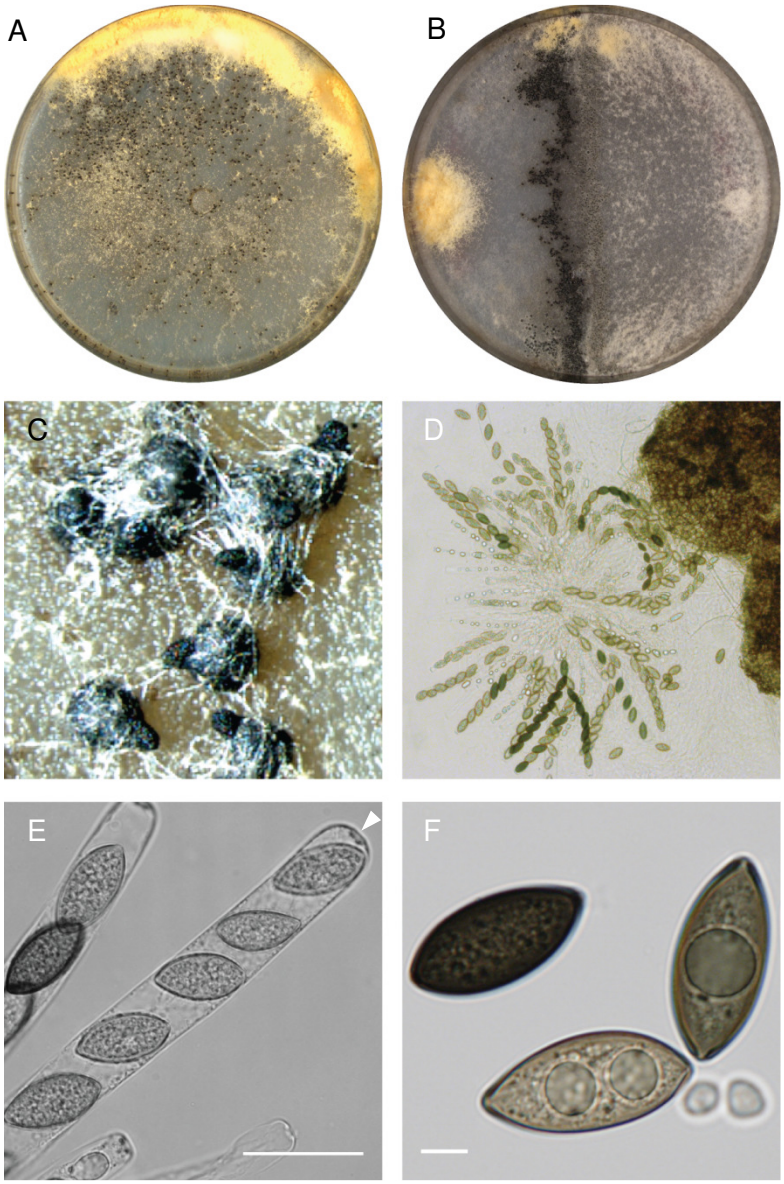

Figure 6.2 Perithecium and ascospore morphogenesis of *Neurospora crassa*. (A) Dry-fertilization of protoperithecia with opposite mating type conidia usually results in perithecia

developing dispersed across the whole plate. **(B)** In mating type compatible confrontation crosses (strains of opposite mating type inoculated on either side of the Petri dish) perithecia develop in the contact zone between both mycelia. **(C)** Mature, highly melanised perithecia which have started to eject ascospores 12 days after fertilization. **(D)** Ascus rosette released from a squashed perithecium. Each ascus contains eight ascospores, sometimes at different developmental stages. **(E)** Brightfield image of an ascus with the apical pore visible at the top (arrowhead). Scale bar, 50 µm. **(F)** Ejected ascospores collected from the Petri dish lid. Spore wall pigmentation increases with maturation. The two blurry objects are macroconidia below the focal plane. Scale bar, 10 µm.

6.2.2. The role of hyphal fusion during early fruitbody development

In stark contrast to the roles of cell fusion during the late stages of the sexual cycle of *Neurospora*, i.e. hyphal fusion inducing crozier formation in the ascogenous tissue and mating cell fusion (section 1.6), our knowledge about hyphal fusion events occurring during the early stages of protoperithecial morphogenesis is lacking. One likely explanation is the small size and thus notoriously limited accessibility of the involved structures. Protoperithecial development begins with an ascogonial coil of about 10 µm in diameter, and ends with the mature protoperithecium, which usually does not expand beyond 80 µm. Furthermore, internal tissues are tightly packed within the melanised protoperithecial wall making it very difficult to experimentally access cellular processes inside the living structure. Unfortunately, TEM sections of developing protoperithecia of *N. crassa*, which could provide first clues to whether or not fusion occurs between hyphal compartments inside, have not yet been reported. All fusion mutants identified so far in *N. crassa* display pleiotropic phenotypes [44]. However, a common defect in these mutants is female sterility. Progression through the sexual cycle, including differentiation and maintenance of the female fruitbody, is the most complex process in the life of a filamentous fungus. Therefore, it is conceivable that sexual development is an easily-disrupted target of mutational defects. But at what stage a defect in hyphal fusion might contribute to the termination of fruitbody development is currently unanswered. In order to establish reasons why hyphal

fusion mutants fail to produce fully functioning protoperithecia we defined four main stages of development, with the fourth being the mature, fertilizable protoperithecium (Fig. 6.3). Each main stage can be subdivided into smaller steps.

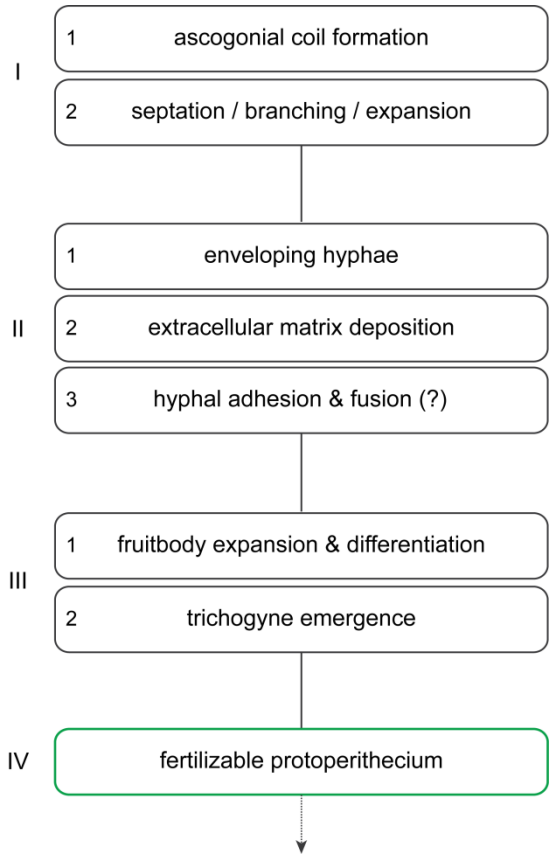

Figure 6.3 Main stages of protoperithecial development. (I) The ascogonium is a specialized, coiled hyphal branch that emerges from the vegetative mycelium. It septates and sends out more branches which envelop it. **(II)** Additional, secondary enveloping hyphae from neighboring areas of the mycelium aggregate and form a protective casing. Secretion of extracellular matrix is a precursor to hyphal adhesion during that process, and possibly involves hyphal fusion. **(III)** Fruitbody expansion, cellular differentiation and emergence of the trichogyne mark the final stage of protoperithecium maturation. Fusion might also occur during this stage. **(IV)** The end product is a fully functional, fertilizable protoperithecium. Most steps comprise even smaller morphological changes which are indicated as I.1, I.2, II.1, etc..

Our current understanding of how far a number of known fusion mutants of *N. crassa* progress in the sexual cycle when acting as females is summarized in Table 6.1. Although all of these mutants - except Δ*prm-1* – have been found to be male fertile, i.e. ascospores were produced when conidia of the mutant were used as fertilizing agent on an opposite mating type female wt, decreased ascospore viability was generally observed in the recovered progeny [44]. Nevertheless, the production of meiotic progeny unambiguously demonstrates successful completion of the sexual cycle. Impairment of ascospore germination due to genetic defects of the mutant progeny is, by our definition, a problem associated with the subsequent vegetative growth phase.

Table 6.1 Fruitbody development in *N. crassa* gene deletion mutants. Mutants were used as females in heterozygous crosses with wt. Green indicates completed developmental stages; yellow indicates stages which were found to be severely impaired; red are those stages identified as being fully blocked. White represents unknown areas.

References	[15, 34]	[49]	[16, 19, 28]	[16, 19, 28]	[16, 19, 28]	[28, 31]	[28]	[27, 28, 31]	[27]	[28, 32]	[28, 32]	[28, 32]	[8]	[8]	[14]
Ascospore germination															
Ascospore ejection															
Neck/ostiole development															
Ascospore production/ maturation															
Ascogenous hyphae															
Crozier fusion															
Perithecium differentiation															
Nuclear transit/ fertilization															
Trichogyne homing and fusion															
Fertilizable protoperith.															
Trichogyne emergence															
Fruitbody expansion															
ECM deposition/ hyphal adhesion															
Enveloping hyphae															
Septation/ branching															
Ascogonial coil formation															
Protein	**unknown**	**membrane protein**	**MAPKKK**	**MAPKK**	**MAPK**	**MAPKKK**	**MAPKK**	**MAPK**	**transcription factor**	**MAPKKK**	**MAPKK**	**MAPK**	**NADPH-oxidase**	**NOX regulator**	**membrane protein**
Locus	**NCU02794**	**NCU03727**	**NCU03071**	**NCU00587**	**NCU07024**	**NCU06182**	**NCU04612**	**NCU02393**	**NCU00340**	**NCU02234**	**NCU06419**	**NCU09842**	**NCU02110**	**NCU07850**	**NCU09337**
Gene	***so***	***ham-2***	***os-4***	***os-5***	***os-2***	***nrc-1***	***mek-2***	***mak-2***	***pp-1***	***mik-1***	***mek-1***	***mak-1***	***nox-1***	***nor-1***	***prm-1***

Most interestingly, when Δ*prm-1* was used as male in such a heterozygous cross, although fertilization took place and perithecial differentiation was initiated, fruitbody development arrested before perithecial necks and ostioles developed. Any sexual cross (homozygous or heterozygous) involving Δ*prm-1* always resulted in the production of barren perithecia, i.e. perithecia lacking asci [38, 39], indicating a major defect during crozier formation [14]. PRM-1 is therefore the first example of a protein with confirmed roles during vegetative and sexual cell fusion. As it is highly unlikely that *prm-1* is the only gene with this shared function in *N. crassa*, the identification of other candidates and potential interaction partners of PRM-1 will be an important research objective in the future.

Certain stages during sexual development are experimentally more readily accessible than others. This is mainly based on the feasibility of simple optical/microscopical observation to verify whether fertilizable protoperithecia have been developed, if further perithecial differentiation has been initiated upon fertilization, or whether produced ascospores generate viable colonies on selection medium. In case these key stages (highlighted in grey in Table 6.1) are not achieved in a particular mutant strain, it is very difficult to determine the intermediate stage at which sexual development is blocked. Protocols which assess trichogyne-conidium homing and mating cell fusion, or crozier formation and fusion have been established, and recently successfully applied [14]. However, these experiments evaluate fusion events post protoperithecial maturation. The white areas in Table 6.1 indicate the early stages of protoperithecial development for which information is missing in most cases. Work presented in this chapter presents initial attempts to approach these early developmental stages experimentally in order to verify the potential connection between vegetative hyphal fusion and fruitbody morphogenesis in *N. crassa*.

6.3. Results

6.3.1. Defects in hyphal fusion primarily affected female fertility

Some of the previous work on sexual development in *N. crassa* has been performed with mutant strains generated by different methods and obtained from a variety of sources (references in Table 6.1). Therefore we decided to verify earlier findings in gene deletion strains generated by homologous recombination and obtained from one source only (the FGSC, Table 2.1). Analysis was extended with selected novel fusion mutants identified within this project (Table 3.7), and new gene deletion strains deposited as replacements for older, probably incorrect strains. The absence of intended target loci was verified by PCR in house for all KO strains (Fig. 2.1). All tested fusion mutants did not generate progeny when used as a female in heterozygous crosses with a wild type male (Table 6.2). Whereas, ascospores were produced in reciprocal and confrontation crosses (section 2.4.2.3) – where the mutant effectively acted as male - suggesting that male fertility is uncoupled from vegetative fusion defects (Table 6.3). Mating type dependent effects were not observed.

Table 6.2 Mutant strains of *N. crassa* selected for the analysis of protoperithecial development.

Strain	FGSC/strain number	Locus	Mating type	Protein
wild type	FGSC2489	_	A	-
wild type	FGSC4200	_	a	-
Δso	FGSC11292	NCU02794.2	a	WW domain protein
Δso	FGSC11293	NCU02794.2	A	WW domain protein
Δham-2	FGSC12091	NCU03727.2	A	transmembrane protein
*Δos-4**	FGSC18202	NCU03071.2	a	MAPKKK
*Δos-5**	FGSC18203	NCU00587.2	a	MAPKK
*Δos-2**	FGSC17933	NCU07024.2	A	MAPK
Δnrc-1	FGSC11466	NCU06182.2	a	MAPKKK
Δmek-2	FGSC11524	NCU04612.2	a	MAPKK
Δmak-2	FGSC11482	NCU02393.2	a	MAPK
Δpp-1	FGSC21335	NCU00340.2	a	transcription factor
Δmik-1	FGSC11326	NCU02234.2	A	MAPKKK
Δmik-1	FGSC11327	NCU02234.2	a	MAPKKK
Δmek-1	FGSC11318	NCU06419.2	a	MAPKK
Δmek-1	FGSC11319	NCU06419.2	A	MAPKK
Δmak-1	FGSC11320	NCU09842.1	A	MAPK
Δmak-1	FGSC11321	NCU09842.1	a	MAPK
Δnox-1	FGSC12867	NCU02110.2	a	NADPH oxidase
Δnox-1	FGSC12868	NCU02110.2	A	NADPH oxidase
Δnor-1 (HP)	this study	NCU07850.2	a	NOX regulator
Δrac-1 (HP)	this study	NCU02160.2	a	Rho GTPase
Δgdh-1	FGSC13417	NCU00461.2	a	glutamate dehydrogenase
Δgdh-1	FGSC13418	NCU00461.2	A	glutamate dehydrogenase
Δlao	FGSC13350	NCU05113.2	a	laccase
Δlao	FGSC13351	NCU05113.2	A	laccase

* Δ*os* strains are vegetative hyphal fusion competent

Table 6.3 Fertility assays. Successful mating was assessed by the production of ascospores within 14 days after fertilization on SCM and LSA (Tables 2.15 and 2.16). Fertilization was achieved either by addition of 'male' macroconidia onto a 5 day old 'female' culture, or confrontation of two opposite mating type colonies on one plate (section 2.4.2.3). Ascospores were only produced when the fusion defective KO strain acted as male (green). Interactions in which the KO mutant acted as female blocked sexual progression during or shortly after the protoperithecial stage (red). Results were consistent for all triplicates prepared for each strain, and independent of the mating type. All controls gave expected results (black).

ascospores produced?		*mat A*			
		wt ♀	wt ♂	KO ♀	KO ♂
mat a	wt ♀	-	+	-	+
	wt ♂	+	-	-	-
	KO ♀	-	-	-	-
	KO ♂	+	-	-	-

6.3.2. Protoperithecial maturation in hyphal fusion mutants was blocked at different stages

Assessment of fruitbody development using the stereomicroscope showed that all tested fusion mutants developed protoperithecium-like structures beyond the stage of ascogonial coils, which are hardly visible at this level of magnification (Fig. 6.4). In comparison to the wt which formed quite regular, spherical protoperithecia of about 65-75 µm diameter, the size and shape of developing protoperithecia varied considerably between different fusion mutants grown under identical conditions. Abundance and morphological definition of these structures was generally improved when strains were grown on LSA compared to SCM (Tables 2.15 and 2.16). Furthermore, the more efficient suppression of conidiogenesis on LSA greatly facilitated observability and sample preparation for microscopy.

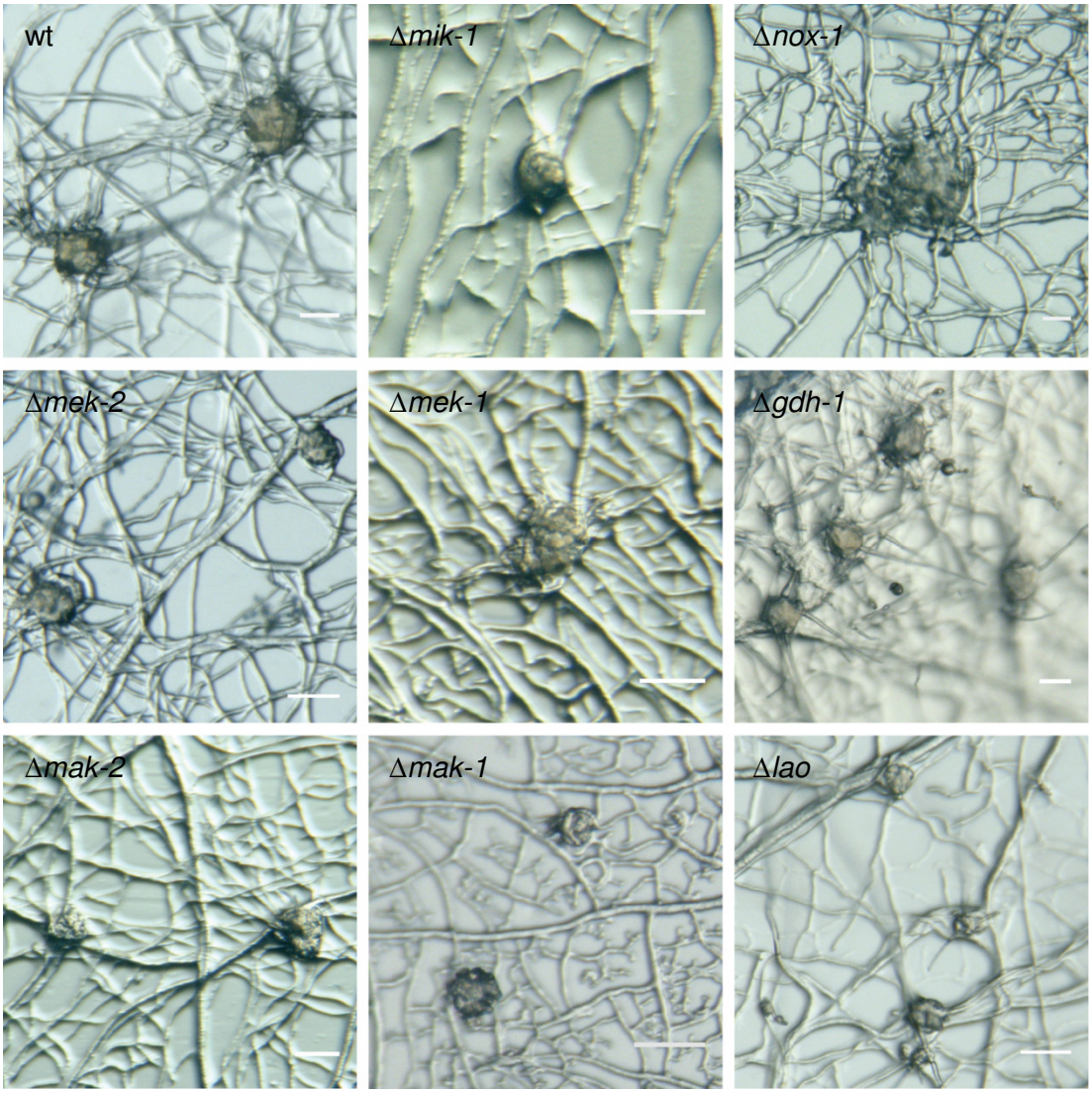

Figure 6.4 Protoperithecial development in *N. crassa* fusion mutants. In comparison to the wt which formed regular, spherical protoperithecia of about 65-75 µm diameter, protoperithecial structures formed by the gene deletion mutants varied considerably in size, shape and degree of pigmentation. All strains have been grown for 7 days at 25°C on LSA plates overlaid with cellophane to facilitate sample preparation for subsequent cryoSEM analysis (Fig. 6.5). Images were taken on a Nikon stereomicroscope fitted with a digital colour camera (section 2.12.1). Scale bars, 50 µm.

To verify the observed morphological differences between strains in greater detail a higher magnification was required. To facilitate rapid sample preparation for LTSEM analysis, strains were grown on cellophane as described in section 2.12.8. The observed morphologies of protoperithecial-like structures comprised loose 'knots' with evident gaps between intertwining hyphae (e.g. Δ*nox-1*), small dense

knots covered in extracellular matrix (ECM) (e.g. Δ*rac-1*), and fruitbodies of wt-like appearance which sent out straight hyphae resembling trichogynes (e.g. Δ*gdh-1*) (Fig. 6.5).

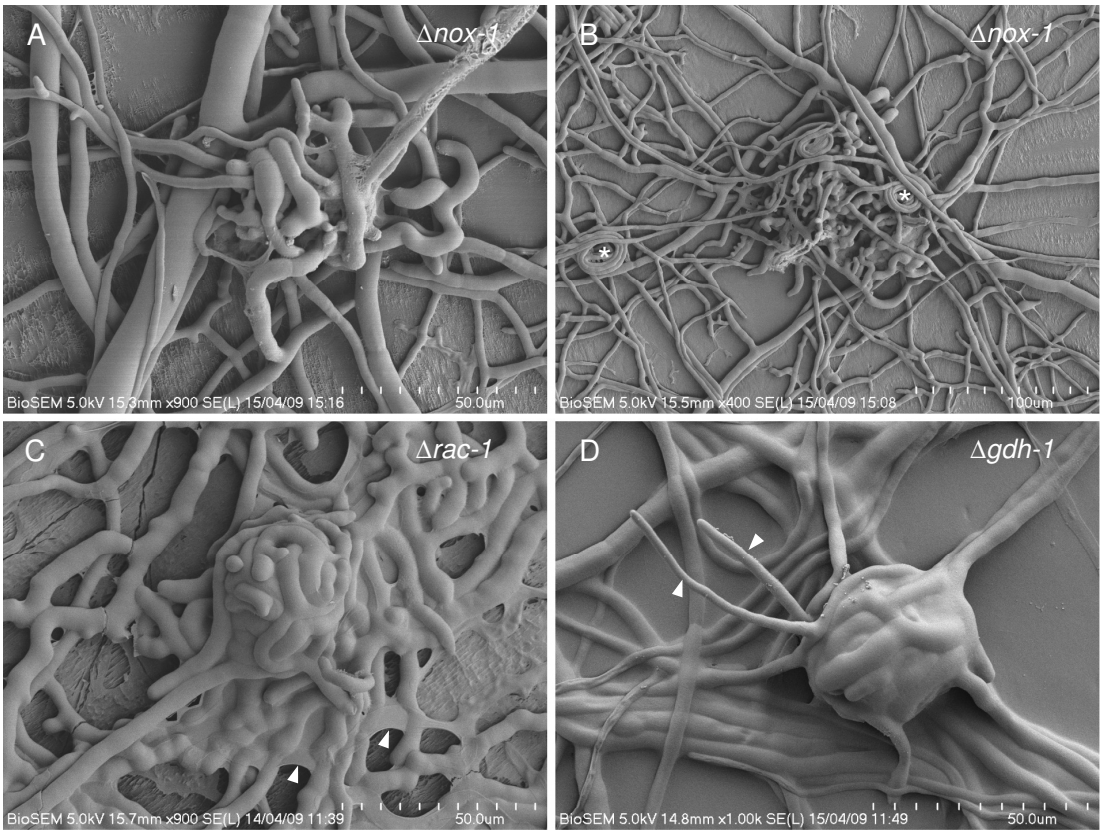

Figure 6.5 Protoperithecial structures of *N. crassa* fusion mutants. (A and B) Lose hyphal aggregations lacking ECM deposition were observed in Δ*nox-1*. Lassos are commonly observed in the wt, too, of unknown function but most likely not connected to sexual development (asterisks in B). **(C)** A densely packed protoperithecium of Δ*rac-1*, with pronounced deposition of extracellular matrix, especially in the surrounding mycelium (arrowheads). **(D)** Wt-like protoperithecia of Δ*gdh-1* send out straight, unbranched hyphae which resembled trichogynes (arrowheads). Images taken by A. Lichius and C.E. Jeffree.

Taken together, the analysis showed that a VHF defect does not lead to disruption of protoperithecial development at a conserved stage, but that blockage occurs at different stages in different mutants. Thus, similar to the analysis of different phases of cell and vegetative hyphal fusion processes (Figs. 1.4 and 1.7),

comparison of protoperithecial and perithecial development in gene deletion mutants can help to dissect signalling pathways that regulate fruitbody formation.

6.3.3. Defects in hyphal aggregation and adhesion aborted protoperithecial morphogenesis in MAPK mutants

Signalling through the pheromone response (PR) and cell wall integrity (CWI) MAPK pathways is essential for hyphal fusion and so far the best understood examples in *N. crassa* [44] (chapter 5). Previous reports [27, 28, 31, 32], as well as our own analysis (Fig. 6.4) suggest a major role for MAPK signalling during early protoperithecial development. To verify the functional relationship between both processes, further cryoSEM analysis was focused on these MAPK mutants. The observed phenotypic defects during protoperithecial development were conserved within each MAPK cascade, but slight differences occurred between them (Fig. 6.6). CWI mutants progressed beyond ascogonial coil formation and expansion, but failed to form tightly packed protoperithecia (Fig. 6.6B). These strains terminated fruitbody development as lose hyphal aggregates. Mutants of the PR pathway progressed slightly further, and formed more densely packed protoperithecia (Fig. 6.6C). The most interesting difference between mutants of both pathways was the absence and presence of ECM, respectively. CWI MAPK mutants did not seem to produce any ECM, whereas mutants of the PR cascade did. This apparently correlated with protoperithecial development. Compared to other mutants and the wt (Figs. 6.5 and 6.6A), densely packed, spherical protoperithecia were only found in those mutants that secreted ECM; not only directly on the fruitbody, but also within the vegetative mycelium. This suggests that the secretion of extracellular matrix facilitates adhesion of enveloping hyphae, and that both are requirements for protoperithecium maturation.

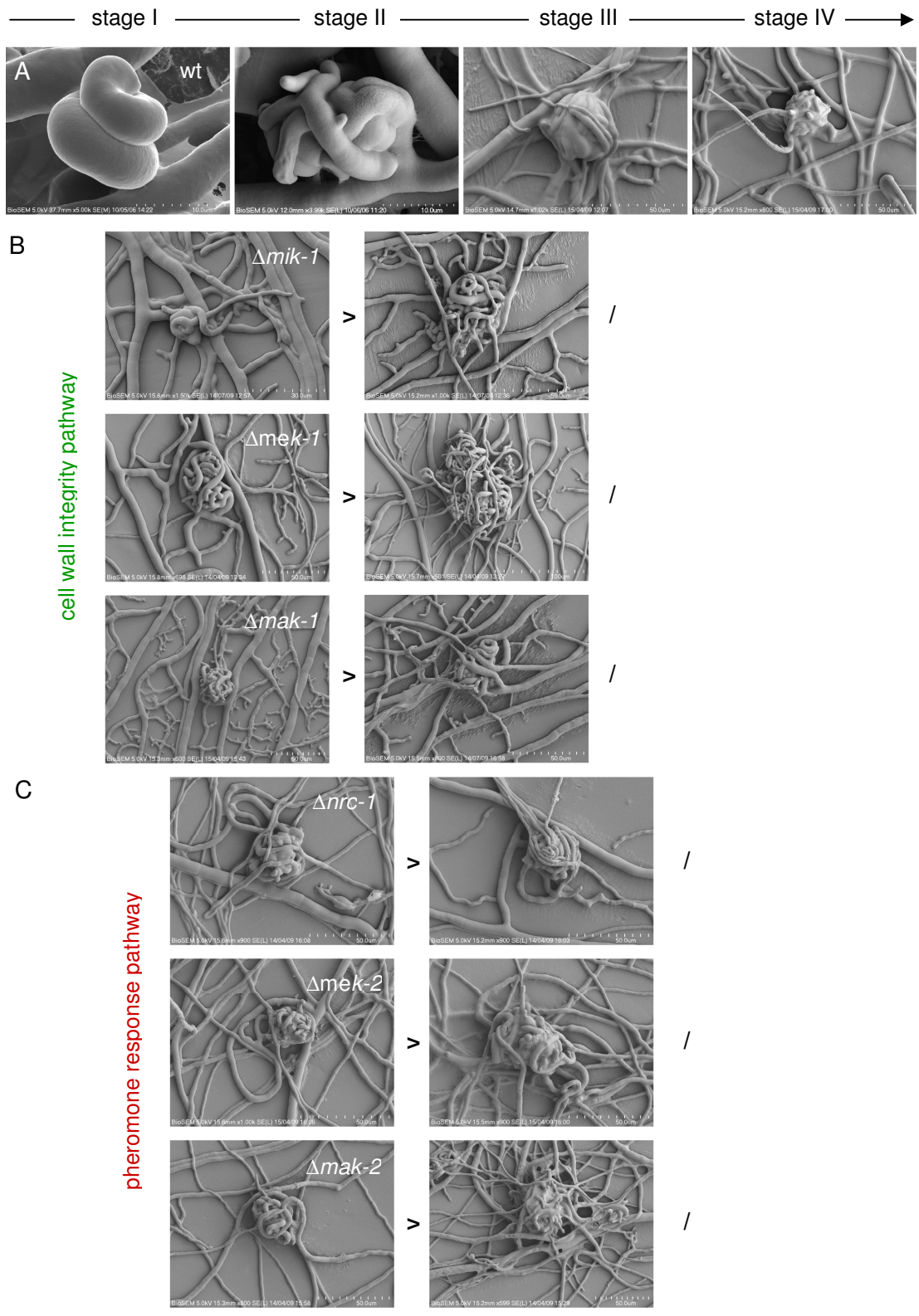

Figure 6.6 Extracellular matrix deposition and hyphal adhesion were required for the organized assembly of enveloping hyphae. Developmental stages I – IV refer to Fig. 6.3. **(A)** In the wild type, ascogonial coils became enveloped with tightly packed hyphae to form functional protoperithecia, which send out trichogynes. Hyphal adhesion is achieved by secretion of ECM. **(B)** MAP kinase mutants of the CWI pathway (Δ*mik-1*/Δ*mek-1*/Δ*mak-1)*

also formed ascogonial coils and enveloping hyphae, but they remained loose hyphal aggregations which lacked deposition of ECM. Developmental progression beyond this stage was not observed (indicated by '/'). **(C)** MAP kinase mutants of the PR pathway (Δ*nrc-1*/Δ*mek-2*/Δ*mak-2*) on the other hand produced ECM, and hyphal aggregations showed a higher degree of organization and appeared spherical; almost resembling 'early-stage' protoperithecia. So far, the emergence of trichogyne-like hyphae has not been observed in any of these strains. Images taken by A. Lichius, K.M. Lord and C.E. Jeffree.

6.3.4. Prematurely aborted protoperithecia in CWI MAPK mutants underwent rapid autolysis

The CWI pathway responds to cell wall stress during vegetative growth and hyphal morphogenesis (chapter 5). Common phenotypes in MIK-1/MEK-1/MAK-1 mutants include altered cell walls, cell-cell adhesion defects and increased autolysis [4, 28, 32]. This directly affected fruitbody development and its analysis (Fig. 6.7).

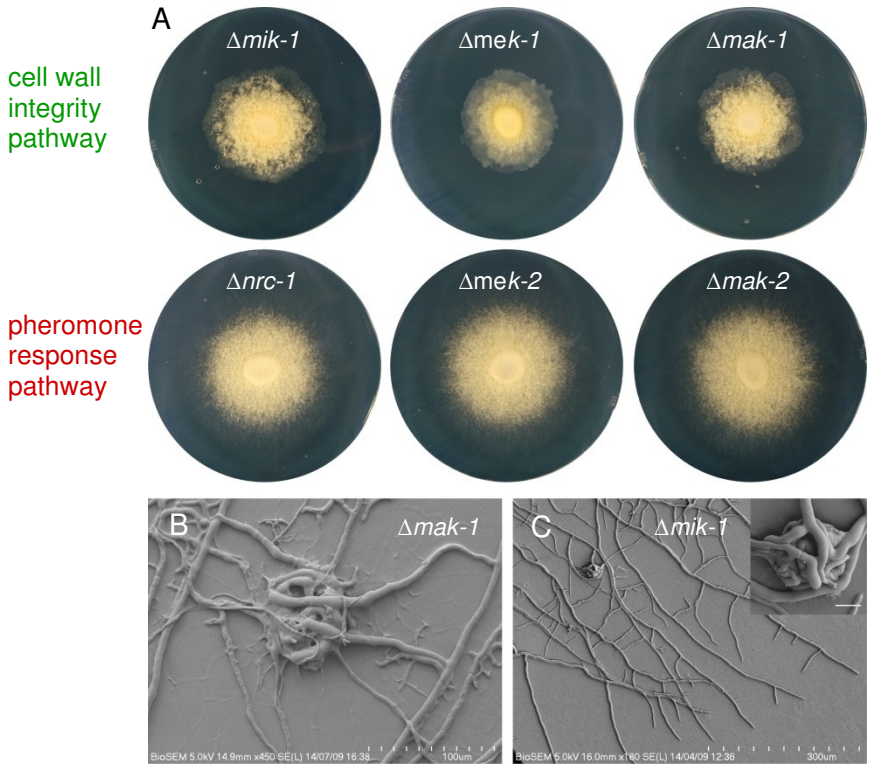

Figure 6.7 Consequences of early hyphal autolysis on colony morphology and fruitbody development. (A) Mutants in the CWI pathway showed increased autolysis resulting in rosetta-like colony growth on nutrient rich medium. Mutants in the PR pathway

did not show this defect. All cultures were incubated for 3 days at 30°C on VM. **(B)** Immature and developmentally aborted fruitbodies in the colony centre and subperiphery autolysed and the material was reabsorbed by the colony. **(C)** Interestingly, Δ*mik-1*/Δ*mek-1*/Δ*mak-1* strains showed early onset initiation of fruitbody development at the colony periphery. Intact protoperithecial structure magnified in inset. Scale bar, 10 µm. This feature was not observed in the wt or other mutants. LTSEM images taken by A. Lichius, K.M. Lord and C.E. Jeffree.

Immature protoperithecia of CWI MAPK mutants autolysed and the material was reabsorbed by the colony. As a consequence, only very few protoperithecial structures could be observed in the colony centre and the subperiphery. Interestingly, Δ*mik-1*, Δ*mek-1* and Δ*mak-1* mutants showed early onset of fruitbody development at the leading edge of the colony (Fig. 6.7B and C); an unusual feature, which was generally not observed in the wt or mutants of the CWI MAPK pathway. Only limited by the size of available, sterile culture dishes, vegetative colonies of the *N. crassa* wt were grown on LSA medium for more than 4 days and up to a diameter of 30 cm without development of female fruitbodies being initiated. As soon as the colony touched the edge of the plate protoperithecial development started from the colony centre outwards (data not shown).

6.3.5. Ectopic expression of MAK-1-sGFP rescued developmental defects of Δ*mak-1*

Ectopic expression of MAK-1 in a Δ*mak-1* background fully restored wild type-like colony morphology, hyphal fusion, and protoperithecial development (Fig. 6.8). Furthermore, the rescued strains strongly expressed MAK-1-sGFP (under control of the inducible *ccg-1* promoter) inside mature protoperithecia, which also successfully differentiated into perithecia and produced ascospores upon fertilization with wt conidia (data not shown).

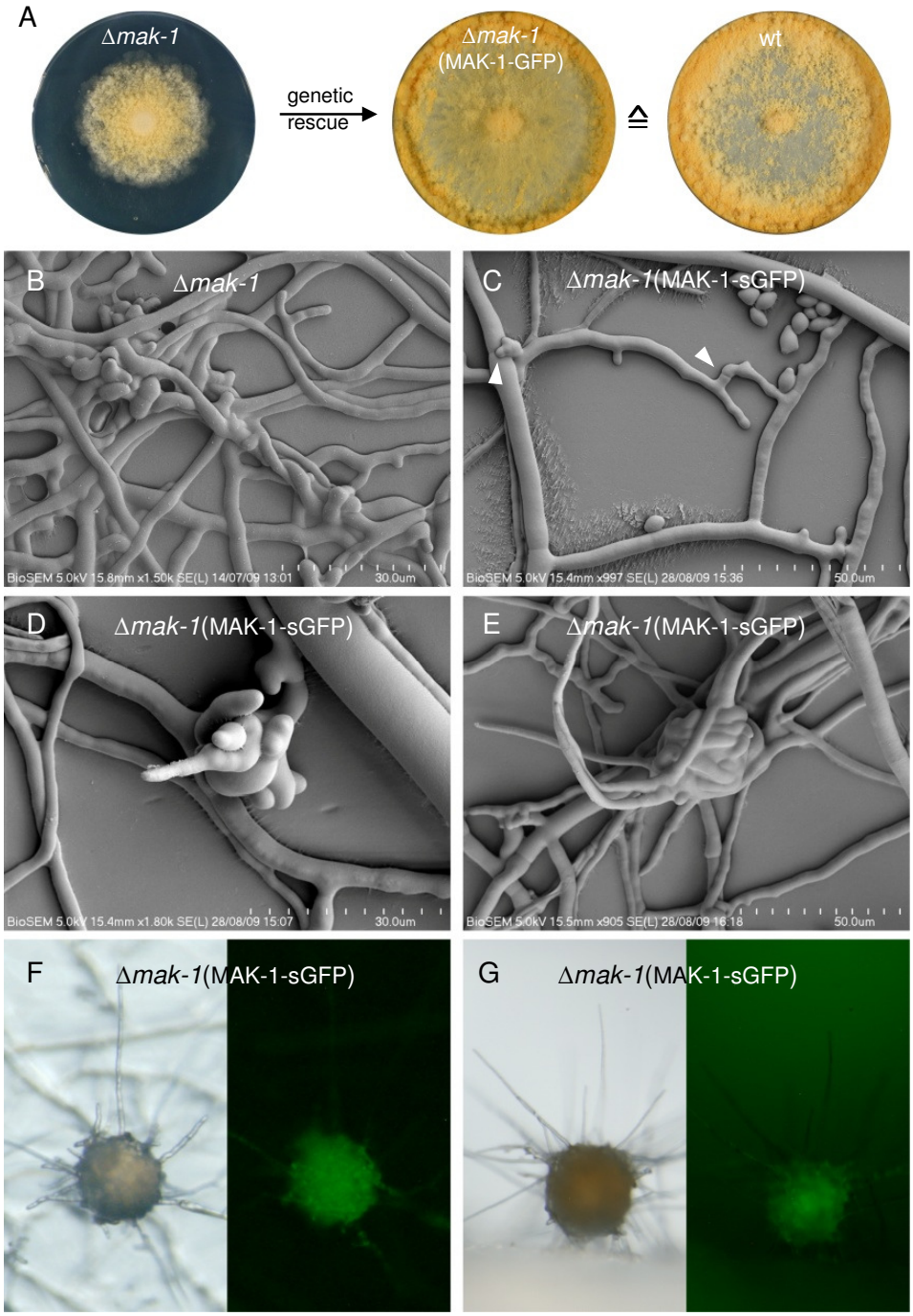

Figure 6.8 Recovery of developmental defects in genetically rescued Δ*mak-1*. **(A)** A wt-like colony phenotype without early onset of autolysis was restored in rescued Δ*mak-1*(MAK-1-sGFP) transformants. **(B)** The fusion defect of Δ*mak-1* was also restored in the rescued strains **(C)** (arrowheads mark fusion connections). **(D)** Ascogonial coil formation and **(E)** development of wt-like protoperithecia showing tightly wrapped enveloping hyphae embedded in ECM (compare with morphological defects in Fig. 6.6B). **(F and G)** Expression of MAK-1-sGFP under control of the *ccg-1* promoter inside mature protoperithecia. LTSEM images taken by A. Lichius, K.M. Lord and C.E. Jeffree.

6.4. Discussion

Cell fusion is fundamental for the establishment of an interconnected mycelial network in the ascomycete *Neurospora crassa*. Cell fusion also plays a critical role during sexual development and progress beyond certain points in the sexual cycle cannot be made unless a fusion event has occurred. Studies so far, have concentrated on cell fusion events during crozier fusion of ascogenous hyphae and mating cell (conidium-trichogyne) fusion. In contrast, only little is known about how cell fusion is involved in other aspects of sexual morphogenesis of the female fruitbody (perithecium). Gene deletion mutants blocked in vegetative cell fusion, revealed interesting phenotypic defects affecting early protoperithecial development, suggesting that the cell fusion machinery has additional roles during the initial stages of sexual development that are not obviously associated with hyphal fusion. Identified proteins indicate that secretion of extracellular matrix and hyphal adhesion are essential for the initiation of multicellular development in filamentous fungi. Our findings also revealed developmental checkpoints, which when not satisfied resulted in abortion, degradation and recycling of immature fruitbodies. Although potential functional connections between VHF and sexual development became clearer, the notion that hyphal fusion does occur during protoperithecial development still remains to be proven.

Hyphal fusion defects which impact on sexual progression mainly affected the female partner. All fusion mutants investigated within this project were blocked in sexual development only when used as females in heterozygous crosses with the wt. Using conidia of mutant strains as the male fertilizing agent on opposite mating type wt females, or sporulating vegetative colonies as partners in compatible confrontation crosses with the wt did not block sexual development. Successful completion of the sexual cycle was assessed by the production of ascospores (Table 6.3). All tested strains were male fertile, but female sterile which is consistent with earlier findings [8, 31, 32, 49], and confirms asymmetry in female

and male function during mating in *N. crassa* [1]. Mutant strains that are highly male fertile, but completely female sterile, are not a surprising find, as the female function is in general more complex and presents a larger mutational target than the male function. The female function is therefore more easily lost through deleterious mutations than is the male function [26]. When assuming that a defect in hyphal fusion is responsible for the termination of sexual development in these strains, the fact that only the female structure was affected implies a number of important findings regarding the function of the disrupted gene, and the role of the male partner in this interaction. Firstly, if the blockage occurred before mature, fertilizable protoperithecia were formed, the gene must function during early fruitbody (protoperithecial) morphogenesis, and fusion events are likely to be necessary for progression beyond the achieved stage. Secondly, if mature protoperithecia with trichogyne-like hyphae were formed by the mutant colony, the missing gene product has no essential role in early fruitbody morphogenesis. This has for example been shown for *so* [15]. Thirdly, if fusion defective mutant conidia are male fertile, the deleted gene is not required for mating fusion from the male side. As this was observed for all tested mutant strains it suggests that the male partner, apart from releasing sex pheromone to guide trichogyne homing [20, 22, 23], has a passive role during mating cell fusion. One recently identified exception to that role is *prm-1* which when removed from the male conidium caused a 25% decrease in heterozygous non-self fusion, and due to a block in subsequent perithecial maturation never lead to the production of ascospores [14]. Thus Δ*prm-1* is the first male sterile fusion mutant identified in *N. crassa*. This is interesting because in theory, male sterility cannot exist in nature in a filamentous fungus with asymmetric mating [1]. Male sterility would block transmission of the nuclear genome and the production of meiotic progeny, and thus prevent spread of the responsible gene defect. This might explain, why the observed fusion associated defects in Δ*prm-1* mutants is only partial [14].

Taken together, these findings suggest that the vast majority of VHF genes play a range of different roles during early fruitbody morphogenesis and many of these notably do not involve cell fusion. This functional diversity is reflected by the distribution of developmental blocks during protoperithecial morphogenesis identified in the various mutant strains shown in Tables 6.1 and 6.5. It will be interesting to determine whether mating fusion occurs between wt conidia and the trichogyne-like hyphae found in Δ*gdh-1* (Fig. 6.5D), and if so at what stage upon fertilization perithecial development of Δ*gdh-1* arrests.

LTSEM revealed novel aspects of defects during early stages of protoperithecial development. Light microscopy showed that all fusion mutants under investigation formed protoperithecium-like structures beyond the stage of ascogonial coils, but mostly did not develop to a mature stage; judged by size and degree of pigmentation compared with the wt structure (Fig. 6.4). For some of these mutant strains, e.g. CWI MAPK and NOX mutants, the existence of protoperithecium-like structures developed to these advanced stages has so far not been reported (Table 6.1). Furthermore, evident morphological differences indicated functional differences of the deleted genes during protoperithecial morphogenesis, and provided a more detailed description than previously achieved. These features, however, could only be resolved using the higher magnification power and rapid sample preparation of the LTSEM. Surface water covering the light microscopy samples was removed by partial freeze-drying following cryo-fixation, and revealed two essential characteristics of developmentally arrested mutant protoperithecia: (1) enveloping hyphae which were only arranged as loose knots with huge gaps between them, and (2) the absence of ECM deposition. Loose knit protoperithecia were observed for the MAPK mutants of the CWI pathway, but also for Δ*nox-1* (Figs. 6.5 and 6.6). It was recently found that high levels of *nox-1* mRNA coincided with the formation of protoperithecia supporting a crucial function of this protein in fruitbody development [8]. Furthermore, these mutants did not deposit ECM, which

in contrast appeared pronounced in Δ*rac-1* (Fig. 6.5), was present to a lesser degree in MAPK mutants of the PR pathway (Fig. 6.6), and clearly visible in Δ*gdh-1* and of course the wt (Figs. 6.5 and 6.6). This suggests that for the formation of a spherical protoperithecium, organized assembly and adhesion of enveloping hyphae is essential. If hyphal adhesion was possible, as for example in the PR MAPK mutants, protoperithecial development progressed further. However, emergence of obvious trichogyne-like hyphae was not observed in these strains, suggesting that fruitbody development aborted before a mature stage was reached. This was different for the wt-like protoperithecia of Δ*gdh-1*, which did send out trichogyne-like hyphae (Fig. 6.5). Nevertheless, fertilization with male wt conidia did not result in the production of ascospores, thus blockage must occur at a later stage, yet to be determined.

Taken together, we propose the inability of enveloping hyphae to assemble a tightly packed hyphal aggregate by hyphal adhesion and ECM deposition as one cause for the disruption of protoperithecial morphogenesis in some of the presented strains. Hyphal attachment following tip growth arrest is a precursor to hyphal fusion and might provide an important trigger for the activation of the fusion machinery (Fig. 1.7). The lack of contact-induced tip growth arrest and hyphal tip attachment is a common phenotype observed in VHF mutants, including CWI and PR MAPK mutants (Fig. 3.3). Therefore, the inability to attach and trigger the transition to the next morphogenetic stage may provide a functional connection between VHF and fruitbody development. This, however, applies only to a group of mutants, as other fusion mutants (e.g. Δ*gdh-1*) which essentially show the same VHF phenotype, progress further in sexual development. For this reason it has to be concluded that a direct connection between a defect in hyphal fusion and the arrest of protoperithecial development seems unlikely at this early stage. A defect in hyphal attachment might be associated to an altered production of hydrophobins. Hydrophobins are small secreted fungal proteins that play a role in a broad range of developmental processes in filamentous fungi, such as the formation of aerial structures and for the attachment of hyphae to hydrophobic surfaces [21, 47, 48].

Table 6.4 Summary of sexual development in gene deletion mutants of *N. crassa*. AC = ascogonial coil formation; AS = ascospore production; PP = formation of protoperithecia. Completed stages of development are indicated in brackets: II.1 enveloping hyphae; III.1 fruitbody expansion and differentiation; III.2 trichogyne emergence; IV fertilizable protoperithecium (for details see Figs. 6.3 and 6.6). * OS mutants are fusion competent.

Strain	female KO x male wt	female wt x male KO	confrontation cross	SEM observation
wild type	AS	AS	AS	fertilizable PP (IV)
Δso	x	AS(?)	AS	fertilizable PP (IV) ?
Δham-2	x	?	AS	?
*Δos-4**	x	AS	AS	loose hyphal knots (II.1)
*Δos-5**	x	AS	AS	loose hyphal knots (II.1)
*Δos-2**	x	AS	AS	loose hyphal knots (II.1)
Δnrc-1	x	AS	AS	dense hyphal knots (III.1)
Δmek-2	x	AS	AS	dense hyphal knots (III.1)
Δmak-2	x	AS	AS	dense hyphal knots (III.1)
Δpp-1	?	?	?	?
Δmik-1	x	AS	AS	loose hyphal knots (II.1)
Δmek-1	x	AS	AS	loose hyphal knots (II.1)
Δmak-1	x	AS	AS	loose hyphal knots (II.1)
Δnox-1	x	AS	AS	loose hyphal knots (II.1)
Δnor-1 (HP)	x	AS	AS	?
Δrac-1 (HP)	x	AS	AS	dense hyphal knots (III.1)
Δgdh-1	x	AS	AS	dense hyphal knots with trichogyne (III.2)
Δlao	x	AS	AS	?

Gene deletion mutants of two *N. crassa* hydrophobin genes (*eas* and the ortholog of *Mhp-1* from *M. oryzae* [3, 25, 45]), however, did not show impairment in VHF (Table 3.6). Reassessment of fruitbody development in these strains, however, might be worthwhile.

Nevertheless, the conducted morphological analysis provided valuable information about when particular genes become activated during fruitbody

development. The emerging order appears to be: *nox-1* and CWI MAPK genes > PR MAPK genes > *rac-1* > *gdh-1*. Table 6.4 summarizes the present findings, including genes currently under investigation.

Increased autolysis in CWI mutants resulted in rapid degradation of prematurely aborted protoperithecia. Another aspect of the Δ*mik-1*/Δ*mek-1*/Δ*mak-1* phenotype that influenced fruitbody development and its analysis, respectively, was the early onset of autolysis in the colony (Fig. 6.7). This phenomenon has been reported for a number of CWI MAPK mutants in different fungal species and is generally regarded as one determining feature of fungal cell wall mutants [4, 11, 28]. Alternatively, this autolytic phenotype could be the result of premature senescence caused by repressed TOR signalling in the absence of CWI MAP kinases (see Fig. 5.5). In *N. crassa*, early autolysis resulted in very quick degradation of aborted protoperithecia in the centre and subperiphery of the colony. This impeded experimental analysis of fruitbody development, and potentially is one reason why these structures have probably not been recognized during earlier investigations. Surprisingly, intact protoperithecial aggregates could be found and analysed close to the colony edge, before the mycelium reached the edge of the culture dish (Fig. 6.7C). As mentioned earlier, this was a surprising find, as wt colonies can extend to considerable sizes before initiating protoperithecial development in response to physical confinement at the colony edge. Furthermore, in the wt development of protoperithecia progresses from the centre outwards, but never the other way around. Although less frequently, autolysis of immature protoperithecia was also observed in the wt. In summary, this data suggests that if certain developmental checkpoints are not reached during fruitbody morphogenesis, further development is aborted and the material becomes reabsorbed and recycled within the colony. This has important implications for the preparation and timing of experimental analysis of these strains.

That this phenomenon is a direct effect of *mak-1* loss-of-function was demonstrated by complete phenotypic rescue upon reintroduction of MAK-1 (Fig. 6.8). Genetically complemented transformants developed normally on minimal medium and hyphal fusion was restored (Fig. 6.8A). Furthermore, female fertility was recovered resulting in the formation of mature protoperithecia (Fig. 6.8D to G), which differentiated into perithecia upon fertilization and produced ascospores in heterozygous crosses (data not shown). These results are consistent with earlier findings [32], but have extended our understanding about the role of the CWI MAPK pathway during early stages of protoperithecial morphogenesis, as they offer an explanation as to why fruitbody development is disrupted.

The CWI pathway acts upstream of the PR pathway during fruitbody morphogenesis. MAPK mutants from the cell wall integrity pathway abort in protoperithecial development earlier when compared to MAPK mutants from the pheromone response pathway (Fig. 6.6). This suggests that signalling through the CWI pathway is required earlier during protoperithecial development than signalling through the PR pathway. CWI MAPK mutants displayed defects which suggest that signalling through this cascade is required for ECM deposition and adhesion of enveloping hyphae during stage II of protoperithecial formation (Fig. 6.3). The PR pathway is known to regulate chemotropic interaction of mating partners leading to non-self fusion and fertilization [24], processes which occur after stage IV (fertilizable protoperithecium) has been completed. NRC-1/MEK-2/MAK-2 mutants have been reported to display only mild cell wall defects and to progress further in fruitbody development [28]. This notion could be confirmed by our analysis, which due to the absence of trichogyne-like hyphae, further suggests that the PR pathway might also act on the transition from stage III to stage IV (differentiation of a chemoattractive trichogyne)(Figs. 6.3 and 6.6). Thus, signalling through the PR pathway might not only be involved in trichogyne homing and mating cell fusion, but also in the initiation of trichogyne formation. Fig. 6.9

summarizes the distinguished roles of both pathways schematically. As trichogyne formation occurs in the wt (Fig. 6.1C) - and presumably other mutants such as Δ*gdh-1* (Fig. 6.5C) – in the absence of opposite mating type pheromone, the involvement of a self-signalling molecule which triggers morphogenetic transitions up until this point (stage IV) is indicated. Cross talk between all three *Neurospora* MAPK pathways (thus including the HOG pathway) during regulation of female sexual development is very likely and has been suggested previously [28, 32], but is not depicted in the diagram.

Previous reports suggested the complete absence of protoperithecia in MAPK mutants of the osmoregulatory pathway [16, 19], which presumably refers to mature, fertilizable, stage IV fruitbodies visible with the naked eye. At what stage protoperithecial morphogenesis is blocked and whether this phenotype is only a secondary effect of osmotic intolerance has not been determined. In a more recent paper the presence of small, curled side branches, typical of early stages during ascogonial formation have been reported for Δ*os-2* [28]. Our preliminary data, however, indicates that all three HOG MAPK mutants (Δ*os-4*/Δ*os-5*/Δ*os-2*) progress much further into fruitbody development, showing phenotypes similar to CWI MAPK mutants, including early abortion of enveloping hyphal aggregates (data not shown). Interesting is the fact that these mutants were not blocked in VHF based on our analyses. Whether the impairment in fruitbody development, therefore, is only an indirect defect of the general reduction in fitness, or indeed associated with OS protein function requires further investigation. Development of functional protoperithecia that progress through sexual development after fertilization, however, was fully restored after re-introduction of OS-2-sGFP into a Δ*os-2* strain background (data not shown).

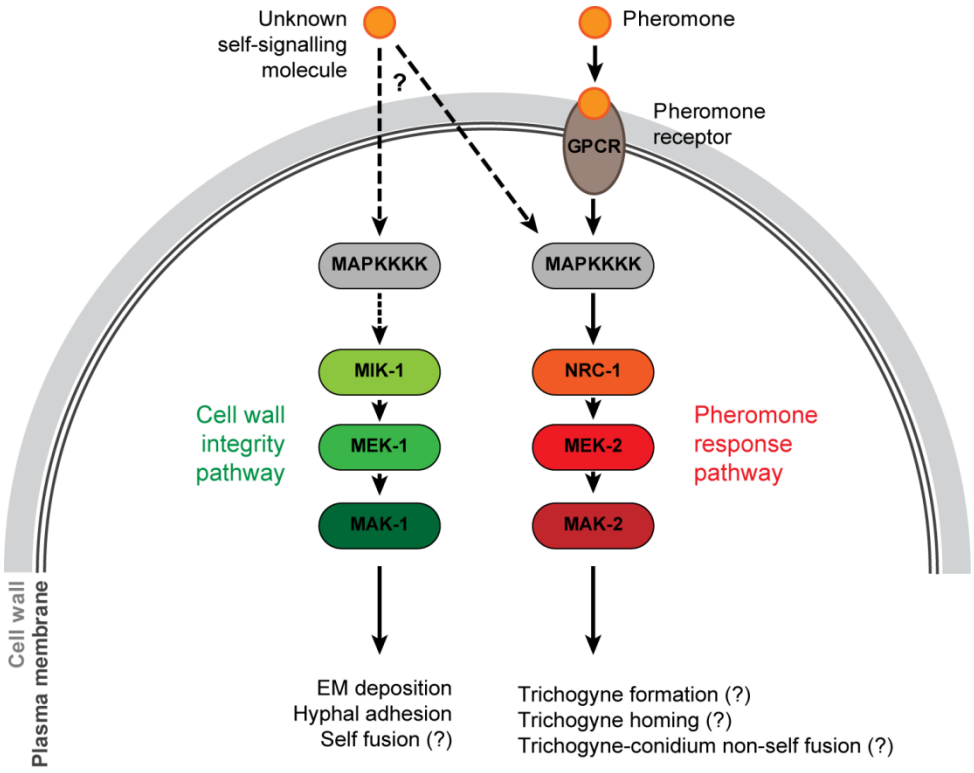

Figure 6.9 Suggested roles of two MAPK pathways in protoperithecial morphogenesis. Deletion mutants of any of the six MAP kinases cannot undergo hyphal fusion [24, 28]. Upstream components of the pheromone response pathway, e.g. the pheromones or subunits of the associated GPCRs are not required for cell fusion but are essential for male fertility, trichogyne homing and mating cell fusion [20, 23]**.** Mutants of the MIK-1/MEK-1/MAK-1 cascade are blocked at a slightly earlier stage of protoperithecial development than mutants of the NRC-1/MEK-2/MAK-2 cascade, potentially reflecting separate roles in self fusion during protoperithecial development and non-self fusion prior to fertilization.

Nevertheless, the conclusion that MAPK mutants of the CWI and HOG pathways are blocked at an earlier stage of sexual development compared to those of the PR MAPK pathway is also supported by our data. More detailed analysis involving double gene deletion mutants will be necessary to resolve this issue. Table 6.5 provides an updated view on sexual development in hyphal fusion mutants, including novel gene deletion strains analysed within this study, such as the VHF competency Δ*os-4*, Δ*os-5* and Δ*os-2* mutants.

Table 6.5 Fruitbody development in *N. crassa* gene deletion mutants. Mutants were used as females in heterozygous crosses with wt. Green indicates completed developmental stages; yellow indicates stages which were found to be severely impaired; red are those stages identified as being fully blocked. White represents unknown areas.

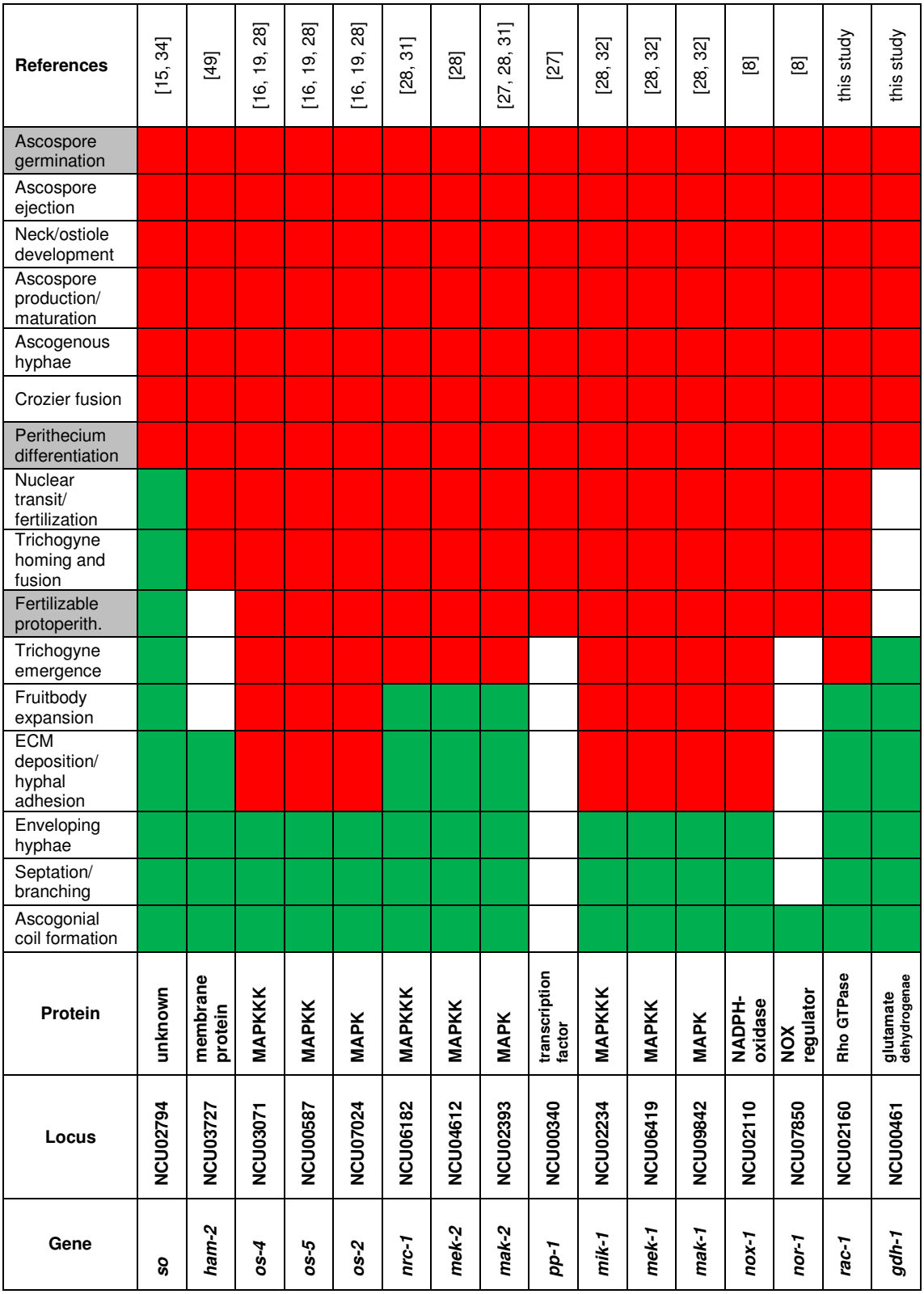

6.5. Summary

This chapter included the first detailed genetic and ultrastructural analysis of the early stages of sexual fruitbody morphogenesis in vegetative hyphal fusion mutants of *N. crassa*. Major findings include:

- LTSEM revealed new ultrastructural details of protoperithecial development which remain obscured in light microscopical samples covered in surface water
- protoperithecial morphogenesis comprises various stages which can be individually blocked in different gene deletion mutants
- increased autolysis of aborted protoperithecia in the colony centre and subperiphery of CWI MAPK mutants obscured previous analyses; early onset of fruitbody formation at the colony edge however, allowed detailed investigations of sexual development in these mutants
- defects in extracellular matrix deposition and hyphal adhesion are correlated with abortion of protoperithecial development and possibly provide a functional link to morphogenetic transitions prior to VHF in the mature colony
- although female sterility is a conserved defect amongst fusion mutants of *N. crassa*, the defect in VHF did not manifest in a conserved phenotypic defect during early stages of fruitbody morphogenesis
- morphogenetic analysis of gene deletion mutants provided clues about when particular genes become activated during protoperithecial development
- a number of gene deletion mutants progressed further in protoperithecial development than previously thought, such as the MAPK CWI mutants

6.6. References

1. **Anderson, J. B., and L. M. Kohn.** 2007. Dikaryons, diploids, and evolution, p. 333-348. *In* J. Heitman (ed.), Sex in fungi: molecular determination and evolutionary implications. American Society of Microbiology, Washington D.C.

2. **Backus, M. P.** 1939. The mechanics of conidial fertilization in *Neurospora sitophila*. Bulletin of the Torrey Botanical Club **1939:**63-67.

3. **Bell-Pedersen, D., J. C. Dunlap, and J. J. Loros.** 1992. The *Neurospora* circadian clock-controlled gene, *ccg-2*, is allelic to *eas* and encodes a fungal hydrophobin required for formation of the conidial rodlet layer. Genes and Development **6:**2382-2394.

4. **Birkaya, B., A. Maddi, J. Joshi, S. J. Free, and P. J. Cullen.** 2009. Role of the cell wall integrity and filamentous growth mitogen-activated protein kinase pathways in cell wall remodeling during filamentous growth. Eukaryotic Cell **8:**1118-1133.

5. **Bistis, G. N.** 1981. Chemotropic interactions between trichogynes and conidia of opposite mating-type in *Neurospora crassa*. Mycologia **73:**959-975.

6. **Bistis, G. N., D. D. Perkins, and N. D. Read.** 2003. Different cell types in *Neurospora crassa*. Fungal Genetics Newsletter **50:**17-19.

7. **Busch, S., and G. H. Braus.** 2007. How to build a fungal fruit body: from uniform cells to specialized tissue. Molecular Microbiology **64:**873-876.

8. **Cano-Dominguez, N., K. Alvarez-Delfin, W. Hansberg, and J. Aguirre.** 2008. NADPH oxidases NOX-1 and NOX-2 require the regulatory subunit NOR-1 to control cell differentiation and growth in *Neurospora crassa*. Eukaryotic Cell **7:**1352-1361.

9. **Coppin, E., R. Debuchy, S. Arnaise, and M. Picard.** 1997. Mating types and sexual development in filamentous ascomycetes. Microbiological and Molecular Biological Reviews **61:**411-428.

10. **Davis, R. H.** 2000. *Neurospora*: contributions of a model organism. Oxford University Press, Oxford.

11. **de Nobel, H., H. van den Ende, and F. M. Klis.** 2000. Cell wall maintenance in fungi. Trends in Microbiology **8:**344-345.

12. **Ferreira, A., S. Saupe, and N. L. Glass.** 1996. Transcriptional analysis of the *mt A* idiomorph of *Neurospora crassa* identifies two genes in addition to *mt A-1*. Molecular and General Genetics **250:**767-774.

13. **Ferreira, A. V. B., Z. An, R. L. Metzenberg, and N. L. Glass.** 1998. Characterization of *mat A-2*, *mat A-3* and Δ*matA* mating-type mutants of *Neurospora crassa*. Genetics **148:**1069-1079.

14. **Fleißner, A., S. Diamond, and N. L. Glass.** 2009. The *Saccharomyces cerevisiae* PRM1 homolog in *Neurospora crassa* is involved in vegetative and sexual cell fusion events but also has postfertilization functions. Genetics **181:**497-510.

15. **Fleißner, A., S. Sarkar, D. J. Jacobson, G. M. Roca, N. D. Read, and N. L. Glass.** 2005. The *so* locus is required for vegetative cell fusion and postfertilization events in *Neurospora crassa*. Eukaryotic Cell **4:**920-930.

16. **Fujimura, M., N. Ochiai, M. Oshima, T. Motoyama, A. Ichiishi, R. Usami, K. Horikoshi, and I. Yamaguchi.** 2003. Putative homologs of SSK22 MAPKK kinase and PBS2 MAPK kinase of *Saccharomyces cerevisiae* encoded by *os-4* and *os-5* genes for osmotic sensitivity and fungicide resistance in *Neurospora crassa*. Bioscience, Biotechnology, and Biochemistry **67:**186-191.

17. **Griffiths, A. J. F.** 1982. Null mutants of the *A* and *a* mating-type allels of *Neurospora crassa*. Canadian Journal of Genetics and Cytology **24:**167-176.

18. **Johnson, T. E.** 1976. Analysis of pattern formation in *Neurospora* perithecial development using genetic mosaics. Developmental Biology **54:**23-36.

19. **Jones, C. A., S. E. Greer-Phillips, and K. A. Borkovich.** 2007. The response regulator RRG-1 functions upstream of a mitogen-activated protein kinase pathway impacting asexual development, female fertility, osmotic stress, and fungicide resistance in *Neurospora crassa*. Molecular Biology of the Cell **18:**2123-2136.

20. **Kays, A. M., and K. A. Borkovich.** 2004. Severe impairment of growth and differentiation in a *Neurospora crassa* mutant lacking all heterotrimeric G-alpha proteins. Genetics **166:**1229-1240.

21. **Kershaw, M. J., G. Wakley, and N. J. Talbot.** 1998. Complementation of the Mpg1 mutant phenotype in *Magnaporthe grisea* reveals functional relationships between fungal hydrophobins. EMBO J **17:**3838-3849.

22. **Kim, H., and K. A. Borkovich.** 2004. A pheromone receptor gene, *pre-1*, is essential for mating type-specific directional growth and fusion of trichogynes and female fertility in *Neurospora crassa*. Molecular Microbiology **52:**1781-1798.

23. **Kim, H., and K. A. Borkovich.** 2006. Pheromones are essential for male fertility and sufficient to direct chemotropic polarized growth of trichogynes during mating in *Neurospora crassa*. Eukaryotic Cell **5:**544-554.

24. **Kothe, G. O., and S. J. Free.** 1998. The isolation and characterization of *nrc-1* and *nrc-2*, two genes encoding protein kinases that control growth and development in *Neurospora crassa*. Genetics **149:**117-130.

25. **Lauter, F. R., V. E. Russo, and C. Yanofsky.** 1992. Developmental and light regulation of *eas*, the structural gene for the rodlet protein of *Neurospora*. Genes and Development **6:**2373-2381.

26. **Leslie, J. F., and K. K. Klein.** 1996. Female fertility and mating type effects on effective population size and evolution in filamentous fungi. Genetics **144:**557-567.

27. **Li, D., P. Bobrowicz, H. H. Wilkinson, and D. J. Ebbole.** 2005. A mitogen-activated protein kinase pathway essential for mating and contributing to vegetative growth in *Neurospora crassa*. Genetics **170:**1091-1104.

28. **Maerz, S., C. Ziv, N. Vogt, K. Helmstaedt, N. Cohen, R. Gorovits, O. Yarden, and S. Seiler.** 2008. The nuclear Dbf2-related kinase COT1 and the mitogen-activated protein kinases MAK1 and MAK2 genetically interact to regulate filamentous growth, hyphal fusion and sexual development in *Neurospora crassa*. Genetics **179:**1313-1325.

29. **Nelson, M. A., and R. L. Metzenberg.** 1992. Sexual development genes of *Neurospora crassa.* Genetics **132:**149-162.

30. **Nowrousian, M., and U. Kück.** 2006. Comparative gene expression analysis of fruiting body development in two filamentous fungi. FEMS Microbiology Letters **257:**328-335.

31. **Pandey, A., G. M. Roca, N. D. Read, and N. L. Glass.** 2004. Role of a mitogen-activated protein kinase pathway during conidial germination and hyphal fusion in *Neurospora crassa*. Eukaryotic Cell **3:**348-358.

32. **Park, G., S. Pan, and K. A. Borkovich.** 2008. Mitogen-activated protein kinase cascade required for regulation of development and secondary metabolism in *Neurospora crassa*. Eukaryotic Cell **7:**2113-2122.

33. **Perkins, D. D.** 1992. *Neurospora*: The organism behind the molecular revolution. Genetics **130:**687-701.

34. **Perkins, D. D., A. Radford, and M. S. Sachs.** 2001. The *Neurospora* compendium: chromsomal loci. Academic Press, San Diego, California.

35. **Philley, M. L., and C. Staben.** 1994. Functional analyses of the *Neurospora crassa* MT a-1 mating type polypeptide. Genetics **137:**715-722.

36. **Pöggeler, S., and U. Kück.** 2000. Comparative analysis of the mating-type loci from *Neurospora crassa* and *Sordaria macrospora*: identification of novel transcribed ORFs. Molecular and General Genetics **263:**292-301.

37. **Raju, N. B.** 1992. Genetic control of the sexual cycle in *Neurospora*. Mycological Research **96:**241-262.

38. **Raju, N. B.** 1980. Meiosis and ascospore genesis in *Neurospora*. European Journal of Cell Biology **23:**208-223.

39. **Raju, N. B., and D. D. Perkins.** 1978. Barren perithecia in *Neurospora crassa*. Canadian Journal of Genetics and Cytology **20:**41-59.

40. **Read, N. D.** 1994. Cellular nature and multicellular morphogenesis of higher fungi, p. 254-271. *In* D. Ingram and A. Hudson (ed.), Shape and Form in Plants and Fungi. Academic Press, London.

41. **Read, N. D.** 1983. A scanning electron microscopic study of the external features of perithecium development in *Sordaria humana*. Canadian Journal of Botany **63:**3217-3229.

42. **Read, N. D., and A. Beckett.** 1985. The anatomy of the mature perithecium in *Sordaria humana* and its significance for fungal multicellular development. Canadian Journal of Botany **63:**281-296.

43. **Read, N. D., and A. Beckett.** 1996. Ascus and ascospore morphogenesis. Mycological Research **100:**1281-1314.

44. **Read, N. D., A. Fleißner, M. G. Roca, and N. L. Glass.** 2010. Hyphal fusion. *In* K. A. Borkovich and D. Ebbole (ed.), Cellular and Molecular Biology of Filamentous Fungi. American Society of Microbiology, Washington DC.

45. **Soonok, K., A. Il-Pyung, R. Hee-Sool, and L. Yong-Hwan.** 2005. *MHP1*, a *Magnaporthe grisea* hydrophobin gene, is required for fungal development and plant colonization. Molecular Microbiology **57:**1224-1237.

46. **Webster, J., and R. Weber.** 2007. Introduction to Fungi, 3rd ed. Cambridge University Press, Cambridge.

47. **Winefield, R. D., E. Hilario, R. E. Beever, R. G. Haverkamp, and M. D. Templeton.** 2007. Hydrophobin genes and their expression in conidial and aconidial *Neurospora* species. Fungal Genetics and Biology **44:**250.

48. **Wösten, H. A. B.** 2001. Hydrophobins: multipurpose proteins. Annual Review of Microbiology **55:**625-646.

49. **Xiang, Q., C. Rasmussen, and N. L. Glass.** 2002. The *ham-2* locus, encoding a putative transmembrane protein, is required for hyphal fusion in *Neurospora crassa*. Genetics **160:**169-180.

50. **Zickler, D.** 2009. Observing meiosis in filamentous fungi: *Sordaria* and *Neurospora*, p. 91-114. *In* S. Kenney (ed.), Meiosis - cytological methods, vol. 2. Humana Press, Heidelberg.

Chapter 7 – Redox signalling in cell fusion

7.1. Abstract

This chapter reviews aspects of how redox signalling influences fungal development, and in particular which roles reactive oxygen species (ROS) play during cell differentiation in *Neurospora crassa*. Novel implications of ROS functions in cell signalling and cell wall remodelling during CAT-mediated cell fusion will be presented, and discussed in the context of modulated NADPH-oxidase (NOX) activity during morphogenetic transitions in other fungal model systems. The key finding of NOX-1 localisation to the perinuclear ER, and its involvement in maintaining a low extracellular redox state demonstrate an important role for ROS-mediated signalling in CAT formation and homing. Parts of this work, involving the development of bioluminescent assays using the ultra-sensitive ROS detector Pholasin® have been carried out in close collaboration with Knight Scientific Ltd., Plymouth. Sincere thanks go to Dr. Jan Knight and Dr. James Reeves for their invaluable advice, support and encouraging interest in *Neurospora*.

7.2. Introduction

Over evolutionary times early heterotrophic organisms learned to adapt and exploit increasing levels of photosynthetic dioxygen (O_2) in the forming atmosphere. The development of antioxidant compounds, such as catalase, superoxide dismutase (SOD) or glutathione peroxidase (GPx), protected cells from damaging influences of ROS, which were inevitably formed when O_2 was chemically reduced or excited by radiation energy, such as UV light. The next step was to use O_2 as a final electron acceptor which enabled cells to colonize aerobic niches, obtain four times more energy from reduced carbon through respiration, and thus attain faster growth. The controlled production of ROS was then adopted to kill or control the growth of other organisms, such as microbial pathogens. Through further refinement of these 'ROS protection mechanisms' the originally life-damaging molecules became endogenous signals for the regulation of cell growth, differentiation, and programmed cell death.

7.2.1. Redox processes in eukaryotes

Reduction-oxidation (redox) biochemistry is simply based on the movement of electrons between molecules, i.e. reduction (gain of electrons) and oxidation (loss of electrons) of cellular compounds. Prominent redox-driven cellular processes are ATP synthesis inside mitochondria, carbohydrate production in chloroplasts, as well as oxidative lysis of phagocytosed pathogens in the mammalian immune system or oxidative bursts during plant defence responses.

In mitochondria and chloroplasts, transfer of high energy electrons generated either by the oxidation of a food source or oxidation of water through the absorption of sunlight, respectively, establish proton (H^+) gradients across membranes [2]. These gradients provide sufficient electron-motive force to enable subsequent electron transfer for the reduction of carbon dioxide (CO_2) into

carbohydrates, in the case of chloroplasts, or reduction of O_2 into H_2O, in the case of mitochondria. Thus, the same basic principle is used to gain energetically opposite products. Whereas carbohydrate molecules and O_2 are inputs for mitochondria in order to generate cellular energy in the form of ATP through respiration, carbohydrates and O_2 are the products of 'energy-fixation' in chloroplasts during photosynthesis. In any biological system, both processes are intrinsically linked (Fig. 7.1).

Upon engulfment by immune cells, microbial pathogens are destroyed through the rapid production of large quantities of ROS inside the phagosome [24]. This respiratory burst is generated by NADPH-oxidases (NOX) which transfer electrons from cytoplasmic NADPH through the membrane onto O_2 inside the phagosomal lumen, generating superoxide radicals ($O_2^{\bullet -}$) [37, 48]. Free radicals are molecules with unpaired electrons, and thus highly unstable, i.e. they are very reactive. When reacting with another molecule the second molecule loses an electron to the free radical that now, with a full complement of paired electrons, is more stable. However, in the process, the second molecule itself becomes a reactive free radical and a chain reaction is thus initiated, which is only broken when two free radicals combine. In case the second molecule is essential for a particular cellular process, its oxidation by the ROS can be detrimental for the cell. A good example are polyunsaturated lipids constituting biological membranes. Attack by a free radical on one of the carbon-to-carbon double bonds can lead to the formation of the corresponding lipid peroxyl radical and the initiation of a chain reaction in which the final product, lipid peroxides, no longer maintain the integrity of the plasma membrane [5], which eventually leads to cell death.

The oxidative action of $O_2^{\bullet -}$ mainly develops after its dismutation into hydrogen peroxide (H_2O_2) in the presence of H^+. Both ROS are not much more reactive than O_2 already, but usually give rise to the production of singlet oxygen ($^1O_2$) and hydroxyl radicals ($^{\bullet}OH$), which form in the presence of transition metals, such as iron and copper. Both metals are abundant co-factors of many enzymes (e.g.

cytochromes or oxidases), and therefore always present inside cells [35]. The •OH is the most reactive molecule on the planet and probably will react with the first molecule it encounters. Together with other ROS, these molecules comprise a 'deadly' oxidizing cocktail utilized for cell defence. Oxygen-dependent degradation is usually assisted by oxygen-independent degradation processes through the release of proteolytic granules (a process called 'degranulation') into the phagosome/lyzosome, which contain enzymes such as defensins and lysozymes. Other antimicrobial peptides are present in these granules, including lactoferrin which sequesters additional iron thereby boosting •OH production [47].

Similar to the mammalian immune system, plants use oxidative bursts to prevent pathogen entry and host tissue colonization. Pathogen recognition stimulates rapid $O_2^{\bullet -}$ and H_2O_2 generation which triggers programmed cell death in and surrounding the initial site of pathogen attack, strengthens the plant cell wall through oxidative cross-linking, and often induces systemic resistance [3, 43]. In a recent study, the rapid and transient increase in ROS production and activity of the antioxidative enzymes SOD, catalase and ascorbate peroxidase (APX) were measured in tomato plants in response to attack by the fungal pathogen *Fusarium oxysporum* [55]. 24 h post-inoculation (hpi) the H_2O_2 concentration increased 2.6-fold, 48 hpi SOD activity increased 2.9-times, and lipid peroxidation was 4.4-times higher 72 hpi. Remarkably, this oxidative burst was not sufficient to ward of the pathogen, which suggests that *F. oxysporum*, being a necrotrophic pathogen, induced ROS production in the plant tissue to facilitate host killing. This is a phenomenon which demonstrates that redox signalling is highly conserved among eukaryotes and works across kingdoms.

The above mentioned redox processes lead to the production and turnover of huge amounts of ROS, which is the reason why they are confined to specialized organelles or occur extracellularly. Although ROS produced in mitochondria and chloroplasts are not believed to act directly as signalling molecules, they contribute to the overall redox status of the cell, and thus indirectly influence ROS signalling

processes. Intra- and intercellular redox signalling processes which regulate cell differentiation and development of the organism usually involve much smaller concentrations of reactive molecule species.

7.2.2. Redox-mediated signal transduction

ROS are ideally suited as signalling molecules because they are small, can quickly diffuse short distances and some readily cross biological membranes. H_2O_2 due to its nonpolar nature crosses biological membranes especially well [89], whereas $O_2^{\bullet-}$ cannot penetrate a phospholipid bilayer. Furthermore, as signalling molecules they need to fulfil the following criteria [33]:

- they need to be produced where they are needed;
- they need to be produced rapidly and only when they are needed;
- they need to be perceived specifically, and their presence acted upon; and
- they need to be removed rapidly, so that the signal is not sustained.

Production: sources for ROS and RNS. ROS are produced either by excitation or reduction and include key molecules, such as singlet oxygen ($^1O_2$) superoxide ($O_2^{\bullet-}$), hydroxyl radical ($^{\bullet}OH$) and hydrogen peroxide (H_2O_2) (Fig. 7.1). Besides, the nitric oxide radical ($NO^{\bullet}$) and other reactive nitrogen species (RNS) derived from $NO^{\bullet}$, such as the peroxynitrite anion ($ONOO^-$), are additional main compounds involved in redox-signal transduction (Fig. 7.2) [21]. A variety of sources exist for the generation of ROS and RNS in eukaryotes and prokaryotes [20]. These, however, cannot easily be summarized in defined pathways but rather depend on the cellular context the molecules of interest act in. Nevertheless, a primary source of $NO^{\bullet}$ production are nitric oxide synthases, which are flavin- or haem-containing enzymes that use arginine as substrate.

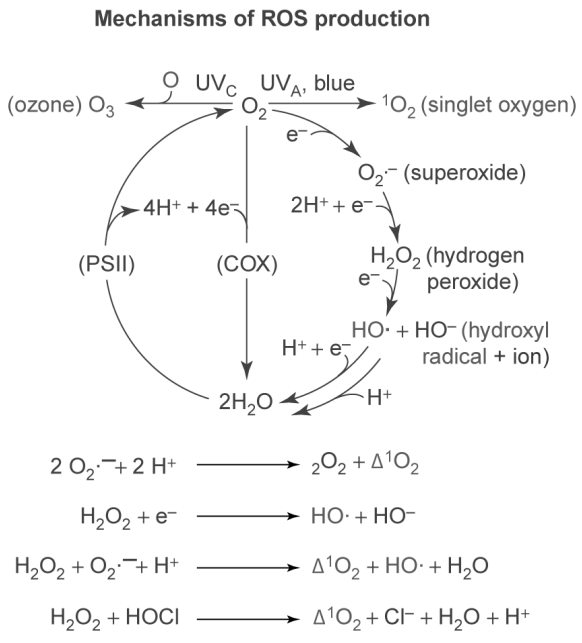

Figure 7.1 Mechanisms of ROS production. ROS are produced either by excitation of oxygen (O_2) through UV light, or its successive univalent reduction. O_2 is generated by photosystem II (PSII) in plants and is reduced by the repiratory chain cytochrome oxidase (COX) in mitochondria. Superoxide ($O_2^{\bullet-}$) reacts with itself, nitric oxide (see Fig. 7.2), and other radicals. H_2O_2 reacts with iron-sulfur centres and deprotonated cysteines of proteins. Importantly, both $O_2^{\bullet-}$ and H_2O_2 can spontaneously form singlet oxygen ($^1O_2$) and hydroxyl radicals ($^{\bullet}OH$), the most reactive ROS. Main reactions for $^1O_2$ and $^{\bullet}OH$ are shown below. Diagram modified from [1].

Other redox enzymes, such as xanthine oxidoreductase and nitrate reductase, are molybdenum-based and generate $NO^{\bullet}$ from nitrite; the latter in plants [62]. ROS also can arise from a number of different cellular sources, the most prominent ones being electron transport chains in mitochondria and chloroplasts, as well as NADPH-oxidases, and non-enzymic processes in fungal and plant cell walls. Comprehensive summaries on this topic are provided by references [4, 12]. The main substrates for ROS and RNS, oxygen, NADPH, arginine and nitrite, are abundant cellular compounds, and thus ROS and RNS generation can usually occur very rapidly and locally defined, provided the production pathway is specifically activated.

Most of the oxygen- or nitrogen-derived species are produced at low levels by normal aerobic metabolism and cellular damage they cause is constantly repaired or immediately prevented. This balanced cellular redox environment is preserved by antioxidants that maintain the reduced state through constant input of metabolic energy. Thus, redox signalling and cell metabolism are tightly linked. At this point it has to be noted that the terms ROS and RNS are vague terms and not in

all cases describe the chemical properties of the named molecules accurately. Recent reviews provide detailed descriptions of the chemical properties of $O_2^{\bullet-}$, $^{\bullet}OH$, $NO^{\bullet}$, NO^+, $NO_2^{\bullet}$ and $ONOO^-$ as signalling messengers in biological systems [27, 86]. Of special interest is the $NO^{\bullet}$/ $O_2^{\bullet-}$ regulatory system, in which the interaction of both radicals comprise a redox system as part of the cellular signalling network [27, 86]. Key points of this regulatory system are summarized in the following two paragraphs in order to exemplify the paradox and fascinating nature of redox signalling systems.

Signalling by $NO^{\bullet}$ requires only nanomolar levels of the compound because the affinity to its soluble receptor guanylyl cyclase (sGC) is extremely high and ligand binding leads to a 400-fold increase in sGC activity [66]. sGC becomes activated in the cytoplasm through S-nitrosylation (-SNO) by $NO^{\bullet}$, and converts GTP into cGMP, which is an important second messenger for several enzymes, including protein kinase G, which elicit cellular responses (Fig. 7.2A). A rise in intracellular cGMP levels can be counteracted through activation of phosphodiesterases, which hydrolyse cGMP into GMP, thereby switching of the signal. Besides this indirect negative regulation of $NO^{\bullet}$ via phosphodiesterase, other ROS can regulate $NO^{\bullet}$ signalling. $O_2^{\bullet-}$ can act as a direct antagonist by trapping $NO^{\bullet}$ as peroxynitrite (Fig. 7.2Ba). Dependent on the molar ratio between $NO^{\bullet}$ and $O_2^{\bullet-}$, this reaction can favour the conversion of $O_2^{\bullet-}$ into peroxynitrite when high levels of $NO^{\bullet}$ are present. As the non-enzymic complexation $O_2^{\bullet-}$ into $ONOO^-$ is faster than its enzymic dismutation into H_2O_2 by SOD [7], $NO^{\bullet}$ also plays an important role as antioxidant (Fig. 7.2Bb). Due to its immediate effects on $NO^{\bullet}$, intracellular $O_2^{\bullet-}$ levels as well need to be kept at nanomolar concentrations, otherwise $NO^{\bullet}$ would be complexed as $ONOO^-$ before it could reach its target enzyme sGC and elicit wanted cellular functions. This explains one crucial role of SOD in providing the chemical equilibrium that allows redox signalling through the $NO^{\bullet}/O_2^{\bullet-}$ system to work. Finally, $O_2^{\bullet-}$ can also act as antioxidant by reducing –SNO groups, thereby deactivating S-nitrosylated enzymes (Fig. 7.2Bc).

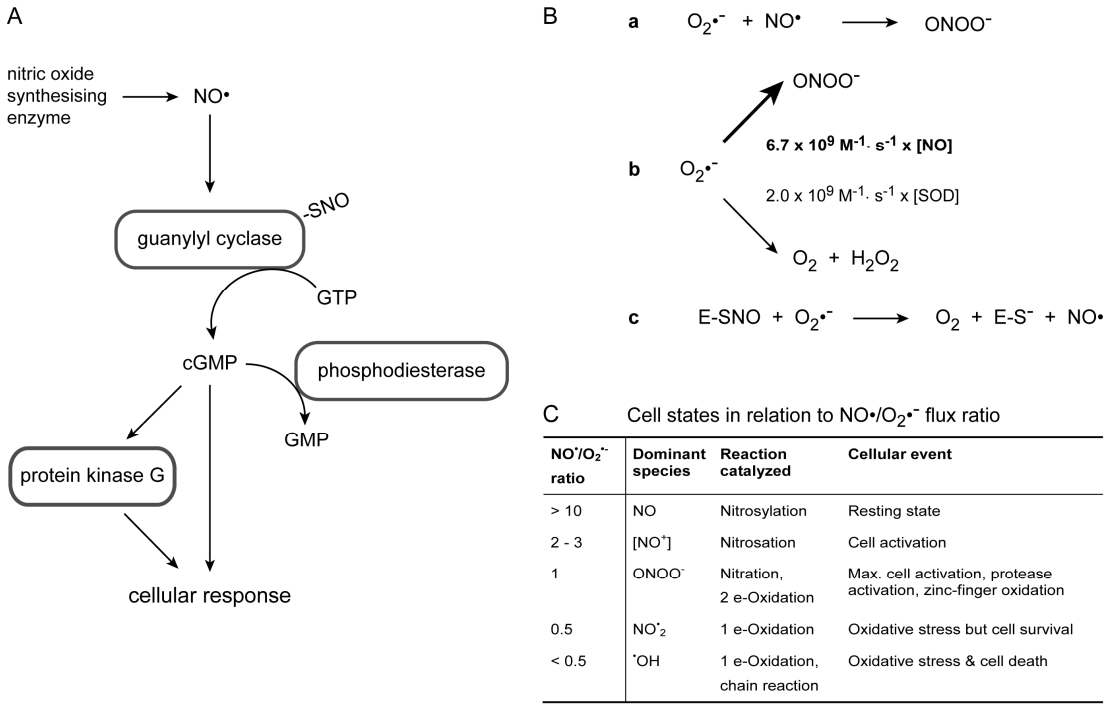

$NO^{\bullet}/O_2^{\bullet-}$ ratio	Dominant species	Reaction catalyzed	Cellular event
> 10	NO	Nitrosylation	Resting state
2 - 3	$[NO^+]$	Nitrosation	Cell activation
1	$ONOO^-$	Nitration, 2 e-Oxidation	Max. cell activation, protease activation, zinc-finger oxidation
0.5	$NO^{\bullet}_2$	1 e-Oxidation	Oxidative stress but cell survival
< 0.5	$^{\bullet}OH$	1 e-Oxidation, chain reaction	Oxidative stress & cell death

Figure 7.2 The $NO^{\bullet}/O_2^{\bullet-}$ regulatory redox system. (A) $NO^{\bullet}$ induces cell responses by activating cGMP production through guanylyl cylcase S-nitrosylation. cGMP acts as second messenger on downstream targets, such as protein kinase G. The signal is switched off by cGMP degradation through phosphodiesterase. **(B) (a)** Formation of peroxynitrite ($ONOO^-$) from superoxide ($O_2^{\bullet-}$) and nitric oxide ($NO^{\bullet}$). **(b)** The fate of $O_2^{\bullet-}$ is controlled by its reaction rate with $NO^{\bullet}$ and SOD, respectively. During steady-state, SOD is present in µM concentrations and the major drain for $O_2^{\bullet-}$ from the cell. However, when $NO^{\bullet}$ levels increase, it can effectively compete with SOD due to its > 3-times faster rate constant (bold). In this case, $NO^{\bullet}$ acts as an antioxidant. **(c)** $O_2^{\bullet-}$ can also act as antioxidant when it removes S-nitrosylation groups from target enzymes through reduction. **(C)** The ratio of $NO^{\bullet}/O_2^{\bullet-}$ flux determines the cellular state, which can range from relaxed (i.e. steady-state) to cell death. Diagrams modified from [7, 33, 86].

Superoxide not only acts as trap for $NO^{\bullet}$, but also can influence enzyme activity directly, for example that of sGC or the phosphatase calcineurin. $O_2^{\bullet-}$-mediated inhibition can be completely reverted by ascorbate and hence comprises a regulatory connection between protein function and the redox state of the cell. Interestingly, ascorbate can also act as prooxidant. This has been shown for apoplastic ascorbate, which as antioxidant (ROS scavenger) prevents oxidative cross-linking of plant cell wall polymers, but as prooxidant (ROS producer) induces the formation of $^{\bullet}OH$ which loosen the cell wall [29, 30]. Balancing both processes

has crucial implications for the regulation of plant cell elongation growth [49]. The double occupancy of certain molecules acting as pro- and antioxidants is generally dependent on the oxidative state of the cellular microenvironment, which for effective redox signalling to work should generally be low, thus adjust the cell at a reduced steady state. High levels or sustained levels cause overstimulation of the cell until the regulatory antioxidant system is exhausted. This point marks the transition from a steady-state redox signalling system to oxidative stress, which can severely damage or kill the cell. This is best demonstrated by changes in the $NO^{\bullet}/O_2^{\bullet-}$ flux ratio which alter the redox equilibrium of the cell, and consequently progress the system through various states, ranging from cell activation to cell death (Fig. 7.2C). It is becoming more and more apparent, that the cellular redox status is crucial to the correct functioning of many enzymes, hence its alteration is suspected to act as a signalling mechanisms in itself [21].

Perception: protein modification through ROS/RNS signalling. ROS and RNS signals can either be produced intracellularly or arrive from the outside. In any case, the current understanding is that these molecules, primarily due to their small size, do not engage in 'classical' ligand-receptor interactions, but rather pass on their signal by direct chemical modification of specific target proteins [27, 33]. One of the main points of action is the thiol group of cysteines. The reaction of cysteineyl thiolates with H_2O_2 can lead to the formation of different modifications, such as sulphenic acid (–SOH), sulphinic acid ($–SO_2H$), and sulphonic acid ($–SO_3H$), as well as disulphide bond formation (–S–S–) and glutathiolation (–S–GSH) (Fig. 7.3) [40, 65].

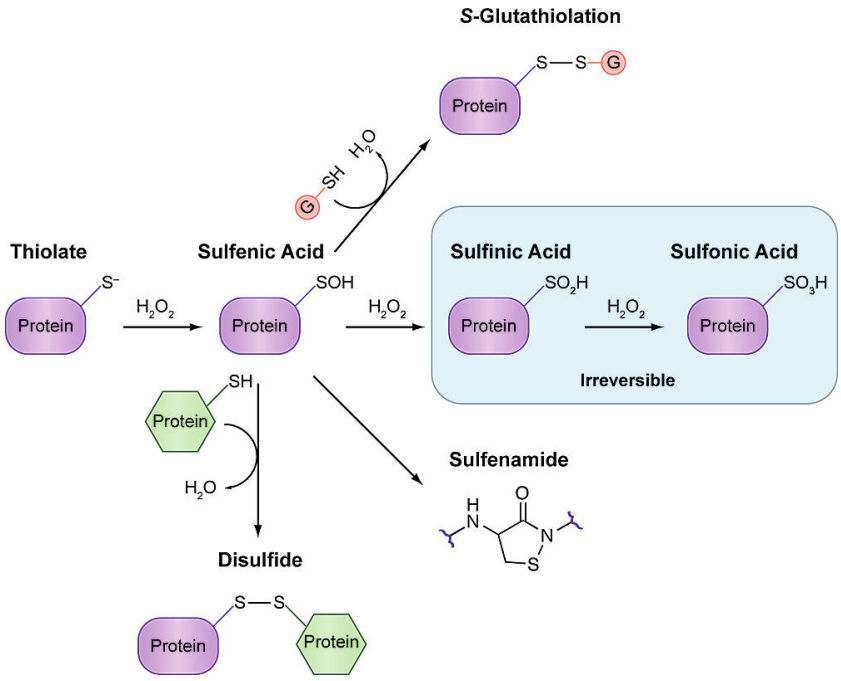

Figure 7.3 Oxidative modifications of protein cysteine residues. Low p*K*a cysteines are present in the cell as thiolates (-S^-) and form a sulphenic acid (-SOH) upon reaction with H_2O_2. Once formed, the -SOH can react with a second cysteine either in the same or a second protein to yield a disulphide bond. Alternatively, a -SOH group can react with the low molecular weight thiol glutathione (GSH) (pink circle) to form a special disulphide known as *S*-glutathiolation. In the event that a neighboring cysteine or glutathione are absent, the amide nitrogen of the neighboring residue can attack the -SOH to form a sulphenamide. Each of these oxoforms can be reduced by the GSH/glutathione reductase or thioredoxin/thioredoxin reductase systems to regenerate the thiols (see Fig. 7.4). The -SOH can also further react with H_2O_2 to generate the irreversible sulphenic (-SO_2H) and sulphonic (-SO_3H) oxoforms. Reproduced from [65].

Alternatively, reaction of $NO^{\bullet}$ with a thiol group can lead to S-nitrosylation (-SNO) [33]. These modifications alter protein activity by changing the oxidative status of the target molecule, influence protein stability, or generate intra- and intermolecular disulphide bonds. These modifications are of equal importance to other post-translational protein modifications, such as phosphorylation or ubiquitination. Each modification will have a different effect on each particular protein - or protein complex - and competition for the protein's limited number of thiol groups is likely to be an important regulatory mechanism of ROS and RNS

action. Therefore, balancing the exact ROS, RNS and glutathione concentrations will dictate the final outcome of the modified cellular function.

Known and putative protein targets for ROS and RNS include the previously mentioned guanylyl cyclase, phospholipases, ion channels and sensor kinases, as well as PKC, MAPKs and glyceraldehydes 3-phosphate dehydrogenase (GAPDH), and many more [4, 12, 27]. Besides the $NO^{\bullet}/O_2^{\bullet-}$ regulatory system introduced earlier, the NADPH/$NADP^+$-dependent glutathione and thioredoxin systems are other redox-cycling mechanisms of great significance for H_2O_2-mediated cell signalling (Fig. 7.4); especially due to their multicompartmental nature. NADPH/$NADP^+$ turnover in both systems is tightly linked to the pentose phosphate pathway, thus to the cell's metabolism, and components of both systems have been located in the cytosol, mitochondria, the nucleus and the endoplasmic reticulum (ER) [13, 36]. In a recent review a total of 183 established and potential plant protein targets for thioredoxin alone have been listed [12]. Of those, the cytoskeletal components tubulin, actin and profilin, components likely to act on the cell wall, such as ascorbate peroxidase/ascorbate oxidase and chitinase, proteins directly associated to metabolism, including glutamate dehydrogenase (GDH) and GAPDH, and the ROS scavenging enzymes SOD and catalase are of special interest for work presented in this thesis.

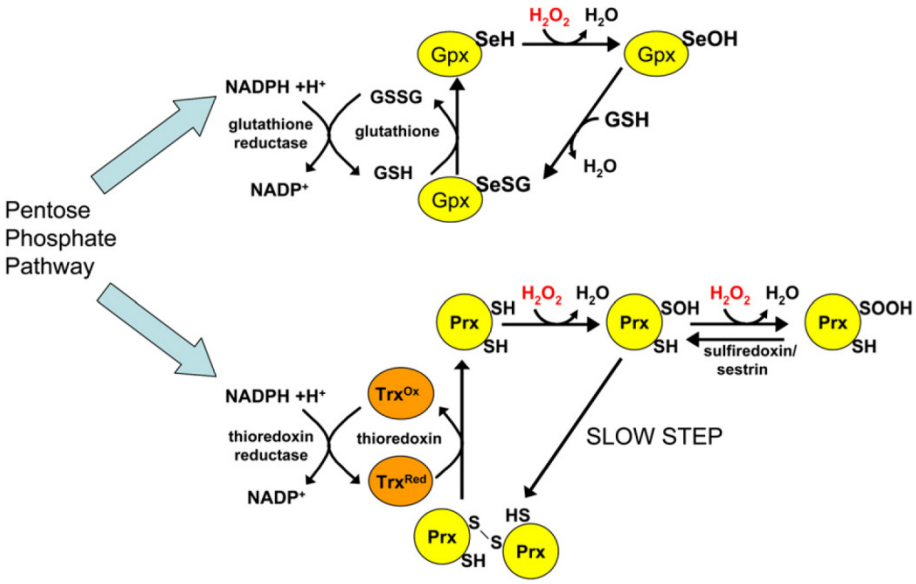

Figure 7.4 The Redox-cycling reactions involved in the catalytic removal of hydrogen peroxide by the glutathione peroxidase and thioredoxin peroxidase systems.The catalytic reduction of hydrogen peroxide (H_2O_2) by glutathione peroxidases (Gpx) and thioredoxin peroxidases involves the oxidation of catalytic thiol groups on selenocysteine (SeH) or cysteine (SH) residues in Gpx, and cysteine residues in thioredoxin peroxidases/peroxiredoxins. The recycling of oxidized peroxidase enzymes involves oxidation of reduced glutathione (GSH) or thioredoxin (Trx). The reduction of oxidized glutathione and Trx are coupled to NADPH by glutathione reductase or thioredoxin reductase, respectively. The pentose phosphate pathway provides NADPH for reduction, and hence antioxidant capacity is tightly linked to cellular metabolism. One class of peroxiredoxin, the typical 2-Cys Prx (Prx), contains two highly conserved cysteine residues that are involved in the thioredoxin-coupled catalytic reduction of H_2O_2. In the first step the peroxidatic cysteine residue becomes oxidized to sulphenic acid (-SOH), then forms a disulphide bond with the resolving cysteine residue on the partner protein in the homodimer preventing further oxidation. However, in eukaryotic 2-Cys Prx disulphide bond formation is slow and as a result the -SOH form of the peroxidatic cysteine residue is sensitive to further oxidation to the sulphinic acid ($-SO_2H$) derivative which can be reduced by either sulphiredoxin or sestrin enzymes [38]. Reproduced from [89].

NADPH-oxidases (NOX), which comprise the main source for endogenously produced $O_2^{\bullet-}$ and consequently H_2O_2, are assembled and localized to specific subcellular compartments in a highly regulated manner [16, 87]. First described and best studied are NOX located in the plasma membrane [26, 44] (see following section 7.2.3). But NOX complexes also localize to internal membrane systems, such as the ER [17], the newly discovered redox active endosomes (redoxosomes) [63],

and were found in the nucleus [88], indicating their involvement in redox-responsive gene expression. Interestingly, in the mammalian system, exogenously added H_2O_2 has been reported to be less effective at eliciting signal responses than endogenously produced H_2O_2 [18]. Furthermore, enzymes located in the cytoplasm have been found to be more susceptible to inactivation by exogenous H_2O_2 than those in the nucleus [10], underpinning the short range transmission nature of this molecule. Regulatory effects on gene transcription are signalled via thioredoxin peroxidase (Tpx)-mediated oxidation and reduction (Fig. 7.4). Under low levels of H_2O_2, Tpx is active and induces nuclear translocation and activation of one transcription factor. Under high levels of H_2O_2 Tpx is inhibited, preventing activation of that transcription factor, but instead increasing activation of MAPK, which in turn activates an alternative transcription factor by phosphorylation [89]. This results in a different response than under low H_2O_2 conditions (also see Fig. 5.6). This is one example of how redox signalling is integrated with other signalling pathways in the cell. In the same review [89], further molecular mechanisms required for H_2O_2-sensitive signalling are discussed in more detail. Of immediate interest might be the fact that proteins with deprotonated cysteine residues are more susceptible to oxidation by H_2O_2, than those that are fully protonated. This is important when considering that dependent on the pH of the subcellular environment (cytoplasmic pH 7.1–7.5, vacuolar pH 5.7–6.1 [46, 64]) proteins might be protonated and therefore unable to react with/sense H_2O_2. Consequently, so far identified H_2O_2 sensor proteins contain cysteine residues with generally low p*K*a which can be readily, specifically and reversibly oxidized at their thiol group (Fig. 7.3 and 7.4). In addition to reversible oxidation of deprotonated cysteine residues, H_2O_2 can also regulate protein activity by reacting with Fe^{2+}-containing cofactors or by oxidation (= inactivation) of antioxidants. Both strategies subsequently lead to functional changes of associated pathway components. Besides further molecular details, recent reviews covering these topics also highlight the current models of redox signalling networks [56, 65, 80]. The latest insights show that transient

phosphorylation of peroxiredoxin I inhibit its H_2O_2-detoxifying activity at the plasma membrane, thereby allowing transient accumulation of NOX-generated H_2O_2 and its interaction with downstream components concentrated at the signalling site [93]. The confined production within a subcellular region provides an answer to the paradox how the cell can generate increased levels of H_2O_2 and make it a useful signalling molecule, whilst preventing toxic effects for the rest of the cell [84]. Again, intracellular compartementalization of redox processes is the key strategy in creating signalling specificity whilst avoiding toxicity.

Removal: cellular protection against oxidative damage and reversal of redox modifications. Disposal of ROS and RNS on the one hand protects the cell from oxidative damage, but also provides means of reversing redox modifications, and thus has crucial importance for the downregulation of redox signals. All antioxidants play multiple roles, and function not only as ROS/RNS decomposers, but in doing so also as sensors and regulators of redox signalling. These compounds can generally be divided into two groups: non-enzymic antioxidants, such as ascorbic acid (vitamin C), tocopherols (vitamin E) or carotenoids, and antioxidant enzymes, such as SOD, catalase, and glutathione and thioredoxin peroxidases (Fig. 7.4). As some of these peroxidases use both, thioredoxin (Trx) and glutaredoxin (Grx) as proton donor, they are commonly referred to as peroxiredoxins [73]. Activity of antioxidant enzymes is particularly directed at disposing of $O_2^{\bullet-}$ and H_2O_2 (Fig. 7.5), primarily to prevent formation of $^1O_2$ and $^\bullet OH$ (Fig. 7.1), but also to regulate their intracellular levels and facilitate cell signalling. Covalent modifications of cysteine thiols by oxidation can be reversed by reduction, thereby ablating the signalling function of the modified protein. In case a disulphide bond has been created by ROS reduction, thioredoxins and glutaredoxins can act as protein disulphide reductases splitting this bond and resolving the signalling complex [19, 76].

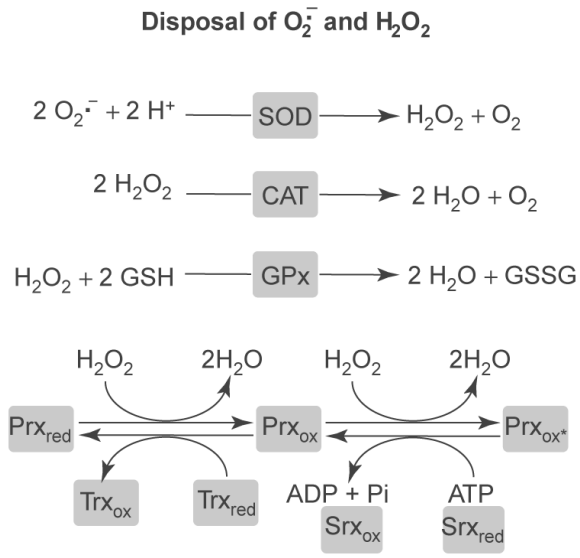

Figure 7.5 Mechanisms of ROS disposal. Superoxide dismutase (SOD) converts $O_2^{\bullet-}$ into H_2O_2, which is then decomposed by catalase (CAT) and peroxidases, such as glutathione peroxidase (Gpx) and peroxiredoxins (Prx). The thiol of a sensitive cysteine in Prx is oxidized to a Cys-sulphenic acid (Prx_{ox}) and reduced by reduced thioredoxin (Trx_{red}). The Cys-sulphenic acid in Prx_{ox} can further be oxidized by H_2O_2 to Cys-sulphinic acid (Prx_{ox*}), which is reduced back by the reduced sulphiredoxin (Srx_{red}) under ATP consumption. Diagram modified from [1].

As for their production, specificity of ROS/RNS decomposition and reversal of protein modifications is generated through different catalytic mechanisms of the involved enzymes, restricted subcellular localization, and co-regulation through associated pathways. Especially compartementalization of antioxidant enzymes provides a mechanism for restricting increases in H_2O_2 to a particular cellular region or organelle. Molecular details of catalytic removal of H_2O_2 have been extensively reviewed elsewhere [89]. In summary, compartmentalized subcellular colocalization of ROS/RNS production and degradation via enzymic and non-enzymic processes does ensure spatial confinement and rapid removal of generated signals, and prevents overoxidation and saturation of the system.

7.2.3. Functions of NADPH-oxidase-derived ROS in the regulation of fungal development

Based on the observation that during conidiogenesis in *Neurospora crassa* redox enzymes, including glutamine synthetase and glutamate dehydrogenase, and related compounds, such as NADPH and glutathione, are rapidly oxidized,

Hansberg and Aguirre proposed that cell differentiation occurs in response to oxidative stress [1, 34, 35]. According to this theory, undifferentiated and differentiated states are stable conditions in which low levels of ROS are maintained by balancing ROS generation (e.g. by NOX) and neutralization (e.g. by antioxidant enzymes). The definition of 'undifferentiated' and 'differentiated' state is arguable and depends on the personal interpretation of the morphogenetic stage under investigation. Important in the context of this study is that transition between these states occurs when a transient, unstable hyperoxidant state is induced, in which ROS generation increases beyond the steady-state redox equilibrium of the cell, triggering morphogenetic changes (Fig. 7.6).

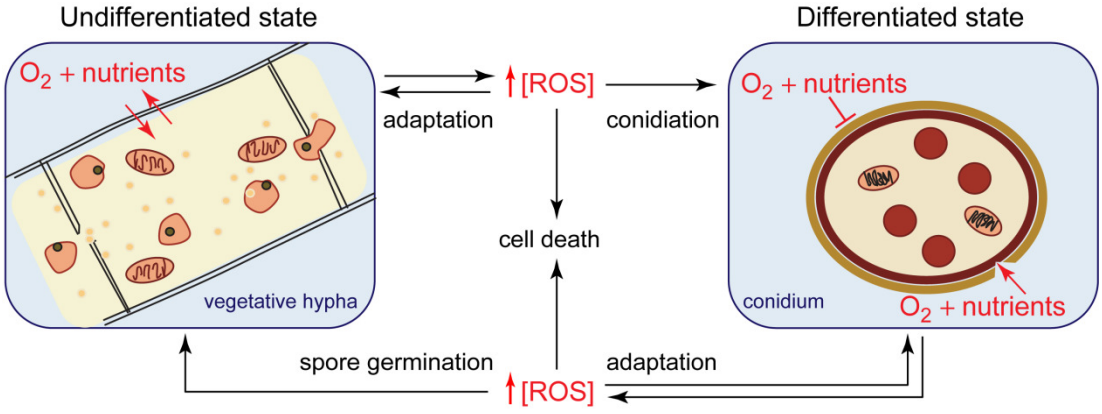

Figure 7.6 Hyperoxidant state cell differentiation model. The undifferentiated state is represented by a hypha of the vegetative mycelium (left). The differentiated state is represented by a conidium (right). Most importantly, both are morphologically stable states. Two differentiation processes are shown, that require transition through an unstable hyperoxidant state to occur. **Conidiation:** occurs when in response to an increase in ROS, cells of the vegetative mycelium insulate themselves from external oxidizing and reducing sources (O_2 and nutrients), and differentiate into asexual spores (conidia). **Spore germination:** occurs when conidia break insulation from external O_2 and nutrients, in order to develop a hyperoxidant state, progress through it by giving rise to the new mycelium, and quasi-simultaneously compensate this state with reducing power derived from nutrient utilization. **Adaptation:** both transitions can be blocked, when the rise in ROS is compensated with antioxidants, including reducing power from nutrients, before morphogenetic changes can occur. The cell returns to the previous stable state and adapts to the more oxidizing conditions without having morphogenetically changed. **Cell death**: occurs when cell differentiation or adaptation cannot take place. The reduced internal medium equilibrates with the oxidized environment and the cell dies. Modified from [1, 35].

Since its first formulation, this model has been supported by a number of findings in *N. crassa* and other microbial model organisms. The onset of conidial germination in *Neurospora* was accompanied by an increase in singlet oxygen, which caused oxidation of catalase 1 and accumulation of *cat-1* mRNA transcript, suggesting that a hyperoxidant state induces its own negative feedback-regulation through gene transcription [50, 51]. Interestingly, addition of exogenous H_2O_2 was sufficient to induce germination in an oxygen-free environment that otherwise did not allow morphogenetic transition from a latent spore to a growing hypha. Recently, similar findings have been made in *Candida albicans*. Yeast-to-hypha transition was induced by subtoxic concentrations (0.4-1 mM) of exogenously applied H_2O_2, which needed to be raised or diminished to induce morphogenesis in case antioxidants were present or absent, respectively [61]. In the filamentous fungus *Podospora anserina*, blockage of endogenous ROS production by mutational inactivation of the two NOX, *PaNox1* and *PaNox2*, abrogated development of sexual fruitbodies and ascospore germination, respectively [54]. Specificity of phenotypic defects between both mutants strongly suggests functional differences between the two NOX isoforms. This has also been documented for Nox1 and Nox2 of *Magnaporthe oryzae* [23]. Although appressoria were formed, appressorium-mediated cuticle penetration was non-functional in both gene deletion mutants, due a defect in penetration peg formation. Further findings showed that only *Δnox1* and *Δnox1Δnox2* double mutants failed to grow invasively *in planta* upon wound inoculation but not Δ*nox2*. This implied that Nox2 is not required for the later stages of infection, and thus is functionally distinct from Nox1. Inactivation of the *noxA* gene in *Aspergillus nidulans*, in fact the first fungal NOX to be recognized, dramatically decreased ROS generation and inhibited formation of cleistothecia at early stages of development, stimulated vegetative, mycelial growth, and suppressed conidiogenesis [45]. Interestingly, no other NOX isoform has so far been identified in *A. nidulans*. In the same organism, recent studies revealed a role for NOX-derived ROS in the regulation of apical dominance, i.e. the suppression of

secondary polarity axes in the general vicinity of a growing hyphal tip [79]. Contrasting earlier findings, which showed that NoxA (but not NoxB) dependent ROS production by the fungal endophyte *Epichloe festucae* regulates *in planta* growth [83] and requires direct interaction between the NOX regulator NoxR and the small GTPase RacA for NOX activation [82], Semighini and Harris [79], suggested an alternative NOX regulation pathway model. In this model, RacA can act as activator of NOX independently of NoxR. Instead, the interaction of NoxR with Cdc42 in a parallel pathway is suggested to regulate NOX localization. Another study, based on yeast-two-hybrid assays, suggested physical interaction between MgRac1 and its effectors Chm1, Nox1 and Nox2 in *M. oryzae* [15]. Here, the Chm1-MgRac1 interaction was associated with conidiogenesis, whereas the Nox1/2-MgRac1 interaction was necessary for appressorium morphogenesis and thus pathogenicity of the rice blast fungus. Although these studies provide compelling evidence for the crucial role of NOX-derived ROS in various aspects of fungal development, they also indicate that the details of underlying molecular regulation might differ amongst species. Recent reviews provide further insights into this topic and also highlight important biological functions of fungal antioxidants that counteract the consequences of NOX activation [28, 77, 81].

The most recent data from *N. crassa*, identified the NOX regulator NOR-1 as essential for the function of both NOX isoforms, NOX-1 and NOX-2, during sexual development [14]. Notably, mutant phenotypes, including female sterility and the absence of aerial hyphae, caused by genetic elimination of NOX-1 were not observed in NOX-2 mutants, suggesting both isoforms are functionally distinct in *N. crassa*. Female fruitbody development was normal in Δ*nox-2* strains, however, recovered ascospores from homozygous crosses did not germinate, even in the presence of exogenous oxidants which should induce a hyperoxidant state artifically. The mutant phenotype of Δ*nor-1*, however, was indistinguishable from that of Δ*nox-1*. This data supports a model in which NOR-1 does regulate NOX-1 and NOX-2 activity, but at different stages of sexual development. A closer

functional relationship between NOX-1 and NOR-1 was further supported by the fact that both proteins were required for normal development of aerial hyphae and condiogenesis, whereas NOX-2 appeared to be dispensable.

In the above presented studies, an increase of ROS, either due to endogenous activation of NOX or exogenous application of oxidants, was associated with cellular differentiation. Consequently, ROS increase leads to an up-regulation of antioxidant enzymes, such as catalases, SODs, peroxidases and peroxiredoxins, and in several of these cases, supplementation with antioxidants inhibited development. The hyperoxidant state cell differentiation model (Fig. 7.6), therefore, provides a plausible basis for the investigation of how changes in the cellular redox state through the alteration of ROS signalling pathway components affect cellular development. From this, a general hypothesis for the analysis of gene deletion mutants arises: null mutants in antioxidant enzymes can be expected to show increased levels of development, whereas development is reduced or completely abolished in mutants affected in prooxidant enzymes [35].

A central role for NADPH-oxidases in ROS-mediated development in fungi is obvious, even though the precise molecular machinery is not yet well understood, and most likely species and process specific. It is worth mentioning, that the presence of *nox* genes in fungi correlates with multicellularity. Phylogenetic analysis within the kingdom showed that the number of *nox* homologes ranges from none in unicellular and some in dimorphic fungi, to one, two and three in different filamentous species [81]. Noteworthy is the presence of the third NOX isform, NoxC, so far identified in seven ascomycete species, including several plant pathogens, such as *M. oryzae* and *F. graminearum* [81]. The C-terminal part of all NoxC proteins contains EF-hand motives which are thought to engage in Ca^{2+}-dependent protein-protein interactions. However, although *N. crassa* does not posses a NoxC ortholog, presence of NoxC is not exclusive to pathogenic fungi. The function of this particular isoform in fungi, however, remains to be discovered.

7.3. Results

7.3.1. Redox signalling components were required for hyphal fusion and CAT homing in *N. crassa*

The two NADPH-oxidase isoforms, NOX-1 and NOX-2, and the regulatory protein NOR-1 of *N. crassa* were identified by comparative genome analysis (section 2.5) with NOX components from *M. oryzae* [23] and *E. festucae* [82, 83]. Gene deletion strains for all three loci were obtained from the FGSC (Table 2.1), genetically verified by PCR (section 2.7) and homokaryon purified if required (section 2.8), before being phenotypically analysed for defects in hyphal fusion (section 3.3.3).

Δ*nox-1* and Δ*nor-1* strains were found to be fusion defective, whereas Δ*nox-2* even after several rounds of homokaryon purification remained fusion competent and showed no obvious phenotype change (Fig. 7.7). Genetic verification of Δ*nox-2* clones recovered after four generations of single spore isolation, however, revealed that *nox-2* was still present in the genome, indicating that it might be an essential gene required for spore germination, and thus generation of viable Δ*nox-2* homokaryons might not be possible with this method. Consequently, the putative Δ*nox-2* strains were excluded from further investigations. Colony morphologies of Δ*nox-1* and Δ*nor-1* strains were indistinguishable from each other, and characterized by dense mycelial growth, lack of aerial hyphae and pale orange colour (data not shown). Features, consistent with the equivalent mutant strains generated and reported by Caño-Dominguez and colleagues [14]. Most interestingly, fusion defects were also identified in two gene deletion mutants lacking enzymes closely associated with redox regulation: NAD^+-dependent glutamate dehydrogenase (Δ*gdh-1*) and a laccase resembling L-ascorbate oxidase (Δ*lao*). The fusion defective phenotype of Δ*lao* was very similar to that observed in Δ*nox-1* and Δ*nor-1*, including the formation of CAT-like protrusions, whereas similar structures were not observed in conidial germlings of Δ*gdh-1* (Fig. 7.8).

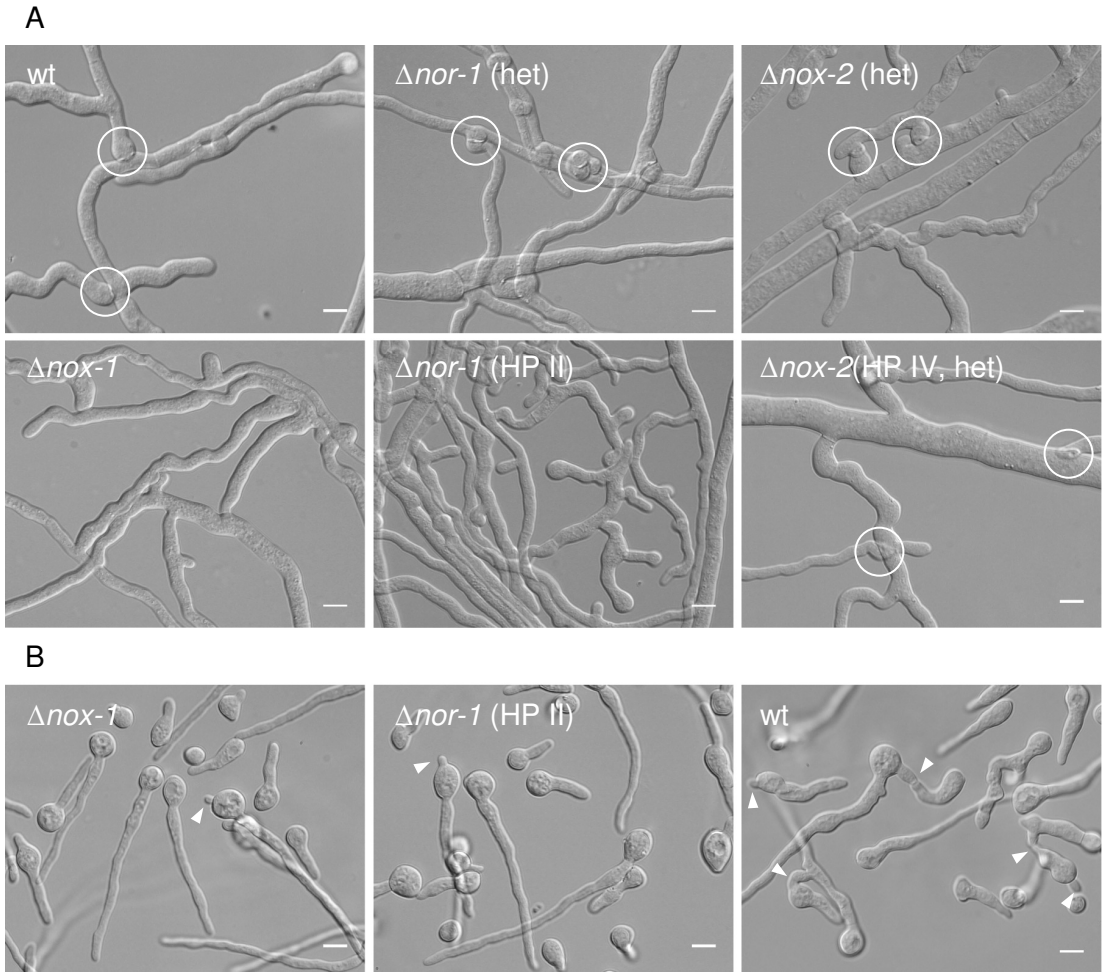

Figure 7.7 NOX-1 and NOR-1 are required for hyphal fusion in *N. crassa*. (A) Vegetative hyphal fusion was blocked in Δ*nox-1* and Δ*nor-1* strains. Δ*nor-1* was generated from the originally heterokaryotic strain by two successive homokaryon purification (HP) steps. A homokaryotic Δ*nox-2* strain could so far not be obtained, potentially indicating that NOX-2 is essential for spore germination. However, a phenotype change, including a VHF defect was not observed in any of the progressively selected clones. Fusion connections are circled. **(B)** The VHF defects of Δ*nox-1* and Δ*nor-1* could be confirmed in germling fusion assays. Both mutants formed long, thin and predominantly unbranched germ tubes (GTs), but did not establish cell fusion, although they formed CAT-like protrusions (arrowheads). CATs and cell fusion connections in the wt are indicated with arrowhead. Scale bars, 10 µm.

CAT formation assays, utilizing the microtubule depolymerising drug benomyl which prevents germ tube (GT) elongation but not CAT formation and cell fusion in the wt (section 4.3.6), suggested that Δ*nox-1*, Δ*nor-1* and Δ*lao* strains were able to form CATs, although with much lower efficiency compared to the wt (Fig. 7.9).

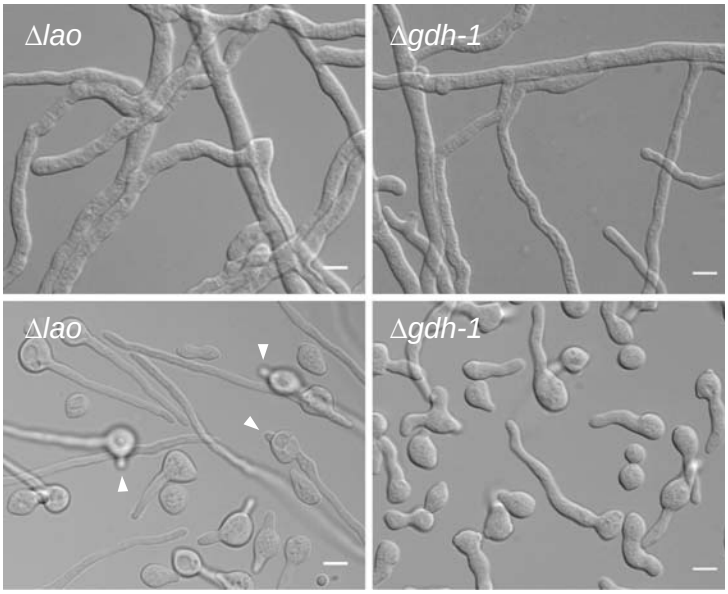

Figure 7.8 Fusion defects in Δ*lao* and Δ*gdh-1*. The fusion defective phenotype of Δ*lao* was very similar to that of Δ*nox-1* and Δ*nor-1*, in both the mature colony and conidial germlings. Δ*lao* germlings also formed CAT-like protrusions (arrowheads). Similar to other fusion mutants, hyphae of Δ*gdh-1* lacked contact-induced tip growth arrest. Conidial germlings of Δ*gdh-1* developed very slowly, but did not form CAT-like protrusions. Scale bars, 10 µm.

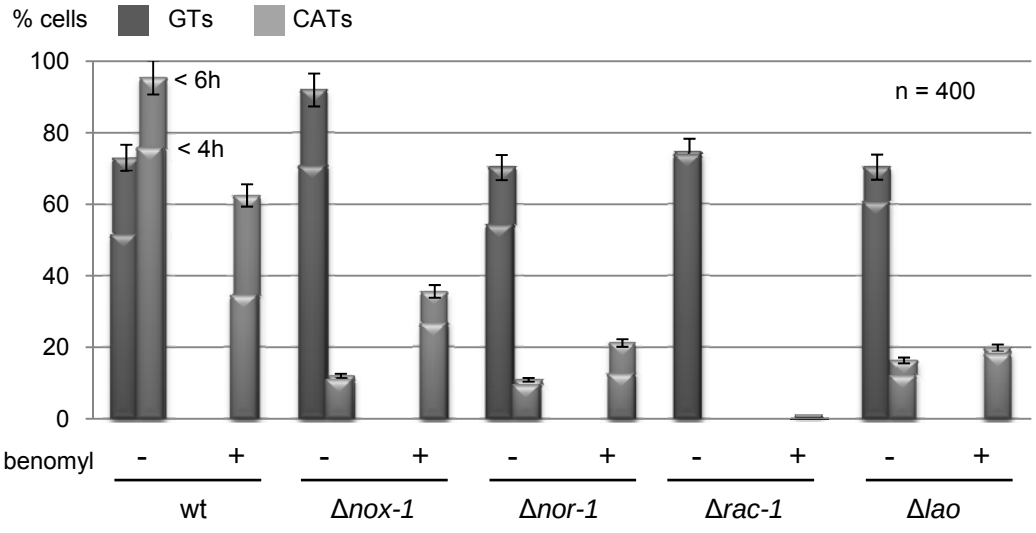

Figure 7.9 CAT formation in redox signalling mutants. The microtubule disrupting drug benomyl was used to distinguish CAT formation in gene deletion mutants involved in redox signalling. Wt cells, which undergo CAT-mediated cell fusion in the presence of benomyl

were used as positive control, whereas Δ*rac-1* cells, which do not form CATs at all, served as negative control (see Fig. 4.10). The number of cells forming GTs and CATs was quantified after 4 and 6 h of incubation in the absence or presence of ~3 µg/ml benomyl. Δ*nox-1*. Δ*nor-1* and Δ*lao* cells formed small cell protrusions in the presence of benomyl, suggesting these structures were CATs.

Taken together, these findings pointed towards an important role for NOX-generated ROS in hyphal fusion in *Neurospora crassa*, and indicate that NOX-1 and NOR-1 act during CAT formation and homing, potentially together with the L-ascorbate oxidase-like protein LAO. Additionally, NAD-dependent GDH-1 also appeared to have an important role in cell fusion, very likely associated to CAT induction. The notion that NOX-2 has no essential role in cell fusion requires further verification.

7.3.2. Genetic rescue of Δ*nox-1* and Δ*nor-1* mutants by ectopic expression of fluorescent NOX-1 and NOR-1 fusion constructs

To confirm that NOX activity was required for cell fusion, fluorescent NOX-1 and NOR-1 fusion constructs were generated, intended to rescue the gene deletion phenotype of Δ*nox-1* and Δ*nor-1* strains, respectively. *N. crassa* expression plasmids pAL1-NOX-1 and pAL1-NOR-1 were constructed by amplifying the coding regions for *nox-1* and *nor-1* from *N. crassa* wt cDNA using oligonucleotides nox1_if_*BamH*I_fw 5′-TTTCCTCGACGGATCCGCCAACATGAGTCTCCTC-3′ and nox1_if_*Pac*I_rv 5′-TTGCTCACCATGTTAATTAAAAAGTGTTCCTTCCAGAACC-3′, and noxR_if_*BamH*I_fw 5′-TTTCCTCGACGGATCCCACCTCAACATGTCGCTAAAAC-3′ and noxR_if_*Pac*I_rv 5′- TTGCTCACCATGTTAATTAATATCTCCTGGACCCAGACCT-3′, respectively (*BamH*I and *Pac*I restriction sites underlined), and subcloning these into *Bam*HI/*Pac*I linearized pAL1 in-frame to sGFP using In-Fusion® PCR cloning (section 2.6.8), whilst omitting endogenous stop codons of both genes. (Note: in

accordance to the nomenclature in other filamentous fungi I initially named the NOX regulator gene *noxR*, but this locus has been officially named *nor-1* in the meantime [14].)

pAL1-NOX-1 and pAL1-NOR-1 plasmids recovered after *E. coli* transformation (section 2.9) were verified by sequencing (section 2.6.10) and transformed into wt, Δ*nox-1* and Δ*nor-1* conidia of *N. crassa* by electroporation (section 2.10). Transformants were selected on Ignite medium and expression of the fusion proteins assessed in 12 clones per strain under the stereomicroscope, and in greater detail by epi-fluorescence and CLSM (section 2.12). In the process, two wrongly annotated introns within the *nor-1* locus were identified, which lead to disruption of the crucial NOX activation domain in the software-predicted transcript sequence. The correctly spliced *nor-1* mRNA transcript encodes a protein of 518 amino acids. *Nox-1* has been correctly predicted and annotated by the software, and encodes a 554 amino acids protein with five transmembrane domains. These findings are consistent with recently published results [14].

NOX-1-sGFP and NOR-1-sGFP showed distinct but consistent subcellular localization patterns when expressed in wt cells and transformants of Δ*nox-1* and Δ*nor-1*, respectively. NOX-1-sGFP was expressed at relatively high levels in germlings of wt and Δ*nox-1* tranformants, and localized to intracellular compartments (Fig. 7.10A and C). Pronounced vacuolar accumulation was noticeable, indicating extensive recycling of the membrane protein. NOR-1-sGFP was generally expressed at much lower levels, cytoplasmically localized and excluded from vacuolar compartments (Fig. 7.10B and D). Most importantly, labelling patterns of both fusion constructs were identical in transformants of the wt and corresponding gene deletion mutants, and furthermore, fusion defects were rescued in both Δ*nox-1*(NOX-1-sGFP) and Δ*nor-1*(NOR-1-sGFP) transformant strains, respectively, indicating correct function of the fusion constructs (Fig. 7.10C and D).

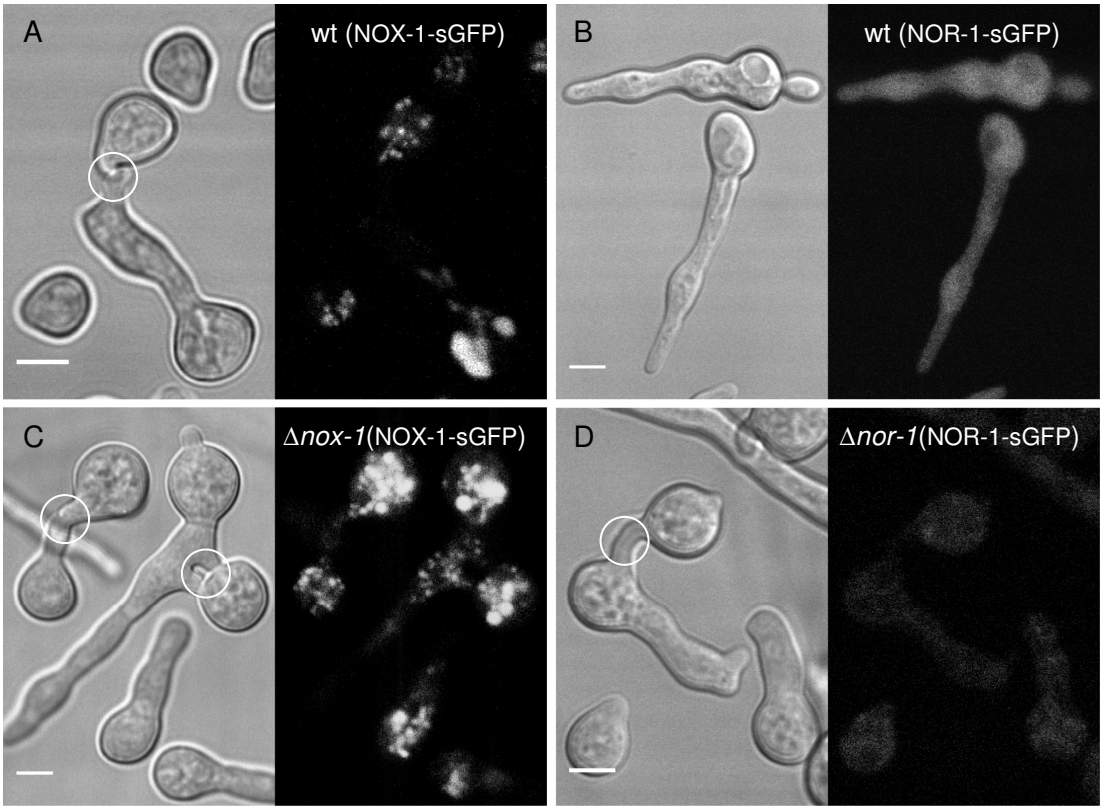

Figure 7.10 Localization patterns of NOX-1-sGFP and NOR-1-sGFP. Brightfield images of conidial germlings alongside intracellular localization of ectopically expressed NOX-1-sGFP and NOR-1-sGFP, respectively, recorded by CLSM. **(A)** Ectopically expressed NOX-1-sGFP localized to small organelles and vacuoles in the wt. **(B)** NOR-1-sGFP expressed in the wt localized to the cytoplasm and excluded from vacuoles. **(C)** Reintroduction of NOX-1-sGFP rescued the fusion defect of Δ*nox-1* cells and showed an intracellular labelling pattern identical to that observed in wt cells. **(D)** Although cytoplasmic expression of NOR-1-sGFP was generally very low in all transformants, the fusion defect of Δ*nor-1* cells was rescued. Cell fusion connections are circled. Scale bars, 5 µm.

7.3.3. NOX-1 localized to the perinuclear ER

Unfortunately, the expression of NOR-1-sGFP was too low in rescued transformants to allow detailed subcellular localization studies. NOX-1-sGFP, on the other hand, revealed an interesting labelling pattern when observed by epifluorescence microscopy (Fig. 7.11). NOX-1 localized to internal ring-like membranes, and tubular components very similar to the labelling pattern of the BEM46 homolog of *Neurospora* which has been localized to the ER and the plasma

membrane [58]. Perinuclear ER localization of NOX-1 was supported by co-staining with DAPI, which confirmed that the ring like structures were nuclei (Fig. 7.11C). Localization of NOX-1-sGFP to other internal membranes, such as vacuolar membranes or the plasma membrane, requires further analysis.

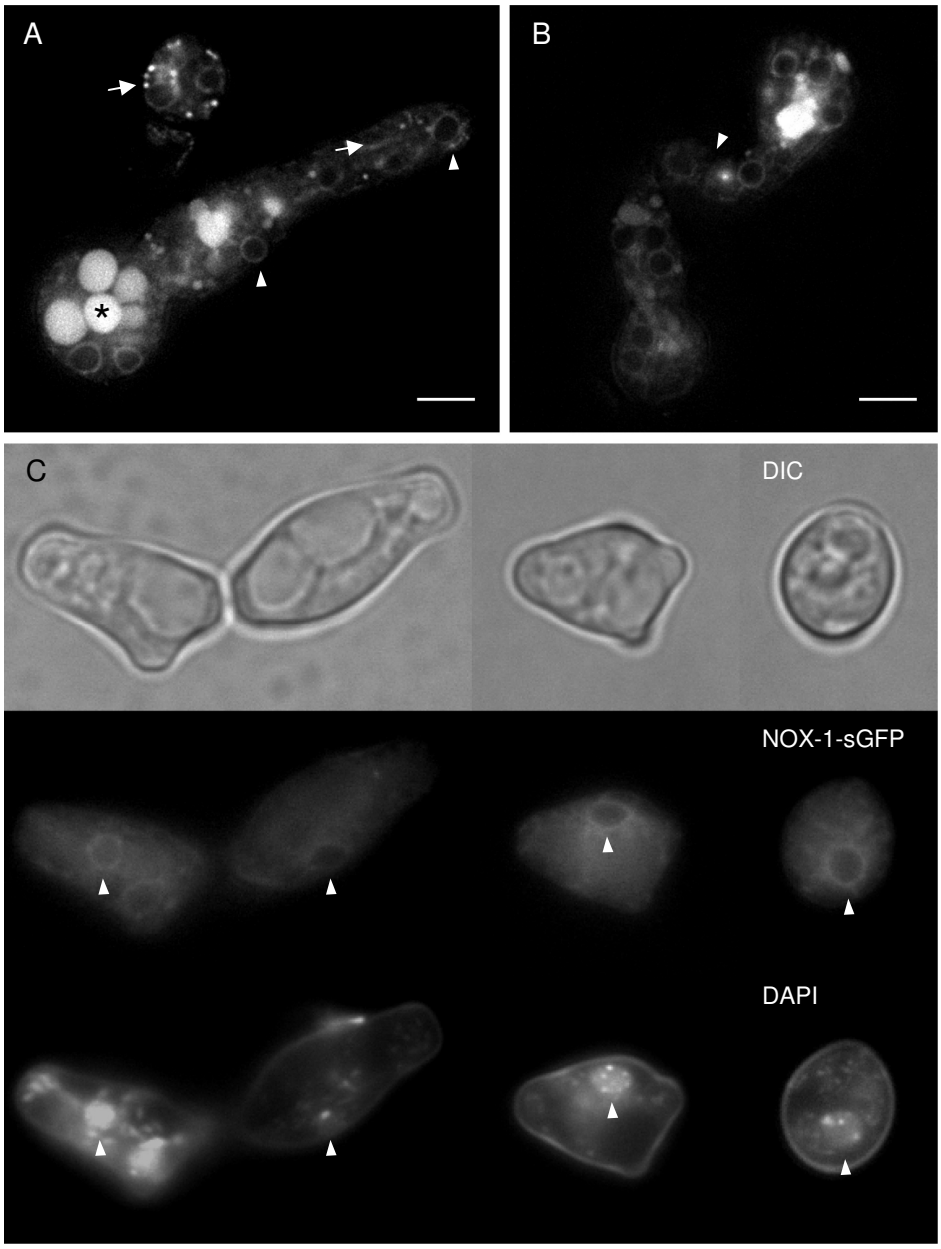

Figure 7.11 Subcellular localization of NOX-1-sGFP. (A) Deconvolved optical section of *N. crassa* germling expressing NOX-1-sGFP. NOX-1 localized to ring-like internal membranes (arrowheads) and clustered in small, bright dots potentially resembling cross sections of tubular vacuoles (arrows) (see supplementary movie 7.1 for full stack).

Furthermore, fluorescence was accumulated inside large vacuoles (asterisk) indicating recycling of the membrane complex. Scale bar, 5 µm. **(B)** Relocation or specific recruitment of NOX-1-sGFP during cell fusion to CAT tips was not observed. The CAT fusion site is indicated by an arrowhead (see supplementary movie 7.2 for full stack). Scale bar, 5 µm. **(C)** Optical sections of ungerminated conidia expressing NOX-1-sGFP. Co-staining with DAPI visualized nuclei (arrowheads) and showed that the ring-like membrane structures labelled with NOX-1-sGFP most likely resembled the perinuclear ER. Vacuolar accumulation of NOX-1-sGFP fluorescence was absent from ungerminated conidia. See supplementary movies 7.3-7.6 for full sequences.

Specific recruitment of NOX-1-sGFP during CAT-mediated cell fusion was not observed. Furthermore, fluorescence accumulated in large vacuoles of conidial germlings (Fig. 7.11A and B). This however, was absent in ungerminated conidia (Fig. 7.11C), indicating that recycling of NOX membrane complexes correlates with increased metabolic activity during germination.

7.3.4. H_2O_2 selectively inhibited CAT formation and cell fusion

To test whether or not changes of the reduced redox equilibrium influenced cell morphology and CAT-mediated cell fusion in particular, cellular development of *N. crassa* germlings was monitored on H_2O_2 gradient plates (section 2.11.3). Two starting concentrations were tested (application of 25 µl of 4.9M or 9.8M H_2O_2 solutions), which would lead to a theoretical final maximum concentration of 6 and 12 mM, respectively, when assuming homogenous diffusion throughout the 20 ml of solidified agar medium. Up to 10 mM H_2O_2 are commonly used to induce oxidative stress in filamentous fungi and yeasts [31, 52, 61], although much lower concentrations (0.3–0.5 mM) have also been reported to effectively induce oxidative stress in budding yeast [53, 94].

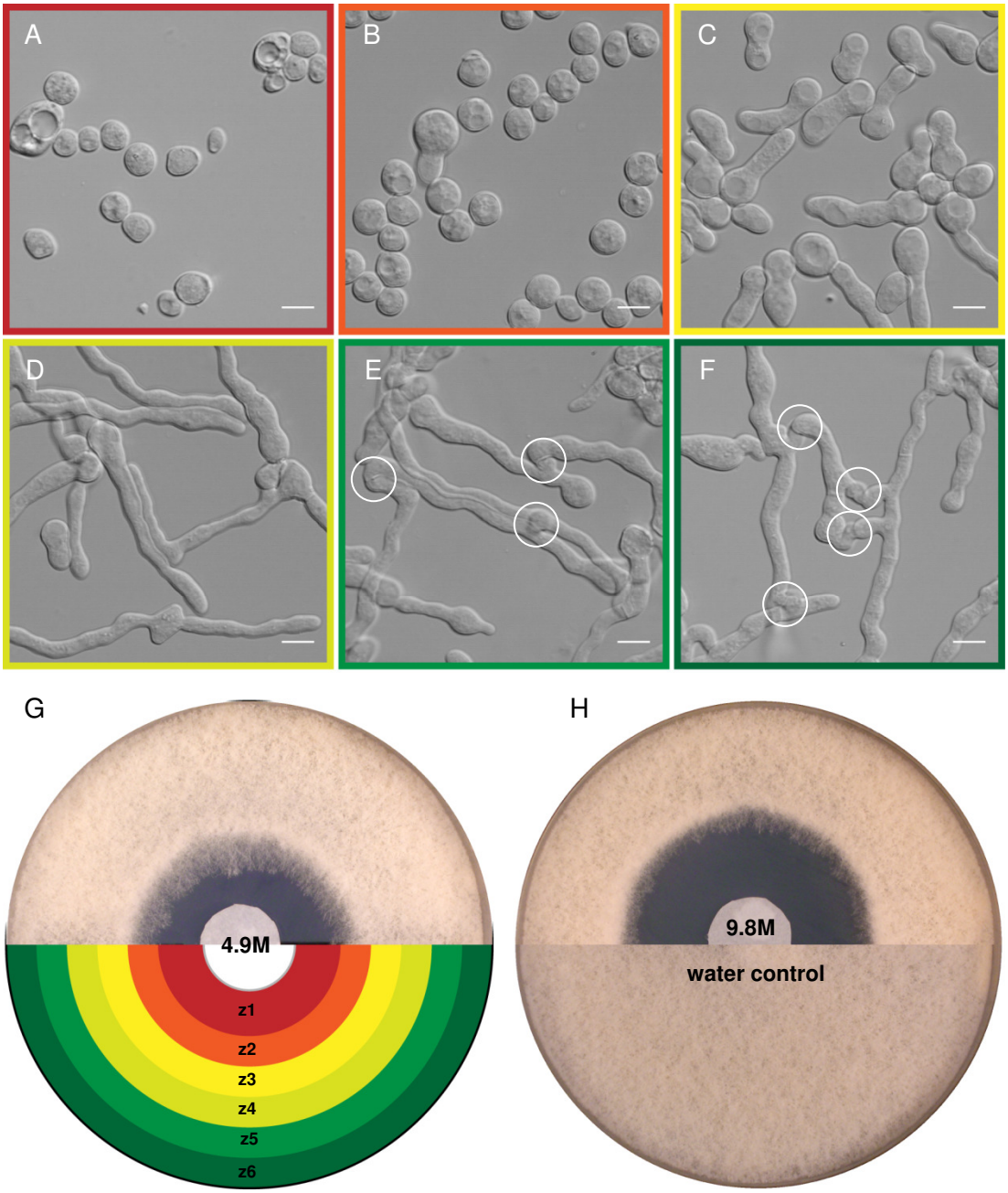

Figure 7.12 CAT formation and cell fusion were specifically inhibited on H_2O_2 gradient plates. A 1.5 cm diameter filter paper soaked with 25 µl of a 4.9 M H_2O_2 solution was placed in the centre of a 20 ml Vogel's medium plate, on which conidia of *N. crassa* wt were evenly distributed. Cellular development was recorded after 3 and 7 h of incubation at 35°C; images A to F show examples after 7 h. **(A) Zone 1:** closest to the H_2O_2 source, cells did not germinate and were presumably killed. **(B) Zone 2:** cells showed isotropic expansion and occasional germination. **(C) Zone 3:** the majority of conidia germinated, but formed only short swollen GTs, no CATs and did not fuse. **(D) Zone 4:** all conidia germinated and formed normal looking GTs, but did not form CATs or fusion connections. **(E) Zone 5:** although CATs were not clearly differentiated, fusion between conidial germlings was functional (circled). **(F) Zone 6:** germination, CAT formation and fusion occurred normally (fusion connections are circled). **(G)** Top: growth inhibition halo on gradient plate set up with 4.9 M

H_2O_2 after 22 h of incubation. Bottom: Schematic representation of the six developmental zones on the H_2O_2 gradient plates, drawn to scale of the six measured zones shown in A-F. Red colours indicate areas with no or only little germination; yellow colours indicate areas in which GTs but not CATs developed, whereas green marks areas in which germination and cell fusion occurred. Remarkable is the direct correlation between inhibition of germination and oxidative stress tolerance of mature hyphae which grew inwards into zone 2, but avoided zone 1. **(H)** Top: growth inhibition halo on gradient plate set up with 9.8 M H_2O_2 after 22 h of incubation; untreated water control below.

Six zones could be identified, in which conidial germlings reached different developmental stages (Fig. 7.12). Width and distance of these zones from the H_2O_2 source changed dependent on chemical concentration (compare growth inhibition halos in Figs. 7.12G and H). To better resolve morphological differences, plates with the shallower gradient, i.e. with the lower starting (4.9 M) and thus final concentration of H_2O_2, were analysed. From immediately at until about 7.5 mm away from the source (zone 1) conidial germination was completely inhibited (Fig. 7.12A), and cells presumably killed as no growth occurred even after > 20 h of incubation (Fig. 7.12G). 7.5–12.5 mm away from the source (zone 2) conidia grew isotropically and occasionally germinated, showing they were alive but inhibited to polarize and develop GTs. Zone 3 ranged from 12.5–17.5 mm, and allowed germination of the majority of the cells. CAT formation and thus cell fusion, however, were completely blocked. Furthermore, GT growth progressed slowly, resulting in only short and swollen GTs after 7.5 h of incubation (Fig. 7.12C). In zone 4, 17.5–22.5 mm away from the source, all conidia germinated and GT elongation progressed normally. Interestingly, CAT formation and thus cell fusion were still inhibited (Fig. 7.12D). Cell fusion first occurred 22.5 mm away from the source. In this fifth zone however, CATs were not clearly distinguishable, indicating that they were not fully differentiated (Fig. 7.12E). Furthermore, cell fusion occurred less frequently. The normal CAT phenotype and full rate of cell fusion were achieved from > 27.5 mm away from the source (Fig. 7.12F). The quantification of GT formation and cell fusion under these conditions is shown in Fig. 7.13.

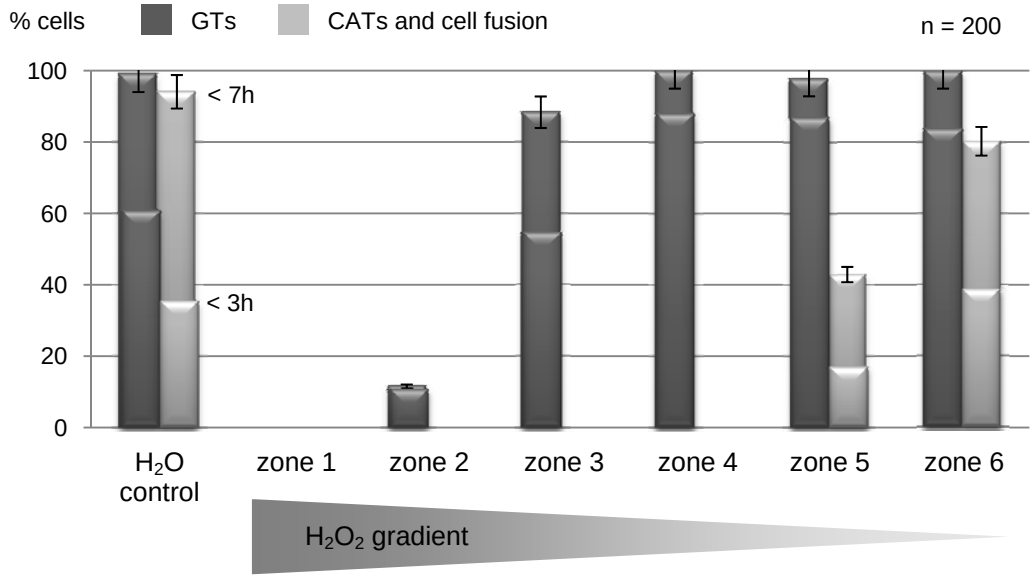

Figure 7.13 Low concentrations of H_2O_2 inhibited CAT formation and cell fusion, but not germination and GT elongation. Quantification of spore germination and CAT-mediated cell fusion after 3 and 7 h of incubation on H_2O_2 gradient plates as shown in Fig. 7.12. The transition from zone 3 to zone 4 marked a H_2O_2 concentration which no longer interfered with normal GT development. CAT formation and cell fusion, however, were still suppressed. The transition from zone 4 to zone 5 represented a H_2O_2 concentration below which CAT formation and cell fusion was again possible.

To determine the minimal concentration of H_2O_2 required to specifically block CAT formation and cell fusion, germling assays were performed in liquid cultures (section 2.4.2.2) (Figs. 7.14 and 7.15). Defined amounts of H_2O_2 were added as either 0.1 M, 0.01 M or 0.001 M aqueous stock solutions yielding final concentrations between 5 μM to 10 mM H_2O_2. 1 mM H_2O_2 effectively blocked CAT formation and cell fusion without inhibiting germination and GT growth (Fig. 7.14). In this experiment, H_2O_2 was added after 1.5 h of incubation, which explains the approx. 20% of initial germination in the 5 mM and 10 mM samples occuring before addition of the chemical. Addition of $\geq$ 2 mM H_2O_2 directly from the incubation start completely blocked spore germination (Fig. 7.15A, below). More than 5 mM H_2O_2 lead to vacuolation indicative of cell stress, and more than 10 mM completely blocked isotropic growth and germination, and presumably were lethal.

Here, germination is defined as the event of cell symmetry breaking leading to the emergence of any protrusion, i.e. GTs or CATs, from the spore after an initial phase of isotropic expansion. CAT-mediated cell fusion usually does not start before 2 h of incubation at 35°C in the wt, and was completely inhibited upon addition of 5 and 10 mM H_2O_2; as was further germination and GT elongation. Addition of 4 U catalase abrogated the inhibitory effects of H_2O_2 dependent on its overall concentration (Fig. 7.14).

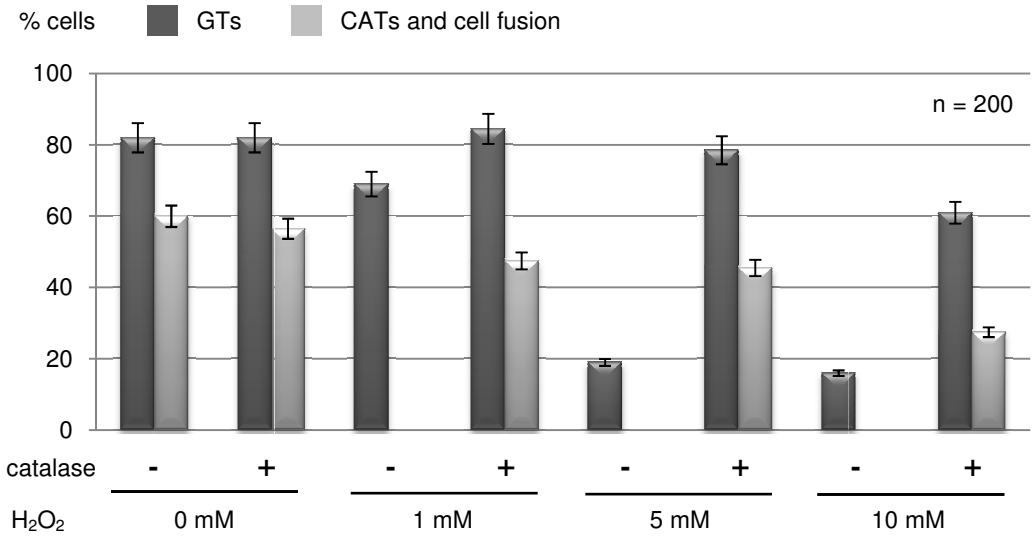

Figure 7.14 Specific inhibition of CAT-mediated cell fusion by H_2O_2 occured in the sub-mM range and could be rescued by the addition of catalase. Aqueous stock solutions of H_2O_2 were added to growing *N. crassa* germlings after 1.5 h of incubation at 35°C, to yield the indicated final concentrations. GT formation and CAT-mediated cell fusion were recorded and quantified 2.5 h after chemical addition (4 h total). As a control, 4 U catalase were simultaneously added with H_2O_2. Addition of catalase alone had no effect on germination and cell fusion. More than 1 mM H_2O_2 completely inhibited CAT formation and thus cell fusion. Concentrations above 1 mM furthermore inhibited germination and GT elongation. Dependent on the total concentration of H_2O_2, its inhibitory effects were abrogated by the addition of catalase.

Most interestingly, addition of 0.05 mM H_2O_2 inversed the GT/CAT ratio, i.e. promoted the formation of elongated GTs (GTs which are at least three times as long as the spore diameter), and suppressed CAT formation and cell fusion. Not surprisingly, this effect was stronger with increasing H_2O_2 concentration, and led to

the complete inhibition of CAT formation above 0.1 mM H_2O_2 (Fig. 7.15A). The minimal H_2O_2 concentration which induced detectable changes in the GT/CAT ratio was 10 µM. Obvious morphological changes, however, occurred between 25 and 50 µM H_2O_2 (Fig. 7.15B).

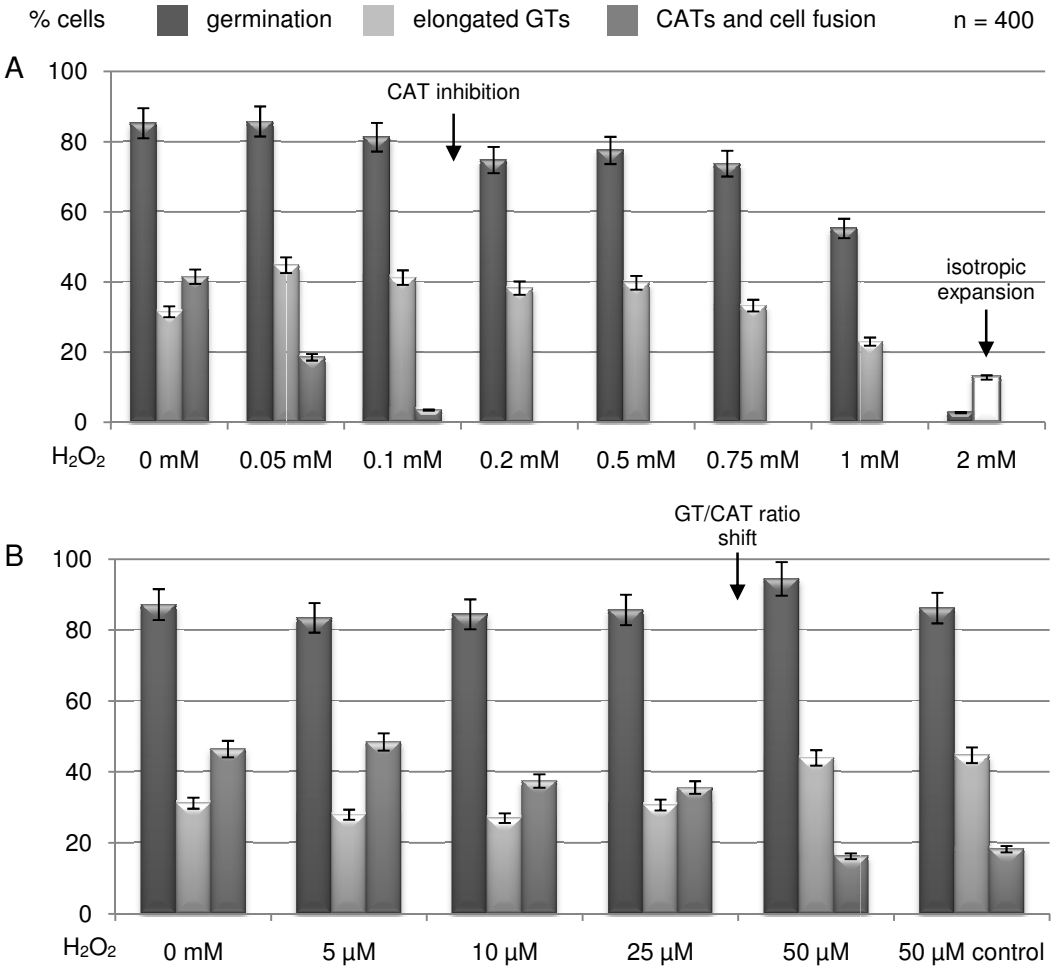

Figure 7.15 Micromolar concentrations of H_2O_2 induced morphogenetic changes in conidial germlings. Quantification of (1) cell germination, i.e. protrusion of GTs or CATs, (2) formation of elongated GTs, i.e. GTs that are at least three times as long as the spore diameter, and (3) formation of CATs and cell fusion connections, after 3 h of incubation at 35°C in the presence of exogenous H_2O_2. **(A)** Without exogenous H_2O_2 cells favoured the formation of CATs over the production of elongated GTs, resulting in a higher percentage of fused cells. Addition of 0.05 mM H_2O_2 inversed the GT/CAT ratio, now promoting the formation of elongated GTs and thus suppressing cell fusion. This effect was stronger with increasing H_2O_2, and lead to the complete inhibition of CAT formation above 0.1 mM H_2O_2. In the presence of 2 mM H_2O_2 germination was almost completely blocked, although extended isotropic expansion occurred, showing that the cells were still viable, but unable to break cell symmetry. **(B)** The minimal H_2O_2 concentration which induced detectable changes

in the GT/CAT ratio was 10 µM. The clear morphological shift, however, occurred between 25 and 50 µM H_2O_2. Note: the '50 µM' condition was generated by diluting a 0.001 M H_2O_2 stock solution 1:20. To control for pipetting inaccuracy, the '50 µM control' condition was generated by diluting a 0.01 M H_2O_2 stock solution 1:200.

Fig. 7.16 shows the aberrant spore morphologies which developed under the influence of H_2O_2, and were quantified in Figs. 7.14 and 7.15. Interestingly, identical phenotypes were observed when cells were treated with some *a priori* antioxidants. Whereas known H_2O_2 scavengers, such as catalase and potassium iodine (KI), as well as the putative $^{\bullet}OH$ scavenger mannitol showed no effects in the tested concentration ranges, addition of > 1 mM ascorbic acid showed clear effects, as did the flavocytochrome (including NOX) inhibitor diphenyleneiodonium (DPI) (Fig. 7. 17). In the presented experiment, however, additive effects due to the presence of 1% DMSO, certainly played a role, and thus need to be corrected in future applications. Nevertheless, the suppression of CAT-mediated cell fusion was significantly stronger in the sample containing 20 µM DPI compared to the 1% DMSO control.

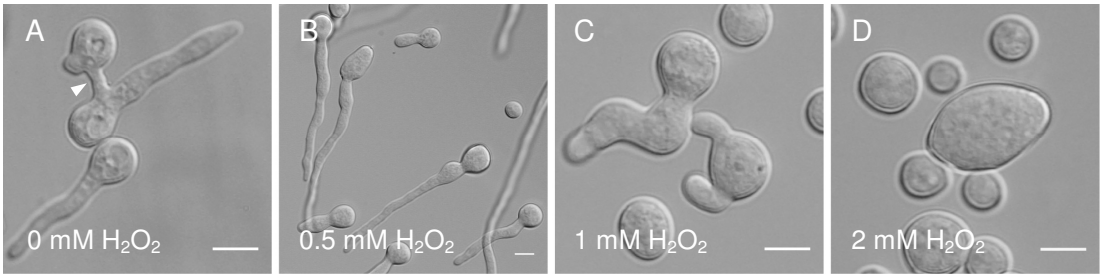

Figure 7.16 Developmental stages of *N. crassa* germlings reached under the influence of H_2O_2. All images were taken after 3 h of incubation at 35°C in liquid medium w/o H_2O_2. **(A)** In the absence of exogenous H_2O_2 conidial germlings formed GTs and CAT fusion connections (arrowhead). **(B)** In the presence of 0.5 mM H_2O_2 CAT formation was blocked and growth of elongated GTs was promoted. **(C)** 1 mM H_2O_2 significantly reduced the germination rate and lead to noticable isotropic swelling of conidia. **(D)** In the presence of 2 mM H_2O_2 cell polarisation was completely inhibited and cells only expanded isotropically, up to four times of their normal diameter (compare A and D). Scale bars, 10 µm.

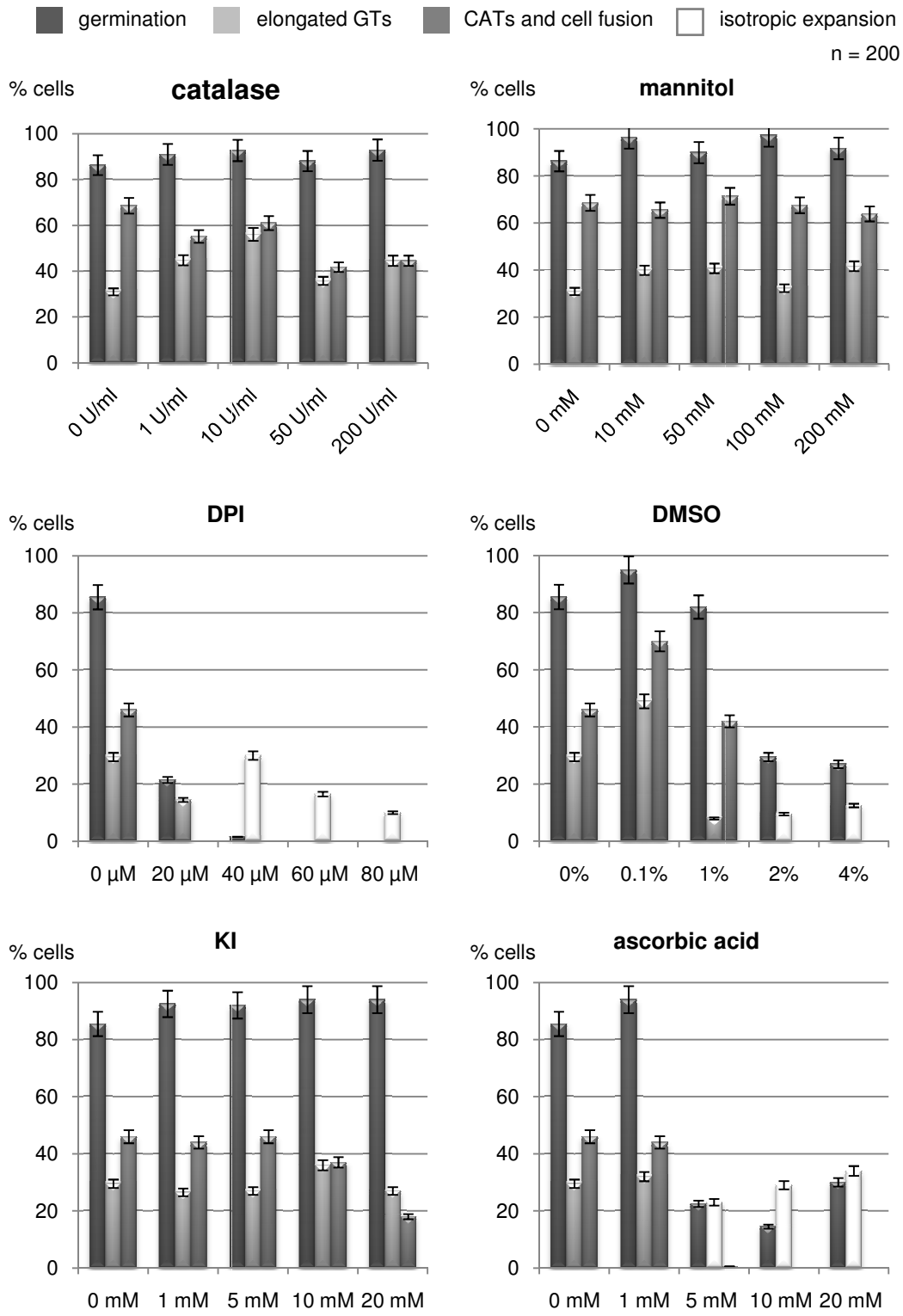

Figure 7.17 Effects of ROS scavengers on cellular development. Cellular development in the presence of various ROS scavengers was assessed as described for Fig. 7.15. Both H_2O_2 scavengers catalase and potassium iodine (KI), as well as the $^{\bullet}OH$ scavenger mannitol had no apparent influence on germling development including CAT-mediated cell fusion. 20 µM of the flavocytochrome, and thus NOX, inhibitor diphenyleneiodonium (DPI) did inhibit

germination and CAT fusion. Higher concentrations (≥ 40 µM) complete blocked cell polarisation and only allowed isotropic expansion of conidida. However, effects in this experiment were likely to be additive to those of dimethyl sulfoxide (DMSO), which was used as solvent for DPI and present at final concentrations of ≥ 1%. 1% DMSO alone significantly reduced GT elongation, but not CAT formation and fusion. More than 1%, however, inhibited cell polarisation resulting in extended isotropic expansion of ungerminated spores. DMSO acts as an unspecific ROS scavenger, but is believed to mainly remove $^{\bullet}OH$ [74, 75]. Ascorbic acid which removes various ROS by being stepwise oxidized into dehydroascorbate [39], also strongly inhibited cell polarisation and thus prevented CAT-mediated cell fusion above a concentration of 1 mM.

Taken together, these experiments clearly demonstrated that changes in the cellular redox state interfere with the developmental program of conidial germlings. Low concentrations of H_2O_2 (< 0.2 mM) and of certain antioxidants (e.g. < 5mM ascorbic acid) were capable of causing a conditional CAT induction defect in wt cells of *N. crassa*. As germination and GT elongation progressed unhindered under these conditions, it seems likely that these subtle redox changes did not stress the cells in the classical sense, but specifically prevented morphogenetic changes required for cell fusion. This notion is strongly supported by the finding that the GT/CAT ratio could be altered through the addition of very low amounts of exogenous H_2O_2 in the range of 25–50 µM. Symptoms indicative of oxidative stress, such as increased vacuolation (Figs. 7.12A and B), were not observed for H_2O_2 concentrations ≤ 2 mM.

7.3.5. Conidial germlings of *N. crassa* maintained low levels of extracellular ROS in the growth medium

To monitor levels of ROS generated during the time course of conidial germination and germling fusion, chemiluminescent assays were developed for *N. crassa*, using the reporter protein Pholasin® (section 2.13.2). In brief, Pholasin® emits light when it becomes oxidized to oxypholasin by ROS. This reaction is irreversible and every Pholasin® molecule reacts only once. Therefore, the

emitted light is proportional to the amount of ROS present and, in contrast to fluorescent reporters which tend to accumulate background signal with time, decreases in ROS are accurately detected as well. Pholasin® is an ultrasensitive detector for superoxide, and emits measurable levels of light in the presence of nanomolar concentrations of $O_2^{\bullet-}$ (and other ROS), whereas it is insensitive for H_2O_2 [41, 67]. As Pholasin® cannot enter the cell it exclusively measures extracellular ROS.

The standardly used growth medium of *N. crassa*, Vogel's minimal medium (VM) (Table 2.9) contains a variety of iron, copper, bromine and chlorine compounds with a very high potential to generate free radicals, such as ferryl radicals, as well as hypobromous and hypochlorous acid which generate ROS in secondary reactions. Its suitability as an assay medium was assessed by measuring the resting glow of Pholasin® in different dilutions of VM, and in the presence or absence of *N. crassa* cells (Fig. 7.18). This was crucial for subsequent experimental analysis, as a larger resting glow level would negatively influence the dynamic range and consequently the sensitivity and accuracy of the assay. These simple measurements confirmed the highly prooxidant nature of VM, and showed that the half diluted medium (50% VM) was an appropriate choice for assay development. A delay or significant reduction in germination and cellular development in the 50% VM was not observed (Fig. 7.19). Also significant for assay development was the finding that freshly harvested conidia immediately released huge amounts of antioxidants into the medium, which further reduced the resting glow of Pholasin®. To correct for this, pre-conditioned VM (VMpc) was used as standard assay medium whenever applicable.

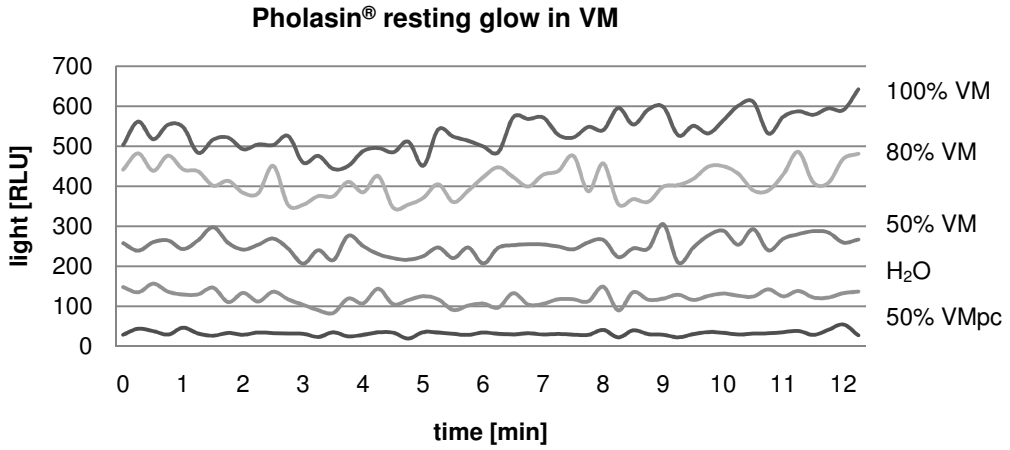

Figure 7.18 Resting glow of Pholasin® in diluted VM. The prooxidant nature of VM raises the resting glow of Pholasin® the higher its concentration. Pre-conditioning the medium (VMpc) with freshly harvested *N. crassa* conidia for 10-15 min (before removing them by centrifugation and using the cell-free supernatant) significantly reduced the resting glow below that in pure water. This demonstrated that ungerminated cells immediately released huge amounts of antioxidants into the medium. Graphs represent mean averages of triplicate measurements.

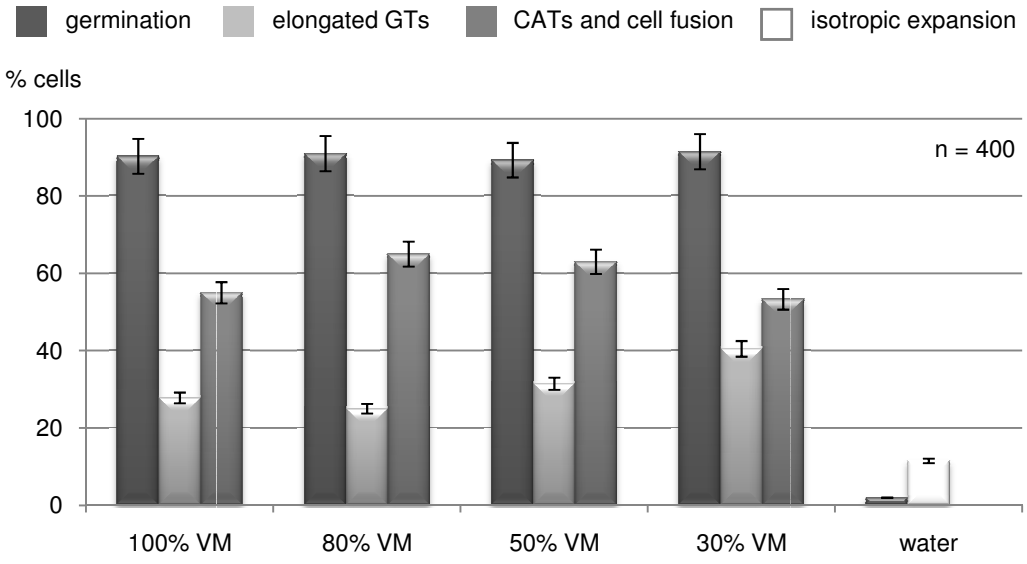

Figure 7.19 Germination and CAT-mediated cell fusion occured normally in half-diluted VM. Germination and cell fusion were quantified after 4 h of incubation at 35°C in different dilutions of VM. Cellular development occurred normally in 80% and 50% VM. Noticeable changes in the GT/CAT ration started to show in 30% VM. Apart from occasional isotropic expansion, spore germination was almost completely inhibited in pure water.

Measuring the level of extracellular ROS over the 6 h time course of cell germination and germling network development showed that wt cells of *N. crassa* very effectively reduced the amount of extracellular ROS in the medium and maintained a ROS level about 4-5-times below the cell-free control (Fig. 7.20).

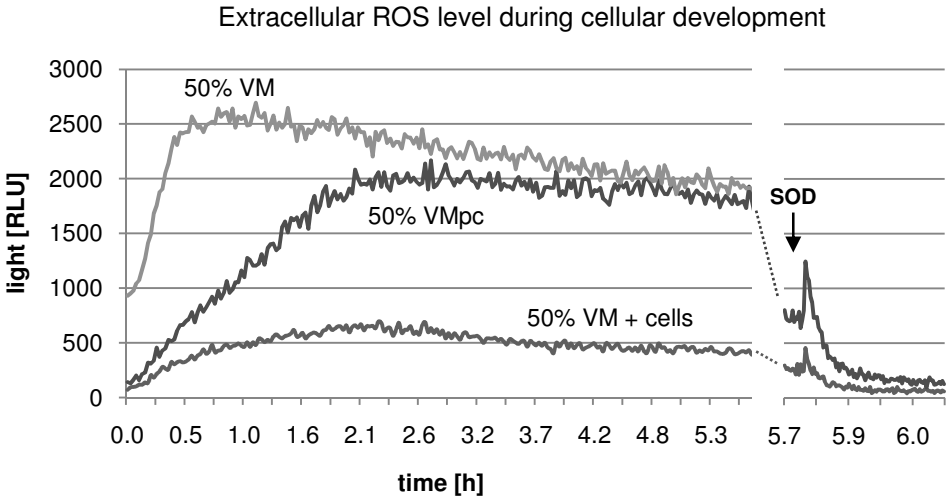

Figure 7.20 Growing cells maintained a low level of extracellular ROS. In plain medium (50% VM) the amount of detectable ROS quickly increased within the first 30 min of incubation, presumably fuelled by the uptake of O_2 into the medium. With time, generated ROS were gradually consumed by oxidizing Pholasin®. Pre-conditioned medium (50% VMpc) contained enough antioxidants to immediately decrease the resting glow and dampen the rapid increase in ROS, which reached equilibrium after about 2 h. In the presence of cells, extracellular ROS level increased only a little and were stably maintained 4–5-fold below the cell-free control (50% VM) for more than 4 h. In both, pre-conditioned medium and in the presence of cells, the resting glow of Pholasin® at the beginning of the measurement was immediately reduced by a factor of about 100x. Addition of SOD (3 u/ml) at the end of the experiment lead to a rapid drop in signal confirming that superoxide was still present in the media.

7.3.6. NOX-1 activity was required to adjust extracellular ROS level

To assess effects on extracellular ROS levels caused by the lack of the NADPH-oxidase complex components NOX-1, NOR-1 and RAC-1, the amounts of ROS in the growth medium of the corresponding gene deletion mutants were analysed. For this, medium samples were taken from growing germling cultures at four different time points and measured for 20 min in plate assays using Pholasin® as chemiluminescent reporter (Fig. 7.21). Although there was little difference between media from the wt and Δ*rac-1* cells, deletion of *nox-1* or *nor-1* genes, caused a significant increase of the amounts of detectable ROS in the respective media. As indicated in Fig. 7.20, wt cells decreased the amount of ROS in the medium below the resting glow of Pholasin® in the pre-conditioned control (50% VM + cells vs. 50% VMpc). This effect was consistent with measurements presented in Fig. 7.21, which furthermore showed that the reduction of extracellular ROS was dependent on the cell number. The more cells were present in the culture, the less ROS were detected after 3 and 5 h of incubation. Similar results were obtained for the Δ*rac-1* mutant. In both NOX mutants, however, ROS levels remained significantly higher. Signal intensity remained 3–10 times above the Pholasin® resting glow recorded in cell-free control medium (black dashed line in all graphs in Fig. 7.21), and compared to ROS levels detected in wt culture supernatants. As seen before, this effect was cell number dependent, but this time the more cells were present the higher the measurable ROS levels were. Fig. 7.22 provides a direct comparison between all four tested strains. Control samples containing cells but no Pholasin® (bottom line in every graph) confirmed that recorded signals were due to cellular activity and not a result of detector noise or other external influences.

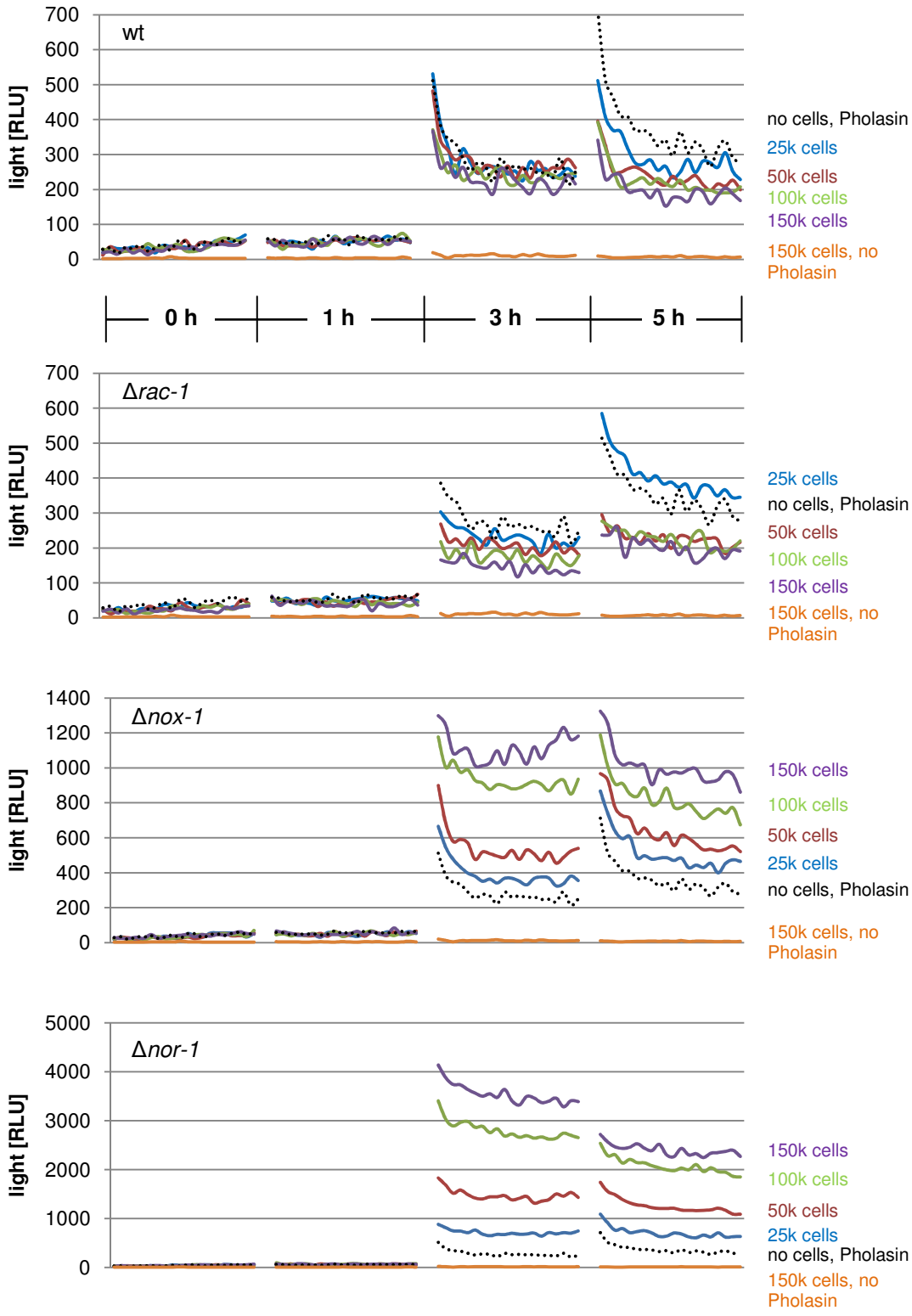

Figure 7.21 Δ*nox-1* and Δ*nor-1* cells maintained much higher extracellular ROS level than wt and Δ*rac-1*. ROS levels were measured in growth medium samples at four different time points (0, 1, 3 and 5.5 h) from continuously incubated germling cultures of *N. crassa*

gene deletion mutants. In the medium of wt and Δ*rac-1* cells low ROS levels, below the resting glow of Pholasin® in the pre-conditioned but cell-free control medium (dotted black lines), were maintained over more than 5 h. In the contrary, much higher amounts of ROS were detected in the medium of Δ*nox-1* and Δ*nor-1* cells incubated under identical conditions and on the same plate. Both effects were strictly cell number dependent; much more obvious, however, for Δ*nox-1* and Δ*nor-1* than for wt and Δ*rac-1*.

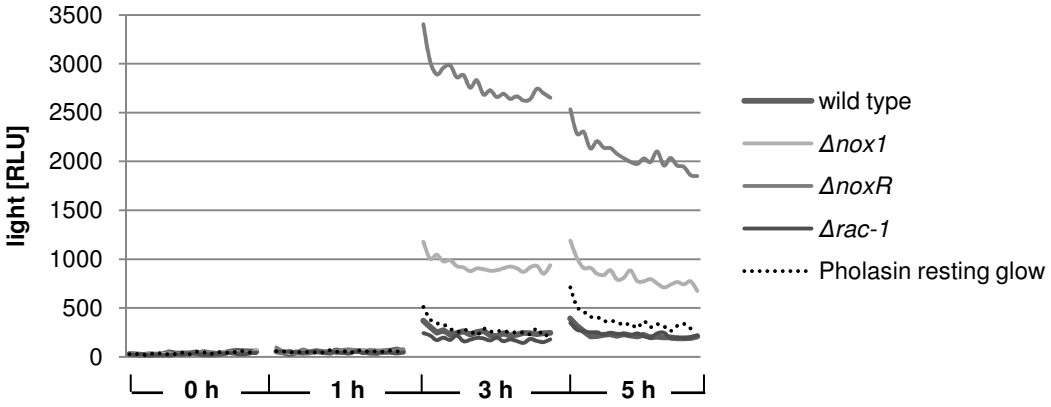

Figure 7.22 Comparison of extracellular ROS levels detected in continuously incubated germling cultures of 100,000 cells/well of wt, Δ*rac-1*, Δ*nox-1* and Δ*nor-1*. See text in Fig. 7.21.

To confirm these result, measurements of extracellular ROS levels were conducted in continuous, this time undisturbed germling cultures (100000 cells/well) of all four previously used strains, plus the putative L-ascorbate oxidase mutant Δ*lao* (Fig. 7.23A). Pre-conditioned medium was prepared for each strain individually and measured on the same plate to record 'background' signal, i.e. any changes in ROS level in the absence of cells, but in a medium that contained antioxidants released from ungerminated conidia. These 'background-control' measurements (Fig. 7.23B) were then subtracted from the measurements obtained from the growing cell cultures (Fig. 7.23A), in order to plot the final graph representing changes in extracellular ROS levels resulting exclusively from cellular activity (Fig. 7.23C). The raw (not-background corrected) measurements confirmed that extracellular ROS levels remained higher in cultures of Δ*nox-1* and Δ*nor-1* cells, compared to wt, but suggested that Δ*rac-1* cells managed to even further reduce the

redox state of the culture medium (Fig. 7.23A). Cells of Δ*lao* appeared to behave similar to Δ*nox-1* and Δ*nor-1* mutants. The 'background-corrected' graph, however, more clearly showed that Δ*nox-1* and Δ*nor-1* cells failed to reduce extracellular ROS level as effectively as the wt, and that Δ*rac-1* cells actually behaved similarly (Fig. 7.23B). Interestingly, Δ*lao* cells initially maintained even higher ROS levels in the medium than seen for the other three mutants, but adjusted to comparable levels after about 2 h. In conclusion, all four cell fusion mutants did not reduce the amount of extracellular ROS to wt levels within 6 h of incubation.

Blocking NOX activity with the flavocytochrome inhibitor DPI, prevented germination and the attenuation of extracellular ROS levels in all four tested gene deletion backgrounds and the wt (Fig. 7.24). This confirmed that the decrease of extracellular ROS is connected to cellular activity during germination, and required NOX activity. The fact that DPI inhibition had the same effect in all tested strains, including Δ*nox-1* and Δ*nor-1* mutants, furthermore indicates involvement of a second redox regulatory pathway, potentially involving NOX-2.

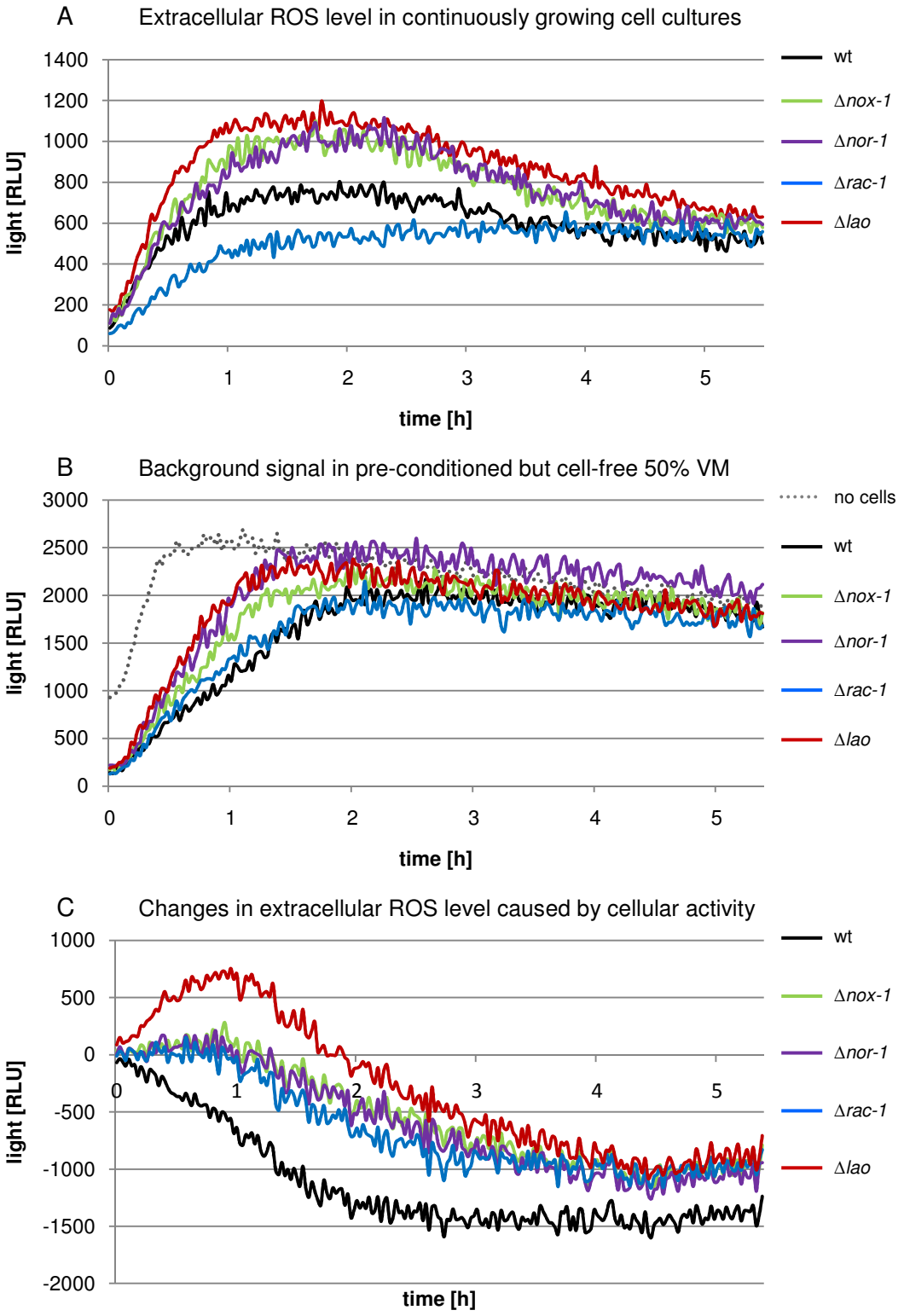

Figure 7.23 Attenuation of the extracellular ROS level occurred less efficiently in cell fusion mutants compared to the wt. (A) 'Raw' Pholasin® signal recorded from cell cultures of *N. crassa* gene deletion mutants and wt control continuously grown for 6 h at 30°C. **(B)** Background signal generated in pre-conditioned 50% VM in the absence of cellular activity.

(C) Background-corrected graphs generated by the subtraction of signals in (B) from signals in (A). Changes in Pholasin® signal and thus extracellular ROS level should exclusively result from cellular activity during germination, GT growth and CAT-mediated cell fusion.

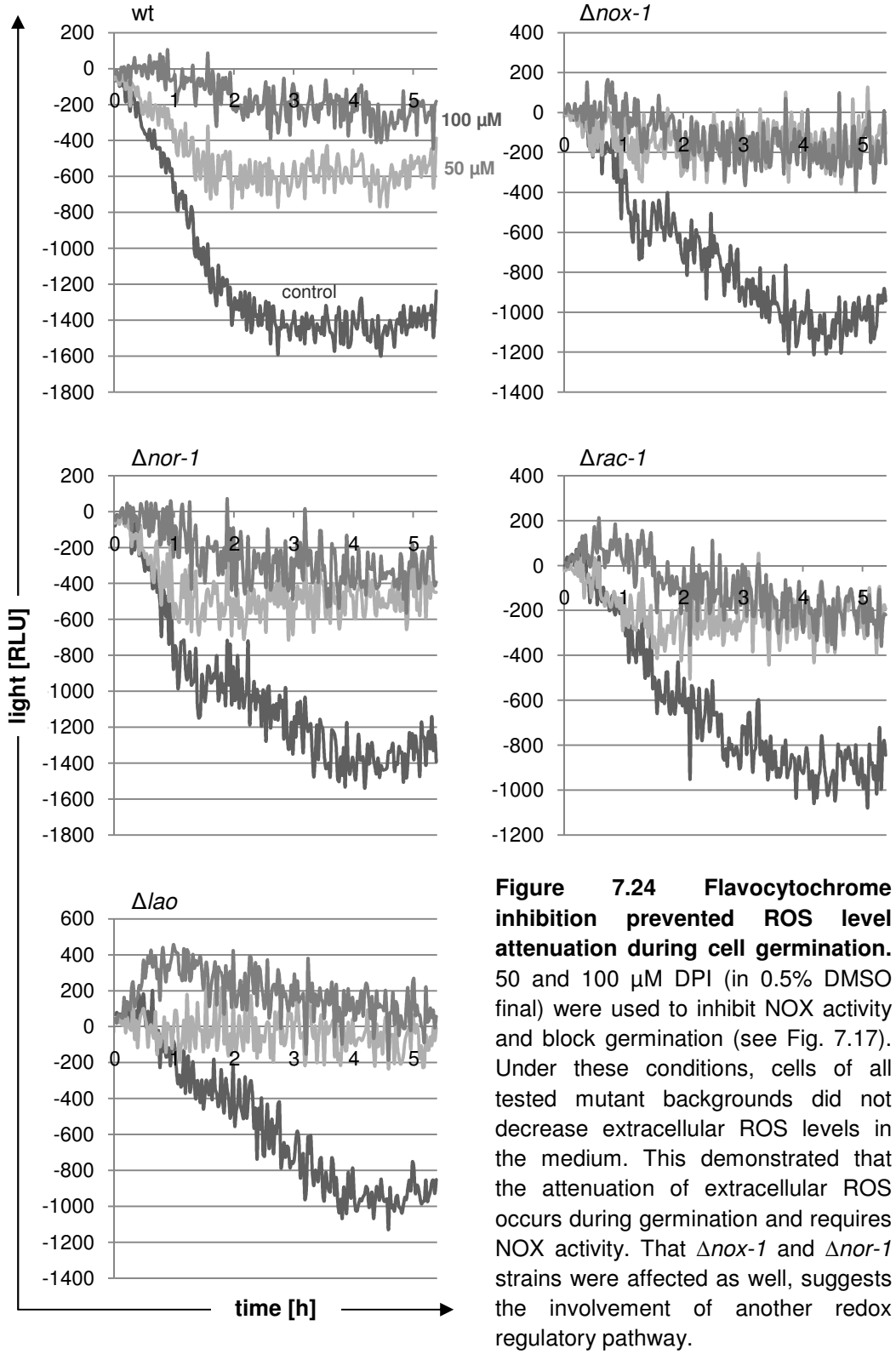

Figure 7.24 Flavocytochrome inhibition prevented ROS level attenuation during cell germination. 50 and 100 µM DPI (in 0.5% DMSO final) were used to inhibit NOX activity and block germination (see Fig. 7.17). Under these conditions, cells of all tested mutant backgrounds did not decrease extracellular ROS levels in the medium. This demonstrated that the attenuation of extracellular ROS occurs during germination and requires NOX activity. That Δ*nox-1* and Δ*nor-1* strains were affected as well, suggests the involvement of another redox regulatory pathway.

7.3.7. NOX activation occurred through receptor-independent but PKC-dependent signalling

In mammals, certain soluble substances, such as, platelet activating factor (PAF), tumor necrosis factor (TNF) and formyl-leucyl-methionyl-phenylalanine (fMLP), can activate NOX complexes at the plasma membrane. For continuous activation the ligand molecule must remain in contact with the receptor, and consequently removal of the stimulus shuts down oxidase activity. Moreover, the phosphorylation state of the NOX and its regulatory components is an additional and essential control element in the activation process [32]. Receptor-mediated NOX activation is Ca^{2+}-dependent but PKC-independent [92]. Consequently, PKC inhibitors have no influence on NOX activation through this pathway. Addition of tyrosine kinase inhibitors, such as erbstatin, or the fungal PI3-kinase inhibitor 17-hydroxywortmannin, specifically inhibit receptor-mediated NOX activation [6, 60].

Alternatively, NOX assembly and activation can be triggered through direct activation of PKC by diacylglycerol (DAG) analogues. Consequently, receptor-independent NOX activation can be blocked through PKC inhibitors [92]. A potent agonist of PKC, and thus NOX activator, is phorbol-12-myristate-13-acetate (PMA). In contrast to fMLP, PMA is membrane-permeable and directly activates PKC in the cytoplasm, leading to a fully functional assembled NOX complex in leukocytes [57]. In phagocytic macrophages, PMA-mediated PKC activation also induces degranulation, i.e. fusion of secondary granules with the plasma membrane in order to release superoxide into the phagosome. Receptor-independent NOX activation is furthermore Ca^{2+}-independent. Interestingly, simultaneous addition of fMLP and PMA triggers a combined response through both the receptor-dependent and receptor-independent pathways leading to a much stronger activation of NOX in human blood cells [42].

To test whether NOX activation in *N. crassa* was receptor-mediated or receptor-independent, cell activation assays were developed which measured

superoxide production in response to fMLP or PMA stimulation. For this, cells were pre-cultured in 96-well plates at 30–35°C for the desired time (usually 0-4 h) and transferred into the plate reader. Pholasin® (2.5 ng/µl final) reconstituted in pre-conditioned medium (50% VMpc) was injected, and the background signal recorded until stable resting glow was established (usually after 2 min). Both, fMLP (0.4 µg/ml final) and PMA (0.5 µg/ml final) were as well reconstituted in 50% VMpc to avoid the addition of exogenous ROS. Upon injection of the chemicals changes in Pholasin® signal were recorded over the following 30 min (Fig. 7.25). Whereas, fMLP did not elicit a response, PMA caused an immediate signal increase, which gradually decreased back to resting glow over the following 15 min (Fig. 7.25B).

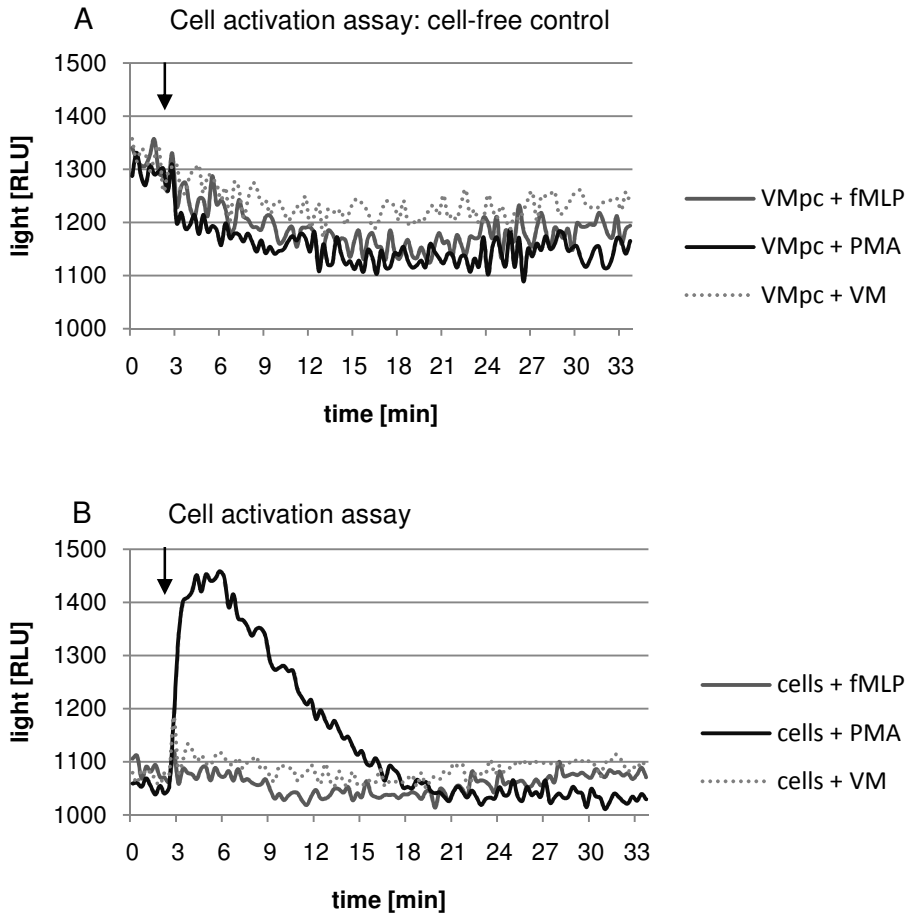

Figure 7.25 Cell activation assay. (A) Addition of fMLP or PMA (arrow) to pre-conditioned, but cell-free medium (50% VMpc) did not cause unspecific signal increase. **(B)** Addition of PMA to cells of *N. crassa* however did produce a rapid increase in extracellular superoxide,

whereas addition of fMLP had no effect. This indicated that NOX activation in conidial germlings can occur by direct stimulation of PKC, and thus is independent of receptors located in the plasma membrane.

To verify the initial finding of PMA-mediated NOX stimulation in *N. crassa*, the assay was adapted for the BioOrbit tube luminometer (section 2.13.2.1), and repeated using two different cell concentrations (Fig. 7.26). The tube luminometer allowed a 4-times higher temporal resolution, allowing the detection of a rapid and transient fMLP response, that might have occurred but have been missed between the 20 sec measurement intervals on the plate reader.

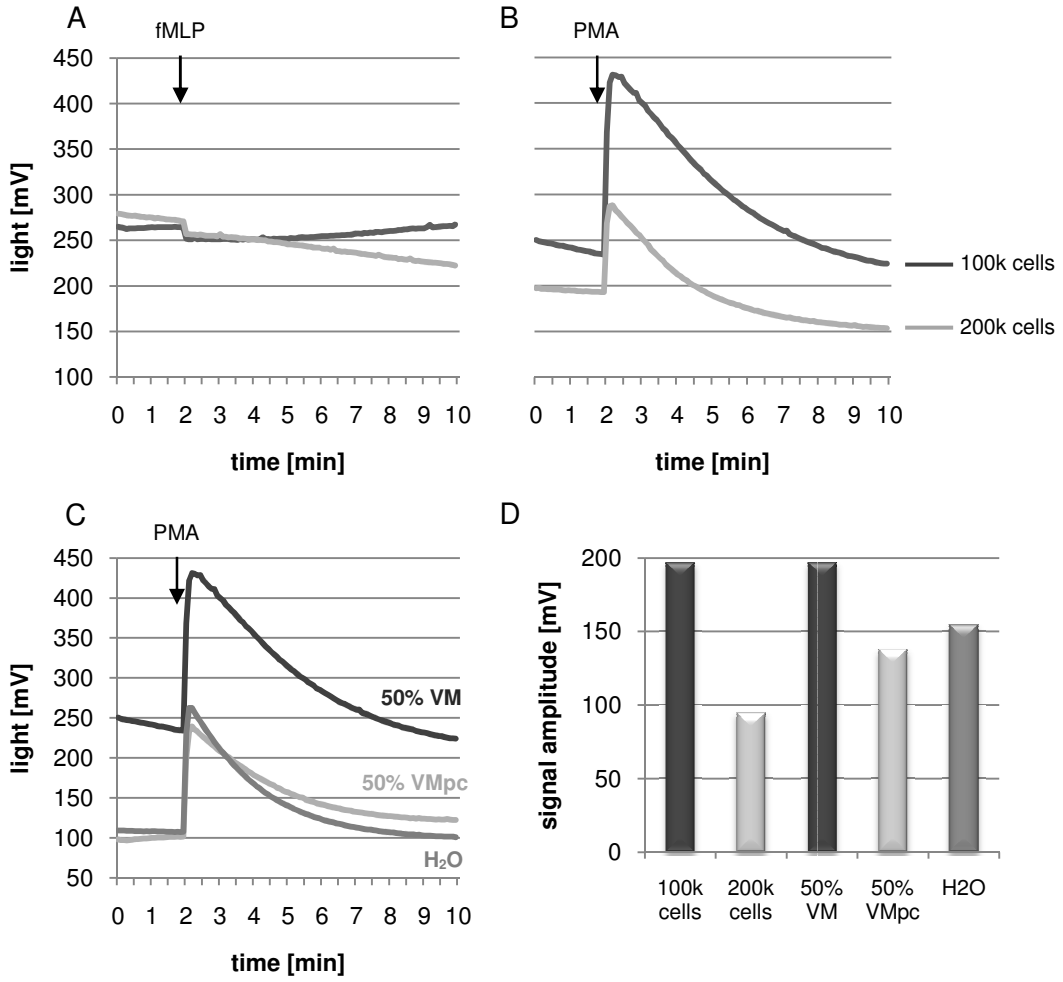

Figure 7.26 Verification of cell activation assay. (A) Addition of fMLP (arrow) did not trigger NOX activation and superoxide release. **(B)** Addition of PMA (arrow) induced the immediate release of superoxide confirming NOX activation. Pholasin® resting glow and signal amplitude upon PMA addition depended on cell number and the assay medium **(C)**.

(D) Signal amplitudes, i.e. signal increase upon PMA addition above resting glow of measurements shown in (B) and (C). The more oxidants were present in the assay medium, either due to a lower cell number (100k cells) or the use of unconditioned medium (50% VM), the higher the resulting signal increase upon PMA stimulation.

PMA cell activation measurements in the tube luminometer were consistent with data obtained with the plate reader set up. Both demonstrated that NOX activation in *N. crassa* can occur through a receptor-independent, but PKC-mediated pathway, but cannot be initiated through fMLP. In addition, the general dependency of assay performance and signal read out on cell number and pro-/antioxidative status of the assay medium itself were confirmed and further characterized. Preliminary data indicates that PMA-induced ROS production is significantly attenuated in Δ*nox-1* and Δ*nor-1* backgrounds (data not shown). This however needs to be repeated and confirmed in future experiments.

7.3.8. Detection of superoxide in conidial germlings

Nitroblue tetrazolium (NBT) which forms a dark-blue water-insoluble formazan precipitate upon reduction by superoxide radicals [59], was used to visualize accumulation of $O_2^{\bullet-}$ in conidial germlings of *N. crassa* (Fig. 7.27). Polarised tip growth of GTs coincided with the apical accumulation of superoxide in all tested strains, including wt, Δ*nox-1* and Δ*nor-1*. Initial evidence for increased levels of superoxide was also collected for CATs (Fig. 7.27F). However, the accumulation of superoxide in CATs seemed to be transient and presumably restricted until the post-contact phase of cell fusion. As soon as a individual cell-cell connections or germling networks were successfully established, NBT staining did no longer detect superoxides at the fusion sites (Fig. 7.27B and G). Simultaneous addition of the NBT dye solution with the NOX inhibitor DPI, prevented staining in a concentration dependent manner (data not shown).

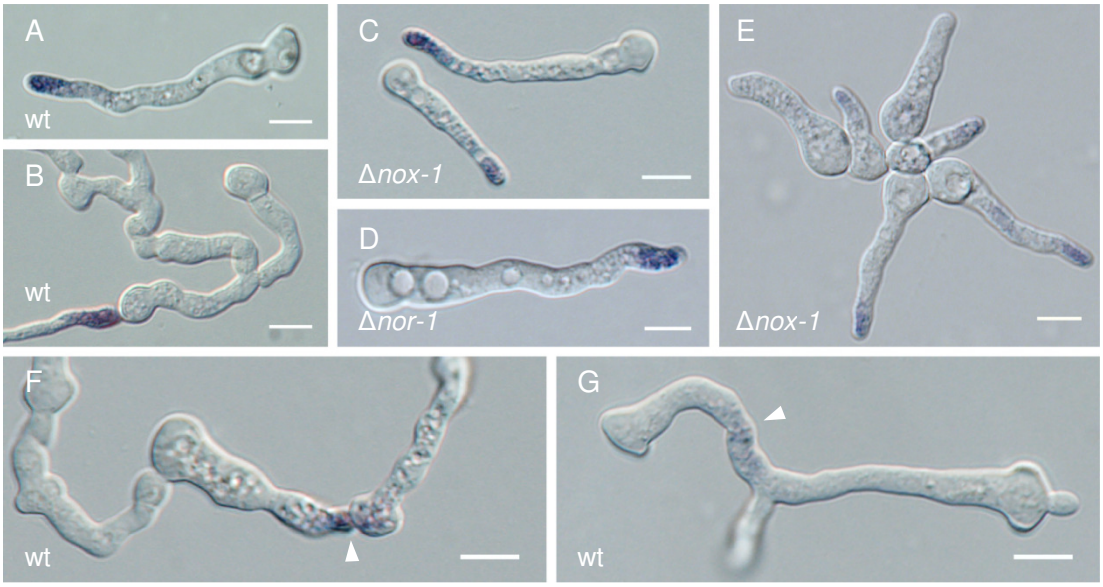

Figure 7.27 NBT staining of conidial germlings of *N. crassa*. All cells were pre-incubated for 3 h at 30°C. Aqueous nitroblue tetrazolium (NBT) solution was added (0.05% w/v final concentration) and incubation continued for another hour before imaging. **(A)** Wt germling with superoxides concentrating at the GT tip. **(B)** Accumulation of superoxides at fusion connections was not observed in established germling networks. **(C and D)** Accumulation of superoxides in the GT tips of Δ*nox-1* and Δ*nor-1* cells. **(E)** Group of Δ*nox-1* germlings that display negative chemotropism and have accumulated superoxides at their GT tips. **(F)** During cell fusion NBT precipitate also located to CAT tips (arrowhead). **(G)** As soon as cytoplasmic continuity was established local concentrations of superoxide at the fusion site (arrowhead) seemed to rapidly decrease, as at this stage only very weak staining was occasionally observed. Scale bars, 10 µm.

Taken together, this data indicated that NOX-dependent superoxide production accompanied polarised tip growth of GTs and CATs, and was independent of NOX-1 and NOR-1 function. As GTs are in most cases continuously elongated, and therefore apical ROS are present at all times, NBT staining gave consistent and reliable staining results. Polarised growth of CATs on the other hand occurs only transiently; hence the detection of superoxide in these protrusions was less consistent and unsuitable for quantification.

7.4. Discussion

Our understanding of how regulated production of ROS through NADPH oxidases influences cellular differentiation and the development of multicellular structures in filamentous fungi has considerably increased over the past decade [77]. Major roles for NOX-generated ROS have been identified in processes, such as fruitbody morphogenesis and spore germination, but also in controlled differentiation associated with fungal symbiosis and pathogenesis, as well the regulation of polarised hyphal growth. Work presented in this chapter, revealed a novel aspect of NOX activity, which is its essential role during CAT-mediated cell fusion in *N. crassa*. Furthermore, two additional components providing functional links between metabolism and the regulation of redox signalling processes, NAD^+-dependent glutamate dehydrogenase (GDH-1(NAD)) and the L-ascorbate oxidase-like laccase (LAO), were also indentified to be involved in cell fusion.

Key components of the redox signalling machinery are required for CAT-mediated cell fusion in *N. crassa*. Gene deletion mutants lacking the NOX components NOX-1, NOR-1 and RAC-1, or the above mentioned enzymes GDH-1 or LAO implicated in the regulation of ROS signalling were unable to establish fusion between conidial germlings and fusion hyphae of the mature colony (Figs. 7.7 and 7.8). Interestingly, Δ*nox-1*, Δ*nor-1* and Δ*lao* strains formed CATs, although with much reduced efficiency compared to the wt (Fig. 7.9), but these were non-functional and did not chemotropically interact to establish cell fusion. Germlings of Δ*gdh-1* appeared to be blocked in CAT induction (Fig. 7.8), which was also the case for the Δ*rac-1* mutant (Figs. 4.10 and 7.9). Based on findings in other filamentous fungi which demonstrated that the small GTPase Rac is required for a functional NOX complex [15, 72, 83, 90], it is very likely that RAC-1 is also a crucial regulator of NOX assembly and activity in *Neurospora*. Experimental evidence for the molecular interaction between RAC-1 and NOR-1/NOX-1 in *Neurospora*, however, is still missing. Nevertheless, a picture is beginning to emerge, in which NOX activity

is required to induce morphogenetic changes leading to CAT-mediated cell fusion. NOX-generated $O_2^{\bullet-}$ and its secondary reaction products, such as H_2O_2 or $^{\bullet}OH$ (Fig. 7.1), have been shown to act as intracellular second messengers in mammals [68, 69], and thus are likely to elicit similar functions in *Neurospora.* In addition, ROS could be involved in modulating cell wall plasticity required for tip extension and fusion pore formation. Of particular interest in the context of ROS signalling during CAT chemoattraction is the notion that a variety of cell surface receptors, including GPCRs [69], could induce H_2O_2 production by activating NOX, and that its downregulation most likely occurs through peroxiredoxins [70]. Both classes of molecules are under current investigation for their participation in CAT-mediated cell fusion in *N. crassa*. As H_2O_2 can readily cross biological membranes, even if its production occurs inside the cell, e.g. through ER localized NOX-1, it could easily diffuse outside and be perceived by cells in the vicinity, and function as intercellular signalling molecule. However, our own findings that addition of catalase did not interfere with CAT chemoattraction and cell fusion (Fig. 7.17) suggests that might not be the case.

Overall, the general hypothesis that null mutants in antioxidant enzymes can be expected to show increased levels of development, whereas development is reduced or completely abolished in mutants affected in prooxidant enzymes [35] (section 7.2.3), is interesting to reconsider based on our findings. Mutants lacking components of the prooxidant NOX complex (Δ*nox-1*, Δ*nor-1* and Δ*rac-1*) or the ROS production fuelling GDH-1(NAD) Δ*gdh-1*, indeed showed a reduced level of development as they were all blocked in CAT-mediated cell fusion. However, so was the Δ*lao* strain lacking an ascorbate oxidase-like protein, which could be considered to be an antioxidant enzyme. But dependent on the redox microenvironment in the CAT 'compartment' LAO might also act as prooxidant. This again reflects the general complexity of redox enzymes, which in many cases can act as pro- or antioxidants, depending on the subcellular redox state. It would therefore be interesting to quantify whether CAT-mediated cell fusion is increased

in gene deletion mutants of 'known' antioxidant enzymes, such as catalase. Cells of the SOD mutant Δ*sod* are able to undergo fusion (Table 3.6). And again the question arises is SOD a pro- or antioxidant enzyme? As it breaks down superoxide it acts as an antioxidant, but at the same time as prooxidant it generates H_2O_2. Hence it depends which of the two ROS constitutes the functionally redox signalling molecule in that particular process.

NOX-1 localized to internal membranes, supporting its role in intracellular redox signalling. Rescue of the fusion defects in both, Δ*nox-1* and Δ*nor-1* strains was accomplished through ectopic expression of the fluorescently labelled fusion constructs NOX-1-sGFP and NOR-1-sGFP, respectively (Figs. 7.10 and 7.11). A potentially alternative subcellular localization of NOR-1-sGFP, apart from it being cytoplasmic (Fig. 7.10B), still needs to be determined. The somewhat unexpected finding that NOX-1 resides in the perinuclear ER, would suggest that its regulatory factor NOR-1 becomes recruited from the cytoplasm to the same location as soon as NOX activation is induced. But whether NOR-1-sGFP shuttles to the perinuclear ER prior to NOX assembly has so far not been determined. Similarly, whether NOX-1 as well resides in the plasma membrane requires a more detailed analysis. In case NOX-1 not only shares its ER localization with BEM46, but also its role in the regulation of polarized growth [58], a population of NOX-1 recruited to the plasma membrane can be expected. This would furthermore support the suggested role of NOX-1 in polarized tip growth and apical dominance [79]. PMA-induced NOX activation of Δ*nox-1*(NOX-1-sGFP) transformants co-expressing NOR-1-TagRFP-T (Figs. 7.25 and 7.26) offers a possibility to address this important question. Compartmentalization of NOX-1 function through ER localization supports its suggested role in intracellular redox signalling. For the mammalian Nox4 it has recently been demonstrated that its ER localization is required for redox-mediated signalling towards protein tyrosine phosphatase and subsequent epidermal growth factor (EGF) regulation [17, 24]. Furthermore, as both NOX-1 and NOR-1 are

dispensable for spore germination, which has been demonstrated to require an oxidative burst in *Neurospora* [35, 51], it must be considered that the generation of intense oxidative bursts might be an exclusive function of NOX-2. The fact that we were unable to isolate growing colonies of homokaryotic Δ*nox-2* mutants might support this notion. It will be interesting to analyse Δ*nox-2* mutants generated elsewhere [14] for cell fusion defects, and furthermore, determin the intracellular localization of fluorescently labelled NOX-2, which we expect to reside in the plasma membrane. These will be important next step in dissecting the presumably separate functions of NOX-1 and NOX-2 in *N. crassa*.

NOX-mediated redox signalling depends on metabolic regeneration of internal NADPH stores, but also requires feedback regulation. The catabolic GDH-1(NAD) is required to generate NADPH in the cell. In *Neurospora*, GDH-1(NAD) activity was found to be rapidly upregulated at the onset of a hyperoxidant state preceding germination and aerial hyphae formation, whilst activity of its anabolic counterpart NADPH-dependent GDH (GDH(NADPH)) immediately decreased [85]. This shuts down the nitrogen assimilation pathway which otherwise would quickly consume ATP and NADPH. GDH-1(NAD) activity, on the other hand, replenishes NADPH which thereby becomes available to fuel increased NOX-mediated ROS production. Consequently, removing GDH-1(NAD) from the genome should theoretically stall NOX-mediated redox signalling and create a phenotype similar to Δ*nox-1*. This is supported by our phenotypic analysis of the Δ*gdh-1* mutant strain (Fig. 7.9). Δ*gdh-1* cells were unable to establish cell fusion, and initial results indicate a CAT induction defect. This however needs to be verified with CAT formation assays involving the GT blocker benomyl (Fig. 4. 10). The metabolic link between GDH-1 function and NOX activity might explain why GDH-1(NAD) is required during cell fusion. GDH-1 is likely to be involved in switching between nutrient sensing and uptake, and hyphal growth and colony extension (Kim Hammond-Kosack, pers. comm.). Removing this sensor potentially disables the cells

to switch to the fusion program, leading to uninterrupted tip growth as seen in the vegetative colony (Fig. 7.8). Consequently, one would predict that the anabolic counterpart GDH(NADPH) is dispensable for CAT formation and cell fusion. This, however, remains to be tested.

The laccase mutant Δ*lao*, missing an L-ascorbate oxidase-like protein, showed a phenotype very similar to that of Δ*nox-1* and Δ*nor-1* (Fig. 7.9). As antioxidant, L-ascorbate oxidase increases the removal of ROS by catalysing the oxidation of ascorbate into dehydroascorbate [39]. Its putative fungal analog LAO could therefore function as a ROS scavenger and thus have an important function in the downregulation of the NOX-generated redox signal. Alternatively or in addition, LAO could aid in cell wall remodelling during CAT attachment and fusion pore opening. As antioxidant it could suppress or slow down wall tightening by preventing oxidative cross-linking of cell wall polymers. When acting as pro-oxidant and •OH generator [25], LAO activity could amplify the effects of NOX-generated ROS and act in cell wall loosening through oxidative polymer scission [74]. That ascorbate has a significant influence on cellular development is well established in various filamentous fungi. Germination and appressorium formation in *M. oryzae*, for example, were inhibited or at least greatly impaired in the presence of 10–100 mM ascorbic acid [23]. Other common phenotypes include abolished GT differentiation and extensive cell swelling, thus a block in cell symmetry breaking and polarised bud protrusion. Identical effects were observed when treating conidia of *N. crassa* with > 5 mM ascorbic acid (Figs. 7.16 and 7.17). Our analysis furthermore showed that smaller amounts between 1-5 mM ascorbic acid were sufficient to prevent GT and CAT formation (Fig. 7.17). The exact minimal concentration which suppresses spore morphogenesis still needs to be determined. Also, whether this effect is due to ascorbate acting as pro- or antioxidant is not yet understood. Other tested *a priori* antioxidants, including the H_2O_2 scavengers catalase and KI, as well as the •OH decomposer mannitol, showed no effects on conidial development in *N. crassa* within the tested concentrations ranges (Fig. 7.17).

In this context, it has to be noted that some of these scavengers are not specific for a particular ROS, and are likely to give pleiotropic effects dependent on the redox state of the cells and their environment [91].

H_2O_2 selectively inhibited CAT formation and cell fusion in the µM range. The most interesting effect was observed when treating conidial germlings with low amounts of H_2O_2. High concentrations inhibited GT elongation (> 1 mM H_2O_2) and ultimately blocked germination completely (> 2 mM) (Fig. 7.15). The cells were not dead as isotropic expansion still occurred and resulted in spores of about 3–4-times the usual diameter, but cell symmetry breaking and consequently polarised protrusion of a germ tube bud were no longer possible. A connection between cell polarisation and ROS signalling has recently been established in *A. nidulans*, where ROS accumulation at the GT tip correlated with apical dominance [79]. These findings are consistent with NBT staining results obtained in *N. crassa*, which visualized huge accumulations of superoxide at GT tips (Fig. 7.27A-E). ROS accumulation was also detected in CATs, whereas here superoxide production appeared to be transient and could only be observed during CAT homing and fusion, but not post-fusion (Fig. 7.17F). In successfully established germling networks, sustained NBT staining at the fusion sites was not observed (Fig. 7.27B and G). Apical accumulation of superoxide has also been described prior to germination and appressorium formation in *M. oryzae* [22, 23], both key morphogenetic events during the establishment of rice blast pathogenesis. A concentration of 50 µM H_2O_2 effectively blocked CAT induction without stressing the cells and without inhibiting GT elongation (Fig. 7.15B). Below 50 µM the rate of CAT formation and cell fusion depended on the microenvironment of the cell, i.e. under locally high cell density cell fusion occurred more frequently than when cells were spaced out and thus H_2O_2 break down in the population was slower (data not shown). Taken together, this demonstrated that small changes in the cellular redox state can prevent morphogenetic changes required for CAT-mediated cell fusion.

The effective H_2O_2 concentration to suppress CAT formation was at 50 μM at least a 100-times lower than what is commonly used to induce oxidative stress in fungi (5-7 mM H_2O_2) [31, 52, 61]. This is in line with the notion that a very small shift in the cellular redox state might act as a signal in itself, as it can cause changed activity of redox sensitive proteins, i.e. proteins with deprotonated cysteine residues (section 7.2.2).

Conidia of *N. crassa* actively adjusted the redox level of their environment prior to germination and kept it constantly low for several hours. Initial measurements of extracellular ROS level using the ultra-sensitive bioluminescent ROS reporter Pholasin® showed three main points: (1) the standardly used culture medium for *Neurospora* (VM) is highly prooxidant, which needed to be accounted for in assay design, (2) freshly harvested, ungerminated conidia immediately released huge amounts of antioxidants into the medium, and (3) cellular activity adjusts the amount of extracellular ROS at a constantly low level over the 6 h period of germination and cell fusion.

The adjustment of extracellular ROS level appeared to be an essential prerequisite for cell germination; more precisely for the induction of morphogenetic transitions leading to GT and CAT protrusion. As discussed above, raising the oxidative status of the medium by the addition of > 0.1 mM H_2O_2 led to a decrease in germination (Fig. 7.15). The same effect was observed when lowering the ROS level in the medium beyond a certain threshold by diluting VM below 50% (Fig. 7.19). In pure water, germination was almost completely inhibited, which of course was also a result of the lack of nutrients. However, together, these simple experiments indicate that an optimum oxidant level exists which needs to be maintained to allow morphogenesis. The lower the redox state of the medium - and presumably therefore the intracellular redox state as well – prior to germination, the lower the required amount of ROS needs to be in order to create a hyperoxidant state and induce morphogenesis. Furthermore, our findings show that CATs were much more

sensitive to changes in the extracellular, and consequently intracellular, redox state than GTs. Addition of 50 μM exogenous H_2O_2 readily blocked CAT formation, but left GT development unaffected (Fig. 7.19). At this point it has to be emphasised that measurements using Pholasin® on its own do not record changes in H_2O_2, as Pholasin does not react with hydrogen peroxide. Hence an increase in hydrogen peroxide which might constitute the hyperoxidant state, would not be monitored with the current assay set up. Continued efforts are focussed on the optimization of a bioluminescent assay that exclusively detects fluctuations in H_2O_2 in *N. crassa* germling cultures (section 2.14.2.2). Initial results show that concentrations of as low as 0.5 μM H_2O_2 can be measured, which is 100 times below the concentration required to block CAT formation (data not shown).

The inability of the tested gene deletion mutants to adjust extracellular ROS as efficiently as the wt (Figs. 7.21-7.23), in that respect, is consistent with their inability to fuse, and strongly supports the function of redox signalling in the process of CAT-mediated cell fusion. Interestingly, this defect could be mimicked in the wt through DPI-mediated flavocytochrome inhibition (Fig. 7.24), which furthermore aggravated the phenotype in the fusion mutants. As NOX complex mutants were equally affected, involvement of a second ROS regulatory pathway can be suggested. This might involve NOX-2, which in a Δ*nox-1* background potentially might substitute for the loss of NOX-1 function. So far unsolved is the question which regulatory component would activate NOX-2 in the absence of NOR-1. In a recent study, it was suggested that NOR-1 equally regulates NOX-1 and NOX-2 activities, based on the finding that a cross between Δ*nor-1* and Δ*nox-2* did not result viable progeny [14]. Molecular evidence for an interaction between NOX-2 and NOR-1, however, has not been provided. In the same study, obvious differences between the phenotypes of NOX-2 mutants and NOX-1/NOR-1 mutants have been reported, and are consistent with our findings. Therefore, one needs to keep an open mind that regulation of NOX-2 might occur in a different way than

that of NOX-1 and potentially does not involve NOR-1, but a yet unidentified regulator.

NOX activation was dependent on PKC, and thus occurs through receptor-independent signalling. Addition of PMA triggered the immediate production of ROS in the *N. crassa* wt (Figs. 7.25 and 7.26), strongly suggesting that NOX activation occurs in a PKC dependent way. PMA acts as diacylgycerol analogue activating PKC directly and leads to a fully functional assembled complex of proteins making up the NOX system [78]. A preliminary test, comparing ROS production upon PMA stimulation in the wt with that in the NOX mutants, indicated a significantly weaker response in Δ*nox-1* and Δ*nor-1*, respectively (data not shown). This, however, needs to be repeated and confirmed in subsequent experiments, and ideally compared with PMA stimulation in a Δ*nox-2* background, in order to determine whether the observed increase in ROS production is attributed to NOX-1 or NOX-2 activity, or due to combined activation. Nevertheless, the fact that NOX activity can be stimulated by PMA but not fMLP, demonstrates that plasma membrane receptors are most likely not involved in this pathway. This makes sense considering the localization of NOX-1 in the perinuclear ER. Studies in various mammalian cells have identified a role for PKC in the activation and membrane translocation of NADPH oxidase [8, 9, 11]. Interestingly, the response pattern of *N. crassa* conidia upon PMA stimulation is very similar to the fast receptor-mediated and Ca^{2+}-dependent NOX activation known from mammalian neutrophils [42, 57, 92]. However, in *Neurospora* there is no third NOX isoform containing a Ca^{2+}-sensitive EF-hand motif, such as Nox3 from *M. oryzae*, and to date a connection between ROS and Ca^{2+} signalling, although suggested [14, 71], has not been established in filamentous fungi.

7.5. Summary

Work in this chapter represents the first identification and functional description of redox signalling components involved in cell fusion in *Neurospora crassa*. The discovery that NADPH-oxidase-derived ROS play an important role in the induction of morphogenetic processes required for CAT formation and chemoattraction adds a new layer of complexity to the process of cell-cell fusion in filamentous fungi. Key findings were:

- Identification of the NOX complex components NOX-1, NOR-1 and RAC-1 provided the first evidence for the involvement of redox signalling in cell fusion in filamentous fungi
- Identification of the two enzymes GDH-1(NAD) and the L-ascorbate-oxidase-like laccase LAO implied that positive and negative regulation of NOX-derived ROS signalling is tightly linked to the cell metabolism
- Complementation of the mutant phenotypes through ectopic expression of NOX-1-sGFP and NOR-1-sGFP fusion constructs confirmed the direct involvement of NOX in VHF and CAT-mediated cell fusion
- Subcellular localization of NOX-1 to the perinuclear ER and of NOR-1 to the cytoplasm are consistent with a role for NOX in intracellular redox signalling
- Selective suppression of CAT formation through the addition of micromolar concentrations of H_2O_2 demonstrated that slight changes in the reduced redox state can alter the morphogenetic program of the cell
- A new Pholasin®-based chemiluminescent assay for filamentous fungi revealed that cell fusion incompetency correlated with a defect in adjusting the extracellular ROS level in the tested mutants
- PMA cell activation assays provided the first evidence that NOX activation in *Neurospora* can occur through direct stimulation of PKC, indicating that

assembly of the functional NOX complex does not involve upstream membrane receptors

- Visualization of superoxide accumulation in the tips of Δ*nox-1* and Δ*nor-1* GTs demonstrated that the NOX-1 complex is not required for polarised growth of germ tubes, and thus appears to have a primary function in CAT-mediated cell fusion

7.6. References

1. **Aguirre, J., M. Rios-Momberg, D. Hewitt, and W. Hansberg.** 2005. Reactive oxygen species and development in microbial eukaryotes. Trends in Microbiology **13:**111-118.

2. **Alberts, B., A. Johnson, J. Lewis, M. Raff, K. Roberts, and P. Walter.** 2008. Energy conversion: mitochondria and chloroplasts, p. 813-878. *In* M. Anderson and S. Granum (ed.), Molecular biology of the cell, 5th ed. Garland Science, New York.

3. **Alvarez, M. E., R. I. Pennell, P.-J. Meijer, A. Ishikawa, R. A. Dixon, and C. Lamb.** 1998. Reactive oxygen intermediates mediate a systemic signaling network in the establishment of plant immunity. Cell **92:**773-784.

4. **Apel, K., and H. Hirt.** 2004. Reactive oxygen species: metabolism, oxidative stress, and signal transduction. Annual Review of Plant Biology **55:**373-399.

5. **Atkinson, J., R. F. Epand, and R. M. Epand.** 2008. Tocopherols and tocotrienols in membranes: a critical review. Free Radical Biology and Medicine **44:**739-764.

6. **Baggiolini, M., and M. P. Wymann.** 1990. Turning on the respiratory burst. Trends in Biochemical Science **15:**69-72.

7. **Beckman, J. S., and W. H. Koppenol.** 1996. Nitric oxide, superoxide, and peroxynitrite: the good, the bad, and ugly. American Journal of Physiology and Cell Physiology **271:**C1424-1437.

8. **Bedard, K., and K. H. Krause.** 2007. The NOX family of ROS-generating NADPH oxidases: physiology and pathophysiology. Physiological Reviews **87:**245-313.

9. **Bedard, K., B. Lardy, and K. H. Krause.** 2007. NOX family NADPH oxidases: not just in mammals. Biochimie **89:**1107-12.

10. **Bossis, G., and F. Melchior.** 2006. Regulation of SUMOylation by reversible oxidation of SUMO conjugating enzymes. Molecular Cell **21:**349-357.

11. **Brennan, A. M., S. Won Suh, S. Joon Won, P. Narasimhan, T. M. Kauppinen, H. Lee, Y. Edling, P. H. Chan, and R. A. Swanson.** 2009. NADPH oxidase is the primary source of superoxide induced by NMDA receptor activation. Nature Neuroscience **12:**857-863.

12. **Buchanan, B. B., and Y. Balmer.** 2005. Redox regulation: a broadening horizon. Annual Reviews of Plant Biology **56:**187-220.

13. **Buchanan, B. B., P. Schürmann, R. A. Wolosiuk, and J.-P. Jacquot.** 2002. The ferredoxin/thioredoxin system: from discovery to molecular structures and beyond. Photosynthetic Research **73:**215-222.

14. **Cano-Dominguez, N., K. Alvarez-Delfin, W. Hansberg, and J. Aguirre.** 2008. NADPH oxidases NOX-1 and NOX-2 require the regulatory subunit NOR-1 to control cell differentiation and growth in *Neurospora crassa*. Eukaryotic Cell **7:**1352-1361.

15. **Chen, J., W. Zheng, S. Zheng, D. Zhang, W. Sang, X. Chen, G. Li, G. Lu, and Z. Wang.** 2008. Rac1 is required for pathogenicity and Chm1-dependent conidiogenesis in rice fungal pathogen *Magnaporthe grisea*. PLoS Pathog **4:**e1000202.

16. **Chen, K., S. E. Craige, and J. F. Keaney.** 2009. Downstream targets and intracellular compartmentalization in Nox signaling. Antioxidants and Redox Signaling **11:**2467-2480.

17. **Chen, K., M. T. Kirber, H. Xiao, Y. Yang, and J. F. Keaney, Jr.** 2008. Regulation of ROS signal transduction by NADPH oxidase 4 localization. Journal of Cell Biology **181:**1129-1139.

18. **Choi, M. H., I. K. Lee, G. W. Kim, B. U. Kim, Y.-H. Han, D.-Y. Yu, H. S. Park, K. Y. Kim, J. S. Lee, C. Choi, Y. S. Bae, B. I. Lee, S. G. Rhee, and S. W. Kang.** 2005. Regulation of PDGF signalling and vascular remodelling by peroxiredoxin II. Nature **435:**347-353.

19. **Couturier, J., J.-P. Jacquot, and N. Rouhier.** 2009. Evolution and diversity of glutaredoxins in photosynthetic organisms. Cellular and Molecular Life Sciences **66:**2539-2557.

20. **D'Autreaux, B., and M. B. Toledano.** 2007. ROS as signalling molecules: mechanisms that generate specificity in ROS homeostasis. Nature Reviews Molecular Cell Biology **8:**813-824.

21. **Dröge, W.** 2002. Free radicals in the physiological control of cell function. Physiological Review **82:**47-95.

22. **Egan, M. J., and N. J. Talbot.** 2008. Genomes, free radicals and plant cell invasion: recent developments in plant pathogenic fungi. Current Opinion in Plant Biology **11:**367-372.

23. **Egan, M. J., Z. Y. Wang, M. A. Jones, N. Smirnoff, and N. J. Talbot.** 2007. Generation of reactive oxygen species by fungal NADPH oxidases is required for rice blast disease. Proceedings of the National Academy of Sciences of the USA **104:**11772-7.

24. **Forman, H. J., and M. Torres.** 2002. Reactive oxygen species and cell signaling: respiratory burst in macrophage signaling. American Journal of Respiratory and Critical Care Medicine **166:**S4-8.

25. **Fry, S. C.** 1998. Oxidative scission of plant cell wall polysaccharides by ascorbate-induced hydroxyl radicals. Biochemical Journal **332:**507-515.

26. **Geiszt, M., and T. L. Leto.** 2004. The Nox Family of NAD(P)H Oxidases: Host Defense and Beyond. Journal of Biological Chemistry **279:**51715-51718.

27. **Genestra, M.** 2007. Oxyl radicals, redox-sensitive signalling cascades and antioxidants. Cellular Signalling **19:**1807-1819.

28. **Gessler, N. N., A. A. Aver'yanov, and T. A. Belozerskaya.** 2007. Reactive oxygen species in regulation of fungal development. Biochemistry (Moscow) **72:**1091-1109.

29. **Green, M. A., and S. C. Fry.** 2005. Apoplastic degradation of ascorbate: Novel enzymes and metabolites permeating the plant cell wall. Plant Biosystems - An International Journal Dealing with all Aspects of Plant Biology: Official Journal of the Societa Botanica Italiana **139:**2-7.

30. **Green, M. A., and S. C. Fry.** 2005. Vitamin C degradation in plant cells via enzymatic hydrolysis of 4-O-oxalyl-l-threonate. Nature **433:**83-87.

31. **Greene, V., H. Cao, F. A. X. Schanne, and D. C. Bartelt.** 2002. Oxidative stress-induced calcium signalling in *Aspergillus nidulans*. Cellular Signalling **14:**437-443.

32. **Groemping, Y., and K. Rittinger.** 2005. Activation and assembly of the NADPH oxidase: a structural perspective. Biochemical Journal **386:**401-416.

33. **Hancock, J. T.** 2009. The role of redox mechanisms in cell signalling. Molecular Biotechnology **43:**162-166.

34. **Hansberg, W., and J. Aguirre.** 1990. Hyperoxidant states cause microbial cell differentiation by cell isolation from dioxygen. Journal of Theoretical Biology **142:**201-221.

35. **Hansberg, W., J. Aguirre, M. Rios-Momberg, P. Rangel, L. Peraza, Y. Montes de Onca, and N. Cano-Dominquez.** 2008. Cell differentiation as a response to oxidative stress, p. 235-258. *In* S. Avery and M. Stratford (ed.), Stress in yeast and filamentous fungi, 1st ed. Elsevier Academic Press, Amsterdam.

36. **Holmgreen, A.** 1985. Thioredoxins. Annual Review of Biochemistry **54:**237-271.

37. **Huang, J., V. Canadien, G. Y. Lam, B. E. Steinberg, M. C. Dinauer, M. A. O. Magalhaes, M. Glogauer, S. Grinstein, and J. H. Brumell.** 2009. Activation of antibacterial autophagy by NADPH oxidases. Proceedings of the National Academy of Sciences of the USA **106:**6226-6231.

38. **Jönsson, T. J., and W. T. Lowther.** 2007. The peroxiredoxin repair proteins. Subcellular Biochemistry **44:**115-141.

39. **Kärkönen, A., and S. C. Fry.** 2006. Effect of ascorbate and its oxidation products on H_2O_2 production in cell-suspension cultures of *Picea abies* and in the absence of cells. Journal of Experimental Botany **57:**1633-1644.

40. **Kiley, P. J., and G. Storz.** 2004. Exploiting thiol modifications. PLoS Biol **2:**e400.

41. **Knight, J.** 1999. Reactions of Pholasin with superoxide and peroxidases: applications to cellular chemiluminescence, p. 251-254. *In* A. Roda, L. J. Kricka, and P. E. Stanley (ed.), Bioluminescence and chemiluminescence. Perspectives for the 21st century. John Wiley & Sons, Chichester, New York.

42. **Knight, J., and A. McCafferty.** 1997. Pholasin monitors neutrophil degranulation and activation, p. 334-337. *In* J. W. Hastings, L. J. Kricka, and P. E. Stanley (ed.), Bioluminescence and Chemiluminescence: molecular reporting with photons. John Wiley & Sons, Chishester, New York.

43. **Lam, E.** 2004. Controlled cell death, plant survival and development. Nature Reviews Molecular Cell Biology **5:**305-315.

44. **Lambeth, J. D.** 2004. NOX enzymes and the biology of reactive oxygen. Nat Rev Immunol **4:**181-189.

45. **Lara-Ortiz, T., H. Riveros-Rosas, and J. Aguirre.** 2003. Reactive oxygen species generated by microbial NADPH oxidase NoxA regulate sexual development in Aspergillus nidulans. Molecular Microbiology **50:**1241-1255.

46. **Legerton, T. L., K. Kanamori, R. L. Weiss, and J. D. Roberts.** 1983. Measurements of cytoplasmic and vacuolar pH in *Neurospora* using nitrogen-15 nuclear magnetic resonance spectroscopy. Biochemistry **22:**899-903.

47. **Legrand, D., A. Pierce, E. Elass, M. Carpentier, C. Mariller, and J. Mazurier.** 2008. Lactoferrin structure and functions, p. 163-194. *In* Z. Bösze (ed.), Bioactive Components of Milk, vol. 606. Springer Verlag, New York.

48. **Leto, T. L., S. Morand, D. Hurt, and T. Ueyama.** 2009. Targeting and regulation of reactive oxygen species generation by Nox family NADPH oxidases. Antioxidants and Redox Signaling **11:**2607-2619.

49. **Liszkay, A., E. van der Zalm, and P. Schopfer.** 2004. Production of reactive oxygen intermediates ($O_2^{\cdot-}$, H_2O_2, and •OH) by maize roots and their role in wall loosening and elongation growth. Plant Physiology **136:**3114-3123.

50. **Lledias, F., P. Rangel, and W. Hansberg.** 1998. Oxidation of catalase by singlet oxygen. Journal of Biological Chemistry **273:**10630-10637.

51. **Lledías, F., P. Rangel, and W. Hansberg.** 1999. Singlet oxygen is part of a hyperoxidant state generated during spore germination. Free Radical Biology and Medicine **26:**1396-1404.

52. **Maerz, S., C. Ziv, N. Vogt, K. Helmstaedt, N. Cohen, R. Gorovits, O. Yarden, and S. Seiler.** 2008. The nuclear Dbf2-related kinase COT1 and the mitogen-activated protein kinases MAK1 and MAK2 genetically interact to regulate filamentous growth, hyphal fusion and sexual development in *Neurospora crassa*. Genetics **179:**1313-1325.

53. **Mahmud, S. A., T. Hirasawa, and H. Shimizu.** Differential importance of trehalose accumulation in *Saccharomyces cerevisiae* in response to various environmental stresses. Journal of Bioscience and Bioengineering **109:**262-266.

54. **Malagnac, F., H. Lalucque, G. Lepère, and P. Silar.** 2004. Two NADPH oxidase isoforms are required for sexual reproduction and ascospore germination in the filamentous fungus Podospora anserina. Fungal Genetics and Biology **41:**982-997.

55. **Mandal, S., A. Mitra, and N. Mallick.** Biochemical characterization of oxidative burst during interaction between *Solanum lycopersicum* and *Fusarium oxysporum f. sp. lycopersici*. Physiological and Molecular Plant Pathology **72:**56-61.

56. **Martinez-Ruiz, A., and S. Lamas.** 2007. Signalling by NO-induced protein S-nitrosylation and S-glutathionylation: convergences and divergences. Cardiovascular Research **75:**220-228.

57. **Meenan, B. J., J. McConnell, J. Knight, A. Boyd, and A. Bell.** 2002. Development of a sensitive whole blood chemiluminescence method for assessing the bioactivity of calcium phosphate powders. Biomaterials **23:**2431-2445.

58. **Mercker, M., K. Kollath-Leiss, S. Allgaier, N. Weiland, and F. Kempken.** 2009. The BEM46-like protein appears to be essential for hyphal development upon ascospore

germination in *Neurospora crassa* and is targeted to the endoplasmic reticulum. Current Genetics **55:**151-61.

59. **Munkres, K.** 1990. Histochemical detection of superoxide radicals and hydrogen peroxide by *age-1* mutants of *Neurospora*. Fungal Genetics Newsletter **37**.

60. **Naccache, P. H., C. Gilbert, A. C. Caon, M. Gaudry, C. K. Huang, V. A. Bonak, K. Umezawa, and S. R. McColl.** 1990. Selective inhibition of human neutrophil functional responsiveness by erbstatin, an inhibitor of tyrosine protein kinase. Blood **76:**2098-2104.

61. **Nasution, O., K. Srinivasa, M. Kim, Y.-J. Kim, W. Kim, W. Jeong, and W. Choi.** 2008. Hydrogen peroxide induces hyphal differentiation in *Candida albicans*. Eukaryotic Cell **7:**2008-2011.

62. **Neill, S. J., R. Desikan, and J. Hancock.** 2003. Nitric oxide signalling in plants. New Phytologist **159:**11-35.

63. **Oakley, F. D., D. Abbott, Q. Li, and J. F. Engelhardt.** 2009. Signaling components of redox active endosomes: the redoxosomes. Antioxidants and Redox Signaling **11:**1313-1333.

64. **Parton, R. M., S. Fischer, R. Malho, O. Papasouliotis, T. C. Jelitto, T. Leonard, and N. D. Read.** 1997. Pronounced cytoplasmic pH gradients are not required for tip growth in plant and fungal cells. Journal of Cell Science **110:**1187-98.

65. **Paulsen, C. E., and K. S. Carroll.** 2009. Orchestrating redox signaling networks through regulatory cysteine switches. ACS Chemical Biology **5:**47-62.

66. **Poulos, T. L.** 2006. Soluble guanylate cyclase. Current Opinion in Structural Biology **16:**736-743.

67. **Reichl, S., S. Bernard, J. Arnhold, J. Schiller, and K. Arnold.** 1999. Factors inlfuencing the Pholasin chemiluminescence, p. 280-283. *In* A. Roda, L. J. Kricka, and P. E. Stanley (ed.), Bioluminescence and Chemiluminescence. Perspectives for the 21st century. John Wiley & Sons, Chichester, New York.

68. **Reth, M.** 2002. Hydrogen peroxide as second messenger in lymphocyte activation. Nature Immunology **3:**1129-34.

69. **Rhee, S. G., T. S. Chang, Y. S. Bae, S. R. Lee, and S. W. Kang.** 2003. Cellular regulation by hydrogen peroxide. Journal of the American Society of Nephrology **14:**S211-5.

70. **Rhee, S. G., S. W. Kang, W. Jeong, T. S. Chang, K. S. Yang, and H. A. Woo.** 2005. Intracellular messenger function of hydrogen peroxide and its regulation by peroxiredoxins. Current Opinion in Cell Biology **17:**183-9.

71. **Rittentour, W. R., H. Si, and S. D. Harris.** 2009. Hyphal morphogenesis in *Aspergillus nidulans*. Fungal Biology Reviews **23:**20-29.

72. **Rolke, Y., and P. Tudzynski.** 2008. The small GTPase Rac and the p21-activated kinase Cla4 in *Claviceps purpurea*: interaction and impact on polarity, development and pathogenicity. Molecular Microbiology **68:**405-423.

73. **Rouhier, N., E. Gelhaye, P.-E. Sautiere, A. Brun, P. Laurent, D. Tagu, J. Gerard, E. de Fay, Y. Meyer, and J.-P. Jacquot.** 2001. Isolation and characterization of a new peroxiredoxin from poplar sieve tubes that uses either glutaredoxin or thioredoxin as a proton donor. Plant Physiology **127:**1299-1309.

74. **Schopfer, P.** 2001. Hydroxyl radical-induced cell-wall loosening *in vitro* and *in vivo*: implications for the control of elongation growth. The Plant Journal **28:**679-688.

75. **Schopfer, P., C. Plachy, and G. Frahry.** 2001. Release of reactive oxygen intermediates (superoxide radicals, hydrogen peroxide, and hydroxyl radicals) and peroxidase in germinating radish seeds controlled by light, gibberellin, and abscisic acid. Plant Physiology **125:**1591-1602.

76. **Schürmann, P., and J. P. Jacquot.** 2000. Plant thioredoxin systems revisited. Annual Review of Plant Physiology and Plant Molecular Biology **51:**371-400.

77. **Scott, B., and C. J. Eaton.** 2008. Role of reactive oxygen species in fungal cellular differentiations. Current Opinion in Microbiology **11:**488-493.

78. **Segal, A. W., and A. Abo.** 1993. The biochemical basis of the NADPH oxidase of phagocytes. Trends in Biochemical Science **18:**43-7.

79. **Semighini, C. P., and S. D. Harris.** 2008. Regulation of apical dominance in *Aspergillus nidulans* hyphae by reactive oxygen species. Genetics **179:**1919-1932.

80. **Spadaro, D., B. W. Yun, S. H. Spoel, C. Chu, Y. Q. Wang, and G. J. Loake.** 2010. The redox switch: dynamic regulation of protein function by cysteine modifications. Physiologia Plantarum **138:**360-71.

81. **Takemoto, D., A. Tanaka, and B. Scott.** 2007. NADPH oxidases in fungi: diverse roles of reactive oxygen species in fungal cellular differentiation. Fungal Genetics and Biology **44:**1065-1076.

82. **Takemoto, D., A. Tanaka, and B. Scott.** 2006. A p67Phox-like regulator is recruited to control hyphal branching in a fungal-grass mutualistic symbiosis. The Plant Cell **18:**2807-2821.

83. **Tanaka, A., M. J. Christensen, D. Takemoto, P. Park, and B. Scott.** 2006. Reactive oxygen species play a role in regulating a fungus-perennial ryegrass mutualistic interaction. The Plant Cell **18:**1052-1066.

84. **Toledano, M. B., A.-G. Planson, and A. Delaunay-Moisan.** 2010. Reining in H_2O_2 for Safe Signaling. Cell **140:**454-456.

85. **Toledo, I., J. Aguirre, and W. Hansberg.** 1994. Enzyme inactivation related to a hyperoxidant state during conidiation of *Neurospora crassa*. Microbiology **140:**2391-2397.

86. **Ullrich, V., and R. Kissner.** 2006. Redox signaling: bioinorganic chemistry at its best. Journal of Inorganic Biochemistry **100:**2079-2086.

87. **Ushio-Fukai, M.** 2009. Compartmentalization of redox signaling through NADPH oxidase-derived ROS. Antioxidants and Redox Signaling **11:**1289-1299.

88. **Ushio-Fukai, M.** 2006. Localizing NADPH oxidase-derived ROS. Science STKE **2006:**re8-.

89. **Veal, E. A., A. M. Day, and B. A. Morgan.** 2007. Hydrogen Peroxide Sensing and Signaling. Molecular Cell **26:**1-14.

90. **Virag, A., M. P. Lee, H. Si, and S. D. Harris.** 2007. Regulation of hyphal morphogenesis by *cdc42* and *rac1* homologues in *Aspergillus nidulans*. Molecular Microbiology **66:**1579-1596.

91. **Vreeburg, R. A. M., and S. C. Fry.** 2005. Reactive oxygen species in cell walls, p. 215-249. *In* N. Smirnoff (ed.), Antioxidants and Reactive Oxygen Species in Plants. Blackwell, Oxford.

92. **Watson, F., J. Robinson, and S. W. Edwards.** 1991. Protein kinase C-dependent and -independent activation of the NADPH oxidase of human neutrophils. Journal of Biological Chemistry **266:**7432-7439.

93. **Woo, H. A., S. H. Yim, D. H. Shin, D. Kang, D.-Y. Yu, and S. G. Rhee.** 2010. Inactivation of peroxiredoxin I by phosphorylation allows localized H_2O_2 accumulation for cell signaling. Cell **140:**517-528.

94. **Zähringer, H., M. Burgert, H. Holzer, and S. Nwaka.** 1997. Neutral trehalase Nth1p of *Saccharomyces cerevisiae* encoded by the NTH1 gene is a multiple stress responsive protein. FEBS Letters **412:**615-620.

Chapter 8 – Overall summary

The key motivation for this project was the small number of known hyphal fusion mutants in *Neurospora crassa,* which comprised only five reported proteins at the beginning of this study. The first hyphal anastomosis mutant (HAM-1) was identified in 1999 by Wilson & Dempsey [29], and was later on found to be allelic with SO and further characterized [5-7]. Shortly after, HAM-2 was identified and its function also described in more detail in the following years [11, 22, 30]. The other three hyphal fusion mutants known at the time were all defective in components of the pheromone response MAPK pathway, and included the MAP kinases NRC-1 and MAK-2, as well as the associated transcription factor PP-1 [12, 16, 20]. Subsequent studies revealed that only Δ*soft* was generally able to form CATs, but defective in CAT homing [7, 22]. All other fusion mutants have been found to be defective in CAT formation. In order to identify novel fusion mutants and thereby expand our knowledge about the underlying regulatory mechanisms, a functional comparative genomics screen of *N. crassa* gene deletion mutants was conducted at the beginning of my PhD research. From the 19 new fusion mutants identified, a selection of candidate proteins was subjected to a more detailed molecular analysis. To achieve a better understanding of the signalling pathways constituting the positive chemotropism underlying CAT-mediated cell fusion, the identification of more CAT homing mutants was of particular interest. Four confirmed and two putative novel CAT homing mutants were identified (Table 3.7). During the course of this study, a number of the initially formulated questions, as well as new questions that arose from the results obtained (section 1.8) could be addressed, and now provide us with a more complete picture of the cell fusion process in *Neurospora crassa*. The key findings and proposed future work leading on from these results are summarized in the following section.

8.1. Key findings and future work

Functional conservation between *M. oryzae* and *N. crassa* is focused on MAPK, Rho GTPase and redox signalling, and suggests that a more detailed analysis of upstream receptor components is required. The functional conservation of the molecular mechanism required for appressorium-mediated host infection of *Magnaporthe oryzae* and CAT-mediated cell fusion of *Neurospora crassa* was about 37%, when considering both essential and non-essential signalling pathway components. All tested core components of the MAPK pheromone response (PR) and cell wall integrity (CWI) pathways were essential for the named processes in both species, whereas MAP kinases of the high-osmolarity glycerol (HOG) pathway were equally non-essential. Furthermore, components constituting NADPH-oxidase complexes were found to be required. However, a final conclusion about the role of NOX-2 in *N. crassa* and its functional distinction to NOX-1 could not yet be fully established (see below). Interestingly, mutants from the CWI MAPK pathway, as well as the redox mutants Δ*nox-1*, Δ*nor-1* and Δ*lao,* were able to form CATs at low frequency but did not chemotropically interact. This indicates that these pathways are mainly active after CAT formation and required during CAT homing and fusion. Other proteins that share functional significance in both fungi included NAD^+-dependent glutamate dehydrogenase which is associated with redox signalling, as well as Rho and Ras GTPase signalling components. A more detailed functional analysis of these proteins in cell fusion is urgently required. Due to lethality of certain gene deletion mutants in both species, or currently unavailable homokaryotic KO strains in either species, the estimated number of unknown components functionally shared between appressorium-mediated infection and hyphal fusion is around 10%. An interesting finding was that, although crucially important for the induction of appressorium morphogenesis in *M. oryzae*, all 12 tested components of the cAMP response pathway were found to be dispensable for hyphal fusion. The role of cAMP signalling in *N. crassa* was found to be connected to the control of conidiogenesis, and might indicate regulatory divergence associated

to the different life styles of both species. Overall, the comparative analysis most importantly resulted in the identification of redox signalling components involved in hyphal fusion. As upstream components which transduce signals into the PR and CWI MAPK cascades, and which are essential for hyphal fusion, have not yet been identified, future investigations should consider a more rigorous analysis of the at least 10 GPCRs identified in *Neurospora* [1]. This should also include 8 candidate proteins containing CFEM domains of GPCRs (PTH-11 like proteins) initially described in *Magnaporthe* [4, 13, 14]. Other upstream elements that might relay contact-induced signals into MAPK signalling, such as WSC-type mechanosensors, also require further investigation. The generation and analysis of selected double KOs needs to be taken into serious consideration as well, especially for G-protein signalling components, which so far analysed as single KOs only resulted in negative data. This however might be misleading due to the potentially high functional redundancy of pathway components, such as Gα-subunits [17].

Novel live-cell imaging marker for F-actin and activated Rho GTPases revealed new aspects of the structural and physiological distinction between GTs and CATs. Another milestone of this study was the development of the two novel live-cell imaging markers for F-actin (Lifeact-FPs) and activated Rho GTPases (CRIB-sGFP). Lifeact-TagRFP/-T allowed the detailed analysis of F-actin cable and patch dynamics during the establishment and maintenance of polarized growth of GTs and CATs. As a result, the primary role of F-actin in cell symmetry breaking, as well as its exclusive requirement for CAT-mediated cell fusion could be demonstrated. Furthermore, co-expression with the microtubule marker BML-sGFP showed that both cytoskeletal elements cooperate during polarisation site selection, but also have functionally distinct roles in GTs and CATs. Disruption of microtubules did not prevent CAT formation, but it greatly impaired polarisation fidelity and prevented elongation of GTs. The CRIB-sGFP biosensor, especially in combination with Lifeact-TagRFP-T and the application of the small molecule Rac-

specific inhibitor NSC23766, indicated for the first time that differential recruitment of CDC42 and RAC-1, respectively, are key determinants of which type of cell protrusion is formed and maintained. Addition of NSC23766 specifically blocked CAT formation and lead to immediate CRIB-sGFP dispersal from growing CAT, but not from GT tips. Moreover, blocking CAT formation by GTPase inhibition promoted GT elongation, suggesting that cells which are unable to engage into the cell fusion program default into a 'GT growth' pathway with potentially increased CD42 activity. Together these findings strongly suggest that RAC-1 has an exclusive role in CAT-mediated cell fusion, whereas CDC42 has a primary role in GT growth. If similar to what has been demonstrated in *Claviceps purpurea* [23], the Cla4p-homolog PAK CHM-1 is likely to be specifically activated by RAC-1 but not CDC42. Future investigations will focus on a more detailed functional dissection of how both GTPases coordinate the interplay between perception of the chemotropic signal, dislocation of GTPase activity at the cell cortex and subsequent rearrangement of the actin cytoskeleton to permit chemotropic tip re-orientation in GTs and CATs. This will include the generation of a RAC-1 specific biosensor derived from the RAC-specific TPR interaction domains of NOR-1 [3, 10, 15, 27], as well as the generation of a CDC42-specific biosensor derived from the unique Cdc42 GTPase-binding domain (GBD) of the cell polarity protein Par6 [8]. A worthwhile test might include expression of CRIB-sGFP in a Δ*rdi-1* backround lacking the Rho GDI RDI-1 of *Neurospora*. GDI proteins are rather catalysts of GTPase shuttling than mere inhibitors [9, 26], thus absence of RDI-1 should result in a stronger activation of RAC-1 activity at the membrane and thus theoretically lead to an increase in CAT formation. The same principle applies for mutants lacking Rho GAPs, such as Δ*rgd-1* or Δ*lrg-1*, which have a crucial role in deactivation and membrane extraction of activated GTPases [9]. Live-cell imaging analyses of CRIB-sGFP dynamics in Δ*cdc42* and Δ*rac-1* backgrounds are additional possibilities, but due to the severe defects of these strains, recovery of transformants is expected to be problematic. The possibility of comparing GTPase behaviour during opposite chemotropisms of GTs

and CATs will greatly facilitate functional analyses. If experimentally accessible, for example by comparing gas chromatograms of lipid extracts from germling cultures grown in the presence and absence of the CAT-inhibitor NSC23766, the biochemical analysis of a suspected differential lipid composition in GT and CAT tips might be another big step forward towards a more comprehensive understanding of the physiological differences between both types of cell protrusions. Furthermore, the use of additional inhibitors, such as secramine which confers Rho GDI-dependent Cdc42p inhibition at the plasma membrane [21], or toxin B from *Clostridium difficile*, which inhibits all three types of Rho GTPases [24, 25], might assist the dissection of functional differences between RAC-1 and CDC42 in comparison to RHO-1 to RHO-4 GTPases during CAT-mediated cell fusion in *Neurospora crassa*.

An essential role of the CWI MAPK pathway includes regulation of the organized assembly of the F-actin cytoskeleton during CAT-mediated cell fusion. Another striking difference between GTs and CATs revealed in this study is the different requirement of the CWI MAP kinase MAK-1. Although colonies of the Δ*mak-1* gene deletion mutant show a phenotype typically associated with cell wall defects, MAK-1 is not required to promote GT growth and general colony establishment. MAK-1 however is required for CAT formation and essential for CAT homing and cell fusion. The detailed functional analysis of MAK-1 showed that its intrinsic kinase activity is necessary for its own recruitment to homing CAT tips, but even more so, upon contact-induced accumulation at the fusion site. MAK-1 remained present during fusion pore opening, suggesting that it functions in localized cell wall degradation processes whilst at the same time preventing cell leakage by reinforcement of the cell wall connection. Another striking observation was the recruitment of MAK-1 into cortical clusters, which appeared to coincide with chemoattractive cell interaction and also required MAK-1 kinase activity. Although the function of these clusters is currently unknown, similar observations have been made with MAK-2, where appearance/disappearance of cortical clusters

coincided with the oscillatory recruitment of the kinase [6]. Whether kinase activity was required for MAK-2 cluster formation has not been reported. If so, it would suggest that phosphorylation of interaction partners is necessary and possibly involved in membrane binding of the kinase. MAK-1 cluster formation was not observed in cells that only grew GTs or were treated with the 1NM-PP1 inhibitor, which blocked CAT formation and CAT fusion in sensitive strains dependent on the timing of kinase inhibition. Being able to induce the Δ*mak-1* phenotype through addition of 1NM-PP1 at will was a substantial step forward for the functional analysis of the protein. Another key finding was that absence of MAK-1 also affected F-actin organization. Expression of Lifeact-TagRFP in a Δ*mak-1* background, provided the first evidence for a functional relationship between CWI MAPK signalling and recruitment of F-actin, and thus offers an explanation for the reduced frequency of CAT formation and defects in cell fusion in this mutant. Future studies will follow up the functional connection between MAK-1 kinase activity and F-actin organization at the fusion site in more detail. This will include live-cell imaging analysis of the effects rapamycin has on MAK-1 recruitment and on F-actin organisation. Furthermore, the upstream MAP kinases MEK-1 and MIK-1, as well as the associated PKC, will be subjected to closer analyses with respect to their role in CAT homing. An interesting approach to further dissect the involvement of PKC signalling potentially offers the PKC/cAMP-dependent protein kinase inhibitor secalonic acid D [28]. In addition, an inhibitable allele of *pkc* is urgently required to facilitate 1NM-PP1-mediated inactivation of PKC and by-pass problems with the lethality of Δ*pkc-1* strains.

The ultrastructural analysis of fruitbody development reveals defects associated with but not dependent on hyphal fusion. The ultrastructural analysis of the initial stages of female sexual development in fusion mutants showed that defects in extracellular matrix deposition and hyphal adhesion are important determinants for protoperithecial morphogenesis and can lead to early abortion of

developing fruitbodies. Removal of surface water from the specimens by partial freeze-drying was found to be essential to reveal these morphological defects. Gene deletion strains that were able to produce extracellular matrix and assembled enveloping hyphae in an organized way generally proceeded further in protoperithecial development. In these cases, developmental blockage appeared to be associated with defects in trichogyne differentiation. The observed defects provided functional links between morphogenetic transitions preceding vegetative hyphal fusion and organization of the developing fruitbody. The unifying fusion defect of all analysed mutants, however, did not manifest in a conserved phenotype during sexual development. Although, for a number of strains the stage at which fruitbody development was blocked could be defined in more detail than previously appreciated, physical fusion between hyphae that gave rise to the protoperithecium could not be demonstrated with this approach. Nevertheless, the morphological comparison of protoperithecial development in hyphal fusion mutants allowed us to start building a model describing in which order the affected signalling pathways might function during fruitbody morphogenesis. Future investigations will concentrate on assessing hyphal fusion within the developing fruitbody invasively and non-invasively. Firstly, sections of protoperithecia that have been fixed and resin-embedded will be examined by light microscopy and TEM. Secondly, the cell walls of developing fruitbodies will be stained with the live-cell imaging dye CFW and optically sectioned by CLSM. Similar analyses of fruitbody development in Δ*os* mutants (HOG pathway), which are not fusion defective, complemented with 3D ultrastructural cryo-SEM data will complete our understanding of the role MAPK signalling has in the process.

Redox processes are essential for CAT-mediated cell fusion, but further studies need to verify the indicated functional distinction between the NOX-1 and NOX-2 isoforms. A number of findings demonstrated that redox processes play important roles in morphogenetic events required for CAT formation and

subsequent cell fusion: (1) CAT formation was blocked or significantly impaired in mutants lacking proteins associated with ROS generation and turn over, and (2) could be selectively suppressed through the addition of micromolar amounts of H_2O_2. (3) NOX-1-sGFP was localized to internal membranes constituting the perinuclear ER suggesting the production of only small localized amounts of ROS, and thus indicating a function in redox signalling rather than in the generation of extracellular oxidative bursts. (4) The enzymes GDH-1 and LAO were identified which could act as positive or negative regulators of ROS activity thereby providing a functional link to the cell's metabolism. Furthermore, using the bioluminescent ROS reporter Pholasin® (5), fusion mutants were found to be impaired in adjusting extracellular ROS level as efficiently as the wt, and (6) NOX-mediated ROS production could be triggered through direct activation of PKC, suggesting that NOX assembly and activation occurs through a receptor-independent pathway. An important task of future investigations will be to functionally dissect the role of NOX-2 in comparison to the date obtained for NOX-1. For this, all experiments presented here will be repeated with a Δ*nox-2* gene deletion strain, which although not successfully generated within this study, has recently been reported to be viable as 'partial' gene deletion mutant [3]. Furthermore, to better verify subcellular regions of ROS production the reduction-oxidation sensitive GFP variant roGFP [18, 19] will be ratio-imaged in the wt and various mutant backgrounds during the process of CAT formation and CAT-mediated cell fusion. To further verify linkage between NOX activity and metabolism, the fusion phenotype of a mutant lacking NADPH-dependent glutamase dehydrogenase needs to be assessed. Deletion of this anabolic enzyme that rather consumes ATP and NADPH, should not influence cell fusion, and in that case would provide supporting evidence for the notion that cell fusion is a morphogenetic event which requires energy- and ROS-dependent transition through a hyperoxidant state. Finally, to resolve the subcellular localization and timing of NOX assembly in more detail, rescued Δ*nox-1*(NOX-1-sGFP) transformants co-expressing sufficient amounts of NOR-1-TagRFP-T need to

be generated and stimulated with PMA. If NOX-1, and not only NOX-2, is activated by PMA, addition of the drug should result in an increased co-localization of NOR-1-TagRFP-T and NOX-1-sGFP in the perinuclear ER and possibly the plasma membrane. Control experiments should include PMA activation of redox gene deletion mutants including Δ*nox-2*, and tests with the NOX2 inhibitor apocynin [2].

8.2. References

1. **Borkovich, K. A., L. A. Alex, O. Yarden, M. Freitag, G. E. Turner, N. D. Read, S. Seiler, D. Bell-Pedersen, J. Paietta, N. Plesofsky, M. Plamann, M. Goodrich-Tanrikulu, U. Schulte, G. Mannhaupt, F. E. Nargang, A. Radford, C. Selitrennikoff, J. E. Galagan, J. C. Dunlap, J. J. Loros, D. Catcheside, H. Inoue, R. Aramayo, M. Polymenis, E. U. Selker, M. S. Sachs, G. A. Marzluf, I. Paulsen, R. Davis, D. J. Ebbole, A. Zelter, E. R. Kalkman, R. O'Rourke, F. Bowring, J. Yeadon, C. Ishii, K. Suzuki, W. Sakai, and R. Pratt.** 2004. Lessons from the genome sequence of *Neurospora crassa*: tracing the path from genomic blueprint to multicellular organism. Microbiological and Molecular Biological Reviews **68:**1-108.

2. **Brennan, A. M., S. Won Suh, S. Joon Won, P. Narasimhan, T. M. Kauppinen, H. Lee, Y. Edling, P. H. Chan, and R. A. Swanson.** 2009. NADPH oxidase is the primary source of superoxide induced by NMDA receptor activation. Nature Neuroscience **12:**857-863.

3. **Cano-Dominguez, N., K. Alvarez-Delfin, W. Hansberg, and J. Aguirre.** 2008. NADPH oxidases NOX-1 and NOX-2 require the regulatory subunit NOR-1 to control cell differentiation and growth in *Neurospora crassa*. Eukaryotic Cell **7:**1352-1361.

4. **DeZwaan, T. M., A. M. Carroll, B. Valent, and J. A. Sweigard.** 1999. *Magnaporthe grisea* Pth11p is a novel plasma membrane protein that mediates appressorium differentiation in response to inductive substrate cues. Plant Cell **11:**2013-2030.

5. **Fleißner, A., and N. L. Glass.** 2007. SO, a protein involved in hyphal fusion in *Neurospora crassa*, localizes to septal plugs. Eukaryotic Cell **6:**84-94.

6. **Fleißner, A., A. C. Leeder, M. G. Roca, N. D. Read, and N. L. Glass.** 2009. Oscillatory recruitment of signaling proteins to cell tips promotes coordinated behaviour during cell fusion Proceedings of the National Academy of Sciences of the USA **106:**19387–19392.

7. **Fleißner, A., S. Sarkar, D. J. Jacobson, G. M. Roca, N. D. Read, and N. L. Glass.** 2005. The *so* locus is required for vegetative cell fusion and postfertilization events in *Neurospora crassa*. Eukaryotic Cell **4:**920-930.

8. **Garrard, S. M., C. T. Capaldo, L. Gao, M. K. Rosen, I. G. Macara, and D. R. Tomchick.** 2003. Structure of Cdc42 in a complex with the GTPase-binding domain of the cell polarity protein, Par6. EMBO Journal **22:**1125-1133.

9. **Goryachev, A. B., and A. V. Pokhilko.** 2008. Dynamics of Cdc42 network embodies a turing-type mechanism of yeast cell polarity. FEBS letters **582:**1437-1443.

10. **Grizot, S., J. Faure, F. Fieschi, P. V. Vignais, M. C. Dagher, and E. Pebay-Peyroula.** 2001. Crystal structure of the Rac1-RhoGDI complex involved in NADPH oxidase activation. Biochemistry **40:**10007-10013.

11. **Hickey, P. C., D. J. Jacobson, N. D. Read, and N. Louise Glass.** 2002. Live-cell imaging of vegetative hyphal fusion in *Neurospora crassa*. Fungal Genetics and Biology **37:**109-119.

12. **Kothe, G. O., and S. J. Free.** 1998. The isolation and characterization of *nrc-1* and *nrc-2*, two genes encoding protein kinases that control growth and development in *Neurospora crassa*. Genetics **149:**117-130.

13. **Kulkarni, R. D., H. S. Kelkar, and R. A. Dean.** 2003. An eight-cysteine-containing CFEM domain unique to a group of fungal membrane proteins. Trends in Biochemical Science **28:**118-21.

14. **Kulkarni, R. D., M. R. Thon, H. Pan, and R. A. Dean.** 2005. Novel G-protein-coupled receptor-like proteins in the plant pathogenic fungus *Magnaporthe grisea*. Genome Biology **6:**R24.1-14.

15. **Kwong, C. H., A. G. Adams, and T. L. Leto.** 1995. Characterization of the effector-specifying domain of Rac involved in NADPH oxidase activation. Journal of Biological Chemistry **270:**19868-72.

16. **Li, D., P. Bobrowicz, H. H. Wilkinson, and D. J. Ebbole.** 2005. A mitogen-activated protein kinase pathway essential for mating and contributing to vegetative growth in *Neurospora crassa*. Genetics **170:**1091-1104.

17. **Li, L., S. J. Wright, S. Krystofova, G. Park, and K. A. Borkovich.** 2007. Heterotrimeric G protein signaling in filamentous fungi. Annual Reviews in Microbiology **61:**423-52.

18. **Meyer, A. J., and T. Brach.** 2009. Dynamic redox measurements with redox-sensitive GFP in plants by confocal laser scanning microscopy. Methods in Molecular Biology **479:**93-107.

19. **Meyer, A. J., T. Brach, L. Marty, S. Kreye, N. Rouhier, J. P. Jacquot, and R. Hell.** 2007. Redox-sensitive GFP in *Arabidopsis thaliana* is a quantitative biosensor for the redox potential of the cellular glutathione redox buffer. Plant Journal **52:**973-86.

20. **Pandey, A., G. M. Roca, N. D. Read, and N. L. Glass.** 2004. Role of a mitogen-activated protein kinase pathway during conidial germination and hyphal fusion in *Neurospora crassa*. Eukaryotic Cell **3:**348-358.

21. **Pelish, H. E., J. R. Peterson, S. B. Salvarezza, E. Rodriguez-Boulan, J.-L. Chen, M. Stamnes, E. Macia, Y. Feng, M. D. Shair, and T. Kirchhausen.** 2006. Secramine inhibits Cdc42-dependent functions in cells and Cdc42 activation *in vitro*. Nature Chemical Biology **2:**39-46.

22. **Roca, G. M., J. Arlt, C. E. Jeffree, and N. D. Read.** 2005. Cell biology of conidial anastomosis tubes in *Neurospora crassa*. Eukaryotic Cell **4:**911-919.

23. **Rolke, Y., and P. Tudzynski.** 2008. The small GTPase Rac and the p21-activated kinase Cla4 in *Claviceps purpurea*: interaction and impact on polarity, development and pathogenicity. Molecular Microbiology **68:**405-423.

24. **Sehr, P., G. Joseph, H. Genth, I. Just, E. Pick, and K. Aktories.** 1998. Glucosylation and ADP ribosylation of rho proteins: effects on nucleotide binding, GTPase activity, and effector coupling. Biochemistry **37:**5296-304.

25. **Servant, G., O. D. Weiner, P. Herzmark, T. Balla, J. W. Sedat, and H. R. Bourne.** 2000. Polarization of chemoattractant receptor signaling during neutrophil chemotaxis. Science **287:**1037-40.

26. **Slaughter, B. D., A. Das, J. W. Schwartz, B. Rubinstein, and R. Li.** 2009. Dual modes of cdc42 recycling fine-tune polarized morphogenesis. Developmental Cell **17:**823-35.

27. **Takemoto, D., A. Tanaka, and B. Scott.** 2006. A p67Phox-like regulator is recruited to control hyphal branching in a fungal-grass mutualistic symbiosis. The Plant Cell **18:**2807-2821.

28. **Wang, B. H., and G. M. Polya.** 1996. The fungal teratogen secalonic acid D is an inhibitor of protein kinase C and of cyclic AMP-dependent protein kinase. Planta Medicina **62:**111-4.

29. **Wilson, J. F., and J. A. Dempsey.** 1999. A hyphal fusion mutant in *Neurospora crassa*. Fungal Genetics Newsletter **46:**31.

30. **Xiang, Q., C. Rasmussen, and N. L. Glass.** 2002. The *ham-2* locus, encoding a putative transmembrane protein, is required for hyphal fusion in *Neurospora crassa*. Genetics **160:**169-180.

Appendices

Appendix I - Supplementary material on CD

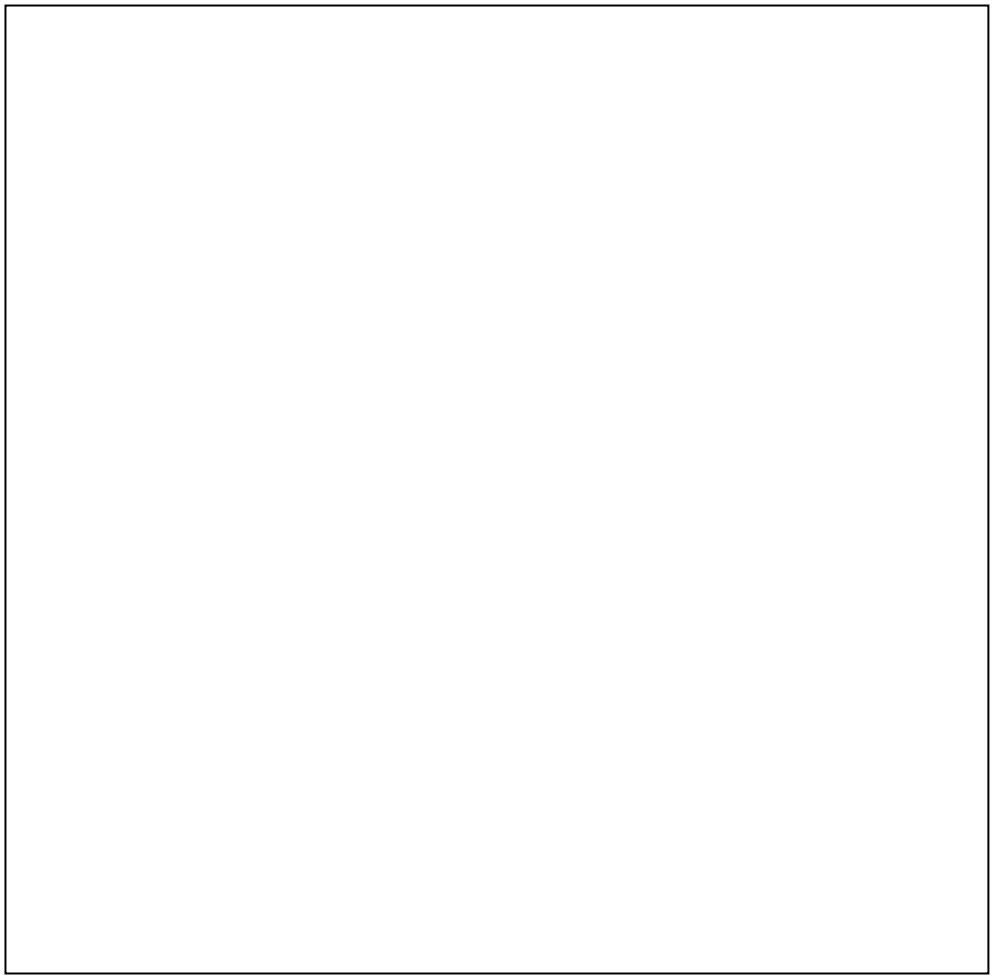

Appendix II - Oral and poster presentations

Oral presentations

Alex Lichius and Nick D. Read. Functional gene analysis during hyphal fusion in *Neurospora crassa*. Annual Scientific Meeting of the British Mycological Society, Ecology of Fungal Communities, 9th–12th September 2007, University of Manchester, England, UK.

Alex Lichius and Nick D. Read. Building networks: functional gene analysis during hyphal fusion in *Neurospora crassa*. 9th European Conference on Fungal Genetics (ECFG9), 5th – 8th April 2008, Edinburgh, Scotland, UK.

Alex Lichius and Nick D. Read. The MAP kinase MAK1 is required for homing and pore formation during cell fusion in *Neurospora crassa.* Annual Meeting of the British Mycological Society, The Fungal Cell, 1st – 4th September 2009, Dundee, Scotland, UK.

Alex Lichius and Nick D. Read. The *Neurospora* cell wall integrity MAPK MAK-1 in cell fusion and early fruitbody development. *Neurospora* Satellite Meeting of the 10th European Conference on Fungal Genetics (ECFG10), 28th March 2010, Leiden, The Netherlands.

Alex Lichius and Nick D. Read. Tip-focused RhoGTPase activity and the actin cytoskeleton regulate directional growth of *Neurospora crassa* germlings. 10th European Conference on Fungal Genetics (ECFG10), 29th March – 2nd April 2010, Leiden, The Netherlands.

Alex Lichius, Andrew B. Goryachev and Nick D. Read. Differential activation of the RhoGTPases CDC42 and RAC-1 of *Neurospora crassa* determines formation and chemotropism of germ tubes and CATs. 9th International Mycological Congress (IMC9), 1st - 6th August 2010, Edinburgh, Scotland, UK.

Poster presentations

Alex Lichius, Nick D. Read. What does the biochemical machinery involved in hyphal fusion have in common with that involved in infection structure differentiation? 9th International Fungal Biology Conference & 16th *New Phytologist* Symposium, Impact of genomics on fungal biology, 18th - 20th September 2006, Nancy, France.

Alex Lichius, Nick D. Read. Identification of novel genes involved in hyphal fusion in filamentous fungi. 24th Fungal Genetics Conference (FGCXXIV), 20th - 25th March 2007, Asilomar, Pacific Grove, USA.

Alex Lichius, Nick D. Read. Identification of novel genes involved in hyphal fusion in filamentous fungi. 8th International Botanical Microscopy Meeting, 31st March – 5th April 2007, University of Salzburg, Austria.

Jun-ya Shoji, **Alex Lichius**, Andrew B. Goryachev and Nick D. Read. Functional analysis of the small GTPase RAC-1 of *Neurospora crassa.* 25th Fungal Genetics Conference (FGCXXV), 17th – 22nd March 2009, Asilomar, Pacific Grove, USA.

Alex Lichius and Nick D. Read. Redox regulation of cell fusion in the filamentous fungus *Neurospora crassa*. British Society for Cell Biology Spring Meeting, The Dynamic Cell, 1st – 4th April 2009, University of Edinburgh, Scotland, UK.

Alex Lichius and Nick D. Read. The MAP kinase MAK1 is required for homing and pore formation during cell fusion in *Neurospora crassa.* Gordon Research conference (GRC) Cell-Cell Fusion, 19th – 24th July 2009, New London, New Hampshire, USA.

Alex Lichius, Kathryn M. Lord, Chris E. Jeffree and Nick D. Read. Sex and fusion in *Neurospora crassa*. Annual Meeting of the British Mycological Society, The Fungal Cell, 1st – 4th September 2009, Dundee, Scotland, UK.

Adokiye Berepiki, **Alex Lichius** and Nick D. Read. Live-cell imaging of the actin cytoskeleton in *Neurospora crassa.* Annual Meeting of the British Mycological Society, The Fungal Cell, 1st – 4th September 2009, Dundee, Scotland, UK.

Alex Lichius, Kathryn M. Lord, Chris E. Jeffree and Nick D. Read. Sex and fusion in *Neurospora crassa*. 37th Scottish Microscopy Group Symposium, 4th November 2009, University of Glasgow, Scotland, UK.

Alex Lichius and Nick D. Read. The MAP kinase MAK1 is required for homing and pore formation during cell fusion in *Neurospora crassa.* 37th Scottish Microscopy Group Symposium, 4th November 2009, University of Glasgow, Scotland, UK.

Alex Lichius, Kathryn M. Lord, Chris E. Jeffree and Nick D. Read. Sex and fusion in *Neurospora crassa*. From Darwin to Evo-Devo, A symposium in honour of the 150th anniversary of Darwin's 'The Origin of Species", 23rd -24th November 2009, Technion Israel Institute of Technology, Haifa, Israel.

Appendix III - PDF versions of publications

The following papers are bound into the back of the thesis:

Read, N. D., A. Lichius, J. Shoji, and A. B. Goryachev. 2009. Self-signalling and self-fusion in filamentous fungi. Current Opinion in Microbiology **12:**608-615.

Berepiki, A., A. Lichius, J.-y. Shoji, J. Tilsner, and N. D. Read. 2010. F-actin dynamics in *Neurospora crassa*. Eukaryotic Cell **9:**547-57.

Roca, M. G., H.-C. Kuo, A. Lichius, M. Freitag, and N. D. Read. 2010. Nuclear dynamics, mitosis and the cytoskeleton during the early stages of colony initiation in *Neurospora crassa*. Eukaryotic Cell (in press).

Appendix IV - Awards received

Sincere thanks to the following institutions for their generous support:

Edinburgh University School of Biological Sciences Ph.D. Studentship Award, September 2006 – September 2009

Royal Microscopical Society Travel Bursary, February 2007

James Rennie Bequest, Edinburgh University, March 2007

Federation of European Microbiological Societies (FEMS) Meeting Grant, March 2008

Best Postgraduate Oral Presentation/Microscopy Prize, BMS Fungal Cell Meeting, Dundee, UK, September 2009

Poster prize, BMS Fungal Cell Meeting, Dundee, UK, September 2009

Technion Israel Institute of Technology Fellowship Travel Award, October 2009

Poster prize, From Darwin to Evo-Devo Symposium, Technion Israel Institute of Technology, Haifa, Israel, November 2009

Poster prize, 37th Scottish Microscopy Group Symposium, University of Glasgow, UK, November 2009

British Mycological Society Small Grant, November 2009

James Rennie Bequest, Edinburgh University, March 2010

Royal Microscopical Society Travel Bursary, March 2010

Available online at www.sciencedirect.com
ScienceDirect
Current Opinion in Microbiology

Self-signalling and self-fusion in filamentous fungi

Nick D Read, Alexander Lichius, Jun-ya Shoji and Andrew B Goryachev

The formation of interconnected hyphal networks is central to the organisation and functioning of the filamentous fungal colony. It is brought about by the fusion of specialised hyphae during colony initiation and mature colony development. These hyphae are normally genetically identical, and hence this process is termed hyphal self-fusion. The conidial anastomosis tube (CAT) functions in forming networks of conidial germlings during colony initiation. This hyphal type in *Neurospora crassa* is being used as a model for studies on hyphal self-signalling and self-fusion in filamentous fungi. Extraordinary new insights into the process of self-signalling that occurs during CAT self-fusion have recently been revealed by live-cell imaging of genetically engineered strains of *N. crassa*. A novel form of signalling involving the oscillatory recruitment of signal proteins to CAT tips that are communicating and growing towards each other has been observed. This 'ping-pong' mechanism operates over a very short time scale and comparisons with non-self-signalling during yeast cell mating indicate that this mechanism probably does not involve transcriptional regulation. It is proposed that this mechanism has evolved to increase the efficiency of fusion between genetically identical cells that are non-motile.

Address
Institute of Cell Biology, University of Edinburgh, Edinburgh EH9 3JH, United Kingdom

Corresponding author: Read, Nick D (Nick.Read@ed.ac.uk)

Current Opinion in Microbiology 2009, **12**:608–615

This review comes from a themed issue on
Growth and development: eukaryotes
Edited by Judith Berman

Available online 26th October 2009

1369-5274/$ – see front matter

DOI 10.1016/j.mib.2009.09.008

Introduction

Hyphal self-fusion is a defining feature of the lifestyle of most filamentous fungi because the majority form a colony composed of a supracellular network of genetically identical hyphae interconnected by prolific hyphal 'self-fusion' (Figures 1 and 2). This interconnected state allows the fungal colony to operate as a coordinated individual and to regulate its overall homeostasis by the interchange of nutrients, water, signalling molecules, nuclei and other organelles [1,2,3•]. The only group of 'filamentous fungi' that has not been reported to undergo vegetative cell fusion are yeasts which can undergo filamentous growth (e.g. *Candida albicans* and *Ashbya gossypii*). Interestingly, even the oomycetes, which are not true fungi but members of the Kingdom Stramenopila with a filamentous lifestyle, also undergo hyphal self-fusion. Although hyphal fusion has been studied in a wide range of different fungi, most recent work has focused on the fungal model *Neurospora crassa* [3•].

Self-fusion is brought about by specialised hyphae at two stages of colony development

During colony establishment specialised hyphae, which are distinct from germ tubes, are involved in fusion. The most studied hyphae of this type are those formed from conidia and conidial germ tubes, and which have been termed *conidial anastomosis tubes* (CATs) [3•,4,5•,6]. CAT fusion creates an interconnected germling network during the initiation of colony development (Figure 1a–c). At later stages in the mature colony a different but related process of self-fusion occurs behind the peripheral zone of leading hyphae involved in colony extension. In this subperipheral region, specialised *fusion hyphae* arise as branches from established hyphae and these branches grow towards each other and fuse (Figure 1d,e).

CAT fusion provides a model for studying self-signalling and self-fusion

The CAT system in *N. crassa* provides a simple, experimentally amenable and genetically tractable system to study self-signalling and self-fusion in filamentous fungi [3•]. The whole process of CAT fusion can be analysed within six hours, which makes mutant screening, live-cell imaging and physiological experiments very easy to perform. CAT fusion can be divided into a continuum of events: CAT induction, CAT chemoattraction, cell–cell adhesion, cell wall remodelling/degradation, plasma membrane merger and the achievement of cytoplasmic continuity between CATs [3•] (Figure 2). Each of these processes is being analysed in detail [3•,5•,6,7,8••].

Currently the most exciting research on self-fusion is on understanding the mechanism of self-signalling. In order to orchestrate the whole process of CAT fusion, exquisite spatio-temporal coordination of signalling is necessary. However, there is an essential requirement for this mechanism of self-signalling, resulting in mutual chemotropism of CATs towards each other, to work: the two genetically identical CATs must generate physiological and functional differences between themselves. Presently we do not know what self-signalling ligands are

Figure 1

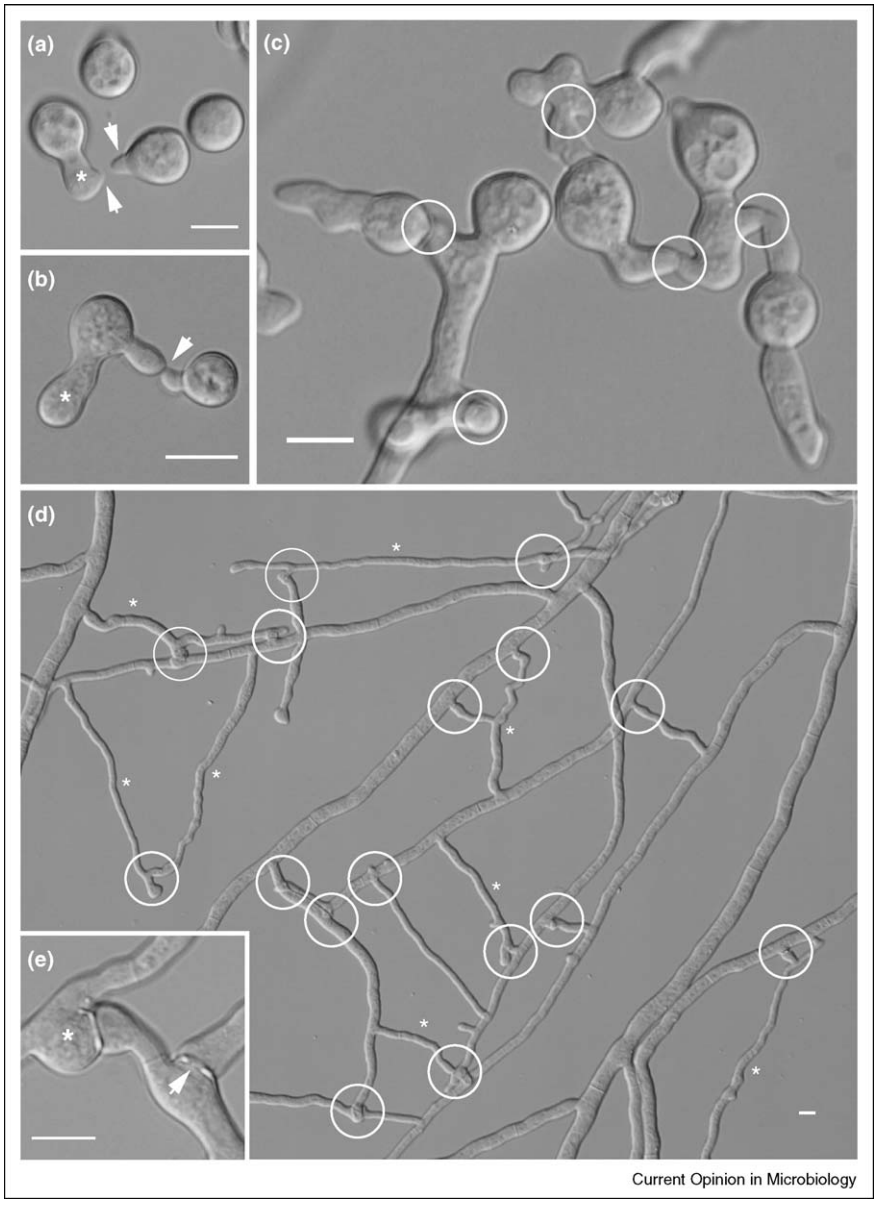

Self-fusion in *Neurospora crassa* occurs during early and late stages of colony development. **(a)** After an initial phase of isotropic expansion conidia of *N. crassa* polarise leading to the outgrowth of germ tubes (asterisk) and conidial anastomosis tubes (CATs) that can arise directly from conidia or from germ tubes (arrowheads). In this situation, the tip of the right hand CAT seems to have induced the formation of the CAT on the germ tube. **(b)** CATs chemotropically attract and become attached to each other (arrowhead indicates site of contact). Upon contact, tip growth arrests and a fusion pore is formed. **(c)** Each cell can interact with several neighbouring cells, thereby creating an interconnected germling network (CAT connections are circled). **(d)** In the subperipheral region of the mature colony (i.e. about 1–2 cm behind the leading edge of the mycelium) specialised fusion hyphae (marked with asterisks) fuse with other hyphae to establish a colony network (fusion connections circled) in a process very similar to CAT fusion. **(e)** Detail of hyphal fusion connections showing isotropic swelling upon contact (asterisk) and a fusion pore (arrowhead). Scale bars = 10 μm.

involved in CAT induction and chemoattraction, but it is likely that they are the same molecule [3•]. Furthermore, the receptor of this self-signalling molecule has not been identified and thus at this stage it remains an open question whether it is located in the plasma membrane, an internal organelle membrane or the cytoplasm.

CAT induction involves MAP kinase signalling, HAM-2 and SO

CAT induction probably involves an extracellular CAT inducer produced by ungerminated conidia [3•,5•] or from the tips of other CATs in the vicinity (Figure 1a). CAT induction involves the NRC-1/MEK-2/MAK-2 mitogen-

Figure 2

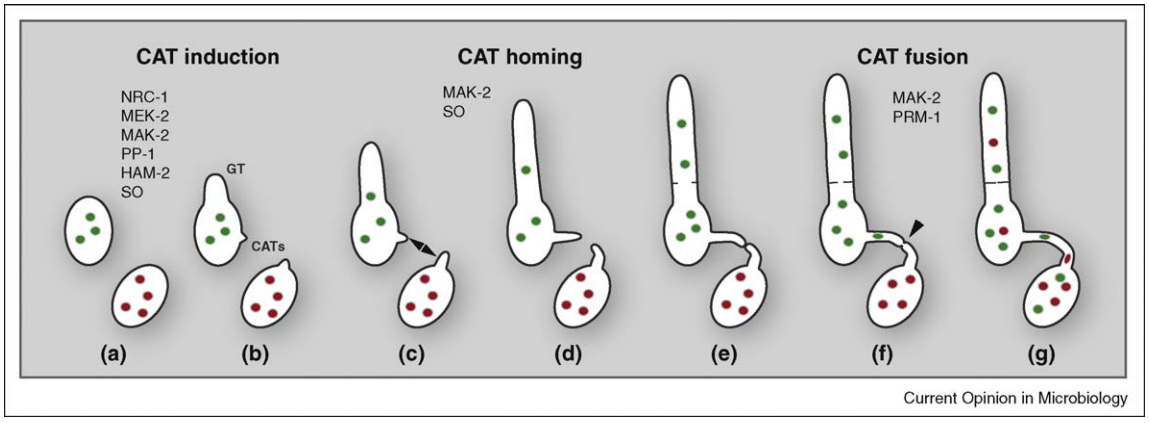

CAT-mediated cell–cell fusion in *Neurospora crassa* and proteins involved. The three major phases of CAT-mediated cell–cell fusion are CAT induction, CAT homing and CAT fusion, and progress through a subset of consecutive stages: **(a)** Ungerminated conidia contain on average three to six nuclei (shown here in green and red to indicate their origin from different but genetically identical germlings), and initially grow exclusively by isotropic expansion. **(b)** Cell polarisation leads to the outgrowth of a germ tube (GT) and conidial anastomosis tubes (CATs). Germ tubes tend to avoid each other and are unable to fuse. **(c)** Genetically identical cells communicate by releasing an unknown chemoattractant from their tips which is perceived by opposing CAT tips (arrowheads). **(d)** Orientation along this chemoattractant gradient results in CATs growing towards each other to establish cell wall contact. **(e)** Upon contact, tip growth arrests and CATs adhere to each other, and this most likely involves adhesive secretion and the buildup of new cell wall material around the contact site in order to prevent leakage during subsequent pore formation. **(f)** Fusion pore formation (arrowhead) includes localised cell wall remodelling/degradation and plasma membrane merger. **(g)** Upon establishment of cytoplasmic continuity, organelles, including nuclei, become mixed between fused germlings. Signalling and structural molecules involved at different stages of the process are indicated (see text for details).

activated protein (MAP) kinase pathway and the transcription factor PP-1 [3•,6,9]. Orthologues of these proteins are components of the pheromone response pathway in budding yeast (Figure 3). Phosphorylation of the MAP kinase MAK-2 was found to increase during the period when CAT induction is most prolific [9]. CAT induction also involves a putative transmembrane protein called HAM-2 [10], which is an orthologue of the yeast Far11 [11], and involves a filamentous ascomycete-specific WW domain protein called SO. In contrast to *mak-2*, *nrc-1*, *pp-1* and *ham-2* mutants which all lack CATs [3•], mutants defective in *so* still form CATs but not as efficiently as the wild type [7].

CAT chemoattraction is regulated by a novel 'ping-pong' signalling mechanism involving MAK-2 and SO

CATs exhibit marked positive chemotropism towards each other. This has been most unambiguously demonstrated using optical (laser) tweezers to micromanipulate CATs which, after having their relative positions changed, readjusted their growth direction to make contact and fuse at their tips [5•,7,12]. These results provide compelling evidence for a diffusible chemoattractant released from CAT tips and for a chemoattractant receptor located at CAT tips.

If the assumption is correct that the CAT inducer and chemoattractant are the same molecule, then the findings that conidia of *mak-2*, *nrc-1*, *ham-2* and *so* mutants fail to attract wild type CATs suggest that the proteins encoded by these genes are involved in either the chemoattractant release or chemoattractant response pathways [3•]. Recent results have provided much stronger evidence for MAK-2 and SO being involved in signalling during CAT chemoattraction [8••]. Previous evidence had shown that a Δ*mak-2* mutant lacks CATs [5•] whilst a Δ*so* mutant produced CATs which were unable to undergo chemotropic growth towards other CATs [7]. It is now clear that CATs that are growing towards each other rapidly alternate between two different physiological states that may be associated with alternating signal delivery and response. This mechanism (which we have termed the '*ping-pong mechanism*') involves the rapid, anti-phase, oscillatory recruitment of MAK-2 and SO to CAT tips. It results in the simultaneous localisation of MAK-2 and SO in opposing CAT tips that are homing towards each other. This highly coordinated, oscillatory recruitment of signalling proteins is initiated when CATs are $<15\ \mu m$ apart, the period of the oscillation is 6–12 min, and each of these proteins can be repeatedly recruited to a single CAT tip four to six times during chemotropic growth. The proteins become concentrated in particulate complexes ~ 300 nm in diameter that mostly concentrate in cortical regions closest to their partner cells. Such spatio-temporal coordination of signalling allows genetically identical and developmentally equivalent cells to avoid self-stimulation and coordinate their behaviour to ultimately achieve cell fusion. A prediction resulting from this ping-pong mechanism of

signalling, in which each CAT alternates between being signal sender and signal receiver (Figure 4), is that the unidentified chemoattractant will be released in a pulsatile manner [8••].

Further insights into the functional role of MAK-2 in the ping-pong mechanism have been gained by using a variant of MAK-2 that is sensitive to inhibition by the ATP-competitor 1NM-PP1. This powerful technique [13] has allowed us to provide strong evidence that MAK-2 activity is not required for the recruitment of SO to the opposing tip but is required for its subsequent delocalisation [8••].

The final stages of CAT fusion involve MAK-2 and PRM-1

Upon making contact with each other, CATs cease tip growth and adhere to each other (Figure 2f). This is followed by fusion pore formation that involves localised cell wall remodelling and degradation, and the merging of the plasma membranes of the two CATs (Figure 2g). MAK-2 also seems to play a role in fusion pore formation [8••] and the plasma membrane protein, PRM-1 is involved in membrane merger [14]. With the development of a fusion pore, cytoplasmic continuity is achieved between the two CATs and organelles, including nuclei, interchange between the two germlings.

Other components have been revealed in studies on hyphal fusion

As indicated earlier, vegetative hyphal fusion also occurs behind the periphery of mature fungal colonies. All CAT fusion mutants so far investigated have also been found to be defective in hyphal fusion in the mature colony which supports the use of CAT fusion as a general model for studies on vegetative hyphal fusion [3•]. However, there are some morphological, developmental and physiological differences between these two processes and therefore one needs to be cautious about extrapolating from one system to the other. Nevertheless, it is tempting to speculate that proteins involved in hyphal fusion in the mature colony, including two additional MAP kinase pathways (the MIK-1/MEK-1/MAK-1 cell wall integrity pathway and the OS-4/OS-5/OS-2 osmosensing pathway), the serine–threonine protein kinase, COT-1 and GPI-anchored proteins [3•,15,16] are also involved in CAT fusion.

What can studies on yeast mating tell us about self-signalling in filamentous fungi?

Budding yeast mating is the most studied example of cell–cell signalling in fungi and results in non-self-fusion. During this process, pheromone binding to cognate G-protein-coupled receptors (GPCRs) leads to phosphorylation of Fus3 MAP kinase [17,18,19••] (Figure 3). Phosphorylated Fus3 arrests cells in G1 phase, promotes actin nucleation and polymerisation leading to polarised outgrowth of mating projections, and also induces expression of mating-related proteins that are involved in the formation of mating projections and cell–cell fusion. Once mating projections from two cells of opposite mating types have physically made contact, their cell walls become attached via GPI-anchored agglutinin proteins. Build up of new cell wall material around the contact site stabilises attachment and prevents leakage during subsequent fusion steps. Cell wall remodelling and local degradation of their intervening cell walls form a pore that allows the merging of plasma membranes, a process mediated by the plasma membrane protein Prm1 [19••]. As described in the previous sections, hyphal fusion in *N. crassa* also involves MAP kinase signalling and a PRM-1 protein. This indicates that in spite of their different physiological roles, molecular mechanisms underlying mating cell fusion in yeast and vegetative cell fusion in *Neurospora* are highly conserved. However, the unknown upstream signal transduction components involved in *Neurospora* self-signalling seem to be significantly different from those in budding yeast because they do not involve sex pheromone–GPCR signalling [3•] (Figure 3).

Somewhat analogous to the oscillatory recruitment of MAK-2 during CAT fusion, Fus3 exhibits oscillatory phosphorylation, and thus activation, during yeast mating [20]. Active Fus3 also preferentially localises to mating projection tips [21,22] but oscillatory recruitment of Fus3 to these tips has not been reported. However, a key difference in the oscillatory MAP kinase behaviour of yeast compared with that in *Neurospora* is the period of MAP kinase oscillation/activity. Whereas the oscillatory recruitment of MAK-2 in *Neurospora* has a period of 6–12 min [8••], the oscillatory phosphorylation of Fus3 in yeast has a period of ~150 min. This much longer period of oscillation in yeast is achieved by transcriptional negative feedback of Fus3 mediated by Sst2 (which regulates G-protein signalling) and the Fus3 phosphatase Msg5 whose expression is upregulated by active Fus3 [20]. In addition, non-transcriptional negative feedback regulates the active Fus3 level to fine-tune the pheromone signalling during yeast mating. This feedback regulation is mediated by the inhibition of MAP kinase scaffold recruitment by active Fus3, and achieves an initial increase and a subsequent decrease to a plateau in the active Fus3 level within 5–7 min [23], a timescale similar to that of the MAK-2 oscillation period.

Other examples of biochemical oscillations mediated by transcriptional negative feedback have been reported to have periods greater than 90 min [24,25], whereas oscillations involving non-transcriptional negative feedback tend to have much shorter periods of ~10 min [26,23]. Thus, the oscillatory recruitment of MAK-2 is most likely achieved by negative feedback regulation that involves protein–protein interaction but not transcription (Figure 3).

Figure 3

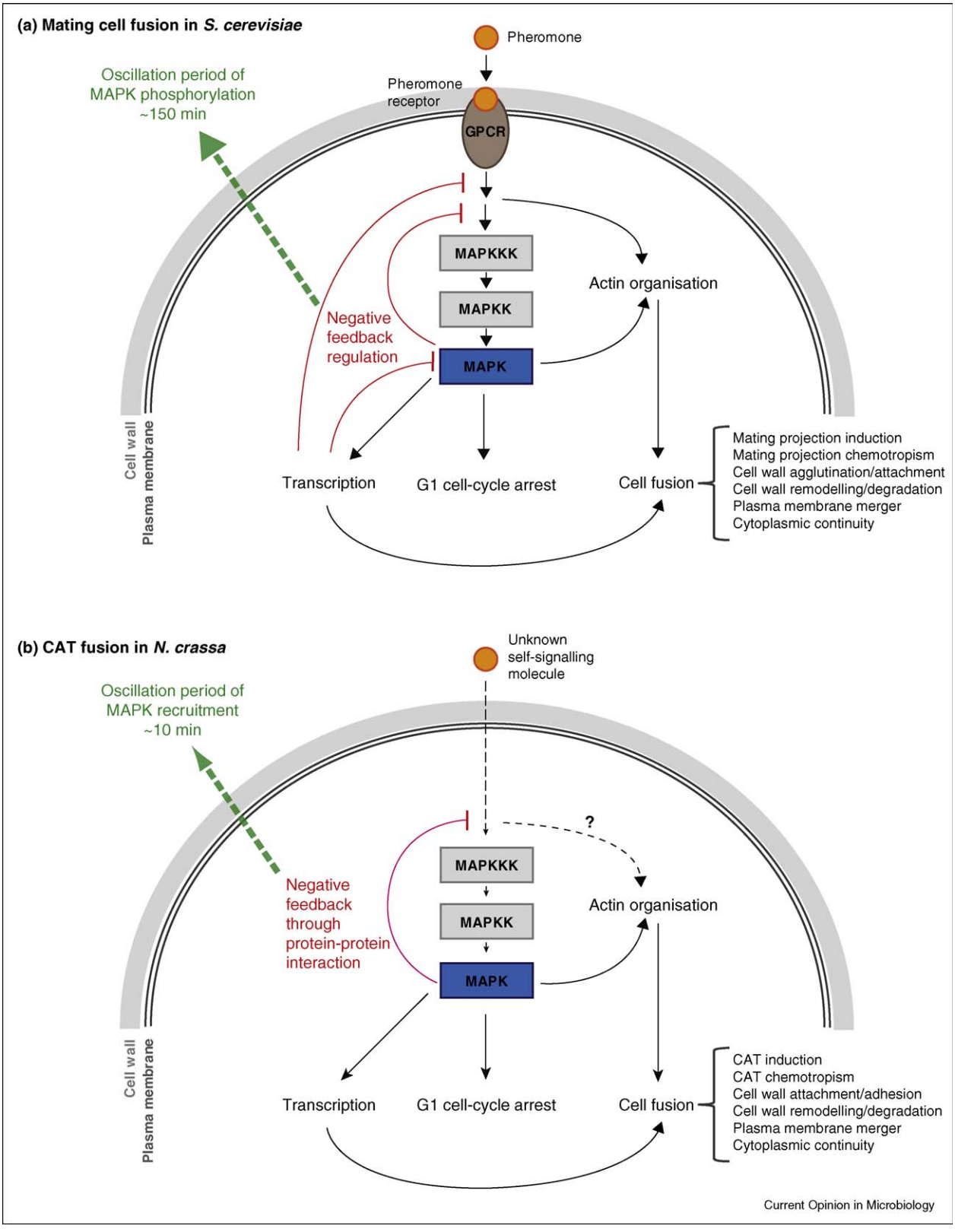

Comparison of non-self-signalling during mating in *Saccharomyces cerevisiae* and self-signalling during CAT fusion in *Neurospora*. **(a)** Pheromone signalling in budding yeast. Pheromone binding to cognate G-protein-coupled receptors (GPCRs; Ste2 and Ste3) leads to activation of the MAP kinase

Figure 4

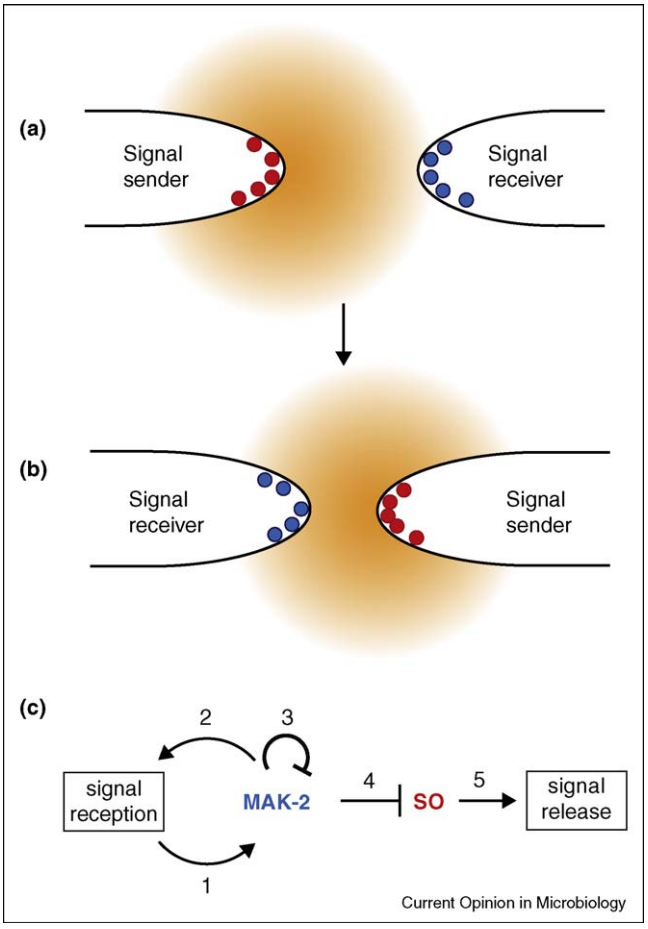

Ping-pong mechanism of self-signalling during CAT chemoattraction. **(a)** In the first half-period of the periodic signalling, the CAT tip on the left releases the chemoattractant signal while the one on the right responds to the signal by adjusting its growth direction along the gradient of the signalling molecule. **(b)** In the second half-period the roles reverse. **(c)** Proposed mechanism of intracellular signalling: (1) a chemoattractant–receptor complex induces local recruitment and activation of MAK-2; (2) a hypothetical positive feedback inherent in MAP kinase modules [38,39] amplifies the received signal; (3) as its local concentration increases, MAK-2-p2 (MAK-2 activated by double phosphorylation) downregulates itself by inducing disassembly of the MAP kinase protein complex through phosphorylation of its upstream components [40,39]; (4) the resulting decrease in MAK-2-p2 derepresses the accumulation of SO and leads to the formation of SO-containing protein complexes at the CAT tip; and (5) SO-stimulated chemoattractant release occurs. As the other CAT tip responds to the released chemoattractant, the sequence (1)–(5) will be repeated until the two tips physically meet [8••].

During yeast mating, negative feedback regulation of the Fus3 MAP kinase pathway is essential for the formation of multiple mating projections if the first projection fails to fuse with a mating projection from another cell [20,27••]. This suggests that downregulation of Fus3 activity is crucial for cells to respond to new pheromone stimulation. In a similar manner, downregulation of the signalling cascade involved in CAT chemoattraction may be important for MAK-2 to be dispersed from CAT tips allowing CATs to respond to the chemoattractant secreted by the opposing cell again, and thus undergo repeated ping-pong self-signalling (Figure 4).

Relationship between self-signalling and self-fusion in fungi and other organisms

Chemoattraction between genetically identical cells, often followed by cell–cell fusion, is widely present in eukaryotes from amoebae to humans [19••,28•]. Three contrasting examples in other organisms that provide interesting comparisons with fungal self-signalling and self-fusion are, where there is, first, chemoattraction without cell fusion (e.g. *Dictyostelium*); second, chemoattraction with fusion between developmentally different cells (e.g. myoblasts); and third, chemoattraction with fusion between developmentally similar cells (e.g. macrophages).

A dramatic example of self-signalling at the cell population level, which does not lead to cell fusion, is displayed by the slime mould *Dictyostelium discoideum*. In response to starvation, *Dictyostelium* unicellular amoebae initiate the pulsatile release of cAMP and follow its gradient to form large cell aggregates that eventually differentiate into multicellular fruiting bodies [29]. In contrast to chemoattraction between two CATs in *Neurospora*, self-signalling in *Dictyostelium* amoebae is a long-range phenomenon that involves thousands of cells. Thus periodic signalling in *Dictyostelium* during chemoattraction is cell-autonomous unlike in *Neurospora* where the periodic response is induced by the presence of another CAT [8••]. Moreover, cAMP signalling in *Dictyostelium* results in an in-phase synchronisation of nearby cells while the oscillatory recruitment of MAK-2 (or SO) to homing CAT tips of *Neurospora* are always out-of-phase in the opposing CAT tips by half a period as necessitated by the ping-pong mechanism of self-signalling (see Figure 4).

(Figure 3 Legend Continued) cascade (MAPKKK; Ste11, MAPKK; Ste7, MAPK; Fus3). Activated Fus3 causes G1 cell-cycle arrest, and promotes actin nucleation and polymerisation to form mating projections. Through activation of the Ste12 transcription factor, Fus3 also induces expression of mating-related proteins which are required for mating projection formation, attachment between two cells of opposite mating types and ultimately cell–cell fusion. The signalling pathway also involves negative feedback loops (red lines) consisting of transcriptional and non-transcriptional feedback regulation, which are crucial for cells to optimally respond to the pheromone stimulus. The transcriptional negative feedback loop leads to oscillatory phosphorylation of Fus3 with a period of ~150 min. **(b)** Signalling during CAT fusion in *Neurospora*. An unidentified chemoattractant is recognised by an unknown receptor(s), and activates the MAP kinase cascade (MAPKKK = NRC-1; MAPKK = MEK-2; MAPK = MAK-2). Downstream events in CAT fusion, which are probably regulated by MAK-2, seem to be similar to those of yeast mating, and involve G1 cell-cycle arrest, actin organisation, cell wall attachment and cell fusion. Somewhat analogous to the oscillatory phosphorylation of Fus3, MAK-2 shows oscillatory recruitment to CAT tips. A key difference to signalling during yeast mating is the period of the MAK-2 oscillation which is markedly shorter (~10 min) than that of Fus3, suggesting a distinct regulatory mechanism for the signalling pathway which does not involve transcriptional feedback loops (see text for details).

One of the most intriguing phenomena involving chemoattraction between developmentally different cells is the fusion of stem cells with differentiated tissue cells which may potentially result in the reversal of cellular senescence and tissue regeneration [30]. Fusion of muscle progenitor cells (myoblasts) during muscle development and regeneration is perhaps the best-characterised example in this class. In *Drosophila*, fusion is initiated by founder cells that do not fuse with each other but instead attract and fuse with undifferentiated fusion-competent myoblasts [31]. This initial fusion event results in a nascent myotube that subsequently grows by 2–25 successive fusion events, the number of which is strictly developmentally regulated. Nascent mammalian myotubes, formed by the initial fusion of several differentiated myoblasts, subsequently grow by releasing cytokine interleukin-4 (IL-4) which chemoattracts more undifferentiated myoblasts with which they fuse [32]. Thus, in contrast to *Neurospora*, both signalling and fusion during muscle development are asymmetric and unilateral. However, all fusion events during myotube elongation are strictly pair-wise and require polarised 'tip-to-tip' attachment of fusing cells, which is a feature in common with hyphal self-fusion.

Perhaps the best-characterised example of self-fusion among developmentally similar cells is the fusion of mammalian macrophages. Uninucleate, macrophages fuse occasionally to form osteoclasts and giant cells. Interestingly, prostaglandins and IL-4, which mediate activation and chemoattraction of myoblasts, are also involved in macrophage fusion that results in the differentiation of osteoclasts and giant cells. Other cytokines and growth factors, such as RANKL and M-CSF, have also been reported to regulate the complex process of macrophage fusion and differentiation [33]. RANKL induces the expression of the dendritic cell-specific transmembrane protein DC-STAMP [34] that is crucial for macrophage fusion during multinucleate osteoclast formation [35]. Interestingly, expression of DC-STAMP in one of the interacting macrophages is sufficient for fusion to occur [35], suggesting that two fusing macrophages are in different physiological states. One cell may take the role of fusion-competent 'founder' cell and expresses DC-STAMP, whilst the other may act as a 'follower' cell that expresses a so far unknown DC-STAMP ligand [36,37]. Thus it seems that macrophages 'differentiate' into founder and follower cells (equivalent to signal sender and receiver cells) to avoid self-stimulation, whereas in CAT chemoattraction two interacting cells rapidly alternate between two physiological states to achieve this. These different strategies to achieve different physiological states in a population of genetically identical cells may be attributed to macrophages being motile and *Neurospora* conidia being non-motile. Thus macrophages are capable of exhibiting migratory movement to a fusion partner [37] whilst sessile conidia depend on being close enough to a potential fusion partner in order to bridge the distance by CAT growth and fusion. The ability to alternate between being a signal sender and receiver allows any fusion-competent cell to fuse with any other fusion-competent cell of similar genetic background in its vicinity. Therefore, the ping-pong mechanism of signalling might function to increase the efficiency of fusion between immobile cells.

Conclusions

Much of the molecular machinery involved in chemotropic growth, cell adhesion and cell fusion during hyphal self-fusion seems to be shared with that involved in non-self-fusion between mating yeast cells. Key differences between these processes appear to lie in the mechanisms of signal perception and regulation in order to ensure cell–cell recognition ultimately leading to cell–cell fusion. It may also have evolved to increase the efficacy of fusion between genetically identical, non-motile cells. The intriguing ping-pong signalling so far seems to be a unique and sophisticated mechanism of self-signalling which allows two genetically identical cells to be in different physiological states. Important challenges for achieving a better understanding of fungal self-signalling in the future will be to identify: firstly, the CAT inducer/chemoattractant and its receptor, secondly, components which act upstream of MAP kinase signalling, thirdly, additional components of the ping-pong mechanism and lastly, the regulatory networks involved in the different stages of cell fusion.

Acknowledgement

This work was supported by funding from the Biotechnological and Biological Sciences Research Council (grant # BB/E010741/1) to NDR.

References and recommended reading

Papers of particular interest, published within the period of review, have been highlighted as:

- • of special interest
- •• of outstanding interest

1. Fricker MD, Boddy L, Bebber D: **Network organisation of filamentous fungi**. In *Biology of the Fungal Cell.* Edited by Howard RJ, Gow NAR. Berlin: Springer-Verlag; 2007:309-330.

2. Read ND: **Environmental sensing and the filamentous fungal lifestyle**. In *Fungi and their Environment.* Edited by Gadd GM, Watkinson SC, Dyer PS. Cambridge, UK: Cambridge University Press; 2007:38-57.

3. • Read ND, Fleißner A, Roca MG, Glass NL: **Hyphal fusion**. In *Cellular and Molecular Biology of Filamentous Fungi.* Edited by Borkovich KA, Ebolle D. Washington DC: American Society of Microbiology; 2010:260-273.
This chapter provides the most comprehensive and up-to-date review of hyphal fusion during vegetative and sexual development in filamentous fungi.

4. Roca MG, Davide LC, Mendes-Costa MC, Wheals A: **Conidial anastomosis tubes in *Colletotrichum***. *Fung Genet Biol* 2003, **40**:138-145.

5. • Roca MG, Arlt J, Jeffree CE, Read ND: **Cell biology of conidial anastomosis tubes in *Neurospora crassa***. *Eukaryot Cell* 2005, **4**:911-919.
This paper was the first study to demonstrate in *N. crassa* that conidial anastomosis tubes are morphologically and physiologically distinct from germ tubes and under separate genetic control.

6. Roca MG, Read ND, Wheals AE: **Conidial anastomosis tubes in filamentous fungi**. *FEMS Microbiol Lett* 2005, **249**:191-198.

7. Fleißner A, Sarkar S, Jacobson DJ, Roca MG, Read ND, Glass NL: **The *so* locus is required for vegetative cell fusion and postfertilization events in *Neurospora crassa***. *Eukaryot Cell* 2005, **4**:920-930.

8. •• Fleißner A, Leeder AC, Roca M.G, Read ND, Glass NL: **Oscillatory recruitment of signaling proteins to cell tips promotes coordinated behavior during cell fusion in *Neurospora crassa***. *Proc Natl Acad Sci USA* (in press).
This paper shows the oscillatory recruitment of the MAK-2 and SO proteins during CAT chemoattraction for the first time.

9. Pandey A, Roca MG, Read ND, Glass NL: **Role of a mitogen-activated protein kinase pathway during conidial germination and hyphal fusion in *Neurospora crassa***. *Eukaryot Cell* 2004, **3**:348-358.

10. Xiang Q, Rasmussen CG, Glass NL: **The *ham-2* Locus, encoding a putative transmembrane protein, is required for hyphal fusion in *Neurospora crassa***. *Genetics* 2002, **160**:169-180.

11. Kemp HA, Sprague GF: **Far3 and five interacting proteins prevent premature recovery from pheromone arrest in the budding yeast *Saccharomyces cerevisiae***. *Mol Cell Biol* 2003, **23**:1750-1763.

12. Wright GD, Arlt J, Poon WCK, Read ND: **Optical tweezer micromanipulation of filamentous fungi**. *Fung Genet Biol* 2007, **44**:1-13.

13. Bishop AC, Ubersax JA, Petsch DT, Matheos DP, Gray NS, Blethrow J, Shimizu E, Tsien JZ, Schultz PG, Rose MD *et al.*: **A chemical switch for inhibitor-sensitive alleles of any protein kinase**. *Nature* 2000, **407**:395-401.

14. Fleißner A, Diamond S, Glass Nl: **The *Saccharomyces cerevisiae PRM1* homolog in *Neurospora crassa* is involved in vegetative and sexual cell fusion events but also has postfertilization functions**. *Genetics* 2009, **181**:497-510.

15. Bowman SM, Piwowar A, Al Dabbous M, Vierula J, Free SJ: **Mutational analysis of the glycosylphosphatidylinositol (GPI) anchor pathway demonstrates that GPI-anchored proteins are required for cell wall biogenesis and normal hyphal growth in *Neurospora crassa***. *Eukaryot Cell* 2006, **5**:587-600.

16. Maerz S, Ziv C, Vogt N, Helmstaedt K, Cohen N, Gorovits R, Yarden O, Seiler S: **The nuclear Dbf2-related kinase COT1 and the mitogen-activated protein kinases MAK1 and MAK2 genetically interact to regulate filamentous growth, hyphal fusion and sexual development in *Neurospora crassa***. *Genetics* 2008, **179**:1313-1325.

17. Dohlman HG, Thorner JW: **Regulation of G protein-initiated signal transduction in yeast: paradigms and principles**. *Annu Rev Biochem* 2001, **70**:703-754.

18. Qi M, Elion EA: **MAP kinase pathways**. *J Cell Sci* 2005, **118**:3569-3572.

19. •• Chen EH, Grote E, Mohler W, Vignery A: **Cell–cell fusion**. *FEBS Lett* 2007, **581**:2181-2193.
This minireview provides the most recent overview on cell–cell fusion in a variety of eukaryotic model systems, including yeast cell mating, somatic cell and gamete fusion in nematodes, myoblast fusion in mammals and flies, as well as macrophage fusion in mammals. Major players of molecular mechanisms involved in cell–cell signalling and plasma membrane fusion are put into context.

20. Hilioti Z, Sabbagh W, Paliwal S, Bergmann A, Goncalves MD, Bardwell L, Levchenko A: **Oscillatory phosphorylation of yeast Fus3 MAP kinase controls periodic gene expression and morphogenesis**. *Curr Biol* 2008, **18**:1700-1706.

21. Maeder CI, Hink MA, Kinkhabwala A, Mayr R, Bastiaens PI, Knop M: **Spatial regulation of Fus3 MAP kinase activity through a reaction-diffusion mechanism in yeast pheromone signalling**. *Nat Cell Biol* 2007, **9**:1319-1326.

22. Slaughter BD, Schwartz JW, Li R: **Mapping dynamic protein interactions in MAP kinase signaling using live-cell fluorescence fluctuation spectroscopy and imaging**. *Proc Natl Acad Sci U S A* 2007, **104**:20320-20325.

23. Yu RC, Pesce CG, Colman-Lerner A, Lok L, Pincus D, Serra E, Holl M, Benjamin K, Gordon A, Brent R: **Negative feedback that improves information transmission in yeast signalling**. *Nature* 2008, **456**:755-761.

24. Lev Bar-Or R, Maya R, Segel LA, Alon U, Levine AJ, Oren M: **Generation of oscillations by the p53–Mdm2 feedback loop: a theoretical and experimental study**. *Proc Natl Acad Sci U S A* 2000, **97**:11250-11255.

25. Hirata H, Yoshiura S, Ohtsuka T, Bessho Y, Harada T, Yoshikawa K, Kageyama R: **Oscillatory expression of the bHLH factor Hes1 regulated by a negative feedback loop**. *Science* 2002, **298**:840-843.

26. Jacquet M, Renault G, Lallet S, De Mey J, Goldbeter A: **Oscillatory nucleocytoplasmic shuttling of the general stress response transcriptional activators Msn2 and Msn4 in *Saccharomyces cerevisiae***. *J Cell Biol* 2003, **161**:497-505.

27. •• Moore TI, Chou CS, Nie Q, Jeon NL, Yi TM: **Robust spatial sensing of mating pheromone gradients by yeast cells**. *PLoS One* 2008, **3**:e3865.
This paper showed detailed observation of *S. cerevisiae* chemotropic growth in response to the pheromone gradient with different steepness and concentration. This paper, along with [21], also raised insight into how negative feedback regulation on the signalling pathway contributes for better sensing the chemoattractant gradient.

28. • Oren-Suissa M, Podbilewicz B: **Cell fusion during development**. *Trends Cell Biol* 2007, **17**:537-546.
This review focuses on ways to identify fusogens that are proteins or protein complexes that directly mediate fusion of lipid bilayers. In this context, proposed models for viral, intracellular and developmental membrane fusion mechanisms are discussed.

29. Rappel WJ, Loomis WF: **Eukaryotic chemotaxis**. *Wiley Interdiscip Rev: Syst Biol Med* 2009, **1**:141-149.

30. Stolzing A, Hescheler J, Sethe S: **Fusion and regenerative therapies: is immortality really recessive?** *Rejuvenation Res* 2007, **10**:571-586.

31. Richardson BE, Nowak SJ, Baylies MK: **Myoblast fusion in fly and vertebrates: new genes, new processes and new perspectives**. *Traffic* 2008, **9**:1050-1059.

32. Jansen KM, Pavlath GK: **Molecular control of mammalian myoblast fusion**. *Methods Mol Biol* 2008, **475**:115-133.

33. Vignery A: **Macrophage fusion: molecular mechanisms**. *Methods Mol Biol* 2008, **475**:149-161.

34. Yagi M, Ninomiya K, Fujita N, Suzuki T, Iwasaki R, Morita K, Hosogane N, Matsuo K, Toyama Y, Suda T, Miyamoto T: **Induction of DC-STAMP by alternative activation and downstream signaling mechanisms**. *J Bone Miner Res* 2007, **22**:992-1001.

35. Yagi M, Miyamoto T, Sawatani Y, Iwamoto K, Hosogane N, Fujita N, Morita K, Ninomiya K, Suzuki T, Miyamoto K *et al.*: **DC-STAMP is essential for cell–cell fusion in osteoclasts and foreign body giant cells**. *J Exp Med* 2005, **202**:345-351.

36. Vignery A: **Macrophage fusion: the making of osteoclasts and giant cells**. *J Exp Med* 2005, **202**:337-340.

37. Ishii M, Saeki Y: **Osteoclast cell fusion: mechanisms and molecules**. *Mod Rheumatol* 2008, **18**:220-227.

38. Kholodenko BN, Birtwistle MR: **Four-dimensional dynamics of MAPK information-processing systems**. *Wiley Interdiscip Rev: Syst Biol Med* 2009, **1**:28-44.

39. Shin SY, Rath O, Choo SM, Fee F, McFerran B, Kolch W, Cho KH: **Positive- and negative-feedback regulations coordinate the dynamic behavior of the Ras–Raf–MEK–ERK signal transduction pathway**. *J Cell Sci* 2009, **122**:425-435.

40. McKay MM, Ritt DA, Morrison DK: **Signaling dynamics of the KSR1 scaffold complex**. *Proc Natl Acad Sci U S A* 2009, **106**:11022-11027.

EUKARYOTIC CELL, Apr. 2010, p. 547–557 Vol. 9, No. 4
1535-9778/10/$12.00 doi:10.1128/EC.00253-09

F-Actin Dynamics in *Neurospora crassa*▽†

Adokiye Berepiki,[1]§ Alexander Lichius,[1]§ Jun-Ya Shoji,[1] Jens Tilsner,[2] and Nick D. Read[1]*

Fungal Cell Biology Group, Institute of Cell Biology, University of Edinburgh, Rutherford Building, Edinburgh EH9 3JH, United Kingdom,[1] and Scottish Crop Research Institute, Invergowrie, Dundee DD2 5DA, United Kingdom[2]

Received 28 August 2009/Accepted 29 January 2010

This study demonstrates the utility of Lifeact for the investigation of actin dynamics in *Neurospora crassa* and also represents the first report of simultaneous live-cell imaging of the actin and microtubule cytoskeletons in filamentous fungi. Lifeact is a 17-amino-acid peptide derived from the nonessential *Saccharomyces cerevisiae* actin-binding protein Abp140p. Fused to green fluorescent protein (GFP) or red fluorescent protein (TagRFP), Lifeact allowed live-cell imaging of actin patches, cables, and rings in *N. crassa* without interfering with cellular functions. Actin cables and patches localized to sites of active growth during the establishment and maintenance of cell polarity in germ tubes and conidial anastomosis tubes (CATs). Recurrent phases of formation and retrograde movement of complex arrays of actin cables were observed at growing tips of germ tubes and CATs. Two populations of actin patches exhibiting slow and fast movement were distinguished, and rapid (1.2 μm/s) saltatory transport of patches along cables was observed. Actin cables accumulated and subsequently condensed into actin rings associated with septum formation. F-actin organization was markedly different in the tip regions of mature hyphae and in germ tubes. Only mature hyphae displayed a subapical collar of actin patches and a concentration of F-actin within the core of the Spitzenkörper. Coexpression of Lifeact-TagRFP and β-tubulin–GFP revealed distinct but interrelated localization patterns of F-actin and microtubules during the initiation and maintenance of tip growth.

Actins are highly conserved proteins found in all eukaryotes and have an enormous variety of cellular roles. The monomeric form (globular actin, or G-actin) can self-assemble, with the aid of numerous actin-binding proteins (ABPs), into microfilaments (filamentous actin, or F-actin), which, together with microtubules, form the two major components of the fungal cytoskeleton. Numerous pharmacological and genetic studies of fungi have demonstrated crucial roles for F-actin in cell polarity, exocytosis, endocytosis, cytokinesis, and organelle movement (6, 7, 20, 34, 35, 51, 52, 59). Phalloidin staining, immunofluorescent labeling, and fluorescent-protein (FP)-based live-cell imaging have revealed three distinct subpopulations of F-actin-containing structures in fungi: patches, cables, and rings (1, 14, 28, 34, 60, 63, 64). Actin patches are associated with the plasma membrane and represent an accumulation of F-actin around endocytic vesicles (3, 26, 57). Actin cables are bundles of actin filaments stabilized with cross-linking proteins, such as tropomyosins and fimbrin, and are assembled by formins at sites of active growth, where they form tracks for myosin V-dependent polarized secretion and organelle transport (10, 16, 17, 27, 38, 47, 48). Cables, unlike patches, are absolutely required for polarized growth in the budding yeast *Saccharomyces cerevisiae* (34, 38). Contractile actomyosin rings are essential for cytokinesis in budding yeast, whereas in filamentous fungi, actin rings are less well studied but are known to be involved in septum formation (20, 28, 34, 39, 40).

Actin cables and patches have been particularly well studied in budding yeast. However, there are likely to be important differences between F-actin architecture and dynamics in budding yeast and those in filamentous fungi, as budding yeasts display only a short period of polarized growth during bud formation, which is followed by isotropic growth over the bud surface (10). Sustained polarized growth during hyphal morphogenesis is a defining feature of filamentous fungi (21), making them attractive models for studying the roles of the actin cytoskeleton in cell polarization, tip growth, and organelle transport.

In *Neurospora crassa* and other filamentous fungi, disruption of the actin cytoskeleton leads to rapid tip swelling, which indicates perturbation of polarized tip growth, demonstrating a critical role for F-actin in targeted secretion to particular sites on the plasma membrane (7, 22, 29, 56). Immunofluorescence studies of *N. crassa* have shown that F-actin localizes to hyphal tips as "clouds" and "plaques" (7, 54, 59). However, immunolabeling has failed to reveal actin cables in *N. crassa* and offers limited insights into F-actin dynamics. Live-cell imaging of F-actin architecture and dynamics has not been accomplished in *N. crassa*, yet it is expected to yield key insights into cell polarization, tip growth, and intracellular transport.

We took advantage of a recently developed live-cell imaging probe for F-actin called Lifeact (43). Lifeact is a 17-amino-acid peptide derived from the N terminus of the budding yeast actin-binding protein Abp140 (5, 63) and has recently been demonstrated to be a universal live-cell imaging marker for F-actin in eukaryotes (43). Here, we report the successful application of fluorescent Lifeact fusion constructs for live-cell imaging of F-actin in *N. crassa*. We constructed two synthetic genes consisting of Lifeact fused to "synthetic" green fluores-

* Corresponding author. Mailing address: Fungal Cell Biology Group, Institute of Cell Biology, University of Edinburgh, Rutherford Building, Edinburgh EH9 3JH, United Kingdom. Phone: 44-131-650-5335. Fax: 44-131-650-5392. E-mail: Nick.Read@ed.ac.uk.

§ A.B. and A.L. contributed equally to this work.

† Supplemental material for this article may be found at http://ec.asm.org/.

▽ Published ahead of print on 5 February 2010.

cent protein (sGFP) (S65T) (henceforth termed GFP) (12) or red fluorescent protein (TagRFP) (33) and expressed these constructs in various *N. crassa* strains. In all strain backgrounds, fluorescent Lifeact constructs clearly labeled actin patches, cables, and rings and revealed a direct association of F-actin structures with sites of cell polarization and active tip growth. Our results demonstrate the efficacy of Lifeact as a nontoxic live-cell imaging probe in *N. crassa*.

MATERIALS AND METHODS

Strains and culture conditions. The *N. crassa* strains generated during this study were derived from FGSC 4200 (wild type [WT] *mat a*), FGSC 2489 (WT *mat A*), FGSC 9717 (*mat A his-3* Δ*mus-51*::*bar*$^+$), and FGSC N2506 (*mat a* β-*tubulin rid his-3*$^+$::*bml-gfp*) strains obtained from the Fungal Genetics Stock Center (FGSC) (School of Biological Sciences, Kansas City, MO). Five strains were constructed: NCAB1721 (*mat A his-3*$^+$::*Pccg-1-Lifeact-gfp* Δ*mus-51*::*bar*$^+$), NCAB1761 (*mat A his-3*$^+$::*Ptef-1-Lifeact-gfp* Δ*mus-51*::*bar*$^+$), NCAL004 (*mat a Pccg-1-Lifeact-tagrfp*::*bar*$^+$), NCAL005 (*mat A Pccg-1-Lifeact-tagrfp*::*bar*$^+$), and NCAL006 (*mat a* β-*tubulin rid his-3*$^+$::*bml-gfp*; *Pccg-1-Lifeact-tagrfp*::*bar*$^+$). The strains were maintained on Vogel's minimal medium (VMM) with 2% sucrose, and all manipulations were performed according to standard *N. crassa* techniques (13).

Plasmid construction. To visualize Lifeact-GFP in *N. crassa*, we constructed a synthetic gene for integration at the *his-3* locus. To construct the Lifeact-GFP plasmid, we designed the *N. crassa* codon-optimized oligonucleotides 5′-GATC TCTAGAATGGGCGTCGCTGACCTCATCAAGAAGTTCGAGTCCATCT CCAAGGAGGAGTTAATTAACTAG-3′ and 5′-CTAGTTAATTAACTCCT CCTTGGAGATGGACTCGAACTTCTTGATGAGGTCAGCGACGCCCAT TCTAGAGATC-3′, which contained the Lifeact sequence, an XbaI site (underlined) at one end, and a PacI site (underlined) at the other end. After being boiled for 5 min, the oligonucleotides were incubated at room temperature for 30 min to anneal them and then digested with XbaI and PacI and inserted into an XbaI- and PacI-digested GFP expression vector, pCCG-1::C-Gly::GFP (24) (obtained from the FGSC), yielding pAB221.

We found that expression of the Lifeact construct from the *ccg-1* promoter did not allow satisfactory visualization of Lifeact-GFP in mature vegetative hyphae. Therefore, the 0.9-kb upstream regulatory region of the *N. crassa* locus NCU02003 (transcriptional elongation factor 1 homolog, *tef-1*) was amplified by PCR and exchanged for *Pccg-1* in the pAL1 GFP expression vector, yielding pTEFsG-2. Following confirmation that the putative *tef-1* promoter provided GFP expression throughout the *N. crassa* life cycle (data not shown), the *Ptef-1* sequence was amplified from pTEFsG-2 using the primers 5′-ACCGCGGTGG CGGCCGCGATATCCCGTGACCACTGAACTA-3′ and 5′-CGACGCCCAT TCTAGATAACCCGGGGATCCGATAT-3′ and integrated into NotI- and XbaI-digested pAB221 using the In-Fusion PCR cloning kit (Clontech, Mountain View, CA), yielding pAB261.

To facilitate dual-labeling studies, we developed a Lifeact-TagRFP fusion construct. A Lifeact-TagRFP fusion was made from the plasmid pGWB460 (T. Nakagawa, Shimane University, Matsue, Japan, unpublished data), which contains the TagRFP (33) open reading frame. TagRFP was altered by the addition of N- and C-terminal amino acids from GFP, increasing its utility for four-dimensional (4D) live-cell imaging (49). TagRFP-specific codons (in italics) and the Lifeact sequence (underlined) were added by PCR using the oligonucleotides 5′-ATGGGTGTCGCAGATTTGATCAAGAAATTCGAAAGCATCTCAAA GGAAGAAGGCTCG*ATGGTGTCTAAGGGCGAA*GAGCTGATTAAGGA GAACATGCAC-3′ and 5′-*TTACTTGTACAGCTCGTCCATGCCATTAAG*TT TGTGCCCCAGTTTGCTAG-3′. In contrast to the Lifeact-GFP construct, the Lifeact sequence in the Lifeact-TagRFP fusion protein was not codon optimized for *N. crassa*. The Lifeact-TagRFP expression vector pAL3-Lifeact was constructed by amplifying the resulting 821-bp fragment encoding Lifeact-TagRFP using the primers 5′-TTTCCTCGACGGATCCATGGGTGTCGCAGATTTG ATCAAGA-3′ and 5′-ATCGATAAGCTTGATATCTTACTTGTACAGCTCG TCCATGCCA-3′ and integrating the purified PCR product into BamHI- and EcoRV-digested pBARGRG1 (36) using the In-Fusion PCR cloning kit (Clontech). DNA sequencing was carried out on all vectors to confirm in-frame cloning of the fusion constructs. Thus, Lifeact-GFP constructs were expressed under the control of the *ccg-1* or *tef-1* promoter and consisted of the Lifeact sequence fused to GFP at its C terminus via a 10-glycine linker, whereas the Lifeact-TagRFP construct was expressed under the control of the *ccg-1* promoter and consisted of the Lifeact sequence fused to TagRFP at its C terminus via a 2-amino-acid (GS) linker.

Transformation and transformant selection. Transformations were performed as described previously (32). To generate strains expressing Lifeact-GFP, NdeI-digested pAB221 and pAB261 were targeted to the *his-3* locus of strain FGSC 9717 (*mat A his-3* Δ*mus-51*::*bar*$^+$). Lifeact-TagRFP-expressing strains were created by introducing pAL3-Lifeact into strains FGSC 4200 (WT *mat a*), FGSC 2489 (WT *mat A*), and FGSC N2506 (*mat a* β-*tubulin rid his-3*$^+$::*bml-gfp*). Transformants were selected either by recovery of histidine prototrophy or on nitrogen-free VMM containing the Ignite (phosphinothricin) selection marker. Southern blotting using a DIG High Prime DNA Labeling and Detection Starter Kit (Roche Diagnostics, Mannheim, Germany), along with a PCR DIG Probe Synthesis Kit (Roche Diagnostics), was performed to check the genotypes of the transformants (see Fig. S1A in the supplemental material).

Lifeact-GFP and Lifeact-TagRFP expression was examined in multiple transformants using a Nikon SMZ1500 stereomicroscope with a GFP (excitation, 470/40 nm; 505-nm long pass dichroic mirror; emission, 530/40 nm) or RFP (excitation, 545/30 nm; 570-nm long pass dichroic mirror; emission, 620/60 nm) filter set. Intracellular expression patterns were analyzed in at least nine transformants per plasmid construct by wide-field fluorescence microscopy. Transformants exhibiting FP expression were selected for subsequent live-cell imaging studies.

Live-cell imaging. Conidia were collected from 3- to 5-day-old cultures and suspended in VMM. In all experiments, unless stated otherwise, conidia were used at a concentration of 10^6 cells per ml. The cells were incubated in VMM in Lab-Tek 8-well chamber slides (Nalge-Nunc International, Rochester, NY) for 2 to 4 h at 35°C and then imaged. To image mature hyphae, conidia were grown in petri dishes containing VMM solidified with 1.5% agar for 16 to 20 h at 24°C and then prepared for imaging using the "inverted agar block method" (23). Imaging was carried out at room temperature. The images were collected using a DeltaVision microscope (Applied Precision, Issaquah, WA) consisting of an Olympus IX70 base, an Olympus 100×/1.4-numerical-aperture (NA) Plan-Apo objective, a 75-W HBO illuminator; a Chroma Sedat Quad ET filter set (for GFP, excitation = 490/20 nm, emission = 528/38 nm; for RFP, excitation = 545/30 nm, emission = 610/75 nm; for FM4-64, excitation = 490/20 nm, emission = 685/40 nm; for calcofluor white, excitation = 360/40 nm, emission = 457/50 nm; Chroma Technology Corp., Rockingham, VT), a CoolSnap HQ charge-coupled-device (CCD) camera (Photometrics, Tuscon, AZ), and SoftWorx software (Applied Precision) for image acquisition. Exposure times ranged from 200 to 400 ms. To acquire 3D (x, y, z) images, 30 to 40 optical sections were obtained at 0.2-μm steps. For 4D imaging (x, y, z, and t), 10 to 15 optical sections were obtained at 0.4- or 0.5-μm steps and 30- to 120-s intervals. The images were processed through 10 iterative deconvolutions using SoftWorx image analysis software. To image actin patch dynamics, time-lapse sequences were captured in one focal plane using 2 × 2 camera binning at 200- to 300-ms intervals. Extension rates, patch velocities, and lifetimes were measured manually using the track object function of the Image Pro-Plus analysis software (version 7.0; Media Cybernetics, Bethesda, MD). The (x, y) coordinates of individual patches or hyphal tips were recorded, and the velocities of objects were calculated as the sum of the distance between points divided by time. The velocities of individual patches were averaged to obtain the mean velocity. Patch lifetimes were determined by multiplying the frame interval by the number of frames in which an individual patch was visible before it moved out of the focal plane. The size of the F-actin-depleted zone was determined using the measurement option of Image Pro-Plus. Projections and further processing steps were carried out with ImageJ software (http://rsbweb.nih.gov/ij/). Some single-plane time-lapse (x, y, t) sequences were processed with an "unsharp mask" filter to aid visualization of fine cytoskeletal details.

Fluorescent staining. Mature hyphae and germlings were labeled for 30 min with either 2 μM FM4-64 (prepared from 200 μM stock in dimethyl sulfoxide [DMSO]; Molecular Probes, Eugene, OR), which stains the plasma membrane and organelle membranes (18, 23), or 0.1 μg/ml calcofluor white (prepared from 1 mg/ml stock in ethanol; Sigma, Welwyn Garden City, United Kingdom), which stains cell walls (23).

Latrunculin A treatment. Latrunculin A (Lat A) (Invitrogen, Carlsbad, CA) was stored as a 1 mM stock in DMSO. For Lat A treatment of growing cells, 25 μl of growth medium was removed from the observation chamber and replaced with 25 μl of medium supplemented with an appropriate volume of the Lat A stock solution or DMSO. Lat A was used at a final concentration of 10 μM. To quantify the effect of Lat A on the presence of patches and cables, cells were incubated in Lab-Tek 8-well chamber slides for 4 h in 250 μl of VMM at a concentration of 10^6 cells/ml. The effect of Lat A treatment was monitored with time-lapse microscopy 1 min after its addition. Cells were scored for the presence

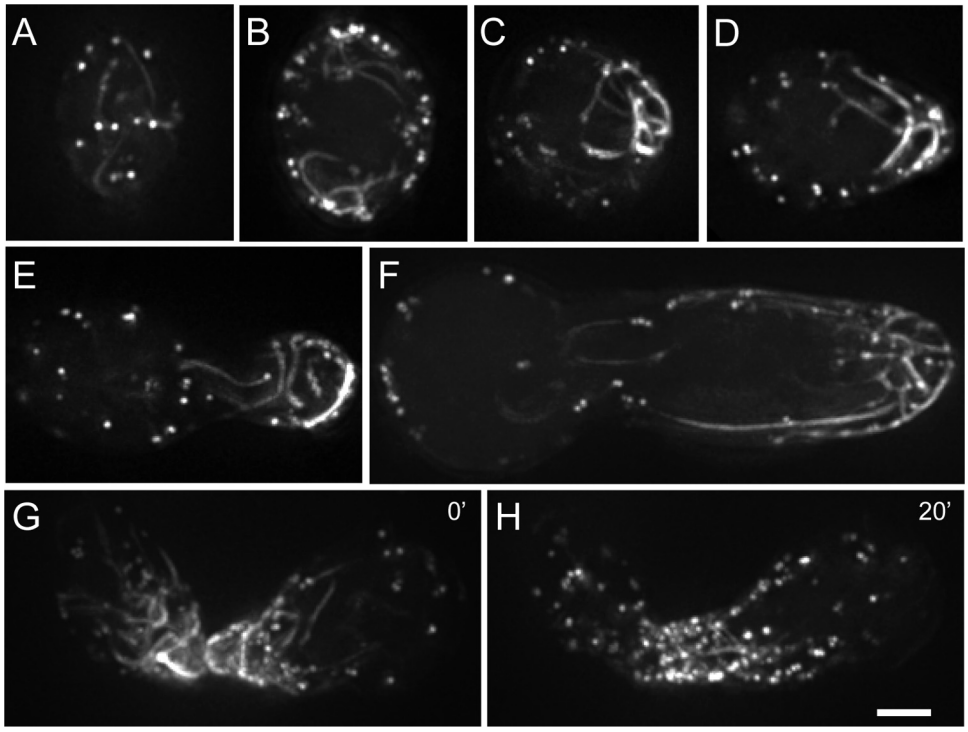

FIG. 1. Lifeact-GFP localization during germ tube emergence and CAT-mediated cell fusion. Maximum-intensity projections of 5 to 10 planes of different conidia at various stages of development are shown. (A and B) Maximum-intensity projections of 6 optical planes from the top (A) and middle (B) of an ungerminated spore. Actin patches and cables are mostly associated with the cell cortex. (C and D) A meshwork-like actin array always marks the site of germ tube emergence. (E, F, and G) Actin arrays persist at sites of active growth. (F) Long actin cables extend longitudinally through the germ tube. (G and H) Maximum-intensity projections of a time-lapse sequence showing enrichment of cables and patches at CAT tips before cell fusion (G) and loss of actin cables after fusion (H). Bar, 2 μm.

or absence of patches or cables at 1-min intervals by visual inspection of time-lapse sequences.

RESULTS

Lifeact-GFP and Lifeact-TagRFP label F-actin in *N. crassa*. We visualized F-actin in *N. crassa* by expressing Lifeact-GFP or Lifeact-TagRFP under the control of the *ccg-1* or *tef-1* promoter. All clones chosen for live-cell imaging studies grew, germinated, and fused at wild-type rates, were healthy and conidiated normally at 25°C and 35°C, and possessed colony morphologies similar to that of the wild type (see Fig. S1 in the supplemental material). Lifeact-TagRFP gave a pattern of actin localization identical to that of Lifeact-GFP and had comparable brightness and photostability. Henceforth, we refer to Lifeact-GFP or Lifeact-TagRFP interchangeably as Lifeact-FP.

To image Lifeact-FP, we used wide-field fluorescence microscopy combined with image deconvolution. Lifeact-FP gave robust labeling of actin patches, cables, and rings (Fig. 1; also see Fig. 5) and displayed a localization pattern of F-actin consistent with previous studies of *N. crassa* using immunofluorescent labeling (7, 22, 54, 59). Latrunculin A treatment, which disrupts the actin cytoskeleton, confirmed F-actin labeling (see below).

F-actin localizes in complex arrays during the establishment and maintenance of polarized growth. Three distinct phases are associated with conidial germination leading to germ tube formation: (i) hydration and isotropic growth, (ii) germ tube emergence, and (iii) germ tube extension (4, 21). During isotropic growth, actin cables were unpolarized and mostly associated with the cell cortex (Fig. 1A and B). Similarly, actin patches were found at the cell periphery but showed no accumulation at particular sites in ungerminated conidia. Prior to germ tube emergence, we observed a strong accumulation of fluorescence that formed a polar cap marking the site of germination (Fig. 1C). Individual cables in this highly dynamic array of F-actin were generally not oriented along the future longitudinal axis but rather followed the curvature of the polarizing cell (Fig. 1C and D). In some instances, this cap disappeared and reformed at a different site on the cell cortex, suggesting that the axis of polarity had not been stably established.

In growing germ tubes, actin cables were mostly found at the cell cortex and organized longitudinally throughout the length of the cell, terminating in a dense meshwork-like array at growing tips (Fig. 1E and F). We commonly observed long (5- to 10-μm) actin cables in germ tubes (Fig. 1F). Occasionally, cables that spanned the entire length of a 25-μm germ tube were visible (see Fig. S2 in the supplemental material). Cortical actin patches were present along the whole length of germ tubes, although, as with cables, they were concentrated at sites of active growth. These observations indicate a close association of actin patches and actin cable arrays with active tip growth. We often observed colocalization of patches and ca-

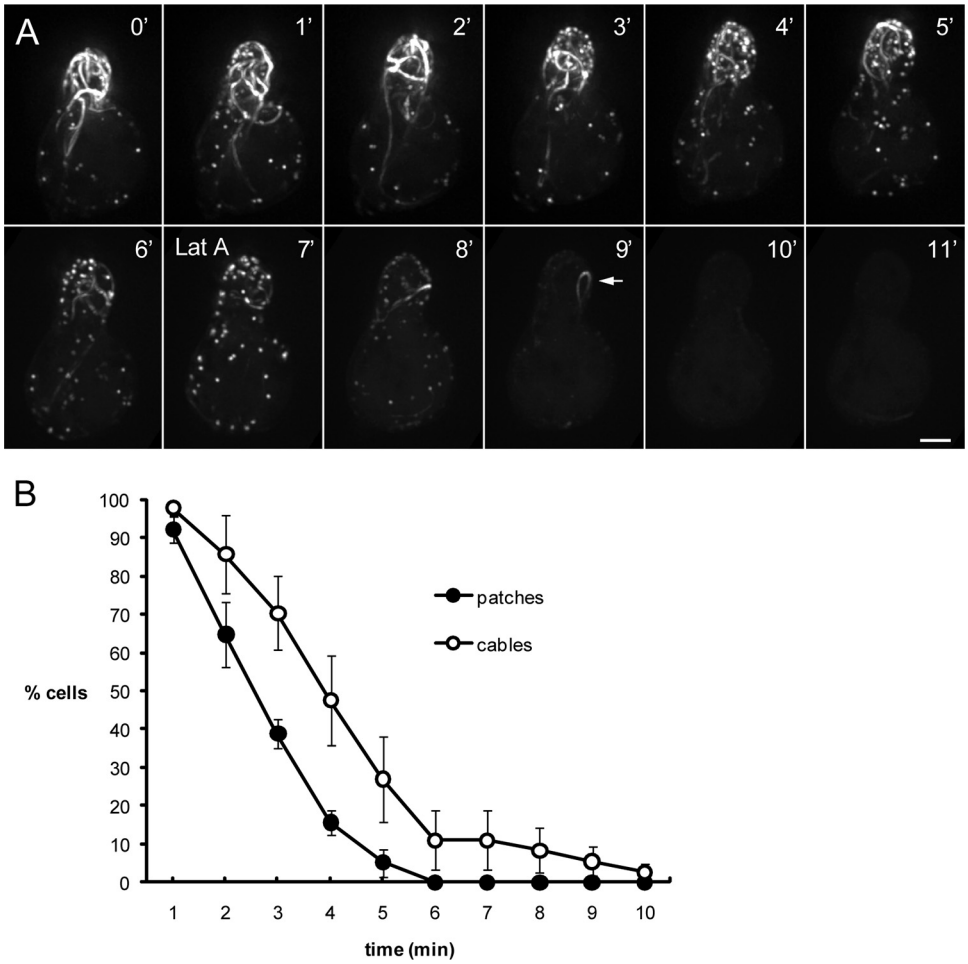

FIG. 2. Lifeact-GFP localization is sensitive to latrunculin A. Growing germ tubes of *N. crassa* were treated with 10 μM Lat A dissolved in DMSO. (A) Maximum-intensity projections of a time-lapse sequence of an elongating germ tube before and after Lat A treatment. Eleven minutes of the full 25-min sequence is shown. Lat A was added at the 7-min (7′) time point and caused a loss of Lifeact-GFP-labeled structures within 4 min. The arrow at the 9-min time point shows a cable that is not tethered to a particular site. The extension rate in the 10 min before Lat A addition was 0.24 μm/min. Following treatment, the extension rate was reduced to 0.005 μm/min. Incubation with an equivalent amount of DMSO (1%) had no effect on Lifeact-GFP localization (not shown). (B) Percentages of cells containing actin patches and actin cables after treatment with 10 μM Lat A (n = 39 cells). Bar, 2 μm. The error bars indicate standard deviations.

bles at the cell periphery and occasionally observed movement of patches along the length of a cable (see below and Fig. 4A and B; see Movie S5 in the supplemental material). The germ tubes analyzed in this study had extension rates of 0.05 to 1.5 μm/min (n = 30).

Latrunculin A caused a rapid loss of Lifeact-FP-labeled structures. Although the Lifeact-FP localization observed here was consistent with previous reports of F-actin distribution in yeast and filamentous fungi, we confirmed the F-actin specificity of the probe using latrunculin A. Latrunculins are potent inhibitors of F-actin polymerization and have been shown to cause rapid disruption of the actin cytoskeleton in fungi (6, 22, 29, 37, 55, 63). We monitored F-actin dynamics in a growing germ tube for 10 min before and after the addition of 10 μM Lat A (Fig. 2A). We found that treatment with Lat A led to a rapid loss of Lifeact-FP fluorescence associated with patches and cables. This confirmed that Lifeact-FP binds to F-actin in *N. crassa*. Germ tube elongation was abrogated by Lat A, emphasizing the importance of F-actin for tip growth (Fig. 2A). Interestingly, upon treatment with Lat A, we occasionally observed a subpopulation of cables that did not appear to be tethered to a particular site (Fig. 2A, arrow at 9 min) and displayed random motion. These cables eventually disassembled, but their initial insensitivity to Lat A showed that the rates of F-actin depolymerization varied within the population of cables. Quantification of the presence of patches and cables following Lat A treatment showed that patches were more sensitive to Lat A, with 83% of cells lacking patches after 4 min compared to 52% of cells lacking cables (n = 39 germlings) (Fig. 2B). Assuming that Lat A only affects actin polymerization (6), this finding also indicates that complete turnover of F-actin in patches and most cables occurs within 4 to 6 min, with cables generally having a longer half-life.

Retrograde movement of actin arrays accompanies polarized growth. Actin cables have been shown to be highly dynamic structures in budding yeast (63). In *N. crassa*, the actin cytoskeleton was in a constant state of flux, with individual actin cables displaying regular kinking and buckling along their

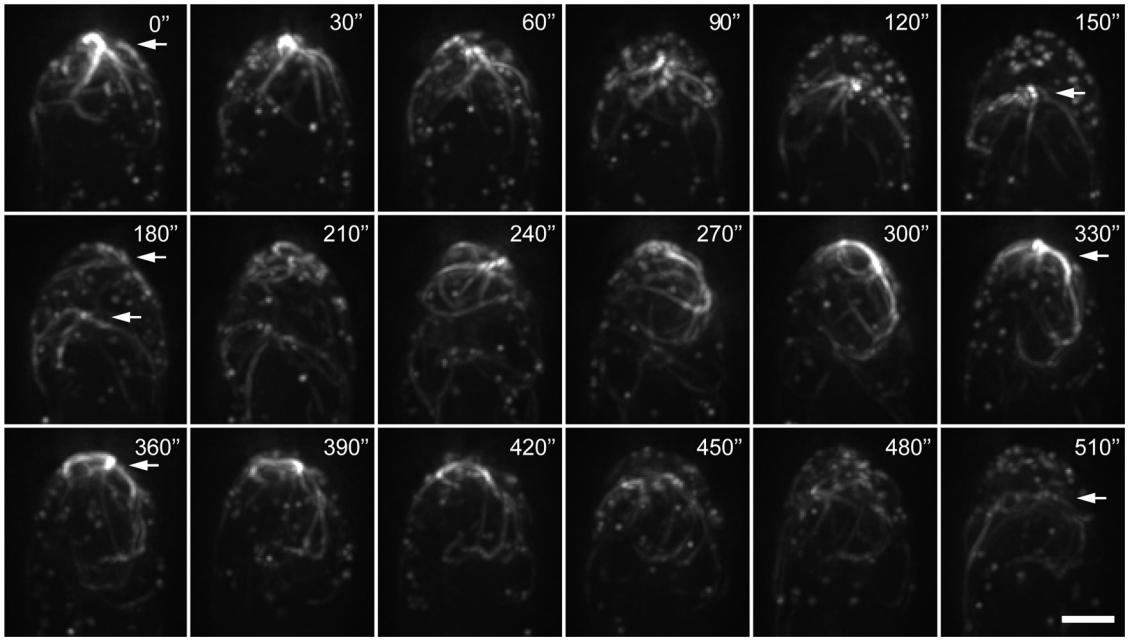

FIG. 3. Retrograde movement of actin cables during germ tube elongation. Maximum-intensity projections of a time-lapse series show actin cable dynamics. The arrow at the 0-s (0″) time point shows an actin array characterized by a bright focal point with cables emanating from it. At the 60-s time point, the actin array started to move back, and by 180 s, the array was no longer present at the germ tube tip. At the 180-s time point, a new actin array (upper arrow) had begun to form, and it subsequently underwent retrograde movement from the tip, as can be seen at the 510-s time point. The extension rate of the germling was 0.18 μm/min. Bar, 2 μm. (See Movies S2 and S3 in the supplemental material.)

lengths. We also observed numerous transient cable-cable interactions and the apparent "exploratory" movement of the untethered ends of individual cables after they were detached or severed (see Movie S1 in the supplemental material).

Another striking aspect of cable dynamics was observed during germ tube emergence and elongation (after 2 to 4 h of incubation). Actin arrays were associated with sites of polarized growth in germlings; intriguingly, these arrays were not static but formed within germ tube tips and underwent recurrent retrograde movement from the elongating tips (Fig. 3). This behavior was commonly observed during germ tube elongation but not during tip extension in mature hyphae (see below and Movies S2, S3, and S4 in the supplemental material). The whole process of actin array formation, retrograde movement, and dissolution generally occurred over a 2- to 10-min period.

Given the dynamic nature of actin cables, we attempted to measure the extension rate of cables from the tips. Yang and Pon (63) used "fiduciary" marks on actin cables to assess cable extension rates. We were unable to find similar stable reference points suitable for such analysis, and generally, quantitative analysis was hindered by the complicated architecture of actin arrays and their highly irregular movements. However, it was apparent that array formation involved the polymerization of cables and that cable extension pushed back the array while tip growth was occurring (see Movies S2 and S3 in the supplemental material).

Actin patches exhibit different types of behavior. Actin patches were visualized throughout the lengths of germlings but were concentrated at sites of active growth. Due to the extremely rapid movement of actin patches, time-lapse observations of patch dynamics were limited to a single focal plane. Consistent with reports on other fungi (3, 26, 37, 55, 57), in *N. crassa*, two types of actin patch movement could be distinguished: slow/nonlinear and fast/linear (Fig. 4; see Movie S5 in the supplemental material). Slow/nonlinear patches formed at the plasma membrane and, following a short period of undirected movement, tracked along actin cables and left the plane of focus, presumably moving to the interior of the cell (Fig. 4A). The mean velocity and lifetime of slow/nonlinear patches were determined to be 0.26 ± 0.08 μm/s and 14 s (n = 23; 6 germlings), respectively. In contrast, the mean velocity of fast/linear patches was 1.2 ± 0.21 μm/s (n = 14; 4 germlings). Fast/linear movement of patches was discontinuous and occurred along the lengths of actin cables, with patches traveling toward and away from the growing tip (Fig. 4B). In some instances, actin patches appeared on the plasma membrane and subsequently underwent directed linear movement along actin cables (see Movie S5 in the supplemental material).

Actin rings assemble prior to septum formation. We monitored the formation and dissipation of actin rings with Lifeact-FP (Fig. 5). Dual labeling with Lifeact-GFP and the cell wall stain calcofluor white showed that ring formation preceded septum formation and that as the septum matured the actin ring was cleaved into two separate accumulations of F-actin and eventually dissipated (Fig. 5A). The duration from initiation to dissipation varied between 30 and 60 min. Formation of these rings occurred by an initially loose accumulation of actin cables in a small area of the hypha, which gradually condensed and shaped itself into an actin ring (see Movie S6 in the supplemental material). Actin cables did not persist around

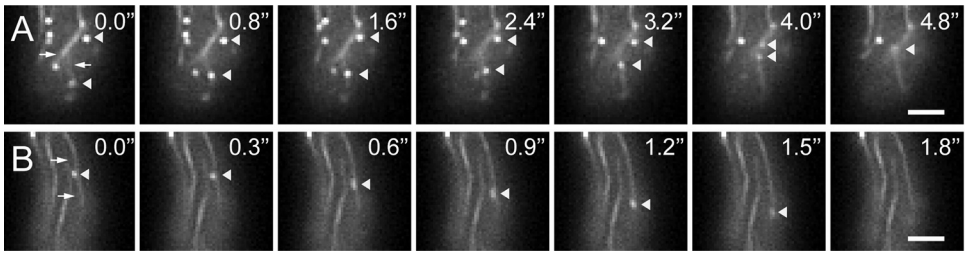

FIG. 4. Actin patches show close association with actin cables. The movement of Lifeact-GFP-labeled patches was monitored by time-lapse microscopy in a single focal plane. (A) Patches (arrowheads) formed at the plasma membrane exhibited a short period of slow/nonlinear movement and then tracked along actin cables (arrows) out of the plane of focus. (B) Fast/linear movement of an actin patch (arrowhead) along an actin cable (arrows). Bars, 2 μm.

the newly formed ring but appeared to be incorporated into its structure (Fig. 5B).

F-actin localization in mature hyphae is distinct from that in germ tubes. Lifeact-FP revealed marked differences in F-actin localization between the tip regions of mature hyphae and germ tubes. In mature hyphae, we observed a concentrated spot of F-actin at the extreme apices of hyphal tips, followed by an F-actin-depleted zone and a collar of actin patches 3.51 ± 1.21 μm ($n = 15$) from the F-actin spot (Fig. 6). The F-actin exclusion zone and spot were present in all actively growing mature hyphae that were observed ($n = 27$). We used the membrane-selective dye FM4-64 to determine whether the F-actin spot localized to the Spitzenkörper (Spk). The Spk is readily stained by FM4-64 and localizes to the tip region of actively growing mature hyphae (18, 23) but is absent from sites of polarized growth in germlings of *N. crassa* (4). Lifeact-FP/FM4-64 colabeling demonstrated that the F-actin spot localized to the core of the Spk, indicating that this may be a center for F-actin organization (Fig. 6B). Notably, actin cables were not visualized in the tip regions of actively growing mature hyphae, although we did observe an accumulation of cables prior to branch formation (Fig. 6C). Cables were present in the new branch for a short period (<10 min), after which the F-actin spot and collar of patches developed and the branches had achieved a linear rate of extension. The leading mature hyphae analyzed in this study exhibited extension rates of 9.1 to 12.4 μm/min ($n = 15$).

Coexpression of Lifeact-TagRFP and β-tubulin–GFP revealed distinct spatial organizations of F-actin and microtubules. In order to investigate the spatial relationship between F-actin and microtubules, we constructed a strain expressing Lifeact-TagRFP and β-tubulin–GFP. Both marker proteins accurately labeled their intended target polymers and showed no nonspecific background staining, cross excitation, or emission bleedthrough (see Movie S7 in the supplemental material). Our initial findings showed that F-actin and microtubules were distinctively organized in conidia and germlings of *N. crassa* (Fig. 7). We commonly observed regions within germlings occupied by F-actin that contained no or only very few microtubules (germ tube a in Fig. 7C), as well as the opposite situation, where microtubules extended into a germ tube tip in which F-actin arrays were absent (germ tube b in Fig. 7C). Recruitment of F-actin to the cell cortex during polarity estab-

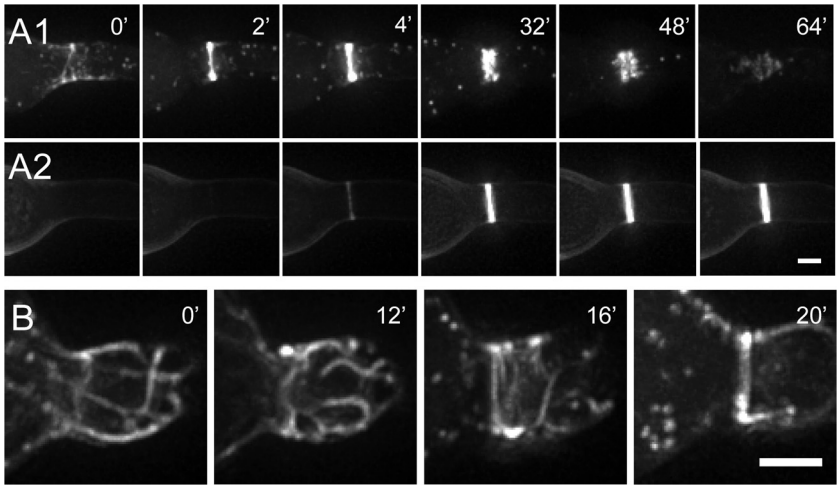

FIG. 5. Actin cables condense to form actin rings. (A1 and A2) Maximum-intensity projections of a time-lapse series showing Lifeact-FP (A1) and calcofluor white (A2) localization during septation. A septum was formed after the appearance of an actin ring. Ring cleavage was visible at the 48-min time point, and F-actin gradually dissipated thereafter. (B) Maximum-intensity projections of a time-lapse series showing actin ring formation. A dense network of actin cables is visible around the future site of ring formation between the 0- and 12-min time points. At 16 min, the cables gradually condensed into an actin ring, which was fully formed 4 min later. Bars, 2 μm.

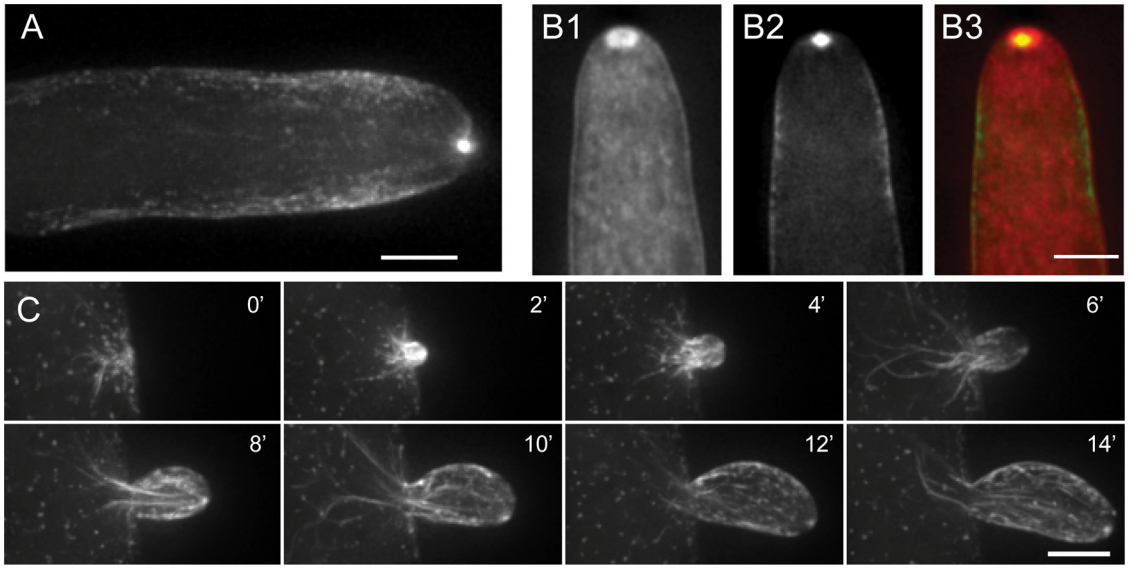

FIG. 6. Lifeact-GFP localization in mature hyphae. (A) Maximum-intensity projection of a hyphal tip. F-actin is concentrated in a spot at the tip, and patches are localized in a subapical collar around the hypha. (B1, B2, and B3) Lifeact-GFP and FM4-64 colabeling of a hyphal tip. (B1) FM4-64. (B2) Lifeact-GFP. (B3) Merged image of both channels with Lifeact-GFP in green and FM4-64 in red. Lifeact-GFP localized to the core of the Spitzenkörper and is shown in yellow where it colocalized with FM4-64. (C) Maximum-intensity projections of a time-lapse sequence showing branch formation. Actin cables were present during early stages of branch outgrowth, but F-actin organization changed as the new branch developed. Bars, 5 μm.

lishment was not accompanied by accumulation of microtubules at that site (ungerminated conidium c in Fig. 7C).

Actin organization during CAT formation is similar to that in germ tube emergence. Conidial anastomosis tubes (CATs) formed by conidia and germ tubes are attracted to and fuse with other CATs to form a germling network (41, 42, 45). The organization of F-actin during CAT formation was in general very similar to that observed during germ tube initiation and outgrowth (see Movie S8 in the supplemental material). CAT formation also coincided with localized accumulation of F-actin at the cell cortex and protrusion of a small bud (Fig. 8, arrowheads). An apical actin cap formed at the bud tip and remained present during CAT extension but eventually disappeared (Fig. 8G to I), suggesting that the CAT had stopped growing as it reached its determinate length (45). In the observed cell, CAT formation coincided with the transient dissolution of the F-actin array present at the germ tube tip (Fig. 8D to H, arrow) and coincided with a decrease in the tip extension rate. In neighboring cells that did not form CATs, actin arrays remained present at the germ tube tips throughout the time course (Fig. 8).

Actin arrays localize to CAT tips during homing and disappear after fusion but are redeployed during germ tube repolarization. During CAT-mediated cell fusion, we found that actin cables and patches localized to CAT tips (Fig. 1G and 9). When two CATs were homing toward each other, equal accumulations of fluorescence in both cell protrusions was typically observed. If only one of the interacting CATs was growing,

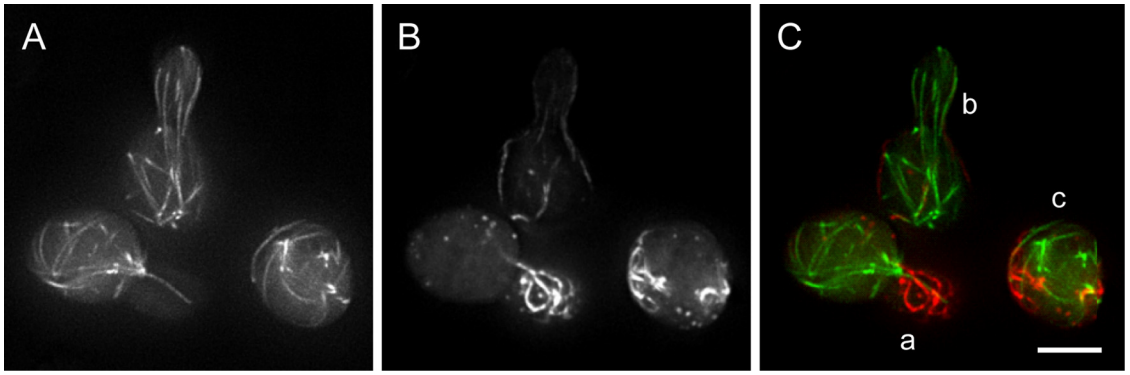

FIG. 7. F-actin and microtubules show distinct spatial organizations in conidia and germlings. (A) β-Tubulin–GFP signal from the middle section of a group of cells showing the distribution of microtubules. (B) Lifeact-TagRFP signal from the same section showing the F-actin distribution. (C) Merged image of panels A and B showing F-actin in red and microtubules in green. (a) Germling with an F-actin array at the tip but only very few microtubules extending into this region. (b) Germling with microtubules extending into the germ tube tip but with no dense accumulation of F-actin currently present. (c) Distribution of F-actin and microtubules in an ungerminated cell. Bar, 5 μm.

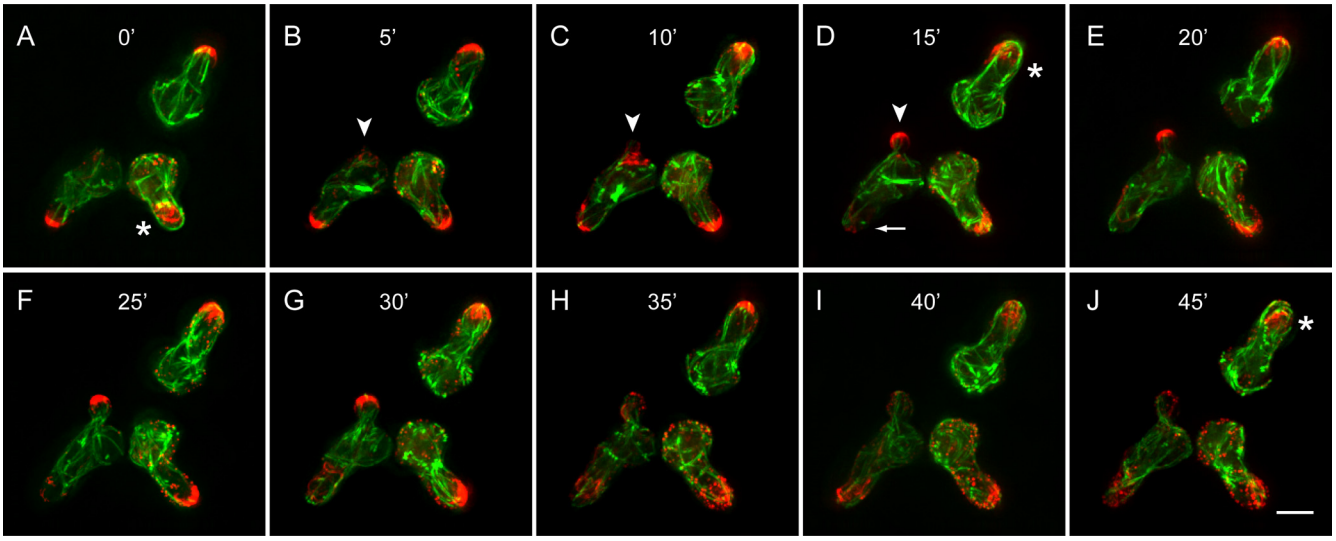

FIG. 8. CAT polarization and protrusion. Microtubules were labeled with β-tubulin–GFP, and F-actin was labeled with Lifeact-TagRFP. (A) Apical F-actin was present at germ tube tips in all three conidial germlings. Over time, these actin caps underwent retrograde movement and dissipation (asterisks) (see Fig. 3 for details). (B) The bottom left germling established a new site of cell polarity, as indicated by the recruitment of F-actin to the cell cortex (arrowhead). (C) Actin array formation coincided with CAT bud emergence. (D) As the CAT elongated, an actin cap formed at its apex. Formation of this CAT coincided with the disappearance of the actin cap in the germ tube tip of the same germling (arrow). (E to J) The CAT extended over the following 10 min but did not elongate beyond 4 to 5 μm in length (E to G), and between 30 and 35 min the actin cap finally disappeared (H to J). (C to H) During the period of CAT formation, germ tube extension was slower (0.04 μm/min) in the germling forming the CAT than in the two germlings that were not forming CATs (0.06 to 0.10 μm/min). CAT elongation, on the other hand, was more rapid (0.14 μm/min). Bar, 5 μm.

pronounced actin arrays were observed only in that one (Fig. 9). Upon contact, actin cables gradually disappeared from the fusion site, which was coincident with the cessation of polarized tip growth. Residual actin cables, however, persisted at the fusion site, suggesting that they may be involved in a later stage of the fusion process. Once cytoplasmic continuity was fully established, actin cables had disappeared from the fused CATs (Fig. 1H and 9H and I), whereas cortical actin patches remained (Fig. 1H). At this stage, germ tube extension resumed, which coincided with the formation of an apical actin array (Fig. 9E, arrowhead). Subsequent to F-actin redeployment, further elongation of the germ tube involved the dynamic re-

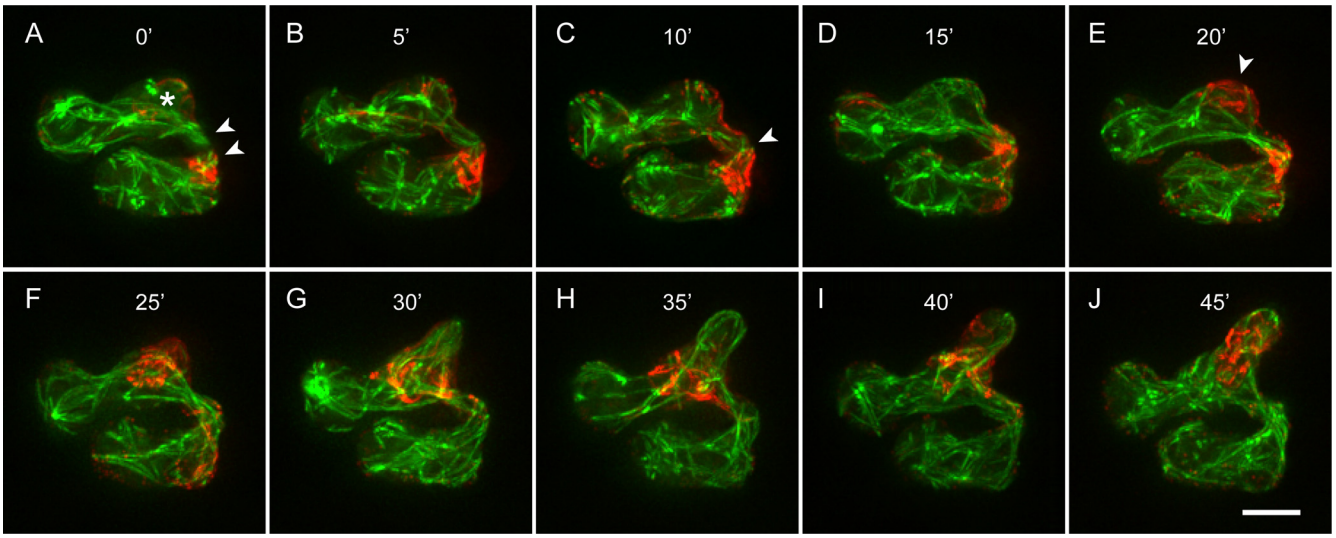

FIG. 9. F-actin dynamics during CAT-mediated cell fusion and germ tube reinitiation. Microtubules were labeled with β-tubulin–GFP, and F-actin was labeled with Lifeact-TagRFP. (A) Two CATs establishing cell-cell contact. The CATs are indicated by arrowheads; the germ tube is indicated by an asterisk. (B to E) Gradual repolarization of F-actin from the fusion site (arrowhead in panel C) to the germ tube tip (arrowhead in panel E). (F to J) F-actin undergoes dynamic rearrangement, while microtubules extend into the growing germ tube. In this instance, germ tube extension increased by a factor of 9 after cell fusion was completed (0.02 μm/min before fusion [A to E] and 0.18 μm/min after fusion [E to J]). Bar, 5 μm.

arrangement of the actin array (Fig. 9G to I). The reinitiation of germ tube growth was also accompanied by extension of microtubules into the tip (Fig. 9G to J).

DISCUSSION

Considerable effort has been expended in attempts to visualize F-actin distribution and dynamics in living fungal cells, and these attempts have mostly relied on fusions between FPs and actin or ABPs (14, 60, 63). The use of FP-actin fusions as reporters for F-actin is problematic, as only a fraction of actin is present in microfilaments, resulting in a low signal-to-noise ratio, and more importantly, the relatively large FP moiety has been shown to perturb actin dynamics in a variety of cell types (2, 43, 62). Thus, FP-actin fusion constructs are likely to alter actin dynamics in filamentous fungi. Fluorescent-protein tagging of ABPs is preferable, as there is generally less perturbation of actin dynamics *in vivo*, but this approach may reveal only a small population of F-actin and the fusion protein may compete with unlabeled endogenous ABPs (11, 61). Therefore, we utilized the Lifeact peptide as a reporter for F-actin in *N. crassa*, which has been shown to provide clear labeling of F-actin in various cell types without interfering with actin dynamics (5, 15, 43, 58, 63). Expression of Lifeact-FP from the *ccg-1* or *tef-1* promoter had no noticeable effect on radial extension rates, cell morphology, germination or cell fusion rates, colony development, or conidiation. The pattern of actin localization revealed by Lifeact-FP was consistent with previous reports on filamentous fungi using immunofluorescence, phalloidin staining, and FP-based live-cell imaging (3, 28, 55, 57) and allowed visualization of F-actin reorganization and polarization in *N. crassa*. Coexpression of Lifeact-TagRFP with β-tubulin–GFP allowed 4D reconstruction of the entire cytoskeleton during early stages of development in living cells of *N. crassa*. To our knowledge, this is the first report of simultaneous visualization of the dynamic interaction of F-actin and microtubules in living fungal cells.

We confirmed the specificity of Lifeact-FP for F-actin with the drug latrunculin A, which prevents F-actin polymerization (6). Treatment with 10 μM Lat A led to a rapid loss of Lifeact-FP-labeled patches and cables, demonstrating a high rate of F-actin turnover in *N. crassa*. Interestingly, although all cables disassembled within 10 min of Lat A treatment, some cables appeared to be initially insensitive to Lat A, implying that different subpopulations of actin cables with different turnover rates exist in *N. crassa*.

In budding yeast, actin cables form tracks for myosin-V-dependent transport of secretory vesicles, whereas actin patches are involved in endocytosis and membrane invagination (34). Both patches and cables localize to new buds in *S. cerevisiae*, but only actin cables are required for polarized secretion (26, 38, 63). The localization of actin patches and cables to the tips of germ tubes and CATs in *N. crassa* suggests active exo- and endocytosis in those regions and indicates a tight coupling of the two processes at this stage of development. Accumulation of actin cables and patches at sites of active growth in *N. crassa* confirms that polarization of the actin cytoskeleton underlies apical extension. Interestingly, the marked differences we observed in F-actin architecture in tip growing regions suggest that the spatial organization of exo- and endocytosis changes during development. A bright focal point of F-actin, colocalizing with the core region of the Spk, and an F-actin-depleted zone followed by a collar of actin patches were present in the tips of mature hyphae compared to the actin arrays and concentration of patches at the extreme apices of germ tubes. The F-actin spot could represent formin-mediated actin nucleation, creating tracks for exocytic vesicles; the formin SepA is found as a spot at hyphal tips that colocalizes with F-actin in *Aspergillus nidulans* (50). In contrast, subapical collars of actin patches are known to be involved in endocytosis in filamentous fungi (3, 57). Thus, it seems the sites of exo- and endocytosis are well separated in mature hyphae while they have tight association in germlings. Extension rates in mature hyphae are 10-fold more rapid than in germlings (4), and the spatial segregation of endocytosis and exocytosis indicates that reorganization of the secretory machinery underlies rapid extension, as has been reported in *Ashbya gossypii* (30).

Consistent with models of actin cable-mediated transport of secretory vesicles in budding yeast, in *N. crassa*, we found that dense arrays of actin cables were present at sites of germ tube emergence and branch formation. Interestingly, cable arrays persisted at the tips of elongating germ tubes and CATs, whereas during branch formation and outgrowth in the mature colony, cables were gradually lost from the tip to be replaced by an F-actin spot and a collar of patches. Lifeact-FP allowed us to monitor the formation of these complex arrays of actin cables during germ tube elongation and to observe their subsequent retrograde movement. This phenomenon was recurrent and was commonly observed during the initial stages of germ tube emergence and elongation but was not observed during branch formation or tip extension in the mature colony. The formation of actin arrays probably represents *de novo* assembly of cables at the tip, eventually leading to backflow of cable arrays. It was possible to observe the movement of a relatively intact array along the length of a germ tube and to monitor its eventual dissolution. It is likely that the disassembly of actin arrays is necessary for reincorporation of the resulting actin subunits into new cables at sites of active growth.

The importance of actin cables for polarized growth is also highlighted by cable localization during and after CAT-mediated cell fusion; dense actin arrays were shown to assemble at the cell cortex prior to CAT formation and to intensify during CAT extension and homing. Shortly after cell fusion, actin cables gradually disappeared from the fusion site while patches persisted. It has been proposed that the polarized secretion of biosynthetic materials is compensated for by endocytosis, maintaining the polarized state of cortical markers and receptors (31, 53, 57). Given the role of actin patches in endocytosis, it is possible that the accumulation of actin patches at the tips of homing CATs and their persistence shortly after fusion facilitates the recycling of membrane receptors and polarity factors no longer required at this site.

Furthermore, Lifeact-FP also showed that actin cables are not always associated with tip growth but have an additional role in septum formation. A formin homolog, SepA, is required for actin ring formation and septation in *A. nidulans*, and it is likely that the *N. crassa* SepA homolog plays a similar role (50). Interestingly, in *N. crassa*, actin rings were formed by the gradual accumulation of preexisting actin cables and their concentration into a ring rather than by *de novo* assembly of

F-actin into a ring. This suggests that ring formation involves both formin-mediated cable production and regulation of the spatial organization of actin cables postproduction.

Coexpression of Lifeact-TagRFP and β-tubulin–GFP revealed distinct but coordinated recruitment of F-actin and microtubules during different stages of cell polarization and tip extension during colony initiation. Previous studies using microtubule-depolymerizing drugs showed that germ tube emergence (but not elongation) can be achieved in *N. crassa* without microtubules (7). Our data showing that polarization of F-actin always preceded polarization of microtubules further reinforces the notion that germ tube emergence and elongation is a two-step process (9, 21) that first involves F-actin to establish a polarized bud and maintain tip polarity but subsequently requires microtubules for further extension. In contrast, CATs are thinner than germ tubes, show determinate growth (45), and do not require microtubules to facilitate cell fusion (46). Consistently, we observed the dynamic rearrangement of actin organization during CAT formation and fusion, suggesting a predominant role for actin in these processes. This notion is supported by findings in *Ustilago maydis*, where it has been demonstrated that cell-cell recognition and cell-cell fusion exclusively depend on F-actin during all stages of polar growth whereas microtubules are required only for long-distance growth of hyphae (19). The function of CATs is to connect cells that are less than 10 to 12 μm apart, i.e., CATs do not need to extend further than 5 to 6 μm. The F-actin cytoskeleton is apparently sufficient to support this short-distance growth and to facilitate fusion. Our observations suggest that recruitment of both cytoskeletal elements occurs in a distinct but coordinated manner and might influence which protrusion is being formed and maintained at any point in time.

Three-dimensional reconstruction and time-lapse microscopy demonstrated a close association of patches and cables (Fig. 1 and 4). Generally, we observed two types of patch behavior: slow/nonlinear and fast/linear movement. Patch formation occurred at the cell cortex and was followed by a short period of undirected movement; then, the patches traveled out of the plane of focus, presumably toward the interior of the cell. The measured velocities and lifetimes of slow/nonlinear patches, 0.26 μm/s and 14 s, respectively, were similar to values obtained for endocytic patches of *A. nidulans* (velocity, 0.19 μm/s; lifetime, 24 s), *Schizosaccharomyces pombe* (velocity, 0.31 μm/s; lifetime, not determined), and *S. cerevisiae* (velocity, 0.1 to 0.5 μm/s; lifetime, 10 to 20 s), and thus, these patches probably represent endocytic vesicles decorated with F-actin (3, 26, 34, 37, 55, 57, 60). Lifeact-FP-labeled patches also underwent directional movement along cables in a discontinuous manner, and occasionally we observed the movement of patches from the cell surface onto actin cables, along which they were transported. These observations strongly indicate that in *N. crassa*, F-actin-decorated endocytic vesicles form at the plasma membrane and, following invagination and scission, can be transported along actin cables. Our observations of patch dynamics in *N. crassa* are consistent with current models of patch formation, which describe how patch movement is correlated with their maturation state (34).

The movement of actin patches along cables has been shown in budding yeast and fission yeast, and in *A. nidulans* actin patches have been shown to undergo linear directed movement along unidentified structures (26, 37, 57). Most interestingly, in *N. crassa*, patches were transported towards and away from the tip, which contrasts with the findings of Huckaba et al. (26), who reported that in budding yeast directional movement of patches along cables is always retrograde to the site of polarized growth. Based on their findings, Huckaba et al. (26) concluded that retrograde patch movement is coupled with the retrograde flow of cables. The saltatory nature and high speed (1.2 μm/s) of actin patch transport along cables in *N. crassa* suggest the involvement of motor proteins (presumably myosins), and the bidirectionality of patch movement implies that F-actin-decorated vesicles can travel toward and away from regions of active growth. The possibility that Lifeact-FP may be labeling "patch-like" structures containing F-actin that are not bona fide endocytic patches should also be considered. Lifeact may be labeling a class of actin-coated microvesicles, termed filasomes (25), that have been shown at the ultrastructural level in fungal hyphae (8, 44).

In conclusion, Lifeact-FP gave clear and robust labeling of F-actin in *N. crassa* without any detectable toxic side effects and provided novel insights into the dynamic reorganization and polarization of the actin cytoskeleton during tip growth and cell fusion. We predict that Lifeact-FP will become a useful tool for studying the regulation, dynamics, and organization of the fungal actin cytoskeleton in the future.

ACKNOWLEDGMENTS

We thank David Kelly from the Centre Optical Instrumentation Laboratory (COIL) at Edinburgh University for help with the DeltaVision system.

Funding for this project was provided by a Biotechnology and Biological Sciences Research Council grant BB/E010741/1 to N.D.R.

REFERENCES

1. **Adams, A., and J. Pringle.** 1984. Relationship of actin and tubulin distribution to bud growth in wild-type and morphogenetic-mutant *Saccharomyces cerevisiae*. J. Cell Biol. **98:**934–945.
2. **Aizawa, H., M. Sameshima, and I. Yahara.** 1997. A green fluorescent protein-actin fusion protein dominantly inhibits cytokinesis, cell spreading, and locomotion in *Dictyostelium*. Cell Struct. Funct. **22:**335–345.
3. **Araujo-Bazán, L., M. A. Peñalva, and E. A. Espeso.** 2008. Preferential localization of the endocytic internalization machinery to hyphal tips underlies polarization of the actin cytoskeleton in *Aspergillus nidulans*. Mol. Microbiol. **67:**891–905.
4. **Araujo-Palomares, C. L., E. Castro-Longoria, and M. Riquelme.** 2007. Ontogeny of the Spitzenkörper in germlings of *Neurospora crassa*. Fungal Genet. Biol. **44:**492–503.
5. **Asakura, T., T. Sasaki, F. Nagano, A. Satoh, H. Obaishi, H. Nishioka, H. Imamura, K. Hotta, K. Tanaka, H. Nakanishi, and Y. Takai.** 1998. Isolation and characterization of a novel actin filament-binding protein from *Saccharomyces cerevisiae*. Oncogene **16:**121–130.
6. **Ayscough, K. R., J. Stryker, N. Pokala, M. Sanders, P. Crews, and D. G. Drubin.** 1997. High rates of actin filament turnover in budding yeast and roles for actin in establishment and maintenance of cell polarity revealed using the actin inhibitor Latrunculin-A. J. Cell Biol. **137:**399–416.
7. **Barja, F., M.-L. Chappuis, and G. Turian.** 1993. Differential effects of anticytoskeletal compounds on the localization and chemical patterns of actin in germinating conidia of *Neurospora crassa*. FEMS Microbiol. Lett. **107:**261–266.
8. **Bourett, T. M., and R. J. Howard.** 1991. Ultrastructural immunolocalization of actin in a fungus. Protoplasma **163:**199–202.
9. **Brand, A., and N. A. R. Gow.** 2009. Mechanisms of hypha orientation of fungi. Curr. Opin. Microbiol. **12:**350–357.
10. **Bretscher, A.** 2003. Polarized growth and organelle segregation in yeast: the tracks, motors, and receptors. J. Cell Biol. **160:**811–816.
11. **Burkel, B. M., G. von Dassow, and W. M. Bement.** 2007. Versatile fluorescent probes for actin filaments based on the actin-binding domain of utrophin. Cell Motil. Cytoskel. **64:**822–832.
12. **Chiu, W., Y. Niwa, W. Zeng, T. Hirano, H. Kobayashi, and J. Sheen.** 1996. Engineered GFP as a vital reporter in plants. Curr. Biol. **6:**325–330.

13. **Davis, R. H.** 2000. *Neurospora*: contributions of a model organism, Oxford University Press, New York, NY.
14. **Doyle, T., and D. Botstein.** 1996. Movement of yeast cortical actin cytoskeleton visualized *in vivo*. Proc. Natl. Acad. Sci. U. S. A. **93:**3886–3891.
15. **Era, A., M. Tominaga, K. Ebine, C. Awai, C. Saito, K. Ishizaki, K. T. Yamato, T. Kohchi, A. Nakano, and T. Ueda.** 2009. Application of Lifeact reveals F-actin dynamics in *Arabidopsis thaliana* and the liverwort, *Marchantia polymorpha*. Plant Cell Physiol. **50:**1041–1048.
16. **Evangelista, M., D. Pruyne, D. C. Amberg, C. Boone, and A. Bretscher.** 2002. Formins direct Arp2/3-independent actin filament assembly to polarize cell growth in yeast. Nat. Cell Biol. **4:**32–34.
17. **Fehrenbacher, K. L., H. C. Yang, A. C. Gay, T. M. Huckaba, and L. A. Pon.** 2004. Live-cell imaging of mitochondrial movement along actin cables in budding yeast. Curr. Biol. **14:**1996–2004.
18. **Fisher-Parton, S., R. M. Parton, P. C. Hickey, J. Dijksterhuis, H. A. Atkinson, and N. D. Read.** 2000. Confocal microscopy of FM4-64 as a tool for analyzing endocytosis and vesicle trafficking in living fungal hyphae. J. Microsc. **198:**246–259.
19. **Fuchs, U., I. Manns, and G. Steinberg.** 2005. Microtubules are dispensable for the initial pathogenic development but required for long-distance hyphal growth in the corn smut fungus *Ustilago maydis*. Mol. Biol. Cell **16:**2746–2758.
20. **Harris, S. D., J. L. Morrell, and J. E. Hamer.** 1994. Identification and characterization of *Aspergillus nidulans* mutants defective in cytokinesis. Genetics **136:**517–532.
21. **Harris, S. D.** 2006. Cell polarity in filamentous fungi: shaping the mold. Int. Rev. Cytol. **251:**41–77.
22. **Heath, I. B., G. Gupta, and S. Bai.** 2000. Plasma membrane-adjacent actin filaments, but not microtubules, are essential for both polarization and hyphal tip morphogenesis in *Saprolegnia ferax* and *Neurospora crassa*. Fungal Genet. Biol. **30:**45–62.
23. **Hickey, P. C., S. R. Swift, M. G. Roca, and N. D. Read.** 2005. Live-cell imaging of filamentous fungi using vital dyes and confocal microscopy, p. 63–87. *In* T. Savidge and C. Pothoulakis (ed.), Methods in microbiology, vol. 34. Elsevier Academic Press, London, United Kingdom.
24. **Honda, S., and E. U. Selker.** 2009. Tools for fungal proteomics: multifunctional *Neurospora* vectors for gene replacement, protein expression and protein purification. Genetics **182:**11–23.
25. **Howard, R. J.** 1981. Ultrastructural analysis of hyphal tip cell growth in fungi: Spitzenkörper, cytoskeleton and endomembranes after freeze-substitution. J. Cell Sci. **48:**89–103.
26. **Huckaba, T. M., A. C. Gay, L. F. Pantalena, H. C. Yang, and L. A. Pon.** 2004. Live-cell imaging of the assembly, disassembly, and actin cable-dependent movement of endosomes and actin patches in the budding yeast, *Saccharomyces cerevisiae*. J. Cell Biol. **167:**519–530.
27. **Karpova, T. S., K. Tatchell, and J. A. Cooper.** 1995. Actin filaments in yeast are unstable in the absence of capping protein or fimbrin. J. Cell Biol. **131:**1483–1493.
28. **Knechtle, P., F. Dietrich, and P. Philippsen.** 2003. Maximal polar growth potential depends on the polarisome component AgSpa2 in the filamentous fungus *Ashbya gossypii*. Mol. Biol. Cell **14:**4140–4154.
29. **Knechtle, P., J. Wendland, and P. Philippsen.** 2006. The SH3/PH domain protein AgBoi1/2 collaborates with the Rho-type GTPase AgRho3 to prevent nonpolar growth at hyphal tips of *Ashbya gossypii*. Eukaryot. Cell **5:**1635–1647.
30. **Köhli, M., V. Galati, K. Boudier, R. W. Roberson, and P. Philippsen.** 2008. Growth-speed-correlated localization of exocyst and polarisome components in growth zones of *Ashbya gossypii* hyphal tips. J. Cell Sci. **121:**3878–3889.
31. **Marco, E., R. Wedlich-Soldner, R. Li, S. J. Altschuler, and L. F. Wu.** 2007. Endocytosis optimizes the dynamic localization of membrane proteins that regulate cortical polarity. Cell **129:**411–422.
32. **Margolin, B. S., M. Freitag, and E. U. Selker.** 1997. Improved plasmids for gene targeting at the *his-3* locus of *Neurospora crassa* by electroporation. Fungal Genet. Newsl. **44:**34–36.
33. **Merzlyak, E. M., J. Goedhart, D. Shcherbo, M. E. Bulina, A. S. Shcheglov, A. F. Fradkov, A. Gaintzeva, K. A. Lukyanov, S. Lukyanov, T. W. Gadella, and D. M. Chudakov.** 2007. Bright monomeric red fluorescent protein with an extended fluorescence lifetime. Nat. Methods **4:**555–557.
34. **Moseley, J. B., and B. L. Goode.** 2006. The yeast actin cytoskeleton: from cellular function to biochemical mechanism. Microbiol. Mol. Biol. Rev. **70:**605–645.
35. **Novick, P., and D. Botstein.** 1985. Phenotypic analysis of temperature-sensitive yeast actin mutants. Cell **40:**405–416.
36. **Pall, M. L., and J. P. Brunelli.** 1994. New plasmid and lambda/plasmid hybrid vectors and a *Neurospora crassa* genomic library containing the bar selectable marker and the Cre/lox site-specific recombination system for use in filamentous fungi. Fungal Genet. Newsl. **41:**63–65.
37. **Pelham, R. J., and F. Chang.** 2001. Role of actin polymerization and actin cables in actin-patch movement in *Schizosaccharomyces pombe*. Nat. Cell Biol. **3:**235–244.
38. **Pruyne, D. W., D. H. Schott, and A. Bretscher.** 1998. Tropomyosin-containing actin cables direct the Myo2p-dependent polarized delivery of secretory vesicles in budding yeast. J. Cell Biol. **143:**1931–1945.
39. **Rasmussen, C. G., and N. L. Glass.** 2005. A rho-type GTPase, *rho-4*, is required for septation in *Neurospora crassa*. Eukaryot. Cell **4:**1913–1925.
40. **Rasmussen, C. G., and N. L. Glass.** 2007. Localization of RHO-4 indicates differential regulation of conidial versus vegetative septation in the filamentous fungus *Neurospora crassa*. Eukaryot. Cell **6:**1097–1107.
41. **Read, N. D., A. Lichius, J. Y. Shoji, and A. B. Goryachev.** 2009. Self-signalling and self-fusion in filamentous fungi. Curr. Opin. Microbiol. **12:**608–615.
42. **Read, N. D., A. Fleißner, M. G. Roca, and N. L. Glass.** 2010. Hyphal fusion. *In* K. A. Borkovich and D. Ebbole (ed.), Cellular and molecular biology of filamentous fungi. ASM Press, Washington, DC.
43. **Riedl, J., A. H. Crevenna, K. Kessenbrock, J. H. Yu, D. Neukirchen, M. Bista, F. Bradke, D. Jenne, T. A. Holak, Z. Werb, M. Sixt, and R. Wedlich-Soldner.** 2008. Lifeact: a versatile marker to visualize F-actin. Nat. Methods **5:**605–607.
44. **Roberson, R. W.** 1992. The actin cytoskeleton in hyphal cells of *Sclerotium rolfsii*. Mycologia **84:**41–51.
45. **Roca, M. G., J. Arlt, C. E. Jeffree, and N. D. Read.** 2005. Cell biology of conidial anastomosis tubes in *Neurospora crassa*. Eukaryot. Cell **4:**911–919.
46. **Roca, M. G., H.-C. Kuo, A. Lichius, M. Freitag, and N. D. Read.** 5 March 2010. Nuclear dynamics, mitosis, and the cytoskeleton during the early stages of colony initiation in *Neurospora crassa*. Eukaryot. Cell doi:10.1128/EC.00329-09.
47. **Sagot, I., S. K. Klee, and D. Pellman.** 2002. Yeast formins regulate cell polarity by controlling the assembly of actin cables. Nat. Cell Biol. **4:**42–50.
48. **Schott, D. H., R. N. Collins, and A. Bretscher.** 2002. Secretory vesicle transport velocity in living cells depends on the myosin-V lever arm length. J. Cell Biol. **156:**35–39.
49. **Shaner, N. C., M. Z. Lin, M. R. McKeown, P. A. Steinbach, K. L. Hazelwood, M. W. Davidson, and R. Y. Tsien.** 2008. Improving the photostability of bright monomeric orange and red fluorescent proteins. Nat. Methods **5:**545–551.
50. **Sharpless, K. E., and S. D. Harris.** 2002. Functional characterization and localization of the *Aspergillus nidulans* formin SEPA. Mol. Biol. Cell **13:**469–479.
51. **Shortle, D., J. E. Haber, and D. Botstein.** 1982. Lethal disruption of the yeast actin gene by integrative DNA transformation. Science **217:**371–373.
52. **Shortle, D., P. Novick, and D. Botstein.** 1984. Construction and genetic characterization of temperature-sensitive alleles of the yeast actin gene. Proc. Natl. Acad. Sci. U. S. A. **81:**4889–4893.
53. **Steinberg, G.** 2007. On the move: endosomes in fungal growth and pathogenicity. Nat. Rev. Microbiol. **5:**309–316.
54. **Suei, S., and A. Garrill.** 2008. An F-actin-depleted zone is present at the hyphal tip of invasive hyphae of *Neurospora crassa*. Protoplasma **232:**165–172.
55. **Taheri-Talesh, N., T. Horio, L. Araujo-Bazán, X. Dou, E. A. Espeso, M. A. Peñalva, S. A. Osmani, and B. R. Oakley.** 2008. The tip growth apparatus of *Aspergillus nidulans*. Mol. Biol. Cell **19:**1439–1449.
56. **Torralba, S., M. Raudaskoski, A. M. Pedregosa, and F. Laborda.** 1998. Effect of cytochalasin A on apical growth, actin cytoskeleton organization and enzyme secretion in *Aspergillus nidulans*. Microbiology **144:**45–53.
57. **Upadhyay, S., and B. D. Shaw.** 2008. The role of actin, fimbrin and endocytosis in growth of hyphae in *Aspergillus nidulans*. Mol. Microbiol. **68:**690–705.
58. **Vidali, L., C. M. Rounds, P. K. Hepler, and M. Bezanilla.** 2009. Lifeact-mEGFP reveals a dynamic apical F-actin network in tip growing plant cells. PLoS One **4:**e5744.
59. **Virag, A., and A. J. Griffiths.** 2004. A mutation in the *Neurospora crassa* actin gene results in multiple defects in tip growth and branching. Fungal Genet. Biol. **41:**213–225.
60. **Waddle, J. A., T. S. Karpova, R. H. Waterston, and J. A. Cooper.** 1996. Movement of cortical actin patches in yeast. J. Cell Biol. **132:**861–870.
61. **Washington, R. W., and D. A. Knecht.** 2008. Actin binding domains direct actin-binding proteins to different cytoskeletal locations. BMC Cell Biol. **9:**10.
62. **Wu, J. Q., and T. D. Pollard.** 2005. Counting cytokinesis proteins globally and locally in fission yeast. Science **310:**310–314.
63. **Yang, H. C., and L. A. Pon.** 2002. Actin cable dynamics in budding yeast. Proc. Natl. Acad. Sci. U. S. A. **99:**751–756.
64. **Yokoyama, K., H. Kaji, K. Nishimura, and M. Miyaji.** 1990. The role of microfilaments and microtubules in apical growth and dimorphism of *Candida albicans*. J. Gen. Microbiol. **136:**1067–1075.

Eukaryot Cell. 2010 Mar 5. [Epub ahead of print]

Nuclear dynamics, mitosis and the cytoskeleton during the early stages of colony initiation in Neurospora crassa.

Roca MG, Kuo HC, Lichius A, Freitag M, Read ND.

Fungal Cell Biology Group, Institute of Cell Biology, Rutherford Building, University of Edinburgh, Edinburgh EH9 3JH, UK; Dept. of Biochemistry and Biophysics, Center for Genome Research and Biocomputing, Oregon State University, Corvallis, OR 97331-7305, USA.

Abstract

Neurospora crassa macroconidia form germ tubes that are involved in colony establishment, and conidial anastomosis tubes (CATs) that fuse to form interconnected networks of conidial germlings. Nuclear and cytoskeletal behavior were analyzed in macroconidia, germ tubes and CATs in strains that expressed fluorescently labelled proteins. Heterokaryons formed by CAT fusion provided a rapid method for imaging multiple labelled fusion proteins, and minimised the potential risk of overexpression artefacts. Mitosis occurred more slowly in non-germinated macroconidia (1.0-1.5 h) than in germ tubes (16-20 min). The nucleoporin SON-1 was not released from the nuclear envelope during mitosis, which suggests that N. crassa exhibits a form of 'closed mitosis'. During CAT homing, nuclei did not enter CATs and mitosis was arrested. Benomyl treatment showed that CAT induction, homing and fusion, as well as nuclear migration through fused CATs, do not require microtubules or mitotis. Three ropy mutants (ro-1, ro-3 and ro-11) defective in the dynein/dynactin microtubule motor were impaired in nuclear positioning but nuclei still migrated through fused CATs. Latrunculin B treatment, imaging F-actin in living cells using Lifeact-RFP, and analysis of mutants defective in the Arp2/3 complex demonstrated that actin plays important roles in CAT fusion.

PMID: 20207852 [PubMed - as supplied by publisher]